Base-Promoted Aryl Carbon-Halogen Bond Cleavages by Iridium(III) Porphyrins

CHEUNG, Chi Wai

A Thesis Submitted

in Partial Fulfillment of the Requirements for the Degree of

Doctor of Philosophy

in

Chemistry

The Chinese University of Hong Kong

December 2010

UMI Number: 3492039

UMI®

Dissertation Publishing

UMI 3492039

ProQuest®

<u>Thesis / Assessment Committee</u>

Professor SHING, Tony Kung Ming (Chair)

Professor CHAN, Kin Shing (Thesis Supervisor)

Professor LEE, Hung Kay (Committee Member)

Professor HSU, Hsiu-fu (External Examiner)

Table of Contents

Acknowledgement

First and foremost, I would like to express my most sincere gratitude to my supervisor, Prof. Kin Shing Chan, for his invaluable advice, patient guidance, enthusiasm, and continuous encouragement throughout my undergraduate and postgraduate studies. He lets me recognize the importance of fundamental chemical researches to the societies. He also helps me broaden my horizon and deepen my interest in chemistry.

Thanks are also given to all members of the Department of Chemistry for their kindly help and technical supports in all circumstances.

I would also like to thank all my seniors: Dr. Fuk Yee Kwong, Dr. Siu Kwan Yeung, Dr. Lirong Zhang, Dr. Xinzhu Li, and Ms. Cheuk Man Lau for their advices, supports, and encouragements in my research life.

Last but not least, I have to thank all my dear former and current group members: Mr. Peng Fai Chiu, Dr. Baozhu Li, Dr. Tsz Ho Lai, Dr. Yun Wai Chan, Dr. Jenkins Yin Ki Tsang, Ms. Xu Song, Mr. Kwong Shing Choi, Mr. Man Ho Lee, Mr. Hong Sang Fung, Mr. Chung Yin Chan, Ms. Ching Chi Au, Ms. Siu Yin Lee, Ms. Yingying Qian, Mr. Ching Tat To, and Mr. Chung Sum Chan for their encouragements, helpful discussions, and inspirations of research ideas. I wish them continued success in their researches and careers.

September, 2010.

Chi Wai Cheung

Department of Chemistry

The Chinese University of Hong Kong

Abbreviations

δ	chemical shift	m	multiplet (NMR)
λ	wavelength (nm)	*m-*	*meta-*
ΔG	Gibbs free energy change	mg	milligram(s)
ΔH	enthalpy change	min	minutes(s)
ΔS	entropy change	mL	millimeter(s)
μL	microliter(s)	mmol	millimole(s)
^1H NMR	proton NMR spectroscopy	M	molarity
^{13}C NMR	carbon 13 NMR spectroscopy	M^+ / M	molecular ion
acac	acetoacetate anion	Me	CH_3, methyl
Anal	analytical	MHz	megahertz
Ar	aryl	MS	mass spectrometry
Bn	benzyl	nm	nanometer
BDE	bond dissociation energy	NMR	nuclear magnetic resonance
br	broad singlet (NMR)	*o-*	*ortho-*
Bu	*tert*-butyl	OAc	acetate anion
Calcd	calculated	ppm	part per million
C-X	carbon-halogen bond(s)	PPh_3	triphenylphosphine
CCA	carbon-carbon bond activation	Ph	phenyl
CHA	carbon-hydrogen bond activation	Phth	phthalimide
COD	1,5-cyclooctadiene	por	porphyrin dianion
Cp	cyclopentadienyl	py	pyridine
d	day(s)	*p-*	*para-*
d	doublet (NMR)	q	quartet (NMR)
dd	doublet of doublet (NMR)	r t	room temperature
E	electrochemical potential	R	alkyl group
FAB	fast atom bombardment	s	second(s)
ESI	electrospray ionization	s	singlet (NMR)
g	gram(s)	t	triplet (NMR)
GC-MS	gas chromatography mass spectrometry	temp	temperature
h	hour(s)	TEMPO	2,2,6,6-tetramethylpiperidinoxy
HRMS	high-resolution mass spectrometry	TFA	trifluoroacetic acid
Hz	Hertz	THF	tetrahydrofuran
IR	infrared	TLC	thin-layer chromatography
J	coupling constant	TMS	tetramethylsilane
k	rate constant	$(TMS)_4Si$	tetrakis(trimethylsilyl)silane
K	equilibrium constant	Tol	tolyl
L	ligand	X	halide (F, Cl, Br, I)

Structural Abbreviations of Porphyrins
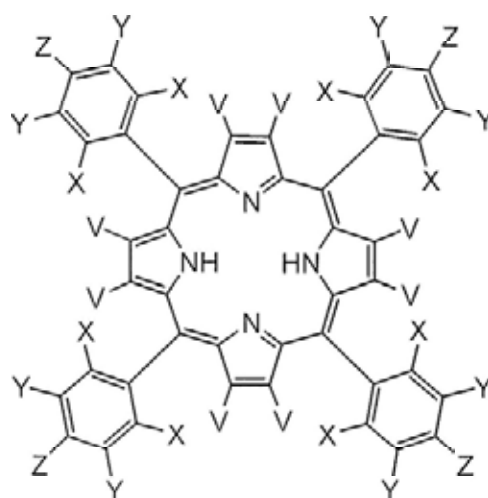
Nomenclature of Porphyrins

Abbreviations	Porphyrins	Substitutions			
		V	X	Y	Z
$H_2(oep)$	2,3,7,8,12,13,17,18-octaethylporphyrin	Et			
$H_2(tpp)$	5,10,15,20-tetraphenylporphyrin	H	H	H	H
$H_2(ttp)$	5,10,15,20-tetrakis(p-tolyl)porphyrin	H	H	H	Me
$H_2(txp)$	5,10,15,20-tetrakis(m-xylyl)porphyrin	H	H	Me	H
$H_2(tmp)$	5,10,15,20-tetramesitylporphyrin	H	Me	H	Me
$H_2(ttepp)$	5,10,15,20-tetrakis(2,4,6-triethylphenyl)-porphyrin	H	Et	H	Et
$H_2(ttipp)$	5,10,15,20-tetrakis(2,4,6-triisopropylphenyl)-porphyrin	H	^iPr	H	^iPr
$H_2(tspp)$	5,10,15,20-tetrakis(p-sulfonatophenyl)-porphyrin	H	H	H	SO_3^-
$H_2(tmps)$	5,10,15,20-tetrakis(3,5-disulfonatomesityl)-porphyrin	H	Me	SO_3^-	Me
$H_2(bocp)$	2,3,7,8,12,13,17,18-octachloro-5,10,15,20-tetrakis(p-$tert$-butylphenyl)porphyrin	Cl	H	H	^tBu
H_2t-3,4,5-tmpp	5,10,15,20-tetrakis(3,4,5-trimethoxyphenyl)-porphyrin	H	H	OMe	OMe
H_2t-2,4,6-tmpp	5,10,15,20-tetrakis(2,4,6-trimethoxyphenyl)-porphyrin	H	OMe	H	OMe
H_2Cl_8tpp	5,10,15,20-tetrakis(2,6-dichlorophenyl)-porphyrin	H	Cl	H	H
$H_2(tap)$	5,10,15,20-tetrakis(p-anisyl)porphyrin	H	H	H	OMe

Abstract

This thesis focuses on the discovery of base-promoted selective aryl carbon-halogen bond (Ar-X, X = Cl, Br, I) cleavages by chloro(carbonyl)(5,10,15,20-tetrakis-(p-tolyl)porphyrinato)iridium(III) (iridium(III) porphyrin carbonyl chloride, $Ir^{III}(ttp)(CO)Cl$ in benzene solvent to give iridium(III) porphyrin aryls ($Ir^{III}(ttp)Ar$) (eq 1).
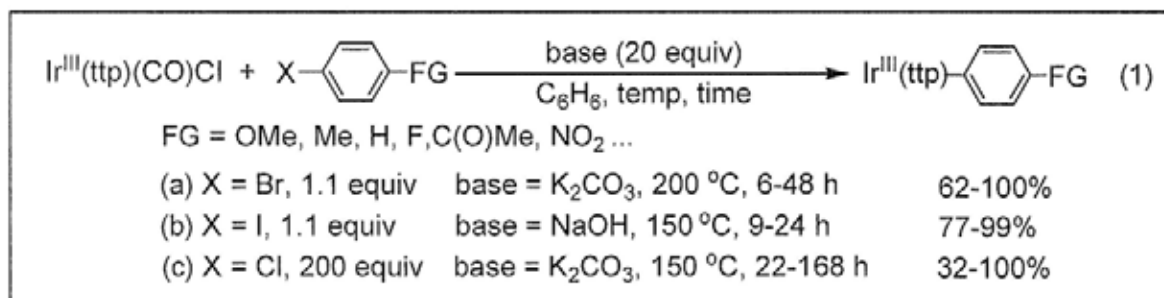
Mechanistic studies suggest that $Ir^{III}(ttp)(CO)Cl$ initially reacts with base (NaOH, K_2CO_3) in benzene to form iridium(III) porphyrin hydroxo complex ($Ir^{III}(ttp)OH$). The hydroxo ligand and the residual water in benzene act as a reducing agent and a protonating source, respectively, to promote the reduction of $Ir^{III}(ttp)OH$ to iridium(III) porphyrin hydride ($Ir^{III}(ttp)H$) (Scheme 1(i), X = Cl). $Ir^{III}(ttp)H$ can also undergo interconversion with iridium(II) porphyrin dimer ($[Ir^{II}(ttp)]_2$) and iridium(I) porphyrin anion ($Ir^{I}(ttp)^-$) via equilibria in basic benzene media (Scheme 1(ii)).

Scheme 1 Reaction Mechanism of Base-Promoted Ar-X Cleavages with $Ir^{III}(ttp)(CO)Cl$
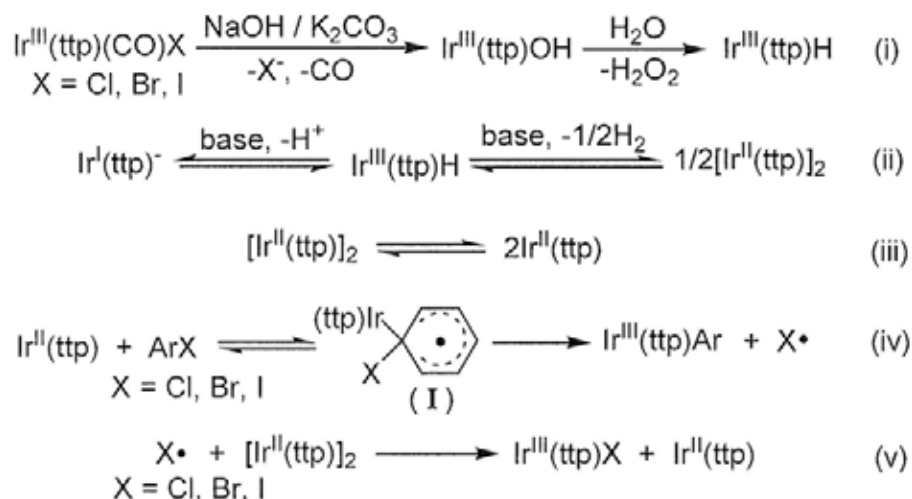
Among the three co-existing iridium porphyrin species ($Ir^{III}(ttp)H$, $[Ir^{II}(ttp)]_2$, $Ir^{I}(ttp)^-$), $[Ir^{II}(ttp)]_2$ is found to be the intermediate for the Ar-X cleavages. $[Ir^{II}(ttp)]_2$ first dissociates into 2 iridium(II) porphyrin metalloradicals ($Ir^{II}(ttp)$) (Scheme 1(iii)). $Ir^{II}(ttp)$ then reacts with Ar-X by radical *ipso*-substitution to form $Ir^{III}(ttp)Ar$ and a halogen atom (X•) via the formation of iridium-porphyrin-cyclohexadienyl radical intermediate (**I**) (Scheme 1(iv)). X• further reacts with $[Ir^{II}(ttp)]_2$ to give iridium(III) porphyrin halide ($Ir^{III}(ttp)X$, X = Cl, Br, I) and $Ir^{II}(ttp)$ for subsequent radical chain propagation (Scheme 1(v)). Radical chain *ipso*-substitution of ArX with $[Ir^{II}(ttp)]_2$ is thus proposed. $Ir^{III}(ttp)X$ (or $Ir^{III}(ttp)(CO)X$ is recycled by undergoing the base-promoted reduction to form $Ir^{III}(ttp)H$ (Scheme 1(i)) for subsequent Ar-X cleavages to give $Ir^{III}(ttp)Ar$ (Scheme 1(ii-v)).

In this thesis, the reaction mechanisms of two newly-discovered reactions are discussed in details:

(1) the redox chemistry of $Ir^{III}(ttp)(CO)X$ (X = Cl, Br, I) in basic benzene media, including the base-promoted reduction of $Ir^{III}(ttp)(CO)X$ to $Ir^{III}(ttp)H$ (Scheme 1(i)), and the base-promoted interconversion among $Ir^{III}(ttp)H$, $[Ir^{II}(ttp)]_2$, and $Ir^{I}(ttp)^-$ (Scheme 1(ii)).

(2) the radical chain *ipso*-substitution of ArX (X= Cl, Br, I) by $[Ir^{II}(ttp)]_2$ to give $Ir^{III}(ttp)Ar$ (Scheme 1(iii-v)).

摘要

本論文主要研究了三價銥羰基氯卟啉絡合物 (Ir^{III}(ttp)(CO)Cl) 在苯容劑中與鹵代苯及其衍生物 (ArX, X = Cl, Br, I) 的反應，發現鹼性添加劑可促進碳-鹵鍵 (Ar-X) 的選擇性斷裂，形成各種銥卟啉芳基絡合物 (Ir^{III}(ttp)Ar) (eq 1)。

機理研究顯示，Ir^{III}(ttp)(CO)Cl 首先跟鹼 (氫氧化鈉、碳酸鉀) 反應，產生三價銥卟啉羥基絡合物 (Ir^{III}(ttp)OH)。 羥基及苯容劑中的剩餘水分別充當還原劑及質子來源，把 Ir^{III}(ttp)OH 還原爲三價銥卟啉氫化物 (Ir^{III}(ttp)H) (Scheme 1(i))。 在鹼性條件下，Ir^{III}(ttp)H 可透過化學平衡，互相轉化成二價銥卟啉二聚絡合物 ([Ir^{II}(ttp)]$_2$) 和一價銥卟啉絡合負離子 (Ir^{I}(ttp)$^-$) (Scheme 1(ii))。

在 Ir^{III}(ttp)H、[Ir^{II}(ttp)]$_2$ 和 Ir^{I}(ttp)$^-$ 當中，我們發現 [Ir^{II}(ttp)]$_2$ 作爲 Ar-X 鍵斷裂的活性中間體。 [Ir^{II}(ttp)]$_2$ 首先分裂爲二價銥卟啉游離基 (Ir^{II}(ttp)) (Scheme 1(iii))，跟 ArX 進行原位取代反應，通過產生環己烷二烯自由基中間體，再生成 Ir^{III}(ttp)Ar 和鹵原子 (X•) (Scheme 1(iv))。 X• 再跟 [Ir^{II}(ttp)]$_2$ 反應，產生三價銥卟啉鹵化物 (Ir^{III}(ttp)X, X = Cl, Br, I) 與 Ir^{II}(ttp) (Scheme 1(v))，繼而發生鏈傳遞反應。 因此，ArX 與 [Ir^{II}(ttp)]$_2$ 發生游離基連鎖原位取代反應。 Ir^{III}(ttp)X (或 Ir^{III}(ttp)(CO)X) 最後跟鹼和水進行還原反應產生 Ir^{III}(ttp)H (Scheme 1(i))，接著進行 Ar-X 鍵斷裂，形成 Ir^{III}(ttp)Ar (Scheme 1(ii-v))。

本論文詳細討論了以下兩個新發現的反應機理：

(1) Ir^{III}(ttp)(CO)X (X = Cl, Br, I) 於鹼性條件下的氧化還原反應，包括了 Ir^{III}(ttp)(CO)X 轉化爲 Ir^{III}(ttp)H 的還原反應 (Scheme 1(i))，以及 Ir^{III}(ttp)H、[Ir^{II}(ttp)]$_2$ 和 Ir^{I}(ttp)$^-$ 的相互轉化反應 (Scheme 1(ii))。

(2) [Ir^{II}(ttp)]$_2$ 與 ArX (X = Cl, Br, I) 之游離基連鎖原位取代反應 (Scheme 1(iii-v))。

Chapter 1   General Introduction

1.1 Macrocycles

In organometallic chemistry, main group metals and transition metals are usually incorporated with ligands to promote various organometallic reactions. Macrocycles are usually bulky, multidendate ligands which can protect the periphery of the metal complexes from external attack and to impose coordination numbers or geometrical constraints to stabilize the metal complexes.[1] Metal macrocycles provide a unique platform for organometallic reactions. Common macrocyclic ligands are Schiff bases, phthalocyanines, porphyrins, corroles, corrins, N-confused porphyrins, and expanded porphyrins.

1.1.1 Schiff Base

Schiff base is a compound with imine or azomethine linkages which are commonly formed by the acid-catalyzed condensation between primary amines and carbonyl groups (Figure 1.1). Schiff base is generally an excellent chelating agent to form stable complexes with most of transition-metals[2] and plays a significant role in coordination, supramolecular, biological, organic, analytical, and industrial chemistry.[3] However, the imine linkage in Schiff base is labile and is easily hydrolyzed in acidic and basic media.[4] Preparation of Schiff bases can take prolonged reaction time and tedious work-up to result in low yield.[5]
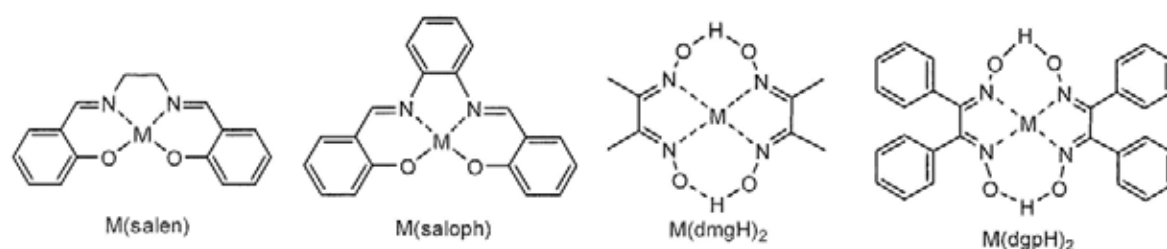
Figure 1.1 Structure of metal Schiff base.

1.1.2 Phthalocyanine

Phthalocyanine is a symmetrical macrocycle with 4 iminoisoindoline units. It contains a central cavity which is sufficiently large to coordinate with different metal ions, thus playing a crucial role in coordination chemistry. It exhibits aromatic behavior due to its planar conjugated system of 18 π-electrons (Fig 1.2),[6] which makes phthalocyanine a deep green or blue compound and is widely applied in dye industry. It is also utilized in photoconductor, nonlinear optical application, and supramolecular chemistry.[7] However, the applications of phathalocyanine are limited by its poor solubility in virtually all solvents, and the difficulties of functionalization of phthalocyanine.[8]

M(pc)
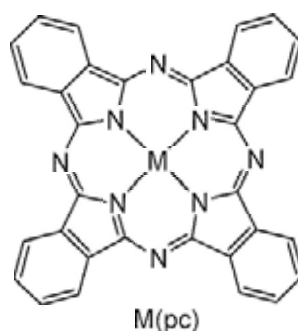
Figure 1.2 Structure of metallophthalocyanine.

1.1.3 Porphyrin

Porphyrin is a heterocyclic macrocycle with 4 pyrrole rings interconnected to methine bridges (Fig 1.3(**A**)). Like phthalocyanine, porphyrin is also a highly conjugated aromatic compound with 18 π-electrons delocalized in the inner 16-membered ring,[9] and it is usually deep purple in color.

(A) Metalloporphyrin   (B) metallocorrole   (C) metallocorrin

Figure 1.3 Structure of metalloporphyrin, metallocorrole, and metallocorrin

Porphyrin is a tetradendate, dianionic ligand which forms stable metalloporphyrins with main group metals and transition metals by replacing the two inner pyrrole protons with metal ions. Metalloporphyrins are commonly used as model compounds to aid the fundamental studies and understandings of the physical and chemical properties of biologically important macromolecules, such as coenzyme B_{12},[10] heme,[11] and chlorophylls.[12] Metalloporphyrins are also utilized in catalytic transformations of organic molecules.[13] Furthermore, porphyrin-based compounds are found in molecular electronics and supramolecular building blocks.[14] Porphyrin shows an extra stability and can be easily accessible and tamable. The steric and electronic properties of metalloporphyrins are thus readily modified.[15]

1.1.4 Corrole

Corrole is a tetradendate, trianionic ligand which is different from the porphyrin analogue by the absence of a *meso* methine carbon (Fig 1.3(**B**)), but it still contains 18 decolalized π-electrons to maintain the aromaticity. Since corrole macrocycle has higher ionic charges and smaller cavity than the porphyrin ring, it usually forms more stable complexes with transition metals with higher oxidation states and smaller sizes.[16] Corrole has been received renewed interests due to the more accessible synthetic procedures.[17] The chemistry of corrole has been studied in the fields of coordination chemistry,[18] chemical transformations,[19] photophysics,[20] and electrochemistry.[21]

1.1.5 Corrin

Corrin is a tetradendate, monoanionic macrocyclic ligand which contains sp^3-carbons to construct the saturated skeletons of the rings (Fig 1.3(**C**)). Corrin can coordinate with transition metals to form metallocorrin complexes.[22] It is also utilized as the construction unit of coenzyme B_{12} for biological rearrangement reactions. Corrin contains 12 π-electrons only and is a non-aromatic macrocycle, which makes the corrin ring non-planar and more flexible than

porphyrin and corrole.[23] Indeed, the presence of sp³-carbons in the corrole ring promotes the steric interactions within the ring.[23] The contracted corrin ring also results in a small cavity size to coordinate tightly with small-sized transition metals,[23] including cobalt ion. These 3 properties are important for the stability of coenzyme B_{12} and the efficiency of coenzyme B_{12}-dependent rearrangement reactions, which involve the cleavage of Co-C bond of the coenzyme B_{12} to initiate the reactions. Metallocorrins are also studied in the fields of optoeletronics and catalytic transformations.[24]

1.1.6 N-Confused Porphyrin

N-Confused porphyrin is the isomer of porphyrin and contains a pyrrole ring jointed to the conjugated system with both α and β-carbons (Figure 1.4(**A**)), which is different from porphyrin involving the pyrrole interconnections with α-carbons only.[25] N-confused porphyrin contains an inner C-H and two *trans*-positioned inner core N-H bonds. In less polar CH_2Cl_2, N-confused porphyrin (Figure 1.4(**A**)) exists as the most stable form. In more polar DMSO, it adopts the less stable tautomeric form with a N-H bond outside the macrocyclic ring (Figure 1.4(**B**)), which can form hydrogen bonding with DMSO to stabilize the tautomer.[26]

The N-confused porphyrin also undergoes the rotation of the α,β-interconnected pyrrole to form an inverted N-confused porphyrin (Figure 1.4(**C**))[25,27] which can further react to form the N-fused porphyrin by forming a C-N bond between the α-carbon of inverted pyrrole and the N-H bond of adjacent pyrrole (Figure 1.4(**D**)).[27]

The N-confused porphyrins and its tautomer,[25,28] inverted N-confused porphyrins,[29] and N-fused porphyrins[30] can form coordination complexes with various metals. These metal macrocycles have been studied in the areas of material sciences and catalysis.[31]

4
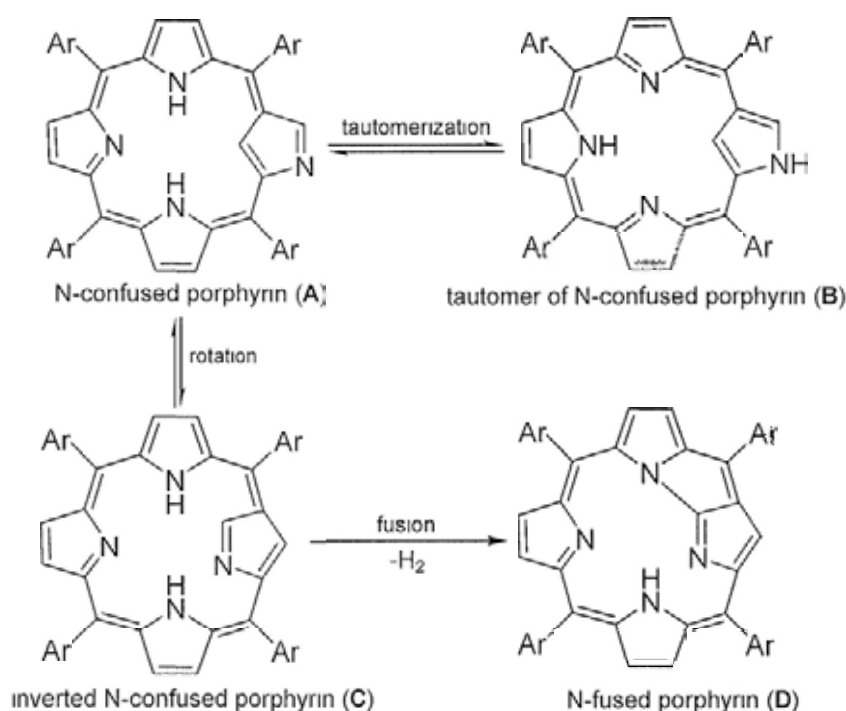
Figure 1.4 Structures of N-confused porphyrin and its tautomer, inverted N-confused porphyrin, and N-fused porphyrin.

1.1.7 Expanded Porphyrin

Expanded porphyrin is the variant form of porphyrin, which contains heterocyclic units (pyrroles, furan, or thiophene) linked together either directly or through spacers, such that the internal ring contains at least 17 atoms (Figure 1.5).[32] Expanded porphyrin contains larger internal cavity and forms stable coordination complexes with larger cations, including those of the lanthanide and actinide series. It also allows the generation of complexes containing multiple cations. The metal-coordinated expanded porphyrins have been widely studied as photosensitizers in photodynamic therapy,[33] contrast agents in magnetic resonance imaging,[34] building blocks in nonlinear optical materials,[35] and enzyme models in bioinorganic chemistry.[36]
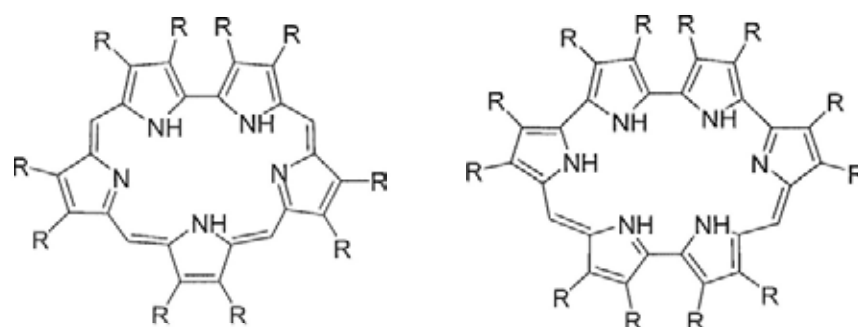
Figure 1.5 Examples of Expanded Porphyrins.

1.2 Group 9 Metalloporphyrins

Group 9 metalloporphyrins (M(por)) are cobalt, rhodium, and iridium porphyrins. They are usually prepared via the metallation of porphyrin ligand with the corresponding metal salts (eq 1.1).

$$M^{n+} \;+\; H_2(por) \xrightarrow{\text{metallation}} M(por) \;+\; 2H^+ \quad (1.1)$$

M = Co, Rh, Ir

Group 9 metalloporphyrins commonly exist in 3 oxidation states: +3 (d^6), +2 (d^7), and +1 (d^8). Figure 1.6 shows the energy level diagrams of the formal square planar complexes of group 9 metalloporphyrin M(por). High-valent M^{III}(por) contains no electron in d_z^2 orbital and is electrophilic. Intermediate-valent M^{II}(por) contains single electron in d_z^2 orbital and is a radical. Low-valent M^{I}(por) contains a pair of electrons in d_z^2 orbital and is nucleophilic. These 3 kinds of metalloporphyrins exhibit different electronic configuration and therefore show tremendously different reactivities (To be discussed in Section 1.7). Group 9 metalloporphyrins in the oxidation states of +4 and +5 are unknown. Indeed, the energy

6

levels of the d_z^2 orbitals in cobalt (3d), rhodium (4d), and iridium (5d) porphyrin complexes are different and lead to different physical and chemical properties among the group 9 metalloporphyrins.

Electrophilic	Radical	Nucleophilic
$d_{x^2-y^2}$	$d_{x^2-y^2}$	$d_{x^2-y^2}$
d_{z^2}	d_{z^2}	d_{z^2}
d_{xy}	d_{xy}	d_{xy}
$d_{xz,\,yz}$	$d_{xz,\,yz}$	$d_{xz,\,yz}$
M^{III}(por), d^6	M^{II}(por), d^7	M^{I}(por), d^8
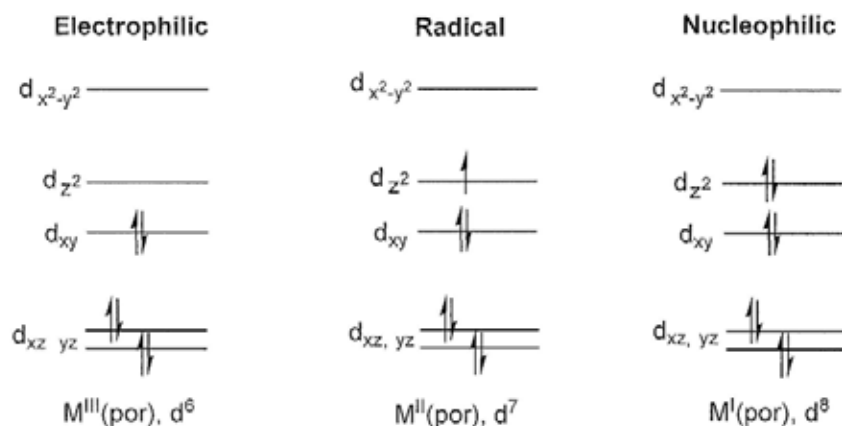
Figure 1.6 Energy level diagrams of square planar group 9 metalloporphyrins.

1.3 Late-Transition-Metal-Alkoxo Complexes

Late transition metals can react with anionic oxygen-containing ligands, such as hydroxides (OH⁻), alkoxides (OR⁻), and aryloxides (OAr⁻),[37] to form late-transition-metal-alkoxo complexes (M-OR). Late-metal-alkoxo complexes has been extensively reported compared with the early-metal-alkoxo complexes due to the much higher reactivities of the late-metal-alkoxo complexes.[38] The general applications of late-metal-alkoxo complexes, and the effect of chemical bondings of early- and late-metal-alkoxo complexes on their tremendously different reactivities, are briefly highlighted below.

1.3.1 General Applications of Late-Transition-Metal-Alkoxo Complexes

(i) As O-Donor Supporting Ligands

Dianionic salen and saloph macrocycles (Fig 1.1) form stable, tetradendate M(salen) and M(saloph) complexes with group 9 transition metals. They serve as chemical models of coenzyme B_{12}.[39] Dianionic acetylacetate (acac) is a bidendate O-donor ligand. Recent

important examples are the iridium(III) complexes, $(O,O\text{-acac})_2Ir^{III}(py)(CH_3)$ and $[(O,O\text{-acac})_2Ir^{III}(C\text{-acac})]_2$ dimer (Figures 1.7(A) and (B)). These iridium(III) complexes have been utilized in stoichiometric C-H bond activations of alkanes, toluenes, and arenes,[40] and act as catalysts or pre-catalysts in hydroarylation of olefins[41] and H/D exchanges of benzenes.[42]

(A)   (B)
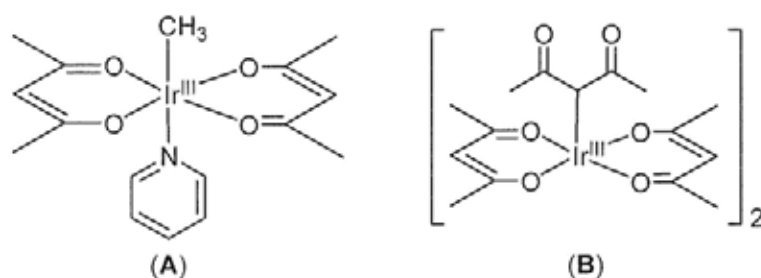
Figure 1.7 Iridium(III) complexes coordinated with O-Donor acetylacetate ligands.

(ii) As Intermediates in C-O Bond Forming Reactions

Transition-metal-catalyzed C-O bond forming reactions between aryl halides and alkoxides are widely applied in the synthesis of precursors of potential drugs and biologically active molecules in pharmaceutical industry.[38,43] One of the examples is the palladium-catalyzed coupling of aryl bromides and chlorides with hydroxide ions to form phenols (eq 1.2).[44] Palladium(II)-aryl-hydroxo complexes are proposed to be the intermediates for C-O couplings via reductive elimination (eq 1.2, species (**I**)). Indeed, palladium(II)-aryl-alkoxo complexes have been demonstrated to undergo the reductive elimination to from C-O bonds (eq 1.3).[45]

(1.2)

$$\text{(1.3)} \quad 87\%$$
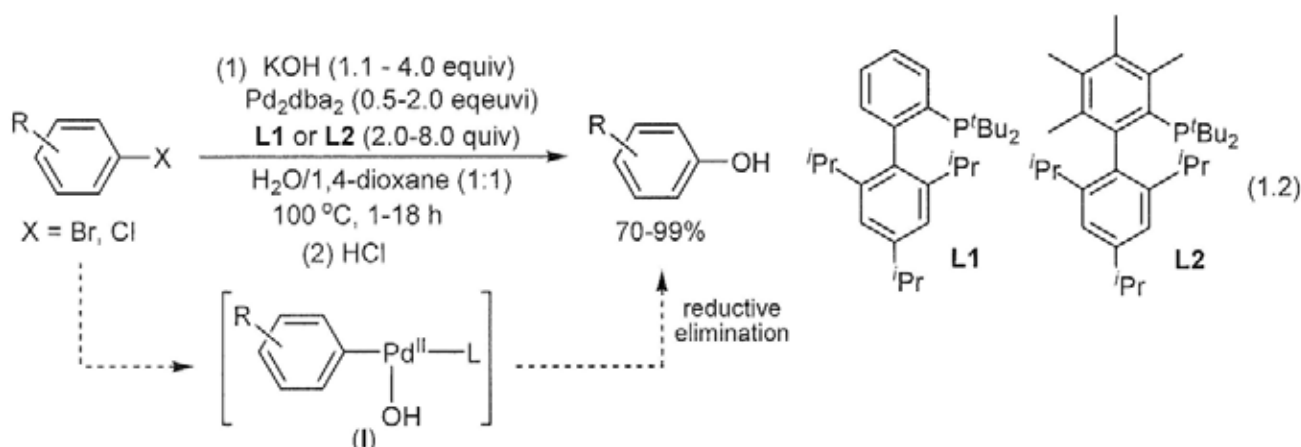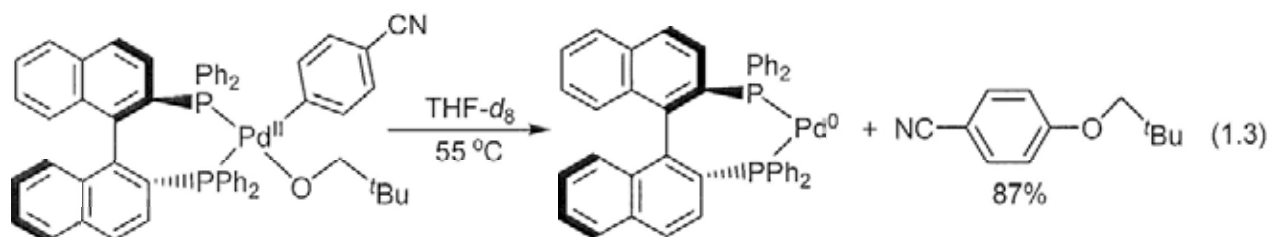
1.3.2 Chemical Bondings of Transition-Metal-Alkoxo Complexes

1.3.2.1 Bond Dissociation Energies of Transition-Metal-Alkoxo Complexes

Both early and late transition metals can form metal-oxygen single bonds (M-O) with various anionic oxygen-containing ligands. Table 1.1 lists some of the homolytic bond dissociation energies (BDEs) of transition-metal-alkoxo complexes obtained by theoretical calculations or experimental elucidations.

Table 1.1 Homolytic Bond Dissociation Energies of Early- and Late-Transition-Metal-Oxygen Single Bonds

entry	transition metal (M)	transition-metal complexes (M-OR)	homolytic bond dissociation energies (kcal mol^{-1})
1		Cl_3Ti^{IV}-OH	108.3 [46]
2		Cl_3Ti^{IV}-OMe	102.0 [46]
3		Cl_3Zr^{IV}-OH	126.0 [46]
4	Early	Cl_3Zr^{IV}-OMe	115.8 [46]
5		Cl_3Hf^{IV}-OH	128.1 [46]
6		Cl_3Hf^{IV}-OMe	121.1 [46]
7		$Cp^*_2(Ph)Zr^{IV}$-OH	115 [47]
8		$Cp^*_2(Ph)Zr^{IV}$-OPh	91 [47]
9		$Cp_2(Cl)Cr^{IV}$-$OSiH_3$	52.2 [48]
10		$Cp_2(Cl)Mo^{IV}$-$OSiH_3$	58.2 [48]
11	Middle	$Cp_2(Cl)W^{IV}$-$OSiH_3$	67.9 [48]
12		$Cp^*(P(CH_3)_3)_2Ru^{II}$-OH	48.9 [49]
13		$Cp^*(P(CH_3)_3)_2Ru^{II}$-OCH_3	33.9 [49]
14		$(CO)_4Co^I$-OH	55.5 [46]
15		(oep)Rh^{III}-OCHRR' ^{a} (R, R' = H, alkyl)	~50-55 [50]
16		(tspp)Rh^{III}-OD ^{b}	~60±3 [51]
17	Late	(tmps)Rh^{III}-OD ^{c}	~60 [52]
18		$(PH_3)_2(CH_3)Ni^{II}$-OH	79.0 [53]
19		$(PH_3)_2(CH_3)Pd^{II}$-OH	77.7 [53]
20		$(PH_3)_2(CH_3)Pt^{II}$-OH	85.9 [53]
21		$(Ph_2PCH_2CH_2PPh_2)(CH_3)Pt^{II}$-OH	40.0 [49]
22		$(Ph_2PCH_2CH_2PPh_2)(CH_3)Pt^{II}$-$OCH_3$	24.7 [49]

^{a} oep = octaethylporphyrin. ^{b} tspp = tetrakis(p-sulfonatophenyl)porphyrin. ^{c} tmps = tetrakis(3,5-disulfonatomesityl)porphyrin.

Early-transition-metal M-O BDEs can be over 100 kcal mol^{-1} and are generally higher than late-metal ones by 30-50 kcal mol^{-1} (Table 1.1).[38] Thus, early-metal-alkoxo complexes usually act as ancillary ligands and exhibit much lower reactivities without undergoing β-hydride elimination,[54] reductive elimination,[47] and migratory insertion.[55] On the other hand, the weaker late-metal-alkoxo complexes exhibit high nucleophilicities and basicities[37,56] and are commonly involved in catalytic transformations in organic synthesis.[56] The tremendously different reactivities between early- and late-metal-alkoxo complexes can be interpreted using the bonding theories.

1.3.2.2 Classifications of Bonding Theories

Three bonding models have been proposed for transition-metal-alkoxo complexes: (i) the hard/soft acid-base principle,[57] (ii) the d_π-p_π model,[58] and (iii) the E-C theory.[59]

1.3.2.2.1 Hard/Soft Acid-Base Principle

The hard/soft acid-base (HSAB) principle was introduced by Pearson in 1960s.[57] The HSAB principle states that hard Lewis acids prefer to bind to hard Lewis bases, whereas soft Lewis acids prefer to bind to soft Lewis bases. For examples, hard early-transition-metals (Group 3-5) bind strongly with hard, anionic oxygen-containing ligands (OR$^-$) to form stronger M-OR bonds, whereas soft late-transition-metals (Group 9-11) bind weakly with OR$^-$ to form weaker M-OR bonds. The model nicely accounts the higher BDEs of M-OR bonds in the early-metal-alkoxo complexes than the late-metal ones (Table 1.1). However, the HSAB principle has its drawbacks. For example, it cannot explain the bond strength order of Ru-X in (PPh$_3$)$_4$Ru^{II}(X)(H): Ru-H > Ru-O(p-Tol) > Ru-NHPh > Rh-CH$_2$Ph. The hard O(p-Tol)$^-$ and NHPh$^-$ ligands form even stronger Ru-X bonds with the soft Ru(II) metal than the soft CH$_2$Ph$^-$ ligand.[60]

1.3.2.2.2 d_π-p_π Model

The d_π-p_π model was then adopted by Caulton in 1994 to interprete both the stabilities and reactivities of transition-metal-alkoxo complexes [58] π-Donation from the lone pair of oxygen of π-symmetry to the empty d orbital of early-transition-metal lowers the ground state energy of M-O bond (Figure 1 8(**A**)). Consequently, the M-O bond strength is enhanced and generally exhibits lower reactivities.
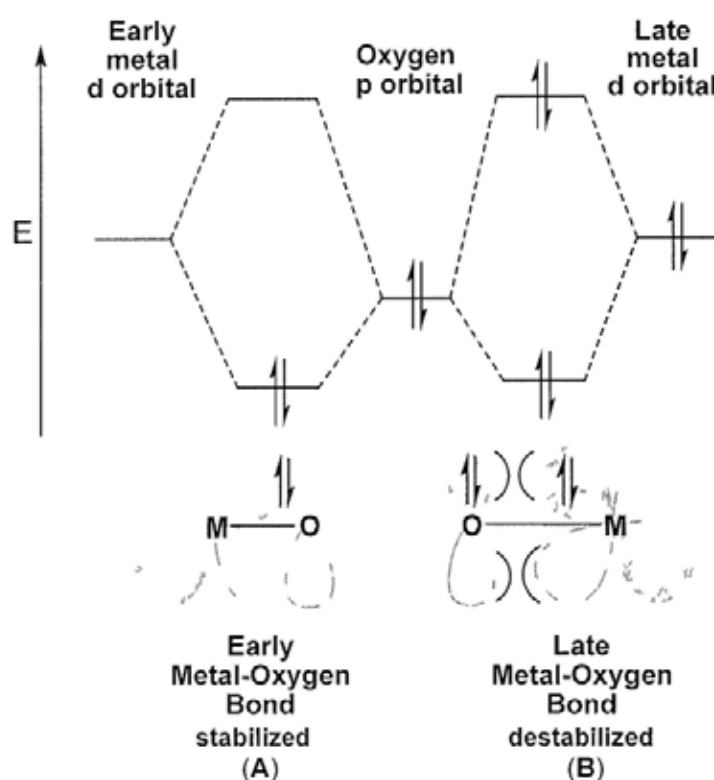
Figure 1.8 Interactions of lone pair of oxygen of π-symmetry with empty d-orbitals of early transition-metal (**A**) and filled d-orbitals of late-transition-metal (**B**).

In contrast, the p_π-d_π repulsion between the lone pair of oxygen and the filled d-orbitals of late-transition-metal increases the ground state energy of M-O bond and makes the oxygen lone pair particularly nucleophilic and basic (Figure 1.8(**B**)). The p_π-d_π model can explain the high reactivity of late-metal-alkoxo complexes, but it still cannot account the unusually strong late-metal-oxygen bonds (Table 1.1, entries 14-20), which are not any weaker than the late-metal-sp^3-carbon (M-C(sp^3)) bonds.[61,62]

1.3.2.2.3 E-C Theory

Both the considerably high bond energies and high reactivities of late-transition-metal-oxygen bonds (M-O) can be explained by the latest E-C theory (electrostatic-covalent theory) proposed by Holland, Andersen, and Bergman in 1999.[59] The E-C theory states that the M-O bond exists in both covalent and ionic forms (Figure 1.9, species **A** and **B**, respectively), and these 2 extreme forms are in resonance. The electropositive late-transition-metal and the electronegative oxygen lead to a low covalent character and a high ionic character and thus the high polarity of the M-O bond. The high polarity of M-O bond sufficiently accounts both the enhanced M-O bond strength as well as the high nucleophilicities and basicities of late-metal-alkoxo complexes, without considering the p_π-d_π repulsion. The E-C theory is now widely adopted to explain both the stabilities and reactivities of late-metal-alkoxo complexes.

$$M\text{—}OR \longleftrightarrow M^+ \ ^-OR$$
$$\qquad A \qquad\qquad\qquad B$$
$$R = H, alkyl, aryl$$
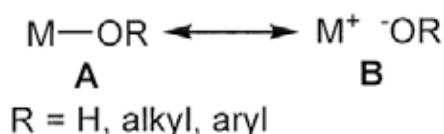
Figure 1.9 Resonance structures of the late-transition-metal-alkoxo bonds.

1.4 Transition Metal Non-Porphyrin Hydroxo Complexes

Many transition-metal non-porphyrin hydroxo complexes have been successfully prepared.[37] They generally exhibit high reactivities due to the high nucleophilicity and basicity of the hydroxo ligands. In this section, group 9 iridium(III)-hydroxo complex (Cp*Ir^{III}(PPh$_3$)Ph(OH)) prepared from the Bergman group,[63] and rhodium(I)-hydroxo complex ((PNP)Rh^I-OH) prepared from the Goldberg group,[64] are mainly used as examples to illustrate various approaches of preparations and reactivities of group 9 late-metal-hydroxo complexes.

1.4.1 Preparation of Transition Metal Non-Porphyrin Hydroxo Complexes

Transition-metal-hydroxo complexes are generally prepared by reacting metal precursors

with various hydroxo sources, such as hydroxide ion, water, and hydrogen peroxide. There are four main types of synthetic pathways of group 9 metal-hydroxo complexes: (1) ligand substitutions with hydroxide ion,[63] (2) protonolysis with water,[64] (3) oxidative addition with water,[65] and (4) oxidative addition with hydrogen peroxide.[66]

1.4.1.1 Ligand Substitutions with Hydroxide Ion

The Bergman group reported that $Cp^*Ir^{III}(PPh_3)(Ph)(OTf)$ complex undergoes ligand substitution with CsOH facilely at room temperature to yield the Ir^{III}-OH complex (eq 1.4).[63]
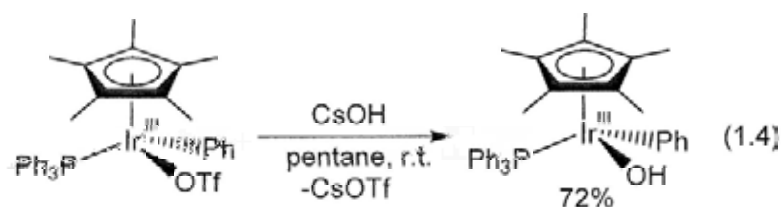
1.4.1.2 Protonolysis with Water

The Goldberg group reported that low-valent pincer-Rh^I-Me complex undergoes protonolysis with water to yield pincer-Rh^I-OH with the concomitant elimination of methane (eq 1.5).[64a]
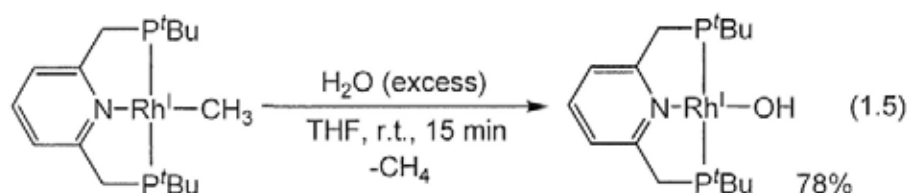
1.4.1.3 Oxidative Addition with Water

The Iridium(I) pincer complex, which is formed by dehydrogenation of iridium(III) dihydrido precursor, undergoes oxidative addition with water to yield iridium(III) hydroxo-hydride complex (eq 1.6).[65a]

13
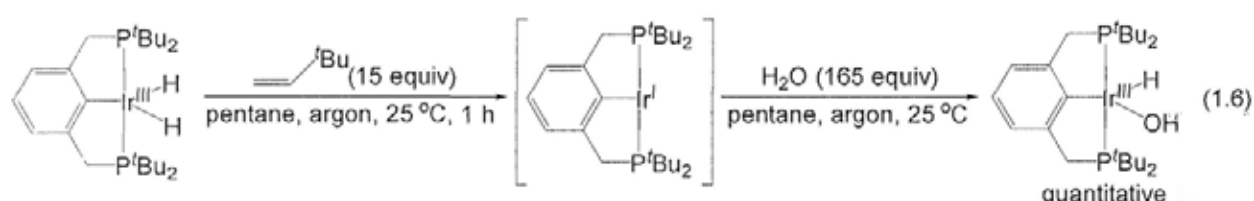
1.4.1.4 Oxidative Addition with Hydrogen Peroxide

The metalloradical, pentacyanocobaltate(II), undergoes bi-metallic oxidative addition with H_2O_2 to form Co^{III}-OH bonds via a radical non-chain mechanism (eq 1.7).[66] Mechanistic studies suggest that Co^{II} radical homolytically cleaves the HO-OH bond to yield Co^{III}-OH and HO• (Scheme 1.1, pathway i). HO• then combines with Co^{II} radical to form another Co^{III}-OH (pathway ii).

$$2[Co^{II}(CN)_5]^{3-} + H_2O_2 \xrightarrow[k = 7.4 \times 10^2 \text{ M}^{-1}\text{s}^{-1}]{25\ ^\circ\text{C, H}_2\text{O}} 2[Co^{III}(OH)(CN)_5]^{3-} \quad (1.7)$$
$$100\%$$
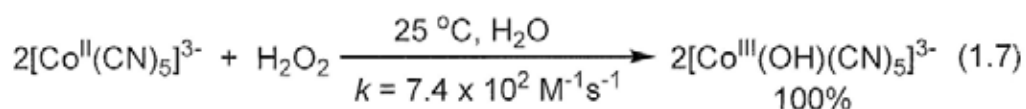
Scheme 1.1 Radical Non-chain Mechanism of $[Co^{III}(OH)(CN)_5]^{3-}$ Formation

$$[Co^{II}(CN)_5]^{3-} + HO\text{-}OH \xrightarrow{\ i\ } [Co^{III}(OH)(CN)_5]^{3-} + HO\bullet$$

$$HO\bullet + [Co^{II}(CN)_5]^{3-} \xrightarrow{\ ii\ } [Co^{III}(OH)(CN)_5]^{3-}$$
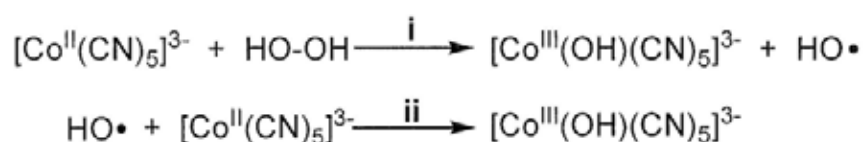
1.4.2 Reactivities of Transition Metal Non-Porphyrin Hydroxo Complexes

Transition-metal-hydroxo complexes can undergo the bond activations and the redox reactions. Late-transition-metal-hydroxo complexes are strongly polarized in ground state (Figure 1.9, species **B**) such that the hydroxo ligand is very nucleophilic and basic for bond activation chemistry. Additionally, the hydroxo ligand can reduce the metal centers by single electron oxidation, or oxidize the metal centers via α-hydrogen elimination, for redox chemistry.

1.4.2.1 Bond Activation Chemistry

1.4.2.1.1 Reacting as Nucleophiles

(i) Iridium(III) Hydroxo Complexes

Iridium(III)-hydroxo complexes, Cp*Ir^{III}(PPh$_3$)(Ph)(OH), undergoes *cis*-1,2-insertion of Ir-OH bond into dimethyl acetylenedicarboxylate (DMAD) via nucleophilic addition to yield

the iridium(III)-enol complex (eq 1.8(a)).[63] Cp*Ir^{III}(PMe$_3$)(Ph)(OH) also hydrolyzes maleic anhydride via nucleophilic substitution to form iridium-maleate (1.8(b)).[63]
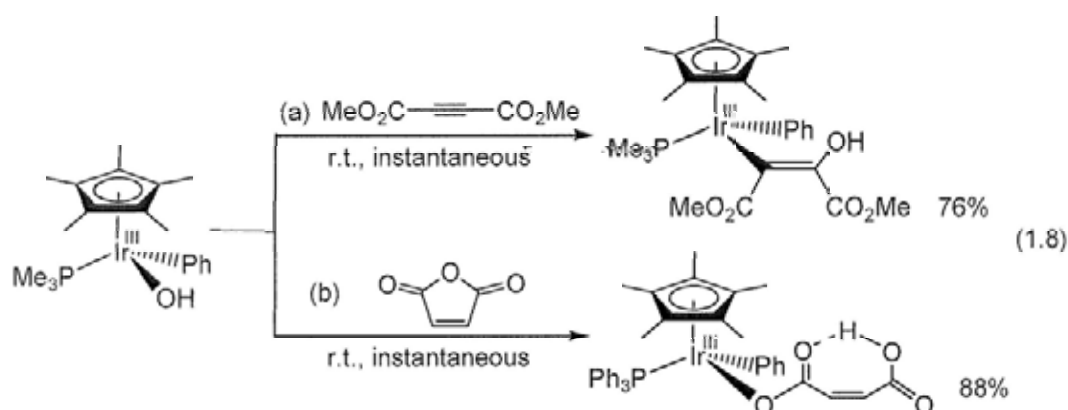
(ii) Cobalt(III)-Hydroxo Complexes

Nucleophilic cobalt(III) macrocyclic hydroxo complexes, Co^{III}(saloph)OH, has been used to catalyze the hydrolytic kinetic resolution (HKR) reactions of racemic terminal epoxides cooperatively with electrophilic Co^{III}(saloph)OTs (eq 1.9).[67] Mechanistic studies suggest that, Co^{III}(saloph)OTs acts as an electrophile to coordinate with the epoxide (Scheme 1.2, pathway i), whereas Co^{III}(saloph)OH coordinates with water to form Co^{III}(saloph)OH(H$_2$O) containing a nucleophilic hydroxo ligand (pathway ii). The hydroxo ligand in Co^{III}(saloph)OH(H$_2$O) attacks the electrophilic β-carbon of coordinated epoxide (pathway iii), and the subsequent protonation with water leads to the formation of stereospecific 1,2-diols and the regeneration of Co^{III}(saloph)(H$_2$O)OH and Co^{III}(saloph)OTs for further catalytic cycles (pathway iv).

15
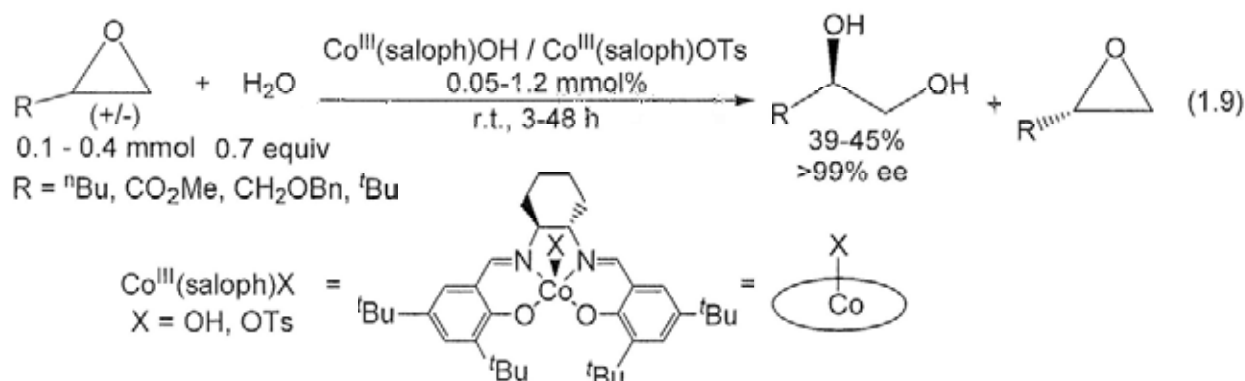
Scheme 1.2 Proposed Mechanism of Hydrolytic Kinetic Resolution of Terminal Epoxides
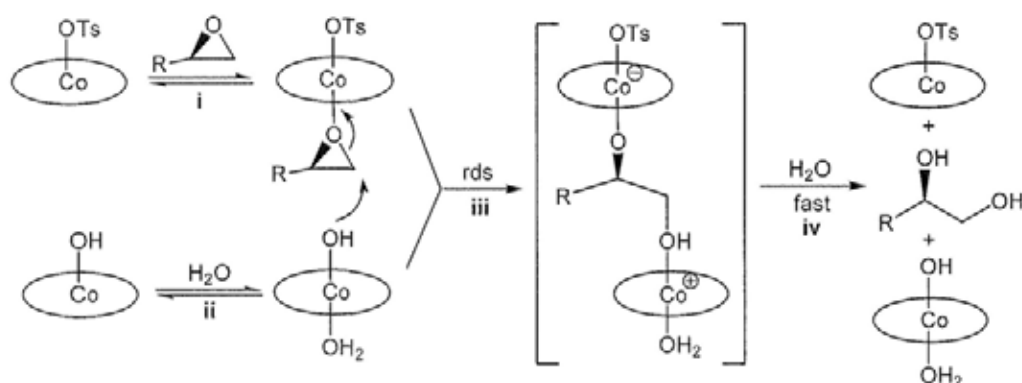
1.4.2.1.2 Reacting as Bases

(i) O-H and N-H Bond Activations

Cp*Ir^{III}(PPh$_3$)(Ph)(OH) reacts with phenol and *p*-toluidine to yield Ir^{III}-OPh and Ir^{III}-N(*p*-Tol) complexes, respectively, via O-H and N-H activations (eqs 1.10(a) and (b)).[63] Mechanistic studies suggest that the activations involve the hydrogen-bonding interaction (Scheme 1.3, pathway **a**) or proton-transfer (pathway **b**) for ligand exchanges, rather than the initial dissociation of Ir-OR to give Ir$^+$ (pathway **c**).[37c]

(1.10)
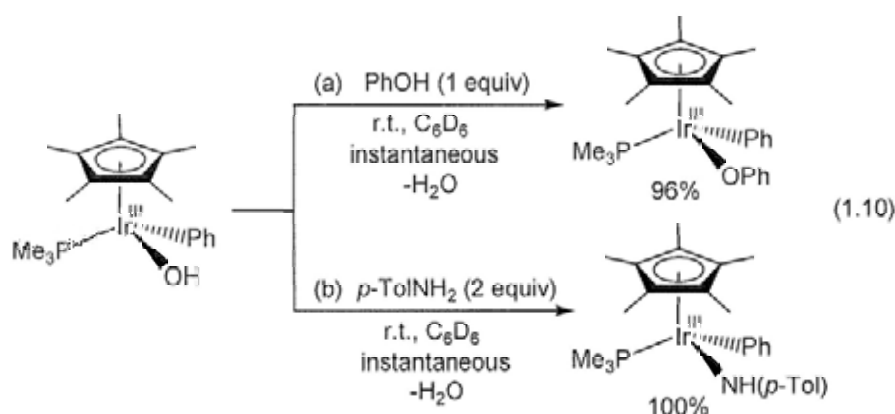
Scheme 1.3 Possible Mechanisms of H-X (X = OR, NHAr) Activations by Ir-OH

16
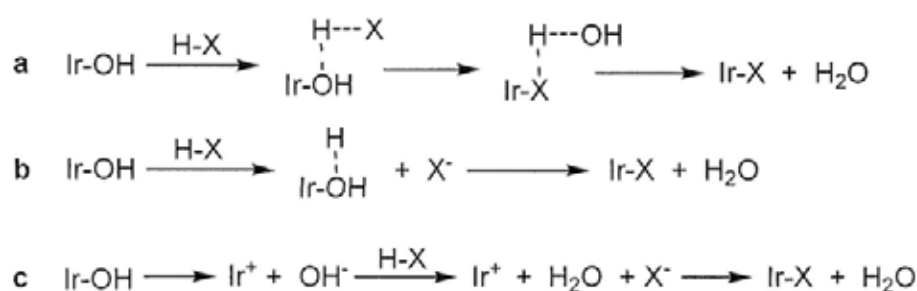
(ii) C-H Activations

The low-valent pincer-rhodium(I)-hydroxo complex undergoes C-H bond activation of benzene-d_6 to afford rhodium(I)-phenyl-d_5 complex (eq 1.11).[64b]
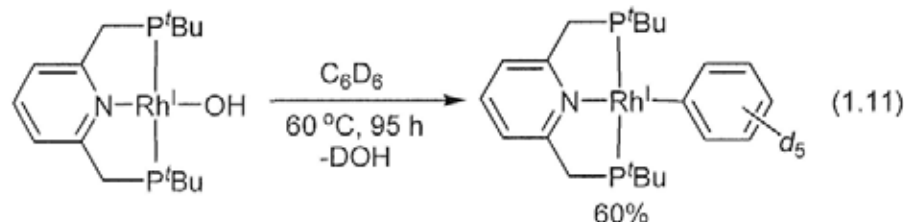
The high-valent O-donor iridium(III)-hydroxo complex, $(O,O\text{-acac})_2Ir^{III}(py)(OH)$, also undergoes C-H bond activation of benzene to form iridium(III)-phenyl complex and water (eq 1.12).[68]
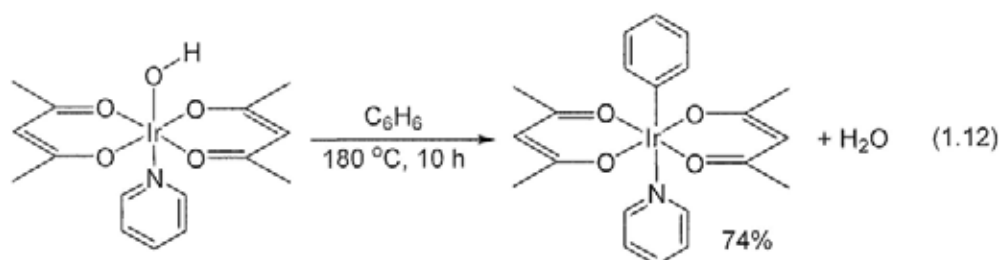
The proposed mechanism of C-H activation of benzene by $(acac\text{-}O,O)_2Ir^{III}(py)(OH)$ is shown in Scheme 1.4.[68] Experimental results and theoretical calculations suggest that $(acac\text{-}O,O)_2Ir^{III}(py)(OH)$ first undergoes ligand dissociation of pyridine (Scheme 1.4, pathway i). The resultant iridium complex isomerizes to provide a *cis*-vacant site for benzene coordination (pathways ii and iii), and Ir-OH cleaves the C-H bond by heterolysis in a transition state resembling σ-bond metathesis (pathway iv) to afford the Ir^{III}-Ph complex and water (pathway v). Addition of pyridine leads to the formation of $(acac\text{-}O,O)_2Ir^{III}(py)Ph$ (pathway vi).

Upon detailed theoretical studies, the interaction between Ir-OH and C-H bond of benzene in the transition states is classified as internal electrophilic substitution (IES)[69] or ambiphilic substitution.[70] During IES or ambiphilic substitution (Scheme 1.5, pathways i-iii), the lone-pair of oxygen atom in Ir-OH donates to the hydrogen atom of C-H bond to form a new O-H bond,

while the orbital making up the Ir-O bond turns into a coordinating lone-pair electrons. Simulataneously, the electrophilic iridium center interacts strongly with the incoming carbon atom to form Ir-C bond. Such bond interaction is a variant of classical σ-bond metathesis, which only involves the breaking of the Ir-O bonding orbital.[70a]

Scheme 1.4 Mechanism of Heterolytic C-H Activation of Benzene by O-Donor Iridium(III)-Hydroxo Complex

Transition state resembling
σ-bond metathesis
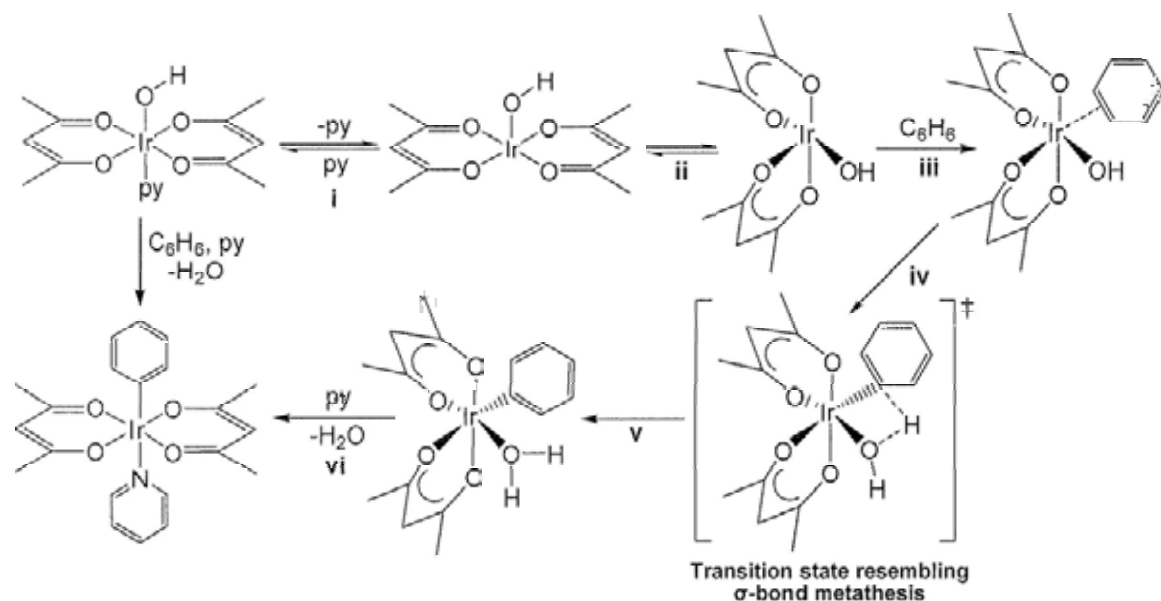
Scheme 1.5 Mechanism of Internal Electrophilic Substitution or Ambiphilic Substitution
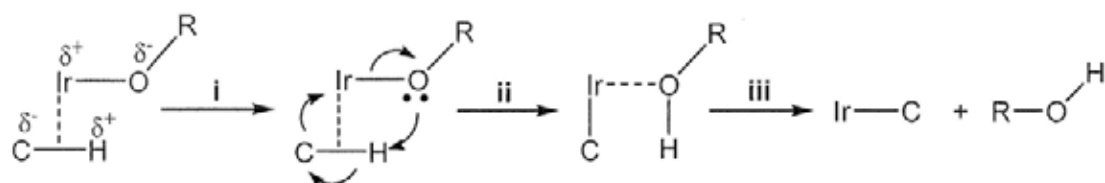
1.4.2.2 Redox Chemistry

1.4.2.2.1 Reacting as Reducing Agents

Reductions of transition-metal non-porphyrin complexes by hydroxide ions have been reported in molybdenum (Mo),[71] tungsten (W),[71] iron (Fe),[72] ruthenium (Ru),[73] and cobalt (Co) complexes.[74,75] OH⁻ reduces the metal centers by an inner sphere electron transfer via the formation of metal-hydroxo complexes, or by an outer-sphere electron transfer. Some of the examples of the OH⁻-promoted reduction of transition-metals are presented below.

(i) Molybdenum(VI) and Tungsten(VI) Complexes

Neutral, high-valent molybdenum(VI) and tungsten(VI) tris-dithiolene complexes are reduced by OH⁻ in THF/water solvent to give mono-anionic Mo^V and W^V complexes (eq 1.13, pathway i).[71] Under high-concentration of OH⁻, di-anionic Mo^{IV} and W^{IV} complexes are formed by further reduction with OH⁻ (pathway ii). OH⁻ is simultaneously oxidized to hydroxo radical (HO•), which dimerizes to form hydrogen poerxide (H_2O_2). H_2O_2 is indirectly detected by reacting with triphenylphosphine to give triphenylphosphine oxide under anaerobic conditions (pathway iii).

$$\text{rate} = -d[ML_3]/dt = k\,[ML_3]\,[Bu_4NOH] \quad (\text{at } 11\ ^oC)$$

$$k \text{ of } MoL_3 = 4.9 \times 10^3\ M^{-1}s^{-1}$$

$$k \text{ of } WL_3 = 1.6 \times 10^5\ M^{-1}s^{-1}$$
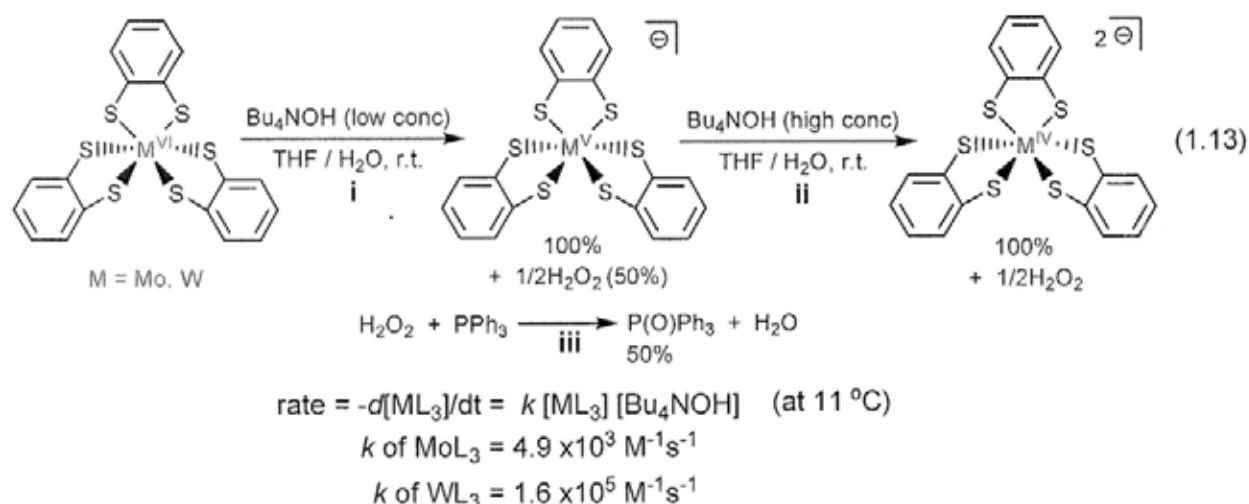
It is proposed that OH⁻ initially coordinates to the M(VI) tris-dithiolene complexes ($M(L)_3$, = Mo, W) to form a 7-coordinated intermediate $[M(L)_3OH]^-$ (Scheme 1.6, pathway i), which either reacts with $M(L)_3$ in the presence of OH⁻ or reacts directly with another $[M(L)_3OH]^-$ to yield 2 M(V) complexes and H_2O_2 (pathway ii).

Scheme 1.6 Proposed Mechanism of Reductions of Mo^{VI} and W^{VI} Tris-dithiolene Complexes by Hydroxide Ions
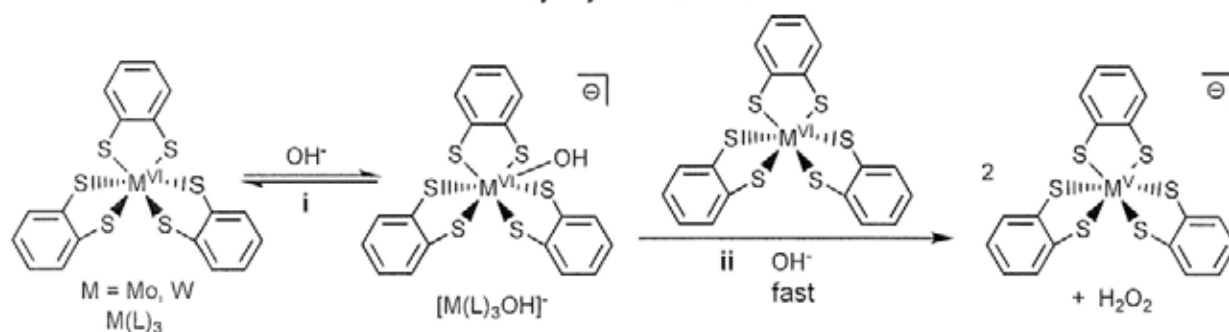
Moreover, the rates of reductions of W(VI) complexes by OH⁻ are much faster than Mo(VI) ones by about 30 times. It is suggested that the bond energy of W-OH is higher than Mo-OH, such that the enthalpy of activation term, $\Delta H^{\ddagger}$, in W-OH is lowered to dictate faster reductions in W-OH complexes.

(ii) Iron(III) and Ruthenium(III) Complexes

Tris(1,10-phenanthroline)iron(III)[72] and tris(2,2'-bipyridyl)iron(III),[73] as well as tris(1,10-phenanthroline)ruthenium(III), are reduced by OH⁻ in aqueous media to form the corresponding iron(II) and ruthenium(II) complexes (eq 1.14 and 1.15). It is reasoned that OH⁻ coordinates to M(III) (M = Fe, Ru), followed by the inner-sphere electron-transfer from OH⁻ to M(III) to give M(II) and HO•. HO• dimerizes to form H_2O_2, which undergoes rapid OH⁻-catalyzed disproportionation in aqueous media to form H_2O and O_2.[76]

$$[Fe^{III}(L)_3]^{3+} + OH^- \xrightarrow[H_2O,\ 6.5\text{-}35\ ^\circ C]{NaOH\ (aq)} [Fe^{II}(L)_3]^{2+} + 1/4 O_2 + 1/2 H_2O \qquad (1.14)$$

L = 1,10-phenanthroline,
    2,2'-bipyridyl

$$[Ru^{III}(bipy)_3](ClO_4)_3 \xrightarrow[r.t.]{NaOH\ (aq)} [Ru^{II}(bipy)_3](ClO_4)_2 + 1/4 O_2 + 1/2 H_2O \quad (1.15)$$

bipy = 2,2'-bipyridyl
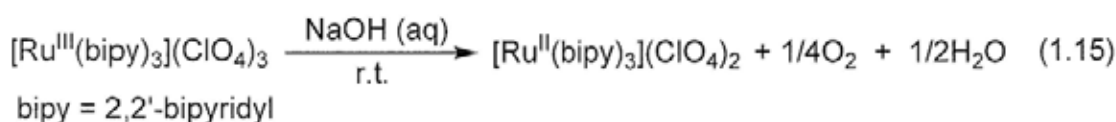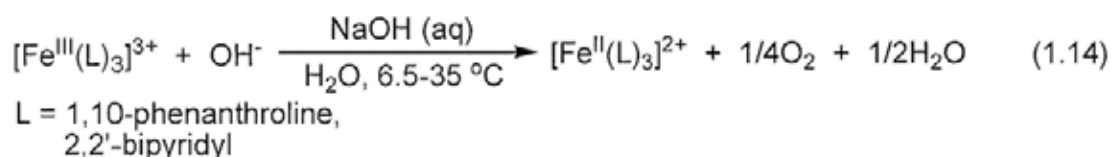
(iii) Cobalt(II) and Cobalt(III) Complexes

Cobalt(II) tetradehydrocorrins are reduced by NaOH in various aprotic solvents to form cobalt(I) tetradehydrocorrins (eq 1.16).[74] An inner-sphere single-electron transfer is proposed.

(a): $R_1 = R_2 = R_3 = Me$ (b): $R_1 = R_3 = Me$ (c): $R_1 = CO_2Et$
     $R_4 = Et$ $R_2 = R_4 = CH_2CH_2CO_2Et$ $R_2 = R_3 = Me$
                                             $R_4 = Et$
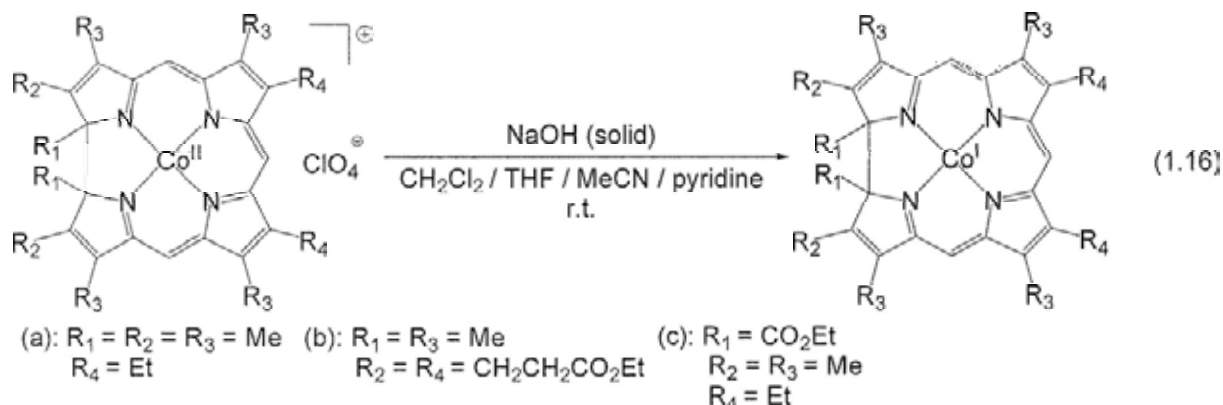
Cobalt(III) corrole is also rapidly reduced by OH⁻ to form cobalt(II) corrole anion in benzene in the presence of olefins (eq 1.17).[75] It is proposed that the olefin coordinates to cobalt(III) to form cobalt(III)-olefin complex. OH⁻ then attacks the olefin and reduces cobalt(III) to cobalt(II) via an inner-sphere electron-transfer. HO• formed further oxidizes the olefin, forming aldehydes or ketones as the observed co-products.

$$(1.17)$$
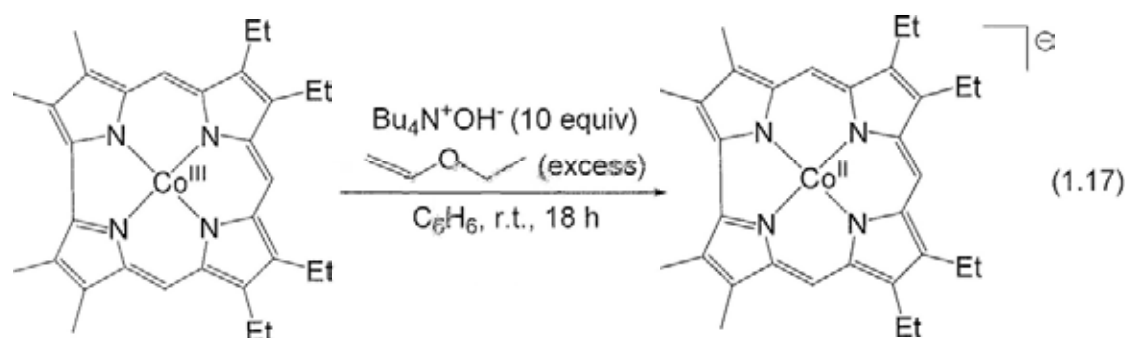
1.4.2.2.2 Reacting as Oxidizing Agents

Tris(acetylene)rhenium(I)-hydroxo complex undergoes oxidation reaction via α-hydrogen migration of hydroxo ligand to form bis(acetylene)rhenium(III)-oxo-hydride complex (eq 1.18).[77] It is proposed that the rearrangement takes place intramolecularly in the coordinatively saturated tris(acetylene)rhenium(I)-hydroxo complex. Hydrogen migration likely takes place either synchronously with or prior to the loss of acetylene ligand.

$$(1.18)$$
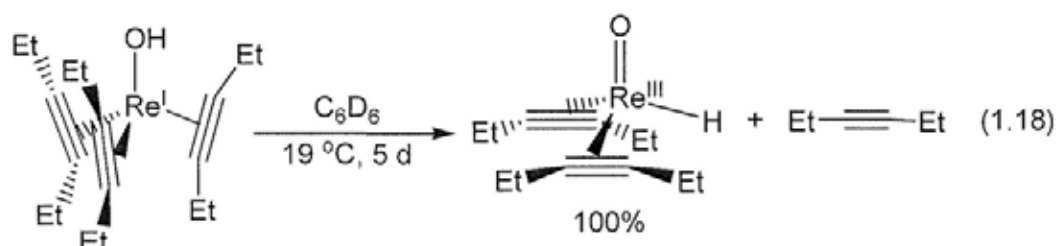
1.5 Transition Metal Porphyrin Hydroxo Complexes

Transition-metal porphyrins can also be converted to metal-hydroxo complexes, which exhibit similar reactivities as the transition-metal non-porphyrin hydroxo complexes. The

preparations and reactivities of some transition-metal porphyrin hydroxo complexes are briefly reviewed below.

1.5.1 Preparation of Transition Metal Porphyrin Hydroxo Complexes

Three major synthetic approaches can be used to prepare metalloporphyrin-hydroxo complexes: (i) Ligand substitution with hydroxide, (ii) deprotonation of aqua ligand, and (iii) oxidative addition with water.

1.5.1.1 Ligand Substitutions with Hydroxide Ions

Metalloporphyrin halides can undergo ligand substitution with hydroxide ions (OH^-) to form metalloporphyrin hydroxo complexes. For examples, sterically hindered $Fe^{III}(tmp)Cl$ (tmp = tetramesitylporphyrin) and $Fe^{III}(t$-$2,4,6$-$tmpp)Cl$ (t-2,4,6-tmpp = tetrakis(2,4,6-trimethoxyphenyl)porphyrin) react with NaOH in toluene to form stable $Fe^{III}(tmp)OH$ and $Fe^{III}(t$-$2,4,6$-$tmpp)OH$, respectively (eq 1.19).[78]

$$Fe^{III}(por)Cl \xrightarrow[\text{toluene, r.t., 1 d}]{\text{NaOH (aq)}} Fe^{III}(por)OH \quad (1.19)$$

$$por = tmp, \ t\text{-}2,4,6\text{-}tmpp$$
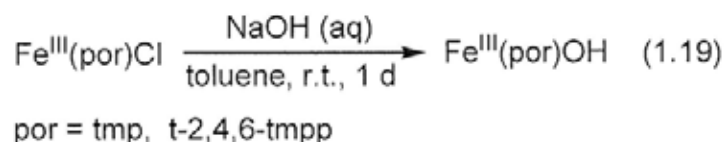
1.5.1.2 Deprotonation of Aqua Ligands

Water-soluble cobalt(III), rhodium(III), and iridium(III) tetrakis(p-sulfonatophenyl)porphyrin complexes ($[M^{III}(tspp)(H_2O)_2]^{3-}$, M = Co, Rh, Ir) contain two aqua ligands which are weak acids.[79] The pK_a values of the aqua ligands in these metalloporphyrin diaqua complexes are listed in Table 1.2. The pK_{a1} values are around 8, whereas the pK_{a2} values are around 11. At slightly alkaline media with pH higher than 9, single aqua ligand is deprotonated, forming metalloporphyrin mono-hydroxo complexes (eq 1.20). At more alkaline conditions with pH higher than 12, the other aqua ligand is further deprotonated to form metalloporphyrin dihydroxo complexes (eq 1.21).

Table 1.2 pK_a Values of Aqua Ligands in $[M^{III}(tspp)(H_2O)_2]^{3-}$

$$[M^{III}(tspp)(H_2O)_2]^{3-} \xrightleftharpoons[pK_{a1}]{H_2O,\ 25\ ^{\circ}C} [M^{III}(tspp)(OH)(H_2O)]^{4-} + H^+$$

$$[M^{III}(tspp)(OH)(H_2O)]^{4-} \xrightleftharpoons[pK_{a2}]{H_2O,\ 25\ ^{\circ}C} [M^{III}(tspp)(OH)_2]^{5-} + H^+$$

$[M^{III}(tspp)(H_2O)_2]^{3-}$	pK_{a1}	pK_{a2}
$[Co^{III}(tspp)(H_2O)_2]^{3-}$	8.06	12.15
$[Rh^{III}(tspp)(H_2O)_2]^{3-}$	7.85	11.55
$[Ir^{III}(tspp)(H_2O)_2]^{3-}$	7.32	10.59

$$[M^{III}(tspp)(H_2O)_2]^{3-} + OH^- \xrightarrow[25\ ^{\circ}C]{H_2O} [M^{III}(tspp)(OH)(H_2O)]^{4-} + H_2O \quad (1.20)$$
M = Co, Rh, Ir

$$[M^{III}(tspp)(OH)(H_2O)]^{4-} + OH^- \xrightarrow[25\ ^{\circ}C]{H_2O} [M^{III}(tspp)(OH)_2]^{5-} + H_2O \quad (1.21)$$
M = Co, Rh, Ir
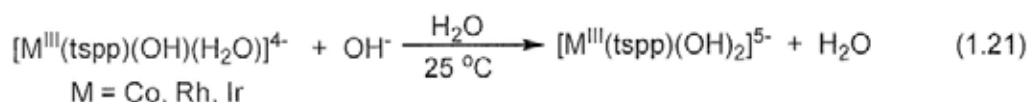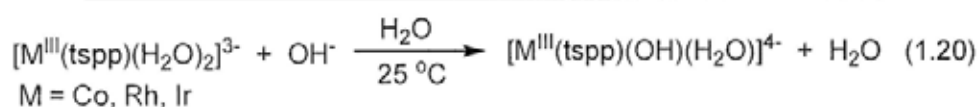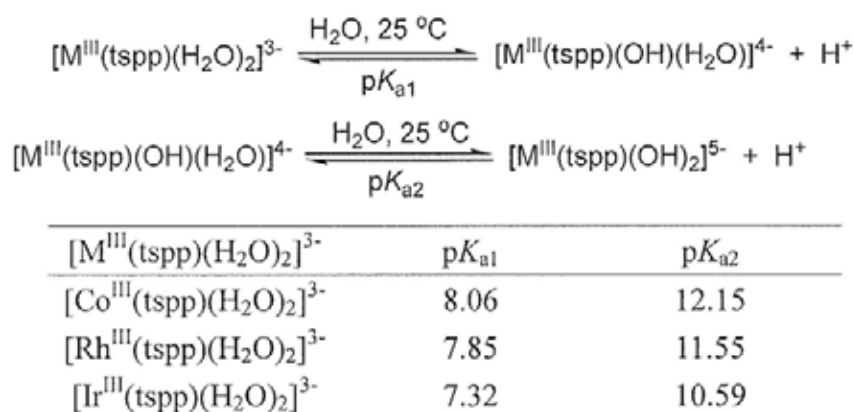
1.5.1.3 Oxidative Addition with Water

Water-soluble monomeric rhodoum(II) tetrakis(3,5-disulfonatomesityl)porphyrin $[Rh^{II}(tmps)(D_2O)_2]^{4-}$ undergoes rapid bimetallic oxidative addition of D_2O to form $[Rh^{III}(tmps)D(D_2O)]^{4-}$ and $[Rh^{III}(tmps)OD(D_2O)]^{4-}$ (eq 1.22).[52] Homolytic cleavage of DO-D bond should not take place due to the strong O-D bond[80] (BDE of DO-D = 121.0 kcal mol^{-1}).[62] It is proposed that D_2O initially promotes the facile disproportionation of rhodium(II) porphyrin to give rhodium(I) porphyrin anion and rhodium(III) porphyrin diaqua complex (Scheme 1.7, pathway i), followed by the deprotonation of rhodium(III) diaqua complex by Rh(I) anion to give Rh^{III}-OD and Rh^{III}-D (pathway ii).[81]

$$2[Rh^{II}(tmps)(D_2O)]^{4-} + D_2O \xrightleftharpoons[D_2O]{25\ ^{\circ}C} [Rh^{III}(tmps)D(D_2O)]^{4-} + [Rh^{III}(tmps)(OD)(D_2O)]^{4-} \quad (1.22)$$
tmps = tetrakis(3,5-disulfonatomesityl)porphyrin $\qquad \triangle G = -2.4$ kcal/mol
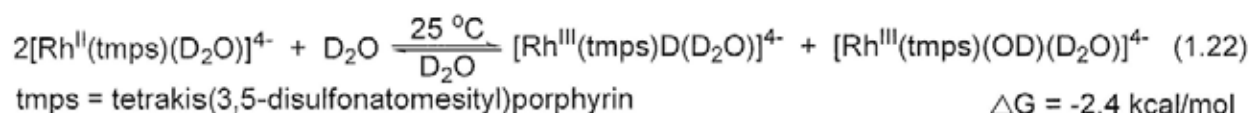
Scheme 1.7 Proposed Mechanism of Oxidative Addition of Water to $[Rh^{II}(tmps)(D_2O)_2)^{4-}]$

$$2[Rh^{II}(tmps)(D_2O)]^{4-} + D_2O \underset{}{\overset{i}{\rightleftharpoons}} [Rh^{III}(tmps)(D_2O)_2]^{3-} + [Rh^{I}(tmps)(D_2O)]^{5-}$$

$$[Rh^{III}(tmps)(D_2O)_2]^{3-} + [Rh^{I}(tmps)(D_2O)]^{5-} \xrightarrow{ii} [Rh^{III}(tmps)(OD)(D_2O)]^{4-} + [Rh^{III}(tmps)-D(D_2O)]^{4-}$$
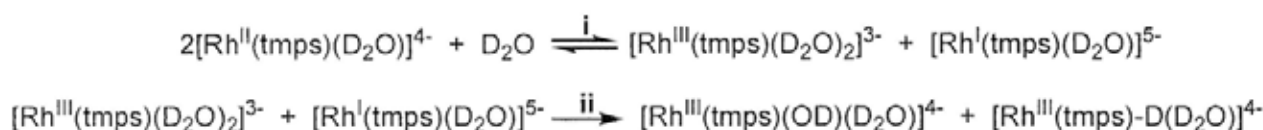
1.5.2 Reactivities of Transition Metal Porphyrin Hydroxo Complexes

The reactivities of metalloporphyrin hydroxo complexes are mostly found in (i) redox reactions and (ii) condensation reactions. OH^- can act as an efficient reducing agent to reduce the metal centers in metalloporphyrins, and to undergo condensation via water elimination to form μ-oxo dimer complexes.

1.5.2.1 Redox Chemistry

The reductions of metal centers in metallporphyrins by hydroxide ion are commonly reported only for the first row transition metals of manganese and iron. To our knowledge, cobalt(III) porphyrin has not been reported to undergo the reduction of metal center by OH^- to give cobalt(II) porphyrin.

(i) Manganese(III) Porphyrin Hydroxo Complexes

Manganese(III) porphyrin chloride, $Mn^{III}(tmp)Cl$ (tmp = tetramesitylporphyrin), reacts with OH^- in aprotic solvents of MeCN and DMSO to yield $[Mn^{II}(tmp)OH]^-$ (eq 1.23).[82a] Scheme 1.8 illustrates the proposed mechanism.[82a] The large excess coordinating solvent molecules (L) promotes the dissociation of Cl^- to form $[Mn^{III}(tmp)(L)_2]^+$ (Scheme 1.8, pathways i and ii), which then reacts with OH^- to yield $Mn^{III}(tmp)(L)OH$ and $[Mn^{III}(tmp)(OH)_2]^-$ (pathways iii and iv). The coordinated OH^- reduces Mn^{III} to Mn^{II} to give $Mn^{II}(tmp)(L)$ and $[Mn^{II}(tmp)OH]^-$, and $HO\bullet$ radical formed likely converts to other oxidation products (pathways v and vii). Dimerization of $HO\bullet$ to H_2O_2 is also proposed in the reduction of $Mn^{III}(Cl_8tpp)Cl$ by OH^- (Cl_8tpp = tetrakis(2,6-dichlorophenyl)porphyrin).[82b] $Mn^{II}(tmp)(L)$ formed finally coordinates with OH^- to give $[Mn^{II}(tmp)OH]^-$ (pathway vi).

$$Mn^{III}(tmp)Cl \xrightarrow[\text{DMSO or MeCN, N}_2\text{, r.t.}]{^nBuN^+OH^- / MeOH} [Mn^{II}(tmp)OH]^- \quad (1.23)$$

24
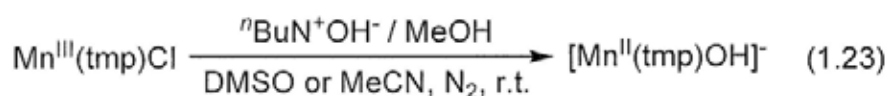
Scheme 1.8 Proposed Mechanism of Reduction of $Mn^{III}(tmp)Cl$ by OH^- to $[Mn^{II}(tmp)OH]^-$

$$Mn^{III}(tmp)Cl + L \xrightleftharpoons{i} [Mn^{III}(tmp)L]^+ + Cl^- \quad (L = MeCN, DMSO)$$

$$[Mn^{III}(tmp)L]^+ + L \xrightleftharpoons{ii} [Mn^{III}(tmp)L_2]^+$$

$$[Mn^{III}(tmp)L_2]^+ + OH^- \xrightleftharpoons{iii} Mn^{III}(tmp)(L)(OH) + L$$

$$Mn^{III}(tmp)(L)(OH) + OH^- \xrightleftharpoons{iv} [Mn^{III}(tmp)(OH)_2]^- + L$$

$$Mn^{III}(tmp)(L)(OH) \xrightarrow{v} Mn^{II}(tmp)(L) + HO\bullet$$

$$Mn^{II}(tmp)(L) + OH^- \xrightleftharpoons{vi} [Mn^{II}(tmp)OH]^- + L$$

$$[Mn^{III}(tmp)(OH)_2]^- \xrightarrow{vii} [Mn^{II}(tmp)OH]^- + HO\bullet$$
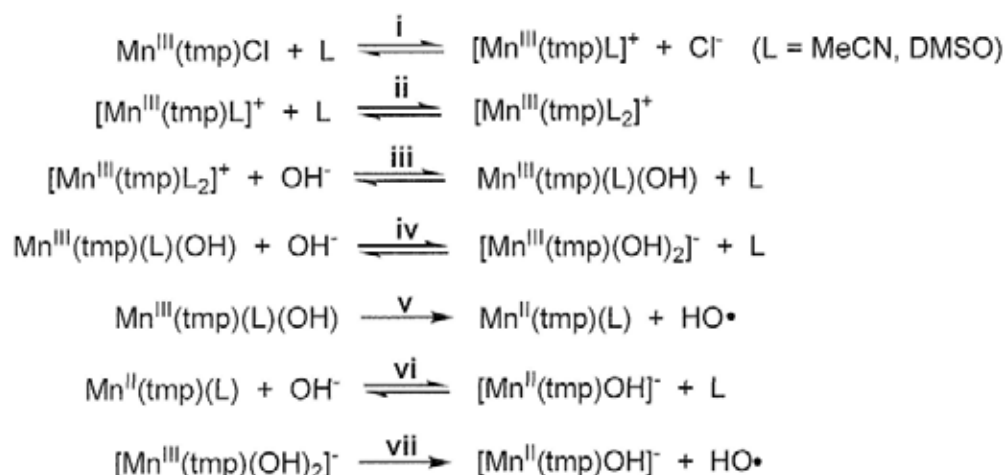
Since the oxidation potential for the half-reaction $OH^- \rightarrow HO\bullet + e^-$ is +0.7 V (vs SCE in DMSO) and the reduction potential for the half-reaction $Mn^{III}(tmp)(ClO_4) + e^- \rightarrow Mn^{II}(tmp)$ is -0.1 V (vs SCE in DMSO),[82a,c] an outer-sphere electron-transfer from OH^- to $Mn^{III}(tmp)^+$ is thermodynamically unfavorable due to the negative E_{rxn} value (E_{rxn} = -0.1 - (+0.7) = -0.8 V).[82a] It has been reported that the oxidation potential of $OH^- \rightarrow HO\bullet$ is shifted to a much negative potential and OH^- becomes more reducing in the presence of $Mn^{III}(tpp)^+$ (tpp = tetraphenylporphyrin) (Table 1.3), due to the stabilization of $HO\bullet$ via the formation of d-p (d_π-$\bullet OH$) covalent bond.[83] Therefore, it is proposed that OH^- coordinates to $Mn^{III}(tmp)^+$ to promote rapid electron transfer from OH^- to Mn center via an inner-sphere electron-transfer (Scheme 1.8, pathways v and vii).[82a]

Table 1.3 Oxidation Potentials of HO•/OH⁻ with and without Metalloporphyrins

$$OH^- \xrightarrow[MeCN, r.t.]{M(por)} HO\bullet + e^- \quad E_{ox}$$

M(por)	E_{ox} (MeCN, vs SCE)	Reducing ability of OH^-
nil	+0.55	low
$Mn^{III}(tpp)^+ClO_4^-$	-0.59	high

(ii) Iron(III) Porphyrin Hydroxo Complexes

Iron(III) porphyrin complex, $[Fe^{III}(tpp)(py)_2]^+$ (tpp = tetraphenylporphyrin), is reduced by OH^- to yield $Fe^{II}(tpp)(py)_2$ (eq 1.24).[84] The coordinated pyridine can act as a bridge to facilitate the reduction of Fe(III) by OH^- to give $Fe^{II}(tpp)(py)_2$ (Scheme 1.9). Oxidized hydroxy-pyridine is a proposed co-product.

$$[Fe^{III}(tpp)(py)_2]^+ \xrightarrow[\text{pyridine, r.t.}]{Et_4N^+OH^- \text{ / MeOH}} Fe^{II}(tpp)(py)_2 + 1/n[p\dot{y}(OH)]_n \quad (1.24)$$
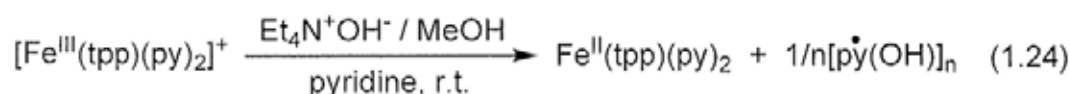
Scheme 1.9 Proposed Mechanism of Reduction of $[Fe^{III}(tpp)(py)_2]^+$ by Hydroxide Ion
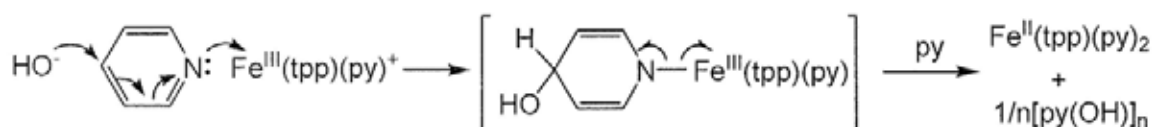
$Fe^{III}(tpp)Cl$ is also reduced by OH^- in aprotic solvent of DMSO to form $[Fe^{II}(tpp)OH]^-$ as the observed product (eq 1.25).[85] Since $Fe^{III}(tpp)Cl$ reacts with OH^- in THF to form $Fe^{III}(tpp)OH$ only without the inner-sphere reduction of Fe^{III}, it is proposed that during the reduction process in DMSO (eq 1.25), OH^- first reduces DMSO to form DMSO radical anion, which then reduces $Fe^{III}(tpp)Cl$ to $Fe^{II}(tpp)$ via an outer-sphere electron-transfer. Further coordination of OH^- to $Fe^{II}(tpp)$ gives $[Fe^{II}(tpp)OH]^-$.

$$Fe^{III}(tpp)Cl \xrightarrow[\text{DMSO-}d_6\text{, argon, r.t.}]{Bu_4N^+OH^- \text{ / MeOH (2 equiv)}} [Fe^{II}(tpp)OH]^- \quad (1.25)$$
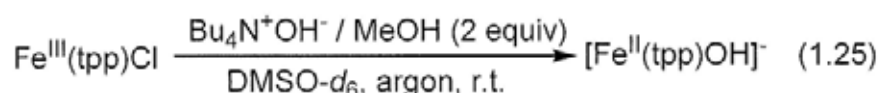
1.5.2.2 Condensation Reactions

Condensation of metalloporphyrin-hydroxo complexes to form μ-oxo dimer has been reported in iron and molybdenum porphyrins.

(i) Formation of Iron(III) Porphyrin μ-Oxo Dimer

Iron(III) porphyrin chloride ($Fe^{III}(por)Cl$) with less sterically-hindered porphyrin ligands

reacts with OH⁻ via ligand substitution to form $Fe^{III}(por)OH$ (eq 1.26), which can further undergo bimolecular condensation to yield iron(III) porphyrin μ-oxo dimer, $Fe^{III}(por)OFe^{III}(por)$ (eq 1.27).[78]

$$Fe^{III}(por)Cl + OH^- \longrightarrow Fe^{III}(por)OH + Cl^- \qquad (1.26)$$

$$2Fe^{III}(por)OH \longrightarrow Fe^{III}(por)OFe^{III}(por) + H_2O \qquad (1.27)$$
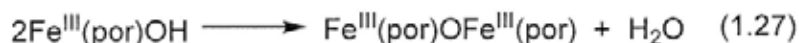
For examples, the more sterically hindered Fe^{III}(t-3,4,5-tmpp)Cl (t-3,4,5-tmpp = tetrakis(3,4,5-trimethoxyphenyl)porphyrin) reacts with OH⁻ to yield both Fe^{III}(t-3,4,5-tmpp)OH and $[Fe^{III}$(t-3,4,5-tmpp)]$_2$O dimer (eq 1.28).[78] On the other hand, the sterically unhindered Fe^{III}(tpp)Cl (tpp = tetraphenylporphyrin) reacts with OH⁻ to yield Fe^{III}(tpp)OH, which further undergoes condensation to yield $[Fe^{III}$(tpp)]$_2$O as the only observed product (eq 1.29).[78] Indeed, the thermodynamically stabilized iron(III) porphyrin μ-oxo dimers do not undergo hydrolysis in excess water at room temperature to give back monomeric $Fe^{III}(por)OH$.[78]

$$Fe^{III}(por)Cl \xrightarrow[\text{toluene, 1 d}]{\text{NaOH (aq)}} Fe^{III}(por)OH + (por)Fe^{III}OFe^{III}(por) \qquad (1.28)$$
$$por = \text{t-3,4,5-tmpp}$$

$$Fe^{III}(tpp)Cl \xrightarrow[\text{toluene, 1 d}]{\text{NaOH (aq)}} (tpp)Fe^{III}OFe^{III}(tpp) \qquad (1.29)$$
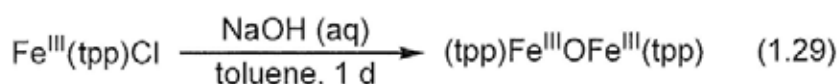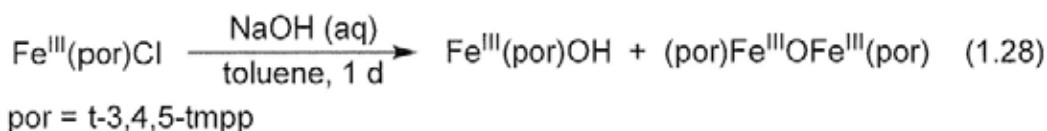
(ii) Formation of Oxo-Molybdenum(V) Porphyrin μ-Oxo Dimer

Molybdenum(V) porphyrin-oxo-hydroxo complex, $O=Mo^V(tpp)OH$ (tpp = tetraphenylporphyrin), can also undergo condensation to form μ-oxo dimer $(O=Mo^V(tpp))_2O$ (eq 1.30).[86]

$$2O=Mo^V(tpp)OH \xrightarrow[\text{r.t.}]{CH_2Cl_2,\ C_6H_6} (O=Mo^V(tpp))_2O + H_2O \qquad (1.30)$$

1.6 Equilibrium Distributions of M^{III}(por), M^{II}(por), and M^{I}(por) of Group 9 Metalloporphyrins in Basic Media

Group 9 metalloporphyrins in the form of metal(III) porphyrin hydroxo (M^{III}(por)OH), metal(III) porphyrin hydride (M^{III}(por)H), metal(II) porphyrin (M^{II}(por)), and metal(I) porphyrin anion (M^{I}(por)) can exist in equilibria and are inter-convertible to one another in a reaction system, depending on the concentrations of OH⁻ (or pH values in aqueous media). Indeed, the Wayland group has studied the detailed equilibrium distributions of water-soluble rhodium(III) and iridium(III) tetrakis(*p*-sulfonatophenyl)porphyrin diaqua complexes, $[Rh^{III}(tspp)(D_2O)_2]^{3-}$ [51] and $[Ir^{III}(tspp)(D_2O)_2]^{3-}$,[79] in basic aqueous media. The equilibria of metalloporphyrins are briefly presented below.

1.6.1 Equilibrium Distributions from $[Rh^{III}(tspp)(D_2O)_2]^{3-}$

When $[Rh^{III}(tspp)(D_2O)_2]^{3-}$ reacts with D_2 in basic aqueous media at 298 K, 6 rhodium porphyrin species are formed in equilibria:[51] (1) the parent $[Rh^{III}(tspp)(D_2O)_2]^{3-}$, (2) $[Rh^{III}(tspp)OD(D_2O)]^{4-}$, (3) $[Rh^{III}(tspp)(OD)_2]^{5-}$, (4) $[Rh^{III}(tspp)D(D_2O)]^{4-}$, (5) $[Rh^{II}(tspp)(D_2O)]_2^{8-}$, and (6) $[Rh^{I}(tspp)(D_2O)]^{5-}$ (Scheme 1.10).

Scheme 1.10 Equilibria of Rh^{III}-OD, Rh^{III}-D, Rh^{II}, and Rh^{I} in the Reaction of $[Rh^{III}(tspp)(D_2O)_2]^{3-}$ with D_2 in Basic Aqueous Media

$[Rh^{III}(tspp)(D_2O)_2]^{3-}$ undergoes deprotonations of aqua ligands to form $[Rh^{III}(tspp)(OD)(D_2O)]^{4-}$ and $[Rh^{III}(tspp)(OD)_2]^{5-}$ (Scheme 1.10, pathways i and ii). The deprotonations become more favorable when the pH value increases. $[Rh^{III}(tspp)(OD)(D_2O)]^{4-}$ reacts facilely with D_2 to form $[Rh^{III}(tspp)-D(D_2O)]^{4-}$ (pathway iii). $[Rh^{III}(tspp)-D(D_2O)]^{4-}$ can further undergo slow dehydrogenative dimerization to form $[Rh^{II}(tspp)(D_2O)]_2^{8-}$ dimer (pathway v) and deprotonation of Rh-H by OH$^-$ to form $[Rh^{I}(tspp)(D_2O)]^{5-}$ (pathway iv). $[Rh^{I}(tspp)(D_2O)]^{5-}$ also reacts with $[Rh^{III}(tspp)(D_2O)_2]^{3-}$ via comproportionation to form $[Rh^{II}(tspp)(D_2O)]_2^{8-}$ (pathway vi). All the rhodium porphyrin species can interconvert to one another via equilibria, and the formation of each species as a major one is highly dependent on the pH values.

1.6.2 Equilibrium Distributions from $[Ir^{III}(tspp)(D_2O)_2]^{3-}$

When $[Ir^{III}(tspp)(D_2O)_2]^{3-}$ reacts with methoxide ion in basic aqueous media at 298 K, 6 iridium porphyrin species are formed in equilibria:[79] (1) the parent $[Ir^{III}(tspp)(D_2O)_2]^{3-}$, (2) $[Ir^{III}(tspp)OD(D_2O)]^{4-}$, (3) $[Ir^{III}(tspp)(OD)_2]^{5-}$, (4) $[Ir^{III}(tspp)(OCH_3)(OD)]^{5-}$, (5) $[Ir^{III}(tspp)-H(OD)]^{5-}$, and (6) $[Ir^{I}(tspp)(OD)]^{6-}$ (Scheme 1.11).

Scheme 1.11 Equilibria of Ir^{III}-OD, Ir^{III}-OCH$_3$, Ir^{III}-H, and Ir^{I} in the Reaction of $[Ir^{III}(tspp)(D_2O)_2]^{3-}$ with Methoxide ion in Basic Aqueous Media

$$[(tspp)Ir^{III}(D_2O)_2]^{3-}$$
$$\Big\updownarrow \quad \text{i } -D^+$$
$$[(tspp)Ir^{III}(OD)(D_2O)]^{4-} \; \underset{\xrightarrow{\hspace{1cm}}}{\overset{\text{ii } -D^+}{\longleftarrow}} \; [(tspp)Ir^{III}(OD)_2]^{5-}$$
$$\Big\updownarrow \quad \text{iii } OCH_3^-, -D_2O$$
$$[(tspp)Ir^{III}(OCH_3)(OD)]^{5-} \; \underset{\xrightarrow{\hspace{1cm}}}{\overset{\text{iv } -HCHO}{\longleftarrow}} \; [(tspp)Ir^{III}-H(OD)]^{5-} \; \underset{\xrightarrow{\hspace{1cm}}}{\overset{\text{v } -H^+}{\longleftarrow}} \; [(tspp)Ir^{I}(OD)]^{6-}$$
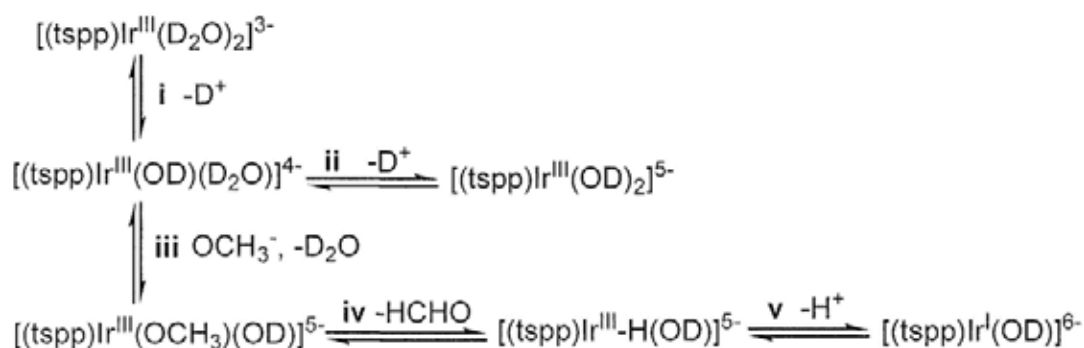
$[Ir^{III}(tspp)(D_2O)_2]^{3-}$ undergoes deprotonations of aqua ligands in basic media to form $[Ir^{III}(tspp)(OD)(D_2O)]^{4-}$ and $[Ir^{III}(tspp)(OD)_2]^{5-}$ (Scheme 1.11, pathways i and ii). $[Ir^{III}(tspp)(OD)(D_2O)]^{4-}$ undergoes facile ligand substitution with OCH_3^- to form $[Ir^{III}(tspp)(OCH_3)(OD)]^{5-}$ (pathway iii), which undergoes β-hydride elimination to form $[Ir^{III}(tspp)\text{-}H(OD)]^{5-}$ (pathway iv). $[Ir^{III}(tspp)\text{-}H(OD)]^{5-}$ can be further deprotonated by OH^- to form $[Ir^{I}(tspp)(OD)]^{6-}$ (pathway v). By controlling the pH values, $[Ir^{III}(tspp)(OCH_3)(OD)]^{4-}$, $[Ir^{III}(tspp)\text{-}D(D_2O)]^{4-}$, and $[Ir^{I}(tspp)(OD)]^{6-}$ can be formed as major products which are the entry points for many chemical transformations.[79]

1.7 Chemistry of Group 9 Metalloporphyrins

Both hydrophilic and lipophilic group 9 metalloporphyrins exhibit rich bond activation chemistry and are briefly reviewed below.

1.7.1 Chemistry of Metal(III) Porphyrins (M^{III}(por))

1.7.1.1 Chemistry of Metal(III) Porphyrin Hydroxo (M^{III}(por)OH)

Recently, group 9 metalloporphyrin hydroxo complexes (M^{III}(por)OH) have been reported to promote the reactions with olefins and bond activations of H-H and C-H bonds to broaden the chemistry of M^{III}(por)OH.

1.7.1.1.1 Reactions with Olefins

$[Rh^{III}(tspp)OD(D_2O)]^{4-}$ reacts with olefins in basic aqueous media at room temperature to form rhodium(III) porphyrin β-hydroxyethyl complexes (eq 1.31), which can further react in aqueous media at elevated temperature to produce ketones (eq 1.32(a)), and to react with KOH in DMSO to form epoxides, respectively (eq 1.32(b)).[87]

$$[Rh^{III}(tspp)\text{-}OD(D_2O)]^{4-} + \underset{\substack{R = {}^{n}Pr, {}^{n}Bu, {}^{n}Pent, \\ Ph, cyclohexyl...}}{\diagup\!\!\!\!=} \underset{\substack{D_2O, r.t. \\ <5\ min - 34\ h}}{\overset{\substack{pH\ 9.0\ buffer \\ solution}}{\rightleftharpoons}} \left[\underset{80\%\ to\ >95\%}{R\overset{OD}{\diagdown}\text{---}Rh^{III}(tspp)(D_2O)} \right]^{4-} \qquad (1.31)$$

$$\left[R\overset{OD}{\diagdown}\text{---}Rh^{III}(tspp)(D_2O) \right]^{4-}_{R = {}^{n}Pr, {}^{n}Bu, {}^{n}Pent}$$

(a) $\xrightarrow[\substack{333\ K\ /\ 353\ K,\ 3\text{-}16.5\ h}]{\substack{pH\ 9.0\ buffer\ solution \\ H_2O,\ degas}}$ $[Rh^{I}(tspp)(D_2O)]^{5-}$ + ketone (quantitative)

(b) $\xrightarrow[\substack{r.t.,\ <5\ min}]{KOH\ /\ DMSO}$ $[Rh^{I}(tspp)(D_2O)]^{5-}$ + epoxide-R (quantitative)

$$(1.32)$$
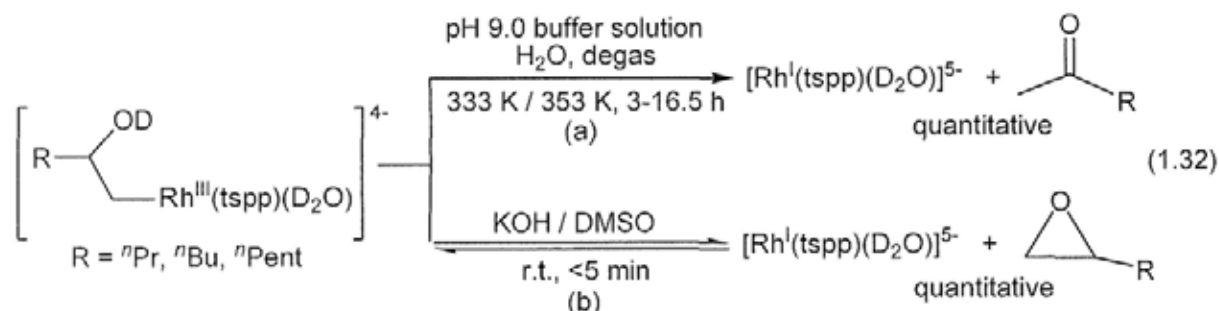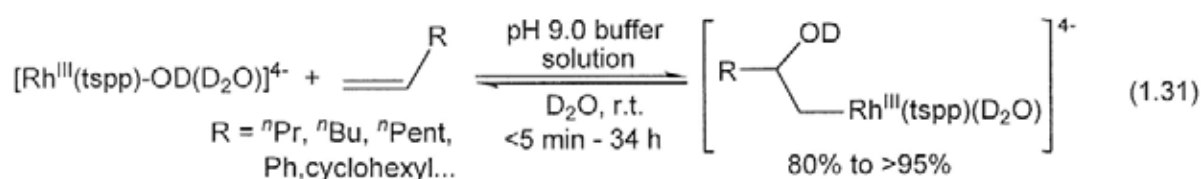
It is proposed that $[Rh^{III}(tspp)OD(D_2O)]^{4-}$ promotes the insertion of olefins in aqueous media to form rhodium(III) porphyrin β-hydroxyethyl intermediate (Scheme 1.12, pathway i), which then undergoes β-hydride elimination at higher temperatures to form rhodium(III) porphyrin hydride and enol in aquesous media (pathway ii). The enol tautomerizes rapidly to generate ketone (pathway vii), and rhodium porphyrin hydride is further deprotonated by OD⁻ to form rhodium(I) porphyrin anion (pathway iii), which can undergo aerobic oxidation to regenerate $[Rh^{III}(tspp)OD(D_2O)]^{4-}$ (pathway iv).

Scheme 1.12 Proposed Mechanism of Rhodium(III) Porphyrin Hydroxo-Mediated Oxidations of Olefins to Form Ketones and Epoxides
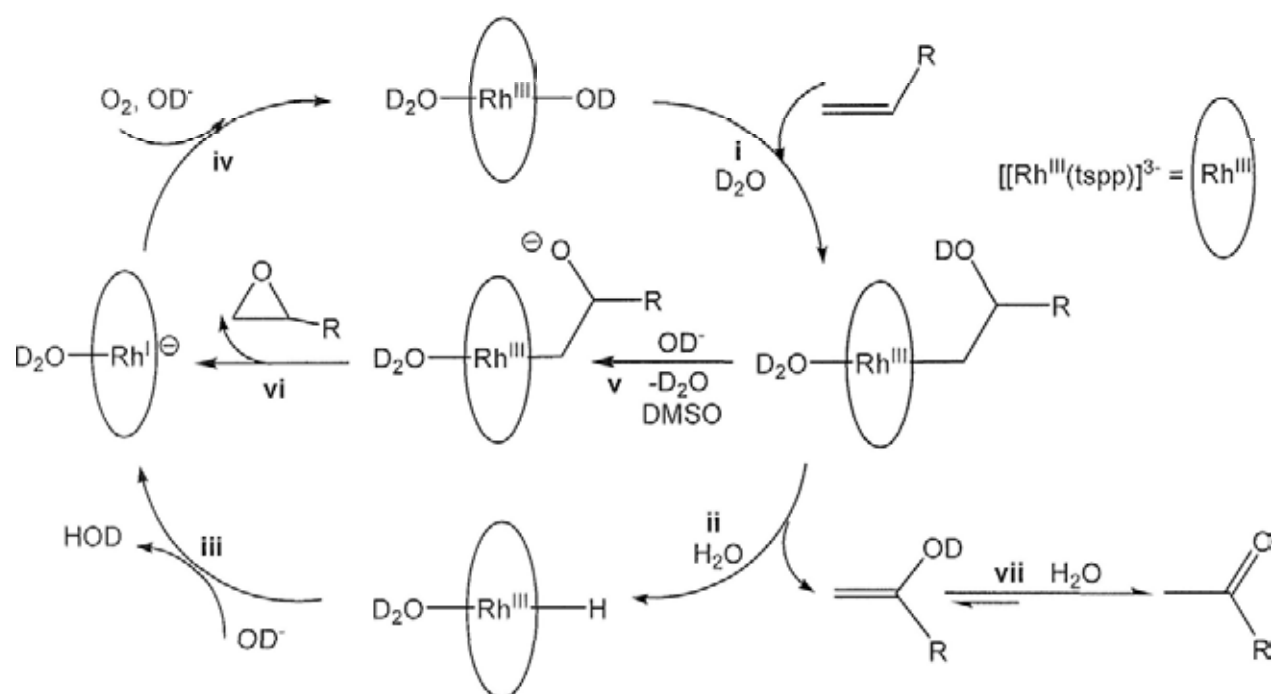
In DMSO, the hydroxo group of rhodium(III) porphyrin β-hydroxyethyl undergoes the deprotonation by OD⁻ to form oxygen anion (pathway v), which then attacks the α-carbon to form epoxide (pathway vi), and Rh^I(tspp)(D$_2$O)]$^{5-}$ formed can be recycled to produce [Rh^{III}(tspp)(D$_2$O)$_2$]$^{3-}$ via the aerobic oxidation (pathway iv).

1.7.1.1.2 Activations of H-H and C-H Bonds

The water-soluble rhodium porphyrin hydroxo complexes, [Rh^{III}(tspp)OD(D$_2$O)]$^{4-}$ and [Rh^{III}(tspp)(OD)$_2$]$^{4-}$, react instantaneously with deuterium (D$_2$) at ambient conditions to form the reduced products, [Rh^{III}(tspp)D(H$_2$O)]$^{4-}$ and Rh^I(tspp)(OD$_2$)]$^{5-}$, respectively (eq 1.33 and 1.34).[51]

$$[Rh^{III}(tspp)(OD)(D_2O)]^{4-} + D_2 \; \underset{25\,°C}{\overset{D_2O}{\rightleftharpoons}} \; [Rh^{III}(tspp)D(D_2O)]^{4-} + D_2O \quad (1.33)$$
$$K = 1.3 \times 10^9 \qquad \triangle G = -12.4 \text{ kcal mol}^{-1}$$

$$[Rh^{III}(tspp)(OD)_2]^{5-} + D_2 \; \underset{25\,°C}{\overset{D_2O}{\rightleftharpoons}} \; [Rh^I(tspp)(D_2O)]^{5-} + D_2O \quad (1.34)$$
$$K = 3.6 \times 10^{13} \qquad \triangle G = -18.5 \text{ kcal mol}^{-1}$$
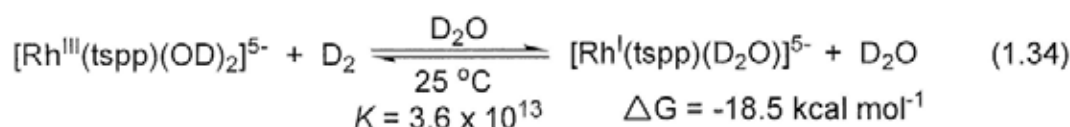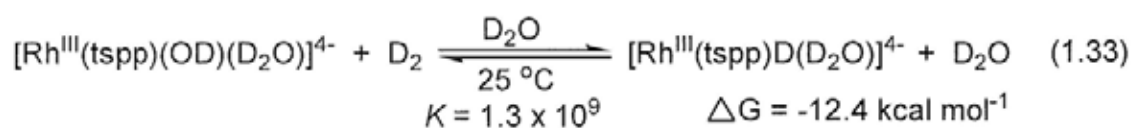
[Rh^{III}(tspp)(OD)(D$_2$O)]$^{4-}$ also undergoes α-C-H bond activation of acetaldehyde and acetone (eq 1.35).[87] It is proposed that the tautomerization of carbonyl compounds produces enols (Scheme 1.13, pathway i). Enols undergoes 1,2-insertion with Rh^{III}(tspp)(OD)(D$_2$O)]$^{4-}$ to form β-dihydoxyalkyl intermediate (pathway ii), which eliminates water to form the observed products (pathway iii).

$$[Rh^{III}(tspp)\text{-}OD(D_2O)]^{4-} + \underset{R\,=\,H,\,CH_3}{\overset{O}{\diagdown}} \; \underset{\substack{\text{r.t.}\\-\text{HOD}}}{\overset{\substack{\text{pH 9.0 buffer}\\\text{solution, D}_2\text{O}}}{\rightleftharpoons}} \; \left[R\overset{O}{\diagdown}\text{—Rh}^{III}(tspp)(D_2O) \right]^{4-} \quad (1.35)$$

Scheme 1.13 Proposed Mechanism of α-C-H bond Activation of Carbonyl Compounds by Rhodium(III) Porphyrin Hydroxo

Moreover, $Rh^{III}(ttp)CH_2CH_2OH$ (ttp = tetra(p-tolyl)porphyrin) added with PPh_3 reacts with benzaldehydes very rapidly at 50 °C to yield $Rh^{III}(ttp)C(O)Ar$ (eq 1.36).[88] $Rh^{III}(ttp)(PPh_3)OH$ is the proposed intermediate for the aldehydic C-H bond activations of benzaldehydes.

It is proposed that PPh_3 promotes the β-hydroxy elimination of $Rh^{III}(ttp)CH_2CH_2OH$ to form $(PPh_3)Rh^{III}(ttp)OH$ (Scheme 1.14, pathways i-iii). $(PPh_3)Rh^{III}(ttp)OH$ may behave as an internal base to heterolytically cleave the aldehydic C-H bond (pathway iv), or dissociate to generate a vacant site for benzaldehyde coordination, followed by proton abstraction by OH⁻ as an external base to yield $Rh^{III}(ttp)C(O)Ar$ (pathways v and vi).

Scheme 1.14 Proposed Mechanism of Aldehydic C-H Activation by $(Ph_3P)Rh^{III}(ttp)OH$

1.7.1.2 Chemistry of Electrophilic Metal(III) Porphyrin ($M^{III}(por)^+$)

Electrophilic rhodium(III) porphyrins ($M^{III}(por)^+$) undergo aromatic C-H bond activations to yield rhodium(III) porphyrin aryls. $Rh^{III}(oep)^+ClO_4^-$ (oep = octaethylporphyrin) reacts with *ortho*, *para*-directing arenes to yield only rhodium(III) porphyrin *para*-substituted aryls (eq 1.37).[89] $Rh^{III}(ttp)Cl$ (ttp = tetrakis(*p*-tolyl)porphyrin) also reacts with *meta*-directing, electron-poor benzonitrile to yield rhodium(III) porphyrin *meta*-cyanophenyl (eq 1.38).[90] These experimental results support the electrophilic aromatic substitution mechanism (S_EAr) (Scheme 1.15).

(1.37) FG = H, OMe, Me, Cl → FG = H: 40%; OMe:46%; Me:46%; Cl:18%

(1.38) 28%
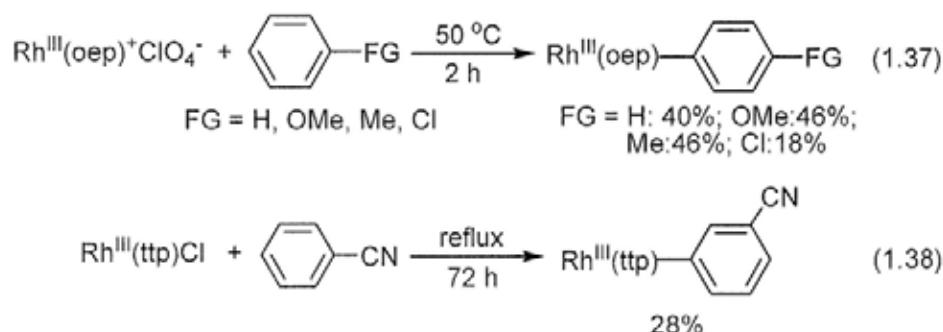
Scheme 1.15 Electrophilic Aromatic Substitution of Rhodium(III) Porphyrins
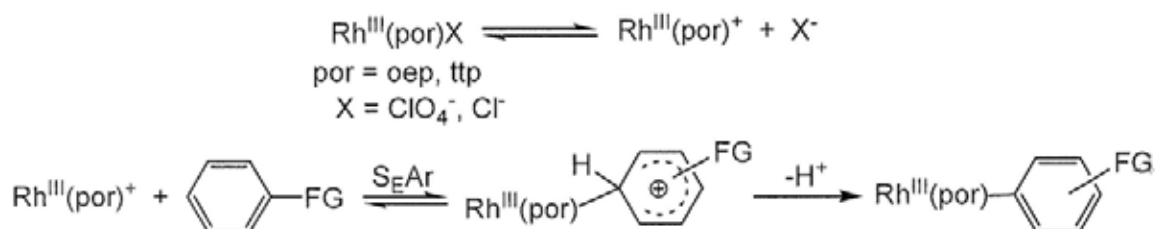
1.7.1.3 Chemistry of Group 9 Metal(III) Porphyrin Hydride ($M^{III}(por)H$)

The chemistry of high-valent group 9 metal(III) porphyrin hydrides ($M^{III}(por)H$) have been studied to explore the different modes of reactivities in small molecule activations[91] and to aid in the understandings of the reaction mechanisms of 1,2-rearrangements catalyzed by coenzyme B_{12}.[39] For examples, cobalt(III), rhodium(III), and iridium(III) porphyrin hydrides show diverse reactivities and mechanisms in the reactions towards styrene and carbon monoxide.

1.7.1.3.1 Reactions with Styrene

Group 9 metallophyrin hydrides have been reported to undergo the insertion of styrene to give metalloporphyrin phenethyl complexes. $Co^{III}(tap)H$ (tap = tetrakis(*p*-anisyl)porphyrin) reacts with styrene to yield 1-phenethyl cobalt(III) porphyrin via a non-chain radical pathway (eq 1.39).[92] Mechanistic studies suggest that Co-H initially dissociates homolytically to yield $Co^{II}(tap)$ and a H atom (Scheme 1.16, pathway i). The very reactive H atom reacts with styrene to yield the more stabilized secondary 1-phenethyl radical (pathway ii), which combines with $Co^{II}(tap)$ to yield the observed product (pathway iii).[93]

(1.39)
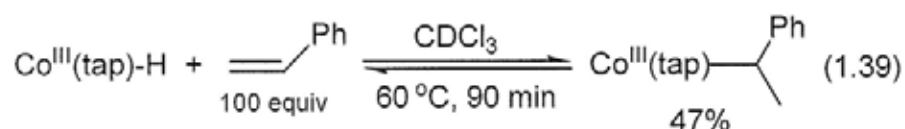
Scheme 1.16 Radical Non-Chain Mechanism of Styrene Insertion to Co(por)H
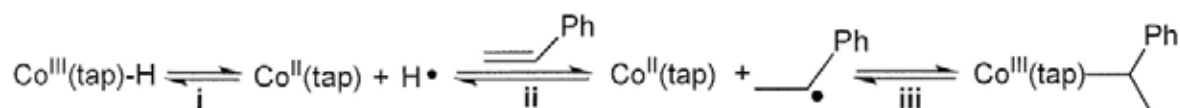
Rhodium(III) porphyrin hydrides, $Rh^{III}(oep)H$[93] and $Rh^{III}(bocp)H$ (bocp = octachloro(4-*tert*-butyl-phenyl)porphyrin),[94] reacted with styrene to give 2-phenethyl rhodium(III) porphyrin complexes (eq 1.40 and 1.41).

(1.40)

(1.41)
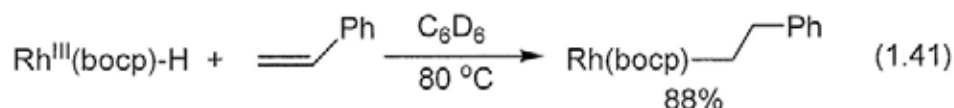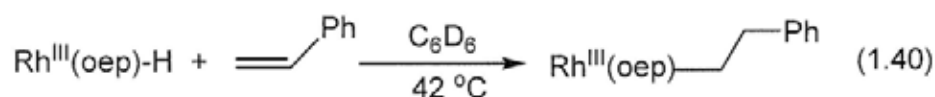
Two mechanisms are suggested. The first mechanism involves the radical chain pathways (Scheme 1.17).[93] $Rh^{III}(oep)H$ initially undergoes dehydrogenation to yield $[Rh^{II}(oep)]_2$ and H_2 via an equilibrium (pathway i). $[Rh^{II}(oep)]_2$ dissociates into 2 $Rh^{II}(oep)$ radicals (pathway ii). $Rh^{II}(oep)$ then reacts with styrene to give a more stable secondary radical intermediate (pathway iii), which abstracts H atom from $Rh^{III}(oep)$-H to yield $Rh^{III}(oep)CH_2CH_2Ph$, and

Rh^{II}(oep) is regenerated for further radical propagation reaction (pathway iv).

Scheme 1.17 Radical Chain Propagation in Styrene Insertion to Rh(por)-H

$$2Rh^{III}(oep)H \underset{i}{\rightleftharpoons} [Rh^{II}(oep)]_2 + H_2$$

$$[Rh^{II}(oep)]_2 \underset{ii}{\rightleftharpoons} 2Rh^{II}(oep)$$
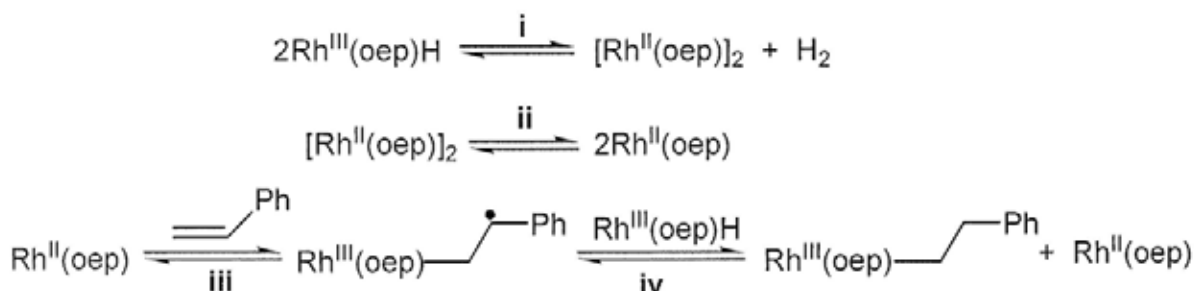
The second mechanism is the concerted insertion of styrene into Rh^{III}(por)-H bond (Scheme 1.18).[94] *Cis*-coordination of styrene to Rh^{III}(bocp)H occurs (pathway i), followed by the breaking of π-bond of styrene and the simultaneous forming of both Rh-C and β-C-H bonds to give Rh^{III}(bocp)CH$_2$CH$_2$Ph (pathways ii and iii).

Scheme 1.18 Concerted Insertion of Styrene to Rh(por)H
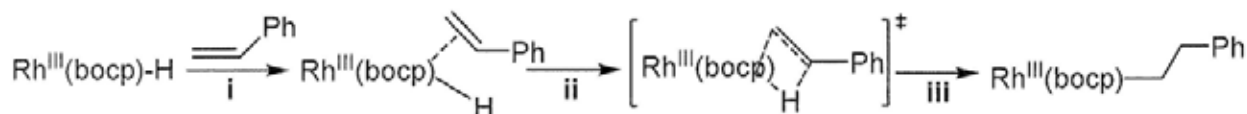
1.7.1.3.2 Reactions with Carbon Monoxide

Rh^{III}(oep)H reacts with CO to yield rhodium(III) porphyrin formyl complexes, Rh^{III}(oep)CHO (eq 1.42).[93]

$$Rh^{III}(oep)H + CO \xrightarrow[\text{instantaneous}]{C_6D_6,\ r.t.} Rh^{III}(oep)CHO \quad (1.42)$$
$$100\%$$
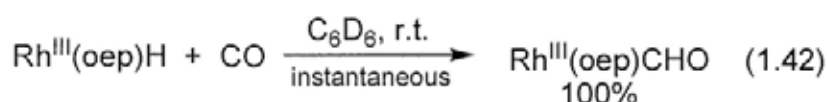
The mechanism of Rh^{III}(oep)CHO formation also involves radical chain reactions (Scheme 1.19).[93] Rh^{II}(oep), generated from the dehydogenative dimerization of Rh^{III}(oep)H (pathways i and ii), reacts with CO to yield the carbon-centered Rh^{III}(oep)(CO) radical (pathway iii), which then abstracts a H atom from Rh^{III}(oep)-H to yield Rh^{III}(oep)CHO and another Rh^{II}(oep) for further radical chain propagation reaction (pathway iv).

Scheme 1.19 Radical Chain Propagation in CO Insertion to Rh(oep)-H

$$2Rh^{III}(oep)H \; \xrightleftharpoons{i} \; [Rh^{II}(oep)]_2 \; + \; H_2$$

$$[Rh^{II}(oep)]_2 \; \xrightleftharpoons{ii} \; 2Rh^{II}(oep)$$

$$Rh^{II}(oep) \; \underset{iii}{\overset{CO}{\rightleftharpoons}} \; Rh^{III}(oep)\overset{\bullet}{C}O$$

$$Rh^{III}(oep)\overset{\bullet}{C}O \; \xrightarrow[iv]{Rh^{III}(oep)H} \; Rh^{III}(oep)H \; + \; Rh^{II}(oep)$$
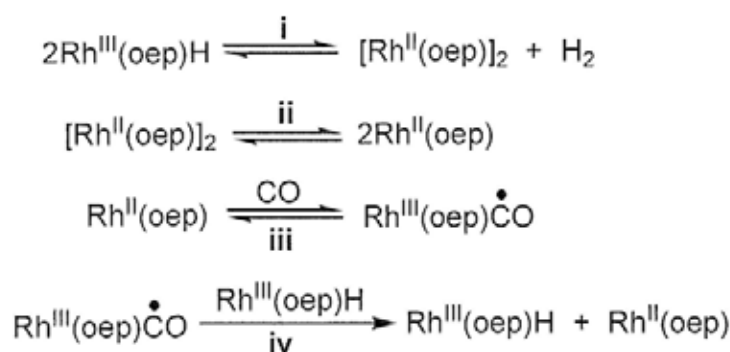
In contrast, $Ir^{III}(oep)H$ reacts with CO to form only CO coordinated complex, $Ir^{III}(oep)H(CO)$ (eq 1.43), due to the thermodynamically unfavorable CO insertion into Ir-H bond to form $Ir^{III}(oep)CHO$.[95]

$$Ir^{III}(oep)H \; + \; CO \; \xrightarrow[\text{instantaneous}]{C_6D_6, \; r.t.} \; Ir^{III}(oep)H(CO) \quad (1.43)$$
$$100\%$$
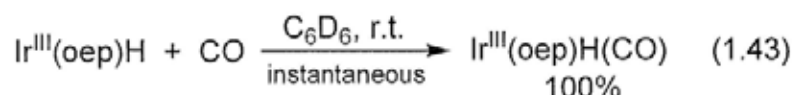
1.7.2 Chemistry of Group 9 Metal(II) Porphyrin (M^{II}(por))

Group 9 metal(II) porphyrins are metalloradicals which exist in monomer or dimer forms, depending on the bulkiness of porphyrin ligands and the nature of metals. These metalloradicals can be used to cleave various chemical bonds.

1.7.2.1 Bond Activations of C-Br, H-H, and C-H Bonds

Rhodium(II) and iridium(II) porphyrins have been used to successfully undergo various efficient bond activations of $C(sp^3)$-Br, H_2, and $C(sp^3)$-H bonds.

$[Rh^{II}(oep)]_2$ reacts with the C-Br bond of benzyl bromide in benzene at room temperature to yield $Rh^{III}(oep)Bn$ and $Rh^{III}(oep)Br$ (eq 1.44).[93] $Rh^{II}(tmp)$ has also been reported to react with H_2 in benzene to give $Rh^{III}(tmp)H$ (eq 1.45),[96] with the C-H bond of methane in benzene to yield $Rh^{III}(tmp)H$ and $Rh^{III}(tmp)CH_3$ (eq 1.46),[97,98] and with the benzylic C-H bond of toluene in benzene to give $Rh^{III}(tmp)H$ and $Rh^{III}(tmp)Bn$ (eq 1.47).[97]

$$[Rh^{II}(oep)]_2 + Br\text{-}CH_2Ph \xrightarrow[\text{instantaneous}]{\text{toluene, 26 °C}} Rh^{III}(oep)Br + Rh^{III}(oep)CH_2Ph \quad (1.44)$$
$$ 50\% \qquad\qquad 50\%$$

$$2Rh^{II}(tmp) + H_2 \xrightarrow[\substack{0.2\text{ -1 atm}\;\; k = 2.5\text{ L}^2\text{ mol}^{-2}\text{ s}^{-1}}]{C_6H_6,\ 23\ °C} 2Rh^{III}(tmp)H \quad (1.45)$$

$$2Rh^{II}(tmp) + CH_4 \underset{K = 1.08}{\overset{C_6H_6,\ 23\ °C}{\rightleftharpoons}} Rh^{III}(tmp)H + Rh^{III}(tmp)CH_3 \quad (1.46)$$
$$1\text{ atm}$$

$$2Rh^{II}(tmp) + CH_3Ph \xrightarrow{C_6H_6,\ 70\ °C} Rh^{III}(tmp)H + Rh^{III}(tmp)CH_2Ph \quad (1.47)$$
$$\text{excess} 50\% \qquad\qquad 50\%$$
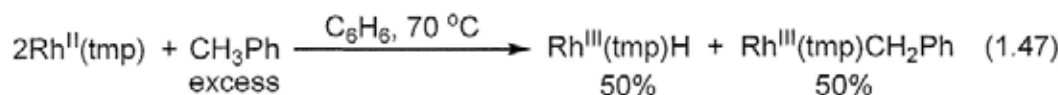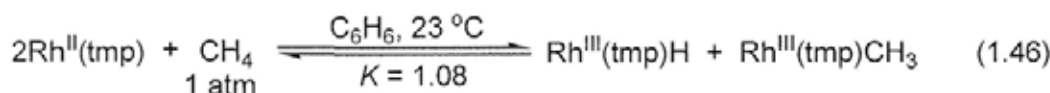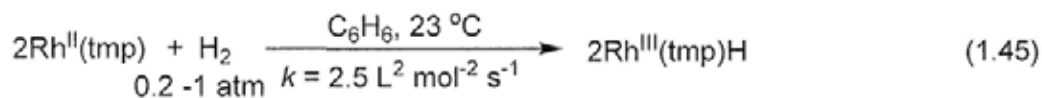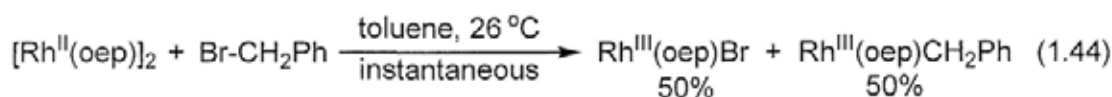
Mechanistic studies suggest that $[Rh^{II}(oep)]_2$ reacts with benzyl bromide via a radical chain mechanism (Scheme 1.20).[93] $[Rh^{II}(oep)]_2$ initially dissociates into 2 $Rh^{II}(oep)$ (pathway i). $Rh^{II}(oep)$ then abstracts Br atom from benzyl bromide, yielding $Rh^{III}(oep)Br$ and benzyl radical (pathway ii), which further reacts with $[Rh^{II}(oep)]_2$ to yield $Rh^{III}(oep)Bn$ and another $Rh^{II}(oep)$ for subsequent Br atom transfer (pathway iii).

Scheme 1.20 Radical Chain Mechanism in the Reaction of $[Rh^{II}(oep)]_2$ with PhCH$_2$Br

$$[Rh^{II}(oep)]_2 \underset{}{\overset{i}{\rightleftharpoons}} 2Rh^{II}(oep)$$

$$Rh^{II}(oep) + Br\text{-}CH_2Ph \xrightarrow{ii} Rh^{III}(oep)Br + PhCH_2\cdot$$

$$PhCH_2\cdot + [Rh^{II}(oep)]_2 \xrightarrow{iii} Rh^{III}(oep)CH_2Ph + Rh^{II}(oep)$$
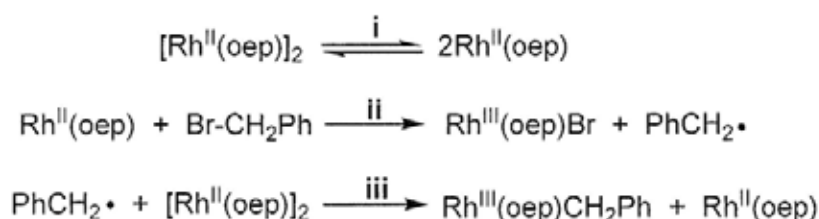
On the other hand, $Rh^{II}(tmp)$ reacts with H_2, the C-H bond of methane, and the benzylic C-H bond of toluene via a termolecular transition state with a rate law: rate = $k\,[Rh^{II}(tmp)]^2\,[H\text{-}X]$ (X = H, CH$_3$, CH$_2$Ph) (Scheme 1.21)[97,98] Indeed, the kinetic isotope effects of C-H bonds in CH$_4$ ($k_H/k_D = 8.2$)[98] and PhCH$_2$-H ($k_H/k_D = 6.5$)[97] support the linear transition states in C-H bond activations by 2 metalloporphyrin radicals.

Scheme 1.21 Bond Cleavages by $Rh^{II}(tmp)$ Involving a Linear Termolecular Transition State

$$2Rh^{II}(tmp) + H\text{-}X \rightleftharpoons \left[(tmp)Rh\text{-}\text{-}H\text{-}\text{-}X\text{-}\text{-}Rh(tmp)\right]^{\ddagger} \rightleftharpoons Rh^{III}(tmp)H + Rh^{III}(tmp)X$$
$$\begin{aligned}&X = H \\ & = CH_3 \quad \text{linear termolecular transition state} \\ & = CH_2Ph \qquad k(CH_4)\,/\,k(CD_4) = 8.2 \\ & k(H\text{-}CH_2Ph)\,/\,k(D\text{-}CD_2C_6D_5) = 6.5\end{aligned}$$
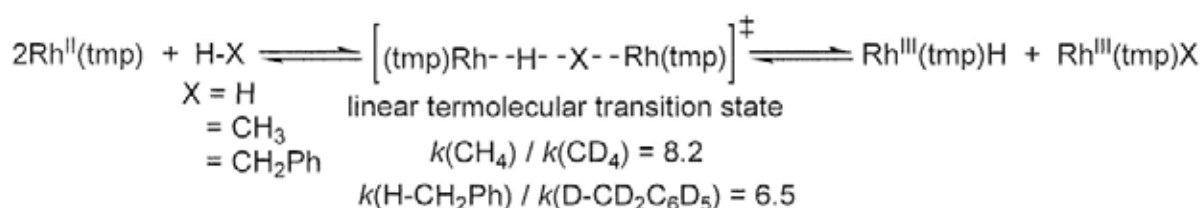
Similarly, $[Ir^{II}(oep)]_2$ reacts with H_2 in benzene to yield $Ir^{III}(oep)H$ (eq 1.48), and with the benzylic C-H bond of toluene to yield $Ir^{III}(oep)H$ and $Ir^{III}(oep)CH_2Ph$ (eq 1.49).[99] It is proposed that $[Ir^{II}(oep)]_2$ initially dissociates to 2 $Ir^{II}(oep)$,[99] which then reacts with H_2 and benzylic C-H bond via the analogous linear termolcular transition state (Scheme 1.21).

$$[Ir^{II}(oep)]_2 \ + \ H_2 \ \xrightarrow[\substack{200\ \text{Torr} \\ \text{instantaneous}}]{C_6D_6,\ 25\ °C} \ \underset{100\%}{2Ir^{III}(oep)H} \qquad (1.48)$$

$$[Ir^{II}(oep)]_2 \ + \ CH_3Ph \ \xrightarrow[\text{instantaneous}]{120\ °C} \ \underset{50\%}{Ir^{III}(oep)H} \ + \ \underset{50\%}{Ir^{III}(oep)CH_2Ph} \qquad (1.49)$$
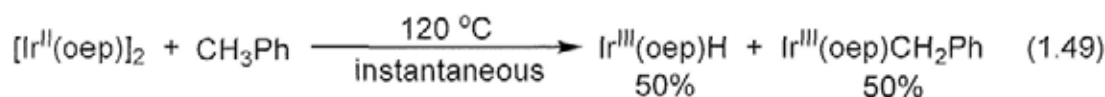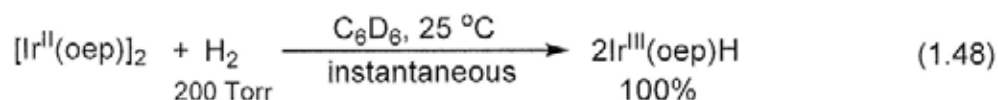
The bond activation reactions by rhodum(II) and iridium(II) porphyrins are driven thermodynamically by the formation of strong $Rh^{III}(por)$-C, $Rh^{III}(por)$-H, and $Ir^{III}(por)$-H bonds (reported bond energies: $Rh^{III}(oep)$-H: 61.8 kcal mol^{-1};[62] $Rh^{III}(tmp)$-H: 60 kcal mol^{-1};[62] $Rh^{III}(tmp)$-CH$_3$: 57.8 kcal mol^{-1};[62] $Ir^{III}(oep)$-H: ~70 kcal mol^{-1} [100]).

1.7.2.2 Reactions with Carbon Monoxide and Ethylene

$[Rh^{II}(oep)]_2$ reacts with CO to yield dirhodium-porphyrin ketone, and can further react with another CO to yield dirhodium-porphyrin diketone (eq 1.50). This is attributed to the formation of 2 strong Rh^{III}-C(O) bond (~55-59 kcal/mol).[101]

$$[Rh^{II}(oep)]_2 \ \underset{r.t.}{\overset{CO}{\rightleftharpoons}} \ Rh^{III}(oep)\overset{O}{\overset{\|}{C}}Rh^{III}(oep) \ \underset{r.t.}{\overset{CO}{\rightleftharpoons}} \ M^{III}(por)\overset{O}{\overset{\|}{C}}\overset{O}{\overset{\|}{C}}M^{III}(por) \qquad (1.50)$$
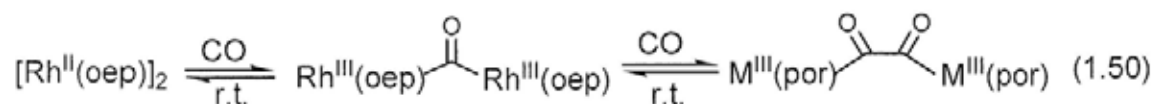
$Rh^{II}(por)$ and $Ir^{II}(por)$ also promote the reductive couplings with 1 or 2 molecules of ethylene, depending on the steric bulkiness of porphyrin ligands (eq 1.51 and 1.52).[101] The coupling reactions are driven by the formation of strong M-C bonds (> 50 kcal/mol).[101] Sterically unhindered $M^{II}(oep)$ (M = Rh, Ir) (oep = octaethylporphyrin) reacts with 1 ethylene to form mono-ethylene activated products (eq 1.51), whereas much more bulky $M^{II}(ttepp)$

(ttepp = tetrakis(2,4,6-triethylphenyl)porphyrin) reacts with 2 ethylene to form di-ethylene activated products (eq 1.52).

$$[M^{II}(oep)]_2 \underset{}{\overset{CH_2=CH_2}{\rightleftharpoons}} (oep)M^{III}\text{-}CH_2CH_2\text{-}M^{III}(oep) \quad (1.51)$$
$$M = Rh, Ir$$

$$2M^{II}(ttepp) \underset{}{\overset{2CH_2=CH_2}{\rightleftharpoons}} (ttepp)M^{III}\text{-}(CH_2)_4\text{-}M^{III}(ttepp) \quad (1.52)$$
$$M = Rh, Ir$$
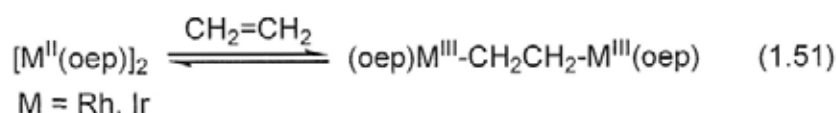
1.7.3 Chemistry of Group 9 Metal(I) Porphyrin Anion ($M^I(por)^-$) as Nucleophile

$M^I(por)^-$, generated by the reduction of $M^{II}(por)$ or $M^{III}(por)Cl$ (M = Co,[102] Rh,[103] Ir[104]), are powerful nucleophiles and undergo nucleophilic substitutions with alkyl halides to yield metalloporphyrin alkyls (eq 1.53-1.55).

$$Co^{II}(oep) \xrightarrow[\text{THF, r.t., overnight}]{Na/Hg} Co^{I}(oep)^- \xrightarrow[\text{r.t., 10 min}]{RI \text{ (excess)}} Co^{III}(oep)R \quad (1.53)$$
$$R = Me, 65\%$$
$$R = Et, 60\%$$

$$Rh^{III}(oep)Cl \xrightarrow[\text{EtOH, Ar, r.t. 3 h}]{NaBH_4 / NaOH} Rh^{I}(oep)^- \xrightarrow[\text{r.t., 10 min}]{RI \text{ (excess)}} Rh^{III}(oep)R \quad (1.54)$$
$$R = Me, 46\%$$
$$R = Et, 60\%$$

$$Ir^{III}(oep)(CO)Cl \xrightarrow[\text{EtOH, Ar, 50 °C, 1 h}]{NaBH_4 / NaOH} Ir^{I}(oep)^- \xrightarrow[\text{r.t., 5 h}]{RI \text{ (excess)}} Ir^{III}(oep)R \quad (1.55)$$
$$R = Me, 72\%$$
$$R = Et, 85\%$$
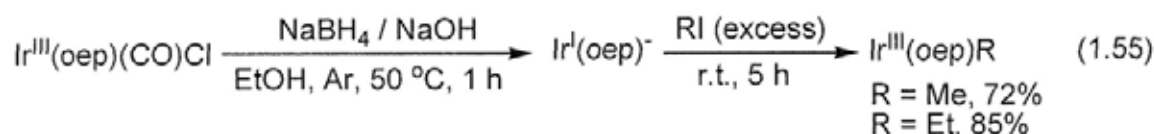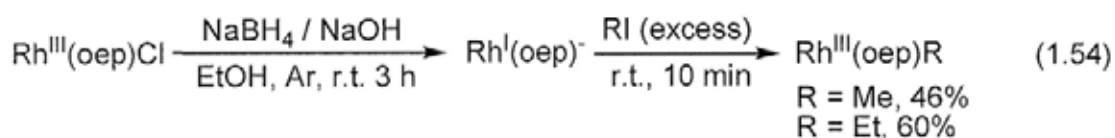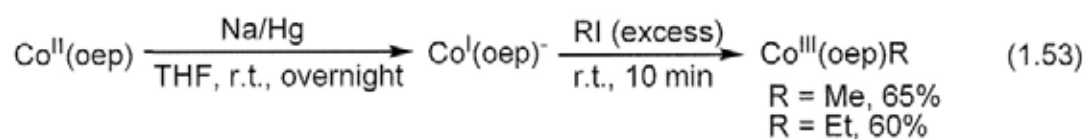
1.8 Bond Activation Chemistry by Group 9 Metal(III) Porphyrin Chlorides in Basic Media

The Chan group has undergone various base-promoted bond activation reactions by group 9 metal(III) porphyrin chlorides ($M^{III}(por)Cl$: $Rh^{III}(ttp)Cl$ and $Ir^{III}(ttp)(CO)Cl$). In basic reaction media, $M^{III}(por)Cl$ is converted to $M^{III}(por)OH$, $M^{III}(por)H$, $M^{II}(por)$, and $M^I(por)^-$ which exist in equilibria. These 4 metalloporphyrin species exhibit different reactivities towards the same

molecules. The relative reactivities of these 4 metalloporphyrins also vary with the nature of metals and the reaction conditions (e.g. polarity of solvents, reaction temperatures). Therefore, the metalloporphyrin intermediates responsible for the bond cleavages change with different reaction systems. Some of the reaction mechanisms of bond activation chemistry by $Rh^{III}(ttp)Cl$ and $Ir^{III}(ttp)(CO)Cl$ are briefly reviewed below.

1.8.1 C-O Bond Cleavage of Methanol: Chemistry of $M^I(por)^-$ Nucleophile

$Rh^{III}(ttp)Cl^{105}$ and $Ir^{III}(ttp)(CO)Cl^{106}$ undergo base-promoted C-O bond cleavages of methanol to yield $Rh^{III}(ttp)CH_3$ and $Ir^{III}(ttp)CH_3$ (eqs 1.56 and 1.57). Mechanistic studies suggest that bases and CH_3OH promote the reduction of $M^{III}(ttp)Cl$ to $M^I(ttp)^-$ (M = Rh, Ir) (pathways i and iv). $Ir^I(ttp)^-$ is a strong nucleophile to react directly with CH_3-OH via nucleophilic substitution (S_N2) to yield $Ir^{III}(ttp)CH_3$ (pathway v). On the other hand, $Rh^I(ttp)^-$ is not nucleophilic enough to react with CH_3-OH. Thus, $Rh^I(ttp)^-$ rapidly protonates with methanol via an equilibrium to produce $Rh^{III}(ttp)H$ (pathway ii), which further reacts with CH_3-OH via metathesis to form $Rh^{III}(ttp)CH_3$ (pathway iii).

$$Rh^{III}(ttp)Cl \xrightarrow[\text{i} \quad 150\,^\circ C,\ 1\ d,\ N_2]{CH_3OH,\ K_2CO_3\ (10\ \text{equiv})} Rh^I(ttp)^- \underset{\text{ii}}{\overset{CH_3O\text{-}H}{\rightleftharpoons}} Rh^{III}(ttp)H \xrightarrow[\text{iii}\ -H_2O]{CH_3\text{-}OH} Rh^{III}(ttp)CH_3 \quad (1.56)$$
$$87\%$$

$$Ir^{III}(ttp)(CO)Cl \xrightarrow[\text{iv}\quad 200\,^\circ C\ 1\ d,\ N_2]{CH_3OH,\ KOH\ (20\ \text{equiv})} Ir^I(ttp)^- \xrightarrow[\text{v}\ -OH^-]{CH_3\text{-}OH} Ir^{III}(ttp)CH_3 \quad (1.57)$$
$$70\%$$
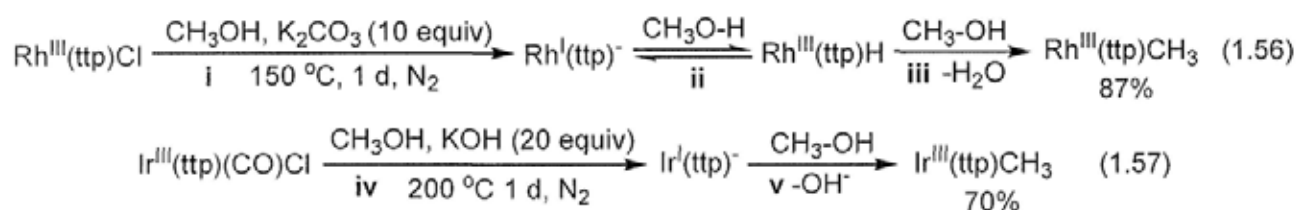
1.8.2 C-C Bond Activation of Cyclooctane: Chemistry of $M^{III}(por)OH$, $M^{III}(por)H$, and $M^{II}(por)$

$Rh^{III}(ttp)Cl$ undergoes base-promoted C-C bond activation of cyclooctane to form rhodium(III) porphyrin n-octyl (eq 1.58).^{107} Mechanistic studies suggest that $Rh^{III}(ttp)Cl$ reacts

with base to form $Rh^{III}(ttp)OH$ (Scheme 1.22, pathway i) which is further reduced to $[Rh^{II}(ttp)]_2$ (pathway ii).[108] $[Rh^{II}(ttp)]_2$ undergoes C-H activation (CHA) to give $Rh^{III}(ttp)H$ and $Rh^{III}(ttp)$-c-octyl (pathway iii), which then undergoes β-hydride elimination to produce $Rh^{III}(ttp)H$ (pathway v). $[Rh^{II}(ttp)]_2$ also undergoes C-C activation (CCA) to yield terminal C-centered radical, $Rh^{III}(ttp)$-$(CH_2)_7CH_2\bullet$, (pathway iv) which abstracts a H atom from $Rh^{III}(ttp)H$ to yield $Rh^{III}(ttp)$-n-octyl (pathway vi).

$$Rh^{III}(ttp)Cl \ + \ \bigcirc \xrightarrow[120\,°C,\ 7.5\ h,\ N_2]{K_2CO_3\ (10\ equiv)} Rh^{III}(ttp)(CH_2)_7CH_3 \quad (1.58)$$
$$33\%$$
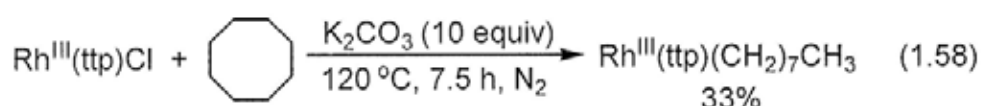
Scheme 1.22 Mechanism of C-H and C-C Activations of Cyclooctane by $Rh^{III}(ttp)Cl$
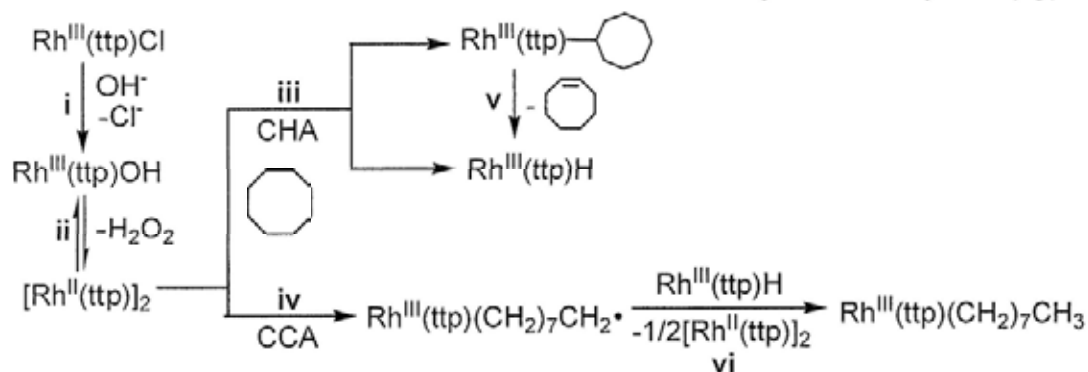
1.8.3 C-H Bond Activation of Alkanes: Chemistry of $M^{III}(por)OH$, $M^{III}(por)H$, and $M^{II}(por)$

$Rh^{III}(ttp)Cl$ undergoes base-promoted C-H bond activation of alkanes (RH) to form rhodium(III) porphyrin alkyls (eq 1.59).[109] Mechanistic studies suggest that $Rh^{III}(ttp)Cl$ is reduced by base to form $Rh^{III}(ttp)OH$ (Scheme 1.23, pathway i) which is further reduced to $[Rh^{II}(ttp)]_2$ (pathway ii).[108] $[Rh^{II}(ttp)]_2$ cleaves the R-H bonds to give $Rh^{III}(ttp)R$ and $Rh^{III}(ttp)H$ (pathway iii). $Rh^{II}(ttp)H$ can further react with R-H to give $Rh^{III}(ttp)R$ (pathway iv), and undergo dehydrogenative dimerization to regenerate $[Rh^{II}(ttp)]_2$ for further reactions (pathway v).

$$\text{Rh}^{III}(\text{ttp})\text{Cl} + \text{R-H} \xrightarrow[\text{120 °C, N}_2,\ 6\text{-}24\ \text{h}]{\text{K}_2\text{CO}_3\ (10\ \text{equiv})} \text{Rh}^{III}(\text{ttp})\text{R} \quad (1.59)$$

$$\text{29-76\%}$$

R = cyclopentyl, cyclohexyl,
n-pentyl, n-hexyl, n-heptyl

Scheme 1.23 Mechanism of C-H Activations of Alkanes by Rh^{III}(ttp)Cl

1.8.4 C-H Bond Activation of Toluenes: Chemistry of M^{III}(por)H and M^{II}(por)

Ir^{III}(ttp)(CO)Cl undergoes base-promoted benzylic C-H bond activation of toluenes to form iridium(III) porphyrin benzyls (eq 1.60).[100] Mechanistic studies suggest that Ir^{III}(ttp)(CO)Cl is reduced to Ir^{III}(ttp)H (Scheme 1.24, pathway i). It is proposed that base promotes the reduction of Ir^{III}(ttp)(CO)Cl by the benzylic C-H bond of toluene to produce Ir^{III}(ttp)H, since the detailed mechanism of the transformation was unclear. Ir^{III}(ttp)H can further undergo dehydrogenative dimerization to form [Ir^{II}(ttp)]$_2$ via an equilibrium (pathway ii). Both Ir^{III}(ttp)H and [Ir^{II}(ttp)]$_2$ undergo benzylic C-H bond activation of toluene to yield Ir^{III}(ttp)Bn (pathways iii and iv).

$$\text{Ir}^{III}(\text{ttp})(\text{CO})\text{Cl} + \text{CH}_3\text{C}_6\text{H}_4(p\text{-FG}) \xrightarrow[\text{0.1-3.5 h}]{\text{K}_2\text{CO}_3\ (20\ \text{equiv})} \text{Ir}^{III}(\text{ttp})\text{CH}_2\text{C}_6\text{H}_4(p\text{-FG}) \quad (1.60)$$

$$\text{FG = Me, H, F, NO}_2 \qquad\qquad\qquad 41\text{-}80\%$$

Scheme 1.24 Mechanism of Benzylic C-H Activations of Toluenes by Ir^{III}(ttp)Cl(CO)

1.9 Summary

The chemistry of group 9 metalloporphyrins in the form of $M^{III}(por)OH$, $M^{III}(por)H$, $M^{II}(por)$, and $M^{I}(por)^-$ discussed above demonstrates that, the oxidation states of metals, the nature of ligands attached to the metals, and the nature of the metals can lead to different product formations, reaction rates, and reaction mechanisms in the bond activation chemistry. Therefore, fundamental reactivity studies of group 9 metalloporphyrins are of importance to aid the understandings of the various interactions of small molecules with transition metal complexes. In a long-term goal, these fundamental studies can facilitate the developments of potential and suitable catalysts in efficient transformations of small molecules to various fine chemicals in both synthetic and industrial chemistry.

Moreover, bases can promote the efficiencies of bond activations using high-valent group 9 metalloporphyrins to form metalloporphyrin alkyls in terms of reaction rates and yields. The use of bases in base-promoted reactions not only reduce the reaction steps for tedious preparations of air- and moisture-sensitive metal species (e.g. $M^{I}(por)^-$, $M^{II}(por)$, Grigard reagents, alkyl lithium) for subsequent chemical transformations, but also reduce the costs in using the more expensive or more toxic reagents (e.g. sodium amalgam, $NaBH_4$).

Indeed, in basic media, metalloporphyrins in the form of $M^{III}(por)OH$, $M^{III}(por)H$, $M^{II}(por)$, and $M^{I}(por)^-$ can exist in equilibria. Each of these metalloporphyrin species can become major or dominant species in the basic reaction systems by controlling the concentrations of bases, solvent polarities, or reaction temperatures for desired selective chemical transformations. Therefore, the investigation of base-promoted reactions can help the discoveries and developments of more advanced and convenient methods for base-promoted catalytic synthesis of various fine chemicals and functionalized compound in more economical and environmentally-friendly ways.

1.10 Scope of Thesis

The objectives of my research focus on the reactivity studies of iridium(III) porphyrins, including:

(1) the redox chemistry of iridium(III) porphyrins in basic media, and

(2) the base-promoted aryl carbon-halogen bond (Ar-X, X = Cl, Br, I) cleavages by iridium(III) porphyrins.

References

(1)   DeWit, D. G. *Coord. Chem. Rev.* **1996**, *147*, 209-246.

(2)   (a) Yamada, S. *Coord. Chem. Rev.* **1966**, *1*, 415-437. (b) Yamada, S. *Coord. Chem. Rev.* **1967**, *2*, 77-81. (c) Costes, J.-P.; Dahan, F.; Donnadieu, B.; Fernandez-Garcia, M.-I.; Rodriguez-Douton, M.-J. *Dalton Trans.* **2003**, *19*, 3776-3779.

(3)   Alexander, V. *Chem. Rev.* **1995**, *95*, 273-342.

(4)   Misra, P.; Mishra, B. K.; Behera, G. B. *Int. J. Chem. Kinet.* **1991**, *23*, 639-654.

(5)   Keypour, H.; Rezaeivala, M.; Fall, Y.; Dehghani-Firouzabadi, A. A. *Solvent-Free Synthesis of Some N_4O_2, N_4S_2 and N_6 Schiff Base Ligands Assisted by Microwave Irradiation.* ARKIVOC, **2009**, X, 292-301.

(6)   Claessens, C. G.; Blau, W. J.; Cook, M.; Hanack, M.; Nolte, R. J. M.; Torres, T.; Wöhrle, D. *Monatsh. Chem.* **2001**, *132*, 3-11.

(7)   (a) Inabe, T.; Tajima, H. *Chem. Rev.* **2004**, *104*, 5503-5533. (b) de la Torre, G.; Vázquez, P.; Agulló-López, F.; Torres, T. *Chem. Rev.* **2004**, *104*, 3723-3750. (c) Beletskaya, I.; Tyurin, V. S.; Tsivadze, A. Y.; Guilard, R.; Stern, C. *Chem. Rev.* **2009**, *109*, 1659-1713.

(8)   (a) Wang, B.; Zuo, X.; Wu, Y.; Chen, Z.; Li, Z. *Mater. Lett.* **2005**, *59*, 3073-3077. (b) Ingrosso, C.; Curri, M. L.; Fini, P.; Giancane, G.; Agostiano, A.; Valli, L. *Langmuir* **2009**,

25, 10305-10313. (c) Chen, X.; Thomas, J.; Gangopadhyay, P.; Norwood, R. A.; Peyghambarian, N.; McGrath, D. V. *J. Am. Chem. Soc.* **2009**, *131*, 13840-13843.

(9) (a) Fleischer, E. B. *Acc. Chem. Res.* **1970**, *3*, 105-112. (b) Ogoshi, H.; Mizutani, T. *Acc. Chem. Res.* **1998**, *31*, 81-89. (c) Kadish, K. M.; Smith, K. M.; Guilard, R. *The Porphyrin Handbook Volume 3*, Eds.; Academic Press: Boston, 2000. (d) Smith, K. M. *Porphyrins and Metalloporphyrins*, Ed.; Elsevier Scientific Pub. Co.: New York, 1975.

(10) (a) Schrauzer, G. N. *Angew. Chem. Int. Ed. Engl.* **1976**, *15*, 417-426. (b) Schrauzer, G. N. *Acc. Chem. Res.* **1968**, *1*, 97-103.

(11) Xu, N.; Campbell, A. L. O.; Powell, D. R.; Khandogin, J.; Richter-Addo, G. B. *J. Am. Chem. Soc.* **2009**, *131*, 2460–2461.

(12) Kunieda, M.; Tamiaki, H. *J. Org. Chem.* **2008**, *73*, 7686-7694.

(13) (a) Nam, W. *Acc. Chem. Res.* **2007**, *40*, 522-531. (b) Xia, Q.-H.; Ge, H.-Q.; Ye, C.-P.; Liu, Z.-M.; Su, K.-X. *Chem. Rev.* **2005**, *105*, 1603-1662.

(14) Oliveri, C. G.; Ulmann, P. A.; Wiester, M. J.; Mirkin, C. A. *Acc. Chem. Res.* **2008**, *41*, 1618-1629.

(15) (a) Shinokubo, H.; Osuka, A. *Chem. Commun.* **2009**, 1011-1021. (b) Kadish, K. M.; Smith, K. M.; Guilard, R. *The Porphyrin Handbook Volume 1*, Eds.; Academic Press: Boston, 2000.

(16) (a) Simkhovich, L.; Goldberg, I.; Gross, Z. *Inorg. Chem.* **2002**, *41*, 5433-5439. (b) Steene, E.; Wondimagegn, T.; Ghosh, A. *J. Phys. Chem. B.* **2001**, *105*, 11406-11413. (c) Meier-Callahan, A. E.; Di Bilio, A. J.; Simkhovich, L.; Mohammed, A.; Goldberg, I.; Gray, H. B.; Gross, Z. *Inorg. Chem.* **2001**, *40*, 6788-6793. (d) Cai, S.; Licoccia, S.; Walker, F. A. *Inorg. Chem.* **2001**, *40*, 5795-5798. (e) Ramdhanie, B.; Zakharov, L. N.; Rheingold, A. R.; Goldberg, D. P. *Inorg. Chem.* **2002**, *41*, 4105-4107.

(17) (a) Paolesse, R.; Nardis, S.; Sagone, F.; Khoury, R. G. *J. Org. Chem.* **2001**, *66*, 550-556. (b) Gross, Z.; Galili, N.; Simkhovich, L.; Saltsman, I.; Botoshansky, M.; Bläser, D.;

Boese, R.; Goldberg, I. *Org. Lett.* **1999**, *1*, 599-602. (c) Mahammed, A.; Gray, H. B.; Meier-Callahan, A. E.; Gross, Z. *J. Am. Chem. Soc.* **2003**, *125*, 1162-1163.

(18) Joseph, C. A.; Ford, P. C. *J. Am. Chem. Soc.* **2005**, *127*, 6737-6743. (c) Collman, J. P.; Wang, H. J. H.; Decréau, R. A.; Eberspacher, T. A.; Sunderland, C. J. *Chem. Commun.* **2005**, 2497-2499.

(19) (a) Saltsman, I.; Mahammed, A.; Goldberg, I.; Tkachenko, E.; Botoshansky, M.; Gross, Z. *J. Am. Chem. Soc.* **2002**, *124*, 7411-7420. (b) Paolesse, R.; Nardis, S.; Venanzi, M.; Mastroianni, M.; Russo, M.; Fronczek, F. R.; Vicente, M. G. H. *Chem. Eur. J.* **2003**, *9*, 1192-1197. (c) Mahammed, A.; Gross, Z. *J. Am. Chem. Soc.* **2005**, *127*, 2883-2887.

(20) (a) Ding, T.; Alemán, E. A.; Modarelli, D. A.; Ziegler, C. J. *J. Phys. Chem. A* **2005**, *109*, 7411-7417. (b) Ventura, B.; Esposti, A. D.; Koszarna, B.; Gryko, D. T.; Flamigni, L. *New J. Chem.* **2005**, *29*, 1559-1566.

(21) Shen, J.; Shao, J.; Ou, Z.; E, W.; Koszarna, B.; Gryko, D. T.; Kadish, K. M. *Inorg. Chem.* **2006**, *45*, 2251-2265.

(22) Cummings, S. C.; Sievers, R. E. *J. Am. Chem. Soc.* **1970**, *92*, 215-217.

(23) Rovira, C.; Kunc, K.; Hutter, J.; Parrinello, M. *Inorg. Chem.* **2001**, *40*, 11-17.

(24) (a) Sessler, J. L. *Angew. Chem. Int. Ed.* **1994**, *33*, 1348-1350. (b) Murayami, Y.; Aoyama, Y.; Hayashida, M. *J. Chem. Soc., Chem. Commun.* **1980**, 501-502. (c) Grodkowski, J.; Neta, P. *J. Phys. Chem. A* **2000**, *104*, 1848-1853.

(25) (a) Furuta, H.; Asano, T.; Ogawa, T. *J. Am. Chem. Soc.* **1994**, *116*, 767-768. (b) Bohle, D. S.; Chen, W.-C.; Hung, C.-H. *Inorg. Chem.* **2002**, *41*, 3334-3336.

(26) Furuta, H.; Ishizuka, T.; Osuka, A.; Dejima, H.; Nakagawa, H.; Ishikawa, Y. *J. Am. Chem. Soc.* **2001**, *123*, 6207-6208.

(27) Furuta, H.; Ishizuka, T.; Osuka, A.; Ogawa, T. *J. Am. Chem. Soc.* **1999**, *121*, 2945-2946.

(28) (a) Jiang, H.-W. Hao, F.; Chen, Q.-Y. Xiao, J.-C.; Liu, S.-B.; Gu, Y.-C. *J. Org. Chem.* **2010**, *75*, 3511-3514. (b) Sripothongnak, S.; Ziegler, C. J. *Inorg. Chem.* **2010**, *49*,

5789–5791.

(29)   Toganoh, M.; Konagawa, J.; Furuta, H. *Inorg. Chem.* **2006**, *45*, 3852-3854.

(30)   Toganoh, M.; Ikeda, S.; Furuta, H. *Inorg. Chem.* **2007**, *46*, 10003-10015.

(31)   (a) Toganoh, M.; Ikeda, S.; Furuta, H. *Chem. Commun.* **2005**, 4589-4591. (b) Kühn, F. E.; Santos, A. M.; Herrmann, W. A. *Dalton Trans.* **2005**, 2483-2591. (c) Lawes, D. J.; Geftakis, S.; Ball, G. E. *J. Am. Chem. Soc.* **2005**, *127*, 4134-4135. (d) Niino, T.; Toganoh, M.; Andrioletti, B.; Furuta, H. *Chem. Commun.* **2006**, 4335-4337. (e) Toganoh, M.; Fujino, K.; Ikeda, S.; Furuta, H. *Tetrahedron Lett.* **2008**, *29*, 1488-1491.

(32)   Sessler, J. L.; Tomat, A. E. *Acc. Chem. Res.* **2007**, *40*, 371–379.

(33)   Sessler, J. L.; Miller, R. A. Texaphyrins. *Biochem. Pharmacol.* **2000**, *59*, 733–739.

(34)   Young, S. W.; Qing, F.; Harriman, A.; Sessler, J. L.; Dow, W. C.; Mody, T. D.; Hemmi, G.W.; Hao, Y. P.; Miller, R. A. *Proc. Natl. Acad. Sci.* **1996**, *93*, 6610–6615.

(35)   Rath, H.; Sankar, J.; PrabhuRaja, V.; Chandrashekar, T. K.; Nag, A.; Goswami, D. *J. Am. Chem. Soc.* **2005**, *127*, 11608–11609.

(36)   Reiter, W. A.; Gerges, A.; Lee, S.; Deffo, T.; Clifford, T.; Danby, A.; Bowman-James, K. *Coord. Chem. Rev.* **1998**, *174*, 343–359.

(37)   For reviews on late-transition-metal-alkoxo complexes, see: (a) Bryndza, H. E.; Tam, W. *Chem. Rev.* **1988**, *88*, 1163-1188. (b) Gilge, J. W.; Roesky, H. W. *Chem. Rev.* **1994**, *94*, 895-910. (c) Fulton, J. R.; Holland, A. W.; Fox, D. J.; Bergman, R. G. *Acc. Chem. Res.* **2002**, 35, 44-56.

(38)   Hartwig, J. F. *Organotransition Metal Chemistry: From Bonding to Catalysis*; Sausalito, CA: University Science Books, 2010.

(39)   For examples, see: (a) Dolphin, D., Ed. *B12*; Wiley: New York, 1982; Vols. 1 and 2. (b) Banerjee, R. *Chemistry and Biochemistry of B12*; Wiley-Interscience: New York, 1999. (c) Halpern, J. *Science* **1985**, *227*, 869-875. (d) Wollowitz, S.; Halpern, J. *J. Am. Chem. Soc.* **1988**, *110*, 3112-3120. (e) Toraya, T. *Chem. Rev.* **2003**, *103*, 2095-2127.

(40) Wong-Foy, A. G.; Bhalla, G.; Liu, X. Y.; Periana, R. A. *J. Am. Chem. Soc.* **2003**, *125*, 14292-14293.

(41) (a) Oxgaard, J.; Muller, R. P.; Goddard, W. A., III; Periana, R. A. *J. Am. Chem. Soc.* **2004**, *126*, 352-363. (b) Oxgaard, J.; Periana, R. A.; Goddard, W. A., III *J. Am. Chem. Soc.* **2004**, *126*, 11658-11665. (c) Bhalla, G.; Liu, X. Y.; Oxgaard, J.; Goddard, W. A., III; Periana, R. A. *J. Am. Chem. Soc.* **2005**, *127*, 11372-11389.

(42) (a) Meier, S. K.; Young, K. J. H.; Ess, D. H.; Tenn, W. J., III; Oxgaard, J.; Goddard, W. A., III; Periana, R. A. *Organometallics* **2009**, *28*, 5293–5304. (b) Young, K. J. H.; Yousufuddin, M.; Ess, D. H.; Periana, R. A. *Organometallics* **2009**, *28*, 3395-3406. (c) Bischof, S. M.; Ess, D. H.; Meier, S. K.; Oxgaard, J.; Nielsen, R. J.; Bhalla, G.; Goddard, W. A., III; Periana, R. A. *Organometallics* **2010**, 29, 742–756.

(43) For example, see: Muci, A. R.; Buchwald, S. L. *Top. Curr. Chem.* **2002**, *219*, 131-209.

(44) Anderson, K. W.; Ikawa, T.; Tundel, R. E.; Buchwald, S. L. *J. Am. Chem. Soc.* **2006**, *128*, 10694-10695.

(45) (a) Widenhoefer, R. A.; Zhong, H. A.; Buchwald, S. L. *J. Am. Chem. Soc.* **1997**, *119*, 6787-6795. (b) Widenhoefer, R. A.; Buchwald, S. L. *J. Am. Chem. Soc.* **1998**, *120*, 6504-6511. (c) Mann, G.; Shelby, Q.; Roy, A. H.; Hartwig, J. F. *Organometallics* **2003**, *22*, 2775-2789.

(46) Ziegler, T.; Tschinke, V.; Versluis, L. *Polyhedron* **1988**, *7*, 1625-2637.

(47) Schock, L. E.; Marks, T. J. *J. Am. Chem. Soc.* **1988**, *110*, 7701-7715.

(48) Luo, L.; Lanza, G.; Fragala, I. L. Stern, C. L.; Marks, T. J. *J. Am. Chem. Soc.* **1998**, *120*, 3111-3122.

(49) Drago, R. S.; Wong, N. M.; Ferris, D. C. *J. Am. Chem. Soc.* **1992**, *114*, 91-98.

(50) Wayland, B. B. *Polyhedron* **1988**, *7*, 1545–1558.

(51) Fu, X.; Wayland, B. B. *J. Am. Chem. Soc.* **2004**, *126*, 2623-2631.

(52) Fu, X.; Li, S. Wayland, B. B. *Inorg. Chem.* **2006**, *45*, 9884-9889.

(53) Macgregor, S. A.; Neave, G. W.; Smith, C.; *Faraday Discuss.* **2003**, *124*, 111–127.

(54) Nugent, W. A.; Overnall, D. W.; Holmes, S. J. *Organometallics* **1983**, *2*, 161-162.

(55) (a) Wu, Z.; Jordan, R. F.; Peterson, J. L. *J. Am. Chem. Soc.* **1995**, *117*, 5867. (b) Carpentier, J.-F.; Wu, Z.; Lee, C. W.; Stroemberg, S.; Christopher, J. N.; Jordan, R. F. *J. Am. Chem. Soc.* **2000**, *122*, 7750-7767. (c) Stoebenau, E. J.; III; Jordan, R. F. *J. Am. Chem. Soc.* **2006**, *128*, 8162-8163.

(56) Glueck, D. S. *Dalton Trans.* **2008**, 5276-5286.

(57) (a) Pearson, R. G. *J. Am. Chem. Soc.* **1963**, *85*, 3533. (b) Pearson, R. G. *J. Chem. Educ.* **1968**, *45*, 581. (c) 270 Pearson, R. G. *J. Chem. Educ.* **1968**, *45*, 643. (c) Pearson, R. G. *Chemical Hardness: Applications from Molecules to Solids*; Wiley-VCH: New York, 1997.

(58) Caulton, K. G. *New. J. Chem.* **1994**, *18*, 25-41.

(59) Holland, P. L.; Andersen, R. A.; Bergman, R. G. *Comments Inorg. Chem.* **1999**, *21*, 115-129.

(60) Hartwig, J. F.; Andersen, R. A.; Bergman, R. G. *Organometallics* **1991**, *10*, 1875-1887.

(61) Bryndza, H. E.; Fong, L. K.; Paciello, R. A.; Tam, W.; Bercaw, J. E. *J. Am. Chem. Soc.* **1987**, *109*, 1444-1456.

(62) Luo, Y.-R. *Comprehensive Handbook of Chemical Bond Energies*; CRC Press: Boca Raton, FL, 2007.

(63) Woerpel, K. A.; Bergman, R. G. *J. Am. Chem. Soc.* **1993**, *115*, 7888-7889.

(64) (a) Kloek, S. M.; Heinekey, D. M.; Goldberg, K. I. *Angew. Chem. Int. Ed.* **2007**, *46*, 4736-4738. (b) Hanson, S. K.; Heinekey, D. M.; Goldberg, K. I. *Organometallics* **2008**, *27*, 1454-1463.

(65) (a) Morales-Morales, D.; Lee, D. W.; Wang, Z.; Jensen, C. M. *Organometallics* **2001**, *20*, 1144-1147. (b) Dorta, R.; Rozenberg, H.; Shimon, L. J. W.; Milstein, D. *J. Am. Chem. Soc.* **2002**, *124*, 188-189.

(66) Chock, P. B.; Dewar, R. B. K.; Halpern, J.; Wong, L.-Y. *J. Am. Chem. Soc.* **1969**, *91*, 82-84.

(67) Nielsen, L., P. C.; Stevenson, C. P.; Blackmond, D. G.; Jacobsen, E. N. *J. Am. Chem. Soc.* **2004**, *126*, 1360-1362.

(68) Tenn, W. J.; III; Young, K. J. H.; Oxgaard, J.; Nielsen, R. J.; William A. Goddard, W. A., III; Periana, R. A. *Organometallics* **2006**, *25*, 5173-5175.

(69) Oxgaard, J.; Tenn, W. J., III; Nielsen, R. J.; Periana, R. A.; Goddard, W. A., III *Organometallics* **2007**, *26*, 1565-1567.

(70) (a) Ess, D. H.; Bischof, S. M.; Oxgaard, J.; Periana, R. A.; Goddard, W. A., III *Organometallics* **2008**, *27*, 6440-6445. (b) Ess, D. H.; Nielsen, R. J.; Goddard, W. A. III; Periana, R. A. *J. Am. Chem. Soc.* **2009**, *131*, 11686–11688.

(71) Cervilla, A. C.; Pérez-Plá, F.; Llopis, E.; Piles, M. *Dalton Trans.* **2004**, 1461-1465.

(72) Nord, G.; Wernberg, O. *J. C. S. Dalton Trans.* **1975**, 845-849.

(73) Creutz, C.; Sutin, N.; *Proc. Nat. Acad. Sci.* **1975**, *72*, 2858-2862.

(74) Murakami, Y.; Aoyama, Y. *Bull. Chem. Soc. Jpn.* **1976**, *49*, 683-688.

(75) Murakami, Y.; Aoyama, Y.; Hayashida, M. *J. Chem. Soc. Chem. Commun.* **1980**, 501-502.

(76) Roberts, J. L., Jr.; Sugimoto, H.; Barrette, W. C., Jr.; Sawyer, D. T. *J. Am. Chem. Soc.* **1985**, *107*, 4556-4557.

(77) Tahmassebi, S. K.; Conry, R. R.; Mayer, J. M. *J. Am. Chem. Soc.* **1993**, *115*, 7553-7554.

(78) Cheng, R.-J.; Latos-Grazynski, L.; Balch, A. L. *Inorg. Chem.* **1982**, *21*, 2412-2418.

(79) Bhagan, S.; Sarkar, S.; Wayland, W. W. *Inorg Chem.* **2010**, *49*, 6734-6739.

(80) Ozeorv, O. V. *Chem. Soc. Rev.* **2009**, *38*, 83-88.

(81) Li, S.; Cui, W.; Wayland, B. B. *Chem. Commun.* **2007**, 4024-4025.

(82) (a) Arasasingham, R. D.; Bruice, T. C. *Inorg. Chem.* **1990**, *29*, 1422-1427. (b) Jeon, S.; Lee, H. K.; Choi. Y. K. *Bull. Korean. Chem. Soc.* **1996**, *17*, 929-934. (c) For

conventional use, the E_{ox} value reported in the literatures were indeed the E_{red} values of the reduction half-equations. For example, for the reduction half-equation: A + e⁻ → A⁻ with a E_{red} value, the E_{red} value is directly adopted as the E_{ox} value in the oxidation half-equation: A⁻ → A + e⁻, without changing the opposite sign (i.e. $E_{ox} = -E_{red}$).

(83)   (a) Sawyer, D. T.; Roberts, J. L. *Acc. Chem. Res.* **1988**, *21,* 469-476. (b) Tsang, P. K. S.: Cofre, P.; Sawyer, D. T. *Inorg. Chem.* **1987**, 26, 3604-3609.

(84)   Srivatsa, G. S.; Sawyer, D. T. *Inorg. Chem.* **1985**, *24,* 1732-1734.

(85)   Shin, K.; Kramer, S. K.; Goff, H. M. *Inorg. Chem.* **1987**, *26,* 4103-4106.

(86)   Ledon, H. J.; Bonnet, M. C.; Yves Brigandat, B.; Varescon, F. *Inorg. Chem.* **1980**, *19,* 3488-3491.

(87)   (a) Zhang, J.; Shan Li, S.; Fu, X.; Wayland, B. B. *Dalton Trans.* **2009**, 3661-3663. (b) Zhang, J.; Wayland, B. B.; Yun, L.; Li, S.; Fu, X. *Dalton Trans.* **2010**, *39,* 477–483.

(88)   Chan, K. S.; Lau, C. M.; Yeung, S. K.; Lai, T. Z. *Organometallics* **2007**, *26,* 1981-1985.

(89)   Aoyama, Y.; Yoshida, T.; Sakurai, K.; Ogoshi, H. *Organometallics* **1986**, *5,* 168-173.

(90)   (a) Zhou, X.; Tse, M. K.; Wu, D.; Mak, T. C. W.; Chan, K. S. *J. Organomet. Chem.* **2000**, *598,* 80-86. (b) Zhou, X.; Li, Q.; Mak, T. C. W.; Chan, K. S. *Inorg. Chem. Acta.* **1998**, *270,* 551-554.

(91)   For examples, see: Cui, C,; Wayland, B. B. *J. Por. Phthal.* **2004**, *8,* 103-110.

(92)   (a) Gridnev, A. A.; Ittel, S. D.; Fryd, M.; Wayland, B. B. *Organometallics* **1993**, *12,* 4871-4880. (b) Woska, D. C.; Xie, Z. D.; Gridnev, A. A.; Ittel, S. D.; Fryd, M.; Wayland, B. B. *J. Am. Chem. Soc.* **1996**, *118,* 9102-9109.

(93)   Paonessa, R. S; Thomas, N. C.; Halpern J. *J. Am. Chem. Soc.* **1985**, *107,* 4333-4335.

(94)   Mak, K. W.; Chan, K. S. *J. Am. Chem. Soc.* **1998**, *120,* 9686-9687.

(95)   Farnos, M. D.; Woods, B. A.; Wayland, B. B. *J. Am. Chem. Soc.* **1986**, *108,* 3659-3663.

(96)   Wayland, B. B; Ba, S.; Sherry, A. E. *Inorg. Chem.* **1992**, *31,* 148-150.

(97)   Wayland, B. B.; Ba, S.; Sherry, A. E. *J. Am. Chem. Soc.* **1991**, *113,* 5305-5311.

(98)   Sherry, A. E.; Wayland, B. B. *J. Am. Chem. Soc.* **1990**, *112,* 1259-1261.

(99)   Del Rossi, K. J.; Wayland, B. B. *J. Chem. Soc. Chem. Commun.* **1986**, 1963-1965.

(100)   Wayland, B. B. University of Pennsylvania, Philadelphia, PA. Personal communication, 2007.

(101)   Cui, W.; Li, S.; Wayland, B. B. *J. Organomet. Chem.* **2007**, *629*, 3198–3206.

(102)   Ogoshi, H.; Watanabe, E.; Koketsu, N.; Yoshisa, Z. *Bull. Chem. Soc. Jpn.* **1976**, *49*, 2529-2536.

(103)   (a) Ogoshi, H.; Setsune, J.; Omura, T.; Yoshida, Z. *J. Am. Chem. Soc.* **1975**, *97*, 6461-6466. (b) Ogoshi, H.; Setsune, J.; Yoshida, Z. *J. Am. Chem. Soc.* **1977**, *99*, 3869-3870.

(104)   Ogoshi, H.; Setsune, J.-I.; Yoshida, Z.-I. *J. Organomet. Chem.* **1978**, *159*, 317–328.

(105)   Fung, H. S.; Chan, Y. W.; Cheung, C. W.; Choi, K. S.; Lee, S. Y.; Qing, Y. Y.; Chan, K. S. *Organometallics* **2009**, *28*, 3981–3989.

(106)   Cheung, C. W.; Fung, H. S.; Lee, S. Y.; Qian, Y. Y.; Chan, Y. W.; Chan, K. S. *Organometallics* **2010**, *29*, 1343–1354.

(107)   Chan, Y. W.; Chan, K. S. *J. Am. Chem. Soc.* **2010**, *132*, 6920-6922.

(108) $Rh^{III}(ttp)OH$ has been recently shown to undergo reduction via dehydroxylative dimerization to form $[Rh^{II}(ttp)]_2$. See Chapter 2, section 2.1 for detailed description: Choi, K. S. Unpublished Results, 2009.

(109)   Chan, Y. W.; Chan, K. S. *Organometallics* **2008**, *27*, 4625-4635.

(110)   Cheung, C. W.; Chan, K. S. *Organometallics* **2008**, *27*, 3043–3055.

Chapter 2   Redox Chemistry of Iridium(III) Porphyrins in Basic Media

2.1 Introduction

2.1.1 Redox Chemistry of Group 9 Metalloporphyrins

In Chapter 1, the redox chemistry of transition metal complexes has been briefly presented. Hydroxide ion (OH$^-$) can act as an efficient single-electron reducing agent to reduce the metal centers of various transition metal complexes (Sections 1.4 and 1.5). Additionally, group 9 metalloporphyrins in different oxidation states, $M^{III}(por)OH$, $M^{III}(por)H$, $M^{II}(por)$, and $M^{I}(por)^-$, can exist in equilibria in basic media (Section 1.6).[1,2]

The electrochemical redox chemistry of group 9 metalloporphyrins has been extensively studied by the Kadish group.[3] The chemically-induced redox chemistry of water-soluble group 9 metalloporphyrins in protic solvents has also been studied. For example, the Wayland group reported the redox chemistry of water-soluble $[Ir^{III}(tspp)(H_2O)_2]^{3-}$ (tspp = tetrakis(p-sulfonatophenyl)porphyrin) in basic aqueous media, and methoxide ion is adopted as a reducing agent to reduce $[Ir^{III}(tspp)(H_2O)_2]^{3-}$ to generate $[Ir^{III}(tspp)H(H_2O)]^{4-}$, which is in an equilibrium with $[Ir^{I}(tspp)(H_2O)]^{5-}$ (Section 1.6.2).[2] However, the chemically-induced redox chemistry of group 9 metalloporphyrins in aprotic solvents, to the best of our knowledge, has not been reported.

Recently, the Chan group has discovered the OH$^-$-promoted reduction of rhodium(III) porphyrin chloride ($Rh^{III}(ttp)Cl$, ttp = tetrakis(p-tolyl)porphyrin) to rhodium(II) porphyrin dimer ($[Rh^{II}(ttp)]_2$) in benzene at 120 °C (eq 2.1).[4] Mechanistic studies suggest that $Rh^{III}(ttp)Cl$ undergoes ligand substitution with OH$^-$ to form $Rh^{III}(ttp)OH$ (Scheme 2.1, pathway i), which then undergoes the reduction via the homolysis of Rh-OH bond to form $Rh^{II}(ttp)$ and H_2O_2 (pathway ii). $Rh^{II}(ttp)$ further dimerizes to form $[Rh^{II}(ttp)]_2$ (pathway iii). $Rh^{III}(ttp)OH$ has also been independently prepared by the reaction of $[Rh^{II}(ttp)]_2$ with H_2O_2 (1 equiv) at room temperature to support the proposed conversion of $Rh^{III}(ttp)OH$ to $[Rh^{II}(ttp)]_2$ at 60 °C (eq 2.2).

$$\text{Rh}^{\text{III}}(\text{ttp})\text{Cl} \xrightarrow[\text{C}_6\text{D}_6,\ 120\ ^\circ\text{C},\ 30\ \text{min}]{\text{KOH (10 equiv)}} \underset{66\%}{[\text{Rh}^{\text{II}}(\text{ttp})]_2} \quad (2.1)$$
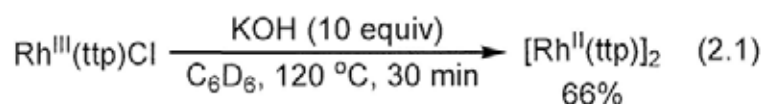
Scheme 2.1 Mechanism of OH⁻-Promoted Reduction of $\text{Rh}^{\text{III}}(\text{ttp})\text{Cl}$ to $[\text{Rh}^{\text{II}}(\text{ttp})]_2$

$$\text{Rh}^{\text{III}}(\text{ttp})\text{Cl} \xrightarrow[120\ ^\circ\text{C}]{\text{i OH}^-,\ \text{-Cl}^-} \text{Rh}^{\text{III}}(\text{ttp})\text{OH} \xrightarrow[120\ ^\circ\text{C}]{\text{ii} \ -1/2\text{H}_2\text{O}_2} \text{Rh}^{\text{II}}(\text{ttp}) \xrightarrow{\text{iii}} 1/2[\text{Rh}^{\text{II}}(\text{ttp})]_2$$

$$[\text{Rh}^{\text{II}}(\text{ttp})]_2 + \underset{1\ \text{equiv}}{\text{H}_2\text{O}_2} \underset{60\ ^\circ\text{C}}{\overset{\text{r.t.}}{\rightleftharpoons}} \underset{\sim56\%}{\text{Rh}^{\text{III}}(\text{ttp})\text{OH}} \quad (2.2)$$
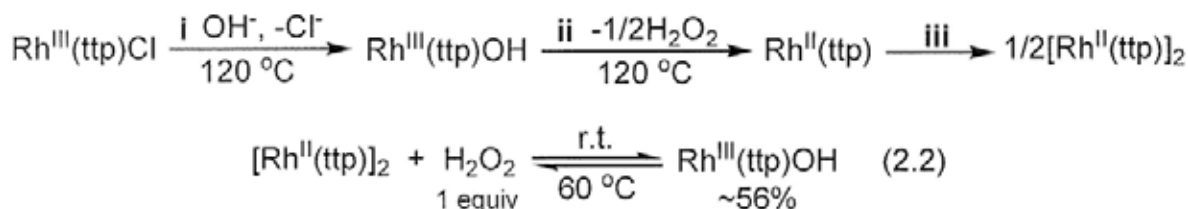
Rhodium(II) porphyrins are essential starting materials for various chemical transformations (Sections 1.7.2 and 1.8). The reduction of $\text{Rh}^{\text{III}}(\text{ttp})\text{Cl}$ by base to form $[\text{Rh}^{\text{II}}(\text{ttp})]_2$ provides a more convenient and cheaper way to produce $[\text{Rh}^{\text{II}}(\text{ttp})]_2$, compared with the traditional synthetic methods via the prolonged photolysis of $\text{Rh}^{\text{III}}(\text{por})\text{-Me}$[5] and the TEMPO-promoted dehydrogenative dimerization of $\text{Rh}^{\text{III}}(\text{por})\text{-H}$.[6]

The Chan group also reported that bases can promote the reduction of iridium(III) porphyrin carbonyl chloride ($\text{Ir}^{\text{III}}(\text{ttp})(\text{CO})\text{Cl}$) to iridium(III) porphyrin hydride ($\text{Ir}^{\text{III}}(\text{ttp})\text{H}$) and iridium(II) porphyrin dimer ($[\text{Ir}^{\text{II}}(\text{ttp})]_2$), which were the observed intermediates for the benzylic C-H bond activation of toluenes to yield iridium(III) porphyrin benzyls (Section 1.8.4).[7] However, the mechanisms of the reduction processes are unclear. Therefore, it is important to investigate the mechanisms of base-promoted reduction of $\text{Ir}^{\text{III}}(\text{ttp})(\text{CO})\text{Cl}$ to $\text{Ir}^{\text{III}}(\text{ttp})\text{H}$ and the redox chemistry of iridium porphyrins in basic aprotic solvent. Hopefully, as a result, the understanding and controlling of the reactivities of iridium complexes in different oxidation states in the chemical reactions can be achieved.[2]

2.1.2 Themes of the Chapter

The themes of this chapter report the results of the discoveries of redox chemistry of iridium porphyrins in basic, aprotic benzene solvent, involving:

(i) the base-promoted reduction of iridium(III) porphyrin halides to produce iridium(III) porphyrin hydride.

(ii) the interconversions among iridium(III) porphyrin hydride, iridium(II) porphyrin dimer, and iridium(I) porphyrin anion.

2.2 Preparations of Iridium Porphyrins

Iridium(III) porphyrin carbonyl chloride, $Ir^{III}(ttp)(CO)Cl$ (**1a**) (ttp = tetrakis(*p*-tolyl)porphyrin), is the starting complex used for various reactivity studies in this thesis. Porphyrin ligand (H_2ttp),[8] the iridium source, iridium(I)(1,5-cyclooctadiene) chloride dimer ($[Ir^I(COD)Cl]_2$),[9] and various iridium porphyrin complexes were prepared according to the literature methods.

$H_2(ttp)$[8] was prepared in 20% yield by refluxing *p*-tolylaldehyde and pyrrole in propionic acid solvent under reflux in 30 minutes (eq 2.3).

$$4 \text{—C}_6\text{H}_4\text{—CHO} + 4 \text{ pyrrole} \xrightarrow[\text{150 °C, reflux, 30 min}]{\text{propionic acid}} H_2(ttp), 20\% \quad (2.3)$$
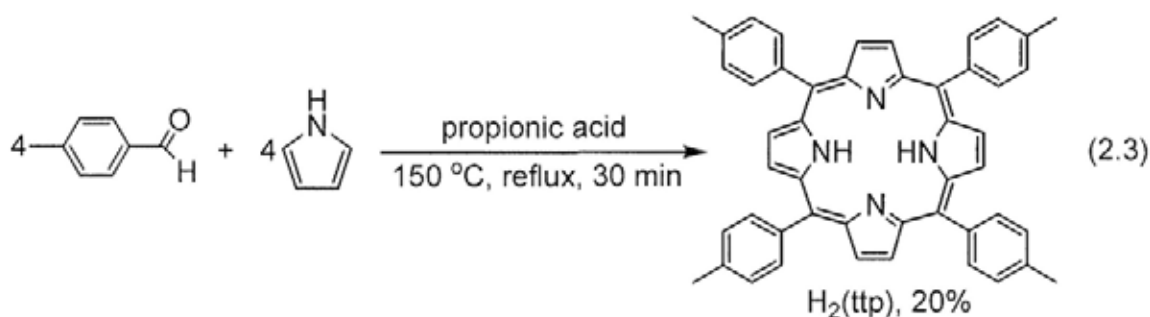
$[Ir^I(COD)Cl]_2$[9] was prepared in 62% yield by reacting iridium(III) trichloride with 1,5-cyclooctadiene in ethanol / water solvent in 1 day (eq 2.4).

$$2 Ir^{III}Cl_3 \cdot 3H_2O + 2COD + 2EtOH \xrightarrow[\text{reflux, 1 d, N}_2]{\text{EtOH / H}_2\text{O}} [Ir^I(COD)Cl]_2 + 4HCl + 2CH_3CHO \quad (2.4)$$
$$62\%$$

56
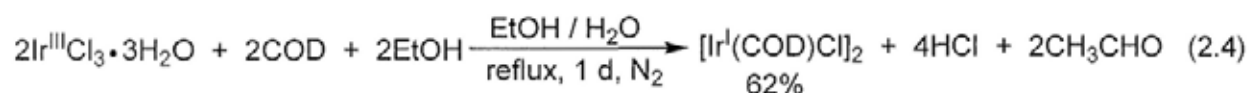
$[Ir^I(COD)Cl]_2$ was subsequently reacted with $H_2(ttp)$ in *p*-xylene under reflux in 4 days to yield $Ir^{III}(ttp)(CO)Cl$ (**1a**)[10] in 64% yield (eq 2.5).

$$2H_2(ttp) + [Ir^I(COD)Cl]_2 \xrightarrow[\text{reflux, 4 d}]{p\text{-xylene}} 2$$
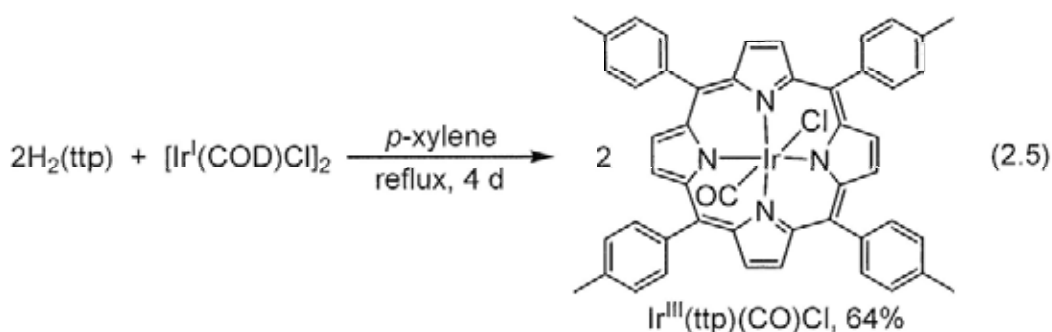
$Ir^{III}(ttp)(CO)Cl$, 64%   (2.5)

$Ir^{III}(ttp)(PPh_3)Cl$ (**1b**) was prepared via the ligand substitution of $Ir^{III}(ttp)(CO)Cl$ with PPh_3 (eq 2.6).

$$Ir^{III}(ttp)(CO)Cl + \underset{\text{(5 equiv)}}{PPh_3} \xrightarrow[200\ ^\circ\text{C, 1 d}]{C_6D_6} \underset{65\%}{Ir^{III}(ttp)(PPh_3)Cl} \quad (2.6)$$
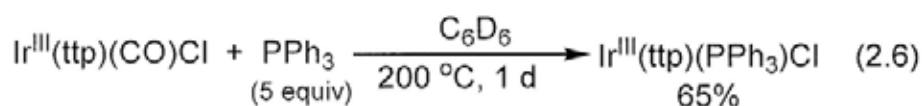
Other iridium(III) porphyrin halides, $Ir^{III}(ttp)(CO)Br$ (**1c**) and $Ir^{III}(ttp)(CO)I$ (**1d**), were discovered to be successfully prepared by reacting $Ir^{III}(ttp)(CO)Cl$ with bromobenzene and iodobenzene in solvent-free conditions at 200 $^\circ$C (eqs 2.7 and 2.8) (See details in Chapter 3).

$$Ir^{III}(ttp)(CO)Cl + \underset{xs}{PhBr} \xrightarrow[\text{2 d, N}_2]{200\ ^\circ\text{C}} \underset{62\%}{Ir^{III}(ttp)(CO)Br} \quad (2.7)$$

$$Ir^{III}(ttp)(CO)Cl + \underset{xs}{PhI} \xrightarrow[\text{2 d, N}_2]{200\ ^\circ\text{C}} \underset{41\%}{Ir^{III}(ttp)(CO)I} \quad (2.8)$$
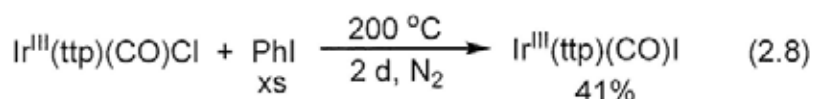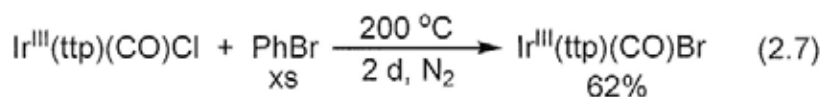
Other iridium(III) porphyrin derivatives, including the electrophilic iridium(III) porphyrin hexafluoroantimonate $(Ir^{III}(ttp)SbF_6)$,[11] iridium(III) porphyrin hydride $(Ir^{III}(ttp)H)$,[7,10a] iridium(II) porphyrin dimer $([Ir^{II}(ttp)]_2)$,[5,6] and iridium(I) porphyrin anion $(Ir^I(ttp)^-)$,[12] are used as the reactants for chemical transformations (Chapter 1, section 1.7), or as the probable intermediates to demonstrate various base-promoted reactions with $Ir^{III}(ttp)(CO)Cl$ (Chapter 1, section 1.8).[7,12] They were prepared by the following methods.

$Ir^{III}(ttp)(CO)Cl$ was reacted with silver hexafluoroantimonate $(AgSbF_6)$ in dichloromethane solvent at room temperature to yield the electrophilic $Ir^{III}(ttp)SbF_6$ (**1e**)[11] (as an inseparable mixture of $Ir^{III}(ttp)SbF_6$ and $[Ir^{III}(ttp)(CO)]SbF_6$ in 2.6-3.4 : 1 ratio)[13] with the weakly

57

coordinating SbF_6^- ligand (eq 2.9).

$$Ir^{III}(ttp)(CO)Cl + \underset{2 \text{ equiv}}{AgSbF_6} \xrightarrow[\text{r.t., 2 h}]{CH_2Cl_2} \underset{\substack{\sim 2.6 - 3.4 \ : \ 1 \\ \text{total yield: 90\%}}}{Ir^{III}(ttp)SbF_6 / [Ir^{III}(ttp)(CO)]SbF_6} + AgCl \quad (2.9)$$
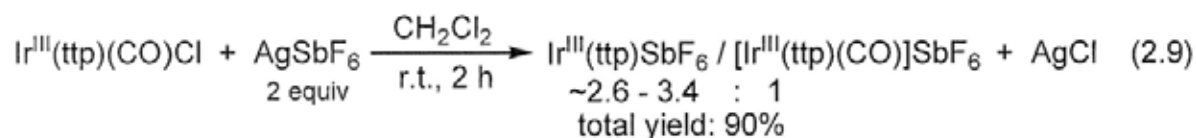
$Ir^{III}(ttp)H$ (**2a**) was prepared by the reductive protonation of $Ir^{III}(ttp)(CO)Cl$.[7,10a] $Ir^{III}(ttp)(CO)Cl$ was initially reacted with $NaBH_4$ / NaOH to yield $Ir^{I}(ttp)^-Na^+$, and was then protonated subsequently with excess HCl (aq) to afford $Ir^{III}(ttp)H$ (eq 2.10).

$$Ir^{III}(ttp)(CO)Cl \xrightarrow[\text{(ii) HCl (aq), r.t., } N_2, \text{ 15 min}]{\text{(i) } NaBH_4 \text{ / 1 M NaOH, THF, 60 °C, } N_2, \text{ 2 h}} \underset{90\%}{Ir^{III}(ttp)H} \quad (2.10)$$
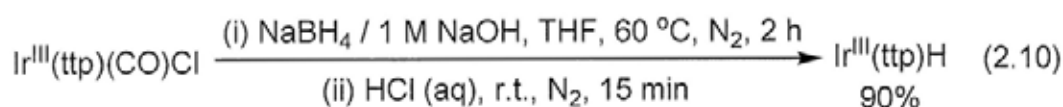
$[Ir^{II}(ttp)]_2$ (**3**)[6,7] was prepared quantitatively by the dehydrogenative dimerization of $Ir^{III}(ttp)H$ with 2,2,6,6-tetramethylpiperidinoxy (TEMPO) (eq 2.11).

$$Ir^{III}(ttp)H \xrightarrow[\text{C}_6\text{D}_6, \text{ r.t., } N_2, <5 \text{ min}]{\text{TEMPO (1.1 equiv)}} \underset{\text{quantitative}}{[Ir^{II}(ttp)]_2} \quad (2.11)$$
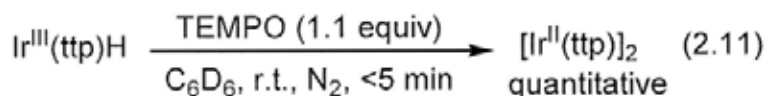
$Ir^{I}(ttp)^-K^+$ (**4a**)[12] was formed quantitatively by the deprotonation of $Ir^{III}(ttp)H$ with KOH in THF-d_8 (eq 2.12).

$$Ir^{III}(ttp)H \xrightarrow[\text{THF-}d_8, \text{ 120 °C, } N_2, \text{ 6 h}]{\text{KOH (20 equiv)}} \underset{\text{quantitative}}{Ir^{I}(ttp)^-K^+} \quad (2.12)$$
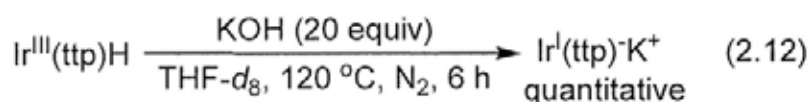
2.3 Base-Promoted Reduction of Iridium(III) Porphyrin Halides to Iridium(III) Porphyrin Hydride

Iridium(III) porphyrin halides ($Ir^{III}(ttp)(CO)X$, X = Cl, Br, I) were discovered to react with bases (KOH, K_2CO_3)[14] or with a trace of residual water in benzene-d_6[15] at elevated temperatures to produce $Ir^{III}(ttp)H$ (eq 2.13). The base is identified as the reducing agent, whereas the water likely acts as the protonating source. The mechanism of this base-promoted reduction of $Ir^{III}(ttp)(CO)X$ to $Ir^{III}(ttp)H$ was investigated and is presented as follows.

$$Ir^{III}(ttp)(CO)X + KOH / K_2CO_3 \xrightarrow[120\text{-}200\,^{\circ}C,\ 1\text{-}50\ h]{H_2O\ (\sim0.2\text{-}1\ equiv),\ C_6D_6} Ir^{III}(ttp)H \quad (2.13)$$
$$X = Cl,\ Br,\ I \qquad 20\ equiv \qquad\qquad\qquad\qquad 71\text{-}100\%$$
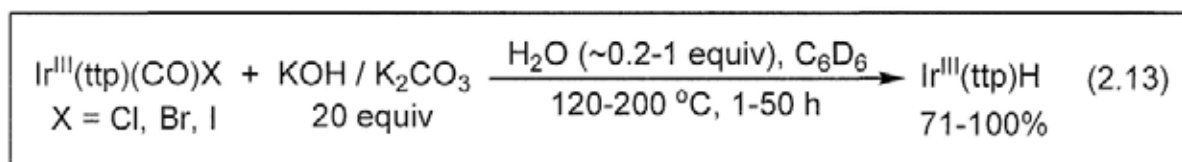
2.3.1 Scope in Base-Promoted Reduction

To understand the base-promoted reduction of $Ir^{III}(ttp)(CO)X$ to $Ir^{III}(ttp)H$, the effects of base strengths, reaction temperatures, and halide ligands of $Ir^{III}(ttp)(CO)X$ on the rates of $Ir^{III}(ttp)H$ formation were initially studied in sealed NMR tubes.

2.3.1.1 Effect of Bases and Temperatures

Without any base, $Ir^{III}(ttp)(CO)Cl$ remained stable in benzene-d_6 at 200 $^{\circ}C$ in 14 days and was recovered quantitatively (Table 2.1, entry 1). When water (100 equiv) was added, $Ir^{III}(ttp)(CO)Cl$ was partially consumed in 10 days to yield $Ir^{III}(ttp)H$ in 16% yield and unreacted $Ir^{III}(ttp)(CO)Cl$ was recovered in 84% yield (Table 2.1, entry 2). When KOH (20 equiv) was added, $Ir^{III}(ttp)(CO)Cl$ reacted at room temperature in 12 hours to form a trace of $Ir^{III}(ttp)H$. At a higher temperature of 200 $^{\circ}C$, $Ir^{III}(ttp)(CO)Cl$ was rapidly consumed in 1 hour to yield $Ir^{III}(ttp)H$ quantitatively (Table 2.1, entry 3). When a weaker base of K_2CO_3 (20 equiv) was added, $Ir^{III}(ttp)(CO)Cl$ reacted more slowly at 200 $^{\circ}C$ in 30 hours to yield $Ir^{III}(ttp)H$ in 95%

yield (Table 2.1, entry 4). Therefore, stronger bases can promote the faster reduction of $Ir^{III}(ttp)(CO)X$ to $Ir^{III}(ttp)H$. At 120 °C, both KOH and K_2CO_3 promoted the reduction of $Ir^{III}(ttp)(CO)Cl$ to $Ir^{III}(ttp)H$ but in slower rates (Table 2.1, entries 5 and 6).

Table 2.1 Effect of Bases and Temperatures on Reduction of $Ir^{III}(ttp)(CO)Cl$

$$Ir^{III}(ttp)(CO)Cl \; + \; \underset{\text{(20 equiv)}}{base} \; \xrightarrow[\text{temp, time}]{H_2O \; (\sim 0.2\text{-}2 \; equiv),^a \; C_6D_6} \; Ir^{III}(ttp)H$$

entry	additive (equiv)	temp/°C	time	yield $Ir^{III}(ttp)H/\%^b$
1	nil	200	14 d	0^c
2	H_2O (100 equiv)	200	10 d	16^d
3	KOH (20)	200	1 h	100^e
4	K_2CO_3 (20)	200	30 h	95
5	KOH (20)	120	5 h	84^f
6	K_2CO_3 (20)	120	23 d	100

^{a} The amount of residual water dissolved in benzene-d_6 was estimated by ^1H NMR spectroscopy. ^{b} NMR yield. ^{c} Unreacted $Ir^{III}(ttp)(CO)Cl$ was recovered quantitatively. ^{d} $Ir^{III}(ttp)(CO)Cl$ was recovered in 84% yield. ^{e} At room temperature, a trace of $Ir^{III}(ttp)H$ was observed in 12 hours. ^{f} $Ir^{I}(ttp)^-K^+$ in 9% yield was also formed.

2.3.1.2 Effect of Halide Ligands

Both $Ir^{III}(ttp)(CO)Cl$ and $Ir^{III}(ttp)(CO)Br$ reacted with KOH (20 equiv) at 120 °C in 5 hours at similar rates to give $Ir^{III}(ttp)H$ in high yields (Table 2.2, entries 1 and 2). $Ir^{III}(ttp)(CO)I$ reacted more slowly at 120 °C in 11 hours to give $Ir^{III}(ttp)H$ (Table 2.2, entry 3). The trend of reactivity is: $Ir^{III}(ttp)(CO)Cl \sim Ir^{III}(ttp)(CO)Br > Ir^{III}(ttp)(CO)I$. Similar trend of reactivity was also observed when K_2CO_3 was used at 200 °C (Table 2.3) (The rationale of the reactivity trend will be discussed in Section 2.3.3(B)). Moreover, in the reactions of $Ir^{III}(ttp)(CO)X$ (X = Cl, Br, I) with KOH, $Ir^{I}(ttp)^-K^+$ or $[Ir^{II}(ttp)]_2$ in modest amount was also formed (Table 2.2, entries 1-3).

Table 2.2 Effect of Halide Ligands (X) on KOH-Promoted Reduction of $Ir^{III}(ttp)(CO)X$

$$Ir^{III}(ttp)(CO)X \ + \ \underset{(20\ equiv)}{KOH} \ \xrightarrow[\ 120\ ^\circ C,\ time\ ]{\ H_2O\ (\sim0.2\text{-}0.8\ equiv),^a\ C_6D_6\ } \ Ir^{III}(ttp)H$$
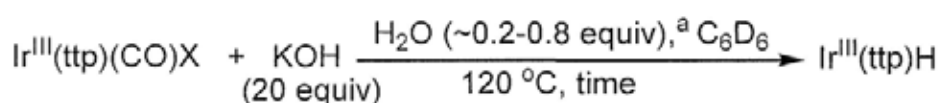
entry	X	time/h	$Ir^{III}(ttp)H$ yield/%[b]
1	Cl	5	84[c]
2	Br	5	71[d]
3	I	11	87[e]

[a] The amount of residual water dissolved in benzene-d_6 was estimated by ^1H NMR spectroscopy [b] NMR yield [c] $Ir^I(ttp)^-K^+$ in 9% yield was also formed [d] $Ir^I(ttp)^-K^+$ in 11% yield was also formed [e] $[Ir^{II}(ttp)]_2$ in 9% yield was also formed

Table 2.3 Effect of Halide Ligands (X) on K_2CO_3-Promoted Reduction of $Ir^{III}(ttp)(CO)X$

$$Ir^{III}(ttp)(CO)X \ + \ \underset{(20\ equiv)}{K_2CO_3} \ \xrightarrow[\ 200\ ^\circ C,\ time\ ]{\ H_2O\ (\sim0.2\text{-}1.1\ equiv),^a\ C_6D_6\ } \ Ir^{III}(ttp)H$$
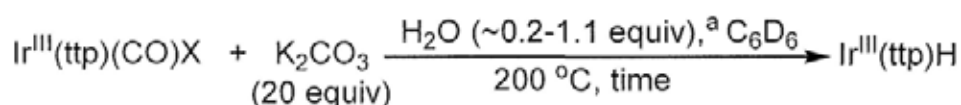
entry	X	time/h	$Ir^{III}(ttp)H$ yield/%[b]
1	Cl	30	95
2	Br	30	97
3	I	50	95

[a] The amount of residual water dissolved in benzene-d_6 was estimated by ^1H NMR spectroscopy [b] NMR yield

The reaction of $Ir^{III}(ttp)(CO)Cl$ with KOH at 120 $^\circ$C (Table 2.2, entry 1) was conveniently enough in time scale to allow close monitor of the reaction by ^1H NMR spectroscopy (Figure 2.1). $Ir^{III}(ttp)(CO)Cl$ (δ(pyrrole H) = 9.07 ppm, Figure 2.1(a)) was observed to be gradually consumed in 2 hours to form $Ir^{III}(ttp)H$ (δ(pyrrole H) = 8.81 ppm) in 55% yield and unreacted $Ir^{III}(ttp)(CO)Cl$ in 45% yield (Figure 2.1(b)). All $Ir^{III}(ttp)(CO)Cl$ was consumed in 5 hours to form $Ir^{III}(ttp)H$ in 84% yield and $Ir^I(ttp)^-K^+$ (δ(pyrrole H) = 8.50 ppm)[16] in 9% yield (Figure 2.1(c)). No intermediates were observed in the course of the reaction as the total yields of $Ir^{III}(ttp)(CO)Cl$ and $Ir^{III}(ttp)H$ were close to 100%. The same high total iridium porphyrin yields were also observed in other base-promoted reductions of $Ir^{III}(ttp)(CO)X$ (Tables 2 1-2.3).
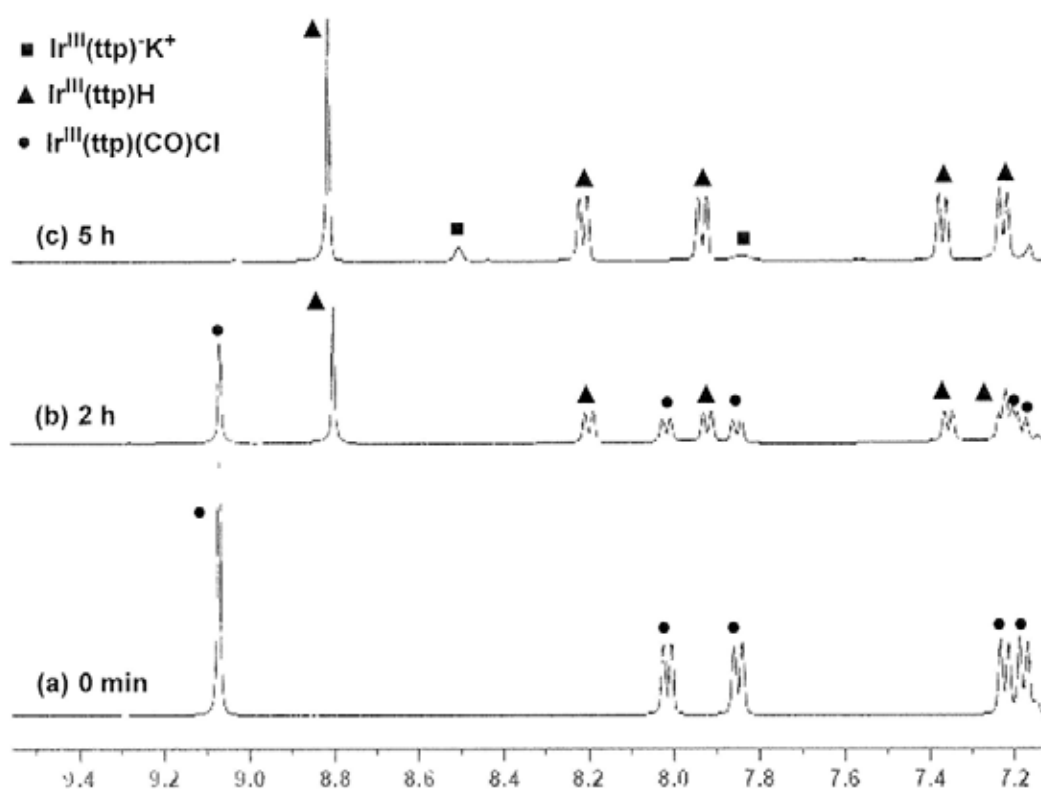
Figure 2.1 Partial ^{1}H NMR profile of the reaction of $Ir^{III}(ttp)(CO)Cl$ with KOH in benzene-d_6 at 120 °C (Table 2.2, entry 1).

2.3.2 Mechanistic Studies of Base-Promoted Reduction

$Ir^{III}(ttp)(CO)X$ (X = Cl, Br, I) were shown to be efficiently reduced to $Ir^{III}(ttp)H$ in the presence of bases (Tables 2.1-2.3). The roles of bases on the reductions of $Ir^{III}(ttp)(CO)X$ to $Ir^{III}(ttp)H$ were thus investigated. Initially, we propose a working reaction mechanism.

2.3.2.1 Overall Reaction Mechanism

Scheme 2.2 depicts a proposed mechanism of the base-promoted reduction of $Ir^{III}(ttp)(CO)X$ to $Ir^{III}(ttp)H$. $Ir^{III}(ttp)(CO)X$ initially undergoes CO dissociation to give $Ir^{III}(ttp)X$ (Scheme 2.2, pathway i). OH$^-$ (from KOH or the thermal hydrolysis of K_2CO_3) then undergoes ligand substitution with $Ir^{III}(ttp)X$ to form $Ir^{III}(ttp)OH$ (pathway ii). $Ir^{III}(ttp)OH$ can exist in an

62

equilibrium with the iridium porphyrin μ-oxo dimer, (ttp)Ir^{III}OIr^{III}(ttp), via the reversible condensation and hydrolysis (pathway iii). Consequently, the hydroxo ligand in Ir^{III}(ttp)OH can act as a single-electron reducing agent to reduce Ir(III) to Ir(II), forming both Ir^{II}(ttp) and hydroxy radical (HO•) (pathway iv), Ir^{II}(ttp) further undergoes the OH$^-$-promoted activation of residual H$_2$O in benzene-d_6[15] to form both Ir^{III}(ttp)H and Ir^{III}(ttp)OH (pathway v). Ir^{III}(ttp)OH is recycled for further Ir^{III}(ttp)H formation (pathways iv and v).

Scheme 2.2 Overall Mechanism of Base-Promoted Reduction of Ir^{III}(ttp)(CO)X

$$Ir^{III}(ttp)(CO)X \underset{}{\overset{i}{\rightleftharpoons}} Ir^{III}(ttp)X + CO$$
$$X = Cl, Br, I$$

$$Ir^{III}(ttp)X + OH^- \xrightarrow{ii} Ir^{III}(ttp)OH + X^-$$

$$2Ir^{III}(ttp)OH \overset{iii}{\rightleftharpoons} (ttp)Ir^{III}OIr^{III}(ttp) + H_2O$$

$$Ir^{III}(ttp)OH \xrightarrow{iv} Ir^{II}(ttp) + HO•$$

$$2Ir^{II}(ttp) + H_2O \overset{OH^-}{\underset{v}{\xrightarrow{\hspace{1cm}}}} Ir^{III}(ttp)H + Ir^{III}(ttp)OH$$
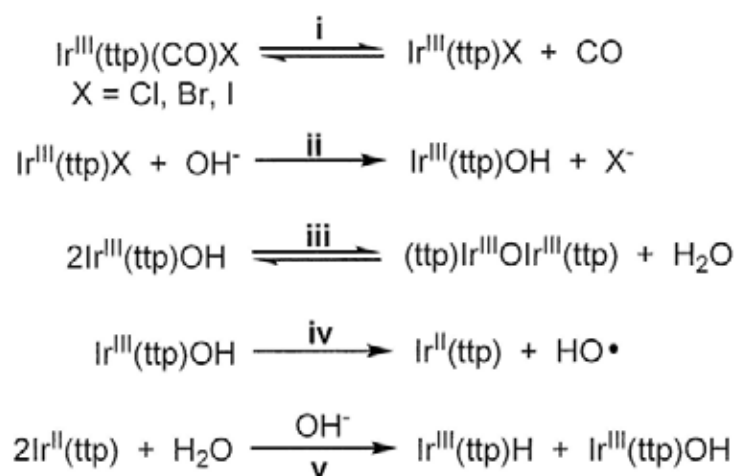
The details of (1) the ligand substitution with OH$^-$ to form Ir^{III}(ttp)OH (pathway ii), (2) the formation and reactivity of iridium(III) porphyrin μ-oxo dimer (pathway iii), and (3) the OH$^-$-promoted conversion of Ir^{III}(ttp)OH to Ir^{III}(ttp)H (pathways iv and v) will be discussed in the following sections.

2.3.2.2 Ligand Substitution of OH$^-$ (1): Formations of Ir^{III}(ttp)OH and (ttp)Ir^{III}OIr^{III}(ttp)

In order to investigate the formation of the proposed Ir^{III}(ttp)OH intermediate via ligand substitution (Scheme 2.2, pathway ii), attempted observation by ^{1}H NMR spectroscopy was carried out. However, the direct observation of Ir^{III}(ttp)OH intermediate was not successful as the total yields of Ir^{III}(ttp)(CO)X and Ir^{III}(ttp)H were always close to 100% (Tables 2.1-2.3). Therefore, the attempted synthesis of Ir^{III}(ttp)OH from the reaction of more electrophilic Ir^{III}(ttp)SbF$_6$ with more nucleophilic CsOH in benzene-d_6 was carried out. Ir^{III}(ttp)SbF$_6$

(δ(pyrrole H) = 9.08 ppm) reacted instantaneously upon mixing with CsOH at room temperature to yield Ir^{III}(ttp)H (δ(pyrrole H) = 8.81 ppm) in 95% yield. No iridium porphyrin intermediate was observed (eq 2.14; Figure 2.2).

$$Ir^{III}(ttp)SbF_6 + CsOH \xrightarrow[\text{r.t., 5 min}]{H_2O\ (\sim2.9\ \text{equiv}),\ C_6D_6} Ir^{III}(ttp)H \quad (2.14)$$
$$\text{3\%} \qquad \text{10 equiv} \qquad\qquad\qquad\qquad \text{95\%}$$

▲ Ir^{III}(ttp)H
● Ir^{III}(ttp)SbF$_6$
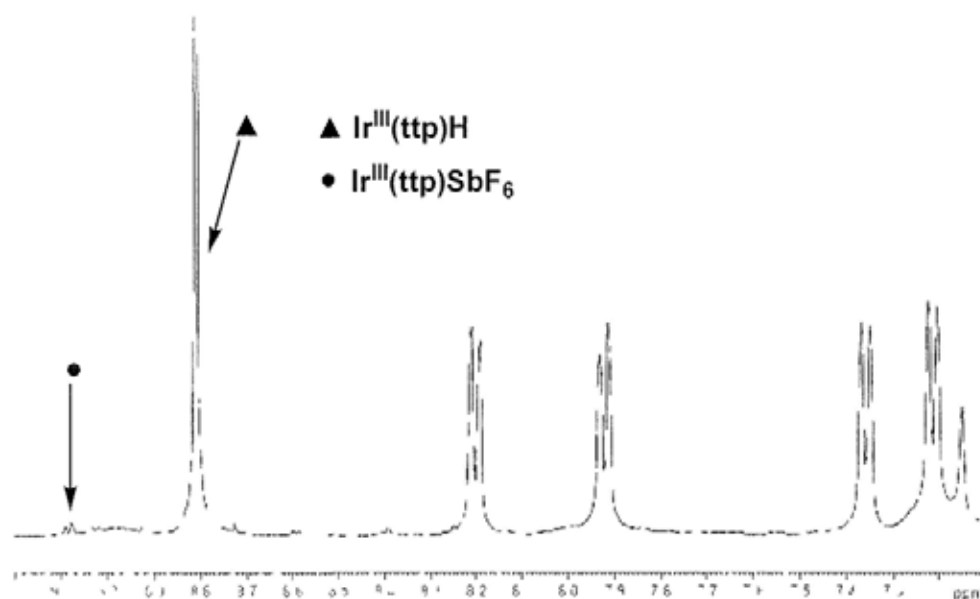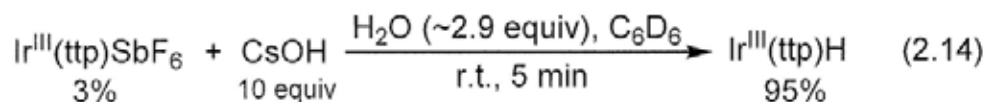
Figure 2.2 Partial ^{1}H NMR profile of reaction of Ir^{III}(ttp)SbF$_6$ with CsOH in 5 minutes (eq 2.14).

Therefore, the more sensitive analytical method of mass spectrometry was used for the detection of Ir^{III}(ttp)OH if indeed it had formed. The crude reaction mixture of Ir^{III}(ttp)SbF$_6$ with CsOH in C$_6$D$_6$ (eq 2.15) was immediately subjected to high-resolution mass spectrometric (HRMS) analysis. To our delight, besides Ir^{III}(ttp)H, both Ir^{III}(ttp)OH (**5**) and (ttp)Ir^{III}OIr^{III}(ttp) (**6**) were also detected (Figures 2.3(a)-(c)). Thus, Ir^{III}(ttp)OH does form as an intermediate via ligand substitution (Scheme 2.2, pathway ii). Most of the Ir^{III}(ttp)OH, however, is converted to Ir^{III}(ttp)H (Scheme 2.2, pathways iv and v). A small amount of Ir^{III}(ttp)OH likely undergoes the concurrent condensation to form (ttp)Ir^{III}OIr^{III}(ttp) (Scheme 2.2, pathway iii). Ir^{III}(ttp)OH is thus very reactive.

$$Ir^{III}(ttp)SbF_6 + CsOH \xrightarrow[\text{r.t., 5 min}]{\text{H}_2\text{O (trace), C}_6\text{D}_6} Ir^{III}(ttp)OH + (ttp)Ir^{III}OIr^{III}(ttp) + Ir^{III}(ttp)H \quad (2.15)$$

	10 equiv			
HRMS calculated		878.2591	1737.5092	
HRMS found		878.2574	1737.5122	
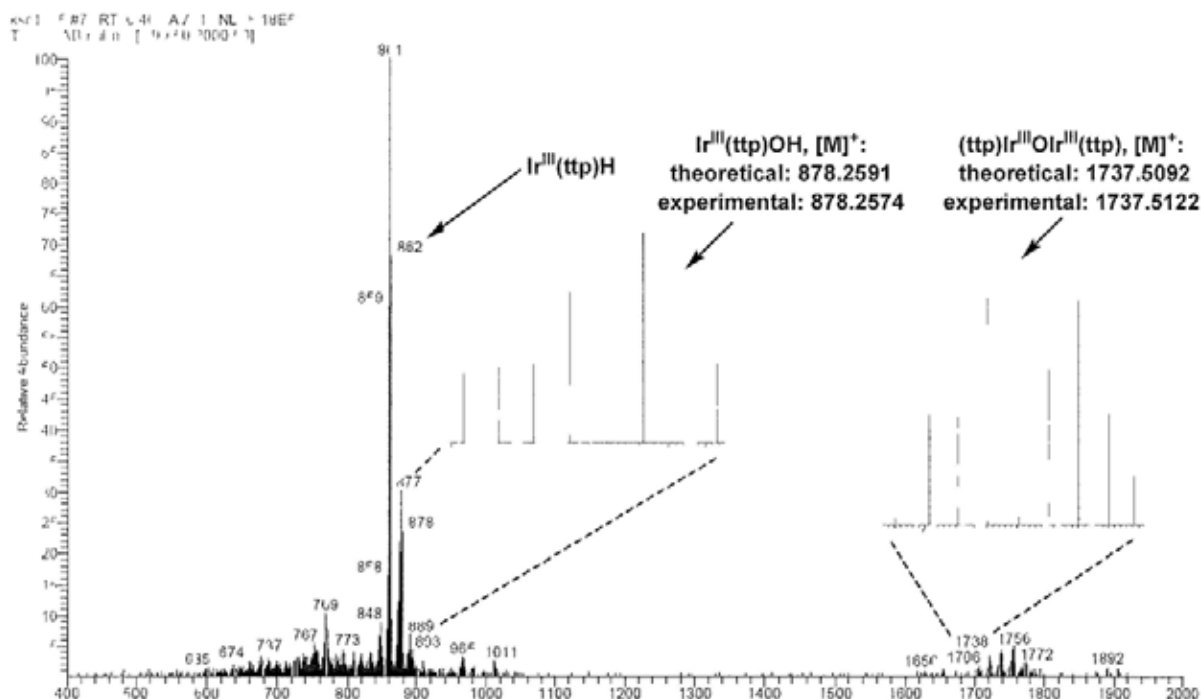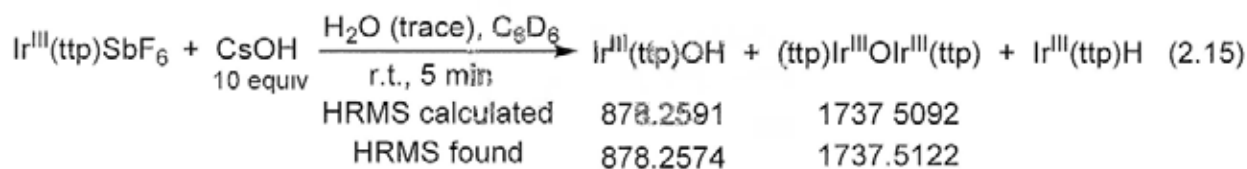
Figure 2.3(a) Mass spectrum of the reaction of $Ir^{III}(ttp)SbF_6$ with CsOH in C_6D_6, showing the concomitant formation of $Ir^{III}(ttp)H$, $Ir^{III}(ttp)OH$, and $(ttp)Ir^{III}OIr^{III}(ttp)$ (eq 2.15).
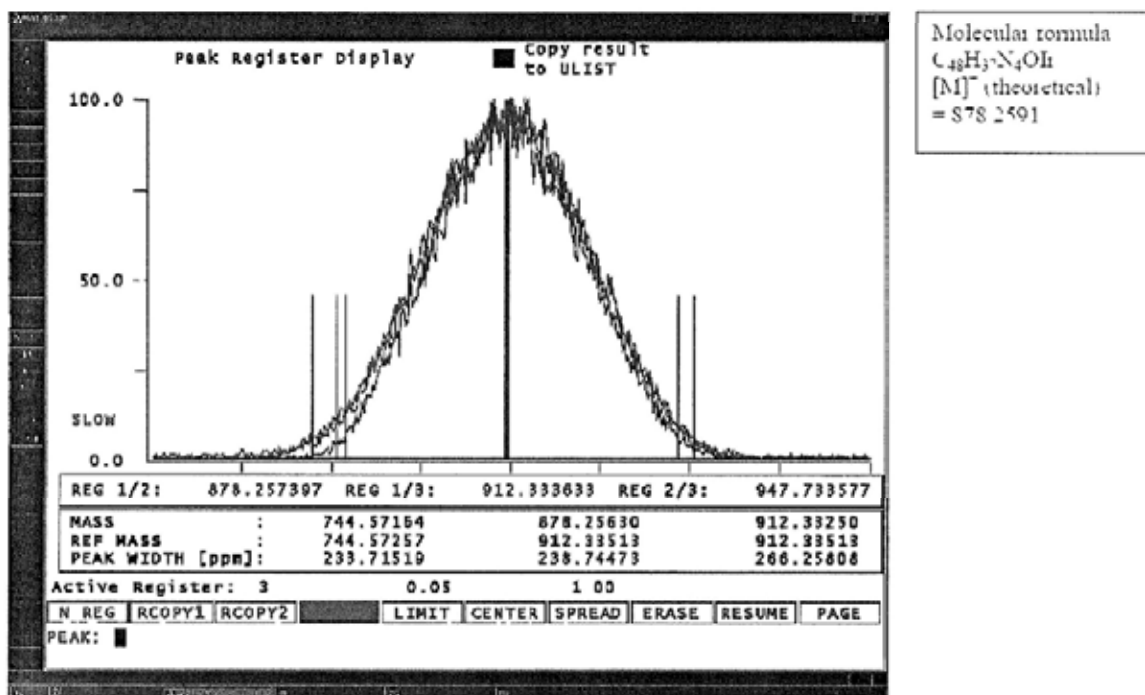
Figure 2.3(b) High-resolution mass spectrum of $Ir^{III}(ttp)OH$ ([M]$^+$: theoretical value = 878.2591; experimental value = 878.2574).
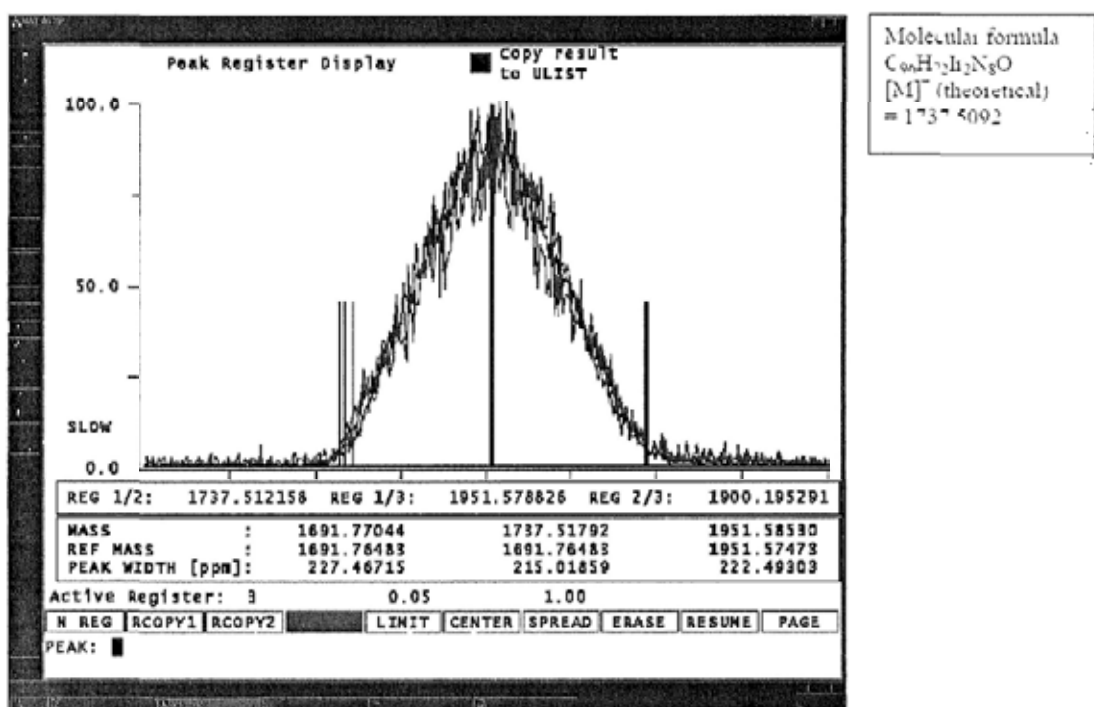
Figure 2.3(c) High-resolution mass spectrum of (ttp)Ir^{III}OIr^{III}(ttp) ([M]$^+$: theoretical value = 1737.5092; experimental value = 1737.5122).

Characterization of (ttp)Ir^{III}OIr^{III}(ttp). To further characterize (ttp)Ir^{III}OIr^{III}(ttp), an authentic sample was prepared using iridium(III) porphyrin β-hydroxyethyl, Ir^{III}(ttp)CH$_2$CH$_2$OH (**7**), as the precursor of Ir^{III}(ttp)OH, since Rh^{III}(ttp)CH$_2$CH$_2$OH has been used as a precursor to generate Rh^{III}(ttp)OH in aldehydic C-H bond activation of benzaldehydes (Chapter 1, section 1.7.1.1.2, Scheme 1.14).[17] Gratifyingly, (ttp)Ir^{III}OIr^{III}(ttp) in the form of (H$_2$O)(ttp)Ir^{III}OIr^{III}(ttp)(OH$_2$) (**6a**) was prepared in 72% yield by heating Ir^{III}(ttp)CH$_2$CH$_2$OH in benzene-d_6 at 120 °C in a sealed NMR tube in 23 days (eq 2.16).

$$\text{Ir}^{III}(\text{ttp})\text{CH}_2\text{CH}_2\text{OH} \xrightarrow[\text{120 °C, 23 d}]{\text{H}_2\text{O (~2.4 equiv), C}_6\text{D}_6} \text{(H}_2\text{O)(ttp)Ir}^{III}\text{OIr}^{III}\text{(ttp)(OH}_2\text{)} \quad (2.16)$$
$$72\%$$
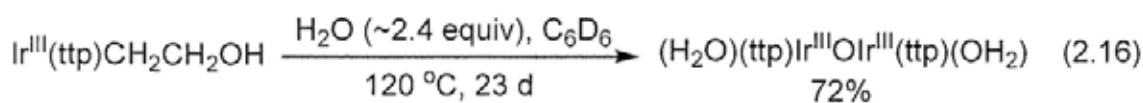
Scheme 2.3 illustrates the proposed mechanism of the condensation of Ir^{III}(ttp)CH$_2$CH$_2$OH to form (H$_2$O)(ttp)Ir^{III}OIr^{III}(ttp)(OH$_2$). Ir^{III}(ttp)CH$_2$CH$_2$OH initially undergoes β-hydroxy elimination[17] to yield Ir^{III}(ttp)OH and ethylene, which was observed in benzene-d_6 by ^{1}H NMR spectroscopy (δ(C$_2$H$_4$) = 5.23 ppm) (pathway i). The π-donating ethylene likely coordinates to

66

Ir^{III}(ttp)OH to form (C$_2$H$_4$)Ir^{III}(ttp)OH[18] to inhibit the conversion of Ir^{III}(ttp)OH to Ir^{III}(ttp)H (pathway ii). (C$_2$H$_4$)Ir^{III}(ttp)OH with a nucleophilic hydroxo ligand then attacks the iridium center of another (C$_2$H$_4$)Ir^{III}(ttp)OH by displacing the ethylene ligand to form the μ-hydroxo-bridged iridium porphyrin dimer, (C$_2$H$_4$)(ttp)Ir^{III}(OH)Ir^{III}(ttp)OH (pathway iii). Hydroxo ligand (OH$^-$) likely dissociates from (C$_2$H$_4$)(ttp)Ir^{III}(OH)Ir^{III}(ttp)OH and ethylene further coordinates to give [(C$_2$H$_4$)(ttp)Ir^{III}(OH)Ir^{III}(ttp)(C$_2$H$_4$)]$^+$ (pathway iv). OH$^-$ further deprotonates the μ-hydroxo ligand to generate μ-oxo iridium porphyrin dimer, (C$_2$H$_4$)(ttp)Ir^{III}OIr^{III}(ttp)(C$_2$H$_4$), and water (pathway v). Coordinations of residual water in benzene-d_6[19] or water generated from the condensation reaction lead to the formation of (H$_2$O)(ttp)Ir^{III}OIr^{III}(ttp)(OH$_2$) (pathway vi).

Scheme 2.3 Proposed Mechansim of Conversion of Ir^{III}(ttp)CH$_2$CH$_2$OH to (ttp)Ir^{III}OIr^{III}(ttp)
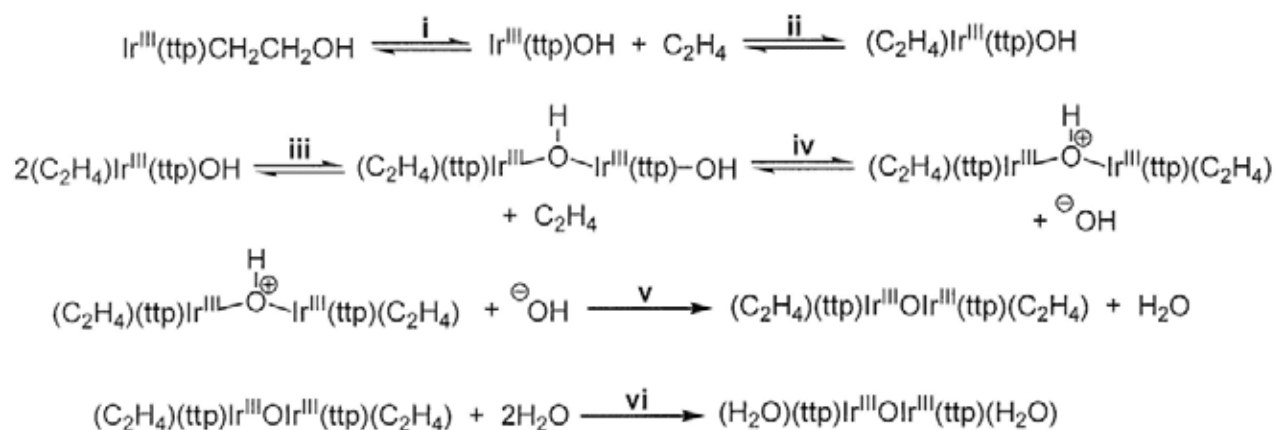
(H$_2$O)(ttp)Ir^{III}OIr^{III}(ttp)(OH$_2$) dissolves very well in benzene-d_6 to form a brown solution. Its formation is supported by the molecular ion in HRMS analysis ([M]$^+$ = 1737.5052) and the upfield porphyrin's pyrrole protons (δ(pyrrole H) = 8.36 ppm) by ^{1}H NMR spectroscopy (Figure 2.4), which is characteristic of μ-oxo-bridged metal macrocyclic complexes.[20] The presence of 2 equivalent upfield coordinated water molecules (δ(H$_2$O) = -10.89 ppm) is supported by the D/H exchange upon the addition of D$_2$O at room temperature (eq 2.17). It is air-sensitive as it completely decomposed in benzene-d_6 solvent under air after 3 days.

$(H_2O)(ttp)Ir^{III}OIr^{III}(ttp)(OH_2)$ was not observed in the reactions of $Ir^{III}(ttp)(CO)X$ (X = Cl, Br, I) and $Ir^{III}(ttp)SbF_6$ with OH^- by ^1H NMR spectroscopy (Tables 2.1-2.3; eq 2.14), as it was likely either formed in a small amount or further hydrolyzed by OH^- at high temperatures to form $Ir^{III}(ttp)OH$ and then $Ir^{III}(ttp)H$ (Scheme 2.2, pathways iv and v).

a   pyrrole H
b   inner *o*-tolyl's H
b' outer *o*-tolyl's H
c   inner *m*-tolyl's H
c' outer *m*-tolyl's H
d   tolyl's methyl H
e   aqua H

$(H_2O)Ir^{III}(ttp)-O-Ir^{III}(ttp)(OH_2)$
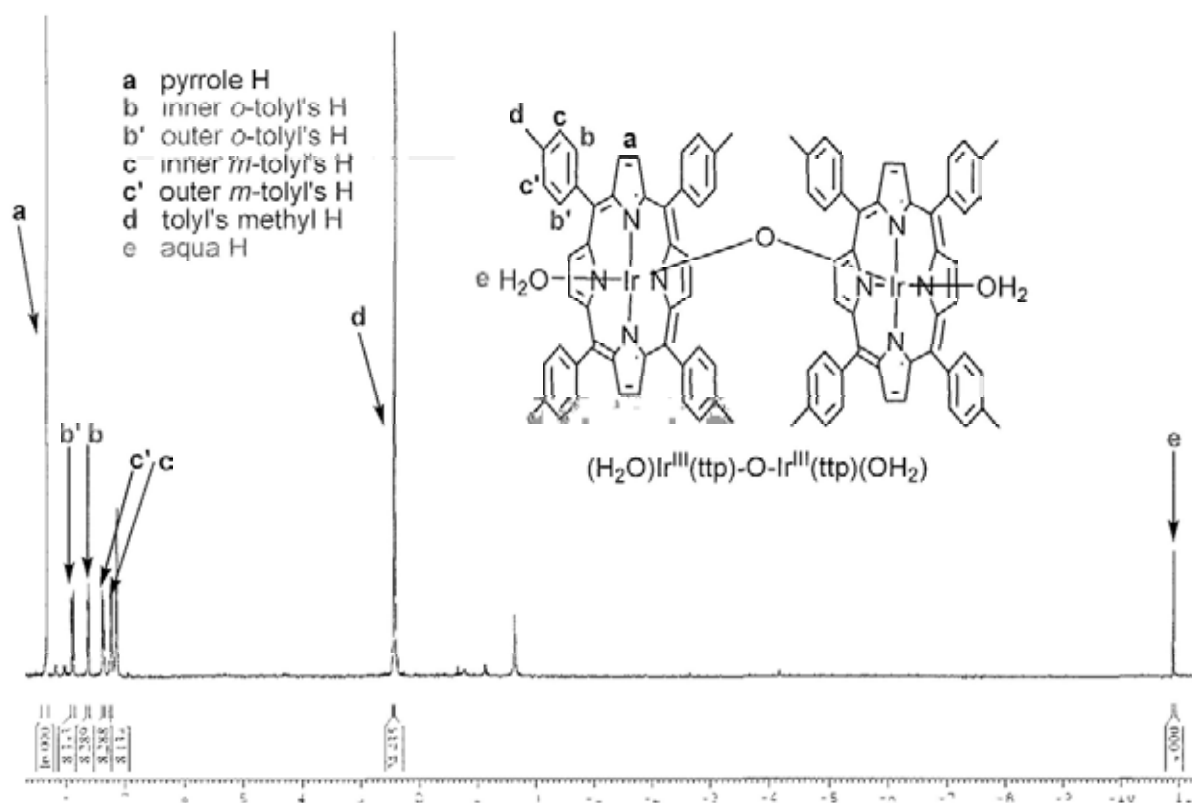
Figure 2.4 ^1H NMR of $(H_2O)(ttp)Ir^{III}OIr^{III}(ttp)(OH_2)$.

$$(H_2O)(ttp)Ir^{III}OIr^{III}(ttp)(OH_2) + \underset{\text{excess}}{D_2O} \xrightarrow[\text{r.t., 1.5 d}]{C_6D_6} (H_nD_{2-n}O)(ttp)Ir^{III}OIr^{III}(ttp)(OH_nD_{2-n}) \quad (2.17)$$
$$n = 0, 1, 2$$
$$D : H \text{ ratio} \sim 2.9 : 1$$
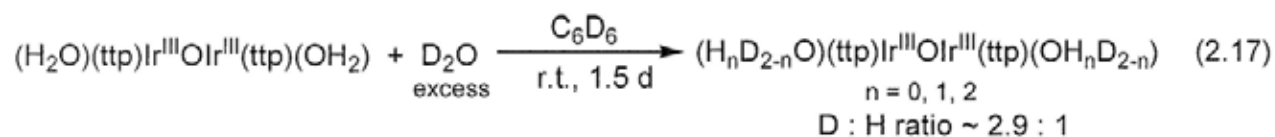
2.3.2.3 Ligand Substitution of OH⁻ (2): Formation of Ir^{III}(ttp)(PPh₃)OH

Since Ir^{III}(ttp)OH was shown to be highly reactive and proved difficult to be observed, the synthesis of coordinatively saturated and more stable Ir^{III}(ttp)(PPh₃)OH (**5a**)[21,22] was attempted from the reaction of Ir^{III}(ttp)(PPh₃)Cl (**1b**) with OH⁻ (Scheme 2.4; Figure 2.5(a)). When Ir^{III}(ttp)(PPh₃)Cl (δ(pyrrole H) = 8.84 ppm) was reacted with KOH in benzene-d_6 at 200 °C in 4 hours, Ir^{III}(ttp)(PPh₃)OH (δ(pyrrole H) = 8.81 ppm) was formed in 96% yield with a trace of Ir^{III}(ttp)(PPh₃)H (**2b**) (δ(pyrrole H) 8.75 ppm) (2%) (Scheme 2.4, pathway i; Figure 2.5(b)).

The formations of Ir^{III}(ttp)(PPh₃)OH and Ir^{III}(ttp)(PPh₃)H are supported by the spin splitting patterns and coupling constants with ^{31}P in both ^{1}H and ^{31}P NMR spectra (^{1}H NMR: (i) (Ph₃P)(ttp)IrO-*H*: doublet, $^3J_{PH}$ = 7.5 Hz; (ii) Ph₃P(ttp)Ir-*H*: doublet, $^2J_{PH}$ = 259 Hz.[12,23] (Figures 2.5(b) and (c)); ^{31}P NMR: (i) Ph₃*P*-(ttp)IrOH: doublet, $^3J_{PH}$ = 7.2 Hz; (ii) Ph₃*P*-(ttp)IrH: doublet, $^2J_{PH}$ = 258 Hz) (Figures 2.5(e) and (f)). The formation of Ir^{III}(ttp)(PPh₃)H is further confirmed by the authentic sample of Ir^{III}(ttp)(PPh₃)H prepared by reacting Ir^{III}(ttp)H with PPh₃ (1 equiv) in benzene-d_6 at room temperature.[12]

Scheme 2.4 Reaction Profile of Ir^{III}(ttp)(PPh₃)Cl with KOH in Benzene-d_6
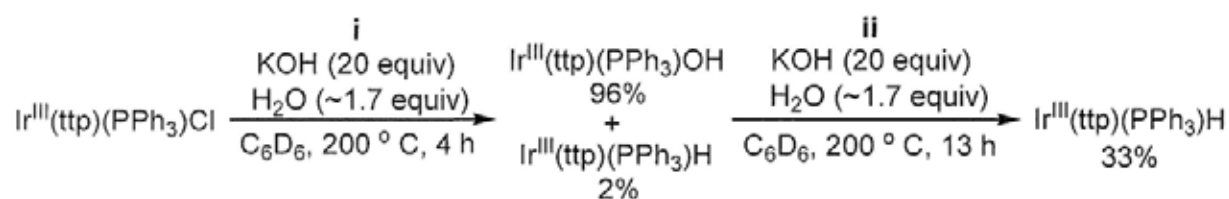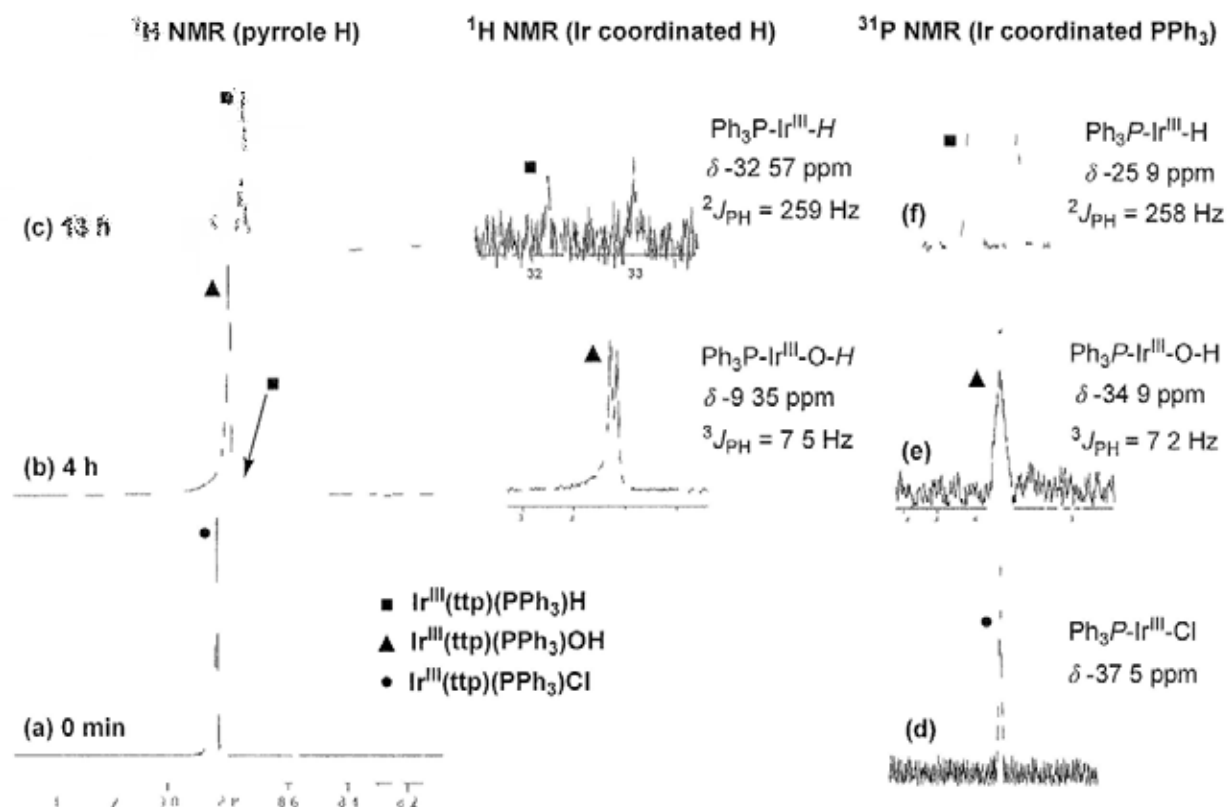
Figure 2.5 (a-c) Partial ^{1}H NMR profile of the reaction of Ir^{III}(ttp)(PPh$_3$)Cl with KOH in benzene-d_6 to form Ir^{III}(ttp)(PPh$_3$)OH (Scheme 2.4). **(d-f)** ^{31}P NMR spectra of Ir^{III}(ttp)(PPh$_3$)Cl, Ir^{III}(ttp)(PPh$_3$)OH, and Ir^{III}(ttp)(PPh$_3$)H.

2.3.2.4 Conversion of Ir^{III}(ttp)(PPh$_3$)OH to Ir^{III}(ttp))(PPh$_3$)H

Upon prolonged heating at 200 °C in 13 hours, Ir^{III}(ttp)(PPh$_3$)OH, which was prepared from the ligand substitution of Ir^{III}(ttp)(PPh$_3$)Cl with KOH, was then slowly and completely converted to Ir^{III}(ttp)(PPh$_3$)H in 33% yield (Scheme 2.4, pathway ii). Thus, Ir^{III}(ttp)(PPh$_3$)OH is the intermediate to give Ir^{III}(ttp)(PPh$_3$)H. The low yield of Ir^{III}(ttp)(PPh$_3$)H may be due to (1) the formation of (Ph$_3$P)(ttp)Ir^{III}OIr^{III}(ttp)(PPh$_3$) from the condensation of Ir^{III}(ttp)(PPh$_3$)OH, and (2) the thermally- and base-promoted decomposition of Ir^{III}(ttp)(PPh$_3$)H. To verify the proposed reactions, independent experiments were then carried out.

(1) The reaction mixture from the reaction of Ir^{III}(ttp)(PPh$_3$)Cl with KOH in benzene-d_6 at 200 °C in a short time of 30 minutes was subjected to HRMS analysis. However, no

$(Ph_3P)_n(ttp)Ir^{III}OIr^{III}(ttp)(PPh_3)_n$ (n = 0, 1) was detected. Moreover, no upfield porphyrin's pyrrole proton signal of iridium porphyrin, which should be due to the characteristic of $(Ph_3P)(ttp)Ir^{III}OIr^{III}(ttp)(PPh_3)$, was observed by ^{1}H NMR spectroscopy (Figure 2.5(c)). Thus, condensation of $Ir^{III}(ttp)(PPh_3)OH$ likely does not occur to form $(Ph_3P)(ttp)Ir^{III}OIr^{III}(ttp)(PPh_3)$. Presumably, the strong coordination of electron-rich PPh_3 in $Ir^{III}(ttp)(PPh_3)OH$ reduces the electrophilicity of iridium center for attack by the hydroxo group of another $(Ph_3P)(ttp)Ir^{III}$-OH to form $(Ph_3P)(ttp)Ir^{III}OIr^{III}(ttp)(PPh_3)$ (eq 2.18).

$$2(Ph_3P)(ttp)Ir^{III}OH \xrightarrow{\quad X \quad} (Ph_3P)(ttp)Ir^{III}OIr^{III}(ttp)(PPh_3) + H_2O \quad (2.18)$$
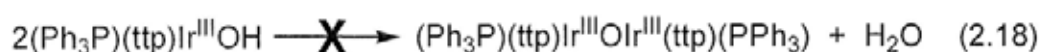
(2) $Ir^{III}(ttp)(PPh_3)H$ was independently prepared[12] and was then heated with KOH in benzene-d_6 at 200 °C (eq 2.19). In 3 days, $Ir^{III}(ttp)(PPh_3)H$ was recovered in 98% yield. Therefore, $Ir^{III}(ttp)(PPh_3)H$ was stable in both thermal and basic conditions without significant decomposition.

$$Ir^{III}(ttp)(PPh_3)H \xrightarrow[\text{C}_6\text{D}_6,\ 200\ ^\circ\text{C, 3 d}]{\text{KOH (20 equiv)}} \begin{array}{c} \text{unreacted} \\ Ir^{III}(ttp)(PPh_3)H \\ 98\% \end{array} \quad (2.19)$$
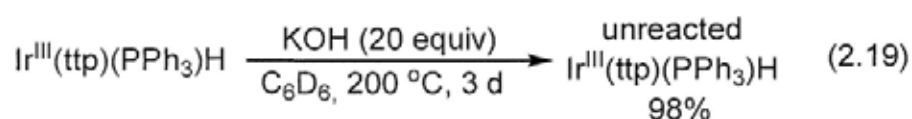
The low yield of $Ir^{III}(ttp)(PPh_3)H$ is neither attributed to the formation of $(Ph_3P)(ttp)Ir^{III}OIr^{III}(ttp)(PPh_3)$ nor the decomposition of $Ir^{III}(ttp)(PPh_3)H$, and the reason is unclear. Presumably, the more reactive, coordinatively saturated $Ir^{III}(ttp)(PPh_3)OH$ is thermally unstable and decomposes considerably upon heating.

2.3.2.5 Reaction Mechanism of Conversion of $Ir^{III}(ttp)(L)OH$ to $Ir^{III}(ttp)(L)H$

Since both $Ir^{III}(ttp)(CO)X$ (X = Cl, Br, I) (Tables 2.1-2.3) and $Ir^{III}(ttp)(PPh_3)Cl$ (Scheme 2.4) react with KOH to yield iridium(III) porphyrin hydride, a common reaction mechanism is assumed (Scheme 2.2). We propose four possible mechanisms for the conversion of $Ir^{III}(ttp)(L)OH$ to $Ir^{III}(ttp)(L)H$ (L = nil, H_2O, PPh_3) as shown in Scheme 2.5. We will examine

one by one.

Scheme 2.5 Possible Mechanisms of Conversion of $Ir^{III}(ttp)(L)OH$ to $Ir^{III}(ttp)(L)H$ (L = nil, H_2O, PPh_3)

(A) C-H Activation of Benzene

$$Ir^{III}(ttp)(L)OH + C_6D_6 \xrightarrow{\text{i}} Ir^{III}(ttp)(L)D + C_6D_5OH$$

$$Ir^{III}(ttp)(L)D \xrightarrow[\text{-HOD}]{\text{ii} \ OH^-} Ir^I(ttp)^- + L \xrightarrow[\text{-OH}^-]{\text{iii} \ H_2O} Ir^{III}(ttp)(L)H$$

$$Ir^{III}(ttp)(L)D \xrightarrow[\text{-HOD}]{\text{iv} \ H_2O} Ir^{III}(ttp)(L)H$$

(B) α-Hydride Elimination

$$(L)(ttp)Ir^{III}\text{-O-H} \xrightarrow{\text{i}} (L)(ttp)Ir^V\!\!\diagdown\!\!\begin{smallmatrix}O\\H\end{smallmatrix} \xrightarrow{\text{ii}} Ir^{III}(ttp)(L)H + 1/2 O_2$$

(C) Water-Gas-Shift Reaction

$$Ir^{III}(ttp)(L)OH + CO \xrightarrow{\text{i}} Ir^{III}(ttp)(L)CO_2H \xrightarrow{\text{ii}} Ir^{III}(ttp)(L)H + CO_2$$

(D) Electron-Transfer from OH⁻

$$(L)Ir^{III}(ttp)OH \xrightarrow{\text{i}} (L)Ir^{II}(ttp) + HO\cdot$$

$$(L)Ir^{III}(ttp)OH + HO\cdot \xrightarrow{\text{ii}} (L)Ir^{II}(ttp) + H_2O_2$$

$$H_2O_2 \xrightarrow{\text{iii} \ OH^-} H_2O + 1/2 O_2$$

$$Ir^{II}(ttp)(L) + OH^- \underset{}{\overset{\text{iv}}{\rightleftharpoons}} [Ir^{II}(ttp)OH]^- + L$$

$$Ir^{II}(ttp)(L) + [Ir^{II}(ttp)OH]^- \underset{}{\overset{\text{v}}{\rightleftharpoons}} \left[(L)(ttp)Ir^{II}\!-\!Ir^{II}(ttp)OH\right]^- \xrightarrow{\text{vi}} Ir^I(ttp)^- + Ir^{III}(ttp)OH + L$$

$$Ir^I(ttp)^- + H_2O + L \xrightarrow{\text{vii}} Ir^{III}(ttp)(L)H + OH^-$$

$$Ir^{III}(ttp)OH + L \xrightarrow{\text{viii}} Ir^{III}(ttp)(L)(OH)$$

Mechanism A: C-H Activation of Benzene by Ir-OH

In principle, $Ir^{III}(ttp)OH$ can undergo C-H activation of C_6D_6, likely via σ-bond metathsis, to yield $Ir^{III}(ttp)D$ and phenol-d_5 (C_6D_5OH) (Scheme 2.5, pathway **A-i**) in an analogous manner with that of $Ir^{III}(acac)_2OH$.[24] $Ir^{III}(ttp)D$ further undergoes the D/H exchange with residual water in benzene solvent either via the deprotonation / protonation process (pathways **A-ii** and **A-iii**) or via the metathesis (pathway **A-iv**) to yield $Ir^{III}(ttp)H$. However, no PhOH was detected by GC-MS analysis in the crude reaction mixture of $Ir^{III}(ttp)(CO)Cl$ with KOH and C_6H_6 either at 200 °C or 120 °C (eq 2.20). Therefore, benzene is neither the hydrogen source nor the reducing agent to form $Ir^{III}(ttp)H$. Mechanism A is ruled out.

$$Ir^{III}(ttp)(CO)Cl \xrightarrow[\substack{C_6H_6,\ N_2 \\ \text{(a) 120 °C, 9 h} \\ \text{(b) 200 °C, 15 min}}]{\text{KOH (20 equiv), H}_2\text{O (trace)}} Ir^{III}(ttp)H, \text{ no PhOH} \quad (2.20)$$
~quantitative
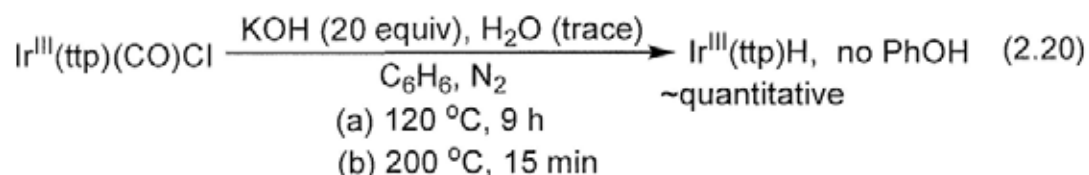
Mechanism B: α-Hydride Elimination of Ir-OH

In principle, the hydroxy group of $Ir^{III}(ttp)$-O-H can undergo α-hydride elimination[25] to form iridium(III) porphyrin-oxo-hydride intermediate, $Ir^{V}(ttp)(H)(O)$ (Scheme 2.5, pathway **B-i**), which then undergoes oxygen elimination to form $Ir^{III}(ttp)H$ (pathway **B-ii**). However, iridium(V) porphyrin complexes are unprecedented, and cis-$(ttp)Ir^{V}(H)(O)$ is too energetically demanding. Therefore, α-hydride elimination of $Ir^{III}(ttp)OH$ unlikely occurs. Mechanism B is disfavored.

Mechanism C: Water-Gas-Shift Reaction between Ir-OH and CO

In transition-metal-catalyzed water-gas-shift reactions, metal-hydride complexes are the commonly accepted intermediates.[26] Wayland also proposed that $[Rh^{II}(oep)]_2$ (oep = octaethylporphyrin) undergoes water-gas-shift reaction with CO and water to form $Rh^{III}(oep)H$ and $Rh^{III}(oep)COOH$ (eq 2.21), which then undergoes decarboxylation to yield $Rh^{III}(oep)H$ and

CO_2 (eq 2.22).[27]

$$[Rh^{II}(oep)]_2 + CO + H_2O \xrightarrow[\mathbf{i}]{C_6D_6, \text{ r.t.}} Rh^{III}(oep)CO_2H + Rh^{III}(oep)H \quad (2.21)$$

$$Rh^{III}(oep)CO_2H \xrightarrow[\mathbf{ii}]{C_6D_6, \text{ r.t.}} Rh^{III}(oep)H + CO_2 \quad (2.22)$$
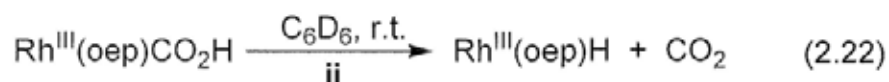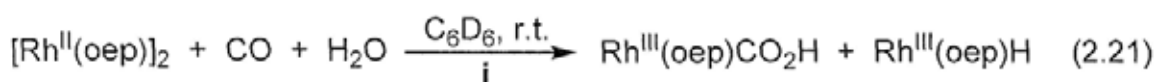
In principle, the CO ligand from $Ir^{III}(ttp)(CO)Cl$ can react with $Ir^{III}(ttp)OH$ via a water-gas-shift reaction to form $Ir^{III}(ttp)CO_2H$ (Scheme 2.5, pathway **C-i**), which further decarboxylates to yield $Ir^{III}(ttp)H$ (pathway **C-ii**). However, $Ir^{III}(ttp)(PPh_3)Cl$, which does not contain any CO ligand, can also react with KOH to yield $Ir^{III}(ttp)(PPh_3)H$ (Scheme 2.4). Thus, the CO ligand is unnecessary to form $Ir^{III}(ttp)H$. Mechanism C is ruled out.

Mechanism D: Electron-Transfer from OH⁻ to Ir(lll)

The hydroxo ligand in $Ir^{III}(ttp)(L)OH$ (L = nil, H_2O, PPh_3) can act as an efficient single-electron reducing agent to rapidly reduce Ir(III) to Ir(II), forming $Ir^{II}(ttp)(L)$ and hydroxy radical (HO•) (Scheme 2.5, pathway **D-i**).[28] The feasibility of the rapid redox reactions can be explained by 3 reasons:

(1) Hydroxide ion is a more efficient reducing agent in aprotic solvents than in water due to the reduced solvation by aprotic solvents.[29] This is reflected by the less positive oxidation potential[30] of HO•/HO⁻ couple in MeCN than that in water ($E_{ox}(OH^- \rightarrow HO•)$ in MeCN = +0.92 V vs NHE; $E_{ox}(OH^- \rightarrow HO•)$ in H_2O = +1.89 V vs NHE).[29] It is assumed that OH⁻ is an even more efficient reducing agent in non-polar benzene.

(2) OH⁻ tends to be more reducing in saturated KOH solution in aprotic solvent and at higher temperature. For example, the oxidation potential[30] of HO•/HO⁻ couple in DMSO containing a low OH⁻ concentration ([OH⁻] = 4.3 mM) at room temperature is reported to be +0.75 V (Table 2.4, entry 1).[31] In saturated KOH / DMSO solution (37 mM),[32] the redox potential is estimated to be +7.0 V at room temperature (refer to **Appendix I** for details), implying that HO⁻ in a

higher concentration is more reducing (Table 2.4, entry 2). At 120 $^{\circ}$C and 200 $^{\circ}$C, the redox poentials in saturated KOH / DMSO solution are estimated to be +0.68 V and +0.66 V, respectively (Table 2.4, entries 3 and 4), showing that OH$^-$ becomes even more reducing at elevated temperatures. It is assumed that OH$^-$ becomes more reducing in saturated KOH / benzene solution (~9 mM)[14] and at 120 $^{\circ}$C and 200 $^{\circ}$C for rapid redox reactions (Tables 2.1-2.3).

Table 2.4 Estimated Redox Potentials of HO•/OH$^-$ in DMSO at Different OH$^-$ Concentrations and Temperatures

$$OH^- \xrightarrow[\text{temp}]{\text{DMSO}} HO\bullet + e^- \quad E_{ox}$$

entry	[OH$^-$] in DMSO (mM)	temperature ($^{\circ}$C)	E_{ox} (V, vs SCE, in DMSO)
1	4.3	24	+0.75^a
2	37^b	25	~ +0.70^c
3	37^{b,d}	120	~ +0.68^c
4	37^{b,d}	200	~ +0.66^c

^{a} Reported experimental value (Ref 31). ^{b} Saturated concentration of KOH in DMSO at 25 $^{\circ}$C (Ref 32). ^{c} Estimated value using the Nernst equation (Refer to Appendix I for details). ^{d} The concentration of KOH is almost the same in DMSO upon the increase of temperature (Ref 32).

(3) Coordinated hydroxo ligand becomes even more reducing. It is proposed that OH$^-$, when coordinated to Mn^{III}(tmp)$^+$ to form Mn^{III}(tmp)OH, becomes much more reducing to reduce the Mn(III) center to form a more stable Mn^{II}(tmp) via more rapid inner-sphere electron-transfer (Section 1.5.2.1).[33] Indeed, the rate of inner-sphere electron-transfer can be much faster than that of outer-sphere electron-transfer in organometallic reactions by a factor of 10^6.[34] Likely, OH$^-$ can efficiently reduce the iridium center in Ir^{III}(ttp)OH via an inner-sphere electron-transfer.

HO• generated may also directly abstract HO• from Ir^{III}(ttp)(L)OH to form Ir^{II}(ttp)(L) and H$_2$O$_2$ (pathway **D-ii**). H$_2$O$_2$ can then undergo base-promoted disproportionation to form H$_2$O and O$_2$ (pathway **D-iii**).[35] Ir^{II}(ttp)(L) further reacts with OH$^-$ to form [Ir^{II}(ttp)OH]$^-$ due to the

thermodynamically favorable coordination of OH⁻ to the Ir centre (pathway **D**-iv).[2] The electron-rich [Ir^{II}(ttp)OH]⁻ rapidly undergoes disproportionation with Ir^{II}(ttp)(L)[36,37] to form Ir^{III}(ttp)OH and Ir^{I}(ttp)⁻ (pathways **D**-v and **D**-vi). Ir^{I}(ttp)⁻ is more basic than OH⁻ (pK_a ((L)Ir^{I}(ttp)-H) > pK_a(H$_2$O) = 15.7 (in H$_2$O)),[38] and it can be protonated with residual water in benzene-d_6[15] and further coordinates with L to form (L)Ir^{III}(ttp)H (pathway **D**-vii). Ir^{III}(ttp)OH coordinates with L to form Ir^{III}(ttp)(L)OH (pathway **D**-viii), which is further recycled for subsequent redox reactions. The supporting lines of mechanistic evidences are presented in the following section.

2.3.2.6 Electron-Transfer Mechanism in Conversion of Ir^{III}(ttp)(PPh₃)OH to Ir^{III}(ttp)(PPh₃)H

Since Ir^{III}(ttp)(PPh₃)OH is more stable than Ir^{III}(ttp)OH,[22] the conversion of Ir^{III}(ttp)(PPh₃)OH to Ir^{III}(ttp)(PPh₃)H (Scheme 2.4, pathway ii) was thus investigated in details.

The conversion of Ir^{III}(ttp)(PPh₃)OH to Ir^{III}(ttp)(PPh₃)H is proposed to occur via the inner-sphere electron-transfer from HO⁻ to Ir(III) to form Ir^{II}(ttp)(PPh₃) and H$_2$O$_2$ (Scheme 2.5, pathways **D**-i and ii). The key evidence for supporting the proposed mechanism can come from the direct detection of co-product, H$_2$O$_2$. However, H$_2$O$_2$ is unstable, especially in alkaline media in which facile disproportionation occurs (Scheme 2.5, pathway **D**-iii).[35,39] Therefore, H$_2$O$_2$ can only be indirectly observed as P(O)Ph₃ via the oxidation reaction with excess PPh₃ (eq 2.23).[40] The demonstration of the trapping of H$_2$O$_2$ was thus carried out.

$$PPh_3 + H_2O_2 \longrightarrow P(O)Ph_3 + H_2O \quad (2.23)$$
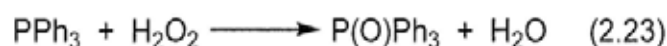
2.3.2.6.1 Trapping of H$_2$O$_2$ by PPh₃

As control experiments, PPh₃ was reacted with various oxygen-containing species likely present to ensure that the sole oxidation of PPh₃ to form P(O)Ph₃ is H$_2$O$_2$ only. These

oxygen-containing species are (1) KOH, (2) O_2, (3) H_2O, and (4) H_2O_2.

PPh$_3$ essentially did not react with (1) KOH, (2) O_2, and (3) H_2O in benzene in 12 hours to produce P(O)Ph$_3$ (Table 2.5, entries 1-3). On the other hand, PPh$_3$ rapidly reacted with (4) H_2O_2 in benzene at 200 °C in 1 hour to yield P(O)Ph$_3$ in 86% yield (Table 2.5, entry 4). Since PPh$_3$ itself did not oxidize in benzene at 200 °C in 12 hours to yield P(O)Ph$_3$ (Table 2.5, entry 5), any P(O)Ph$_3$ being formed in the KOH-promoted reduction of Ir^{III}(ttp)(PPh$_3$)Cl with excess PPh$_3$ most likely comes from the oxidation of PPh$_3$ by H_2O_2 co-product.

Table 2.5 Relative Reactivities of Possible Oxygen Sources with PPh$_3$

$$PPh_3 \xrightarrow[\text{200 °C, C}_6\text{H}_6\text{, N}_2\text{, time}]{\text{oxygen source (equiv)}} P(O)Ph_3$$

Entry	oxygen source (equiv)	time/ h	P(O)Ph$_3$ Yield/%[a]	PPh$_3$ Recovered /%[a]
1	KOH (20)	12	< 1	75
2	O_2 in air (~3)	12	< 1	89
3	H_2O (5)	12	< 1	94
4	H_2O_2 (2)	1	86	0
5	nil	12	< 1	75

[a] NMR yield.

Ir^{III}(ttp)(CO)Cl was then reacted with KOH and excess PPh$_3$ (5 equiv) (as a H_2O_2 trap) in benzene-d_6 at 200 °C in 3 hours (eq 2.24(a)). Ir^{III}(ttp)(PPh$_3$)H and P(O)Ph$_3$ were formed in 42% and 21% yield, respectively. The formation of P(O)Ph$_3$ was firmly established by ^{1}H and ^{31}P NMR spectroscopies (Figures 2.6(a) and (b)) and HRMS analysis with reference to the authentic sample of P(O)Ph$_3$ (Characterization of P(O)Ph$_3$ formed: (i) ^{1}H NMR: δ(o-phenyl H) 7.74 ppm; (ii) ^{31}P NMR: δ 24.9 ppm; (iii) HRMS [M+Na]$^+$: 301.0750). This supports the oxidation of OH$^-$ to produce H_2O_2 (Scheme 2.5, pathways **D**-i and ii), which then oxidizes PPh$_3$ to form P(O)Ph$_3$ (eq 2.23). The low yield of P(O)Ph$_3$ (observed yield: 21%; theoretical yield: 50%) is understandable due to the competititve disproportionation of H_2O_2 by OH$^-$ (Scheme 2.5, pathway **D**-iii).

$$Ir^{III}(ttp)(CO)Cl \ + \ KOH \xrightarrow[\text{200 °C \ C}_6\text{D}_6 \ \text{N}_2]{\substack{\text{PPh}_3 \ \text{(5 equiv)} \\ \text{H}_2\text{O (trace)}}} \ Ir^{III}(ttp)(PPh_3)Cl \ + \ Ir^{III}(ttp)(PPh_3)H \ + \ P(O)Ph_3 \quad (2\ 24)$$
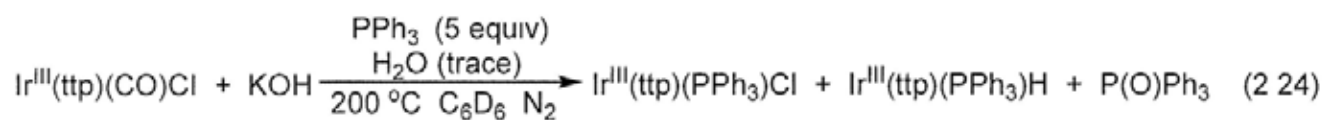
	PPh₃ equiv	time	Ir(ttp)(PPh₃)Cl	Ir(ttp)(PPh₃)H	P(O)Ph₃
(a)	20 equiv	3 h	0%[a]	42%[a]	21%[a]
(b)	0 equiv	12 h	100%[a]	0%[a]	1%[b]

[a] yield based on $Ir^{III}(ttp)(CO)Cl$
[b] yield based on PPh₃

(a) ¹H NMR

$Ir^{III}(ttp)(PPh_3)H$

unreacted PPh₃

P(O)Ph₃

(b) ³¹P NMR

unreacted PPh₃
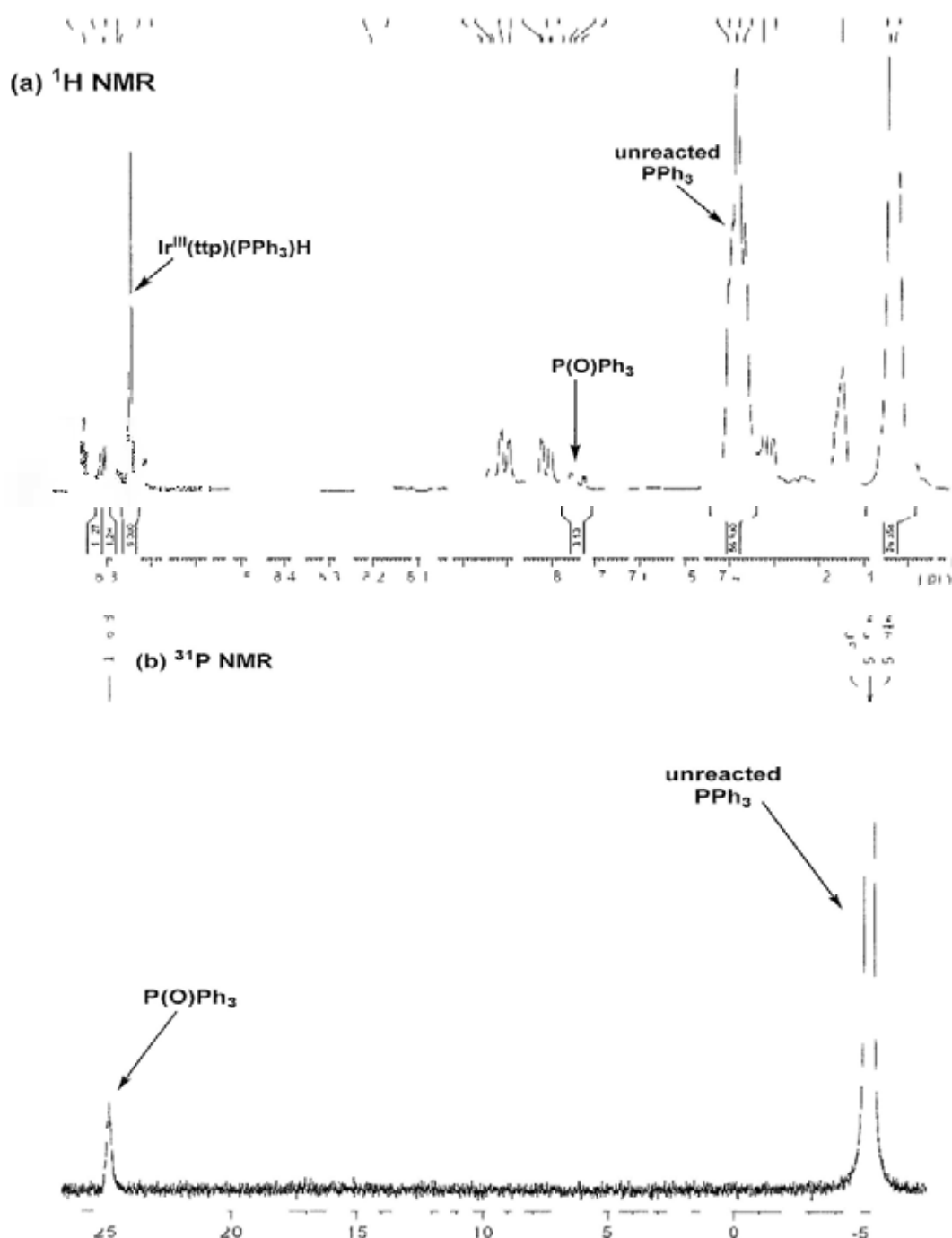
P(O)Ph₃

Figure 2.6 (a) ¹H and **(b)** ³¹P NMR spectra showing the reaction of $Ir^{III}(ttp)(CO)Cl$ with KOH and excess PPh₃ to yield $Ir^{III}(ttp)(PPh_3)H$ and P(O)Ph₃ (eq 2 24(a))

As a further control experiment, in the absence of KOH, PPh$_3$ did not reduce Ir^{III}(ttp)(CO)Cl to form Ir^{III}(ttp)(PPh$_3$)H, and was not oxidized to give P(O)Ph$_3$ (eq 2.24(b)). Therefore, PPh$_3$ is not the reducing agent. Instead, OH$^-$ is the genuine reducing agent in the base-promoted reduction of Ir^{III}(ttp)(PPh$_3$)Cl to form Ir^{III}(ttp)(PPh$_3$)H and P(O)Ph$_3$ (2.24(a)).

2.3.2.6.2 Base-Promoted Conversion of Ir^{II}(ttp)(PPh$_3$) to Ir^{III}(ttp)(PPh$_3$)H

Scheme 2.5(**D**) illustrates the proposed mechanism of the redox reaction of Ir^{III}(ttp)(PPh$_3$)OH at 200 °C to form Ir^{II}(ttp)(PPh$_3$), which further converts to Ir^{III}(ttp)(PPh$_3$)H (pathways **D**-iv-viii). Ir^{II}(ttp)(PPh$_3$) is thus prepared *in-situ* by reacting [Ir^{II}(ttp)]$_2$ with PPh$_3$ at 200 °C for mechanistic study (Table 2.6).

Table 2.6 Effect of KOH on Conversion of [Ir^{II}(ttp)]$_2$ / PPh$_3$ to Ir^{III}(ttp)(PPh$_3$)H

$$1/2[\text{Ir}^{II}(\text{ttp})]_2 + \text{PPh}_3 \xrightarrow[\substack{\text{C}_6\text{D}_6,\ \text{temp, time}}]{\substack{\text{H}_2\text{O (~1 equiv)}^a \\ \text{KOH (equiv)}}} \text{Ir}^{III}(\text{ttp})(\text{PPh}_3)\text{OH} + \text{Ir}^{III}(\text{ttp})(\text{PPh}_3)\text{H}$$

deep brown   1 : 1   deep red   brown

entry	KOH (equiv)	temp/°C	time	Ir^{III}(ttp)(PPh$_3$)OH yield/%^{b}	Ir^{III}(ttp)(PPh$_3$)H yield/%^{b}
1	0	r.t.^{c}	~5 min	scarce	nil
2	0	200	4 h	trace	trace
3	20	r.t.^{c}	~5 min	scarce	nil
4	20	200	4 h	16	15

^{a} The amount of residual H$_2$O (~1 equiv) dissolved in benzene-d_6 was estimated by ^{1}H NMR spectroscopy. ^{b} NMR yield. ^{c} Reddish brown precipitate was observed upon the addition of PPh$_3$, probably due to the formation of [Ir^{II}(ttp)(PPh$_3$)]$_2$.

Upon the addition of PPh$_3$ at room temperature, the deep brown, partially soluble [Ir^{II}(ttp)]$_2$ (δ(pyrrole H) = 8.33 ppm) (Figures 2.7(a) and 2.8(a)) in benzene-d_6 instantaneously turned to an insoluble, reddish brown precipitate, which was probably [Ir^{II}(ttp)(PPh$_3$)]$_2$, and a trace of soluble, deep red Ir^{III}(ttp)(PPh$_3$)OH (δ(pyrrole H) = 8.80 ppm) (Table 2.6, entries 1 and 3,

Figures 2.7(b) and 2.8(b)). No unreacted $[Ir^{II}(ttp)]_2$ and the paramagnetic $Ir^{II}(ttp)(PPh_3)$ monomer with its characteristic broad proton signals were observed.

In the absence of KOH, $[Ir^{II}(ttp)]_2$ / PPh_3 reacted with residual water (~1 equiv) in benzene-d_6[15] at 200 °C in 4 hours to yield $Ir^{III}(ttp)(PPh_3)H$ (δ(pyrrole H) = 8.75 ppm) and $Ir^{III}(ttp)(PPh_3)OH$ (δ(pyrrole H) = 8.80 ppm)[41] only in trace amounts with the considerable formation of unknown iridium porphyrin species (Table 2.6, entry 2; Figure 2.7(c)). $(Ph_3P)(ttp)Ir^{III}OIr^{III}(ttp)(PPh_3)$ was not formed since no characteristic upfield porphyrin's pyrrole proton was observed.

On the other hand, when KOH (20 equiv) was added, $[Ir^{II}(ttp)]_2$ / PPh_3 reacted with OH⁻ and residual water in benzene-d_6 at 200 °C in 4 hours to produce $Ir^{III}(ttp)(PPh_3)H$ (δ(pyrrole H) = 8.75 ppm) in 15% yield and $Ir^{III}(ttp)(PPh_3)OH$ (δ(pyrrole H) = 8.80 ppm) in 16% yield in a nearly 1 : 1 ratio (Table 2.6, entry 4; Figure 2.8(c)).[41] This supports that OH⁻ acts as a strong σ-donating ligand to promote the disproportionation of $Ir^{II}(ttp)(PPh_3)$ to form $Ir^{III}(ttp)(PPh_3)OH$ and $Ir^{I}(ttp)^-$ (eq 2.25; Scheme 2.5, pathways **D**-iv-vi,viii). Indeed, it is reported that the strong σ-donating ligand of pyridine induces the disproportionation of $[Rh^{II}(oep)]_2$ to produce $[Rh^{III}(oep)(py)_2]^+$ and $Rh^{I}(oep)^-$ in an 1 : 1 ratio (eq 2.26).[37] $Ir^{I}(ttp)^-$ further protonates with residual water and then coordinates with PPh_3 to form $Ir^{III}(ttp)(PPh_3)H$ (Scheme 2.5, pathway **D**-vii).

$$[Ir^{II}(ttp)]_2 \text{ / } PPh_3 \; + \; OH^- \rightleftharpoons Ir^{III}(ttp)(PPh_3)OH \; + \; Ir^{I}(ttp)^- \qquad (2.25)$$
$$\sim 1 : 1$$

$$[Rh^{II}(oep)]_2 \; + \; 2py \; \underset{\text{r.t.}}{\overset{py}{\rightleftharpoons}} \; [Rh^{III}(oep)py_2]^+ \; + \; Rh^{I}(oep)^- \qquad (2.26)$$
$$1 : 1$$
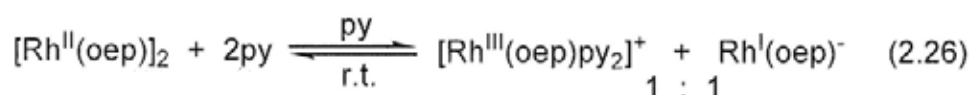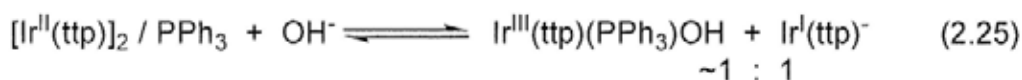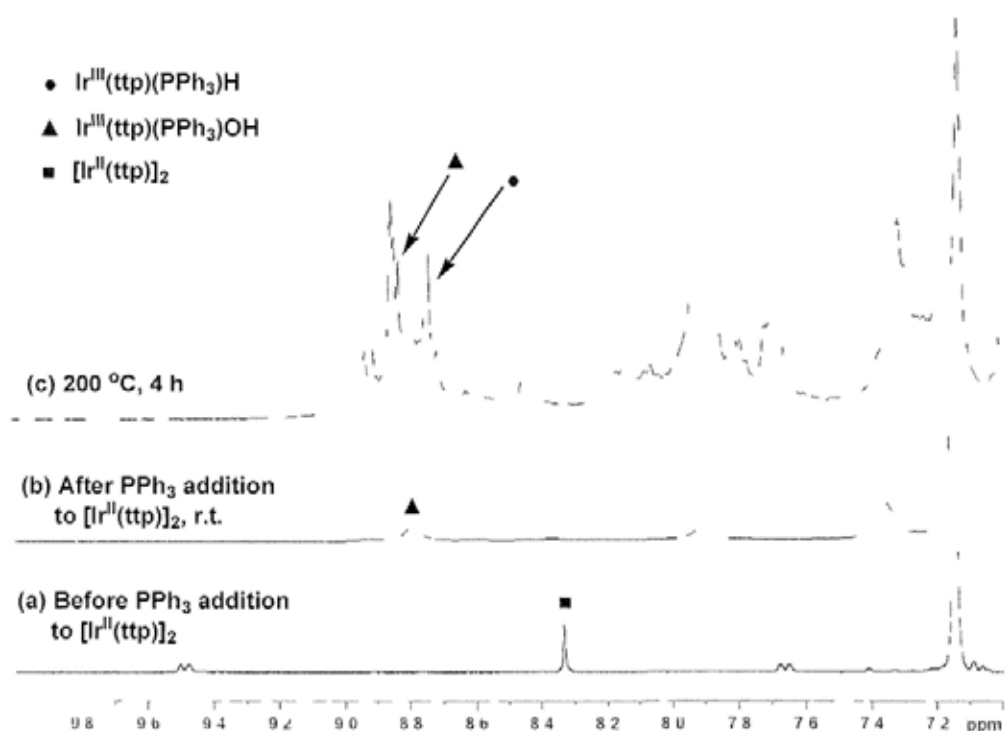
Figure 2.7 ^{1}H NMR time profile of the reaction of $[Ir^{II}(ttp)]_2$ / PPh$_3$ with residual water in benzene-d_6: **(a)** before the addition of PPh$_3$, **(b)** after the addition of PPh$_3$ at room temperature, and **(c)** after heating at 200 °C for 4 hours (Table 2.6, entries 1 and 2).
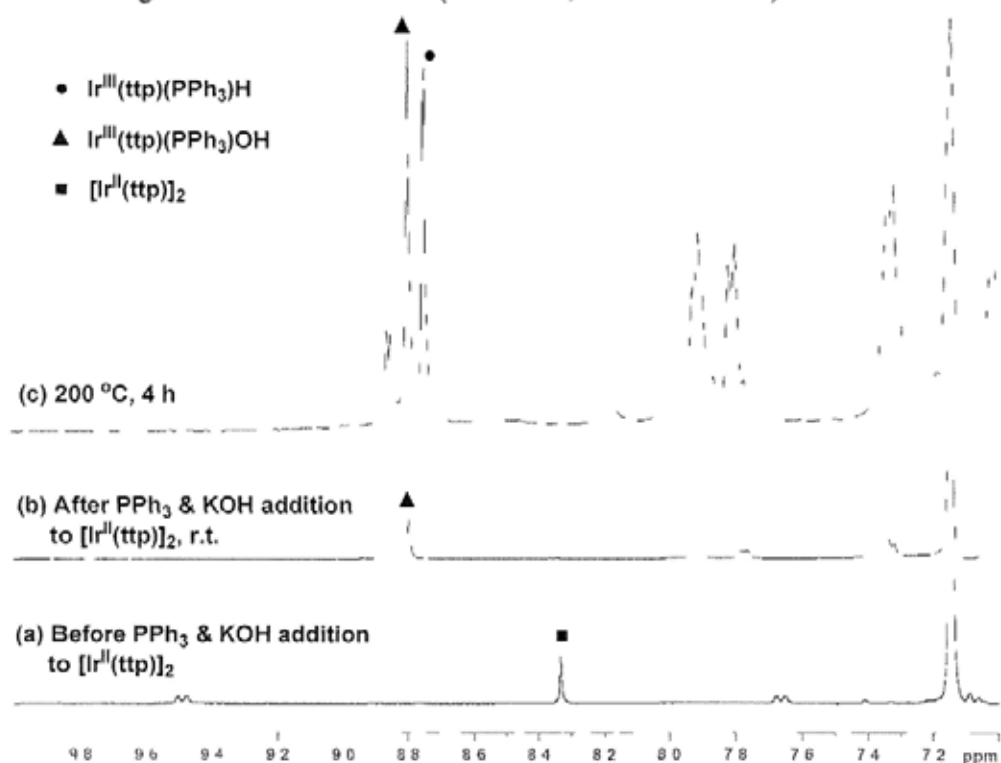
Figure 2.8 Reaction profile of the reaction of $[Ir^{II}(ttp)]_2$ / PPh$_3$ with KOH and residual water in benzene-d_6· **(a)** before the addition of PPh$_3$ and KOH, **(b)** after the addition of PPh$_3$ and KOH at room temperature, and **(c)** after heating at 200 °C for 4 hours (Table 2.6, entries 3 and 4).

2.3.2.7 Possibility of Iridium(III) Porphyrin μ-Oxo Dimer as an Intermediate

Since $(ttp)Ir^{III}OIr^{III}(ttp)$ was detected in the base-promoted conversion of $Ir^{III}(ttp)SbF_6$ to $Ir^{III}(ttp)H$ (eq 2.15), the role of $(ttp)Ir^{III}OIr^{III}(ttp)$ as an intermediate to yield $Ir^{III}(ttp)H$ was further investigated. $(H_2O)(ttp)Ir^{III}OIr^{III}(ttp)(OH_2)$ was found to react with KOH (20 equiv) slowly in benzene-d_6 at 120 °C in 10 days to produce only a small amount of $Ir^{III}(ttp)H$ in 6% yield (eq 2.27(a)). The reaction was further heated at 200 °C, and $(H_2O)(ttp)Ir^{III}OIr^{III}(ttp)(OH_2)$ was slowly consumed in 10 days to yield $Ir^{III}(ttp)H$ in 58% yield (eq 2.27(b)).

Likely, $(H_2O)(ttp)Ir^{III}OIr^{III}(ttp)(OH_2)$ undergoes slow ligand substitution with KOH to yield $Ir^{III}(ttp)OH$ and $Ir^{III}(ttp)O^-$ as a poor leaving group (resembling OR^-) (Scheme 2.6, pathway i). $Ir^{III}(ttp)O^-$ protonates with residual water in benzene-d_6[15] to re-form $Ir^{III}(ttp)OH$ (pathway ii). $Ir^{III}(ttp)OH$ further reacts rapidly in the presence of excess KOH to give $Ir^{III}(ttp)H$ via the redox reactions (pathway iii; Scheme 2.5(**D**)).

$$(H_2O)(ttp)Ir^{III}OIr^{III}(ttp)(OH_2) \xrightarrow[\text{C}_6\text{D}_6]{\text{KOH (20 equiv), H}_2\text{O (~1.9 equiv)}} Ir^{III}(ttp)H \quad (2.27)$$

(a) recovered: 94%	120 °C, 10 d	6%
(b) recovered: 0%	200 °C, 10 d	58%
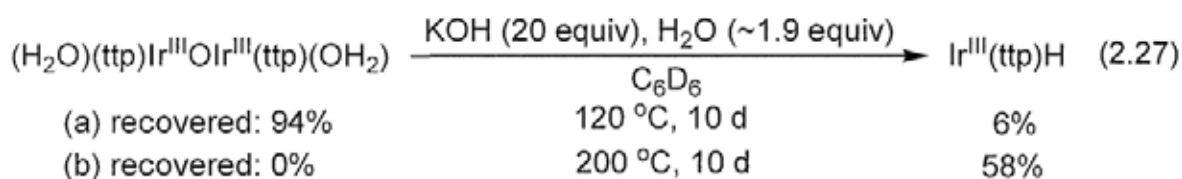
Scheme 2.6 OH^--Promoted Conversion of $(H_2O)Ir^{III}(ttp)OIr^{III}(ttp)(OH_2)$ to $Ir^{III}(ttp)H$

$$(H_2O)(ttp)Ir^{III}OIr^{III}(ttp)(OH_2) + OH^- \underset{}{\overset{i}{\rightleftharpoons}} Ir^{III}(ttp)OH + Ir^{III}(ttp)O^- + 2H_2O$$

$$Ir^{III}(ttp)O^- + H_2O \xrightarrow{ii} Ir^{III}(ttp)OH + OH^-$$

$$Ir^{III}(ttp)OH \xrightarrow{iii\ OH^-} Ir^{III}(ttp)H$$
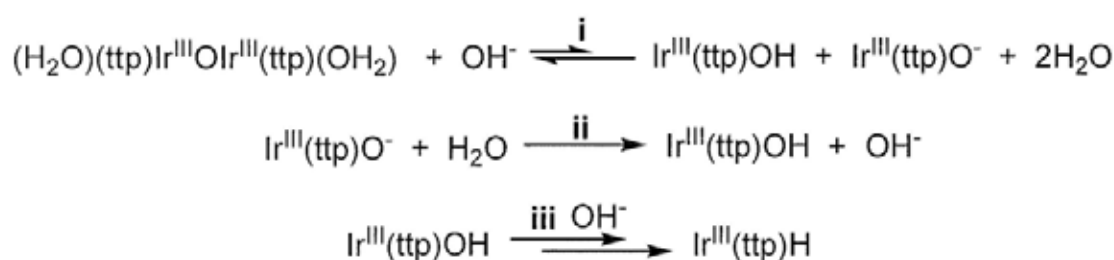
The rate of base-promoted conversion of $(H_2O)(ttp)Ir^{III}OIr^{III}(ttp)(OH_2)$ to $Ir^{III}(ttp)H$ is much slower than the rate of base-promoted reduction of $Ir^{III}(ttp)(CO)X$ (X = Cl, Br, I) and $Ir^{III}(ttp)SbF_6$ to form $Ir^{III}(ttp)H$ (Table 2.1-2.3; eq 2.14). Moreover, $(H_2O)Ir^{III}(ttp)OIr^{III}(ttp)(OH_2)$ was not observed as a major intermediate in the course of

reactions. Thus, $(H_2O)(ttp)Ir^{III}OIr^{III}(ttp)(OH_2)$ is not the major intermediate for $Ir^{III}(ttp)H$ formation. This supports that $Ir^{III}(ttp)OH$, once formed, undergoes rapid redox reactions to form $Ir^{III}(ttp)H$ as the dominant pathway (Scheme 2.2, pathways iv and v; Scheme 2.5(**D**)). $Ir^{III}(ttp)OH$ simultaneously undergoes minor, slow condensation to form $(ttp)Ir^{III}OIr^{III}(ttp)$ (Scheme 2.2, pathway iii), which further undergoes slower base-catalyzed hydrolysis to regenerate $Ir^{III}(ttp)OH$ and then $Ir^{III}(ttp)H$ (Scheme 2.6).

2.3.3 Discussions

The key steps in the base-promoted reduction of $Ir^{III}(ttp)(L)X$ (L = nil, H_2O, PPh_3; X = Cl, Br, I) to $Ir^{III}(ttp)(L)H$ are further discussed in the following parts.

(A) Ligand Substitution of $Ir^{III}(ttp)(L)X$ with OH^- in Benzene-d_6

Concerning the rapid conversion of $Ir^{III}(ttp)SbF_6$ with CsOH to form $Ir^{III}(ttp)H$ (eq 2.14), ligand substitution of OH^- to form $Ir^{III}(ttp)OH$ must be very fast for subsequent conversion. However, the concentration of dissolved OH^- in benzene at room temperature is estimated to be very low and is only nearly 1 equivalent with respect to iridium porphyrin species (Table 2.7, entries 1-4). Therefore, the rapid ligand substitution of $Ir^{III}(ttp)SbF_6$ with CsOH cannot be explained by the high concentration of OH^- in benzene-d_6. Instead, it can only be explained by the high activity of OH^- in benzene-d_6.

Indeed, the basicities of bases are enhanced when the solvent polarities decrease.[42] Since a base with high basicity usually exhibits high nucleophilicity (activity) in an aprotic solvent,[43] the enhanced nucleophilicity of OH^- in the non-polar benzene-d_6 solvent can account the rapid ligand substitution with $Ir^{III}(ttp)X$ (X = C, Br, I, SbF_6) to form $Ir^{III}(ttp)OH$ (Scheme 2.2, pathway ii).

Table 2.7 Concentrations of Solutes in Benzene-d_6

Entry	solute	concentration in C_6D_6 at room temperature (mM)
1	$Ir^{III}(ttp)(CO)X$ (X = Cl, Br, I)	10^a
2	$Ir^{III}(ttp)SbF_6$	5^a
3	$Ir^{III}(ttp)(PPh_3)Cl$	9^a
4	MOH (M = K, Cs)	$\sim9^b$

^{a} The concentration of iridium porphyrin is estimated using the number of mole of iridium porphyrin added in 0.5 mL of benzene-d_6. ^{b} Maximal solubility of NaOH in toluene at 25 °C, and the solubilities of KOH and CsOH in benzene are estimated to be close to that in toluene (Ref 14).

(B) Effect of Halide Ligands on Rates of Base-Promoted Reduction of $Ir^{III}(ttp)(CO)X$

The base-promoted reductions of $Ir^{III}(ttp)(CO)X$ (X = Cl, Br, I) to form $Ir^{III}(ttp)H$ in benzene-d_6 is in the reactivity trend: $Ir^{III}(ttp)(CO)Cl \sim Ir^{III}(ttp)(CO)Br > Ir^{III}(ttp)(CO)I$ (Tables 2.2 and 2.3). It is conceivable that the rate of ligand substitution of $Ir^{III}(ttp)X$ by OH^- to form $Ir^{III}(ttp)OH$ is in the corresponding order: Ir-Cl $\sim$ Ir-Br > Ir-I. Likely, an associative ligand substitution between OH^- and $Ir^{III}(ttp)X$ takes place. Such reactivity trend reflects the extent to which the $(ttp)Ir^{III}$-X bond is weakened in the transition state of the substitution process (rate of Ir^{III}-X cleavage is in the order: Ir^{III}-I ($\sim$64 kcal mol^{-1}) > Ir^{III}-Br ($\sim$76 kcal mol^{-1}) > Ir^{III}-Cl ($\sim$90 kcal mol^{-1}))[44] and the ability of X to increase the electrophilicity of Ir center in $Ir^{III}(ttp)X$ for OH^- attack (electrophilicity of Ir is in the order: Ir^{III}-Cl > Ir^{III}-Br > Ir^{III}-I).[45,46]

(C) Reaction of $Ir^{II}(ttp)(L)$ in the presence of OH^-: Competitive Disproportionation and Dimerization

In principle, $Ir^{II}(ttp)(L)$ (L = nil, H_2O, PPh_3), once formed from $Ir^{III}(ttp)(L)OH$, can initially react with OH^- to form $[Ir^{II}(ttp)OH]^-$ for subsequent base-promoted disproportionation to give $Ir^{III}(ttp)(L)H$ (Scheme 2.7, pathways i and iii; Scheme 2.5(**D**)). Alternatively, $Ir^{II}(ttp)(L)$ can

initially dimerize to form $[Ir^{II}(ttp)(L)]_2$ for subsequent base-promoted disproportionation to give $Ir^{III}(ttp)(L)OH$ (Scheme 2.7, pathways ii, iv, and iii).

Scheme 2.7 Possible Mechanistic Pathways in the Conversion of $Ir^{II}(ttp)(L)$ to $Ir^{III}(ttp)(L)H$
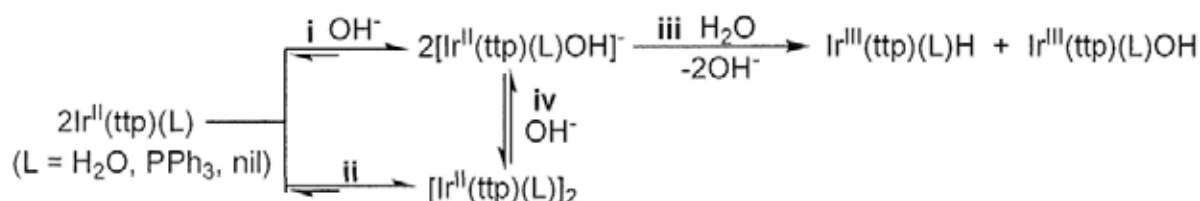
Since $Ir^{III}(ttp)(CO)X$ (X = Cl, Br, I) and $Ir^{III}(ttp)(PPh_3)Cl$ only react with KOH and residual water in benzene-d_6 to form $Ir^{III}(ttp)H$ and $Ir^{III}(ttp)(PPh_3)H$ as the dominant product (Tables 2.1-2.3; Scheme 2.4), it is reasoned that $Ir^{II}(ttp)(L)$, once formed, can rapidly coordinate with highly nucleophilic OH⁻ to give $[Ir^{II}(ttp)(L)OH]^-$, most likely inside a solvent cage, and then undergoes rapid disproportionation to form $Ir^{III}(ttp)(L)H$ (Scheme 2.7, pathways i and iii). On the other hand, $Ir^{II}(ttp)(L)$ unlikely dimerizes initially to give $[Ir^{II}(ttp)(L)]_2$ (Scheme 2.7, pathway ii), as $[Ir^{II}(ttp)]_2$ was not observed as the major species in the base-promoted reactions of $Ir^{III}(ttp)(CO)Cl$ and $Ir^{III}(ttp)SbF_6$ (Tables 2.1-2.3; eq 2.14).

The proposed formation of $[Ir^{II}(ttp)(L)OH]^-$ rather than $[Ir^{II}(ttp)(L)]_2$ dimer can be further supported by 2 reasons:

(1) Favorable coordination of $Ir^{II}(ttp)(L)$ to OH⁻. The magnitude of the exergonicity of OD⁻ coordinations to water-soluble group 9 metalloporphyrins, $[M^{III}(tspp)(H_2O)_2]^{3-}$ (M = Co, Rh, Ir; tspp = tetrakis(p-sulfonatophenyl)porphyrin), is reported to increase down the group $(-\Delta G(Co-OD) < -\Delta G(Rh-OD) < -\Delta G(Ir-OD))$.[2] The coordination of OD⁻ to anionic $[Ir^I(tspp)]^{5-}$ to form $[Ir^I(tspp)(OD)]^{6-}$ is also proposed.[2] Presumably, OH⁻ coordination to $Ir^{II}(ttp)(L)$ in benzene to form $[Ir^{II}(ttp)OH]^-$ should also be very thermodynamically favorable. Indeed, OH⁻ is also shown to promote the disproportionation of $[Ir^{II}(ttp)]_2$ / PPh_3 to give high yields of

$Ir^{III}(ttp)(PPh_3)H$ and $Ir^{III}(ttp)(PPh_3)OH$ (Table 2.6, entry 4; eq 2.25). Thus, $[Ir^{II}(ttp)OH]^-$ is likely the intermediate to produce $Ir^{III}(ttp)(L)H$.

(2) No conversion of $[Ir^{II}(ttp)]_2$ to $Ir^{III}(ttp)H$ was observed. $Ir^{III}(ttp)SbF_6$ reacted with KOH at room temperature in 1.5 days to yield $Ir^{III}(ttp)H$ in 75% yield (eq 2.28). However, $[Ir^{II}(ttp)]_2$ neither reacted with KOH nor water at room temperature in 2 days to yield any $Ir^{III}(ttp)H$ (eq 2.29 and 2.30), supporting that $[Ir^{II}(ttp)]_2$ is unlikely the intermediate to produce $Ir^{III}(ttp)H$. It is conceivable that $[Ir^{II}(ttp)]_2$ only dissociates at room temperature to form $Ir^{II}(ttp)$ monomer in an extremely low concentration, due to the strong Ir-Ir bond in $[Ir^{II}(ttp)]_2$ (BDE ~ 24 kcal mol^{-1})[47] and the resulting very small equilibrium constatnt K (eq 2.31).[48]

$$Ir^{III}(ttp)SbF_6 \ + \ \underset{20 \ equiv}{KOH} \ \xrightarrow[\text{r.t., 1.5 d}]{C_6D_6} \ \underset{75\%}{Ir^{III}(ttp)H} \qquad (2.28)$$

$$[Ir^{II}(ttp)]_2 \ + \ \underset{20 \ equiv}{KOH} \ \xrightarrow[\text{r.t., 2 d}]{C_6D_6} \ \text{no rxn (no } Ir^{III}(ttp)H) \qquad (2.29)$$

$$[Ir^{II}(ttp)]_2 \ + \ \underset{100 \ equiv}{H_2O} \ \xrightarrow[\text{r.t., 2 d}]{C_6D_6} \ \text{no rxn (no } Ir^{III}(ttp)H) \qquad (2.30)$$

$$[Ir^{II}(ttp)]_2 \ \underset{\text{r.t.}}{\overset{C_6D_6}{\rightleftharpoons}} \ 2Ir^{II}(ttp) \quad K = 2.5 \times 10^{-18} \ M \quad (2.31)$$
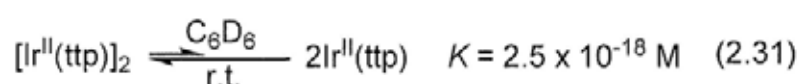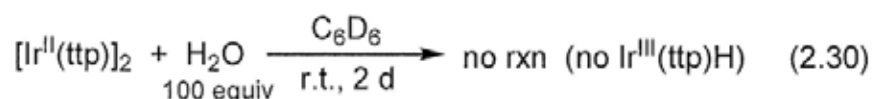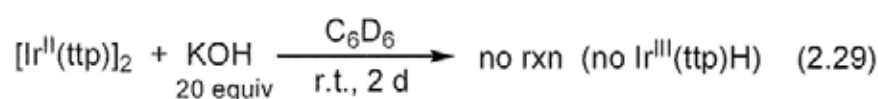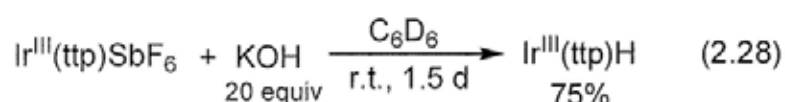
This supports that, $Ir^{II}(ttp)(L)$, once formed, unlikely dimerizes initially to give $[Ir^{II}(ttp)(L)]_2$ (Scheme 2.7, pathway ii), but rather rapidly reacts with OH$^-$ and H_2O via disproportionation to give $Ir^{III}(ttp)(L)H$ (Scheme 2.7, pathways i and iii).

2.3.4 Summary

The reaction mechanism of base-promoted reduction of $Ir^{III}(ttp)(L)X$ (L = nil, CO, PPh$_3$; X = Cl, Br, I, SbF$_6$) to $Ir^{III}(ttp)(L)H$ was discovered. Mechanistic studies suggest that $Ir^{III}(ttp)(L)X$ undergoes ligand substitution with OH⁻ to yield $Ir^{III}(ttp)(L)OH$ (Scheme 2.2, pathway ii). $Ir^{III}(ttp)(L)OH$ likely undergoes the homolysis of Ir-OH bond to form $Ir^{II}(ttp)(L)$ and H$_2$O$_2$ via (i) inner-sphere electron-transfer from OH⁻ to Ir(III) (Scheme 2.5, pathway **D-i**) and (ii) HO• abstraction from $Ir^{III}(ttp)(L)OH$ by another HO• to form H$_2$O$_2$ (Scheme 2.5, pathway **D-ii**). H$_2$O$_2$ can be indirectly detected as P(O)Ph$_3$ by reacting with added PPh$_3$ (eq 2.23). $Ir^{II}(ttp)(L)$ undergoes base-promoted disproportionation to form $Ir^{III}(ttp)(L)OH$ and $Ir^{I}(ttp)^-$ (Scheme 2.5, pathways **D-iv-vi, viii**). $Ir^{I}(ttp)^-$ then protonates with residual water and further reacts with L to form $Ir^{III}(ttp)(L)H$ (Scheme 2.5, pathway **D-vii**). $Ir^{III}(ttp)(L)OH$ is recycled to further give $Ir^{III}(ttp)(L)H$.

$Ir^{III}(ttp)OH$ can also undergo the condensation to form $(ttp)Ir^{III}OIr^{III}(ttp)$ (Scheme 2.2, pathway iii). $(ttp)Ir^{III}OIr^{III}(ttp)$ undergoes slow base-catalyzed hydrolysis to give back $Ir^{III}(ttp)OH$ and then $Ir^{III}(ttp)H$ (eq 2.27, Scheme 2.6).

Indeed, the base-promoted reduction of $Ir^{III}(ttp)(CO)X$ to $Ir^{III}(ttp)H$ can provide a more convenient method for the preparation of iridium(III) porphyrin hydride, without using the more tedious traditional reductive protonation with NaBH$_4$ / NaOH and HCl (eq 2.10).[7,10a]

2.4 Interconversions among $Ir^{III}(ttp)H$, $[Ir^{II}(ttp)]_2$, and $Ir^{I}(ttp)^-$ in Basic Media

In the mechanistic studies of base-promoted reduction of $Ir^{III}(ttp)(CO)X$ (X = Cl, Br, I) in benzene-d_6 at 120 °C, $Ir^{III}(ttp)OH$ is the intermediate to form $Ir^{III}(ttp)H$ as the major product, and $[Ir^{II}(ttp)]_2$ and $Ir^{I}(ttp)^-K^+$ as the minor ones (Table 2.2). This implies that $Ir^{III}(ttp)OH$, $Ir^{III}(ttp)H$, $[Ir^{II}(ttp)]_2$, and $Ir^{I}(ttp)^-$ may exist in equilibria, similar to the interconversions among $[Rh^{III}(tspp)OD(D_2O)]^{4-}$, $[Rh^{III}(tspp)D(D_2O)]^{4-}$, $[Rh^{II}(tspp)(D_2O)]_2^{8-}$, and $[Rh^{I}(tspp)(D_2O)]^{5-}$ in basic aqueous solution (Section 1.6.1).[1] After the mechanism of the conversion of $Ir^{III}(ttp)OH$ to $Ir^{III}(ttp)H$ in benzene-d_6 has been investigated (Section 2.3), the interconversions among $Ir^{III}(ttp)H$, $[Ir^{II}(ttp)]_2$, and $Ir^{I}(ttp)^-$ in benzene-d_6 are further studied.

In this section, the following parts are discussed:

(i) The established equilibria among $Ir^{III}(ttp)H$, $[Ir^{II}(ttp)]_2$, and $Ir^{I}(ttp)^-$.

(ii) The thermodynamic estimations of the interconversions.

(ii) The kinetics of the interconversions.

(iii) The mechanisms of the interconversions.

2.4.1 Established Equilibria among $Ir^{III}(ttp)H$, $[Ir^{II}(ttp)]_2$, and $Ir^{I}(ttp)^-$

The established interconverisons among $Ir^{III}(ttp)H$, $[Ir^{II}(ttp)]_2$, and $Ir^{I}(ttp)^-$ in benzene solvent are illustrated in Scheme 2.8, including (1) the dehydrogenative dimerization of $Ir^{III}(ttp)H$ to form $[Ir^{II}(ttp)]_2$ (pathway **i**), (2) the hydrogenation of $[Ir^{II}(ttp)]_2$ with H_2 to form $Ir^{III}(ttp)H$ (pathway **ii**), (3) the deprotonation of $Ir^{III}(ttp)H$ by OH^- to form $Ir^{I}(ttp)^-$ (pathway **iii**), (4) the protonation of $Ir^{I}(ttp)^-$ with H_2O to form $Ir^{III}(ttp)H$ (pathway **iv**), and (5) the comproportionation between $Ir^{III}(ttp)H$ and $Ir^{I}(ttp)^-$ to form $[Ir^{II}(ttp)]_2$ (pathway **v**). $Ir^{III}(ttp)H$, $[Ir^{II}(ttp)]_2$, and $Ir^{I}(ttp)^-$ can exist in equilibria, based on the reported equilibrium distributions of $[Rh^{III}(tspp)D]^{4-}$, $[Rh^{II}(tspp)(D_2O)]_2^{8-}$, and $[Rh^{I}(tspp)(D_2O)]^{5-}$ (Section 1.6.1).[1] Moreover, the tendencies of interconversions are established based on the relative rates of the reported reactions and the independent reactions with iridium porphyrins.

Scheme 2.8 Equilibrium Distributions among $Ir^{III}(ttp)H$, $[Ir^{II}(ttp)]_2$, and $Ir^{I}(ttp)^-$ in Benzene

$$Ir^{III}(ttp)H \underset{\textbf{ii } H_2}{\overset{\textbf{i } Ir^{III}(ttp)H, -H_2}{\rightleftarrows}} [Ir^{II}(ttp)]_2$$

iii OH⁻
iv H₂O   −H₂O
−OH⁻   **v** $Ir^{III}(ttp)H$, H₂O
                    −H₂, −OH⁻

$Ir^{I}(ttp)^-$
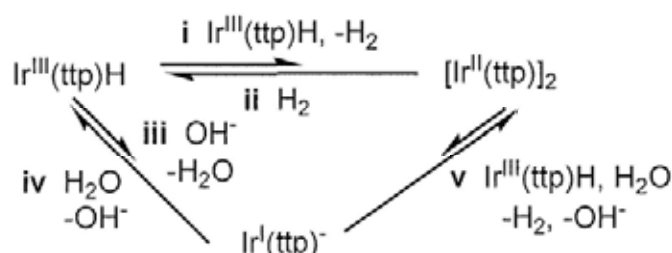
The hydrogenation of $[Ir^{II}(ttp)]_2$ with H_2 to form $Ir^{III}(ttp)H$ is thermodynamically favorable and fast (pathway **ii**), since the reaction of $[Ir^{II}(oep)]_2$ with H_2 is facile at room temperature to form $Ir^{III}(oep)H$ (eq 2.32).[49] On the other hand, the reverse dehydrogenative dimerization of $Ir^{III}(ttp)H$ to $[Ir^{II}(ttp)]_2$ becomes endergonic and slow (pathway **i**).

$$[Ir^{II}(oep)]_2 + H_2 \xrightarrow[\text{instantaneous}]{C_6D_6,\ 25\ ^\circ C} 2Ir^{III}(oep)H \qquad (2.32)$$
$$\text{200 Torr} \qquad\qquad\qquad\qquad 100\%$$
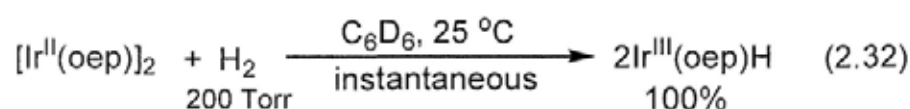
The deprotonation of $Ir^{III}(oep)H$ by NaOH (1 M, aqueous solution) to form $Ir^{I}(oep)^-$ in ethanol at room temperature is very slow due to the low acidity of $Ir^{III}(oep)H$ ($pK_a(Ir^{III}(por)-H)$ > $pK_a(H_2O) = 15.7$)[38] (eq 2.33). Thus, the deprotonation of $Ir^{III}(ttp)H$ by OH⁻ should be slow (pathway **iii**). On the other hand, $Ir^{I}(ttp)^-$ is basic enough to undergo rapid protonation with water to form $Ir^{III}(ttp)H$ (pathway **iv**).

$$Ir^{III}(oep)H + NaOH \underset{}{\overset{EtOH,\ r.t.}{\rightleftarrows}} Ir^{I}(oep)^-Na^+ + H_2O \quad (2.33)$$
$$\text{(1 M, aq)}$$
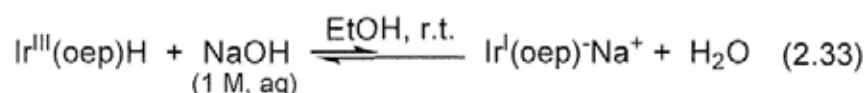
The comproportionation between iridium(III) porphyrin and iridium(I) porphyrin anion in aprotic solvent has not been reported. Therefore, the reaction between $Ir^{I}(ttp)^-K^+$ and $Ir^{III}(ttp)H$ was independently carried out. $Ir^{I}(ttp)^-K^+$ was prepared from the deprotonation of $Ir^{III}(ttp)H$ with KOH in a Teflon screw-capped NMR tube (eq 2.12) and benzene-d_6 was then added under N_2. Both $Ir^{III}(ttp)H$ and $[Ir^{II}(ttp)]_2$ were instantaneously formed in 45% and 18% yields,

respectively, at room temperature (eq 2.34). It is proposed that the protonation of $Ir^I(ttp)^-$ with residual water[15] in benzene-d_6 (eq 2.35) and the comproportionation[50] between $Ir^I(ttp)^-$ and $Ir^{III}(ttp)H$ (eq 2.36) occur concurrently. The result also supports that the concomproportionation between $Ir^I(ttp)^-$ and $Ir^{III}(ttp)H$ is thermodynamically favorable to give $[Ir^{II}(ttp)]_2$ (pathway **v**).

$$Ir^I(ttp)^-K^+ \xrightarrow[\text{r.t., instantaneous}]{H_2O\ (\sim 0.5\ \text{equiv}),\ C_6D_6} \underset{45\%}{Ir^{III}(ttp)H} + \underset{18\%}{1/2[Ir^{II}(ttp)]_2} \quad (2.34)$$

$$Ir^I(ttp)^- + H_2O \longrightarrow Ir^{III}(ttp)H + OH^- \quad (2.35)$$

$$Ir^I(ttp)^- + Ir^{III}(ttp)H + H_2O \longrightarrow [Ir^{II}(ttp)]_2 + H_2 + OH^- \quad (2.36)$$
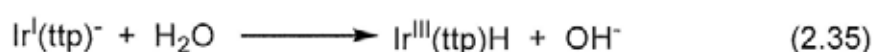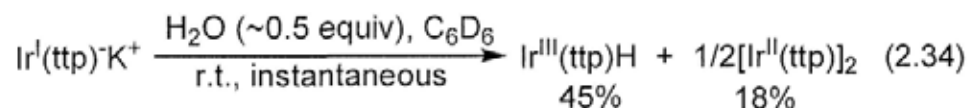
2.4.2 Thermodynamics of Interconversions

The equilibrium distributions of interconversions among $Ir^{III}(ttp)H$, $[Ir^{II}(ttp)]_2$, and $Ir^I(ttp)^-$ are further supported by the thermodynamic estimations using the reported data of bond dissociation energies (BDEs),[47,51,52] entropy changes,[53] and redox potentials (E).[31,54,55] The estimated free energy change (ΔG) of each of the interconverisons at 200 °C is shown in Table 2.8. The thermodynamics calculations are also shown in Scheme 2.9. Indeed, the estimated ΔG supports the established equilibria as shown in Scheme 2.8. It should be noted that the estimated ΔG values only reflect the tendencies of the equilibria, but not the quantifications of the equilibrium constants.

Table 2.8 Reaction Pathways and Estimated Thermodynamics of Interconversions Among $Ir^{III}(ttp)H$, $[Ir^{II}(ttp)]_2$, and $Ir^I(ttp)^-$ at 200 °C

Pathway	Reactions	Estimated ΔG (kcal mol^{-1})
i	$2Ir^{III}(ttp)H \rightleftharpoons [Ir^{II}(ttp)]_2 + H_2$	~ +5.3
ii	$[Ir^{II}(ttp)]_2 + H_2 \rightleftharpoons 2Ir^{III}(ttp)H$	~ -5.3
iii	$Ir^{III}(ttp)H + OH^- \rightleftharpoons Ir^I(ttp)^- + H_2O$	~ +7.2
iv	$Ir^I(ttp)^- + H_2O \rightleftharpoons Ir^{III}(ttp)H + OH^-$	~ -7.2
v	$Ir^I(ttp)^- + Ir^{III}(ttp)\text{-}H + H_2O \rightleftharpoons (ttp)Ir^{II}\text{-}Ir^{II}(ttp) + H\text{-}H + OH^-$	~ -4.9

Scheme 2.9 Thermodynamic Estimations of Established Interconversions at 200 °C

(A) Dehydrogenative Dimerization of $Ir^{III}(ttp)H$ / Hydrogenation of $[Ir^{II}(ttp)]_2$ with H_2

$$2Ir^{III}(ttp)\text{-}H \underset{}{\overset{C_6D_6}{\rightleftharpoons}} Ir^{II}(ttp)\text{-}Ir^{II}(ttp) + H\text{-}H \qquad \triangle G \sim +5.3 \text{ kcal mol}^{-1}$$

(A) Enthalpy change

Bond	BDE (kcal mol^{-1})
$Ir^{III}(ttp)$-H	~70 [51]
$Ir^{II}(ttp)$-$Ir^{II}(ttp)$	~24 [47]
H-H	104.2 [52]

- -

$\triangle H$ = 2 BDE(Ir-H) - BDE(Ir-Ir) - BDE(H-H)

= 2(70) - 24 - 104.2
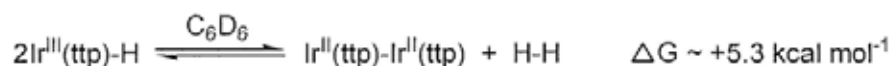
= +11.8 kcal mol^{-1}

(B) Entropy increase from H_2 formation

$T\triangle S(H_2)_{473K} \sim T(S(H_2)^{\circ}_{500K})$[53a]

= (473 K) (145.7 J mol^{-1} K^{-1})

= +68916.1 J mol^{-1}

= +68.9 kJ mol^{-1}

= +16.5 kcal mol^{-1}

(C) Translational entropy decrease of 1 mole from 2 $Ir^{III}(ttp)H$ to 1 $[Ir^{II}(ttp)]_2$

$T\triangle S_{(-1M)} \sim$ -35 eu

$\sim$ -10 kcal mol^{-1} [53b]

$$\triangle G = \triangle H - T\triangle S(H_2)_{473K} - T\triangle S_{(-1M)}$$

$$= (+11.8) - (+16.5) - (-10)$$

$$= +5.3 \text{ kcal mol}^{-1}$$

(B) Deprotonation of $Ir^{III}(ttp)H$ by OH^- / Protonation of $Ir^I(ttp)^-$ with H_2O

$$Ir^{III}(ttp)\text{-}H + OH^- \overset{C_6D_6}{\rightleftharpoons} Ir^I(ttp)^- + HO\text{-}H \qquad \triangle H \sim +7.2 \text{ kcal mol}^{-1}$$

(A) $Ir^{III}(ttp)\text{-}H \longrightarrow Ir^{II}(ttp) + H\bullet \qquad \triangle H = +70 \text{ kcal mol}^{-1}$ [51]

(B) Electron Transfer from OH^- to $Ir^{II}(ttp)$

$OH^- \longrightarrow OH\bullet + e^- \qquad E_{ox} = +0.75 \text{ V (DMSO, vs SCE, } [OH^-] \sim 4 \text{ mM)}$[31]

$Ir^{II}(ttp) + e^- \rightleftharpoons Ir^I(ttp)^- \qquad E_{red} \sim -1.7 \text{ V (CH}_2\text{Cl}_2\text{, vs SCE, } [Ir^{II}(ttp)] = 1 \text{ mM)}$[54]

- -

$Ir^{II}(ttp) + OH^- \longrightarrow Ir(ttp)^- + HO\bullet \qquad E_{Rxn} \sim -2.45 \text{ V}$

$\triangle H = -nFE$

$\sim -(1)(96485)(-2.45)$

$\sim +236.4 \text{ kJ mol}^{-1}$

$\sim +56.5 \text{ kcal mol}^{-1}$

(C) $H\bullet + HO\bullet \longrightarrow HO\text{-}H \qquad \triangle H = -119.3 \text{ kcal mol}^{-1}$ [52]
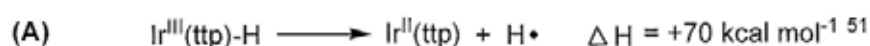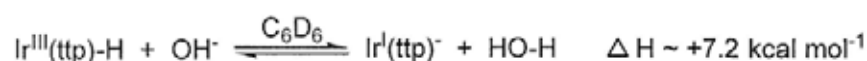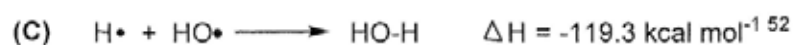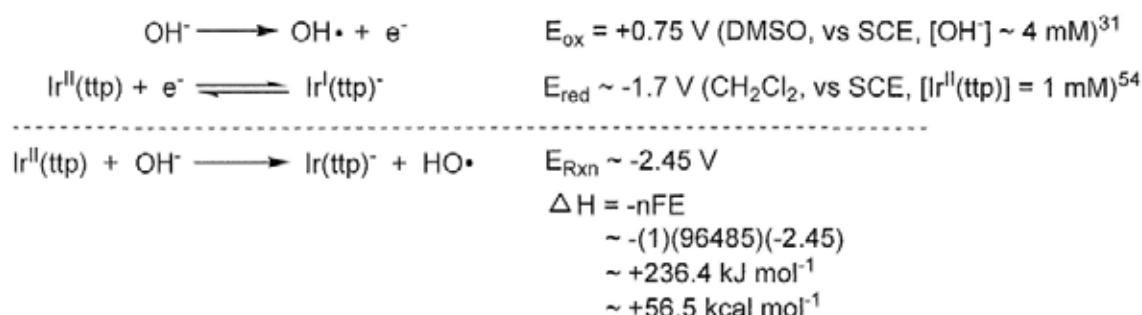
$$\triangle G \sim \triangle H = (A) + (B) + (C)$$

$$= 70 + 56.5 + (-119.3)$$

$$= +7.2 \text{ kcal mol}^{-1}$$

(C) Comproportionation between Ir^I(ttp)$^-$ and Ir^{III}(ttp)H to form [Ir^{II}(ttp)]$_2$

Ir^I(ttp)$^-$ + Ir^{III}(ttp)-H + H$_2$O $\rightleftharpoons$ (ttp)Ir^{II}-Ir^{II}(ttp) + H-H + OH$^-$ ΔH ~ -4.9 kcal mol^{-1}

(A)   Ir^{III}(ttp)-H $\longrightarrow$ Ir^{II}(ttp) + H$\cdot$ ΔH ~ +70 kcal mol^{-1} [51]

(B)   H-OH $\longrightarrow$ H$\cdot$ + HO$\cdot$ ΔH = +119.3 kcal mol^{-1} [52]

(C)   2H$\cdot$ $\longrightarrow$ H-H ΔH = -104.2 kcal mol^{-1} [52]
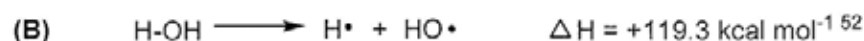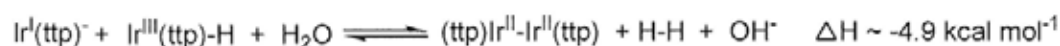
(D) Electron-transfer from Ir^I(ttp)$^-$ to HO$\cdot$

Ir^{II}(ttp) + e$^-$ $\rightleftharpoons$ Ir^I(ttp)$^-$ E_{red} ~ -1.7 V (CH$_2$Cl$_2$, vs SCE, [Ir^I(ttp)$^-$] = 1 mM) [54]

HO$\cdot$ + e$^-$ $\rightleftharpoons$ OH$^-$ E_{red} ~ +1.16 V (MeCN, vs SCE, [OH$^-$] ~ 4 mM) [55]

- -

Ir^I(ttp)$^-$ + HO$\cdot$ $\longrightarrow$ Ir^{II}(ttp) + OH$^-$ E_{Rxn} ~ +2.86 V

ΔH = -nFE

~ -(1)(96485)(2.86)

~ -276.0 kJ mol^{-1}

~ -66.0 kcal mol^{-1}

Ir^I(ttp)$^-$ + HO$\cdot$ $\longrightarrow$ Ir^{II}(ttp) + OH$^-$ ΔH = -66.0 kcal mol^{-1}

(E)   2Ir^{II}(ttp) $\longrightarrow$ (ttp)Ir^{II}-Ir^{II}(ttp) ΔH ~ -24 kcal mol^{-1} [47]
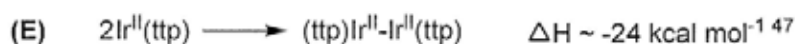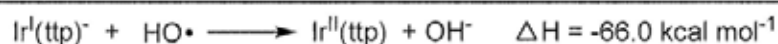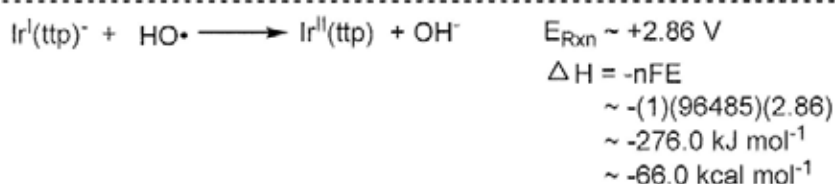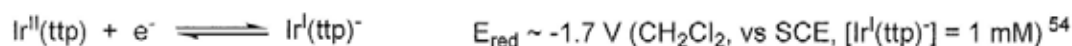
ΔG ~ ΔH = **(A)** + **(B)** + **(C)** + **(D)** + **(E)**

~ 70 + 119.3 + (-104.2) + (-66.0) + (-24)

~ -4.9 kcal mol^{-1}

2.4.3 Kinetics of Interconversions

The kinetics and rates of interconversions among Ir^{III}(ttp)H, [Ir^{II}(ttp)]$_2$, and Ir^I(ttp)$^-$ (Scheme 2.8) were then studied by reacting Ir^{III}(ttp)H in benzene-d_6 without and with bases at 200 °C in sealed NMR tubes.

It should be noted that the co-product, H$_2$ (δ(H$_2$) = 4.47 ppm),[56] could not be observed in benzene-d_6 at room temperature by ^{1}H NMR spectroscopy, as the solubility of H$_2$ in benzene-d_6 is very small under the vacuum atmosphere in sealed NMR tube. It is estimated that when all

$Ir^{III}(ttp)H$ was converted to $[Ir^{II}(ttp)]_2$ (100%) and H_2 (100%), only H_2 in 1% yield is dissolved in benzene-d_6, whereas H_2 in 99% yield is in gaseous phase (Refer to **Appendix I** for the calculation).[57] The incomplete conversion of $Ir^{III}(ttp)H$ to $[Ir^{II}(ttp)]_2$ (19-59% conversion in this studies, Tables 2.9-2.11) implies that the dissolved H_2 in benzene-d_6 is much less than 1%, which is out of the detection limit by ^1H NMR spectroscopy.

The effect of residual O_2 in degassed benzene-d_6 on the oxidation of $Ir^{III}(ttp)H$ to $[Ir^{II}(ttp)]_2$[58,59] was also studied. $Ir^{III}(ttp)H$ was dissolved in degassed benzene-d_6 and was then left at room temperature for 22 days (eq 2.37). A trace of $[Ir^{II}(ttp)]_2$ in 5% yield was observed. Thus, the maximal amount of $[Ir^{II}(ttp)]_2$ formed from the oxidation of $Ir^{III}(ttp)H$ with residual O_2 in degassed benzene-d_6 is assumed to be 5% yield.[60] The amount of $[Ir^{II}(ttp)]_2$ formed higher than 5% yield should come from the thermal and base-promoted dehydrogenative dimerization of $Ir^{III}(ttp)H$ (To be discussed in the following sections).

$$Ir^{III}(ttp)H \xrightarrow[\text{r.t., 22 d}]{C_6D_6} 1/2[Ir^{II}(ttp)]_2 + "1/2H_2" \quad (2.37)$$
$$\text{recovered} \qquad\qquad\qquad\quad 5\%$$
$$95\%$$
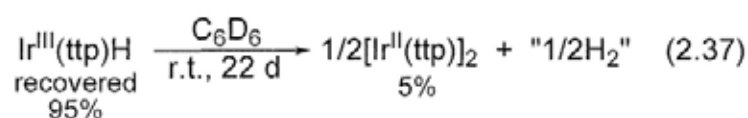
2.4.3.1 Thermal Conversion of $Ir^{III}(ttp)H$ to $[Ir^{II}(ttp)]_2$

The thermal reaction of $Ir^{III}(ttp)H$ in benzene-d_6 was monitored at 200 °C by ^1H NMR spectroscopy (Table 2.9; Figures 2.9(a),(b)). After 2 minutes, $Ir^{III}(ttp)H$ (δ(pyrrole H) = 8.81 ppm) was converted to $[Ir^{II}(ttp)]_2$ (δ(pyrrole H) = 8.33 ppm) in 19% yield (Table 2.9, entry 3) Thus, the thermal dehydrogenative dimerization of $Ir^{III}(ttp)H$ to $[Ir^{II}(ttp)]_2$ is established.

After 5 minutes, $Ir^{III}(ttp)H$ was further consumed, but the yield of $[Ir^{II}(ttp)]_2$ was decreased without the observation of $(H_2O)(ttp)Ir^{III}OIr^{III}(ttp)(OH_2)$ (δ(pyrrole H) = 8.36 ppm) (Table 2.9, entry 4), likely due to the thermal decomposition of $[Ir^{II}(ttp)]_2$ at 200 °C. Indeed, $[Ir^{II}(ttp)]_2$ was shown independently to excessively decompose in benzene-d_6 at 200 °C in 1 hour (eq 2.38).

$$[Ir^{II}(ttp)]_2 \xrightarrow[\text{200 °C, 1 h}]{C_6D_6} \text{decomp.} \quad (2.38)$$
$$\text{recovered}$$
$$26\%$$
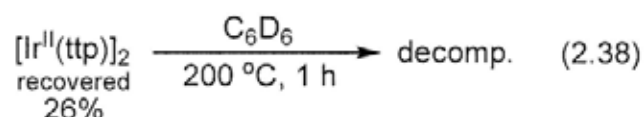
After 1.5 hours, all $[Ir^{II}(ttp)]_2$ was converted back to $Ir^{III}(ttp)H$, most likely by reacting with

the co-product of H_2 at 200 °C (Table 2.9, entries 4-6). Even though H_2 has a low solubility in

benzene-d_6, it is reasoned that the thermodynamically more favorable reaction of $[Ir^{II}(ttp)]_2$

with H_2 (eq 2.32) is much faster at 200 °C to give back $Ir^{III}(ttp)H$. The formation of $Ir^{III}(ttp)H$

was not attributed to the reaction of $[Ir^{II}(ttp)]_2$ with water, as $[Ir^{II}(ttp)]_2$ was shown to react very

slowly at 200 °C in 7 days to give $Ir^{III}(ttp)H$ in only 11% yield (eq 2.39).

$$[Ir^{II}(ttp)]_2 \xrightarrow[\substack{\text{recovered} \\ 0\%}]{\substack{H_2O \ (100 \ equiv) \\ C_6D_6, \ 200\ °C, \ 7\ d}} Ir^{III}(ttp)H \quad (2.39) \\ \text{11\%}$$
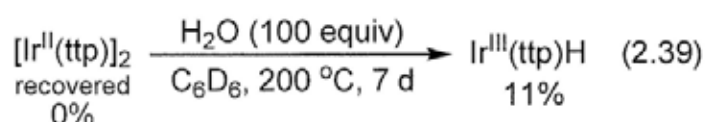
Table 2.9 Reaction Profile of Thermal Conversion of $Ir^{III}(ttp)H$ to $[Ir^{II}(ttp)]_2$
at 200 °C

$$Ir^{III}(ttp)H \xrightarrow[\substack{200\ °C, \ time}]{H_2O \ (\sim 1 \ equiv), \ C_6D_6} \tfrac{1}{2}[Ir^{II}(ttp)]_2 \ + \ "\tfrac{1}{2}H_2"$$
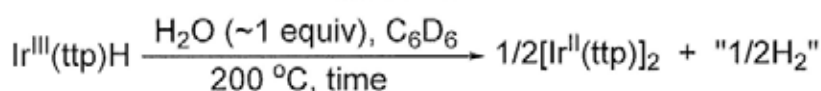
entry	time	$Ir^{III}(ttp)H/\%^a$	$1/2[Ir^{II}(ttp)]_2/\%^a$	total yield/$\%^a$
1	0	100	0	100
2	1 min	81	19	100
3	2 min	81	19	100
4	5 min	67	13	80
5	15 min	70	7	77
6	1.5 h	72	0	72
7	5.0 h	72	0	72
8	15 h	72	0	72

^{a} NMR yield.
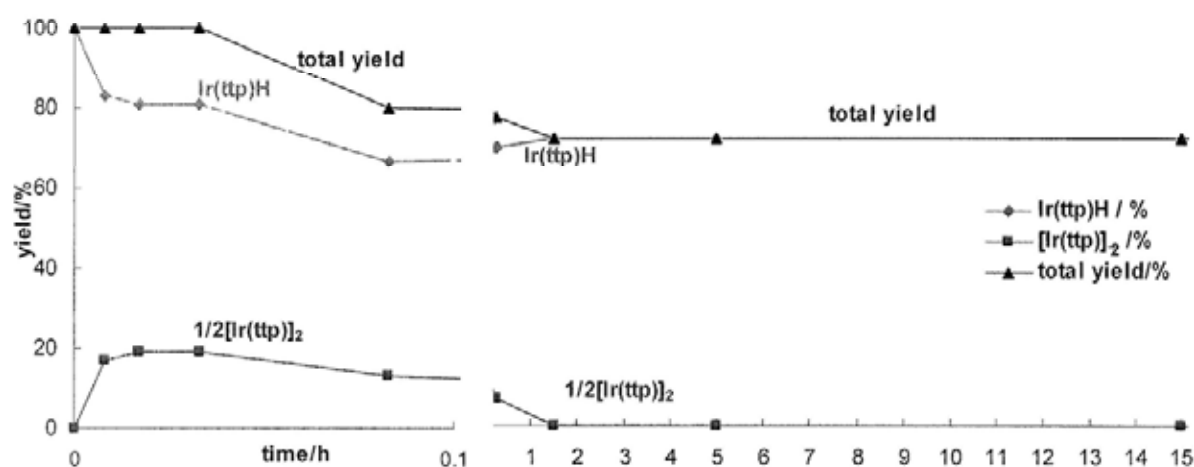
Figure 2.9(a) Time profile of thermal reaction of $Ir^{III}(ttp)H$ at 200 °C (Table 2.9).
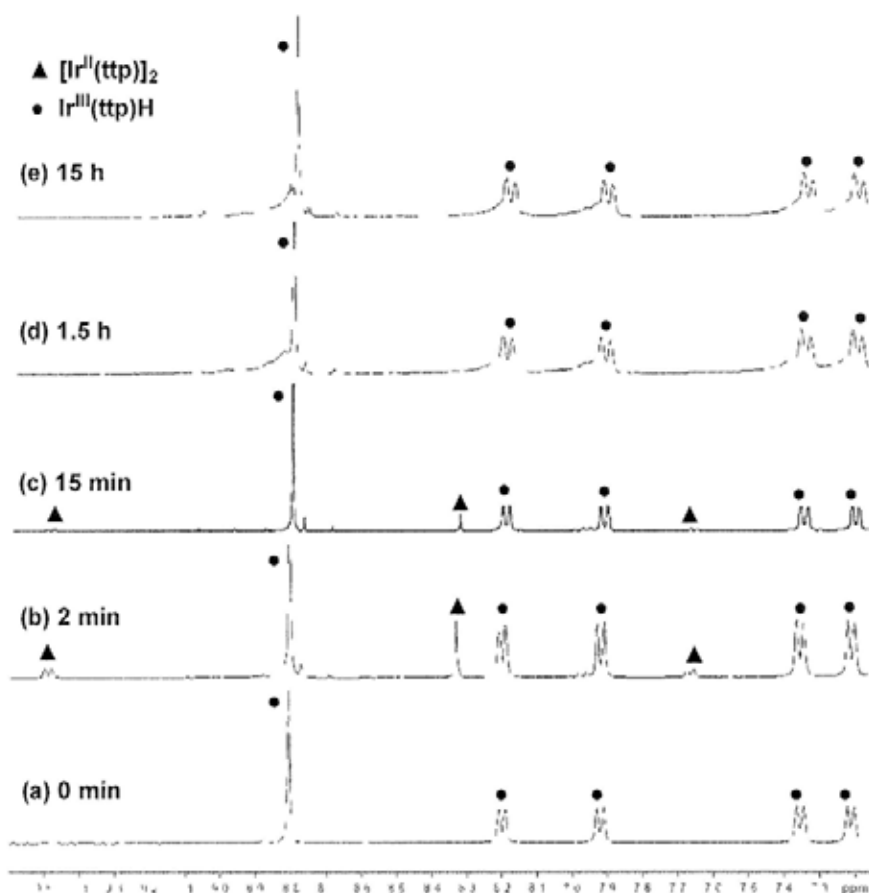
Figure 2.9(b) Partial ^{1}H NMR profile of thermal reaction of Ir^{III}(ttp)H at 200 ^{o}C (Table 2.9).

2.4.3.2 KOH-Promoted Conversion of Ir^{III}(ttp)H to [Ir^{II}(ttp)]$_2$

The reaction of Ir^{III}(ttp)H added with KOH was then monitored at 200 ^{o}C by ^{1}H NMR spectroscopy (Table 2.10; Figures 2.10(a),(b)). After 2 minutes, Ir^{III}(ttp)H (δ(pyrrole H) = 8.81 ppm) reacted with KOH to form [Ir^{II}(ttp)]$_2$ (δ(pyrrole H) 8.33 ppm) in 59% yield (Table 2.10, entry 2). Thus, the KOH-promoted dehydrogenative dimerization of Ir^{III}(ttp)H to [Ir^{II}(ttp)]$_2$ is established.

From 5 to 15 minutes, [Ir^{II}(ttp)]$_2$ was gradually converted back to Ir^{III}(ttp)H likely by reacting with H$_2$ formed (Table 2.10, entries 3 and 4). After 1 hour, a modest amount of Ir^{I}(ttp)$^-$K$^+$ (16%) with a characteristic upfield porphyrin's pyrrole proton signal (δ(pyrrole H) = 8.53 ppm)[16] was also formed via the deprotonation of Ir^{III}(ttp)H with OH$^-$ (Table 2.10, entry 5).

After 2 hours, all $Ir^I(ttp)^-K^+$ was converted back to $Ir^{III}(ttp)H$ via the protonation with residual water in benzene-d_6 (Table 2.10, entry 6), and $Ir^{III}(ttp)H$ was recovered in 74% yield. No $(H_2O)(ttp)Ir^{III}OIr^{III}(ttp)(OH_2)$ (δ(pyrrole H) = 8.36 ppm) was observed in the course of reaction.

Since a higher yield of $[Ir^{II}(ttp)]_2$ can be obtained from $Ir^{III}(ttp)H$ when KOH is added, the KOH-promoted dehydrogenative dimerization of $Ir^{III}(ttp)H$ (Table 2.10) is more efficient at 200 °C compared with the thermal conversion (Table 2.9).

Table 2.10 Reaction Profile of KOH-Promoted Conversion of $Ir^{III}(ttp)H$ to $[Ir^{II}(ttp)]_2$ at 200 °C

$$Ir^{III}(ttp)H \xrightarrow[\text{C}_6\text{D}_6, 200\ ^\circ\text{C, time}]{\substack{\text{KOH (20 equiv)}\\ \text{H}_2\text{O (\textasciitilde1.4 equiv)}}} 1/2[Ir^{II}(ttp)]_2 + Ir^I(ttp)^-K^+ + "1/2H_2"$$
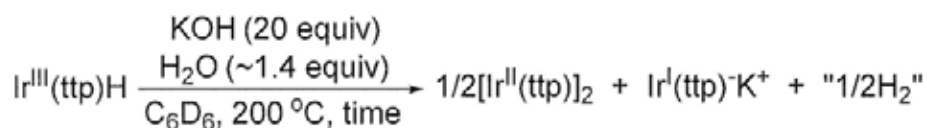
entry	time	$Ir^{III}(ttp)H/\%^a$	$1/2[Ir^{II}(ttp)]_2/\%^a$	$Ir^I(ttp)^-K^+/\%^a$	total yield/$\%^a$
1	0	100	0	0	0
2	2 min	36	59	0	95
3	5 min	46	47	0	93
4	15 min	53	39	0	92
5	1.0 h	56	0	16	72
6	2.0 h	74	0	0	74
7	6.0 h	65	0	0	65
8	14 h	65	0	0	65

^{a} NMR yield.
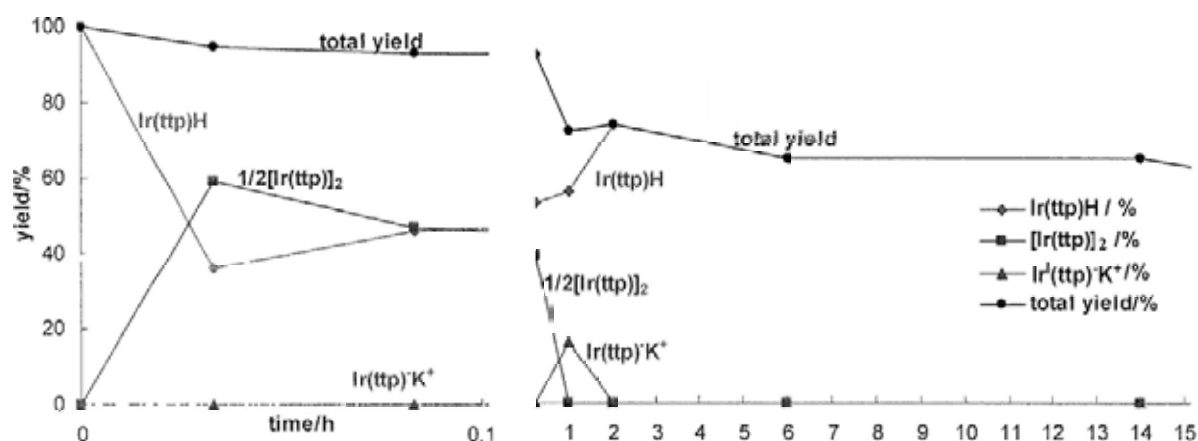
Figure 2.10(a) Time profile of reaction of $Ir^{III}(ttp)H$ with KOH in benzene-d_6 at 200 °C (Table 2.10).
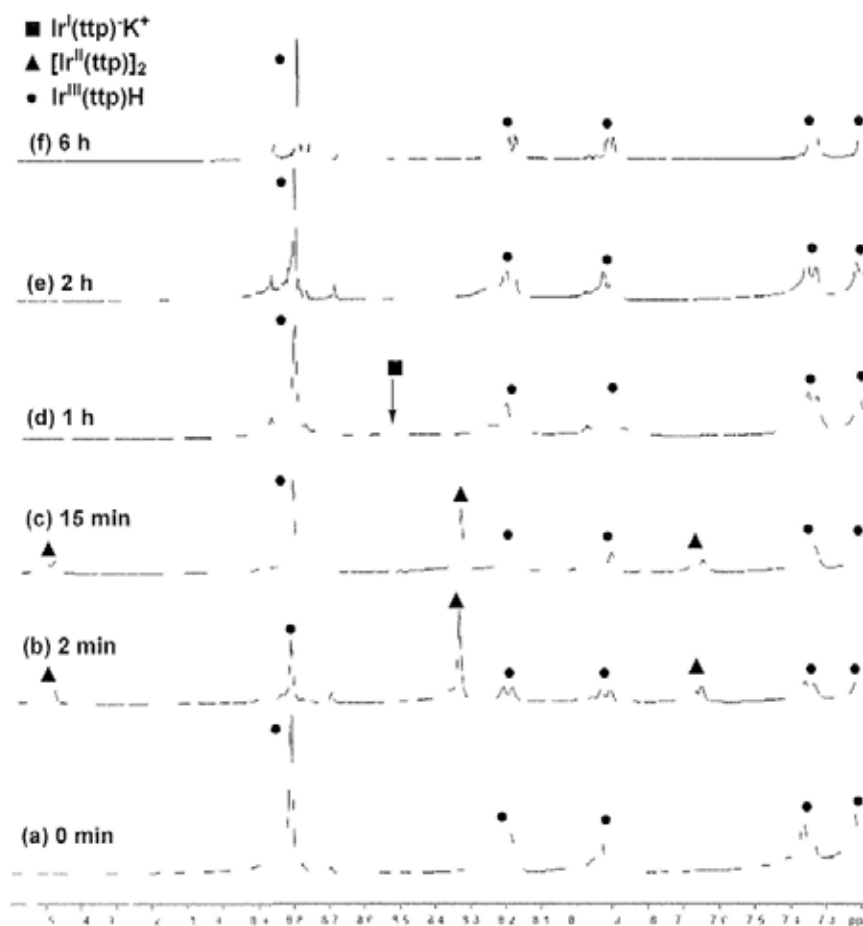
Figure 2.10(b) Partial ^{1}H NMR profile of reaction of Ir^{III}(ttp)H with KOH in benzene-d_6 at 200 °C (Table 2 10)

2.4.3.3 K$_2$CO$_3$-Promoted Conversion of Ir^{III}(ttp)H to [Ir^{II}(ttp)]$_2$

Since K$_2$CO$_3$ was used as an optimal base to promote the aryl C-X bond cleavages by Ir^{III}(ttp)(CO)Cl to form iridium porphyrin aryls via the formation of both Ir^{III}(ttp)H and [Ir^{II}(ttp)]$_2$ (To be discussed in details in Chapter 3), the effect of K$_2$CO$_3$ on the conversion of Ir^{III}(ttp)H to [Ir^{II}(ttp)]$_2$ was also studied

The reaction of Ir^{III}(ttp)H added with K$_2$CO$_3$ was monitored at 200 °C by ^{1}H NMR spectroscopy (Table 2 11, Figures 2 11(a),(b)) After 2 minutes, Ir^{III}(ttp)H (δ(pyrrole H) = 8 81 ppm) was converted to [Ir^{II}(ttp)]$_2$ (δ(pyrrole H) = 8.33 ppm) in 55% yield (Table 2.11, entry 3). Thus, the K$_2$CO$_3$-promoted dehydrogenative dimerization of Ir^{III}(ttp)H to [Ir(ttp)]$_2$ is

established.

From 15 minutes onwards, $[Ir^{II}(ttp)]_2$ gradually reacted with H_2 and converted back to $Ir^{III}(ttp)H$ (Table 2.11, entries 5-8). After 15 hours, $Ir^{III}(ttp)H$ was regenerated in 64% yield.

$Ir^{I}(ttp)^-$ (δ(pyrrole H) ~ 8.53 ppm)[16] was not observed in the course of reaction, probably due to the lower basicity of CO_3^{2-} (pK_a of $HCO_3^- = 10.33$ (in H_2O))[61] than OH^- (pK_a of $H_2O = 15.7$ (in H_2O)),[38] such that the concentration of $Ir^{I}(ttp)^-$ formed by the deprotonation of $Ir^{III}(ttp)H$ with CO_3^{2-} would be too low for observation.

Table 2.11 Reaction Profile of K_2CO_3-Promoted Conversion of $Ir^{III}(ttp)H$ to $[Ir^{II}(ttp)]_2$ at 200 °C

$$Ir^{III}(ttp)H \xrightarrow[C_6D_6,\ 200\,°C,\ time]{\substack{K_2CO_3\ (20\ equiv)\\ H_2O\ (\sim1.8\ equiv)}} 1/2[Ir^{II}(ttp)]_2 + \text{"}1/2H_2\text{"}$$
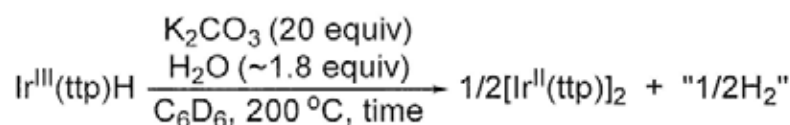
entry	time	$Ir^{III}(ttp)H/\%^a$	$1/2[Ir^{II}(ttp)]_2/\%^a$	total yield/$\%^a$
1	0	95	5^b	100
2	1 min	39	52	91
3	2 min	40	55	95
4	5 min	43	54	97
5	15 min	43	55	98
6	1.5 h	48	24	72
7	5.0 h	62	6	68
8	15 h	64	0	64

^{a} NMR yield. ^{b} The small amount of $[Ir^{II}(ttp)]_2$ formed at room temperature was likely due to the oxidation of $Ir^{III}(ttp)H$ with residual O_2 in degassed benzene-d_6.
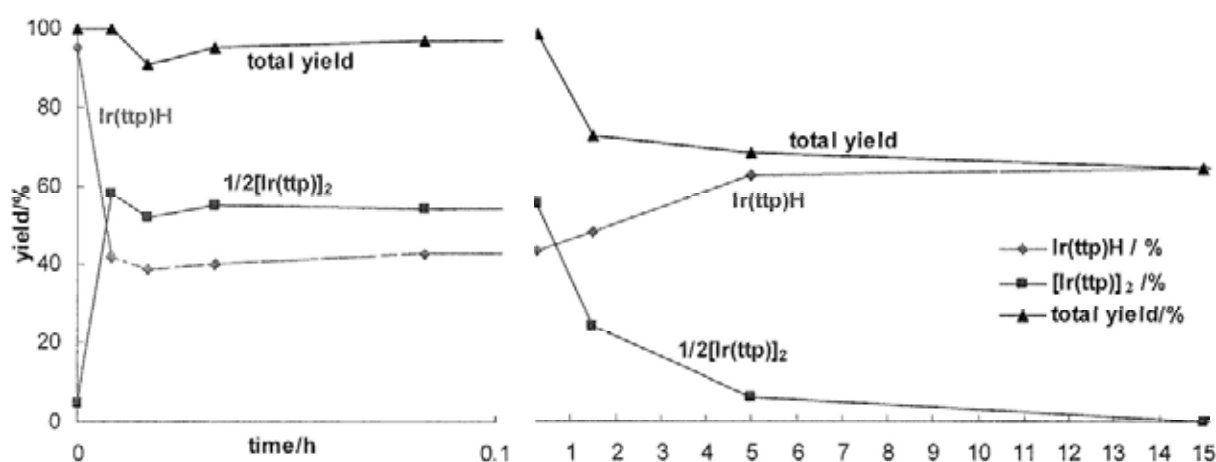
Figure 2.11(a) Time profile of reaction of $Ir^{III}(ttp)H$ with K_2CO_3 at 200 °C (Table 2.11).
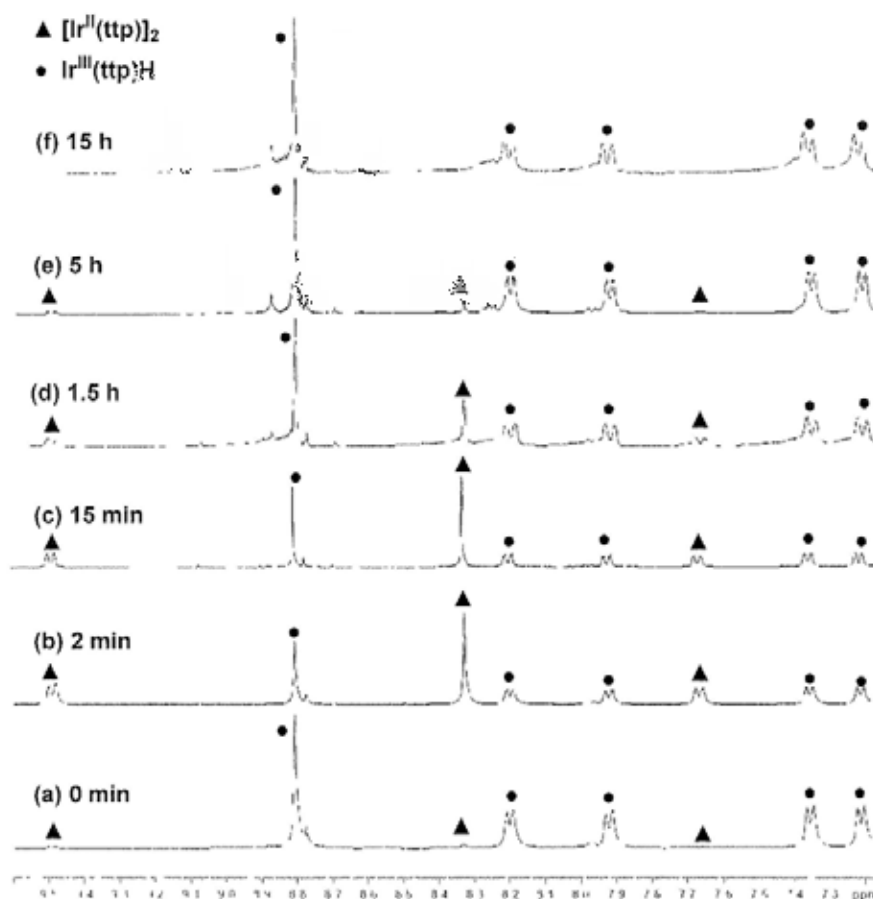
Figure 2.11(b) Partial ^{1}H NMR profile of reaction of Ir^{III}(ttp)H with K$_2$CO$_3$ at 200 ^{o}C (Table 2.11).

2.4.3.4 Rate Comparisons between Thermal and Base-Promoted Conversions of Ir^{III}(ttp)H to [Ir^{II}(ttp)]$_2$

To further support that the base-promoted dehydrogenative dimerization of Ir^{III}(tttp)H is more pronounced than the thermal one to generate [Ir^{II}(ttp)]$_2$ (Tables 2.9-2.11), the ratios of [Ir^{II}(ttp)]$_2$: Ir^{III}(ttp)H at fixed time intervals are compared. After 1 and 2 minutes, the [Ir^{II}(ttp)]$_2$: Ir^{III}(ttp)H ratios are much higher in the base-promoted reactions (Tables 2.12(B) and (C)) than the thermal reaction (Table 2.12(A)), showing that the base-promoted reactions is indeed more efficient than the thermal one. The rates of KOH- and K$_2$CO$_3$-promoted reactions are similar as shown by the similar [Ir^{II}(ttp)]$_2$: Ir^{III}(ttp)H ratios (Tables 2.12(B) and (C)).

Table 2.12 Ratio of [Ir^{II}(ttp)]$_2$: Ir^{III}(ttp)H during the Converison of Ir^{III}(ttp)H to [Ir^{II}(ttp)]$_2$ at 200 °C

		[Ir^{II}(ttp)]$_2$: Ir^{III}(ttp)H Ratio		
		(A)	(B)	(C)
entry	time/min	Themal Conversion (Table 2.9)	KOH-promoted conversion (Table 2.10)	K$_2$CO$_3$-promoted conversion (Table 2.11)
1	1	0.23	1.64	1.33
2	2	0.23	1.02	1.38

2.4.4 Mechanisms of Interconversions

Considering the estimated thermodynamics (Scheme 2.8; Table 2.8) and the results of the interconversions among Ir^{III}(ttp)H, [Ir^{II}(ttp)]$_2$, and Ir^{I}(ttp)$^-$ (Tables 2.9-2.11), Ir^{III}(ttp)H, [Ir^{II}(ttp)]$_2$, and Ir^{I}(ttp)$^-$ can exist in equilibria. The proposed mechanisms of thermal and base-promoted interconversions are summarized in the energetics as shown in Figure 2.12.
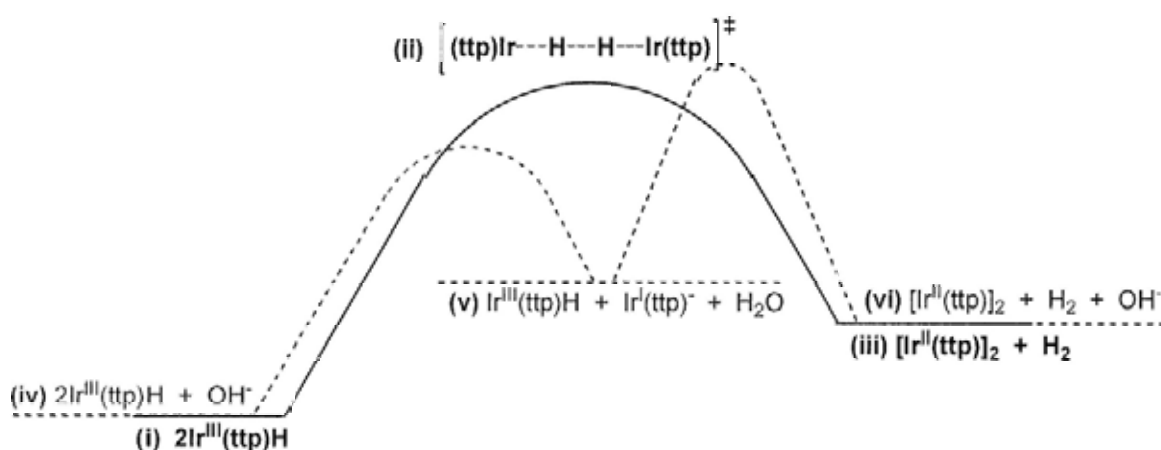
Figure 2.12 Energetics of interconversions among Ir^{III}(ttp)H, [Ir^{II}(ttp)]$_2$, and Ir^{I}(ttp)$^-$.

When no base is added (Table 2.9), Ir^{III}(ttp)H is slowly converted to [Ir^{II}(ttp)]$_2$ at 200 °C likely via a linear termolecular transiton state (Section 1.7.2.1, Scheme 1.21).[49,62] The dehydrogenative dimerization is thermally-promoted and entropically driven by the formation of H$_2$ (Figure 2.12, pathways (i)→(ii)→(iii)).

When KOH or K_2CO_3 is added (Table 2.10 and 2.11), $Ir^{III}(ttp)H$ can be deprotonated at 200 °C to form $Ir^I(ttp)^-$, which undergoes faster comproportionation with $Ir^{III}(ttp)H$ to form $[Ir^{II}(ttp)]_2$ and H_2 (Figure 2.12, pathways **(iv)→(v)→(vi)**; eq 2.34).

The backward hydrogenation of $[Ir^{II}(ttp)]_2$ with H_2 likely occurs simultaneously to give back $Ir^{III}(ttp)H$ via a linear termolecular transiton state (Figure 2.12, pathways **(iii)→(ii)→(i)**).[49,62]

2.5 Conclusions

The redox chemistry of $Ir^{III}(ttp)(L)X$ (L = nil, H_2O, PPh_3; X = SbF_6, Cl, Br, I) in basic benzene-d_6 solvent has been discovered, including: (i) the base-promoted reduction of $Ir^{III}(ttp)(L)X$ to form $Ir^{III}(ttp)(L)H$, and (ii) the interconversions among $Ir^{III}(ttp)H$, $[Ir^{II}(ttp)]_2$, and $Ir^I(ttp)^-$. Detailed mechanisms of these two redox chemistry have been studied.

In the base-promoted reduction of $Ir^{III}(ttp)(L)X$ to form $Ir^{III}(ttp)(L)H$, OH^- likely acts as an reducing agent to reduce Ir(III) to Ir(II) likely via a coordination-assisted inner-sphere electron-transfer, generating $Ir^{II}(ttp)(L)$ and H_2O_2. $Ir^{II}(ttp)(L)$ then activates water to produce $Ir^{III}(ttp)(L)H$ and $Ir^{III}(ttp)(L)OH$ via the OH^--promoted disproportionation of $Ir^{II}(ttp)(L)$. The formation of H_2O_2, and the conversion of $Ir^{II}(ttp)(L)$ intermediate to $Ir^{III}(ttp)(L)H$, are supported by the trapping of H_2O_2 with PPh_3 to form $P(O)Ph_3$, and the independent reaction of $[Ir^{II}(ttp)]_2$ / PPh_3 with KOH and residual water in benzene-d_6 to form $Ir^{III}(ttp)(PPh_3)H$, respectively. $Ir^{III}(ttp)(L)OH$ is recycled for further redox reactions to give $Ir^{III}(ttp)(L)H$.

In the interconversions among $Ir^{III}(ttp)H$, $[Ir^{II}(ttp)]_2$, and $Ir^I(ttp)^-$, $Ir^{III}(ttp)H$ can undergo slower thermal dehydrogenative dimerization and faster base-promoted dehydrogenative dimerization to form $[Ir^{II}(ttp)]_2$ at 200 °C. The thermal reaction of $Ir^{III}(ttp)H$ occurs via a linear termolecular transition state to yield $[Ir^{II}(ttp)]_2$, whereas the base-promoted dimerization occurs via the deprotonation of $Ir^{III}(ttp)H$ to form $Ir^I(ttp)^-$, which then reacts with $Ir^{III}(ttp)H$ and water

to give $[Ir^{II}(ttp)]_2$ and H_2. $[Ir^{II}(ttp)]_2$ likely further reacts with H_2 via a linear termolecular transition state to give back $Ir^{III}(ttp)H$. The reactions studies support that $Ir^{III}(ttp)H$, $[Ir^{II}(ttp)]_2$, and $Ir^{I}(ttp)^-$ can exist in equilibria.

References

(1) Fu, X.; Wayland, B. B. *J. Am. Chem. Soc.* **2004**, *126*, 2623-2631.

(2) Bhagan, S.; Sarkar, S.; Wayland, W. W. *Inorg Chem.* **2010**, *49*, 6734-6739.

(3) Kadish, K. M.; Smith, K. M.; Guilard, R. *The Porphyrin Handbook Volume 9*, Eds.; Academic Press: Boston, 2000.

(4) Choi, K. S. Unpublished Results, 2009.

(5) Wayland, B. B.; Ba, S.; Sherry, A. E. *J. Am. Chem. Soc.* **1991**, *113*, 5305-5311.

(6) Chan, K. S.; Leung, Y.-B. *Inorg. Chem.* **1994**, *33*, 3187.

(7) Cheung, C. W.; Chan, K. S. *Organometallics* **2008**, *27*, 3043–3055.

(8) Wagner, R. W.; Lawrence, D. S.; Lindsey, J. S. *Tetrahedron Lett.* **1987**, *28*, 3069-3070.

(9) van der Ent, A.; Onderdelinden, A. L. *Inorg. Synth.* **1973**, *14*, 92-95.

(10) (a) Ogoshi, H.; Setsune, J.-I.; Yoshida, Z.-I. *J. Organomet. Chem.* **1978**, *159*, 317–328.
   (b) Yeung, S. K.; Chan, K. S. *Organometallics* **2005**, *24*, 6426-6430.

(11) The experimental procedure for the synthesis of $Ir^{III}(ttp)BF_4$ was adopted to prepare $Ir^{III}(ttp)SbF_6$. See: Song, X.; Chan, K. S. *Organometallics* **2007**, *26*, 965-970.

(12) Cheung, C. W.; Fung, H. S.; Lee, S. Y.; Qian, Y. Y.; Chan, Y. W.; Chan, K. S. *Organometallics* **2010**, *29*, 1343–1354.

(13) The ratio of $Ir^{III}(ttp)SbF_6$: $[Ir^{III}(ttp)(CO)]SbF_6$ in the product mixture of $Ir^{III}(ttp)SbF_6$ and $[Ir^{III}(ttp)(CO)]SbF_6$ was estimated by ^1H NMR spectroscopy in $CDCl_3$. The ratio varied in each time of the preparation with the ratio changing from 2.6 : 1 to 3.4 : 1.

(14)   The solubility of NaOH in toluene at 25 °C has been reported to be approximately 9 mM. It is assumed that the solubility of KOH in benzene at 25 °C is also about 9 mM. See: Hradil, J.; Švec, F. *Polym. Bull.* **1983**, *10*, 14-20.

(15)   A trace of residual water ($\delta(H_2O) \sim 0.4$ ppm) was always present in benzene-d_6, even though benzene-d_6 has been distilled over sodium and stored in a Telfon-screwed capped tube under N_2. The bases, the iridium porphyrin species, and other reagents may also contain a trace of water even though they have been dried under vacuum in Teflon screw capped tubes or NMR tubes prior to the reactions. Adventitious water might also be introduced during setting up the reactions. The amount of water in benzene-d_6 ($\sim$0.2-2 equiv with reference to iridium porphyrin species, or $\sim$2-20 mM) is estimated by ^{1}H NMR spectroscopy. The maximal solubility of water in benzene at 25 °C is 36 mM, see: Karlsson, R. *J. Chem. Eng. Data* **1973**, *18*, 290-292.

(16)   The chemical shift of porphyrin's pyrrole proton of $Ir^I(ttp)^-[K(18\text{-crown-}6)]^+$ in benzene-d_6 was 8.58 ppm when the concentration is 0.009 M (See Experimental Section for the preparation of $Ir^I(ttp)^-[K(18\text{-crown-}6)]^+$). The chemical shift of $Ir^I(ttp)^-K^+$ may deviate from that of $Ir^I(ttp)^-[K(18\text{-crown-}6)]^+$ due to the difference in the concentration of $Ir^I(ttp)^-K^+$ and the nature of counter cation.

(17)   Chan, K. S.; Lau, C. M.; Yeung, S. K.; Lai, T. Z. *Organometallics* **2007**, *26*, 1981-1985.

(18) $Ir^{II}(ttipp)$ (ttipp = tetrakis(2,4,6-triisopropylphenyl)porphyrin) is reported to coordinate with π-donating ethylene (C_2H_4) to form iridium(III) porphyrin-centered radical, $Ir^{III}(ttipp)^{\cdot-}$. See: Cui, W.; Li, S.; Wayland, B. B. *J. Organomet. Chem.* **2007**, *629*, 3198–3206. It is assumed that the more electrophilic $Ir^{III}(ttp)OH$ can also coordinate with ethylene to form $(C_2H_4)Ir^{III}(ttp)OH$.

(19)   Water likely binds strongly to iridium porphyrin due to the formation of stronger Ir-O bonds, compared with the Rh-O and Co-O bonds (Ref 2).

(20) μ-Oxo iron(III) porphyrin dimer $((por)Fe^{III}OFe^{III}(por))$ has an upfield pyrrole proton

signal in ^{1}H NMR spectroscopy when compared with $Fe^{III}(por)OH$. An example is $[Fe^{III}(t-3,4,5-tmpp)]_2O$ (t-3,4,5-tmpp = tetrakis(3,4,5-trimethoxyphenyl)porphyrin) (δ(pyrrole H) = 13.7 ppm) and $Fe^{III}(t-3,4,5-tmpp)OH$ (δ(pyrrole H) = 80.2). See: Cheng, R.-J.; Latos-Grazynski, L.; Balch, A. L. *Inorg. Chem.* **1982**, *21*, 2412-2418. Similarly, $(H_2O)(ttp)Ir^{III}OIr^{III}(ttp)(OH_2)$ has a more upfield porphyrin's pyrrole proton signal in benzene-d_6 (δ(pyrrole H) = 8.36 ppm), whereas the monomeric iridium(III) porphyrin complexes have more downfield porphyrin's pyrrole proton signals in benzene-d_6 (e.g. $Ir^{III}(ttp)(PPh_3)OH$: δ(pyrrole H) = 8.80 ppm; $Ir^{III}(ttp)H$: δ(pyrrole H) = 8.81 ppm).

(21) Iridium(III) alkoxo and hydroxo complexes have been reported to become more air- and thermally-stable by coordinating with strong σ-donating pyridine ligand to form coordinatively saturated complexes: (a) Tenn, W. J., III; Young, K. J. H.; Bhalla, G.; Oxgaard, J.; Goddard, W. A., III; Periana, R. A. *J. Am. Chem. Soc.* **2005**, *127*, 14172-14173. (b) Tenn, W. J.; III; Young, K. J. H.; Oxgaard, J.; Nielsen, R. J.; William A. Goddard, W. A., III; Periana, R. A. *Organometallics* **2006**, *25*, 5173-5175.

(22) $Ir^{III}(ttp)OH$ prepared from the reaction of $Ir^{III}(ttp)SbF_6$ with CsOH was very unstable in benzene-d_6 at room temperature under air and decomposed to form an unknown brown precipitate. On the other hand, both $Ir^{III}(ttp)(PPh_3)OH$ and $Ir^{III}(ttp)(py)OH$ were more stable in benzene-d_6 and $CDCl_3$, respectively, at room temperature under air and did not decompose in 12 hours, since the upfield Ir-coordinated hydroxo's proton signals were still observed.

(23) The chemical shift of hydride ligand in $Ir^{III}(oep)(PPh_3)H$ (oep = octaethylporphyrin) (δ(Ir-H) -32.95 ppm) and its coupling constant (^2J(P-Ir-H) = 259 Hz) have been reported and are very similar to that of $Ir^{III}(ttp)(PPh_3)H$. See: Farnos, M. D.; Woods, B. A.; Wayland, B. B. *J. Am. Chem. Soc.* **1986**, *108*, 2659-3663.

(24) The C-H bond activation of benzene by $Ir^{III}(acac)_2OH$ to give $Ir^{III}(acac)_2Ph$ and H_2O has been reported. (Ref 21b).

(25) For the example of the α-H elimination of transition-metal-hydroxo complexes, see: Tahmassebi, S. K.; Conry, R. R.; Mayer, J. M. *J. Am. Chem. Soc.* **1993**, *115*, 7553-7554.

(26) For the example of the transition-metal-catalyzed water-gas-shift reaction, see: Badger, R. C.; D'Acchioli, J. S.; Oudenhoven, T. A.; Walder, B. J. *Organometallics* **2010**, *29*, 1061-1063.

(27) Wayland, B. B.; Woods, B. A.; Pierce, R. *J. Am. Chem. Soc.* **1982**, *104*, 302-303.

(28) For the example of the reduction of metal centres by hydroxo ligands in metalloporphyrin-hydroxo complexes, see: Shin, K.; Kramer, S. K.; Goff, H. M. *Inorg. Chem.* **1987**, *26*, 4103-4106.

(29) Sawyer, D. T.; Roberts, J. L. *Acc. Chem. Res.* **1988**, *21*, 469-476.

(30) For conventional use, the E_{ox} value reported in the literatures were indeed the E_{red} values of the reduction half-equations. For example, for the reduction half-equation: $A + e^- \rightarrow A^-$ with a E_{red} value, the E_{red} value is directly adopted as the E_{ox} value in the oxidation half-equation: $A^- \rightarrow A + e^-$, without changing the opposite sign (i.e. $E_{ox} = -E_{red}$).

(31) The oxidation potential (E_{ox}) of $OH^- \rightarrow HO\bullet + e^-$ in DMSO containing diluted OH^- in 0.0043 M at 24 °C was measured to be +0.75 V. See: Goolsby, A. D.; Sawyer, D. T. *Anal. Chem.* **1968**, *40*, 83-86.

(32) The concentration of KOH in saturated KOH / DMSO solution at 25 °C is reported to be 0.037 M. The concentration of KOH in DMSO does not change upon an increase in temperature when no water is present. See: Trofimov, B. A.; Vasiltsov, A. M.; Amosova, S. V. *Russ. Chem. Bull.* **1986**, *35*, 682-686.

(33) Arasasingham, R. D.; Bruice, T. C. *Inorg. Chem.* **1990**, *29*, 1422-1427.

(34) The rates of inner-sphere electron transfer from N_4-tetradentated Co^{II} complexes (($Co^{II}N_4)^{2-}$) to $[Co^{III}(H_2O)_5Cl]^{2+}$ are much faster than the rates of outer-sphere electron transfer from ($Co^{II}N_4)^{2-}$ to $[Co^{III}(H_2O)_6]^{3+}$ by a factor of 10^4 to 10^6. See: Rotzinger, F. P.; Kumar, K.; Endicott, J. F. *Inorg. Chem.* **1982**, *21*, 4111-4112.

(35) OH⁻ can rapidly catalyze the disproportionation of H_2O_2 in aqueous solution to give H_2O and O_2. See: Roberts, J. L., Jr.; Sugimoto, H.; Barrette, W. C., Jr.; Sawyer, D. T. *J. Am. Chem. Soc.* **1985**, *107*, 4556-4557.

(36) In high concentration of MeOH in benzene, it is proposed that Rh^{II}(tmp) coordinates with MeOH to promote the disproportionation to give $[Rh^{III}(tmp)(MeOH)_2]^+$ and Rh^{I}(tmp)⁻, which further reacts to give Rh^{III}(tmp)OMe(MeOH) and Rh^{III}(tmp)H. See: Li, S.; Cui, W.; Wayland, B. B. *Chem. Commun.* **2007**, 4024-4025. It is assumed that Ir^{II}(ttp) can also coordinate with OH⁻ to promote the disproportionation to give Ir^{III}(ttp)OH and Ir^{I}(ttp)⁻ for subsequent formation of Ir^{III}(ttp)H.

(37) $[Rh^{II}(oep)]_2$ coordinates with pyridine to undergo disproportionation to form $[Rh^{III}(oep)(py)_2]^+$ and Rh^{I}(oep)⁻. See: (a) Wayland, B. B.; Balkus, K. J., Jr.; Farnos, M. D. *Organometallics* **1989**, *8*, 950-955. (b) Wayland, B. B.; Sherry, A. E.; Bunn, A. G. *J. Am. Chem. Soc.* **1993**, *115*, 7675-7684.

(38) Ir^{III}(oep)H remains undissolved and unreacted in NaOH / ethanol solution. It is proposed that the pK_a of Ir^{III}(oep)-H is higher than H_2O (pK_a(Ir^{III}(oep)-H) > pK_a(H_2O) = 15.7 (in H_2O)). Thus, the protonation of the conjugated base, Ir^{I}(oep)⁻, with water becomes very favorable to give Ir^{III}(oep)H (Ref 10(a)). It is likely that the analogous Ir^{I}(ttp)⁻ is a strong base to be rapidly protonated by water to form Ir^{III}(ttp)H. For the pK_a value of H_2O (15.7), see: Lide, D. R., Ed. *CRC Handbook of Chemistry and Physics*, 85th ed; CRC Press: Cleveland, OH, 2004.

(39) When PPh₃ containing KOH (20 quiv) was added with 30% H_2O_2 solution (2 equiv H_2O_2) in benzene at room temperature, gas bubble, which was likely O_2, was evolved. Further heating the reaction mixture at 200 °C in 1 hour only led to the formation of a trace of P(O)Ph₃ in 2% yield and unreacted PPh₃ in 80% yield. Likely, OH⁻ dissolves into the H_2O_2 solution to catalyze the disproportionation of H_2O_2 to O_2 and H_2O, prior to the oxidation of PPh₃ by H_2O_2 to form P(O)Ph₃.

(40) (a) H_2O_2 is a common oxidant in the oxidization of PPh_3 to $P(O)Ph_3$. For example, see: Abu-Omar, M. M.; Espenson, J. H. *J. Am. Chem. Soc.* **1995**, *117*, 272-280. (b) PPh_3 has been used as a H_2O_2 trap in the single electron reduction of Mo(VI) and W(VI) complexes by OH^-. See: Cervilla, A. C.; Pérez-Plá, F.; Llopis, E.; Piles, M. *Dalton Trans.* **2004**, 1461-1465.

(41) Activation of D_2O by water-soluble $[Rh^{II}(tmps)(H_2O)_2]^{4-}$ radical (tmps = tetrakis(3,5-bis(sulfonato)mesityl)porphyrin) to form $[Rh^{III}(tmps)(D)(D_2O)]^{4-}$ and $[Rh^{III}(tmps)(OD)(D_2O)]^{4-}$ in an 1 : 1 ratio has been reported. See: Fu, X.; Li, S. Wayland, B. B. *Inorg. Chem.* **2006**, *45*, 9884-9889.

(42) The basicities of 4-substituted pyridines in the protonation to form pyridinium ion were determined theoretically to increase with the decrease of the solvent polarities due to the reduction of stabilization by solvation. Therefore, the basicity of 4-methylpyridine is highest in non-polar cyclohexane, followed by less polar CH_2Cl_2, and then the most polar MeCN. See: Lee, I.; Kim, C. K.; Han, I. S.; Lee, H. W.; Kim, W. K.; Kim, Y. B.; *J. Phys. Chem. B* **1999**, *103,* 7302-7307.

(43) The rates of bimolecular nucleophilic substitution (S_N2) of benzyl chloride by various nucleophilic carbon and nitrogen bases (C^-, N^-) in DMSO at 25 $^\circ$C increase when the pK_a of the conjugated acids (C-H, N-H) increase. Selected pK_a values of C-H and N-H and the corresponding rate constants (k) are shown: (1) $pK_a(Me(CN)_2C\text{-}H) = 12.5$, $k = 15.2$ M^{-1} s^{-1}; $pK_a(p\text{-}ClC_6H_4(Me)(CN)C\text{-}H) = 21.7$, $k = 1.24 \times 10^4$ M^{-1} s^{-1}; (2) $pK_a(Ph(PhCO)N\text{-}H) = 18.8$, $k = 3.19 \times 10^{-3}$ M^{-1} s^{-1}; $pK_a(Ph(Ac)N\text{-}H) = 21.5$, $k = 0.101$ M^{-1} s^{-1}. Therefore, the rate of substitution reactions can be increased by using the stronger bases (B^-) with higher pK_a values of BH. See: Bordwell, F. G.; Hughes, D. L. *J. Org. Chem.* **1983**, 48, 2206–2215. (b) Bordwell, F. G.; Hughes, D. L. *J. Am. Chem. Soc.* **1984**, *106*, 3234–3240.

(44) The BDEs of Ir^{III}-X bonds (X = Cl, Br, I) from $Cp*(PMe_3)Ir^{III}X_2$ are used for the

comparison of Ir^{III}-X bond strengths. See: Stoutland, P. O.; Newman, L. J.; Buchanan, J. M.; Bergman, R. G. *J. Am. Chem. Soc.* **1987**, *109*, 3143-3145.

(45) Hartwig, J. F. *Organotransition Metal Chemistry: From Bonding to Catalysis*; Sausalito, CA: University Science Books, 2010.

(46) The associative ligand substitution of $[Pt^{II}(dien)X]^+$ (dien = diethylenetriamine) with pyridine (py) to give $[Pt^{II}(dien)(py)]^{2+}$ was in the reactivity trend: Pt-Cl > Pt-Br > Pt-I. See: (a) Basolo, F.; Gray, H. B.; Pearson, R. G. *J. Am. Chem. Soc.* **1960**, *82*, 4200-4203. (b) Gray, H. B.; Olcott, R. J. *Inorg. Chem.* **1962**, *1*, 481-485.

(47) The BDE of Ir-Ir bond in $[Ir^{II}(ttp)]_2$ is estimated to be ~24 kcal mol^{-1} using the reported BDE of Ir-Ir bond in $[Ir^{II}(oep)]_2$. (Ref 18).

(48) The equilibrium constant K for the homolysis of $[Ir^{II}(ttp)]_2$ to form 2 $Ir^{II}(ttp)$ monomer in benzene-d_6 at room temperature can be estimated by using the expression $\Delta G = -RT\ln K$ (where $\Delta G \sim$ BDE of Ir-Ir in $[Ir^{II}(ttp)]_2$ (~24 kcal mol^{-1} = 24 x 4.184 x 1000 J mol^{-1} = 100416 J mol^{-1}), R = 8.314 J K^{-1} mol^{-1}, T = 298 K. K is estimated to be 2.5 x 10^{-18} M, implying that the concentration of $Ir^{II}(ttp)$ in benzene-d_6 is extremely low at room temperature.

(49) Del Rossi, K. J.; Wayland, B. B. *J. Chem. Soc. Chem. Commun.* **1986**, 1963-1965.

(50) The comproportionation between M(I) and M(III) to from M(II) dimer has been reported in group 9 macrocyclic complexes. (a) Rhodium system: Ref 1. (b) Cobalt system: Kaufmann, E. J.; Espenson, J. H. *J. Am. Chem. Soc.* **1977**, *99*, 7051-7054.

(51) The BDE of Ir-H bond of $Ir^{III}(oep)H$ is around 70 kcal mol^{-1}. It is assumed that the BDE of $Ir^{III}(ttp)$-H is similar to that of $Ir^{III}(oep)H$: Wayland, B. B. University of Pennsylvania, Philadelphia, PA. Personal communication, 2007.

(52) For the reported values of BDEs of HO-H (119.3 kcal mol^{-1}) and H-H (104.2 kcal mol^{-1}), see: Luo, Y.-R. *Comprehensive Handbook of Chemical Bond Energies*; CRC Press: Boca Raton, FL, 2007.

(53)   (a) For the entropy of formation of H_2 at 500 K (145.7 J mol^{-1} K^{-1}), see: Lide, D. R., Ed. *CRC Handbook of Chemistry and Physics*, 85th ed; CRC Press: Cleveland, OH, 2004. (b) For the translational entropy decrease of 1 mole at 25 °C (-10 kcal mol^{-1}), see: Page, M. I. *Angew. Chem. Int. Ed.* **1977**, *16*, 449-459.

(54)   The second reduction potentials of Ir^{III}(tpp)(CO)Cl (tpp = tetraphenylporphyrin) (1mM) (i.e. Ir^{II}(tpp) + e$^-$ → Ir^{I}((tpp)$^-$) in CH_2Cl_2 at 25 °C ($E_{red(2nd)}$ = -1.7 V vs SCE) is reported. It is assumed that Ir^{III}(ttp)(CO)Cl has the similar $E_{red(2nd)}$ value. See: (a) Swistak, C.; Cornillon, J. L.; Anderson, J. E.; Kadish, K. M. *Organometallics* **1987**, *6*, 2146-2150. (b) Ref 3.

(55)   The irreversible oxidation potential (E_{ox}) of the oxidation half-reaction OH$^-$ → HO• + e$^-$ ([OH$^-$] ~ 4 mM) in MeCN is +0.92 V vs NHE and +1.16 V vs SCE (estimated by adding 0.24 V to the E value vs NHE) (Ref 29). In order to estimate the redox reaction between Ir^{I}(ttp)$^-$ and HO•, the reversible reduction of HO• to OH$^-$ is assumed to take place with the reduction half-equation: HO• + e$^-$ → HO$^-$ (E_{red} = +1.16 V). The concentration of OH$^-$ in MeCN is ~4 mM for the measurement of the oxidation potential. See: Tsang, P. K. S.; Cofre, P.; Sawyer, D. T. *Inorg. Chem.* **1987**, 26, 3604-3609.

(56)   Fulmer, G. R.; Miller, A. J. M.; Sherden, N. H.; Gottlieb, H. E.; Nudelman, A.; Stoltz, B. M.; Bercaw, J. E.; Goldberg, K. I. *Organometallics* **2010**, *29*, 2176–2179.

(57)   The equation for the calculation of H_2 concentration in benzene as a function of temperature and H_2 pressure has been reported and is applied for estimation of the solubility of H_2 in benzene-d_6. See: Wayland, B. B; Ba, S.; Sherry, A. E. *Inorg. Chem.* **1992**, *31*, 148-150.

(58)   Electrochemical oxidation of Ir^{III}(oep)H (oep = octaethylporphyrin) with O_2 to give [Ir^{II}(oep)]$_2$ is reported. See: (a) Collman, J. P.; Kim, K. *J. Am. Chem. Soc.* **1986**, *108*, 7847-7849. (b) Collman, J. P.; Chng, L. L.; Tyvoll, D. A. *Inorg. Chem.* **1995**, *34*, 1311-1324.

(59)   The aerobic oxidation of $Rh^{III}(tpp)H$ (tpp = tetraphenylporphyrin) to form $[Rh^{II}(tpp)]_2$ is reported. See: Collman, J. P.; Boulatov, R. *Inorg. Chem.* **2001**, *40*, 2461-2464.

(60) $Ir^{III}(ttp)H$ probably does not undergo the dehydrogenative dimerization at room temperature to form $[Ir^{II}(ttp)]_2$, since no $[Ir^{II}(ttp)]_2$ was observed in the base-promoted reductions of $Ir^{III}(ttp)(CO)Cl$ and $Ir^{III}(ttp)SbF_6$ to form $Ir^{III}(ttp)H$ at room temperature (Table 2.1, entry 3; eq 2.14).

(61)   For the pK_a value of HCO_3^-, see: *http://www.chem.wisc.edu/areas/reich/pkatable/index.htm.* Accessed on 8th June, 2010.

(62)   Termolecular transition states have been proposed in rhodium(II) porphyrin systems via the kinetic studies. See: (a) Sherry, A. E.; Wayland, B. B. *J. Am. Chem. Soc.* **1990**, *112*, 1259-1261. (b) Ref 5.

Chapter 3 Base-Promoted Aryl Carbon-Halogen Bond Cleavages by Iridium(III) Porphyrins

3.1 Introduction

3.1.1 General Introduction

3.1.1.1 Definition of Aryl Carbon-Halogen Bond Cleavages by Transition Metals

Aryl carbon-halogen bond (Ar-X, X = F, Cl, Br, I) cleavages by transition metals can be defined as the reactions of Ar-X bonds with the transition metal complexes to form metal-aryl-halide complexes (Scheme 3.1, pathway i), metal-aryl complexes and halide ions (pathway ii), or both metal-aryl and metal-halide complexes (pathway iii), with the concomitant increase in the oxidation states of transition metals by +1 or +2.

Scheme 3.1 Possible Products Formed from Aryl C-X Bond Cleavages by Transition Metal Complexes

3.1.1.2 Physical Properties of Aryl Halides

(i) Polarities of Aryl-Halogen Bonds

The electronegativities of the atoms in halobenzenes (PhX) are shown in Table 3.1.[1] The halogen atoms (X = F, Cl, Br, I) (Table 3.1, entries 3-6) are generally more electronegative than H and C (Table 3,1, entries 1-2), whereas H and C have similar electronegativities. Thus, C-X bonds are generally more polar than C-H bonds via the inductive effect of X ($-I_\sigma$). In C-X

bonds, the electronegativities of X are in the order: F > Cl > Br > I. The polarity of Ph-X bond

and the electrophilicity of the X-bound carbon is thus in the order: C-F > C-Cl > C-Br > C-I.

Table 3.1 Pauling Electronegativities of Halogen Atoms in Halobenzenes

Entry	Atoms in Ph-X	Pauling Electronegativity[1]
1	H	2.20
2	C	2.55
3	F	3.98
4	Cl	3.16
5	Br	2.96
6	I	2.66

(ii) Bond Dissociation Energies of Aryl Halides

The bond dissociation energies (BDEs) of aryl C-H and C-X bonds (Ar-H and Ar-X) in

various aryl halides (ArX) are shown in Table 3.2.[2,3] The BDEs of Ar-X decrease down the

group and are in the order: Ar-F > Ar-Cl > Ar-Br > Ar-I (Table 3.2, enties 1-9). The electronic

effect of functional groups (FG) in ArX does not significantly affect the BDEs of Ar-X. The

BDEs of Ar-X in *para-* and *meta-*substituted ArX are very similar, but the BDE of Ar-X in

*ortho-*substituted ArX are weaker by about 1.4 kcal mol^{-1} due to the steric strain (Table 3.2, FG

= C(O)Me: entries 2, 5, and 8; entries 3, 6, and 9).[4] The corresponding C-X bonds in

2-halo-naphthalenes are weaker than Ph-X bond by about 2.6 kcal mol^{-1} (Table 3.2, entries 10

and 11).[2]

In ArX (X = Cl, Br, I), the Ar-H bonds are generally within 110-114 kcal mol^{-1},[3] which are

stronger than the Ar-X bonds (X = Cl, Br, I) (Table 3.2, entries 2-4). Therefore, the cleavages

of Ar-X bonds are generally kinetically and thermodynamically more favorable than the

cleavages of Ar-H bonds (To be discussed in details in Section 3.1.6). On the other hand, in ArF,

the Ar-F bond is stronger than the Ar-H bond by around 12-16 kcal mol^{-1} (Table 3.2, entry 1),

such that Ar-H bond cleavage is generally a kinetic pathway.[5] Moreover, the formations of

more stable transition-metal-fluoroaryl complexes (M-Ar^F) via Ar^F-H cleavages result in the

thermodynamic Ar^F-H cleavages.[6] However, depending on the natures of the transition metals

and the reaction conditions, Ar-F bond cleavages by transition metals can also take place.

Table 3.2 Bond Dissociation Energies (BDEs, in kcal mol^{-1}) of Aryl C-X Bonds[2]

| entry | X | para-FG | | | | |
		H	C(O)Me	CO$_2$Et	CN	NO$_2$
1	F[3]	125.6				
2	Cl	95.6	95.6	96.3	95.4	95.8
3	Br	80.5	80.3	81.0	80.1	80.1
4	I	65.5	65.5	65.2	65.5	65.5
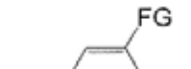
| entry | X | meta-FG | | | | |
		H	C(O)Me	CO$_2$Et	CN	NO$_2$
5	Cl	95.6	95.4			
6	Br	80.5	80.5			
7	I	65.5	65.5			
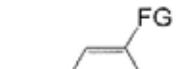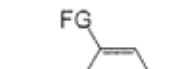
| entry | X | ortho-FG | | | | |
		H	C(O)Me	CO$_2$Et	CN	NO$_2$
8	Cl	95.6	94.2			
9	Br	80.5	79.1			
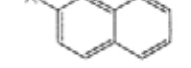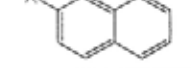
entry	X	H
10	Cl	93.0
11	Br	77.9

3.1.1.3 Applications of Aryl C-X Cleavages

(i) Carbon-Carbon and Carbon-Heteroatom Bond Forming Reactions

Aryl halides have been extensively utilized for various aryl-carbon and aryl-heteroatom bond forming reactions (e.g. C-N, C-P, C-O, C-S) (Scheme 3.2, pathways i-iii) which are applied in pharmaceutical industries, optoelectronics, and polymer sciences.[7]

Scheme 3.2 Bond Coupling Reactions of Aryl Halides with Various Nucleophiles
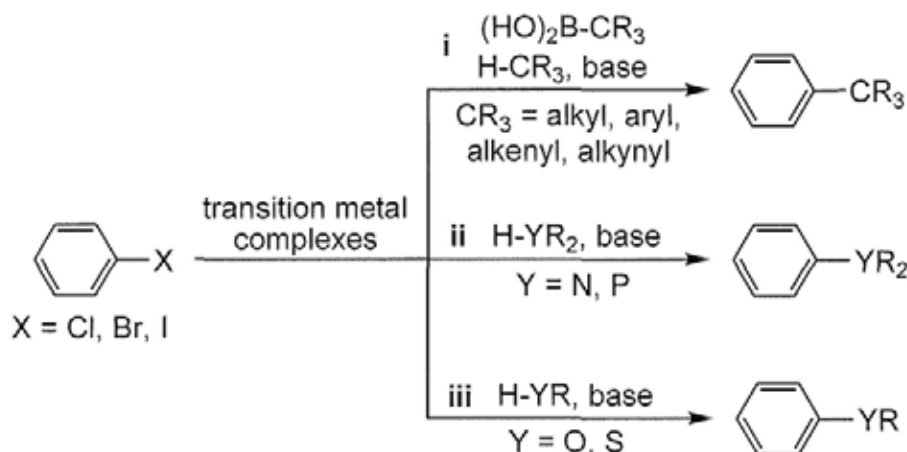
Transition metal complexes (e.g. Pd, Ni, Cu) are commonly applied as catalysts for cross-coupling reactions via the facile metal-mediated Ar-X bond cleavages. During the

coupling reactions, aryl halides react as electrophiles, whereas the alkyl or aryl boronic acid, C-H bonds, and heteroatom-H bonds react as nucleophiles. Bases are usually added to promote the deprotonations of C-H and heteroatom-H bonds and to react with the boronic acids, generating the carbon and heteroatom nucleophiles for the coupling reactions.

(ii) Hydrodehalogenation of Halogenated Compounds for Pollutant Treatments

Halogenated aromatic compounds are also the chemical wastes which cause pollutions to the environments and are hazardous to humans and animals. The most toxic ones are chlorinated dioxins and polyhalogenated biphenyls.[8] Incinerations or oxidations are the common methods of chemical waste treatments of halogenated aromatic compounds. However, those processes result in high energy consumptions and severe CO_2 emission.[9]

Alternatively, the halogenated aromatic compounds can be treated by hydrodehalogenation catalyzed by transition metals. During the hydrodehalogenation, the C-X bonds of the halogenated compounds are cleaved by the transition metal complexes in milder reaction conditions and are subsequently reduced by hydrogen sources (e.g. H_2O, H_2) to form C-H bonds (eq 3.1). Hydrodehalogenation of halogenated aromatic complexes are more environmentally-friendly, more energy-saving, and have the potential to recycle the halogenated wastes into valuable raw materials.[9]

$$\text{Ar}-X \xrightarrow[\text{[H] (e.g. }H_2O,\ H_2)]{\substack{\text{transition metal}\\\text{complexes}}} \text{Ar}-H \qquad (3.1)$$
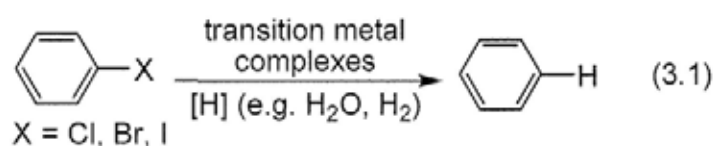
X = Cl, Br, I

3.1.2 Modes of Reactivity of Aryl Carbon-Halogen Bond Cleavages by Transition Metal Complexes

Ar-X (X = Cl, Br, I) bond cleavages can be achieved in one or two transition metal centers (M^n) (Table 3.3). In mono-metallic aryl C-X bond cleavages, 3 major modes of reactivities are

114

generally classified (Table 3.3):

Table 3.3 Classifications of Aryl C-X Cleavages by Transition Metal Complexes

Mono-metallic Aryl C-X Bond Cleavages	
(A) Oxidative Addition (OA) (2 e$^-$ process)	$M^n + Ar\text{-}X \longrightarrow M^{n+2} \begin{smallmatrix} Ar \\ \\ X \end{smallmatrix}$
(B) Nucleophilic Aromatic Substitution (S_NAr) (2 e$^-$ process)	$M^{n\ominus} + Ar\text{-}X \longrightarrow M^{n+2}\!\!-\!\!Ar + X^{\ominus}$
(C) Halogen Atom Transfer (XAT) (1 e$^-$ process)	$M^n\!\!\bullet + Ar\text{-}X \xrightarrow{\text{i}} M^{n+1}\!\!-\!\!X + Ar\bullet$ $Ar\bullet \xrightarrow{\text{ii}} Ar\text{-}Ar$ $Ar\bullet \xrightarrow[\text{iii}]{[H]} Ar\text{-}H$
Bi-metallic Aryl C-X Bond Cleavages	
(D) Oxidative Addition (OA) (1 e$^-$ process)	$2M^n\!\!\bullet + Ar\text{-}X \longrightarrow M^{n+1}\!\!-\!\!X + M^{n+1}\!\!-\!\!Ar$

(A) Oxidative Addition (OA). The Ar-X bond is cleaved by M^n to form both M-Ar and M-X bonds with the concomitant increase of metal oxidation state by +2 (Table 3.3(A)).

(B) Nucleophilic Aromatic Substitution (S_NAr). Anionic M^{n-} acts as a strong nucleophile to attack the electrophilic carbon of the polar Ar-X bond and eliminate the halide ion (X^-) to form M-Ar (Table 3.3(B)).

(C) Halogen Atom Transfer (XAT). The halogen atom ($X\bullet$) of Ar-X is abstracted by the transition metal radical ($M^n\bullet$) to form the M-X bond and the aryl radical ($Ar\bullet$) (Table 3.3(C), pathway i). $Ar\bullet$ can dimerize to form biaryls (Ar-Ar), or react with hydrogen atom source (e.g. solvents) to form arenes (Ar-H) (Table 3.3(C), pathways ii and iii). $Ar\bullet$ can also further react with another $M^n\bullet$ to form M-Ar for the bimetallic oxidative addition of Ar-X (Table 3.3(D)).

Each category of aryl C-X bond cleavages by transition metal complexes is briefly reviewed below.

3.1.2.1 Mono-metallic Aryl C-X Cleavages

3.1.2.1.1 Oxidative Addition

Oxidative addition (OA) of aryl halides (ArX, X = Cl, Br, I) usually takes place with electron-rich, low-valent middle-group 8^{10} and late-group 9^{11} and 10^{12} transition metal complexes.

(i) Palladium(0)

Palladium(0) is one of the commonly studied transition metals for oxidative addition of Ar-X,[13] which is the initial step in the palladium-catalyzed cross-coupling reactions with ArX.[7] For example, $Pd^0(PPh_3)_4$ undergoes oxidation addition of halobenzene (PhX, X = Cl, Br, I) to form $(Ph_3P)_2Pd^{II}(Ph)(X)$ (eq 3.2). Mechanistic studies suggest that $Pd^0(PPh_3)_4$ first undergoes PPh_3 dissociation to form coordinatively unsaturated 14-electron $Pd^0(PPh_3)_2$ (Scheme 3.3, pathway i). PhX then coordinates to $Pd^0(PPh_3)_2$ via η^2 π-interaction (pathway ii), followed by concerted oxidative addition of Ph-X bond to $Pd^0(PPh_3)_2$ via a 3-centered transition state to form $(Ph_3P)_2Pd^{II}(Ph)(X)$ (pathways iii and iv). There is no strong evidence of radical pathways for the oxidative addition process.

$$(PPh_3)_4Pd^0 + X\text{-}C_6H_5 \xrightarrow{-2PPh_3} (Ph_3P)_2Pd^{II}(Ph)(X) \quad X = Cl, Br, I \quad (3.2)$$
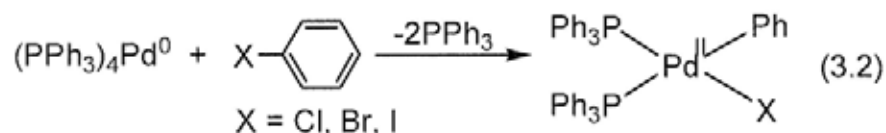
Scheme 3.3 Mechanism of Oxidative Addition of PhX to $Pd^0(PPh_3)_4$
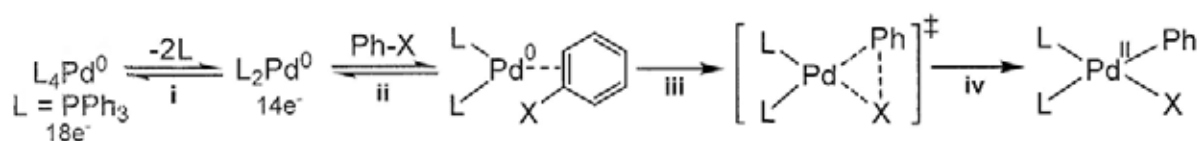
(ii) Nickel(0)

Similar to $Pd^0(PPh_3)_4$, $Ni^0(PEt_3)_4$ can also undergo oxidative addition of ArX to form $Ni^{II}(PEt_3)_2(Ar)(X)$, but with the concomitant formation of $Ni^I(PEt_3)_2X$ (eq 3.3).[14] Mechanistic studies reveal that $Ni^0(PEt_3)_4$ reacts with ArX via electron-transfer. $Ni^0(PEt_3)_4$ first undergoes PEt_3 dissociation to form the coordinatively-unsaturated 16-electron $Ni^0(PEt_3)_3$ (Scheme 3.4, pathway i). $Ni^0(PEt_3)_3$ then coordinates with ArX, followed by the rate-determining electron-transfer from Ni(0) to ArX to generate $[Ni^I(PEt_3)_3]^+$ and ArX radical anion (pathway ii). ArX radical anion either collapses with $[Ni^I(PEt_3)_3]^+$ to form $Ni^{II}(PPh_3)_2(Ar)(X)$ (pathway iii), or undergoes fragmentation to form Ar• and X^- (pathway iv). Ar• can diffuse out of the solvent cage and reacts with solvent to form arenes (Ar-H), and X^- further reacts with $[Ni^I(PEt_3)_3]^+$ to form $Ni^I(PEt_3)_3X$ (pathway v). The insignificant decrease of the rate of oxidative addition of *ortho*-substituted ArX further supports the electron-transfer pathway.
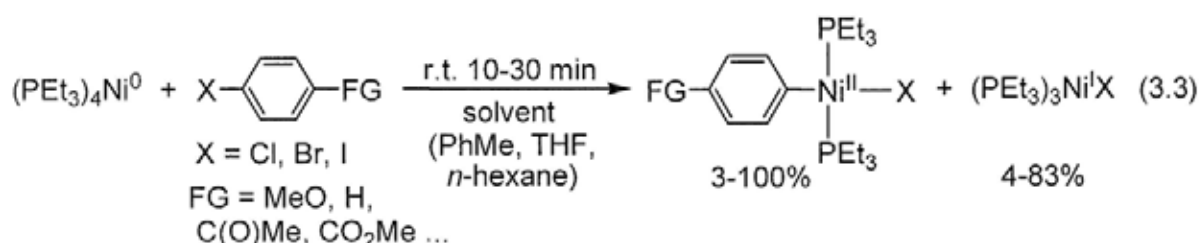
Scheme 3.4 Mechanism of Oxidative Addition of ArX to $Ni^0(PEt_3)_4$
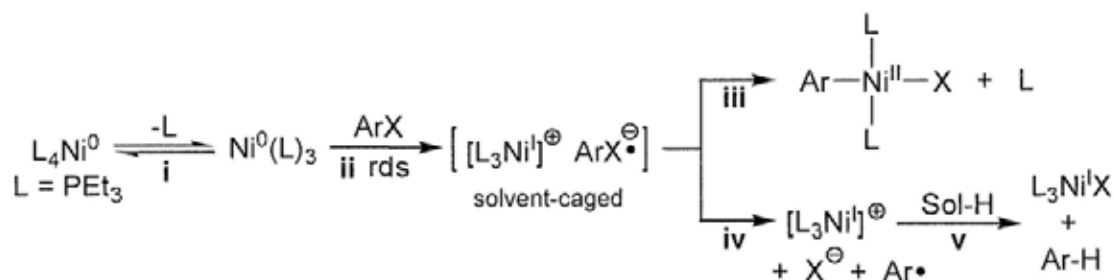
(iii) Iridium(I)

Vaska's complex is a low valent iridium(I) complex. Vaska's complex can undergo oxidative addition of various ArX to form $Ir^{III}(PPh_3)_2(CO)Cl(Ar)(X)$ (eq 3.4).[15] During the reaction,[15b]

Vaska's complex first undergoes PPh$_3$ dissociation to form the coordinatively unsaturated 14-electron Ir^I(PPh$_3$)(CO)Cl (Scheme 3.5, pathway i), which then undergoes unsymmetrical concerted addition of ArX to give Ir^{III}(PPh$_3$)(CO)Cl(Ar)(X) (pathways ii and iii). Coordination of PPh$_3$ yields the observed product (pathway iv). The reactivity of Ar-X is in the order Ar-Cl < Ar-Br < Ar-I in line with the corresponding Ar-X bond energies (Table 3.2).

(3.4)
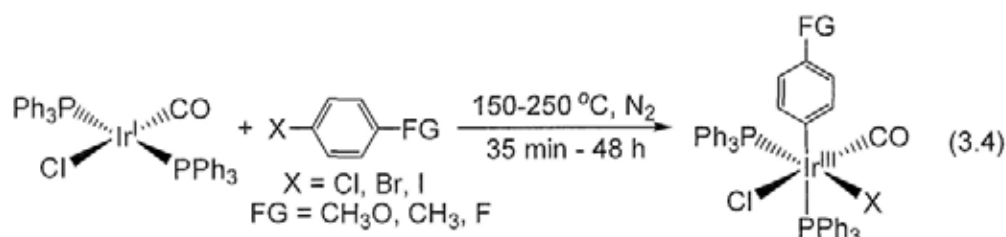
Scheme 3.5 Mechanism of Oxidative Addition of ArX to Vaska's Complex
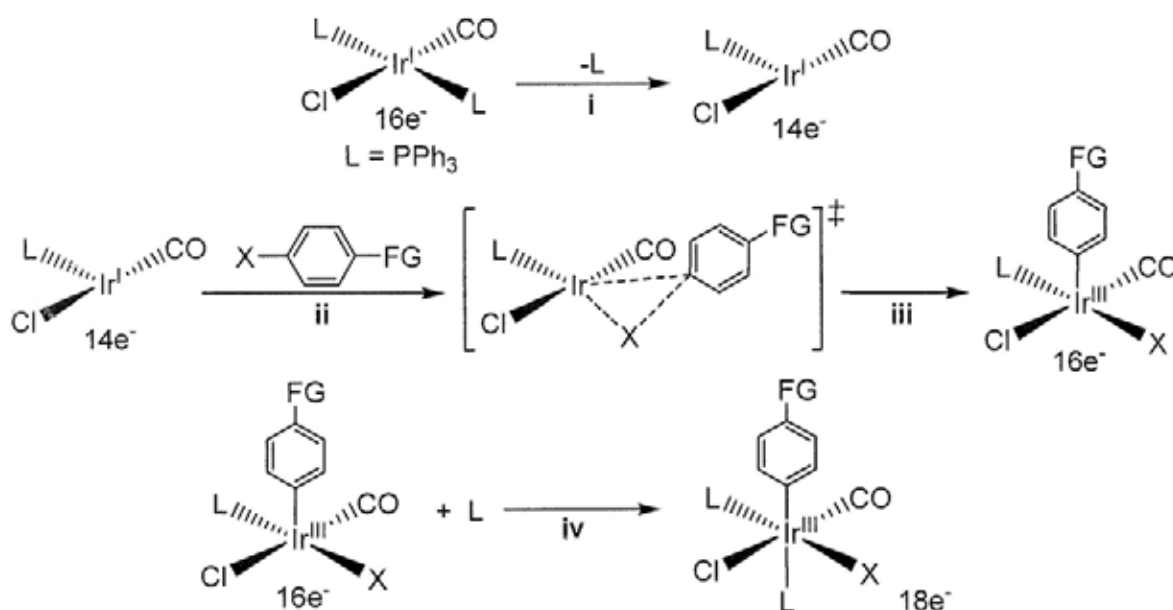
3.1.2.1.2 Nucleophilic Aromatic Substitution

Nucleophilic aromatic substitution (S$_N$Ar) of ArX (X = F, Cl, Br, I) by transition metal complexes is relatively less reported compared with oxidative addition. Classical S$_N$Ar of ArX by transition metals usually involves electron-deficient ArF or ArX bearing the electron-withdrawing substituents, and the electron-rich, anionic transition metals.

(i) Rhodium(I)

Anionic rhodium(I) complex, [Cp*Rh^I(PPh$_3$)H]$^-$, undergoes S$_N$Ar of fluorinated arenes

$(Ar^F\text{-}F)$ to give $Cp^*Rh^{III}(PPh_3)H(Ar^F)$ (eq 3.5).[16] First, $[Cp^*Rh^I(PPh_3)H]^-$ is facilely generated by the deprotonation of $Cp^*Rh^{III}(PPh_3)H_2$ with pyridine (Scheme 3.6, pathway i). $[Cp^*Rh^I(PPh_3)H]^-$ then undergoes S_NAr of $Ar^F\text{-}F$ to give $Cp^*Rh^{III}(PPh_3)H(Ar^F)$ and pyridinium fluoride (pathways ii and iii). Pyridinium fluoride also acts as a strong base to promote the deprotonation of $Cp^*Rh^{III}(PPh_3)H_2$ for subsequent S_NAr of $Ar^F\text{-}F$ (pathway i).

(a) $Ar^F = C_6F_5$, $t_{1/2}$ = 12 h   81%
(b) $Ar^F = p\text{-}HC_6F_4$, $t_{1/2}$ = 20 h   85%
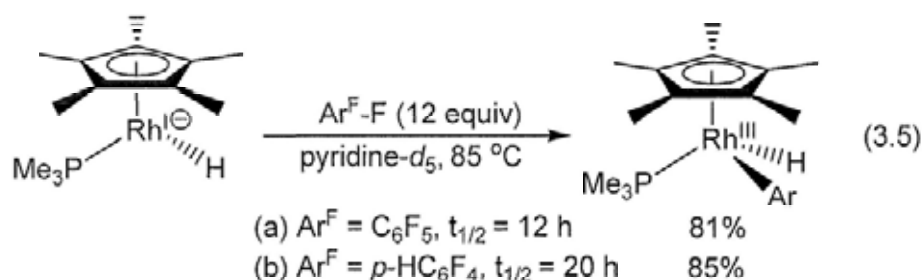
Scheme 3.6 Mechanism of S_NAr of Aryl Fluorides by $Cp^*Rh^I(PPh_3)H^-$

(ii) Cobalt(I)

Anionic tetracyanocobaltate(I) ($[Co^I(CN)_4]^{3-}$) can be prepared *in-situ* by the reaction of pentacyanocobaltate(II) radical ($[Co^{II}(CN)_5]^{3-}$) with H_2 and base (Scheme 3.7, pathway i).[17] $[Co^I(CN)_4]^{3-}$ then undergoes S_NAr of ArBr to form $[Ar\text{-}Co^{III}(CN)_5]^{3-}$ (Scheme 3.7, pathway ii).

Scheme 3.7 S_NAr of ArBr with $[Co^I(CN)_4]^{3-}$
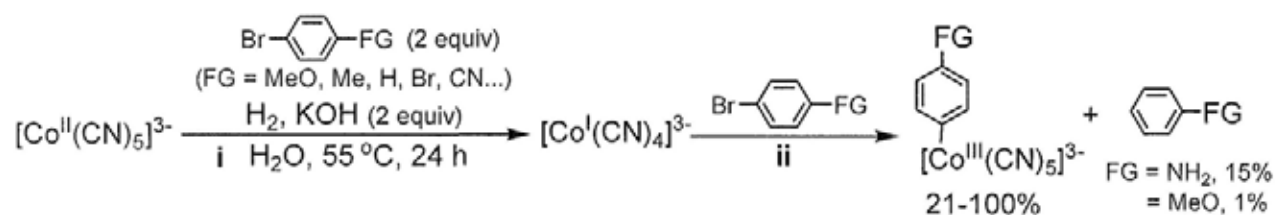
It is proposed that $[Co^{II}(CN)_5]^{3-}$ reacts with H_2 to form $[Co^{III}(CN)_5H]^{3-}$, followed by the deprotonation of OH^- and CN^- dissociation to form $[Co^I(CN)_4]^{3-}$ (Scheme 3.8, pathways i and

ii). $[Co^I(CN)_4]^{3-}$ likely undergoes inner-sphere electron transfer to ArBr to produce $[Co^{II}(CN)_4]^{2-}$ and ArBr radical anion (pathway iii). ArBr radical anion fragments to form Ar• and Br⁻, which further collapses to form $[Ar-Co^{III}(CN)_4Br]^{3-}$ (pathways iv and v). Ligand exchange with CN⁻ finally yields $[Ar-Co^{III}(CN)_5]^{3-}$ (pathway vi). Ar• can also leak from the solvent cage to undergo H atom abstraction from $[Co^{III}(CN)_5H]^{3-}$ to form arenes (pathways vii and viii).

Scheme 3.8 Proposed Mechanism of S_NAr of ArBr with $[Co^I(CN)_4]^{3-}$
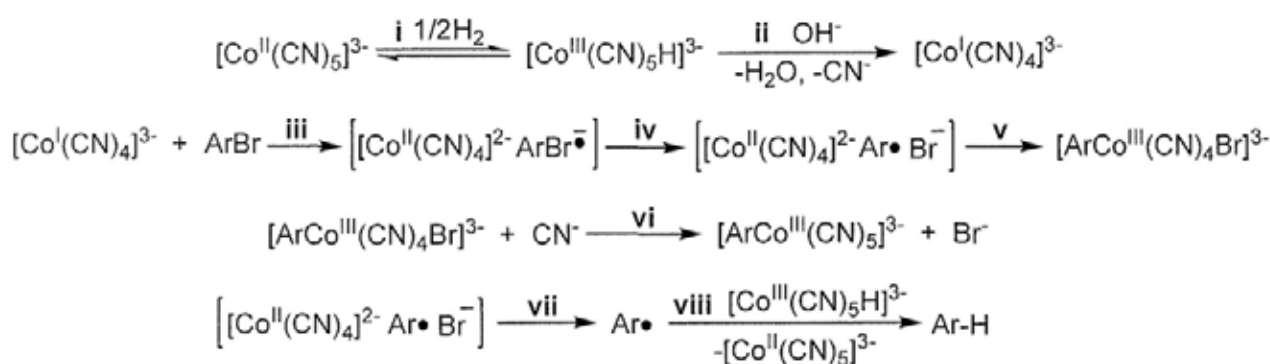
3.1.2.1.3 Halogen Atom Transfer

Halogen atom transfer (XAT) reactions are commonly observed in the reactions of ArX (X = Cl, Br, I) with metalloradicals. Both radical chain and non-chain mechanism are feasible.

(i) Titanium(III)

Titanium(III) complex, $[Cp^*Ti^{III}-N=P^tBu_3]^+$, is a metalloradical formed by the dehydrogenation of $[Cp^*(H)Ti^{IV}-N=P^tBu_3]^+$. It reacts with PhX (X = Cl, Br) by XAT via radical chain propagation mechanism to form $[Cp^*(X)Ti^{IV}-N=P^tBu_3]^+$ (X = Cl, Br) accompanied with the formations of benzene and biphenyl (eq 3.6).[18]

120
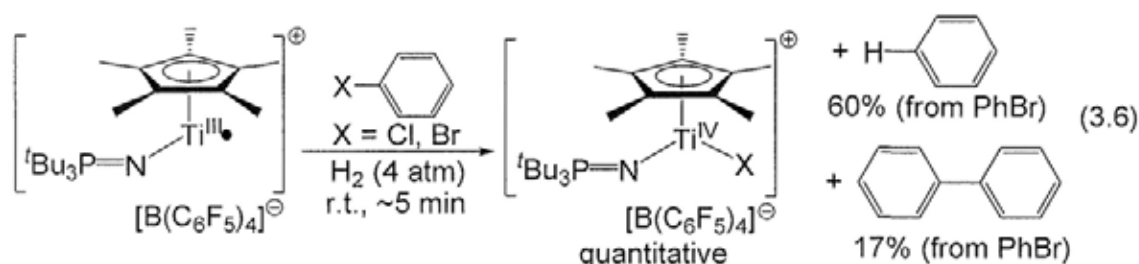
$[Cp^*(H)Ti^{IV}-N=P^tBu_3]^+$ was prepared *in-situ* from the metathesis of $[Cp^*(Me)Ti^{IV}-N=P^tBu_3]^+$ with H_2 (Scheme 3.9, pathway i). Mechanistic studies suggest that $[Cp^*(H)Ti^{IV}-N=P^tBu_3]^+$ undergoes dehydrogenation to form a small amount of $[Cp^*Ti^{III}-N=P^tBu_3]^+$ metalloradical (Scheme 3.9, pathway ii), which then undergoes XAT with PhX to form $[Cp^*(X)Ti^{IV}-N=P^tBu_3]^+$ and a phenyl radical (Ph•) (pathway iv). The resultant Ph• abstracts a H atom from $[Cp^*(H)Ti^{IV}-N=P^tBu_3]^+$ to give benzene and to regenerate $[Cp^*Ti^{III}-N=P^tBu_3]^+$ (pathways v and iii) for subsequent XAT. When the concentration of $[Cp^*(H)Ti^{IV}-N=P^tBu_3]^+$ decreases in the course of reaction, Ph• dimerizes to form biphenyl (pathway vi).

Scheme 3.9 Mechanism of Halogen Atom Transfer of PhX by $[Cp^*Ti^{III}-N=P^tBu_3]^+$
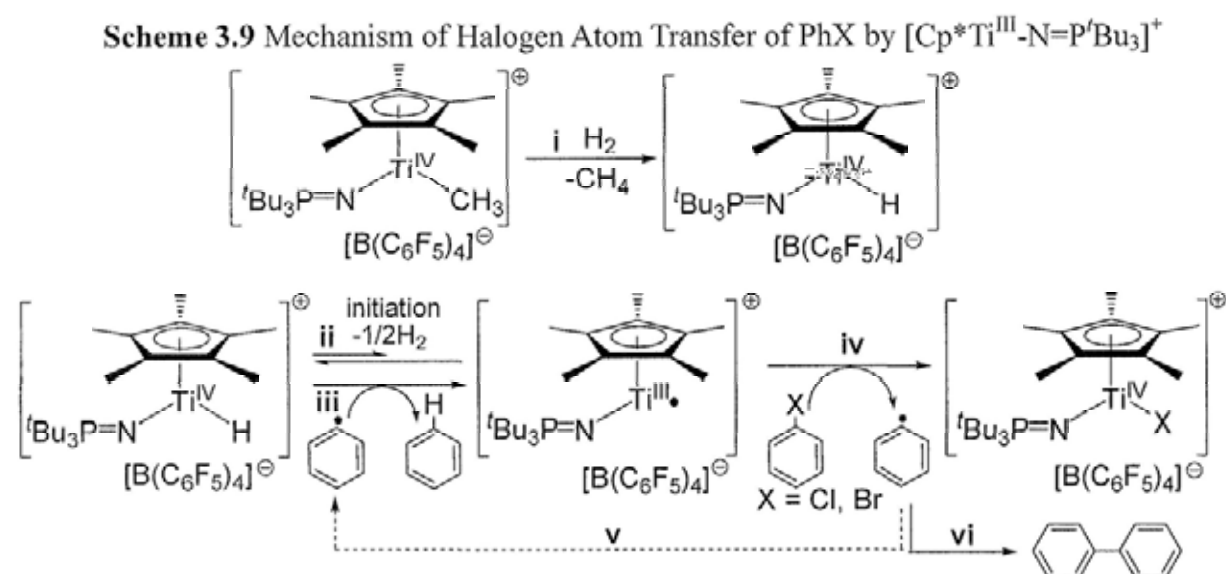
(ii) Rhenium(0)

The 17-electron rhenium(0) complex, $(PMe_3)(CO)_4Re^0$, is a metalloradical which can undergo bromine atom abstraction with 4-bromobenzonitrile and 1-bromonaphthalene to form $(PMe_3)(CO)_4Re^I$-Br as the only organometallic product (eq 3.7).[19]

$$(PMe_3)(CO)_4Re^0\bullet \; + \; R\text{-}Br \xrightarrow[\text{22 °C}]{\text{toluene}} (PMe_3)(CO)_4Re^I(Br) \quad (3.7)$$

$R = $ —⟨ ⟩—CN $\quad k = 0.058$ M s^{-1}
$R = $ 1-naphthyl $\quad k = 0.021$ M s^{-1}
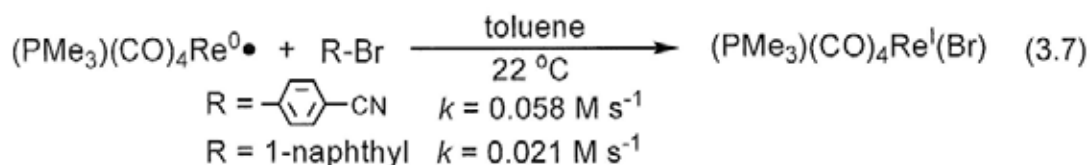
Since the reaction rate constants do not correlate well with the available thermochemical C-Br bond energies, an electron-transfer pathway is more reasonable. First, $(PMe_3)(CO)_4Re^0$

reacts with RBr (R = 4-nitrophenyl, 1-naphthyl) via electron-transfer to form $[(PMe_3)(CO)_4Re^I]^+$ and ArBr radical anion (Scheme 3.10, pathway i). Fragmentation of RBr radical anion forms R• and Br⁻ (pathway ii). Combination between Br⁻ and $[(PMe_3)(CO)_4Re^I]^+$ then gives $(PMe_3)(CO)_4Re^I$-Br (pathway iii). However, the fate of the R• is not reported. Presumably, R• abstracts a H atom from the benzylic C-H bond of toluene to form R-H.

Scheme 3.10 Proposed Mechanism of Br Atom Abstraction by $(PMe_3)(CO)_4Re^0$

$$(PMe_3)(CO)_4Re^0 \ + \ R\text{-}Br \ \underset{}{\overset{i}{\rightleftharpoons}} \ \left[[(PMe_3)(CO)_4Re^I]^+ \ RBr^{\underline{\bullet}} \right]$$
$$R = 4\text{-nitrophenyl, 1-naphthyl}$$

$$\left[[(PMe_3)(CO)_4Re^I]^+ \ RBr^{\underline{\bullet}} \right] \ \xrightarrow{ii} \ \left[[(PMe_3)(CO)_4Re^I]^+ \ Br^- \ R\bullet \right] \ \xrightarrow{iii} \ (PMe_3)(CO)_4Re^I(Br) \ + \ R\bullet$$
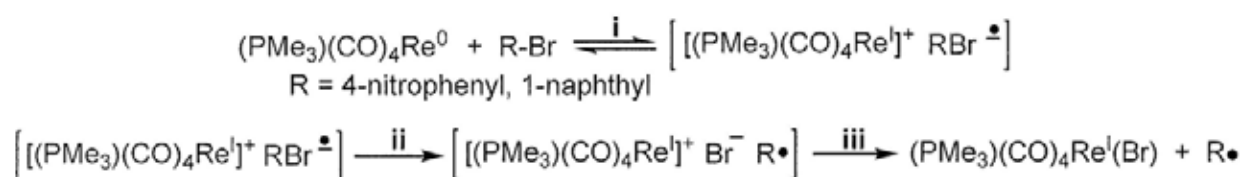
(iii) Platinum(II)

Tetrakis(μ-pyrophosphito)diplatinum(II) complex, $[Pt^{II}_2(\mu\text{-}P_2O_5H_2)_4]^{4-}$, undergoes bromine atom abstraction with C_6F_5Br in photochemical conditions to form $[Br\text{-}Pt^{III}(\mu\text{-}P_2O_5H_2)_4Pt^{III}\text{-}Br]^{4-}$ bearing 2 Pt-Br bonds. (eq 3.8).[20]

$$[Pt^{II}_2(\mu\text{-}P_2O_5H_2)_4Pt^{II}]^{4-} \xrightarrow[\substack{CH_3OH \ / \ H_2O, \ r.t. \\ < 1 \ \mu s}]{\substack{C_6F_5Br \\ h\nu \ (\lambda > 350 \ nm)}} [Br\text{-}Pt^{III}(\mu\text{-}P_2O_5H_2)_4Pt^{III}\text{-}Br]^{4-} \quad (3.8)$$
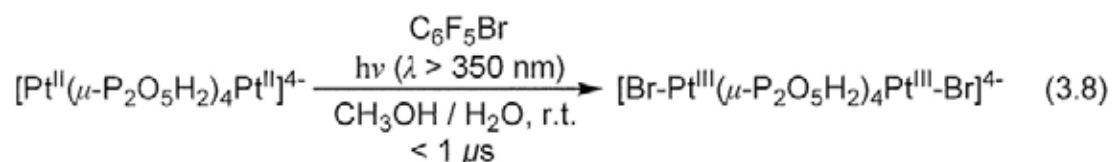
Upon photochemical irridation by laser, $[Pt^{II}_2(\mu\text{-}P_2O_5H_2)_4]^{4-}$ in a singlet state is converted to $[Pt^{II}_2(\mu\text{-}P_2O_5H_2)_4]^{4-\bullet}$ in an excited triplet state with an unpair electron in the d orbital of Pt (Scheme 3.11, pathway i). $[Pt^{II}_2(\mu\text{-}P_2O_5H_2)_4]^{4-\bullet}$ then abstracts a Br atom from C_6F_5Br to form a mixed valence $[Pt^{II}(\mu\text{-}P_2O_5H_2)_4Pt^{III}\text{-}Br]^{4-}$ (pathway ii), which further disproportionates to generate $[Br\text{-}Pt^{III}(\mu\text{-}P_2O_5H_2)_4Pt^{III}\text{-}Br]^{4-}$ and $[Pt^{II}_2(\mu\text{-}P_2O_5H_2)_4]^{4-}$ (pathway iii). $[Pt^{II}_2(\mu\text{-}P_2O_5H_2)_4]^{4-}$ is recycled for further photochemical reactions (pathways i-iii). However, the fate of aryl radical ($C_6F_5\bullet$) is not reported. Presumably, $C_6F_5\bullet$ dimerizes to form biaryl, $C_6F_5\text{-}C_6F_5$.

Scheme 3.11 Photochemially-Induced Br Atom Abstraction of C_6F_5Br by $[Pt^{II}{}_2(\mu\text{-}P_2O_5H_2)_4]^{4-}$

$$[Pt^{II}(\mu\text{-}P_2O_5H_2)_4Pt^{II}]^{4-} \xrightarrow[\text{i}]{h\nu} [Pt^{II}(\mu\text{-}P_2O_5H_2)_4Pt^{II}]^{4-*}$$

$$[Pt^{II}(\mu\text{-}P_2O_5H_2)_4Pt^{II}]^{4-*} \xrightarrow[\text{Br Atom Abstraction}]{C_6F_5Br} [Pt^{II}(\mu\text{-}P_2O_5H_2)_4Pt^{III}\text{-}Br]^{4-} + C_6F_5{}^\bullet$$

<center>ii</center>

$$2[Pt^{II}(\mu\text{-}P_2O_5H_2)_4Pt^{III}\text{-}Br]^{4-} \xrightarrow[\text{iii}]{\text{disproportionation}} [Br\text{-}Pt^{III}(\mu\text{-}P_2O_5H_2)_4Pt^{III}\text{-}Br]^{4-} + [Pt^{II}(\mu\text{-}P_2O_5H_2)_4Pt^{II}]^{4-}$$

3.1.2.2 Bi-metallic Aryl C-X Cleavages

(i) Cobalt(II)

Pentacyanocobaltate(II) ($[Co^{II}(CN)_5]^{3-}$) can undergo oxidative addition with 2-iodopyridine to yield cobalt(III) 2-pyridyl and iodide complexes (eq 3.9).[21]

$$[Co^{II}(CN)_5]^{3-} + \text{(pyridyl-I)} \xrightarrow[\text{H}_2\text{O, 25 °C}]{k \sim 10^{-3}\ M^{-1}s^{-1}} \left[\text{(pyridyl-)}Co^{III}(CN)_5\right]^{3-} + [\text{I-}Co^{III}(CN)_5]^{3-} \quad (3.9)$$
<center>50%   50%</center>

Radical non-chain halogen atom transfer mechanism is suggested (Scheme 3.12). First, $[Co^{II}(CN)_5]^{3-}$ abstracts an I atom from 2-iodopyridine to form $[I\text{-}Co^{III}(CN)_5]^{3-}$ and 2-pyridyl radical (pathway i), which subsequently combines with another $[Co^{II}(CN)_5]^{3-}$ to form $[2\text{-pyridyl-}Co^{III}(CN)_5]^{3-}$ (pathway ii).

<center>**Scheme 3.12** Halogen Atom Abstraction of 2-Iodopyridine by $Co^{II}(CN)_5{}^{3-}$</center>

$$[Co^{II}(CN)_5]^{3-} + R\text{-}I \xrightarrow[\text{i}]{\text{rds}} [I\text{-}Co^{III}(CN)_5]^{3-} + R^\bullet$$

$$R^\bullet + [Co^{II}(CN)_5]^{3-} \xrightarrow{\text{ii}} [R\text{-}Co^{III}(CN)_5]^{3-}$$

$$R\text{-}I = \text{(pyridyl-I)}$$

(ii) Platinum(II)

$[Pt^{II}{}_2(\mu\text{-}P_2O_5H_2)_4]^{4-}$ (($P_2O_5H_2)^{2-}$ = pyrophosphito dianion) also undergoes oxidative addition with PhBr under photochemical conditions to form $[Ph\text{-}Pt^{III}(\mu\text{-}P_2O_5H_2)_4 Pt^{III}\text{-}Br]^{4-}$ (eq 3.10).[22]

$$[Pt^{II}(\mu\text{-}P_2O_5H_2)_4Pt^{II}]^{4-} \xrightarrow[\substack{CH_3OH \ / \ H_2O, \ r.t. \\ < 1 \ \mu s}]{\substack{PhBr \\ h\nu \ (\lambda > 350 \ nm)}} [Ph\text{-}Pt^{III}(\mu\text{-}P_2O_5H_2)_4Pt^{III}\text{-}Br]^{4-} \quad (3.10)$$

It is proposed that the photochemically excited $[Pt^{II}(\mu\text{-}P_2O_5H_2)_4Pt^{II}]^{4-*}$ initially transfers single electron to PhBr to form $[Pt^{II}(\mu\text{-}P_2O_5H_2)_4Pt^{III}]^{3-}$ and PhBr radical anion (Scheme 3.13, pathways i and ii). Fragmentation of PhBr radical anion gives Ph• and Br⁻ (pathway iii), which further collapse with $[Pt^{II}(\mu\text{-}P_2O_5H_2)_4Pt^{III}]^{3-}$ to form $[Ph\text{-}Pt^{III}(\mu\text{-}P_2O_5H_2)_4Pt^{III}\text{-}Br]^{4-}$ (pathway iv).

Scheme 3.13 Mechanism of Oxidative Addition of ArX to $[Pt^{II}_2(\mu\text{-}P_2O_5H_2)_4]^{4-}$

$$[Pt^{II}(\mu\text{-}P_2O_5H_2)_4Pt^{II}]^{4-} \xrightarrow[\text{i}]{h\nu} [Pt^{II}(\mu\text{-}P_2O_5H_2)_4Pt^{II}]^{4-*}$$

$$[Pt^{II}(\mu\text{-}P_2O_5H_2)_4Pt^{II}]^{4-*} + PhBr \xrightarrow{\text{ii}} \left[[Pt^{II}(\mu\text{-}P_2O_5H_2)_4Pt^{III}]^{3-} \ PhBr^{\bullet-}\right] \xrightarrow{\text{iii}} \left[[Pt^{II}(\mu\text{-}P_2O_5H_2)_4Pt^{III}]^{3-} \ Ph\bullet \ Br^{-}\right]$$

$$\left[[Pt^{II}(\mu\text{-}P_2O_5H_2)_4Pt^{III}]^{3-} \ Ph\bullet \ Br^{-}\right] \xrightarrow{\text{iv}} [Ph\text{-}Pt^{III}(\mu\text{-}P_2O_5H_2)_4Pt^{III}\text{-}Br]^{4-}$$
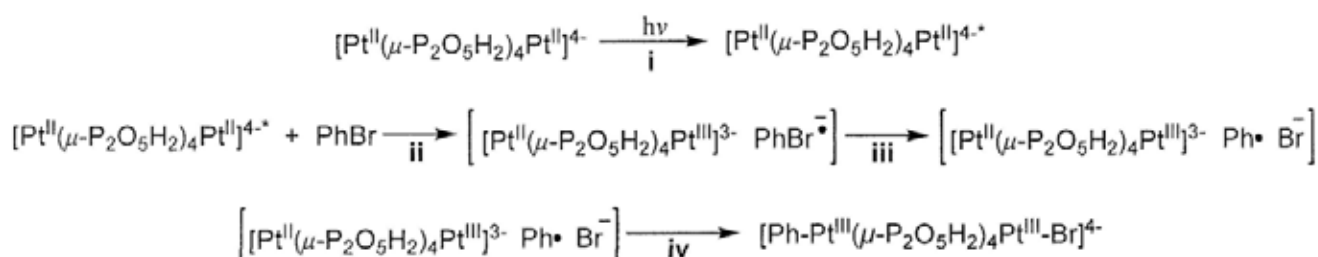
3.1.3 Radical *Ipso*-Substitutions of Aryl C-X Bonds

In principle, transition metal radicals can undergo *ipso*-substitutions with aryl halides (ArX) to form transition metal aryls (M-Ar) and halogen atoms (X•) (eq 3.11). To the best of our knowledge, such reactivity mode of Ar-X cleavages by transition-metal complexes has not been reported. On the other hand, *ipso*-substitutions of aryl halides by non-metal radicals[23] (e.g. carbon-centered radicals,[24] sulfur-centered radicals,[25] halogen atoms[26]) with the concomitant elimination of halogen atoms have been reported (eq 3.12). The characteristics of the radical *ipso*-substitution of aryl halides are briefly summarized below.

$$M\overset{n}{\bullet} + Ar\text{-}X \longrightarrow M\overset{n+1}{\text{---}}Ar + X\bullet \quad (3.11)$$
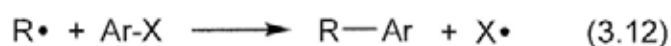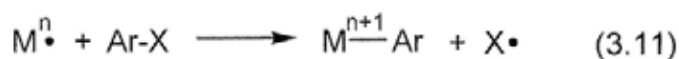
$$R\bullet + Ar\text{-}X \longrightarrow R\text{---}Ar + X\bullet \quad (3.12)$$
$$R = \text{non-metal radical}$$

3.1.3.1 *Ipso*-Substitutions of Dihalobenzenes by Benzyl Radicals

(i) Effect of Natures of Ar-X Bonds

Benzyl radical, which is generated *in-situ* from the thermolysis of mercury(II) di-benzyl, reacts with various 1,4-dihalobenzenes to form diarylmethane as the minor product and the inevitable bibenzyl as the major side product (Table 3.4).[24b] When 1-fluoro-4-bromobenzene and 1-fluoro-4-chlorobenzene are reacted with benzyl radical, only the weaker C-Br and C-Cl bonds, respectively, are cleaved to form the corresponding diarylmethanes (Table 3.4, entries 1 and 2). When 1-chloro-4-bromobenzene is reacted, both the weaker C-Br and the stronger C-Cl bonds are cleaved in around 2.5 : 1 ratio to form the corresponding diarylmethanes (Table 3.4, entry 3). The rates of aryl C-X bond cleavages are thus in the order: C-F < C-Cl < C-Br.

Table 3.4 Radical *Ipso*-Substitutions of Di-halo-substituted Benzenes by Benzyl Radical

entry	Ar-X	Ar-CH$_2$Ph	ArCH$_2$Ph : bibenzyl[a,b]
1	Br—⬡—F	PhCH$_2$—⬡—F	0.023
2	Cl—⬡—F	PhCH$_2$—⬡—F	0.017
3	Br—⬡—Cl	(a) PhCH$_2$—⬡—Cl (b) PhCH$_2$—⬡—Br	(a) 0.069 (b) 0.028

[a] The yield of ArCH$_2$Ph generated was not reported, and only the ratio of ArCH$_2$Ph : bibenzyl was given. [b] ArCH$_2$Ph was formed as a minor product due to the inevitable major dimerization of benzyl radical to form bibenzyl.

Mechanism. It is proposed that the benzyl radical undergoes electron-transfer to ArX to form a benzyl cation and an aryl radical anion (Scheme 3.14, pathway i). The benzyl cation then attacks the *ispo*-carbon of the C-X bond to form the cyclohexadienyl radical intermediate due to the highest electron-density of *ipso*-carbon brought by the σ-withdrawing halogen

substituents (X) (pathway ii). The *ipso*-halogen atom finally eliminates to give diarylmethane (pathway iii).

Scheme 3.14 Proposed Mechanism of *Ipso*-Substitution of Aryl Halides by Benzyl Radical
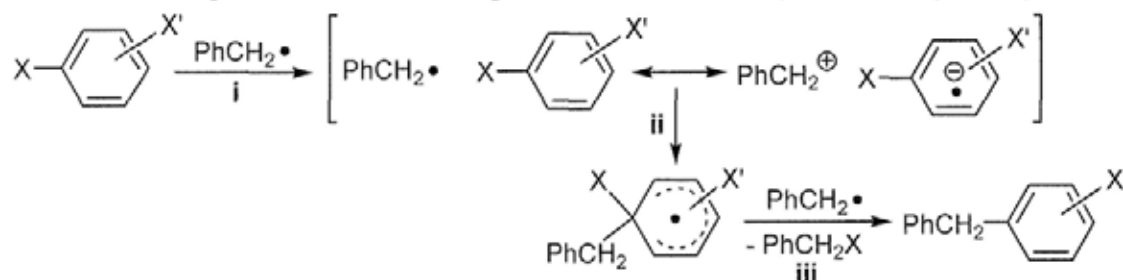
(ii) Electronic Effects of Halogen Substituents

Benzyl radical reacts with 1,2,4-trichlorobenzene via *ipso*-substitution to form diarylmethanes **A**, **B**, and **C** in the relative product ratios of 50%, 39%, and 11%, respectively (Scheme 3.15, pathways i and ii).[24b] Both *ortho*- and *para*-Cl groups can stabilize the cyclohexadienyl radicals via resonance interactions. Among the three cyclohexadienyl radical intermediates (**I**) formed, **I$_A$** is most stabilized by both the *ortho*- and *para*-Cl groups to give product **A** in highest yield (pathways i and ii$_A$). On the other hand, **I$_B$** and **I$_C$** are only stabilized by single *ortho*- and *para*-Cl groups, respectively, to form **B** and **C** as the minor products (pathways i and ii$_{B C}$). **B** is formed more than **C**, as the formation of **I$_B$** is more favorable than that of **I$_C$** by the strain relief of the *ortho*-Cl atom (pathway ii$_B$).[24b]

Scheme 3.15 Product Distributions in *Ipso*-Substitutions of 1,2,4-Trichlorobenzene by Benzyl Radical
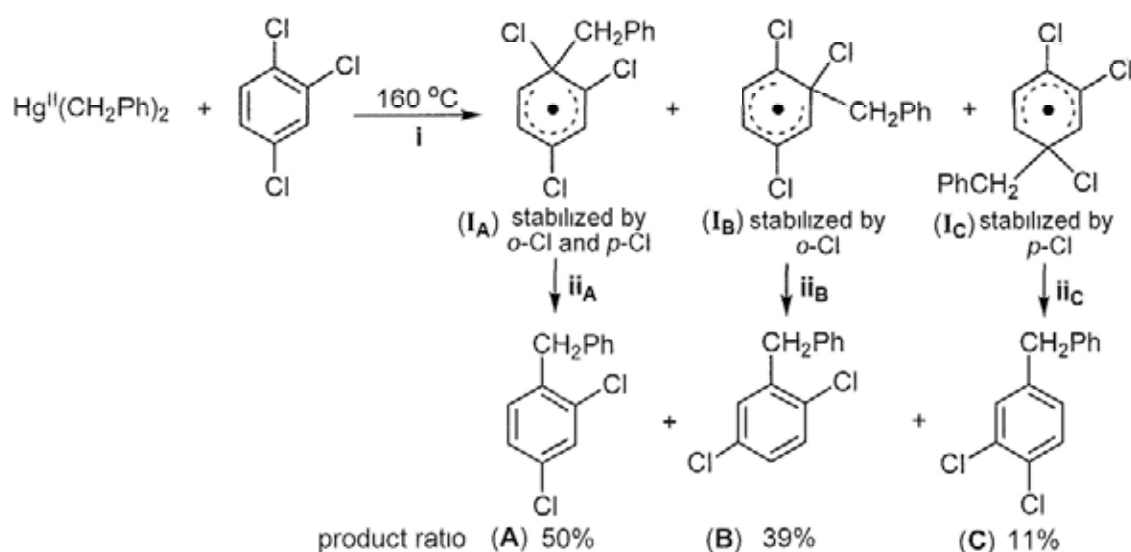
3.1.3.2 *Ipso*-Substitutions of Aryl Halides by Sulfur-Centered Radicals

(i) Effect of Natures of Ar-X Bonds

Arylsulfonyl ($ArSO_2\bullet$) and phenylthio radicals ($PhS\bullet$) can be generated from the thermolysis of $ArSO_2$-I and PhS-SPh, respectively. p-MeC$_6$H$_4$SO$_2\bullet$ reacts with PhX to form p-MeC$_6$H$_4$SO$_2$-Ph in the order of relative reaction rate: Ph-F $\ll$ Ph-Cl $<$ Ph-Br $<$ Ph-I (eq 3.13).[25]

$$p\text{-MeC}_6\text{H}_4\text{SO}_2\bullet \ + \ \text{PhX} \xrightarrow{\;190\,^\circ\text{C}\;} p\text{-MeC}_6\text{H}_4\text{SO}_2\text{—Ph} \quad (3.13)$$

X	relative rate
(a) F	0
(b) Cl	1
(c) Br	5.9
(d) I	18.6
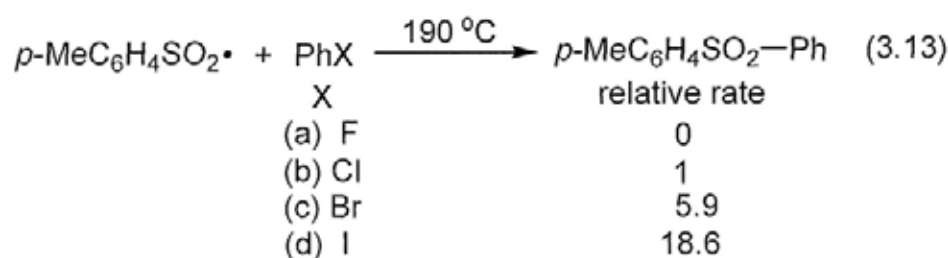
(ii) Electronic Effects of Substituents

Both $PhSO_2\bullet$ and $PhS\bullet$ were used to study the electronic effects of aryl bromide (ArBr) on the relative rates of Ar-Br cleavages (Table 3.5).[25]

Table 3.5 Relative Reactivities of Substituted Bromobenzenes with $PhSO_2\bullet$ and $PhS\bullet$

$$R\bullet \ + \ \text{Br}\!-\!\langle\text{Ar}\rangle\!-\!FG \xrightarrow[\;15\text{ h}\;]{\;190\,^\circ\text{C}\;} R\!-\!\langle\text{Ar}\rangle\!-\!FG$$

R = PhSO$_2\bullet$
PhS$\bullet$
relative rate

entry	FG	$\sigma^{0\,a}$	(A) relative rate (R = PhSO$_2\bullet$)	(B) relative rate (R = PhS$\bullet$)
1	*p*-H	0.00	1	1
2	*p*-OMe	-0.27	8.78	60
3	*p*-Me	-0.17	3.59	1.84
4	*p*-NO$_2$	0.78		3.00
5	*m*-H	0.00	1	1
6	*m*-OMe	0.12	0.68	0.80
7	*m*-Me	-0.07	2.18	1.20
8	*m*-NO$_2$	0.71		0.63

^{a} Hammett constant (Ref 27).

Both electron-donating *para*-substituents (FG = *p*-OMe, *p*-Me) ($\sigma^0 < 0$, Table 3.5, entries 2 and 3) and electron-withdrawing *para*-substituents (FG = *p*-NO$_2$) ($\sigma^0 > 0$, Table 3.5, entries 4)

can promote the reaction rates when compared with the parent PhBr (FG = *p*-H) (Table 3.5, entry 1). π-Donating *p*-OMe also promotes faster reaction rate than the σ-donating *p*-Me (Table 3.5, entries 2 and 3). However, all the *meta*-substituents (FG = *m*-OMe, *m*-Me, *m*-NO$_2$) generally do not promote the reaction rates (Table 3.5, entries 6-8). The rate-promoting effect of FG is in the order: *p*-OMe > *p*-NO$_2$ > *p*-Me > *p*-H = *m*-H ~ *m*-OMe ~ *m*-Me ~ *m*-NO$_2$.

Mechanism. It is suggested that radical *ipso*-substitutions of ArX (X = Cl, Br, I) by PhSO$_2$• and PhS• occur to form PhSO$_2$Ar and PhSAr, respectively. PhSO$_2$• and PhS• attack the *ipso*-carbon of C-X bonds in ArX to form the cyclohexadienyl radicals (**I**) (Scheme 3.16, pathway i), which then either undergoes radical-assisted (pathway ii) or spontaneous elimination of X• (pathway iii) to form PhSO$_2$Ar and PhSAr. Free halogens are also observed. Likely, both the electron-donating and electron-withdrawing *para*-substituents can stabilize the cyclohexadienyl radical (**I**) to favor the formations of *para*-substituted products.

Scheme 3.16 Mechanisms of Radical *Ipso*-Substitution of ArX by Phenylsulfonyl and Phenylthio Radicals
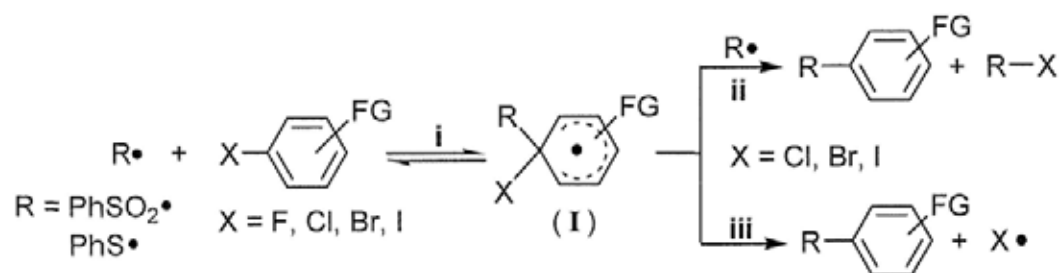
Indeed, the rate of *ipso*-substitution is kinetically controlled by the Ph-X bond strength. Ph-F bond is too strong such that the elimination of F• from the cyclohexadienyl radical intermediate (**I**) is kinetically unfavorable and no reaction occurs (R = PhSO$_2$, PhS) (eq 3.13(a); Scheme 3.16, pathway i). On the other hand, the rate of *ipso*-substitution is in the order: C-Cl < C-Br < C-I (eqs 3.13(b)-(d)), which is in line with the Ph-X bond strengths to dictate the corresponding reaction rates.

3.1.4 Homolytic Aromatic Substitutions of Arenes

The homolytic aromatic substitutions of various arenes by phenyl radical (generated from the thermolysis of benzoyl peroxide) to form biaryls have been studied (Table 3.6).[28] The homolytic aromatic substitution has the following characteristics:

(1) All electron-donating ($\sigma^o < 0$, Table 3.6, entries 2-4) and electron-withdrawing substituents ($\sigma^o > 0$, Table 3.6, entries 5-7) can increase the overall reaction rates of substituted arenes when compared with benzene ($K_{FG} > 1.00$).

(2) All substituents are activating and *ortho/para*-directing ($F_{o/p} > 1$). None of the substituents are deactivating and *meta*-directing ($F_m \sim 1$).

(3) The electronic effects of substituents on the relative rates of homolytic aromatic substitution are much smaller (usually $< 10^1$), compared with that of the electrophilic and nucleophilic aromatic substitutions (usually $> 10^2$).

Table 3.6 Partial Rate Factors of Homolytic Aromatic Substitution of Arenes with Phenyl Radicals

$$\text{Ph}\bullet \ + \ \text{FG}-\!\!\bigcirc \quad \xrightarrow[\text{72 h}]{\text{80 °C}} \quad \text{FG}-\!\!\bigcirc^{\text{Ph}}$$

entry	FG	$\sigma^{o\,a}$	total rate factor $(K_{FG})^b$	partial rate factor (F)		
				F_o	F_m	F_p
1	H	0.00	1.00	1	1	1
2	MeO	-0.27	2.71	5.6	1.23	2.31
3	^{t}Bu	-0.20	1.09	0.70	1.64	1.81
4	Me	-0.17	2.58	4.70	1.24	3.55
5	Cl	0.23	2.20	3.90	1.65	2.12
6	Br	0.23	1.90	3.05	1.70	1.92
7	NO$_2$	0.78	2.94	5.50	0.86	4.90

^{a} Hammett constant (Ref 27). ^{b} The yields of products were not reported, and only the relative total rate was given.

Mechanism. The reaction mechanism of homolytic aromatic substitutions of arenes by phenyl radical (Scheme 3.17)[28b] is similar to that of radical *ipso*-substitutions of aryl halides (Schemes

3.15 and 3.16).[24b,25] The phenyl radical attacks the arenes to form a cyclohexadienyl radical (Scheme 3.17, pathways i$_{a-c}$). Both the *ortho-* and *para*-substituents (FG) can stabilize the cyclohexadienyl radicals to promote the formations of *ortho-* and *para*-products (pathways i$_a$, i$_c$; pathways ii$_a$, ii$_c$). The *meta*-FG cannot stabilize the cyclohexadienyl radicals to disfavor the formation of *meta*-products (pathways i$_b$ and ii$_b$). Radical-assisted H atom abstraction from the cyclohexadienyl radical occurs to yield the products (pathway ii).

Scheme 3.17 Mechanisms of Homolytic Aromatic Substitution of Arenes by Phenyl Radical
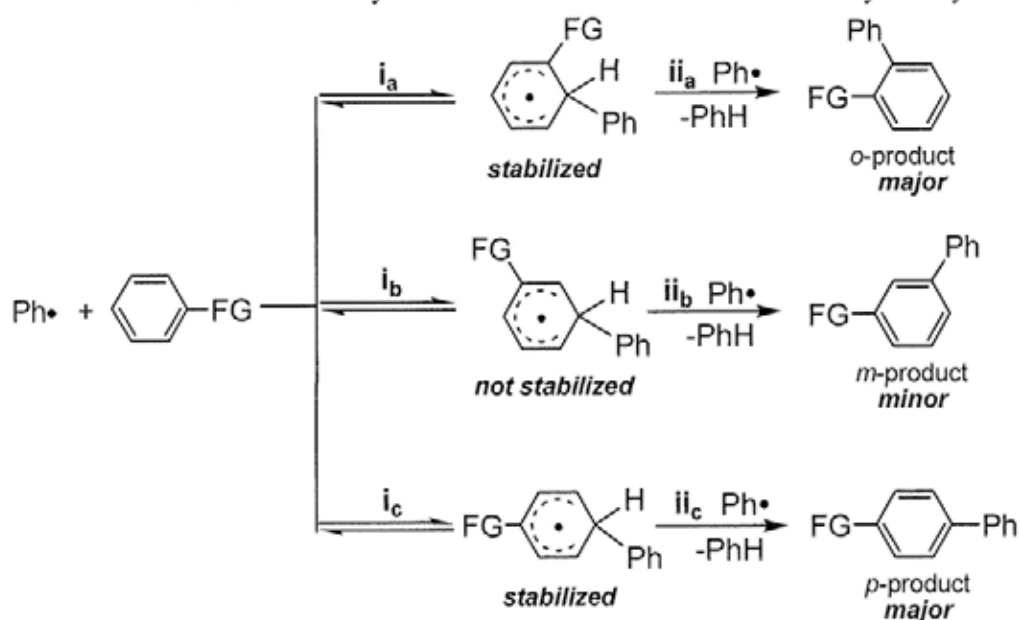
3.1.5 Radical Substituent Effects in Radical Reactions

The radical substituent parameters ($\sigma\bullet$) are obtained from the thermal rearrangements of aryl methylenecyclopropanes (Table 3.7).[29] During the rearrangements of methylenecyclopropanes, benzyl radical intermediates (**I**) are formed. Both the electron-donating *para*-groups ($\sigma_p^o < 0$, Table 3.7, entries 1, 2, 6-8) and electron-withdrawing *para*-groups ($\sigma_p^o > 0$, Table 3.7, entries 4, 10-13) can stabilize the benzyl radical intermediates (**I**), thereby increasing the rate of rearrangements ($k_{rel} > 1$). On the other hands, all the *meta*-groups (σ_m, Table 3.7, entries 5,

14-16) cannot stabilize the benzyl radicals (**I**) and generally do not promote the reaction rates ($k_{rel} \sim 1$).

Table 3.7 Radical Substituent Parameters ($\sigma\bullet$) in the Thermal Rearrangements of Arylmethylenecyclopropanes

(**I**)
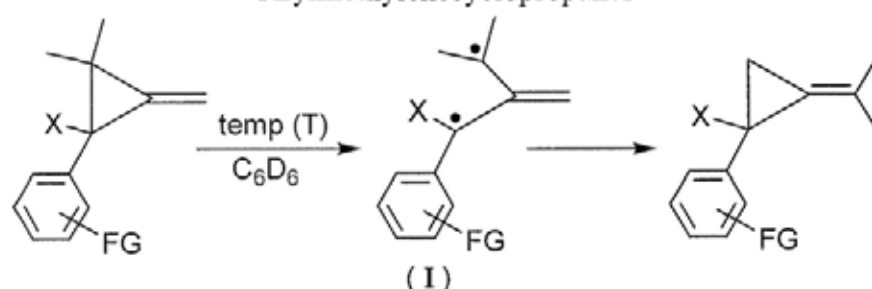
		X = H, T = 80 °C					X = CO$_2$Et, T = 100 °C		
entry	FG	$\sigma^{0\,a}$	$\sigma\bullet$	relative rate (k_{rel})	entry	FG	$\sigma^{0\,a}$	$\sigma\bullet$	relative rate (k_{rel})
1	*p*-NMe$_2$	-0.83	0.90	7.88	6	*p*-OMe	-0.27	0.24	1.72
2	*p*-SiMe$_3$	-0.07	0.18	1.53	7	*p*-^{t}Bu	-0.20	0.13	1.34
3	*p*-H	0.00	0.00	1.00	8	*p*-Me	-0.17	0.11	1.30
4	*p*-NO$_2$	0.78	0.57	3.76	9	*p*-H	0.00	0.00	1.00
5	*m*-NO$_2$	0.71	-0.11	0.77	10	*p*-Cl	0.23	0.12	1.33
					11	*p*-Br	0.23	0.13	1.36
					12	*p*-CO$_2$Me	0.25	0.35	2.26
					13	*p*-CN	0.66	0.46	2.87
					14	*m*-OMe	0.12	-0.02	0.95
					15	*m*-Me	-0.07	0.03	1.07
					16	*m*-CN	0.56	-0.12	0.75

[a] Hammett constant (Ref 27).

The substituents are then assigned the radical substituent parameter ($\sigma\bullet$). The magnitude of $\sigma\bullet$ reflects the ability of the substituent to stabilize the benzyl radical intermediate (**I**) to enhance the reaction rate. Thus, all the electron-donating and electron-withdrawing *para*-groups are activating and have the $\sigma\bullet$ values larger than 0 (Table 3.7, entries 1-4, 6-13), whereas all the unactivating *meta*-groups have the $\sigma\bullet$ values nearly to 0 (Table 3.7, entries 5, 14-16).

Indeed, the $\sigma\bullet$ values, which are originally applied in the reactions involving benzyl radical intermediate (Table 3.7), can partly support the rate-promoting effect by both the electron-donating and electron-withdrawing *para*-groups on the radical *ipso*-substitutions of ArX (Table 3.5, Scheme 3.16) and the homolytic aromatic substitution of arenes (Table 3.6, Scheme 3.17) via the stabilizations of cyclohexadienyl radical intermediates.

3.1.6 Selectivities in Aryl C-X and C-H Bond Cleavages

Halobenzenes (PhX, X = Cl, Br, I) contain both Ar-X and Ar-H bonds. Since Ar-X bonds (66-96 kcal mol^{-1}) (Table 3.2, entries 2-4)[2,3] are weaker than Ar-H bond (110-114 kcal mol^{-1}),[3] the cleavages of Ar-X bonds are usually kinetically more favorable. Moreover, oxidative additions of Ar-X bonds are usually thermodynamically more favorable than that of Ar-H bonds. This can be explained by the more exergonic oxidative addition of Vaska's complex (Ir^{I}(PPh$_3$)$_2$(CO)Cl) to Ph-X than that to XC$_6$H$_4$-H (Scheme 3.18). Therefore, selective Ar-X bond cleavages are much more commonly reported (Section 3.1.2.1).

Scheme 3.18 Thermodynamic Estimations of Oxidative Addition of Ar-X and Ar-H to Vaska's Complex
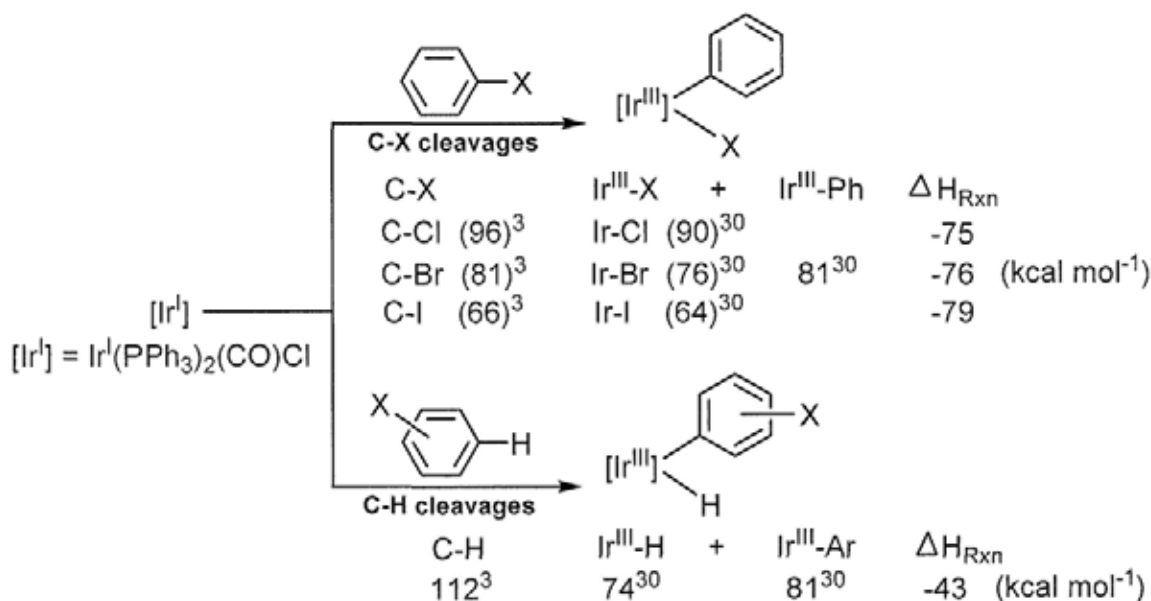
Depending on the natures of metals and ligands in the transition metal complexes and the reaction temperature, selective aryl C-H bond cleavage of halobenzenes can also occur as the kinetic or thermodynamic pathway without the C-X bond cleavage.

Some examples of selective aryl C-X and C-H bond cleavages by group 9 transition metal complexes are presented below.

3.1.6.1 Selective Aryl C-X Bond Cleavages

Rhodium(I) pincer complex (Rh^I(PNP)) undergoes oxidative addition of Ph-X (X = Cl, Br) at room temperature in 1 day to form Rh^{III}(PNP)(Ph)(X) as the thermodynamic product (eq 3.14).[31]

$$(3.14)$$

(a) X = Cl   62%
(b) X = Br   91%
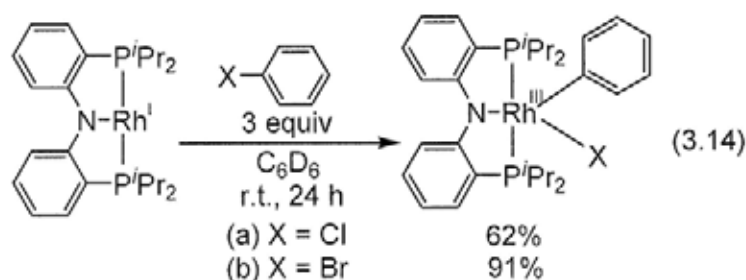
No oxidative addition of Ar-H bond was observed. It was proposed that the kinetic oxidative addition of Ar-H is very facile to hamper the observation of Rh^{III}(PNP)(C$_6$H$_4$X)(H), as the reverse reductive elimination of Rh^{III}(PNP)(C$_6$H$_4$X)(H) prepared *in-situ* was shown to be very fast to generate Rh^I(PNP), which further reacts rapidly with PhX to give Rh^{III}(PNP)(Ph)(X).

3.1.6.2 Kinetic Aryl C-H Bond Cleavages and Thermodynamic Aryl C-X Bond Cleavages

Iridium(I) pincer complex (Ir^I(PNP)) undergoes oxidative additions (OA) of both aryl C-H and C-X bonds of PhX (X = Cl, Br) (eq 3.15).[32]

$$(3.15)$$

	*m-, p-*Cl	*o-*Cl	
(a) r.t., <15 min	84%	11%	5%
(b) 70 °C, 72 h	0%	71%	5%
(c) 120 °C, 24 h	0%	15%	85%

	*o-, m-, p-*Cl	
(d) r.t., instantaneous	79%	15%
(e) 100 °C, 48 h	0%	85%
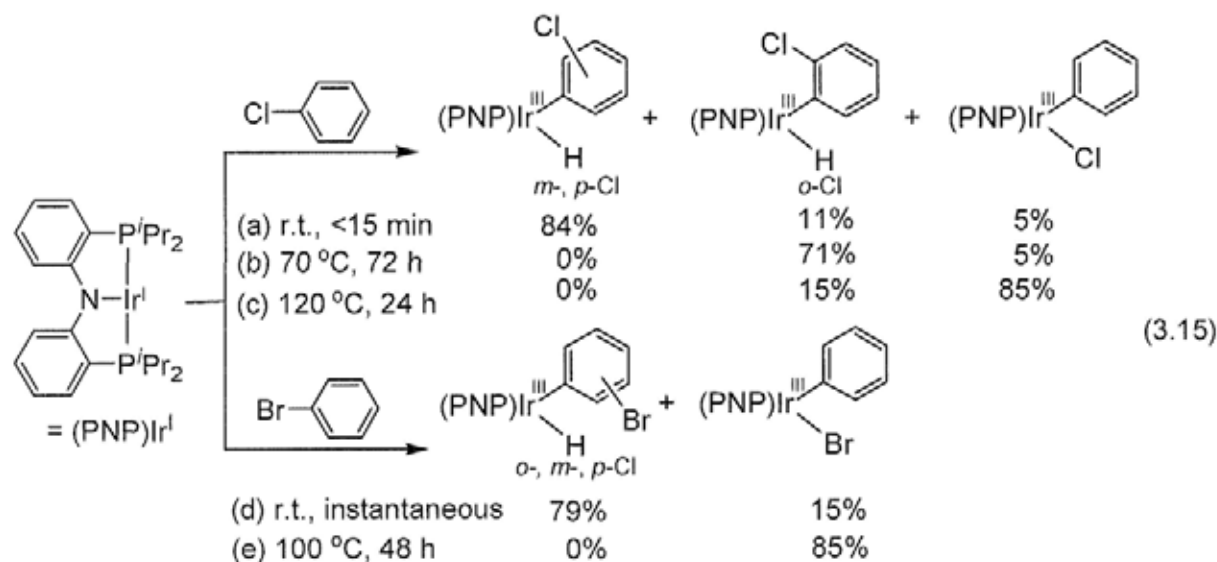
At room temperature, Ir^I(PNP) reacts with the aryl C-H bonds of PhCl to form *o-*, *m-*, and *p-*aryl C-H OA products with a trace of C-X OA product (eq 3.15(a)). At 70 °C, the *m-* and

p-aryl C-H OA products isomerize to form the most stable *o*-C-H OA product in 71% yield, likely due to the stabilization via Ir---*o*-Cl interaction and the strongest Ir-C bond among the isomeric C_6H_4Cl groups (eq 3.15(b)). At 120 °C, aryl C-H OA products are converted to the Ph-Cl OA product (eq 3.15(c)). Thus, C-H OA is the kinetic reaction, whereas C-Cl OA is the thermodynamic reaction. Similarly, Ir[I](PNP) undergoes the kinetic C-H OA and thermodynamic C-X OA of PhBr (eqs 3.15(d) and (e)). Therefore, the selectivities of C-H and C-X cleavages of PhX by Ir[I](PNP) can be controlled by varying the reaction temperature.

3.1.6.3 Selective Aryl C-H Bond Cleavages

Cationic iridium(I) pincer complex (Ir[I](PNP)[+]) underwent oxidative addition (OA) of the C-H bonds of PhX (X = Br, Cl) without OA of C-X bonds (Scheme 3.19).[33]

Scheme 3.19 C-H Bond Cleavages of Halobenzenes by Cationic Iridium(I) Pincer Complex

(a) X = Cl   100%   100%
(*o*- : *m*- : *p*- = 60% : 27% : 13%)

(b) X = Br   100%   70%
(*o*- : *m*- : *p*- = 70% : 20% : 10%)
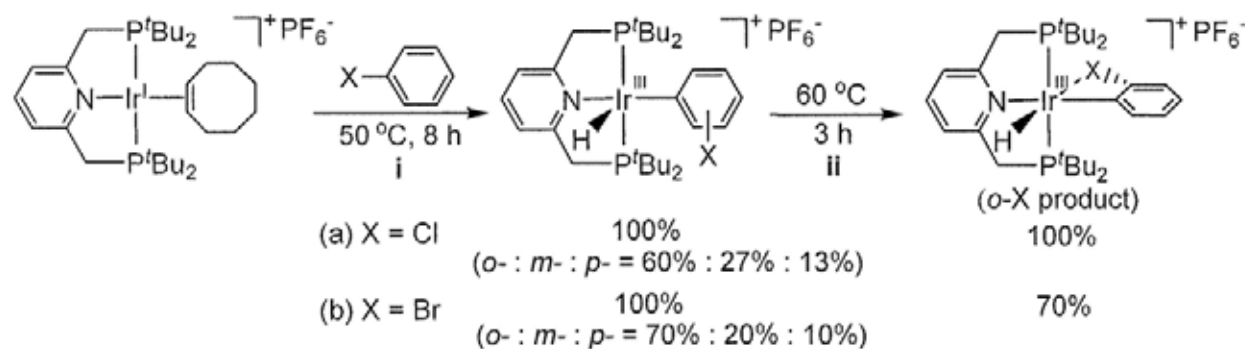
At 50 °C, Ir[I](PNP)[+] reacts with the C-H bonds of PhCl to give *o*-C-H, *m*-C-H, and *p*-C-H OA products in 60%, 27%, and 13% yields, respectively (Scheme 3.19, pathway a-i). The major *o*-C-H OA product is found to be the kinetic and thermodynamic product due to its stabilization by the ligation of *o*-Cl group to the cationic Ir[+]. Upon heating at 60 °C, all *m*-C-H and *p*-C-H OA products isomerize to generate the most stable *o*-C-H OA product (pathway a-ii). Reaction of Ir[I](PNP)[+] with PhBr followed the similar reaction pattern (pathways b-i and b-ii). Selective *o*-C-H cleavage of halobenzenes can thus be achieved.

3.1.7 Aryl C-X Bond Cleavages by Metalloporphyrins

3.1.7.1 Functionalizations of Aryl C-X Bonds by Palladium(II) Porphyrins

Metalloporphyrin-catalyzed cross-coupling reactions with ArX are rare. To our knowledge, only palladium(II) porphyrins have been used in the coupling reactions with aryl halides.[34] For example, water-soluble palladium(II) porphyrin is used as the catalyst in the C-C bond coupling reactions of ArBr with phenylboronic acid (eq 3.16).[34a] However, the reaction mechanism is not reported.

$$R-C_6H_4-Br + (HO)_2B-C_6H_5 \xrightarrow[\substack{K_2CO_3 \ (2 \ equiv) \\ H_2O, \ 100\,^\circ C, \ 1\text{-}4 \ h, \ air}]{Pd^{II}(por) \ (0.1 \ mol\%)} R-C_6H_4-C_6H_5 \quad (3.16)$$

R = OMe, H, CN, NO$_2$ 1.5 quiv   80-100%

$$Pd^{II}(por) = \text{[porphyrin structure]} \qquad Ar = -C_6H_4-O(CH_2)_3CO_2^-K^+$$
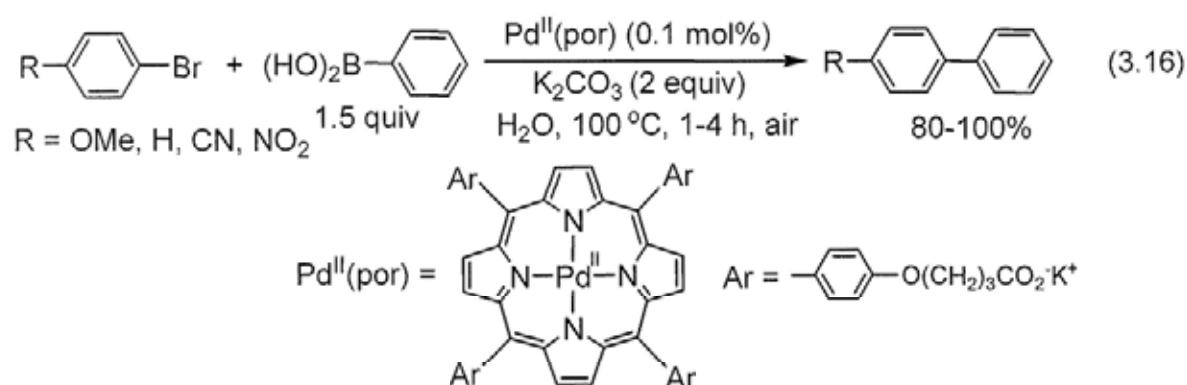
3.1.7.2 Aryl C-X Bond Cleavages by Group 9 Metalloporphyrins

The Chan group has studied the aryl C-Br bond cleavage of aryl bromides (ArBr, Ar = Ph, *p*-Tol) by high-valent rhodium(III) porphyrin (Rh^{III}(ttp)Cl, ttp = tetrakis(*p*-tolyl)porphyrin) to give rhodium(III) porphyrin aryls (Rh^{III}(ttp)Ar, Ar = Ph, *p*-Tol) (Table 3.8).[35] In the absence of base, Rh^{III}(ttp)Cl reacts with PhBr at 120 °C in 3 days to yield Rh^{III}(ttp)Ph and Rh^{III}(ttp)Br in 20% and 48% yields, respectively (Table 3.8, entry 1). When NaOH is added, the reaction rate is faster to give Rh^{III}(ttp)Ph in 86% yield (Table 3.8, entry 2). NaOH also promotes the Ar-Br cleavages of *m*-bromotoluene to yield Rh^{III}(ttp)(*m*-Tol) in 70% yield (Table 3.8, entry 3). However, the reaction mechanism has not been investigated.

Rhodium(III) porphyrin aryls (M^{III}(por)Ar), which are generated by the base-promoted Ar-Br cleavage with Rh^{III}(ttp)Cl (Table 3.8), can be potentially converted to aryl-C or aryl-heteroatom bonds to attain the functionalizations of ArBr. Hopefully, the understanding of

the initial aryl carbon-halogen bond cleavages by group 9 metalloporphyrins can help developing a novel catalytic system for the chemical transformations of ArX using group 9 metalloporphyrins. Iridium(III) porphyrin would be a suitable group 9 metalloporphyrin to study the reaction mechanism of the base-promoted Ar-X bond cleavages, since the iridium porphyrin species (e.g. Ir-C, Ir-H) are generally the most stable among the group 9 metal complexes.[36]

Moreover, to our knowledge, aryl C-X bond cleavages by high-valent group 9 metal(III) complexes have not been reported. The aryl C-X bond cleavages using high-valent group 9 metal(III) porphyrins would be mechanistically intriguing for investigation.

Table 3.8 Base-Promoted Aryl C-Br Bond Cleavages by Rh^{III}(ttp)Cl

entry	FG	NaOH (equiv)	time/h	Rh^{III}(ttp)Ar yield/%	Rh^{III}(ttp)Br yield/%
1	H	0	72	20	48
2	H	10	12	86	0
3	Me	10	24	70	0

3.1.8 Theme of the Chapter

The themes of this chapter report the results of the discoveries of base-promoted aryl carbon-halogen bond (Ar-X, X = Cl, Br, I) cleavages by iridium(III) porphyrin carbonyl chloride (Ir^{III}(ttp)(CO)Cl), involving:

(i) the scope of ArX.

(ii) the detailed mechanism of base-promoted Ar-X cleavages.

3.2 Results of Base-Promoted Aryl Carbon-Halogen Bond Cleavages by Iridium(III) Porphyrins

The base-promoted aryl carbon-halogen bond (Ar-X, X = Cl, Br, I) cleavages by high valent iridium(III) porphyrin carbonyl chloride (Ir^{III}(ttp)(CO)Cl) (**1a**) to form iridium(III) porphyrin aryls (Ir^{III}(ttp)Ar) were discovered. The key synthetic results are summarized in eq 3.17.

$$Ir^{III}(ttp)(CO)Cl \ + \ X\text{—}\underset{}{\bigcirc}\text{—FG} \ \xrightarrow[\text{C}_6\text{H}_6, \text{ temp, time}]{\text{base (20 equiv)}} \ Ir^{III}(ttp)\text{—}\underset{}{\bigcirc}\text{—FG} \quad (3.17)$$

FG = OMe, Me, H, F, C(O)Me, NO_2 ...

(a) X = Br, 1.1 equiv	base = K_2CO_3, 200 °C, 6-48 h	62-100%
(b) X = I, 1.1 equiv	base = NaOH, 150 °C, 9-24 h	77-99%
(c) X = Cl, 200 equiv	base = K_2CO_3, 150 °C, 22-168 h	32-100%
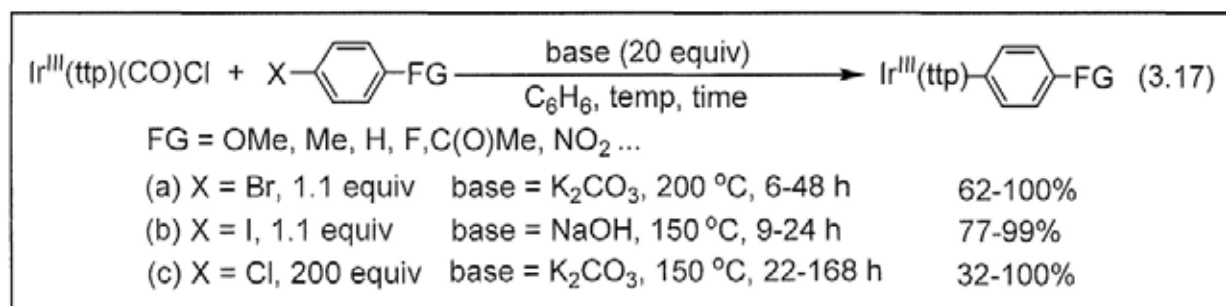
In this section, the following aspects of the reaction of base-promoted aryl C-X bond cleavages with Ir^{III}(ttp)(CO)Cl are discussed:

(i) Optimization of reaction conditions in base-promoted aryl C-X bond cleavages by Ir^{III}(ttp)(CO)Cl.

(ii) Reaction scope.

(iii) Reaction mechanisms.

3.2.1 Effect of Base on Rates of Ph-X Cleavages

Halobenzenes (PhX, X = Cl, Br, I) are used as typical aryl halides to study the aryl C-X bond cleavages by Ir^{III}(ttp)(CO)Cl. The effect of base on the rates of Ph-X bond cleavages by Ir^{III}(ttp)(CO)Cl was initially examined by reacting PhX with Ir^{III}(ttp)(CO)Cl without and with K_2CO_3 in solvent-free conditions (Table 3.9). K_2CO_3 was used since it is the optimal base in the base-promoted benzylic C-H bond cleavages by Ir^{III}(ttp)(CO)Cl to give iridium porphyrin benzyls (Section 1.8.4).[37]

In the absence of base, PhCl reacted with Ir^{III}(ttp)(CO)Cl at 200 °C in 3 days to generate

Ir^{III}(ttp)Ph in 26% yield and unreacted Ir^{III}(ttp)(CO)Cl was recovered in 45% yield (Table 3.9, entry 1). On the other hand, PhBr and PhI reacted with Ir^{III}(ttp)(CO)Cl at 200 °C in 2 days to yield Ir^{III}(ttp)(CO)Br (**1c**) in 62% yield, and Ir^{III}(ttp)(CO)I (**1d**) in 41% yield, respectively (Table 3.9, entries 3 and 5). Ir^{III}(ttp)Ph was also formed in the course of reactions with PhBr and PhI in 12 hours, but it decomposed upon prolonged heating in 2 days to form a black unknown complex (Table 3.9, entries 3 and 5). The reason was unclear. Presumably, PhBr and PhI are more oxidizing than PhCl that lead to the decomposition of Ir^{III}(ttp)Ph in excess PhBr and PhI.[38]

Table 3.9 Effect of Base on Ph-X Cleavage by Ir^{III}(ttp)(CO)Cl in Solvent-Free Conditions

$$Ir^{III}(ttp)(CO)Cl + \underset{xs}{PhX} \xrightarrow[\text{temp, N}_2,\ \text{time}]{K_2CO_3\ (equiv)} Ir^{III}(ttp)Ph + Ir^{III}(ttp)(CO)X$$

entry	PhX^a	K$_2$CO$_3$ (equiv)	temp/ °C	time/ h	Ir^{III}(ttp)Ph yield/%^{b}	Ir^{III}(ttp)(CO)X yield/%^{b}
1	PhCl	0	200	72	26	Ir^{III}(ttp)(CO)Cl (45)
2		20	200	12	84	0
3	PhBr	0	200	48	decomp.^{c}	Ir^{III}(ttp)(CO)Br (62)
4		20	150	12	91^d	0
5	PhI	0	200	48	decomp.^{c}	Ir^{III}(ttp)(CO)I (41)
6		20	150	36	93^e	0

^{a} Reaction in solvent-free conditions. ^{b} Isolated yield. ^{c} Ir^{III}(ttp)Ph was observed in 12 hours by thin-layer chromatography but decomposed in 2 days. ^{d} Ir^{III}(ttp)(CO)Br was observed in the course of reaction by thin-layer chromatography. ^{e} Ir^{III}(ttp)(CO)I was observed in the course of reaction by thin-layer chromatography.

When K$_2$CO$_3$ was added, Ir^{III}(ttp)(CO)Cl reacted with PhCl at 200 °C in 12 hours to give Ir^{III}(ttp)Ph in 84% yield (Table 3.9, entry 2). Ir^{III}(ttp)(CO)Cl also reacted much faster with PhBr and PhI in the presence of K$_2$CO$_3$ even at 150 °C to give Ir^{III}(ttp)Ph in 91% and 93% yields, respectively (Table 3.9, entries 4 and 6). Moreover, Ir^{III}(ttp)(CO)Br and Ir^{III}(ttp)(CO)I were also observed in the course of reaction, and they were further consumed to give Ir^{III}(ttp)Ph (Table 3.9, entries 4 and 6). Therefore, base does promote the Ph-X bond cleavages by

Ir^{III}(ttp)(CO)Cl to give Ir^{III}(ttp)Ph.

The effect of K$_2$CO$_3$ on Ph-X cleavage by Ir^{III}(ttp)(CO)Cl at lower loading of PhX (1.1 equiv) in benzene solvent was then studied (Table 3.10). The rates of Ph-X cleavages are much slower in benzene solution than that in solvent-free conditions (Table 3.9).

Table 3.10 Effect of Base on Ph-X Cleavage by Ir^{III}(ttp)(CO)Cl in Benzene

$$\text{Ir}^{III}\text{(ttp)(CO)Cl} + \underset{\text{1.1 equiv}}{\text{PhX}} \xrightarrow[\text{200 °C, N}_2, \text{ time}]{\text{K}_2\text{CO}_3 \text{ (equiv), C}_6\text{H}_6} \text{Ir}^{III}\text{(ttp)Ph} + \text{Ir}^{III}\text{(ttp)(CO)X}$$
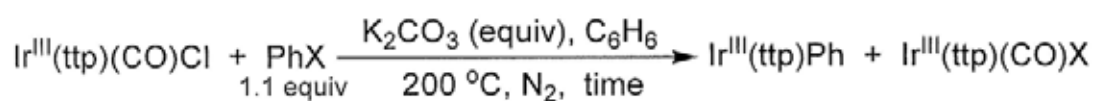
entry	PhX	time/d	K$_2$CO$_3$ (equiv)	Ir^{III}(ttp)Ph yield/%^{a}	Ir^{III}(ttp)(CO)X yield/%^{a}
1	PhCl	7	0	2^b	Ir^{III}(ttp)(CO)Cl (78)
2		1	20	31^c	
3	PhBr	7	0	9^b	Ir^{III}(ttp)(CO)Br (10), Ir^{III}(ttp)(CO)Cl (81)
4		2	20	100^d	
5	PhI	7	0	19^b	Ir^{III}(ttp)(CO)I (5), Ir^{III}(ttp)(CO)Cl (76)
6		3	20	81^e	

^{a} Isolated yield. ^{b} NMR yield. ^{c} Ir^{III}(ttp)(p-C$_6$H$_4$)Ir^{III}(ttp) in 3% yield and Ir^{III}(ttp)CH$_3$ in 3% yield were isolated. ^{d} Ir^{III}(ttp)(CO)Br was observed by thin layer chromatogrpahy in the course of reaction. ^{e} Ir^{III}(ttp)(CO)I was observed by thin-layer chromatography in the course of reaction.

In the absence of K$_2$CO$_3$, Ir^{III}(ttp)(CO)Cl reacted very slowly with PhCl in benzene at 200 °C in 7 days to give a trace of Ir^{III}(ttp)Ph (2%) and unreacted Ir^{III}(ttp)(CO)Cl was recovered in 78% yield (Table 3.10, entry 1). Ir^{III}(ttp)(CO)Cl also reacted very slowly with PhBr in benzene at 200 °C in 7 days to give small amounts of Ir^{III}(ttp)Ph (9%) and Ir^{III}(ttp)(CO)Br (10%), with a high yield of Ir^{III}(ttp)(CO)Cl (81%) remained unreacted (Table 3.10, entry 3). Similarly, Ir^{III}(ttp)(CO)Cl reacted very slowly with PhI in benzene at 200 °C in 7 days to give a modest amount of Ir^{III}(ttp)Ph (19%) and a trace of Ir^{III}(ttp)(CO)I (5%), with a high yield of Ir^{III}(ttp)(CO)Cl (76%) remained unreacted (Table 3.10, entry 5).

When K$_2$CO$_3$ was added, Ir^{III}(ttp)(CO)Cl reacted with PhCl (1.1 equiv) in benzene in 1 day to give Ir^{III}(ttp)Ph in 31% yield with the concomitant formations of small amounts of

$Ir^{III}(ttp)(p\text{-}C_6H_4)Ir^{III}(ttp)$ (3%) and $Ir^{III}(ttp)CH_3$ (3%) (Table 3.10, entry 2). K_2CO_3 also significantly promoted both the rates and yields of Ph-Br and Ph-I cleavages by $Ir^{III}(ttp)(CO)Cl$ to give high yields of $Ir^{III}(ttp)Ph$ in 100% and 91% yields, respectively (Table 3.10, entries 4 and 6). During the reactions with PhBr and PhI, $Ir^{III}(ttp)(CO)Br$ and $Ir^{III}(ttp)(CO)I$ were also formed and further consumed to give $Ir^{III}(ttp)Ph$. Indeed, base can also promote the Ph-X bond cleavages by $Ir^{III}(ttp)(CO)Cl$ in benzene solvent.

To further confirm that $Ir^{III}(ttp)Ph$ does come from Ph-X cleavage rather than the C-H bond activation of benzene,[39] the phenyl exchange of $Ir^{III}(ttp)Ph$ with benzene-d_6 was studied. $Ir^{III}(ttp)Ph$ did not react with K_2CO_3 and benzene-d_6 at 200 °C in 5 days to give any $Ir^{III}(ttp)C_6D_5$, and $Ir^{III}(ttp)Ph$ was recovered in 91% yield (eq 3.18). Therefore, selective Ph-X cleavage by $Ir^{III}(ttp)(CO)Cl$ takes place to give $Ir^{III}(ttp)Ph$.

$$Ir^{III}(ttp)Ph \xrightarrow[\substack{C_6D_6,\ 200\ ^\circ C,\ 5\ d}]{K_2CO_3\ (20\ equiv)} \text{No } Ir^{III}(ttp)C_6D_5 \quad (3.18)$$
$$\substack{\text{recovered} \\ 91\ \%}$$
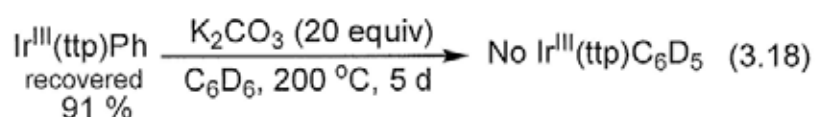
3.2.2 Optimizations of Base-Promoted Reaction Conditions

The base-promoted Ph-X bond cleavages by $Ir^{III}(ttp)(CO)Cl$ were further optimized in terms of (i) the types of bases, (ii) the loadings of bases, (iii) the loadings of PhX, and (iv) the reaction temperatures, in order to attain the highest efficiencies (rates and yields) of Ph-X cleavages.

3.2.2.1 Optimization of Base-Promoted Ph-Br Cleavage

(i) Optimization of Base

Initially, the nature of base on the efficiencies of base-promoted Ph-Br cleavage by $Ir^{III}(ttp)(CO)Cl$ at 150 °C was carried out. Stronger bases of KOH, NaOH, and Cs_2CO_3 reacted faster but gave $Ir^{III}(ttp)Ph$ in lower yields (Table 3.11, entries 1-3). K_3PO_4 gave the highest yield of $Ir^{III}(ttp)Ph$ but reacted most slowly (Table 3.11, entry 5), Therefore, K_2CO_3 was

selected as the optimal base, as it reacted considerably fast to give a high yield of $Ir^{III}(ttp)Ph$ (Table 3.11, entry 4). Likely, the intermediates formed during the reactions are unstable in the strongly basic media when stronger bases are used.

Table 3.11 Optimization of Base in Base-Promoted Ph-Br Cleavage

$$Ir^{III}(ttp)(CO)Cl + PhBr \xrightarrow[150\ ^{\circ}C,\ time,\ N_2]{base\ (20\ equiv)} Ir^{III}(ttp)Ph$$

entry	base	time/h	$Ir^{III}(ttp)Ph$ yield/%[a]
1	KOH	2	75
2	NaOH	2.5	75
3	Cs_2CO_3	3	83
4	K_2CO_3	12	91
5	K_3PO_4	20	97

[a] Isolated yield.

(ii) Optimization of Base Loading

The optimal loading of K_2CO_3 used was found to be 20 equiv (Table 3.12, entry 2), since a lower loading of 10 equiv K_2CO_3 and a higher loading of 30 equiv K_2CO_3 both gave lower yields of $Ir^{III}(ttp)Ph$ (Table 3.12, entries 1 and 3).

Table 3.12 Optimization of Loadings of K_2CO_3 in Ph-Br Cleavage

$$Ir^{III}(ttp)(CO)Cl + PhBr \xrightarrow[150\ ^{\circ}C,\ time,\ N_2]{K_2CO_3\ (equiv)} Ir^{III}(ttp)Ph$$

entry	K_2CO_3 equiv	time/h	$Ir^{III}(ttp)Ph$ yield/%[a]
1	10	24	74
2	20	12	91
3	30	6	84

[a] Isolated yields.

(iii) Optimization of PhBr Loading

Since 1.1 equiv of PhBr was sufficient to react with $Ir^{III}(ttp)(CO)Cl$ in benzene at 150 °C in 4 days to give $Ir^{III}(ttp)Ph$ in a high yield (Table 3.13, entry 1), the loading of PhBr was selected to be 1.1 equiv.

Table 3.13 Optimization of PhBr Loading in Ph-Br Cleavage

$$Ir^{III}(ttp)(CO)Cl + PhBr \xrightarrow[\substack{C_6H_6,\ 150\ ^\circ C,\ N_2 \\ time}]{K_2CO_3\ (20\ equiv)} Ir^{III}(ttp)Ph$$
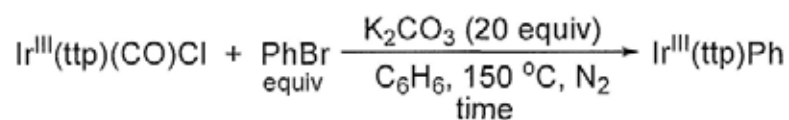
entry	PhBr (equiv)	time/d	$Ir^{III}(ttp)Ph$ yield /%[a]
1	1.1	4	87
2	~550[b]	0.5	91

[a] Isolated yield. [b] The reaction was carried out in solvent-free conditions without the addition of benzene solvent.

(iv) Optimization of Temperature

At 200 °C, $Ir^{III}(ttp)(CO)Cl$ reacted faster with PhBr (1.1 equiv) and K_2CO_3 (20 equiv) in benzene solvent in 2 days to yield $Ir^{III}(ttp)Ph$ quantitatively (Table 3.14, entry 2). At lower temperature of 150 °C, the reaction was slower to gave a lower yield of $Ir^{III}(ttp)Ph$ (Table 3.14, entry 1). 200 °C was thus selected as the optimal temperature in the subsequent studies in benzene solvent.

Table 3.14 Optimization of Temperature in Ph-Br Cleavage

$$Ir^{III}(ttp)(CO)Cl + \underset{1.1\ equiv}{PhBr} \xrightarrow[\substack{C_6H_6,\ temp,\ N_2 \\ time}]{K_2CO_3\ (20\ equiv)} Ir^{III}(ttp)Ph$$
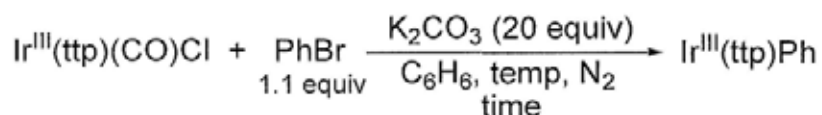
entry	temp/°C	time/d	$Ir^{III}(ttp)Ph$ yield/%[a]
1	150	4	87
2	200	2	100

[a] Isolated yield.

3.2.2.2 Optimization of Base-Promoted Ph-I Cleavage

(i) Optimization of Base

The nature of base on the rate and yield of Ph-I cleavage by $Ir^{III}(ttp)(CO)Cl$ was studied. Strong base of KOH reacted very fast with $Ir^{III}(ttp)(CO)Cl$ and PhI (1.1 equiv) in benzene at 150 °C but gave lower yield of $Ir^{III}(ttp)Ph$ (Table 3.15, entry 1). Cs_2CO_3 and K_3PO_4 also reacted to give lower yields of $Ir^{III}(ttp)Ph$ (Table 3.15, entries 3 and 5). While K_2CO_3 can

enhance both the rate and yield in the Ph-Br cleavage (Table 3.11, entry 4), K_2CO_3 reacted very slowly in 5 days to give $Ir^{III}(ttp)Ph$ in a lower yield (Table 3.15, entry 4). Indeed, NaOH was found to react very fast to give $Ir^{III}(ttp)Ph$ quantitatively (Table 3.15, entry 2). Therefore, NaOH was selected as the optimal base.

Table 3.15 Optimization of base in Ph-I Cleavage

$$Ir^{III}(ttp)(CO)Cl + PhI \xrightarrow[\text{1.1 equiv } 150\,°C,\text{ time, } N_2]{\text{base (20 equiv)}} Ir^{III}(ttp)Ph$$

entry	base	time/d	$Ir^{III}(ttp)Ph$ yield/%[a]
1	KOH	0.5	70
2	NaOH	0.5	99
3	Cs_2CO_3	1	82
4	K_2CO_3	5	78
5	K_3PO_4	1.5	82

[a] Isolated yield.

(ii) Base Loading

NaOH in 20 equiv was found to be the optimal loading in efficiently promoting the rate and yield of Ph-I cleavage (Table 3.16, entry 2). A lower NaOH loading (10 equiv) resulted in a lower rate and yield (Table 3.16, entry 1), while a higher NaOH loading (30 equiv) did not render profound effects in rate and yield enhancements (Table 3.16, entry 3).

Table 3.16 Optimization of Base Loading in Ph-I Cleavage

$$Ir^{III}(ttp)(CO)Cl + PhI \xrightarrow[\text{1.1 equiv } C_6H_6,\ 150\,°C,\ N_2,\text{ time}]{\text{NaOH (equiv)}} Ir^{III}(ttp)Ph$$

entry	NaOH (equiv)	time/h	Ir(ttp)Ph yield /%[a]
1	10	24	87
2	20	12	99
3	30	9	95

[a] Isolated yield.

(iii) Optimization of Temperature

When the reaction temperature was increased from 120 to 200 °C, the rate of Ph-I cleavage

increased (Table 3.17). Since the reaction rate was considerably fast and the yield of Ir^{III}(ttp)Ph was highest at 150 °C, 150 °C was selected as the optimal temperature (Table 3.17, entry 2).

Table 3.17 Optimization of Temperature in Ph-I Cleavage

$$Ir^{III}(ttp)(CO)Cl + \underset{1.1\ equiv}{PhI} \xrightarrow[C_6H_6,\ temp,\ N_2,\ time]{NaOH\ (20\ equiv)} Ir^{III}(ttp)Ph$$

entry	temp/ °C	time/h	Ir^{III}(ttp)Ph yield/%[a]
1	120	20	90
2	150	12	99
3	200	2	97

[a] Isolated yield.

(iv) Optimization of Loading of PhI

1.1 equiv of PhI was adopted as the optimal loading of PhI, since it is sufficient to produce Ir^{III}(ttp)Ph quantitatively (Table 3.17, entry 2).

3.2.2.3 Optimization of Base-Promoted Ph-Cl Cleavage

(i) Optimization of Base

The nature of base on the efficiency of Ph-Cl cleavage was initially studied by reacting Ir^{III}(ttp)(CO)Cl and PhCl (1.1 equiv) at 200 °C with various bases. Ir^{III}(ttp)Ph was isolated as the major product, accompanied with other co-products, Ir^{III}(ttp)(p-C_6H_4)Ir^{III}(ttp) (**9a**) or Ir^{III}(ttp)CH$_3$ (**10**),[40] in smaller amounts (Table 3.18).

Table 3.18 Optimization of Base in Base-Promoted Ph-Cl Cleavage

$$Ir^{III}(ttp)(CO)Cl + \underset{1.1\ equiv}{PhCl} \xrightarrow[\substack{C_6H_6,\ 200\ °C,\ N_2 \\ time}]{base\ (20\ equiv)} Ir^{III}(ttp)Ph + Ir^{III}(ttp)(p\text{-}C_6H_4)Ir^{III}(ttp) + Ir^{III}(ttp)CH_3$$
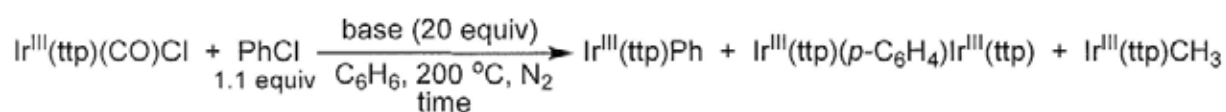
entry	base	time	Ir^{III}(ttp)Ph yield/%[a]	Ir^{III}(ttp)(p-C_6H_4)Ir^{III}(ttp) yield/%[a]	Ir^{III}(ttp)CH$_3$ yield/%[a]	total yield/%[a]
1	NaOH	24	20		6	26
2	KOH	20	18		2	20
3	K_2CO_3	24	31	3	3	37
4	K_3PO_4	96	20		16	36

[a] Isolated yield.

Since K_2CO_3 led to the highest yield of $Ir^{III}(ttp)Ph$, K_2CO_3 was selected as the optimal base for subsequent optimizations (Table 3.18, entry 3).

(ii) Optimization of PhCl Loading

In order to further promote the yield of $Ir^{III}(ttp)Ph$, the effect of PhCl loading was studied. When the amount of PhCl was increased from 1.1 to 200 equiv, the reaction rate and yield of $Ir^{III}(ttp)Ph$ were increased accordingly (Table 3.19, entries 1-4). Further increase of PhCl loading to 300 equiv did not further promote the total yield (Table 3.19, entry 5). Thus, 200 equiv PhCl was chosen as the optimal loading.

Table 3.19 Optimization of PhCl Loading in Base-Promoted Ph-Cl Cleavage
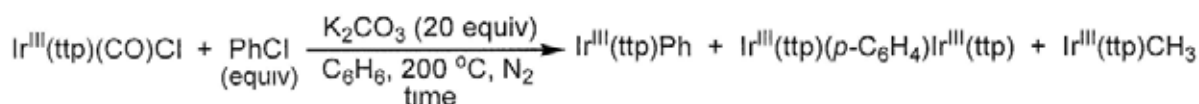
$$Ir^{III}(ttp)(CO)Cl + PhCl \xrightarrow[\substack{C_6H_6,\ 200\ ^{\circ}C,\ N_2 \\ time}]{K_2CO_3\ (20\ equiv)} Ir^{III}(ttp)Ph + Ir^{III}(ttp)(p\text{-}C_6H_4)Ir^{III}(ttp) + Ir^{III}(ttp)CH_3$$

entry	PhCl (equiv)	time/h	$Ir^{III}(ttp)Ph$ yield/%[a]	$Ir^{III}(ttp)(p\text{-}C_6H_4)Ir^{III}(ttp)$ yield/%[a]	$Ir^{III}(ttp)CH_3$ yield/%[a]	total yield/%
1	1.1	24	31	3	3	37
2	50	12	57	3	5	65
3	100	10	62	2	0	64
4	200	7	75	2[b]	0	77[c]
5	300	12	79	1[b]	0	80

[a] Isolated yield [b] NMR yield [c] 1,4-dichlorobenzene in 1% yield was detected by GC-MS analysis

(iii) Optimization of Base Loading

20 equiv K_2CO_3 was selected as the optimal base loading as it was found to efficiently promote the rate and yield of $Ir^{III}(ttp)Ph$ (Table 3.20, entry 2), compared with 10 and 30 equiv K_2CO_3 (Table 3.20, entries 1 and 3).

Table 3.20 Optimization of K$_2$CO$_3$ Loading in Base-Promoted Ph-Cl Cleavage

$$Ir^{III}(ttp)(CO)Cl + \underset{200 \text{ equiv}}{PhCl} \xrightarrow[\text{C}_6\text{H}_6,\ 200\ ^\circ\text{C},\ \text{N}_2]{\text{K}_2\text{CO}_3\ (\text{equiv})} Ir^{III}(ttp)Ph + Ir^{III}(ttp)(p\text{-C}_6\text{H}_4)Ir^{III}(ttp)$$
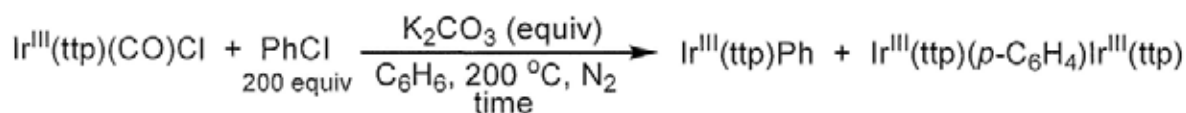
entry	K$_2$CO$_3$ equiv	time/ h	Ir^{III}(ttp)Ph yield/%[a]	Ir^{III}(ttp)(p-C$_6$H$_4$)Ir^{III}(ttp) yield/%[b]	total yield/%
1	10	19	63	2	65
2	20	7	75	2	77[c]
3	30	11	64	2	66

[a] Isolated yield. [b] NMR yield. [c] 1,4-dichlorobenzene in 1% yield was detected by GC-MS analysis.

(iv) Optimization of Temperature

At 150 and 200 $^\circ$C, Ir^{III}(ttp)(CO)Cl reacted with PhCl (200 equiv) and K$_2$CO$_3$ (20 equiv) to give similar yields of Ir^{III}(ttp)Ph (Table 3.21). A trace of 1,4-dichlorobenzene (~1%) was also formed in both reaction conditions. 150 $^\circ$C was selected as the optimal temperature for subsequent study of reaction scope (Table 3.21, entry 1).

Table 3.21 Optimization of Temperature in Base-Promoted Ph-Cl Cleavages

$$Ir^{III}(ttp)(CO)Cl + \underset{200 \text{ equiv}}{PhCl} \xrightarrow[\text{C}_6\text{H}_6,\ \text{temp},\ \text{N}_2]{\text{K}_2\text{CO}_3\ (20\ \text{equiv})} Ir^{III}(ttp)Ph + Ir^{III}(ttp)(p\text{-C}_6\text{H}_4)Ir^{III}(ttp)$$
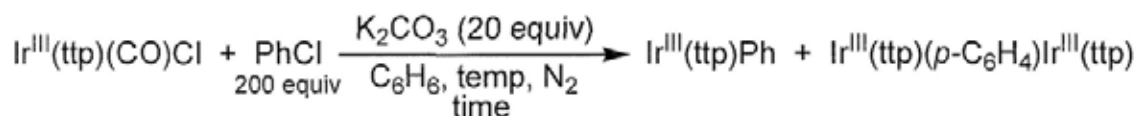
entry	temp/$^\circ$C	time/h	Ir^{III}(ttp)Ph yield/%[a]	Ir^{III}(ttp)(p-C$_6$H$_4$)Ir^{III}(ttp) yield/%[b]	total yield/%
1	150	22	74	5	79[c]
2	200	7	75	2	77[d]

[a] Isolated yield. [b] NMR yield. [c] 1,4-dichlorobenzene in 1% yield was detected by GC-MS analysis. [d] 1,4-dichlorobenzene in <1% yield was detected by GC-MS analysis.

3.2.3 Summary of Optimization of Base-Promoted Ph-X Cleavages by Ir^{III}(ttp)(CO)Cl

The optimized reaction conditions of base-promoted Ph-X bond cleavages in benzene solvent are summarized in Table 3.22. In Ph-Br cleavage, 1.1 equiv of PhBr was sufficient to react with Ir^{III}(ttp)(CO)Cl and K$_2$CO$_3$ at 200 $^\circ$C in 2 days to yield Ir^{III}(ttp)Ph quantitatively

(Table 3.22, entry 1). In Ph-I cleavage, 1.1 equiv of PhI was also enough to react with $Ir^{III}(ttp)(CO)Cl$ and NaOH (20 equiv) at 150 °C in 12 hours to give $Ir^{III}(ttp)Ph$ quantitatively (Table 3.22, entry 2). In Ph-Cl cleavage, a high loading of PhCl (200 equiv) was required to react with $Ir^{III}(ttp)(CO)Cl$ and K_2CO_3 at 150 °C to give a high yield of $Ir^{III}(ttp)Ph$ in 74% yield and a trace of $Ir^{III}(ttp)(p\text{-}C_6H_4)Ir^{III}(ttp)$ (Table 3.22, entry 3). The optimized conditions were then used to study the substrate scope of ArX in base-promoted Ar-X cleavages by $Ir(ttp)(CO)Cl$ (Section 3.2.5).

Table 3.22 Optimized Conditions of Base-Promoted Ph-X Cleavages by $Ir^{III}(ttp)(CO)Cl$

$$Ir^{III}(ttp)(CO)Cl + \underset{equiv}{PhX} \xrightarrow[C_6H_6, \text{ temp, time}]{\text{base (20 equiv)}} Ir^{III}(ttp)Ph$$

entry	PhX (equiv)	base	temp/°C	time	$Ir^{III}(ttp)Ph$ yield /%[a]
1	PhBr (1.1)	K_2CO_3	200	2 d	100
2	PhI (1.1)	NaOH	150	12 h	99
3	PhCl (200)	K_2CO_3	150	22 h	74[b]

[a] Isolated yield. [b] $Ir^{III}(ttp)(p\text{-}C_6H_4)Ir^{III}(ttp)$ in 5% NMR yield was estimated by ^1H NMR spectroscopy, and 1,4-dichlorobenzene in 1% yield was detected by GC-MS analysis.

3.2.4 Comparison of Reactivities of Aryl C-X Bond Cleavages by $Ir^{III}(ttp)(CO)Cl$

To study the effect of nature of halogen group of ArX on the rate of Ar-X cleavages, competition reactions of base-promoted Ar-X cleavages of 1,4-dihalobenzenes containing 2 different halogens were studied. When excess 1-bromo-4-iodobenzene was reacted with $Ir^{III}(ttp)(CO)Cl$ and K_2CO_3 at 200 °C, only the weaker C-I bond was selectively cleaved to yield $Ir^{III}(ttp)C_6H_4(p\text{-}Br)$ (**8i**) (Table 3.23, entry 1). Similarly, only the weaker C-Br bond in 1-bromo-4-chlorobenzene was cleaved to give $Ir^{III}(ttp)C_6H_4(p\text{-}Cl)$ (**8j**) (Table 3.23, entry 2), and only the weaker C-Cl bond in 1-chloro-4-fluorobenzene was cleaved to give $Ir^{III}(ttp)C_6H_4(p\text{-}F)$ (**8h**) (Table 3.23, entry 3). Therefore, the weaker C-X bond does react much faster in base-promoted Ar-X cleavages. The rate of Ar-X cleavage is established to be in the

order: C-F < C-Cl < C-Br < C-I, which is in line with the bond strengths of aryl C-X bonds.

Table 3.23 Competition Reactions in 1,4-Dihalobenzenes

$$Ir^{III}(ttp)(CO)Cl \ + \ X\!-\!\!\langle\ \rangle\!\!-\!X' \ \xrightarrow[\substack{C_6H_6, \ 200\,^{\circ}C, \ N_2 \\ time}]{K_2CO_3 \ (20 \ equiv)} \ Ir^{III}(ttp)\!-\!\!\langle\ \rangle\!\!-\!X'$$

50 equiv $Ir^{III}(ttp)Ar$

entry	$X\!-\!\!\langle\ \rangle\!\!-\!X'$	time/h	$Ir^{III}(ttp)Ar$ (yield/%[a])
1	$I\!-\!\!\langle\ \rangle\!\!-\!Br$	6	$Ir^{III}(ttp)C_6H_4(p\text{-}Br)$ (**8i**) (86)
2	$Br\!-\!\!\langle\ \rangle\!\!-\!Cl$	21	$Ir^{III}(ttp)C_6H_4(p\text{-}Cl)$ (**8j**) (66)
3	$Cl\!-\!\!\langle\ \rangle\!\!-\!F$	24	$Ir^{III}(ttp)C_6H_4(p\text{-}F)$ (**8h**) (66)
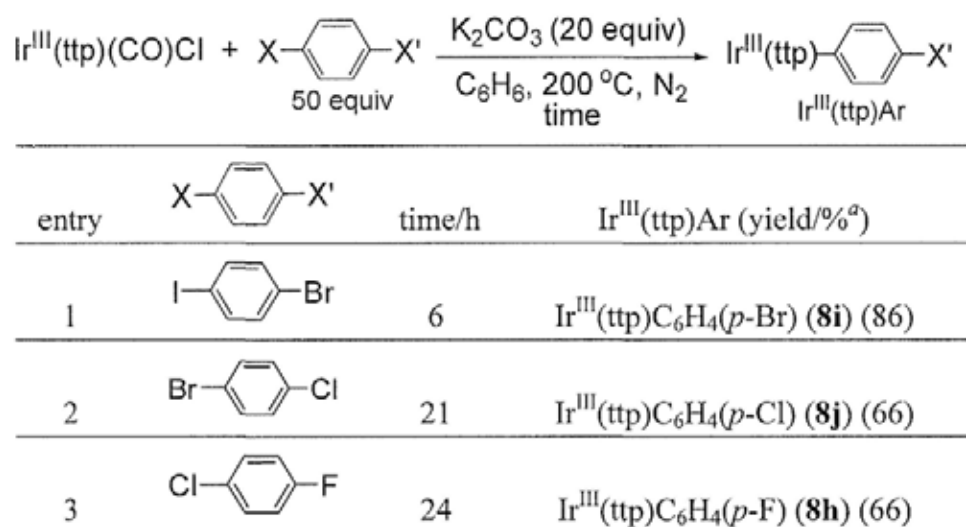
[a] Isolated yield.

3.2.5 Reaction Scope of Base-Promoted Aryl C-X Cleavages by $Ir^{III}(ttp)(CO)Cl$

The substrate scope of base-promoted aryl C-X cleavages by $Ir^{III}(ttp)(CO)Cl$ were further studied by using various 4-substituted aryl halides (ArX) in the optimized base-promoted reaction conditions for Ph-X cleavages (Table 3.22).

3.2.5.1 Reaction Scope of Base-Promoted Ar-Br Cleavage

Generally, all 4-substituted aryl bromides (ArBr) reacted with $Ir^{III}(ttp)(CO)Cl$ and K_2CO_3 at 200 °C to undergo selective Ar-Br bond cleavage to yield iridium(III) porphyrin aryls ($Ir^{III}(ttp)Ar$) in moderate to high yields (Table 3.24). The only exception was 1-bromo-4-iodobenzene, which underwent the more facile, selective C-I bond cleavage to yield $Ir^{III}(ttp)C_6H_4(p\text{-}Br)$ (**8i**) without any C-Br bond cleavages (Table 3.24, entry 10). $Ir^{III}(ttp)(CO)Br$ was also observed by thin-layer chromatography in the course of reactions, and it was further consumed upon further heating to yield $Ir^{III}(ttp)Ar$.

Table 3.24 Reaction Scope of K_2CO_3-Promoted Ar-Br Cleavage by $Ir^{III}(ttp)(CO)Cl$

$$Ir^{III}(ttp)(CO)Cl + Br-\langle\!\!\!\bigcirc\!\!\!\rangle-FG \xrightarrow[200\,^{\circ}C,\ time,\ N_2]{K_2CO_3\ (20\ equiv),\ C_6H_6} Ir^{III}(ttp)-\langle\!\!\!\bigcirc\!\!\!\rangle-FG$$

1.1 equiv $Ir^{III}(ttp)C_6H_4(p\text{-}FG)$

entry[a]	FG	time/h	$Ir^{III}(ttp)Ar$ yield/%[b]	entry[a]	FG	time/h	$Ir^{III}(ttp)Ar$ yield/%[b]
1	NMe$_2$	6	8b$_1$[c] (62)	10	I	19	$Ir^{III}(ttp)C_6H_4(p\text{-}Br)$[e] 8i (88)
2	OMe	9	8c (89)	11	Cl	24	8j (72)
3	^{t}Bu	15	8d (86)	12	CO$_2$Me	36	8k (84)
4	Me	11	8e (73)	13	C(O)Me	19	8l (82)
5	SiMe$_3$	15	8f (80)	14	CHO	11	8m (61)[f]
6	H	48	8a (100)	15	CF$_3$	24	8n (72)
7	NPhth[d]	27	8g (68)	16	CN	24	8o (62)[g]
8	F	20	8h (99)	17	NO$_2$	6	8p (63)
9	Br	36	8i (76)	18	Br—(naphthyl)	19	$Ir^{III}(ttp)$—(naphthyl) 8q (85)
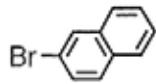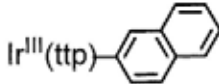
[a] $Ir^{III}(ttp)(CO)Br$ was observed in the course of reaction by thin-layer chromatography, which was further consumed. [b] Isolated yield. [c] PPh$_3$ was added to form $Ir^{III}(ttp)(PPh_3)C_6H_4(p\text{-}NMe_2)$. [d] NPhth: phthalimide. [e] C-I cleavage occurred. [f] PPh$_3$ was added to form $Ir^{III}(ttp)(PPh_3)C_6H_4(p\text{-}CHO)$. [g] PPh$_3$ was added to form $Ir^{III}(ttp)(PPh_3)C_6H_4(p\text{-}CN)$.

4-Bromotoluene and 4-bromobenzaldehyde also reacted to yield only $Ir^{III}(ttp)(p\text{-}Tol)$ (8e) and $Ir^{III}(ttp)C_6H_4(p\text{-}CHO)$ (isolated as $Ir^{III}(ttp)C_6H_4(p\text{-}CHO)(PPh_3)$ (8m)), respectively, via selective C-Br bond cleavage without any benzylic[37,41] and aldehydic C-H[42] bond activations (Table 3.24, entries 4 and 14). Likely, the weaker C-Br bonds (BDE = 80.5 kcal mol^{-1})[2,3] reacts more facilely than the stronger benzylic C-H (BDE = 88.5 kcal mol^{-1})[3] and the aldehylic C-H bonds (BDE ~ 85 kcal mol^{-1}).[3]

Both electron-rich (Table 3.24, entries 1-5) and electron-poor (Table 3.24, entries 7-9, 11-17) reacted smoothly to give $Ir^{III}(ttp)Ar$, showing high functional-group compatibilities. They also generally reacted faster than the parent bromobenzene (Table 3.24, entry 6).

Other halogenated aromatic compound, 2-bromonaphthalene, also underwent the C-Br cleavage to yield $Ir^{III}(ttp)(2\text{-}naphthyl)$ (8q) (Table 3.24, entry 18).

In the reactions with 4-bromobenzaldehyde and 4-bromobenzonitrile (Table 3.24, entries 14 and 16), brown precipitates were initially formed upon the consumption of $Ir^{III}(ttp)(CO)Cl$. The precipitates were insoluble in common solvents for purification by column chromatography or recrystallization. Presumably, $Ir^{III}(ttp)C_6H_4(p\text{-}CHO)$[43] and $Ir^{III}(ttp)C_6H_4(p\text{-}CN)$,[44] once formed, undergo extensive intermolecular coordinations to give insoluble oligomers (eqs 3.19 and 3.20). PPh$_3$ was thus added to generate the isolable, coordinatively-saturated $Ir^{III}(ttp)(PPh_3)C_6H_4(p\text{-}CHO)$ (**8m**) and $Ir^{III}(ttp)(PPh_3)C_6H_4(p\text{-}CN)$ (**8o**).
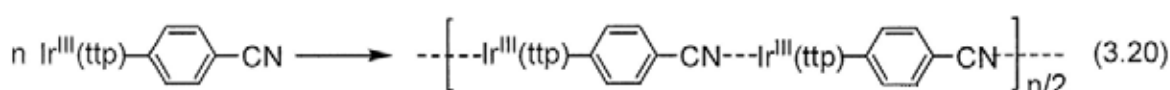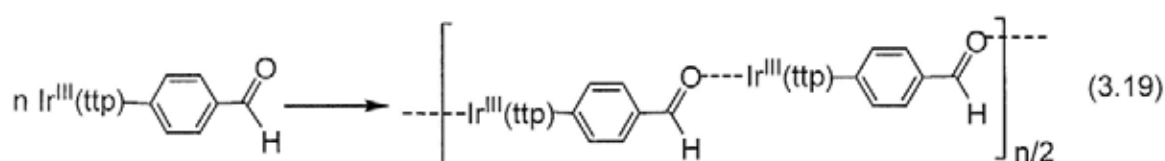
In the reaction with 4-bromo-N,N-dimethyl-aniline (Table 3.24, entry 1), $Ir^{III}(ttp)C_6H_4(p\text{-}NMe_2)$ (**8b**) was initially isolated as confirmed by high-resolution mass spectrometric (HRMS) analysis, but it shows upfield and broad proton signals in CDCl$_3$ by ^{1}H NMR spectroscopy (δ(pyrrole H) = 7.81 ppm) (Figure 3.1).[45] However, its single crystal has not been successfully grown. Presumably, the electron-donating NMe$_2$ group releases single electron[46] to the relatively electron-deficient porphyrin ring to form NMe$_2^{+\cdot}$ and porphyrin anionic radical, which becomes paramagnetic and more electron-rich for the broadening and upfielding effects, respectively, in the proton signals of ^{1}H NMR spectroscopy (Scheme 3.20, pathway i). Upon the addition of PPh$_3$, $Ir^{III}(ttp)(PPh_3)C_6H_4(p\text{-}NMe_2)$ (**8b$_1$**) was formed (Table 3.24, entry 1). The PPh$_3$-coordinated $Ir^{III}(ttp)(PPh_3)C_6H_4(p\text{-}NMe_2)$ enriches the electron density of the porphyrin ring, resulting in the transfer of electron from the porphyrin ring back to the NMe$_2^{+\cdot}$ group (Scheme 3.20, pathway ii) to obtain normal sharp proton signals in ^{1}H NMR spectroscopy.
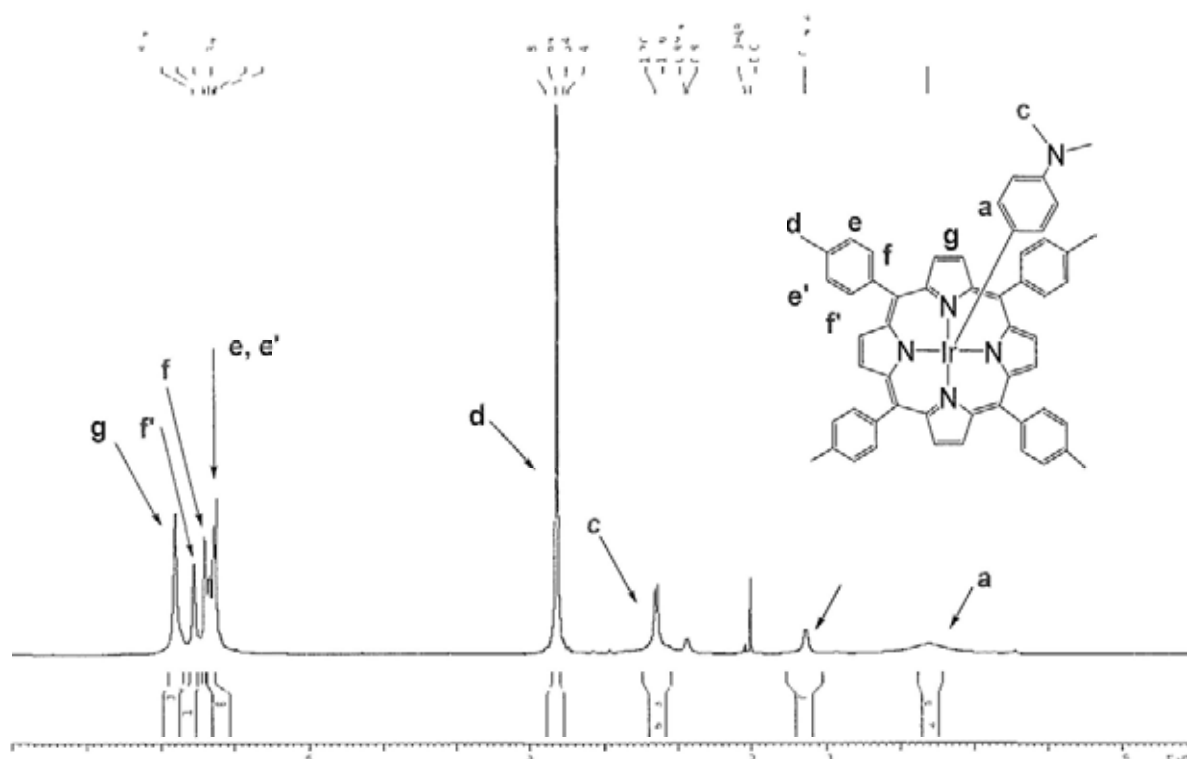
Figure 3.1 ^{1}H NMR spectrum of Ir^{III}(ttp)C$_6$H$_4$(p-NMe$_2$) in CDCl$_3$ with the upfield proton signals

Scheme 3.20 Proposed Mechanism of Single Electron Transfer from NMe$_2$ Group to Porphyrin Ligand of Ir^{III}(ttp)C$_6$H$_4$(p-NMe$_2$) in CDCl$_3$
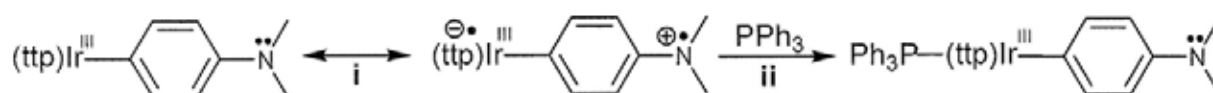
When the substituents in *para*-substituted aryl bromides contain acidic protons (NH$_2$, OH, CO$_2$H), no Ar-Br cleavages occurred to yield Ir^{III}(ttp)Ar (Table 3.25, entries 1, 2, and 4). Instead, Ir^{III}(ttp)(CO)Cl decomposed or unknown products were formed. The reasons of these unsuccessful reactions are unclear Presumably, the acidic proton of NH$_2$, OH, and CO$_2$H further reacts with the intermediates to form unknown products, which further decompose upon heating On the other hand, the C(O)Cl and OSiMe$_3$ groups are likely hydrolyzed by base to form CO$_2$H and OH groups, respectively, which lead to unknown product formations (Table 3 25, entries 3 and 5).

Table 3.25 Substrate Scope of Unsuccessful Base-Promoted Ar-Br Cleavages

$$\text{Ir}^{III}(\text{ttp})(\text{CO})\text{Cl} + \text{Br}\!\!-\!\!\langle\!\!\bigcirc\!\!\rangle\!\!-\!\!\text{FG} \xrightarrow[\text{200 °C, time, N}_2]{\text{K}_2\text{CO}_3 \text{ (20 equiv), C}_6\text{H}_6} \text{No } \text{Ir}^{III}(\text{ttp})\!\!-\!\!\langle\!\!\bigcirc\!\!\rangle\!\!-\!\!\text{FG}$$

1.1 equiv
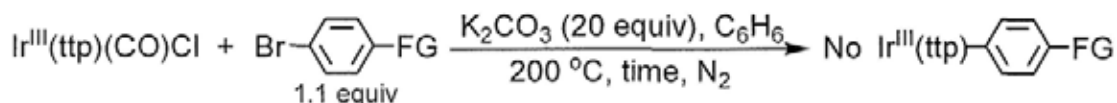
entry	FG	time/h	results[a]	entry	FG	time/h	results[a]
1	NH$_2$	5	decomp.	4	CO$_2$H	9	decomp.
2	OH	9	unknown	5	OSiMe$_3$	16	unknown
3	C(O)Cl	12	unknown				

[a] No characteristic proton signals of iridium porphyrin aryls were observed by ^{1}H NMR spectroscopy.

3.2.5.2 Reaction Scope of Base-Promoted Ar-I Cleavage

NaOH selectively promoted the aryl C-I cleavage of all aryl iodides (ArI) by Ir^{III}(ttp)(CO)Cl to give Ir^{III}(ttp)Ar in high yields (Table 3.26). In 4-iodotoluene, a much weaker C-I bond (BDE = ~65 kcal mol^{-1})[3] was preferentially cleaved without the activation of benzylic C-H bond (BDE ~ 89 kcal/mol)[3] (Table 3.26, entry 2). Double C-X bond cleavages occurred in 1-bromo-4-iodobenzene and 1,4-diiodobenzene to yield a trace of Ir^{III}(ttp)(p-C$_6$H$_4$)Ir^{III}(ttp) (**9a**) (Table 3.26, entries 5 and 6). Ir^{III}(ttp)(CO)I was observed by thin-layer chromatography in the course of reactions and was further consumed to give Ir^{III}(ttp)Ar.

Table 3.26 Substrate Scope of Base-Promoted Ar-I Cleavage

$$\text{Ir}^{III}(\text{ttp})(\text{CO})\text{Cl} + \text{I}\!\!-\!\!\langle\!\!\bigcirc\!\!\rangle\!\!-\!\!\text{FG} \xrightarrow[\text{150 °C, time, N}_2]{\text{NaOH (20 equiv), C}_6\text{H}_6} \text{Ir}^{III}(\text{ttp})\!\!-\!\!\langle\!\!\bigcirc\!\!\rangle\!\!-\!\!\text{FG}$$

1.1 equiv   Ir^{III}(ttp)Ar
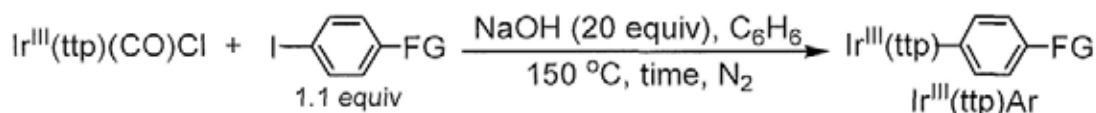
entry[a]	FG	time/h	Ir^{III}(ttp)Ar yield/%[b]	entry[a]	FG	time/h	Ir^{III}(ttp)Ar Yield/%[b]
1	OMe	20	**8c** (89)	5	Br	12	**8i** (77)[c]
2	Me	17	**8e** (84)	6	I	9	**8r** (90)[d]
3	H	12	**8a** (99)	7	C(O)Me	12	**8l** (81)
4	F	24	**8h** (96)	8	NO$_2$	15	**8p** (98)

[a] Ir^{III}(ttp)(CO)I was observed in the course of reaction by thin-layer chromatography, which was further consumed. [b] Isolated yield. [c] Ir^{III}(ttp)C$_6$H$_4$(p-I) in 3% yield and Ir^{III}(ttp)(p-C$_6$H$_4$)Ir^{III}(ttp) in 1% yield were isolated. [d] Ir^{III}(ttp)(p-C$_6$H$_4$)Ir^{III}(ttp) in 3% yield was isolated.

3.2.5.3 Reaction Scope of Base-Promoted Ar-Cl Cleavage

K_2CO_3 could promote the aryl C-Cl bond cleavage of aryl chlorides (ArCl) by $Ir^{III}(ttp)(CO)Cl$ to give $Ir^{III}(ttp)Ar$ in modest to high yields (Table 3.27). However, compared with the aryl C-Br and C-I bond cleavages (Tables 3.24 and 3.26), aryl C-Cl bond cleavage becomes less selective, accompanied with the competitive cleavages of other chemical bonds.

In the reaction with 4-chlorotoluene (Table 3.27, entry 2), besides the cleavage of aryl C-Cl bond (BDE ~ 96 kcal mol^{-1}),[2,3] the weaker benzylic C-H bond (BDE = 88.7 kcal mol^{-1})[3] was also cleaved considerably to yield $Ir^{III}(ttp)Bn(p\text{-}Cl)$ (**11**) in 18% yield. $Ir^{III}(ttp)(p\text{-}Tol)$ (**8e**) and $Ir^{III}(ttp)Bn(p\text{-}Cl)$ in about 2 : 1 ratio were obtained.

In the aryl C-Cl cleavage with 4-chloroanisole (Table 3.27, entry 1) and methyl 4-chlorobenzoate (Table 3.27, entry 6), a trace of $Ir^{III}(ttp)CH_3$ was formed, likely due to the cleavages of the weaker Me-O bonds (BDE of $p\text{-}ClC_6H_4O\text{-}Me$ = 62.4 kcal mol^{-1} [3]; BDE of $p\text{-}ClC_6H_4C(O)O\text{-}Me$ ~ 89.1 kcal mol^{-1} [3]).

In the aryl C-Cl cleavage of 4-chlorobenzaldehyde (Table 3.26, entry 7), the weaker aldehydic C-H bond (BDE = 84.2 kcal mol^{-1})[3] was also cleaved to give a trace of $Ir^{III}(ttp)(PPh_3)C(O)C_6H_4(p\text{-}Cl)$ (**12**).

Table 3.27 Substrate Scope of Base-Promoted Ar-Cl Cleavages

$$Ir^{III}(ttp)(CO)Cl + Cl\text{-}\langle\text{-}\rangle\text{-}FG \xrightarrow[\text{150 °C, time, N}_2]{K_2CO_3 \text{ (20 equiv), C}_6H_6} Ir^{III}(ttp)\text{-}\langle\text{-}\rangle\text{-}FG$$

200 equiv

entry	FG	time/h	$Ir^{III}(ttp)Ar$ yield/%[a]	entry	FG	time/h	$Ir^{III}(ttp)Ar$ yield/%[a]
1	OMe	36	**8c** (76)[b]	6	CO$_2$Me	46	**8k** (70)[b]
2	Me	36	**8e** (32)[c]	7	CHO	22	**8m** (69)[e,f]
3	H	22	**8a** (74)[d]	8	CF$_3$	168	**8n** (68)
4	F	36	**8h** (67)	9	CN	24	**8o** (51)[g]
5	Cl	84	**8j** (100)				

[a] Isolated yield. [b] $Ir^{III}(ttp)CH_3$ in 3% yield was isolated. [c] $Ir^{III}(ttp)Bn(p\text{-}Cl)$ in 18% isolated yield and $Ir^{III}(ttp)CH_3$ in 2% NMR yield were obtained. [d] $Ir^{III}(ttp)(p\text{-}C_6H_4)Ir^{III}(ttp)$ in 5% NMR yield was obtained. [e] $Ir^{III}(ttp)(PPh_3)C_6H_4(p\text{-}CHO)$ was isolated by adding PPh$_3$. [f] Aldehydic C-H activation also occurred to give $Ir^{III}(ttp)(PPh_3)C(O)C_6H_4(p\text{-}Cl)$ in ~1% yield. [g] $Ir^{III}(ttp)(PPh_3)C_6H_4(p\text{-}CN)$ was isolated by adding PPh$_3$.

153

3.2.6 Preparations of Di-Iridium-Porphyrin Substituted Arenes

In the base-promoted reaction of 1,4-diiodobenzene with $Ir^{III}(ttp)(CO)Cl$ (Table 3.26, entry 6), single C-I bond cleavage occurred predominantly to yield $Ir^{III}(ttp)C_6H_4(p$-$I)$, accompanied with a trace of $Ir^{III}(ttp)(p$-$C_6H_4)Ir^{III}(ttp)$ from double C-I bond cleavages. To synthesize $Ir^{III}(ttp)(p$-$C_6H_4)Ir^{III}(ttp)$ in a larger amount, $Ir^{III}(ttp)C_6H_4(p$-$I)$ was initially prepared in a pure and isolated form by reacting excess 1,4-diiodobenzene with $Ir^{III}(ttp)(CO)Cl$ and K_2CO_3. $Ir^{III}(ttp)C_6H_4(p$-$I)$ was then reacted with $Ir^{III}(ttp)(CO)Cl$ (1.1 equiv) and K_2CO_3 for further C-I cleavage reaction to form $Ir^{III}(ttp)(p$-$C_6H_4)Ir^{III}(ttp)$ in 78% yield (Table 3.28, entry 1).

$Ir^{III}(ttp)(p$-$C_6H_4)Ir^{III}(ttp)$ can also be prepared from the double C-Br bond cleavages of 1,4-dibromobenzene. $Ir^{III}(ttp)(CO)Cl$ reacted with 1.4-dibromobenzene and K_2CO_3 to give $Ir^{III}(ttp)C_6H_4(p$-$Br)$, which further reacted with $Ir^{III}(ttp)(CO)Cl$ (1.1 equiv) to give $Ir^{III}(ttp)(p$-$C_6H_4)Ir^{III}(ttp)$ in 59% yield (Table 3.28, entry 2).

Table 3.28 Double C-X Bond Cleavages of 1,4-Dihalobenzenes by $Ir^{III}(ttp)(CO)Cl$
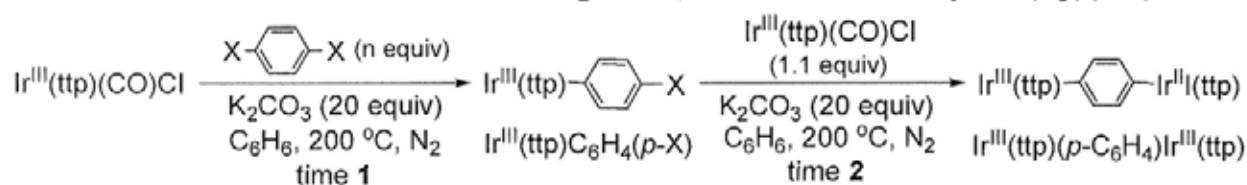
entry	X	n	time 1 /h	$Ir^{III}(ttp)C_6H_4(p$-$X)$ yield/%[a]	time 2 /h	$Ir^{III}(ttp)(p$-$C_6H_4)Ir^{III}(ttp)$ (9a) yield/%[a]
1	I	10	11	**8r** (92)	24	78
2	Br	1.1	36	**8i** (76)[b]	14	59

[a] Isolated yield. [b] Result from Table 3.24, entry 9.

The double C-X bond cleavages of 4,4'-dihalo-biphenyls can also be successfully carried out to synthesize 4,4'-di-iridium-porphyrin biphenyl, $Ir^{III}(ttp)(p$-$C_6H_4)_2Ir^{III}(ttp)$ (**9b**). 4,4'-Dibromobiphenyl and 4,4'-diiodobiphenyl in excess amounts were initially reacted with $Ir^{III}(ttp)(CO)Cl$ and K_2CO_3 to yield $Ir^{III}(ttp)(p$-$C_6H_4)_2(p$-$X)$ (X = I (**8s**), Br (**8t**)), which were

further reacted with $Ir^{III}(ttp)(CO)Cl$ (1.1 equiv) and K_2CO_3 to give $Ir^{III}(ttp)(p-C_6H_4)_2Ir^{III}(ttp)$ (Table 3.29, entries 1 and 2).

Table 3.29 Double C-X Bond Cleavages of 4,4'-Dihalobiphenyls with $Ir^{III}(ttp)(CO)Cl$
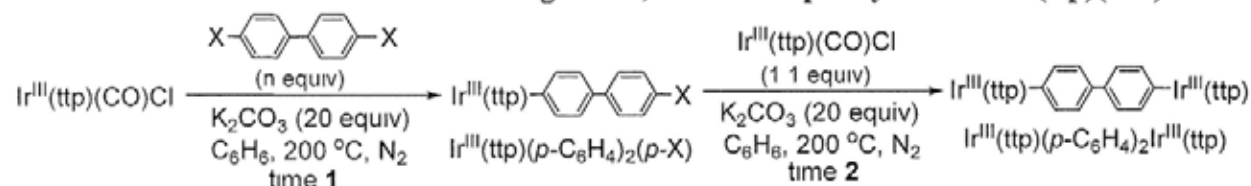
entry	X	n	time **1** /h	$Ir^{III}(ttp)(p-C_6H_4)_2(p-X)$ yield/%[a]	time **2** /h	$Ir^{III}(ttp)(p-C_6H_4)_2Ir^{III}(ttp)$ (**9b**) yield/%[a]
1	I	6	24	**8s** (76)	19	71
2	Br	10	15	**8t** (73)	36	75

[a] Isolated yield.

The one-pot preparation of di-iridium-porphyrin-substituted arenes (eq 3.21) was found to be less efficient than the sequential preparation (Tables 3.28 and 3.29) even though excess $Ir^{III}(ttp)(CO)Cl$ was added. It is supported by the formation of $Ir^{III}(ttp)(p-C_6H_4)_2Ir^{III}(ttp)$ in a low yield of 43% yield from the reaction of 4,4'-dibromobiphenyl with excess $Ir^{III}(ttp)(CO)Cl$ (3.5 equiv) and K_2CO_3 at 200 °C even in 3 days (eq 3.21), compared with the higher yield of $Ir^{III}(ttp)(p-C_6H_4)_2Ir^{III}(ttp)$ obtained in 75% yield by sequential synthesis (Table 3.29, entry 2).
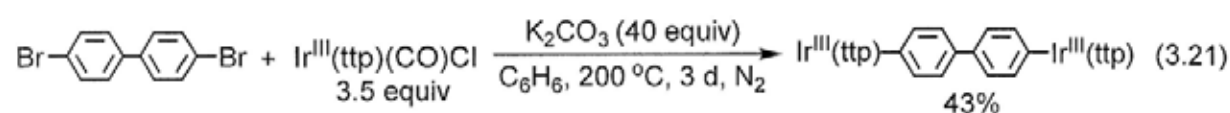
The reason of the low yielding one-pot double C-X bond cleavage reaction is unclear. Likely, the intermediates ($Ir^{III}(ttp)H$ and $[Ir^{II}(ttp)]_2$, which are rapidly generated from base-promoted reduction of $Ir^{III}(ttp)(CO)X$ (Chapter 2, Sections 2.3 and 2.4)) partially decompose prior to the subsequent slower reactions with the sterically more bulky $Ir^{III}(ttp)(p-C_6H_4)_2Br$ (The detailed reaction mechanism of aryl C-X bond cleavages is discussed in section 3.2.8).

155

3.2.7 X-Ray Data of Iridium(III) Porphyrin Aryls

The X-ray crystallographic structures of the iridium(III) porphyrin aryls (Ir^{III}(ttp)Ar), including Ir^{III}(ttp)C$_6$H$_4$(p-OMe) (**8c**), Ir^{III}(ttp)(p-Tol) (**8e**), Ir^{III}(ttp)C$_6$H$_4$(p-NO$_2$) (**8p**), and Ir^{III}(ttp)(p-C$_6$H$_4$)$_2$Ir^{III}(ttp) (**9b**), are shown in Figures 3.2-3.5. They are coordinated with methanol in the single crystals for X-ray crystallography and can be used for direct comparison of the bond distances (Table 3.30).
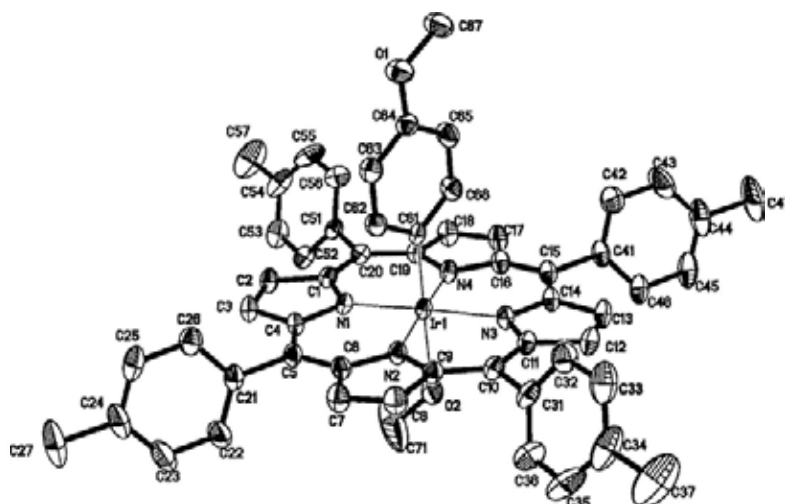
Figure 3.2 ORTEP presentation of the molecular structure for Ir^{III}(ttp)C$_6$H$_4$(p-OMe)(CH$_3$OH) (**8c**) (30% probability displacement ellipsoids).
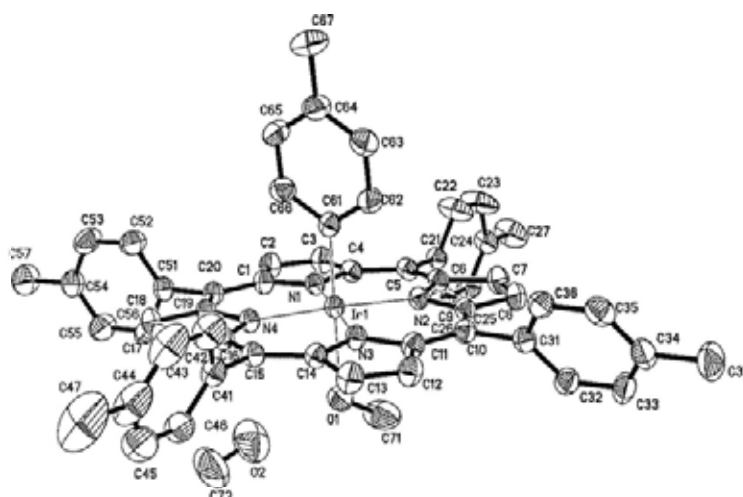
Figure 3.3 ORTEP presentation of the molecular structure for Ir^{III}(ttp)(p-Tol)(CH$_3$OH)•CH$_3$OH (**8e**) (30% probability displacement ellipsoids).

Figure 3.4 ORTEP presentation of the molecular structure with numbering scheme for Ir^{III}(ttp)C$_6$H$_4$(p-NO$_2$)(CH$_3$OH)•CH$_3$OH•CHCl$_3$ (**8p**) (30% probability displacement ellipsoids).

Figure 3.5 ORTEP presentation of the molecular structure for (CH$_3$OH)Ir^{III}(ttp)(p-C$_6$H$_4$)$_2$Ir^{III}(ttp)(CH$_3$OH) (**9b**) (30% probability displacement ellipsoids).

Table 3.30 Selected Bond Distances (Å) for Ir^{III}(ttp)Ar

Entry	Ir^{III}(ttp)Ar	Ir-C (Å)	Ir-N$_{average}$ (Å)
1	Ir^{III}(ttp)C$_6$H$_4$(p-OMe)(CH$_3$OH) (**8c**)	2.023(4)	2.033
2	Ir^{III}(ttp)(p-Tol)(CH$_3$OH) (**8e**)	2.033(5)	2.030
3	Ir^{III}(ttp)C$_6$H$_4$(p-NO$_2$)(CH$_3$OH) (**8p**)	1.990(6)	2.031
4	(CH$_3$OH)Ir^{III}(ttp)(p-C$_6$H$_4$)$_2$Ir^{III}(ttp)(CH$_3$OH) (**9b**)	2.027(8)	2.042

157

Both the *para*-substituted, electron-donating OMe and Me groups and the electron-withdrawing NO_2 group of Ir^{III}(ttp)Ar do not impose significant electronic effects on the bond lengths of Ir-C and Ir-N bonds, since they all have similar Ir-C and average Ir-N bond lengths (Table 3.30, entries 1-3). Moreover, Ir^{III}(ttp)(p-C_6H_4)$_2Ir^{III}$(ttp), which contains 2 bulky iridium porphyrins rings opposite to each other (Table 3.30, entry 4), also has similar Ir-C and Ir-N bond lengths as those of Ir^{III}(ttp)C_6H_4(p-FG) (Table 3.30, entries 1-3). This implies that the steric interactions between the two iridium porphyrins in Ir^{III}(ttp)(p-C_6H_4)$_2Ir^{III}$(ttp), which could lengthen the Ir-C bond, is negligible.

3.2.8 Reaction Mechanism of Base-Promoted Aryl C-X Bond Cleavages by Ir^{III}(ttp)(CO)Cl

3.2.8.1 Reaction Profiles of Base-Promoted Ph-X Cleavages

To elucidate the reaction mechanisms of base-promoted aryl C-X cleavages by Ir^{III}(ttp)(CO)Cl, the reaction profiles were initially studied in sealed NMR tubes using the optimal reaction conditions (Table 3.22) in order to observe the iridium porphyrin intermediates. It is noted that the reactions underwent in NMR tubes are slower by a few times than the reactions carried out in Schlenk tubes (Table 3.22), probably due to the lack of stirring in the NMR tube experiments.[47]

3.2.8.1.1 Reaction Profile of Base-Promoted Ph-Br Cleavage

(i) Reaction with K_2CO_3

Initially, Ir^{III}(ttp)(CO)Cl reacted slowly with PhBr (1.1 equiv) and K_2CO_3 (20 equiv) in benzene-d_6 at 200 °C in 10 days to give Ir^{III}(ttp)Ph in 94% yield (eq 3.22). No other iridium porphyrin intermediates were observed. Likely, the reactive intermediates generated reacted rapidly at 200 °C and could not be observed.

$$Ir^{III}(ttp)(CO)Cl + \underset{1.1\ equiv}{PhBr} \xrightarrow[\text{C_6D_6, 200 °C, 10 d}]{\text{K_2CO_3 (20 equiv)}} \underset{94\%}{Ir^{III}(ttp)Ph} \quad (3.22)$$
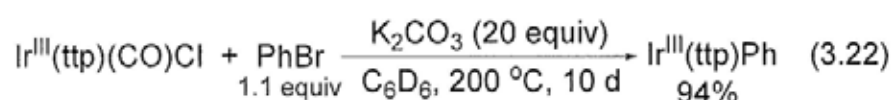
(ii) Reaction with Cs$_2$CO$_3$

To allow the observations of intermediates from the Ph-Br cleavage with Ir^{III}(ttp)(CO)Cl, a stronger base of Cs$_2$CO$_3$ and a lower temperature of 150 ^{o}C were used (Table 3.31; Figures 3.6(a),(b)). In 3 hours, Ir^{III}(ttp)(CO)Cl (δ(pyrrole) = 9.07 ppm) reacted with PhBr (1.1 equiv) and Cs$_2$CO$_3$ (20 equiv) in benzene-d_6 at 150 ^{o}C to give Ir^{III}(ttp)Ph (δ(pyrrole) = 8.80 ppm) in 30% yield via the Ph-Br cleavage, with the concomitant formations of Ir^{III}(ttp)H (δ(pyrrole) = 8.81 ppm) and [Ir^{II}(ttp)]$_2$ (δ(pyrrole) = 8.33 ppm) in 13% and 1% yields, respectively (Table 3.31, entry 4). After 60 hours, all Ir^{III}(ttp)(CO)Cl, Ir^{III}(ttp)H, and [Ir^{II}(ttp)]$_2$ were consumed to give Ir^{III}(ttp)Ph quantitatively (Table 3.31, entry 6). Therefore, Ir^{III}(ttp)H and [Ir^{II}(ttp)]$_2$ are the observed intermediates in the base-promoted Ph-Br cleavage.

Table 3.31 Time Profile of Cs$_2$CO$_3$-Promoted Ph-Br Cleavage by Ir^{III}(ttp)(CO)Cl at 150 ^{o}C

$$\text{Ir}^{III}\text{(ttp)(CO)Cl} + \underset{\text{1.1 equiv}}{\text{PhBr}} \xrightarrow[\text{C}_6\text{D}_6,\ 150\ ^{o}\text{C, time}]{\text{Cs}_2\text{CO}_3\ (20\ \text{equiv})} \text{Ir}^{III}\text{(ttp)H} + [\text{Ir}^{II}\text{(ttp)}]_2 + \text{Ir}^{III}\text{(ttp)Ph}$$

entry[a]	time/h	Ir^{III}(ttp)(CO)Cl[b]/%	Ir^{III}(ttp)H/%	1/2[Ir^{II}(ttp)]$_2$/%	Ir^{III}(ttp)Ph/%	Total yield/%
1	0	100	0	0	0	100
2	0.5	93	4	0	3	100
3	1.5	81	5	0	14	100
4	3.0	56	13	1	30	100
5	26	10	5	0	85	100
6	60	0	0	0	100	100

[a] NMR yield. [b] The yield included Ir^{III}(ttp)(CO)Br but its yield could not be estimated, since both Ir^{III}(ttp)(CO)Cl and Ir^{III}(ttp)(CO)Br have very similar chemical shift in ^{1}H NMR spectroscopy and could not be differentiated.
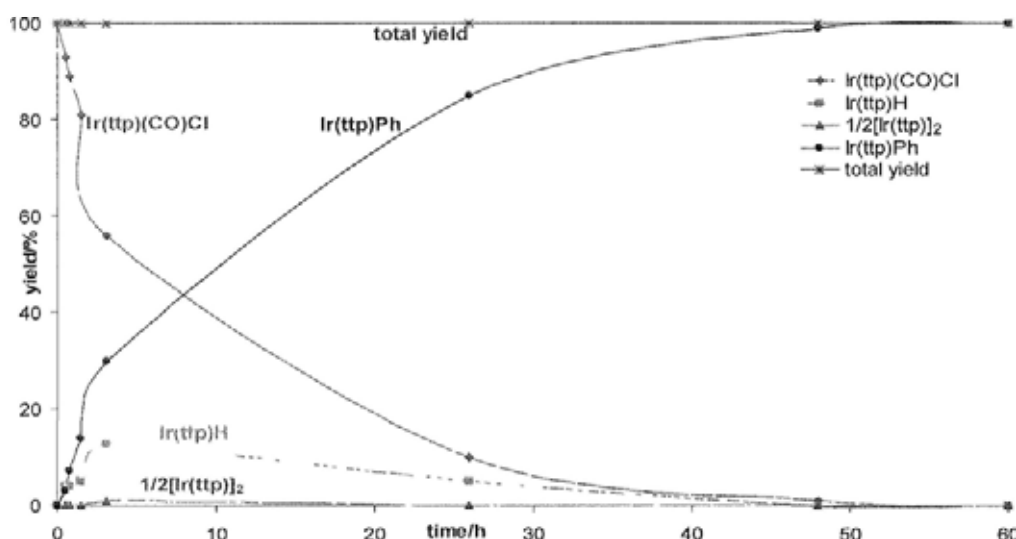
Figure 3.6(a) Time profile of Cs$_2$CO$_3$-promoted Ph-Br cleavage by Ir^{III}(ttp)(CO)Cl at 150 ^{o}C (Table 3.31).
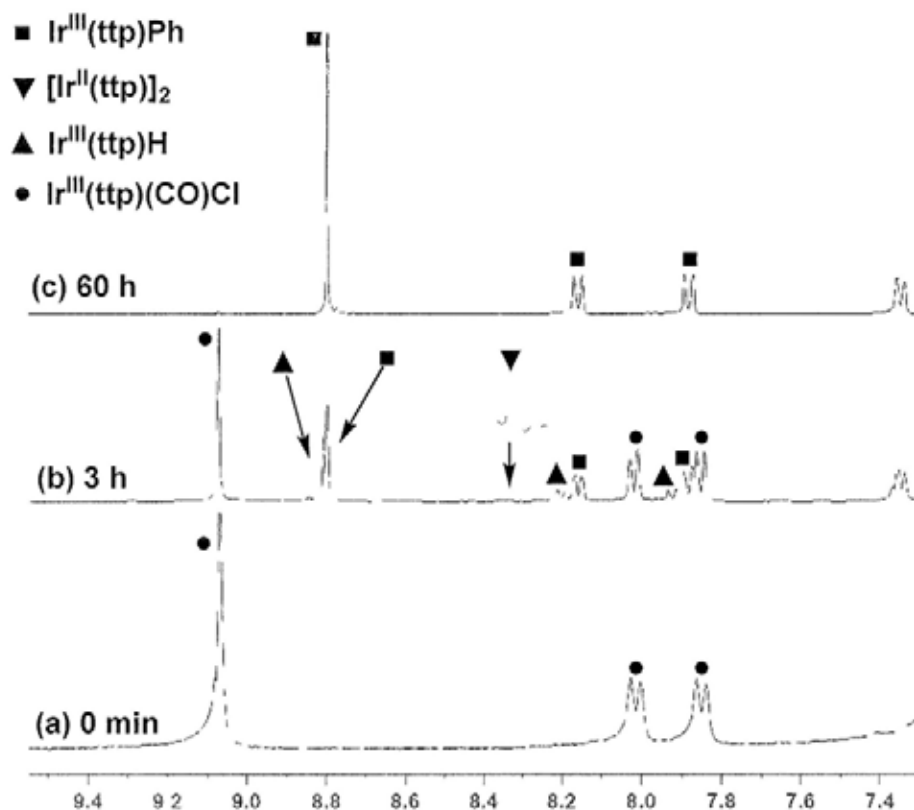
Figure 3.6(b) Partial ^{1}H NMR profile of Cs_2CO_3-promoted Ph-Br cleavage by $Ir^{III}(ttp)(CO)Cl$ in benzene-d_6 at 150 ^{o}C (Table 3.31).

3.2.8.1.2 Reaction Profiles of Base-Promoted Ph-I Cleavage

In order to observe the intermediates in base-promoted Ph-I cleavage by $Ir^{III}(ttp)(CO)Cl$, a stronger base of KOH and a lower temperature of 120 ^{o}C were also used (Table 3.32; Figures 3.7(a),(b)). After 3 hours, $Ir^{III}(ttp)(CO)Cl$ (δ(pyrrole) = 9.07 ppm) reacted with PhI (1.1 equiv) and KOH (20 equiv) in benzene-d_6 at 120 ^{o}C to give $Ir^{III}(ttp)Ph$ (δ(pyrrole) = 8.80 ppm), $Ir^{III}(ttp)H$ (δ(pyrrole) = 8.81 ppm), and $[Ir^{II}(ttp)]_2$ (δ(pyrrole) = 8.33 ppm) in 17%, 62% and 1% yields, respectively (Table 3.32, entry 4). After 38 hours, all $Ir^{III}(ttp)(CO)Cl$, $Ir^{III}(ttp)H$, and $[Ir^{II}(ttp)]_2$ were consumed to give $Ir^{III}(ttp)Ph$ quantitatively (Table 3.32, entry 7). $Ir^{III}(ttp)H$ and $[Ir^{II}(ttp)]_2$ are also the observed intermediates in the base-promoted Ph-I cleavage.

160

Table 3.32 Time Profile of KOH-Promoted Ph-I Cleavage by Ir^{III}(ttp)(CO)Cl at 120 ^{o}C

$$Ir^{III}(ttp)(CO)Cl + PhI \xrightarrow[\text{1.1 equiv}]{\substack{\text{KOH (20 equiv)} \\ C_6D_6,\ 120\ ^oC,\ \text{time}}} Ir^{III}(ttp)H + [Ir^{II}(ttp)]_2 + Ir^{III}(ttp)Ph$$

entry[a]	time/h	Ir^{III}(ttp)(CO)Cl[b]/%	Ir^{III}(ttp)H/%	1/2[Ir^{II}(ttp)]$_2$/%	Ir^{III}(ttp)Ph/%	Total yield/%
1	0	100	0	0	0	100
2	0.5	89	11	0	0	100
3	1.5	50	39	0	11	100
4	3	20	62	1	17	100
5	5	2	38	1	59	100
6	10	0	22	0	78	100
7	38	0	0	0	100	100

[a] NMR yield. [b] The yield included Ir^{III}(ttp)(CO)I but its yield could not be estimated, since both Ir^{III}(ttp)(CO)Cl and Ir^{III}(ttp)(CO)I have very similar chemical shift in ^{1}H NMR spectroscopy and could not be differentiated.
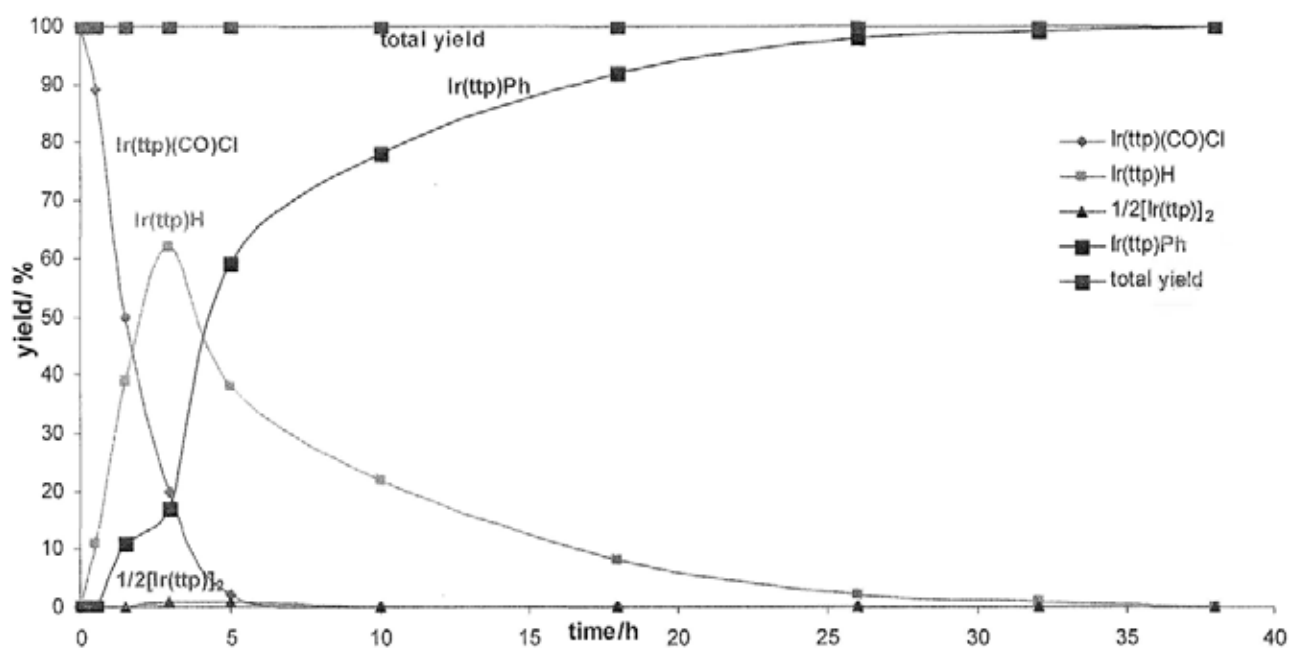
Figure 3.7(a) Time Profile of KOH-Promoted Ph-I Cleavage by Ir^{III}(ttp)(CO)Cl at 120 ^{o}C (Table 3.32).
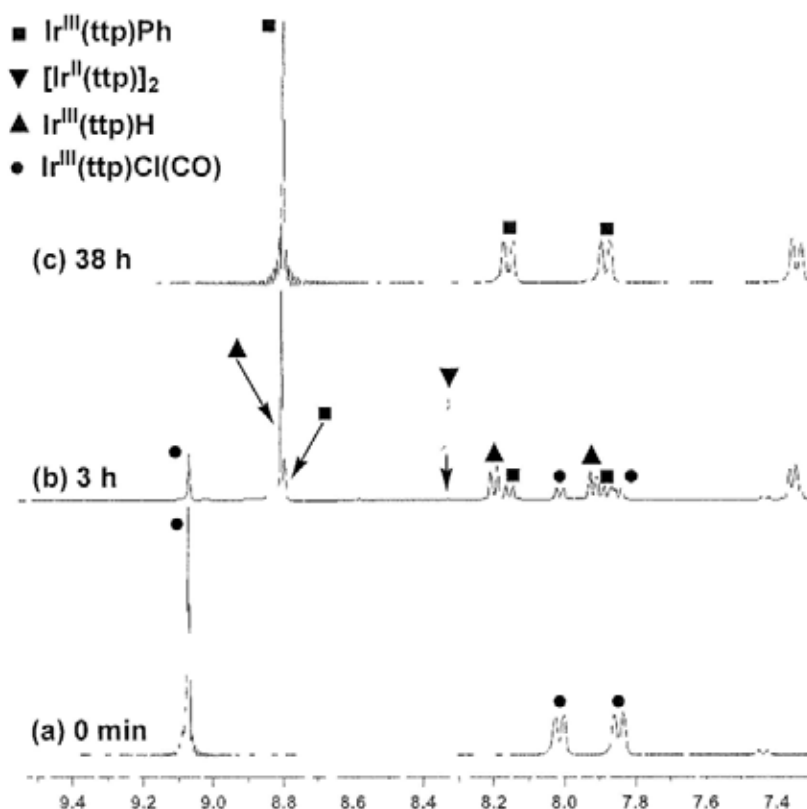
Figure 3.7(b) Partial ^{1}H NMR profile of KOH-promoted Ph-I cleavage by Ir^{III}(ttp)(CO)Cl in benzene-d_6 at 120 ^{o}C (Table 3.32).

3.2.8.1.3 Reaction Profiles of Base-Promoted Ph-Cl Cleavage

The reaction of Ir^{III}(ttp)(CO)Cl with PhCl (50 equiv) and a stronger base of Cs$_2$CO$_3$ (20 equiv) in benzene-d_6 at 150 ^{o}C was also monitored (Table 3.33, Figures 3.8(a),(b)). In 50 minutes, Ir^{III}(ttp)(CO)Cl (δ(pyrrole) = 9.08 ppm) was converted to Ir^{III}(ttp)H (δ(pyrrole) = 8.81 ppm) and [Ir^{II}(ttp)]$_2$ (δ(pyrrole) = 8.33 ppm) in 6% and 3% yields, respectively (Table 3.33, entry 3). After 18 days, Ir^{III}(ttp)Ph (δ(pyrrole) = 8.80 ppm) was formed in 56% yield and unreacted Ir^{III}(ttp)H was recovered in 13% yield, with the concomitant formations of Ir^{III}(ttp)(p-C$_6$H$_4$)Ir^{III}(ttp) (δ(pyrrole) = 8.35 ppm) in 6% yield and Ir^{III}(ttp)CH$_3$ (δ(pyrrole) = 8.77 ppm) in 6% yield (Table 3.33, entry 6). Upon further heating the reaction mixture at 200 ^{o}C in 60 hours, unreacted Ir^{III}(ttp)H was consumed to generate more Ir^{III}(ttp)Ph in a total of 71% yield (Table 3.33, entry 7). Indeed, Ir^{III}(ttp)H and [Ir^{II}(ttp)]$_2$ are also the observed intermediates in the base-promoted Ph-Cl cleavage.

162

Table 3.33 Time Profile of Cs₂CO₃-Promoted Ph-Cl Cleavage by Ir^{III}(ttp)(CO)Cl

$$\text{Ir}^{III}(\text{ttp})(\text{CO})\text{Cl} + \text{PhCl} \xrightarrow[\text{C}_6\text{D}_6,\ \text{temp, time}]{\text{Cs}_2\text{CO}_3\ (20\ \text{equiv})} \text{Ir}^{III}(\text{ttp})\text{H} + [\text{Ir}^{II}(\text{ttp})]_2 + \text{Ir}^{III}(\text{ttp})\text{Ph} +$$
$$\text{50 equiv} \qquad\qquad\qquad\qquad \text{Ir}^{III}(\text{ttp})(p\text{-C}_6\text{H}_4)\text{Ir}^{III}(\text{ttp}) + \text{Ir}^{III}(\text{ttp})\text{CH}_3$$
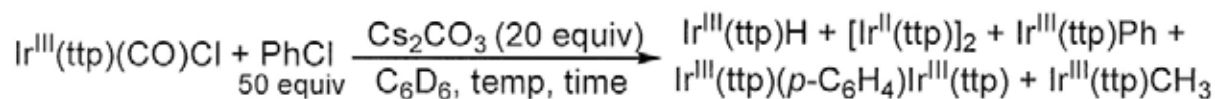
entry[a]	temp /°C	time	Ir(ttp)-(CO)Cl/%	Ir(ttp)H /%	1/2[Ir(ttp)]₂ /%	Ir(ttp)Ph /%	Ir(ttp)(p-C₆H₄)-Ir(ttp)/%	Ir(ttp)CH₃ /%	total yield /%
1		0	100	0	0	0	0	0	100
2		20 min	97	1	2	0	0	0	100
3	150	50 min	91	6	3	0	0	0	100
4		3.5 h	66	26	7	0	1	0	100
5		14 h	0	54	0	15	6	6	81
6		18 d	0	13	0	56	6	6	81
7	200	60 h	0	0	0	71	6	4	81

[a] NMR yield.
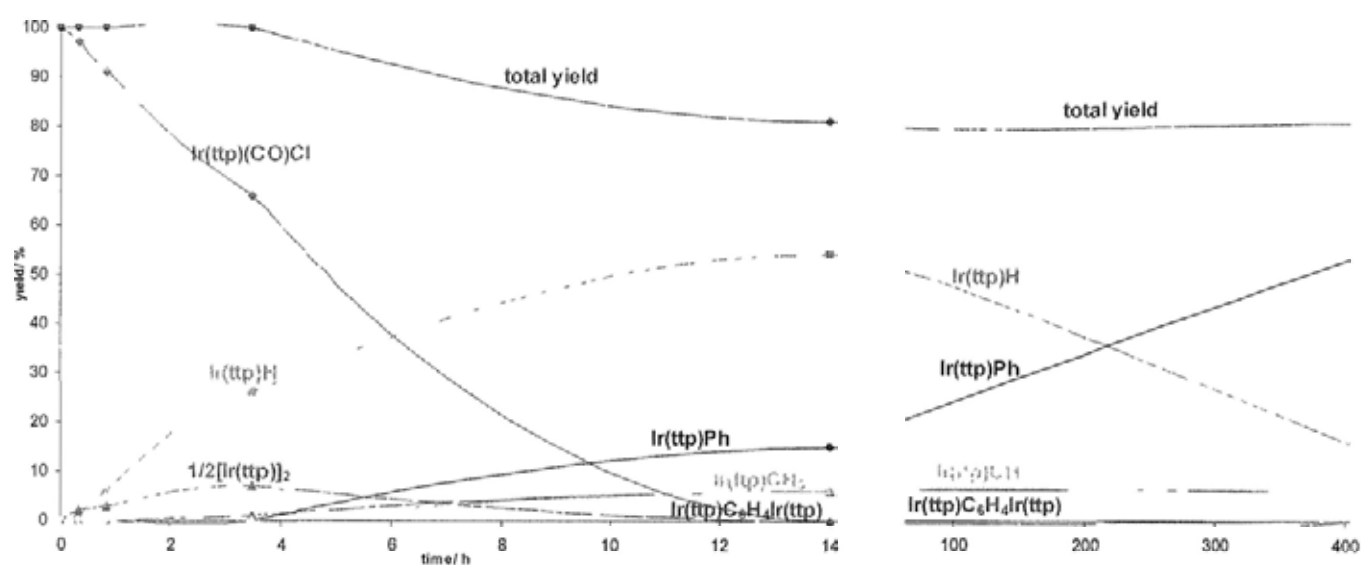
Figure 3.8(a) Time Profile of Cs₂CO₃-Promoted Ph-Cl Cleavage by Ir^{III}(ttp)(CO)Cl at 150 °C (Table 3.33).

163
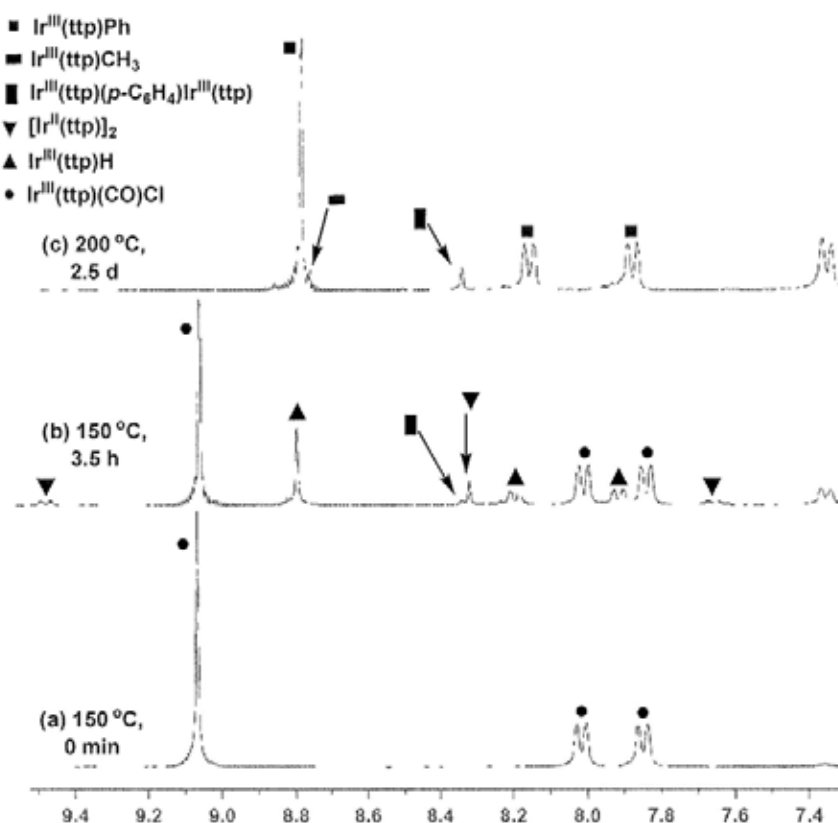
Figure 3.8(b) Partial ^{1}H NMR profile of Cs$_2$CO$_3$-promoted Ph-Cl cleavage by Ir^{III}(ttp)(CO)Cl in benzene-d_6 at 150 $^\circ$C (Table 3.33).

3.2.8.2 General Reaction Mechanism of Base-Promoted Ph-X Cleavages by Ir^{III}(ttp)(CO)Cl

During the base-promoted Ph-X (X = Cl, Br, I) cleavages by Ir^{III}(ttp)(CO)Cl (Tables 3.31-3.33), both Ir^{III}(ttp)H and [Ir^{II}(ttp)]$_2$ are observed as the intermediates. Most likely, Ir^{III}(ttp)(CO)Cl undergoes the base-promoted reduction to form Ir^{III}(ttp)H (Chapter 2, Section 2.3, Tables 2.2 and 2.3), which then undergoes rapid base-promoted dehydrogenative dimerization to give [Ir^{II}(ttp)]$_2$ (Chapter 2, Section 2.4, Tables 2.10 and 2.11).

Ir^{III}(ttp)(CO)X (X = Br, I) is also formed in the base-promoted Ar-Br and Ar-I cleavages, and are further consumed to yield Ir^{III}(ttp)Ph (Tables 3.10, 3.24, and 3.26). Likely, Ir^{III}(ttp)(CO)X (X = Br, I) further undergoes the base-promoted reduction to form Ir^{III}(ttp)H for further

164

reaction (Chapter 2, Section 2.3, Tables 2.2 and 2.3).

Based on these foundings, the general mechanism of base-promoted aryl C-X bond cleavages by $Ir^{III}(ttp)(CO)Cl$ is proposed (Scheme 3.21).

Scheme 3.21 General Mechanism of Base-Promoted Ar-X Cleavages by $Ir^{III}(ttp)(CO)Cl$

$$Ir^{III}(ttp)(CO)Cl \xrightarrow[\text{-Cl}^-,\ \text{-CO}]{\textbf{i}\ \text{base (OH}^-,\ \text{CO}_3^{2-})} Ir^{III}(ttp)OH \xrightarrow[\text{-1/2H}_2\text{O}_2]{\textbf{ii}\ \text{base, H}_2\text{O}} Ir^{III}(ttp)H \underset{}{\overset{\textbf{iii}\ \text{base, -H}_2}{\rightleftharpoons}} [Ir^{II}(ttp)]_2$$

(with **iv** and **v** pathways: Ar-X, X = Cl, Br, I giving $Ir^{III}(ttp)X$ and $Ir^{III}(ttp)Ar$; **vii** base (OH$^-$, CO$_3^{2-}$), -X$^-$ regenerating $Ir^{III}(ttp)OH$; **vi** CO giving $Ir^{III}(ttp)(CO)X$)
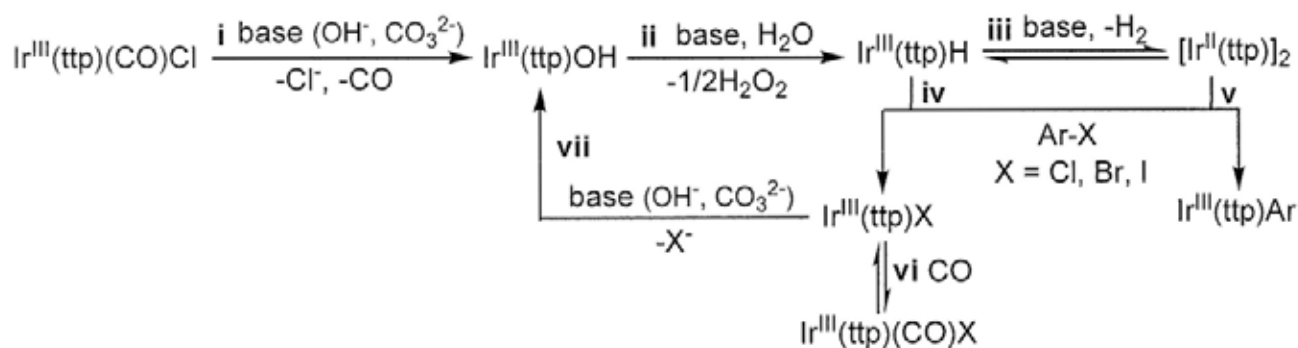
Initially, $Ir^{III}(ttp)(CO)Cl$ undergoes ligand substitution with OH$^-$ (from NaOH and K$_2$CO$_3$) to give $Ir^{III}(ttp)OH$ (Scheme 3.21, pathway i). $Ir^{III}(ttp)OH$ then undergoes redox reactions to give $Ir^{III}(ttp)H$ (pathway ii). $Ir^{III}(ttp)H$ further undergoes both thermal and base-promoted dehydrogenative dimerization to give $[Ir^{II}(ttp)]_2$ (pathway iii; See Chapter 2, Sections 2.3 and 2.4 for detailed mechanistic studies).

Both $Ir^{III}(ttp)H$ and $[Ir^{II}(ttp)]_2$ are the observed and probable intermediates to cleave the Ar-X bond (X = Cl, Br, I) to give $Ir^{III}(ttp)Ar$ and $Ir^{III}(ttp)X$ (pathways iv and v). $Ir^{III}(ttp)X$ further coordinates with CO (dissociated from $Ir^{III}(ttp)(CO)Cl$) to form $Ir^{III}(ttp)(CO)X$ (pathway vi). Both $Ir^{III}(ttp)X$ and $Ir^{III}(ttp)(CO)X$ are recycled via the base-promoted reduction to form $Ir^{III}(ttp)OH$ (pathway vii) for further conversion to $Ir^{III}(ttp)Ar$ (pathways ii-v).

In the following sections, the detailed investigations of the base-promoted aryl C-X bond cleavages are discussed, including:

(i) the identification of the iridium porphyrin intermediate in the Ar-X cleavage step.

(ii) the detailed reaction mechanism of the Ar-X cleavage.

3.2.8.3 Relative Reactivities of Intermediates in Ar-X Cleavages

During the base-promoted Ph-Br, Ph-I, and Ph-Cl bond cleavages, $Ir^{III}(ttp)H$, generated from the base-promoted reduction of $Ir^{III}(ttp)(CO)Cl$ (Scheme 3.22, pathway i), can exist in equilibria with $[Ir^{II}(ttp)]_2$ (via the base-promoted dehydrogenative dimerization) (Scheme 3.22, pathway iii) and $Ir^{I}(ttp)^-$ (via the deprotonation of $Ir^{III}(ttp)H$ with base) (Scheme 3.22, pathway ii). The equilibria have also been demonstrated (Chapter 2, Section 2.4). Therefore, $Ir^{III}(ttp)H$, $[Ir^{II}(ttp)]_2$, and $Ir^{I}(ttp)^-$ are possible intermediates for Ar-X cleavages. Their reactivities toward Ph-X cleavages are thus compared to differentiate the intermediate for Ar-X cleavages.

Scheme 3.22 Mode of Reactivities of Possible Iridium Porphyrin Intermediates
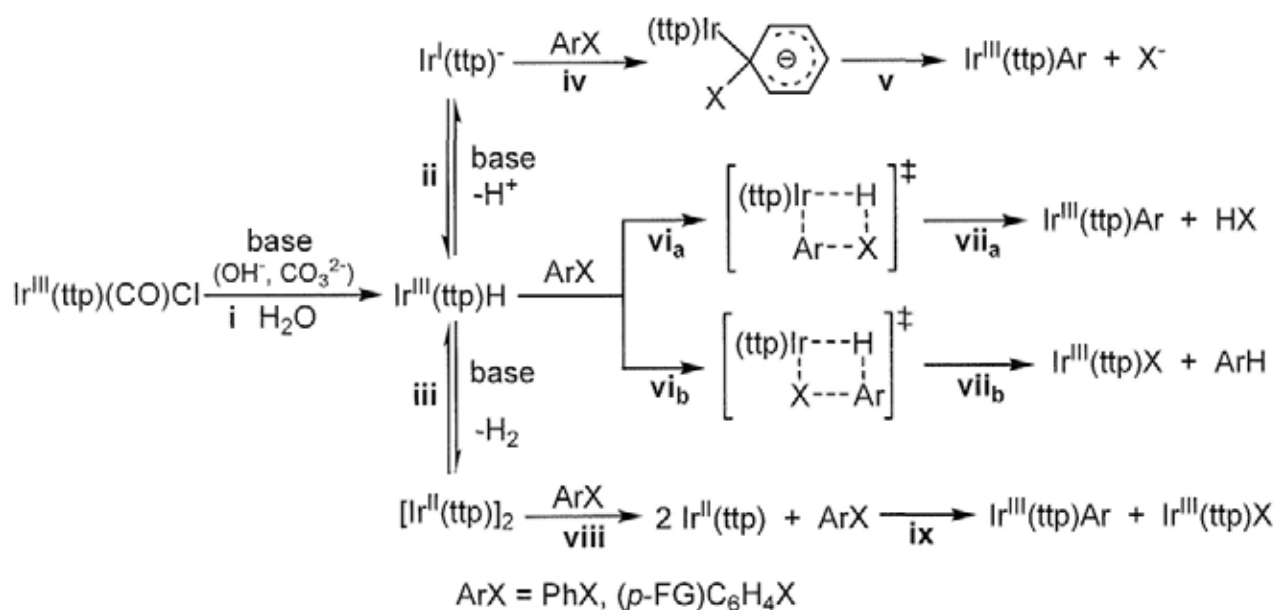
$Ir^{III}(ttp)H,^{37}$ $[Ir^{II}(ttp)]_2,^{37}$ and $Ir^{I}(ttp)^-,^{47,48}$ which were independently prepared in benzene-d_6 in the same concentrations, were reacted with PhX in the identical reaction conditions in sealed NMR tubes, and the reactions were monitored by ^1H NMR spectroscopy. Their reactivities are estimated by comparing the times used for the complete consumptions of the iridium porphyrin species.

3.2.8.3.1 Effect of Halogen Atoms of Halobenzenes

The effect of nature of halogen atoms (X) in PhX on the relative reactivities of $Ir^{III}(ttp)H$, $[Ir^{II}(ttp)]_2$, and $Ir^{I}(ttp)^-$ was investigated (Table 3.34).

Table 3.34 Relative Reactivities of Possible Ir(ttp) Species in Ph-X Cleavages

$$Ir^{III}(ttp)X' + PhX \xrightarrow[\substack{200\ ^{\circ}C,\ time}]{C_6D_6} Ir^{III}(ttp)Ph + Ir^{III}(ttp)X$$
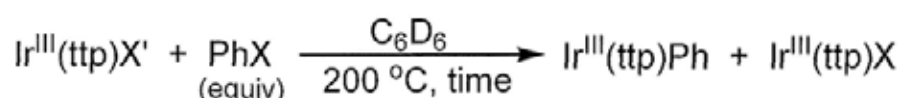
$$\text{(equiv)}$$

entry	$Ir^{III}(ttp)X'$	PhX (equiv)	time	$Ir^{III}(ttp)Ph$ yield/%[a]	$Ir^{III}(ttp)X$ yield/%	$Ir^{III}(ttp)Ph$: $Ir^{III}(ttp)X$ ratio
1	$Ir^{I}(ttp)^-K^{+\,b}$		14 d	38		
2	$Ir^{III}(ttp)H$	PhBr (1.1)	14 h	31	7^c	
3	$1/2[Ir^{II}(ttp)]_2$		2 min	34	32^c	1.1 : 1.0
4	$Ir^{I}(ttp)^-K^{+\,b}$		20 d	25^d		
5	$Ir^{III}(ttp)H$	PhI (1.1)	15 min	34	19^c	
6	$1/2[Ir^{II}(ttp)]_2$		1 min	37	36^c	~1.0 : 1.0
7	$Ir^{I}(ttp)^-K^{+\,b}$		4 d	50		
8	$Ir^{III}(ttp)H$	PhCl (50)	4 d	67	4^e	
9	$1/2[Ir^{II}(ttp)]_2$		5 h	57^f	4^e	14.3 : 1.0

[a] Isolated yield. [b] In form of $Ir^{I}(ttp)^-[K(18\text{-crown-}6)]^+$. [c] Yield was estimated by ^1H NMR spectroscopy since $Ir^{III}(ttp)X$ (X = Br, I) was not stable enough to be isolated by column chromatography. [d] $Ir^{I}(ttp)^-K^+$ in 15% yield remained unreacted. [e] $Ir^{III}(ttp)(CO)Cl$ was isolated. [f] $Ir^{III}(ttp)(p\text{-}C_6H_4)Ir^{III}(ttp)$ was formed in 3% NMR yield.

In the reaction with PhBr (1.1 equiv) in benzene-d_6 at 200 °C, $Ir^{I}(ttp)^-$ reacted very slowly in 14 days with PhBr, probably via nucleophilic aromatic substitution (S_NAr), to give $Ir^{III}(ttp)Ph$ in 38% yield (Table 3.34, entry 1; Scheme 3.22, pathways iv and v). $Ir^{III}(ttp)H$ reacted faster with PhBr in 14 hours to yield $Ir^{III}(ttp)Ph$ and $Ir^{III}(ttp)Br^{49}$ in 31% and 7% yields, respectively, likely via σ-bond metathesis (Table 3.34, entry 2; Figure 3.9(a); Scheme 3.22, pathways vi and vii). $[Ir^{II}(ttp)]_2$ reacted most rapidly with PhBr in 2 minutes to give $Ir^{III}(ttp)Ph$ and $Ir^{III}(ttp)Br^{49}$ in 34% and 32% yields, respectively, in a nearly 1:1 ratio (Table 3.34, entry 3; Figure 3.9(b); Scheme 3.22, pathways viii and ix).

In the reaction with PhI (1.1 equiv) in benzene-d_6 at 200 °C, Ir^{I}(ttp)$^-$ reacted with PhI very slowly even in 20 days to produce Ir^{III}(ttp)Ph in 25% yield and unreacted Ir^{I}(ttp)$^-$ was recovered in 15% yield (Table 3.34, entry 4). Ir^{III}(ttp)H reacted with PhI faster in 15 minutes to yield Ir^{III}(ttp)Ph and Ir^{III}(ttp)I[49] in 34% and 19% yields, respectively (Table 3.34, entry 5; Figure 3.10(a)). [Ir^{II}(ttp)]$_2$ reacted with PhI much faster in 1 minute to obtain Ir^{III}(ttp)Ph and Ir^{III}(ttp)I[49] in 37% yield and 36% yield, respectively, in an almost 1:1 ratio (Table 3.34, entry 6; Figure 3.10(b)).

In the reaction with PhCl (50 equiv) in benzene-d_6 at 200 °C, the reaction rates of Ir^{I}(ttp)$^-$ and Ir^{III}(ttp)H become comparable. Ir^{I}(ttp)$^-$ reacted in 4 days to give Ir^{III}(ttp)Ph in 50% yield (Table 3.34, entry 7), whereas Ir^{III}(ttp)H reacted in 4 days to give Ir^{III}(ttp)Ph in 67% yield and a trace of Ir^{III}(ttp)(CO)Cl (4%) (Table 3.34, entry 8). [Ir^{II}(ttp)]$_2$ reacted fastest in 5 hours to give Ir^{III}(ttp)Ph in 57% yield, and a trace of Ir^{III}(ttp)(CO)Cl (4%) and Ir^{III}(ttp)(p-C$_6$H$_4$)Ir^{III}(ttp) (2%) (Table 3.34, entry 9).

The rates of the three possible iridium porphyrin intermediates in Ph-X cleavages are generally in the reactivity order: [Ir^{II}(ttp)]$_2$ > Ir^{III}(ttp)H > Ir^{I}(ttp)$^-$. Since [Ir^{II}(ttp)]$_2$ is shown to be the most reactive species (Table 3.34, entries 3, 6, and 9), it is most likely the intermediate for Ph-X cleavages. It is reasonable to assume that the base-promoted cleavages of Ph-Br, Ph-I, and Ph-Cl bonds by Ir^{III}(ttp)(CO)Cl go through a common mechanism.

(a) Ir^{III}(ttp)H + PhBr

(b) [Ir^{II}(ttp)]₂ + PhBr
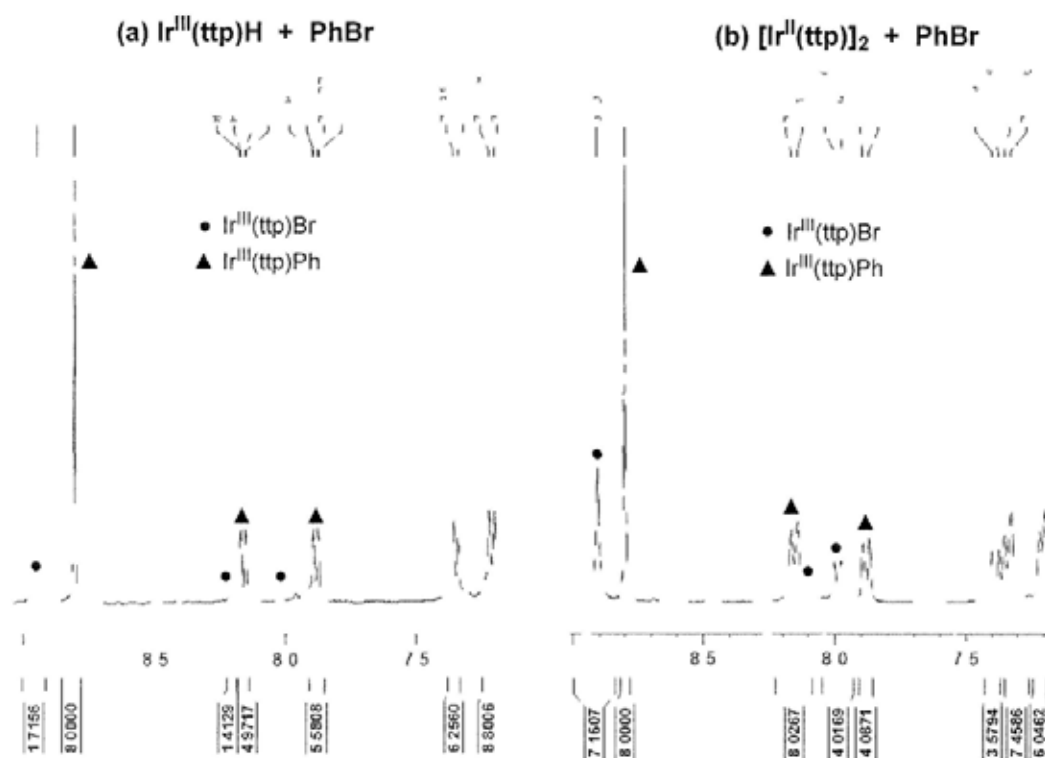
Figure 3.9 Partial ^{1}H NMR profiles of the reaction of PhBr (1.1 equiv) in benzene-d_6 at 200 °C with **(a)** Ir^{III}(ttp)H and **(b)** [Ir^{II}(ttp)]$_2$ (Table 3.34, entries 2 and 3).

(a) Ir^{III}(ttp)H + PhI

(b) [Ir^{II}(ttp)]₂ + PhI
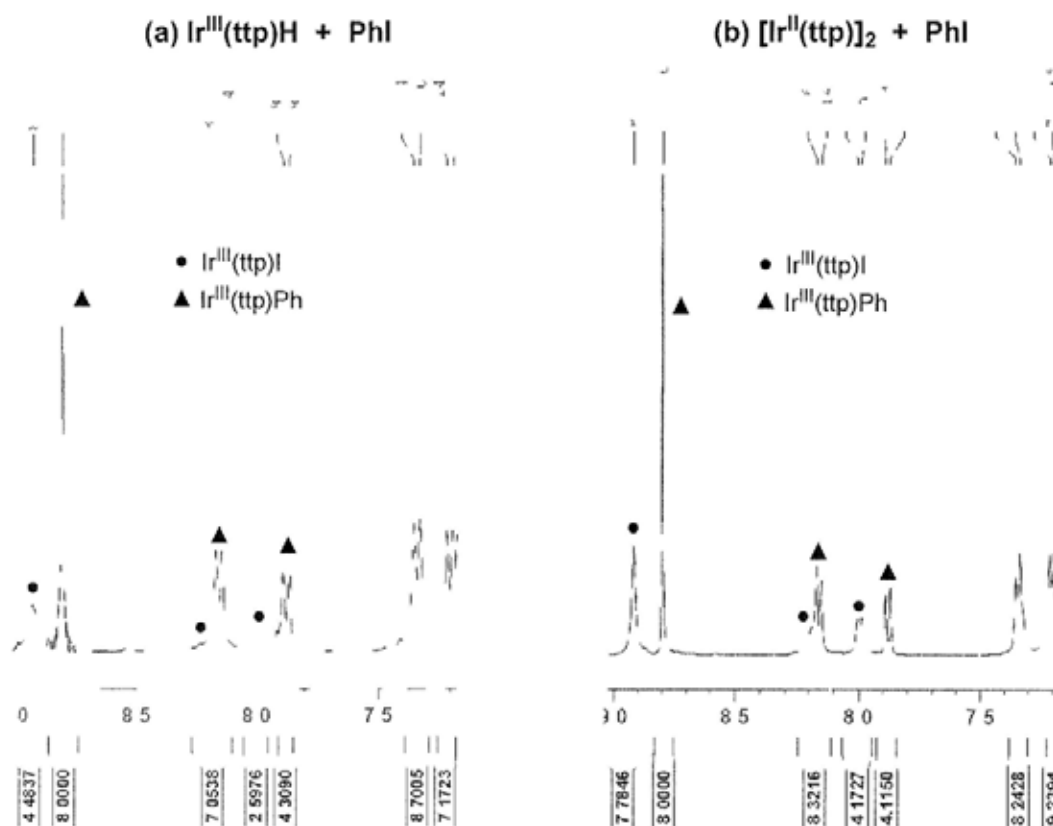
Figure 3.10 Partial ^{1}H NMR profiles of the reaction of PhI (1.1 equiv) in benzene-d_6 at 200 °C with **(a)** Ir^{III}(ttp)H and **(b)** [Ir^{II}(ttp)]$_2$ (Table 3.34, entries 5 and 6).

169

3.2.8.3.2 Electronic Effect of 4-Substituted Aryl Halides

Electron-rich and electron-poor *para*-substituted aryl bromides (ArBr, Ar = p-MeOC$_6$H$_4$, p-NO$_2$C$_6$H$_4$) were reacted with Ir^I(ttp)$^-$, Ir^{III}(ttp)H, and [Ir^{II}(ttp)]$_2$ in benzene-d_6 at 200 °C to investigate the electronic effect of ArX on the reactivities of possible iridium porphyrin intermediates (Table 3.35).

Table 3.35 Relative Reactivities of Possible Ir(ttp) Species in Ar-Br Cleavages

Ir^{III}(ttp)X' + Br–⟨C$_6$H$_4$⟩–FG $\xrightarrow[\text{200 °C, time}]{\text{C}_6\text{D}_6}$ Ir^{III}(ttp)–⟨C$_6$H$_4$⟩–FG + Ir^{III}(ttp)Br

1.1 equiv · · · · Ir^{III}(ttp)Ar

entry	Ir(ttp)X'	FG	time	Ir^{III}(ttp)Ar yield /%^{a}	Ir^{III}(ttp)Br yield/%^{b}
1	Ir^I(ttp)$^-$K$^{+\,c}$		2 d	nil^d	
2	Ir^{III}(ttp)H	MeO	1 h	61	28
3	1/2[Ir^{II}(ttp)]$_2$		2 min	46	31
4	Ir^I(ttp)$^-$K$^{+\,c}$		2 d	27^e	
5	Ir^{III}(ttp)H	H	14 h	31	7
6	1/2[Ir^{II}(ttp)]$_2$		2 min	34	32
7	Ir^I(ttp)$^-$K$^{+\,c}$		2 d	no rxn^f	
8	Ir^{III}(ttp)H	NO$_2$	1 h	44	14
9	1/2[Ir^{II}(ttp)]$_2$		2 min	37	36

^{a} Isolated yield. ^{b} Yield was estimated by ^{1}H NMR spectroscopy since Ir^{III}(ttp)Br was not stable to be isolated by column chromatography. ^{c} In form of Ir^I(ttp)$^-$[K(18-crown-6)]$^+$. ^{d} Ir^{III}(ttp)CH$_3$ in 73% NMR yield was isolated. ^{e} Ir^I(ttp)$^-$K$^+$ in 43% NMR yield also remained unreacted in 2 days, and Ir^I(ttp)$^-$K$^+$ was completely consumed in 14 days to give Ir^{III}(ttp)Ph in 38% isolated yield. ^{f} Ir^I(ttp)$^-$K$^+$ in 75% NMR yield remained unreacted.

In the reaction with p-MeOC$_6$H$_4$Br (1.1 equiv) in benzene-d_6 at 200 °C, Ir^I(ttp)$^-$ reacted slowly in 2 days to give Ir^{III}(ttp)CH$_3$ in 73% yield without the formation of Ir^{III}(ttp)C$_6$H$_4$(p-OMe), likely due to the more favorable nucleophilic substitution of Me-OC$_6$H$_4$(p-Br) (Table 3.35, entry 1).[50] Ir^{III}(ttp)H reacted faster in 1 hour to yield Ir^{III}(ttp)C$_6$H$_4$(p-OMe) and Ir^{III}(ttp)Br[49] in 61% and 28% yields, respectively (Table 3.35, entry 2). [Ir^{II}(ttp)]$_2$ reacted most rapidly in 2 minutes to give Ir^{III}(ttp)C$_6$H$_4$(p-OMe) and Ir^{III}(ttp)Br[49] in 46% and 31% yields, respectively (Table 3.35, entry 3).

In the reaction with p-NO$_2$C$_6$H$_4$Br (1.1 equiv) in benzene-d_6 at 200 °C, Ir^I(ttp)$^-$ did not react

in 2 days to yield any $Ir^{III}(ttp)C_6H_4(p\text{-}NO_2)$, and unreacted $Ir^I(ttp)^-K^+$ was recovered in 75%

yield (Table 3.35, entry 7). $Ir^{III}(ttp)H$ reacted faster in 1 hour to yield $Ir^{III}(ttp)C_6H_4(p\text{-}NO_2)$ and

$Ir^{III}(ttp)Br^{49}$ in 44% and 14% yields, respectively (Table 3.35, entry 8). $[Ir^{II}(ttp)]_2$ reacted most

rapidly in 2 minutes to give $Ir^{III}(ttp)C_6H_4(p\text{-}NO_2)$ and $Ir^{III}(ttp)Br^{49}$ in 37% and 36% yields,

respectively (Table 3.35, entry 9).

Since $[Ir^{II}(ttp)]_2$ was shown to react fastest with $p\text{-}MeOC_6H_4Br$, PhBr, and $p\text{-}NO_2C_6H_4Br$

among the iridium porphyrin intermediates (Table 3.35, entries 3, 6, and 9), it is also

reasonable to assume that the Ar-X cleavages of the electron-rich ArX, the parent PhBr, and the

electron-poor Ar-X go through a common mechanism.

3.2.8.4 Reaction Mechanisms of Ar-X Cleavages by Iridium(II) Porphyrin

$[Ir^{II}(ttp)]_2$ was shown to react with ArX to give both $Ir^{III}(ttp)Ar$ and $Ir^{III}(ttp)X$ (Table 3.34,

entries 3, 6, and 9; Table 3.35, entries 3 and 9). Likely, $[Ir^{II}(ttp)]_2$ dissociates into 2 $Ir^{II}(ttp)$

metalloradicals (Scheme 3.22, pathway viii), which then reacts with ArX via a classical

bi-metallic oxidative addition to give $Ir^{III}(ttp)Ar$ and $Ir^{III}(ttp)X$ (Scheme 3.22, pathway ix).

In principle, Ar-X cleavage by $Ir^{II}(ttp)$ can occur via (A) halgoen atom transfer (Scheme 3.23,

pathways i and ii) and (B) radical *ipso*-substitution (Scheme 3.23, pathways iii-v).

Scheme 3.23 Possible Mechanisms of Ph-X Cleavages by $Ir^{II}(ttp)$

(A) Halogen Atom Transfer

Ir^{II}(ttp) can abstract the halogen atom (X•) from ArX to form Ir^{III}(ttp)X and the aryl radical (Ar•) (Scheme 3.23, pathway i). Ar• then reacts with another Ir^{II}(ttp) to give Ir^{III}(ttp)Ar (Scheme 3.23, pathway ii). The halogen atom transfer pathway can be supported by 2 observations: (1) the formation of biaryls from Ar•, either via the dimerization of Ar• (Scheme 3.23, pathway vi)[18] or the homolytic aromatic substitution of Ar• with benzene solvent (Scheme 3.23, pathway vii; Scheme 3.17),[28b] and (2) the ratio of Ir^{III}(ttp)Ar : Ir^{III}(ttp)X is less than 1, due to the leakage of Ar• for biaryl formations. However, in the reaction of $[Ir^{II}$(ttp)$]_2$ with 4-bromo-*tert*-butyl-benzene (1.1 equiv) in benzene at 200 °C, neither $(p\text{-}^tBu)C_6H_4\text{-}C_6H_4(p\text{-}^tBu)$ nor $(p\text{-}^tBu)C_6H_4\text{-}Ph$ were detected by GC-MS analysis (eq 3.23). Moreover, the Ir^{III}(ttp)Ar : Ir^{III}(ttp)X ratios are generally larger than 1 (Tables 3.34 and 3.35). Therefore, the halogen atom transfer mechanism unlikely takes place.

$$1/2[Ir^{II}(ttp)]_2 \ + \ Br\text{-}\langle \rangle\text{-}^tBu \xrightarrow[200\,^\circ C,\ 5\ min]{C_6H_6,\ N_2} Ir^{III}(ttp)\text{-}\langle \rangle\text{-}^tBu \ + \ Ir^{III}(ttp)Br \ + \ PhBr \quad (3.23)$$

1 1 equiv   47%   ~39%   1%

$^tBu\text{-}\langle \rangle\text{-}\langle \rangle\text{-}^tBu$ (none)

$^tBu\text{-}\langle \rangle\text{-}\langle \rangle$ (none)

(B) Radical *Ipso*-Substitution

Ir^{II}(ttp) can undergo the *ipso*-attack of the carbon center of C-X bond in Ar-X to form Ir(ttp)-cyclohexadienyl radical intermediate (**I**) (Scheme 3.23, pathway iii),[23] which then eliminates X• to generate Ir^{III}(ttp)Ar (Scheme 3.23, pathway iv). X• further reacts with another Ir^{II}(ttp) to form Ir^{III}(ttp)X (Scheme 3.23, pathway v). Several lines of evidences support the radical *ipso*-substitution mechanism. The details of the mechanistic studies are discussed in the following section.

3.2.8.5 Radical Chain *Ipso*-Substitution of Aryl Halides by Iridium(II) Porphyrin

The more detailed mechanisms of the radical *ipso*-substitution of ArX by $[Ir^{II}$(ttp)$]_2$ to form Ir^{III}(ttp)Ar and Ir^{III}(ttp)X are depicted in Scheme 3.24.

172

Scheme 3.24 Proposed Mechanism of Radical Chain *Ipso*-Substitution of ArX with $[Ir^{II}(ttp)]_2$

$$[Ir^{II}(ttp)]_2 \underset{}{\overset{i}{\rightleftharpoons}} 2Ir^{II}(ttp)$$

$$Ir^{II}(ttp) + X\text{—}\langle\text{—}\rangle\text{—FG} \overset{ii}{\rightleftharpoons} (ttp)Ir, X \text{—}\langle\bullet\rangle\text{—FG} \ (\mathbf{I}) \overset{iii}{\longrightarrow} Ir^{III}(ttp)\text{—}\langle\text{—}\rangle\text{—FG} + X\bullet$$

ArX — (I) — $Ir^{III}(ttp)Ar$

$$X\bullet + [Ir^{II}(ttp)]_2 \overset{iv}{\longrightarrow} Ir^{III}(ttp)X + Ir^{II}(ttp)$$

$$2X\bullet + \langle\text{—}\rangle \overset{v}{\longrightarrow} X\text{—}\langle\text{—}\rangle + HX$$

$$2X\bullet + \langle\text{—}\rangle\text{—X} \overset{vi}{\longrightarrow} X\text{—}\langle\text{—}\rangle\text{—X} + HX \quad (o, m, p\text{-}X)$$

$$Ir^{II}(ttp) + X\text{—}\langle\text{—}\rangle \overset{vii}{\longrightarrow} Ir^{III}(ttp)Ph + X\bullet$$

$$Ir^{II}(ttp) + X\text{—}\langle\text{—}\rangle\text{—X} \overset{viii}{\longrightarrow} Ir^{III}(ttp)\text{—}\langle\text{—}\rangle\text{—X} + X\bullet \quad (o, m, p\text{-}X)$$

$$Ir^{II}(ttp) + Ir^{III}(ttp)\text{—}\langle\text{—}\rangle\text{—X} \overset{ix}{\longrightarrow} Ir^{III}(ttp)\text{—}\langle\text{—}\rangle\text{—}Ir^{III}(ttp) + X\bullet$$

Under the high reaction temperature (150-200 °C) (Tables 3.24, 3.26, and 3.27), the intermediate, $[Ir^{II}(ttp)]_2$, initially dissociates into $Ir^{II}(ttp)$ metalloradicals (Scheme 3.24, pathway i).[51] $Ir^{II}(ttp)$ is very reactive and attacks the *ipso*-carbon of C-X bonds in ArX to form the Ir(ttp)-cyclohexadienyl radical intermediate (**I**) (pathway ii),[23] which further eliminates the halogen radical (X•) to form $Ir^{III}(ttp)Ar$ (pathway iii). X• then attacks $[Ir^{II}(ttp)]_2$ to produce $Ir^{III}(ttp)X$, and $Ir^{II}(ttp)$ is regenerated for subsequent radical chain propagation (pathway iv). A radical chain *ipso*-substitution of ArX with $[Ir^{II}(ttp)]_2$ is thus proposed.

Alternatively, X• can leak out and further react with excess benzene solvent and halobenzenes (PhX, FG = H in ArX) via the homolytic aromatic substitution (mechanism similar to Scheme 3.17) to generate the co-products, PhX and dihalobenzene ($C_6H_4X_2$), respectively (pathways v and vi). $Ir^{II}(ttp)$ can further react with PhX and $C_6H_4X_2$ via the

analogous *ipso*-substitution to form Ir^{III}(ttp)Ph and Ir^{III}(ttp)C$_6$H$_4$X, respectively (pathways vii and viii). In case Ir^{III}(ttp)C$_6$H$_4$(*p*-X) is produced, subsequent C-X cleavage by Ir^{II}(ttp) can also occur to give Ir^{III}(ttp)(*p*-C$_6$H$_4$)Ir^{III}(ttp) (pathway ix).

3.2.8.6 Supporting Mechanistic Evidences for Radical-*Ipso* Substitution of ArX by Iridium(II) Porphyrin

Several lines of evidences can support the radical *ipso*-substitution by Ir^{II}(ttp) (Scheme 3.24) and are presented in details in the following sections.

(1) Higher Ratio of Ir^{III}(ttp)Ar : Ir^{III}(ttp)X

The halogen atom (X•), which is eliminated from the Ir(ttp)-cyclohexadienyl radical intermediates (**I**) (Scheme 3.24, pathway iii), mainly reacts with [Ir^{II}(ttp)]$_2$ to form Ir^{III}(ttp)X (Scheme 3.24, pathway iv), but a small amount of X• can also react with excess C$_6$H$_6$ solvent and PhX simultaneously (Scheme 3.24, pathways v and vi). As a result, the ratio of Ir^{III}(ttp)Ar : Ir^{III}(ttp)X should be higher than 1. Indeed, [Ir^{II}(ttp)]$_2$ was shown to react with ArX (X = Cl, Br) to give Ir^{III}(ttp)Ar and Ir^{III}(ttp)X with an Ir^{III}(ttp)Ar : Ir^{III}(ttp)X ratio larger than 1 (Table 3.34, entries 3 and 9; Table 3.35, entries 3 and 9). This partially supports the possibility of the radical *ipso*-substitution mechanism.

(2) Reactions of Halogen Radicals with Benzene or Halobenzenes

The direct evidence of the radical *ipso*-substitution of ArX by Ir^{II}(ttp) to eliminate X• is the formation of organic co-products, halobenzene (PhX), formed from the reaction of X• with benzene solvent (Scheme 3.24, pathway v), or dihalobenzene (C$_6$H$_4$X$_2$), formed from the reaction of X• with excess PhX (Scheme 3.24, pathway vi), via the homolytic aromatic substitutions (mechanism similar to Scheme 3.17) .

174

Cl• and Br•, which can be generated from the thermolysis of SO_2Cl_2 and Br_2, have been reported[52,53] and also demonstrated to react with benzene at 200 °C in 90 minutes to yield PhCl and PhBr in 20% and 83%[54] yields, respectively (eqs 3.24 and 3.25). SO_2Cl_2 also reacted with PhCl in solvent-free conditions at 200 °C in 90 minutes to yield dichlorobenzene and chlorinated biaryls,[55] in which 1,4-dichlorobenzene (1,4-$Cl_2C_6H_4$)[56] was the major product (eq 3.27). However, I_2, a precursor of I•, did not react with benzene at all at 200 °C to yield any PhI due to its very low reactivity (eq 3.26).[57]

$$SO_2Cl_2 + C_6H_6 \xrightarrow[\text{1.5 h, } N_2]{200\ ^\circ C} \underset{20\%}{PhCl} \qquad (3.24)$$

$$Br_2 + C_6H_6 \xrightarrow[\text{1.5 h, } N_2]{200\ ^\circ C} \underset{83\%}{PhBr} \qquad (3.25)$$

$$I_2 + C_6H_6 \xrightarrow[\text{2 h, } N_2]{200\ ^\circ C} No\ Rxn \qquad (3.26)$$

$$(3.27)$$

[Ir^{II}(ttp)]$_2$ was then independently prepared[37] to react with ArBr and PhCl to support the proposed formation of organic co-products.

(i) Reaction of Bromine Radical with C_6H_6

In the reaction of [Ir^{II}(ttp)]$_2$ with 4-bromo-*tert*-butylbenzene in C_6H_6 at 200 °C, Ir^{III}(ttp)C_6H_4(p-^{t}Bu) and Ir^{III}(ttp)Br[49] were obtained in 49% and ~39% yields, repsectively, with the formation of PhBr[58] in 1% yield by GC-MS analysis (eq 3.28). This supports the radical *ipso*-substitution of ArBr by Ir^{II}(ttp) to give Ir^{III}(ttp)Ar and Br•, which further reacts with excess benzene at 200 °C to yield PhBr (Scheme 3.24, pathways ii-v).

$$(3.28)$$

(ii) Reaction of Chlorine Radical with PhCl

In the reaction of $Ir^{III}(ttp)(CO)Cl$ with PhCl (200 equiv) and K_2CO_3 in benzene at 150 and 200 °C, 1,4-dichlorobenzene (1,4-$Cl_2C_6H_4$) was formed in ~1% yield (Table 3.21). Moreover, $[Ir^{II}(ttp)]_2$ was also shown to react with excess PhCl at 200 °C to give $Ir^{III}(ttp)Ph$ in 39% yield, traces of $Ir^{III}(ttp)(CO)Cl$ (4%) and $Ir^{III}(ttp)(p\text{-}C_6H_4)Ir^{III}(ttp)$ (4%), and 1,4-$Cl_2C_6H_4$[59] in 2% yield by GC-MS analysis (eq 3.29) These results support the radical *ipso*-substitution of PhCl by $Ir^{II}(ttp)$ to give $Ir^{III}(ttp)Ph$ and Cl•, which further reacts with excess PhCl to give 1,4-$Cl_2C_6H_4$[59] (Scheme 3.24, pathways ii-iv, vi).

$$1/2[Ir^{II}(ttp)]_2 + PhCl \xrightarrow[\text{30 min, N}_2]{200\ ^\circ C} Ir^{III}(ttp)Ph + Ir^{III}(ttp)(CO)Cl + Ir^{III}(ttp)(p\text{-}C_6H_4)Ir^{III}(ttp) + 1,4\text{-}Cl_2C_6H_4$$

$$\phantom{1/2[Ir^{II}(ttp)]_2 + PhCl \xrightarrow[\text{30 min, N}_2]{200\ ^\circ C}}\ \ 39\%\qquad\qquad 1\%\qquad\qquad\qquad 4\%\qquad\qquad\qquad\qquad 2\%$$

(3.29)
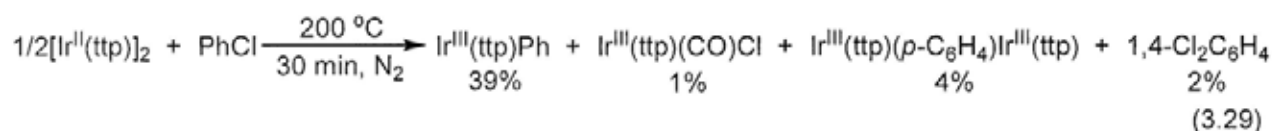
The formation of $Ir^{III}(ttp)(p\text{-}C_6H_4)Ir^{III}(ttp)$ in the reactions of $Ir^{III}(ttp)(CO)Cl$ / K_2CO_3 (Table 3.21) and $[Ir^{II}(ttp)]_2$ (eq 3.29) with PhCl most likely comes from the double C-Cl cleavages of 1,4-$Cl_2C_6H_4$ with $[Ir^{II}(ttp)]_2$ (Scheme 3.24, pathways viii and ix). Indeed, $Ir^{III}(ttp)(CO)Cl$ was shown to react with 1,4-$Cl_2C_6H_4$ (1 equiv) and K_2CO_3 in benzene at 200 °C in 7 hours to give $Ir^{III}(ttp)(p\text{-}C_6H_4)Ir^{III}(ttp)$ in 3% yield (eq 3.30).[60]

$$Ir^{III}(ttp)(CO)Cl + (p\text{-}Cl)C_6H_4Cl \xrightarrow[\substack{C_6H_6,\ N_2 \\ 200\ ^\circ C,\ 7\ h}]{K_2CO_3\ (20\ equiv)} Ir^{III}(ttp)(p\text{-}C_6H_4)Ir^{III}(ttp) + Ir^{III}(ttp)C_6H_4(p\text{-}Cl) + Ir^{III}(ttp)CH_3$$

$$\phantom{Ir^{III}(ttp)(CO)Cl +}\ \ 1\ equiv \qquad\qquad\qquad\qquad\qquad\qquad\qquad 3\%\qquad\qquad\qquad\quad 9\%\qquad\qquad\quad 1\%$$

(3.30)
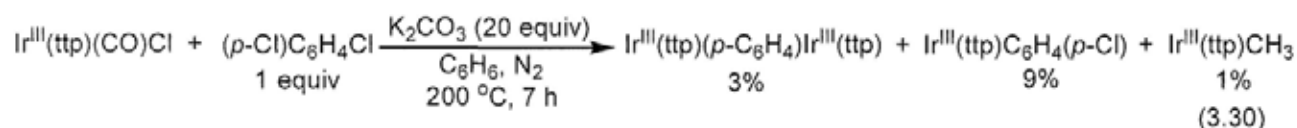
(3) Rate Enhancements in *Para*-Substituted Aryl Halides than Halobenzenes

The electronic effect of *para*-substituted ArX on the rate of base-promoted Ar-X cleavages by $Ir^{III}(ttp)(CO)Cl$ was studied by undergoing the competition reactions between Ar-X and PhX in an equimolar ratio (Tables 3.36-3.38). The $Ir^{III}(ttp)Ar$: $Ir^{III}(ttp)Ph$ ratio reflects the relative rates in Ar-X and Ph-X cleavages. As control experiments, $Ir^{III}(ttp)Ph$ neither underwent deuterium exchange with benzene-d_6 to give $Ir^{III}(ttp)C_6D_5$ nor react with excess 4-bromo-nitrobenzene to give $Ir^{III}(ttp)C_6H_4(p\text{-}NO_2)$ in basic conditions at 200 °C in a long time of 7 days (eqs 3.31 and 3.32). Thus, the $Ir^{III}(ttp)Ar$: $Ir^{III}(ttp)Ph$ ratios obtained in the

competition reactions are indeed the kinetic values.

$$\text{Ir}^{\text{III}}\text{(ttp)Ph} \xrightarrow[\text{C}_6\text{D}_6, \, 200\,^\circ\text{C}, \, 7\,\text{d}]{\text{KOH (20 equiv)}} \text{No Ir}^{\text{III}}\text{(ttp)C}_6\text{D}_5 \quad (3.31)$$
recovered
55%

$$\text{Ir}^{\text{III}}\text{(ttp)Ph} + \text{Br}\!-\!\!\langle\!\!\bigcirc\!\!\rangle\!-\!\text{NO}_2 \xrightarrow[\text{C}_6\text{D}_6, \, 200\,^\circ\text{C}, \, 7\,\text{d}]{\text{KOH (20 equiv)}} \text{No Ir}^{\text{III}}\text{(ttp)}\!-\!\!\langle\!\!\bigcirc\!\!\rangle\!-\!\text{NO}_2 \quad (3.32)$$
recovered
71%   25 equiv
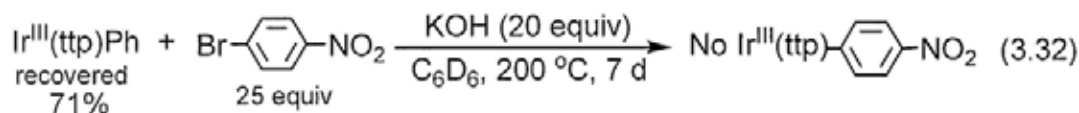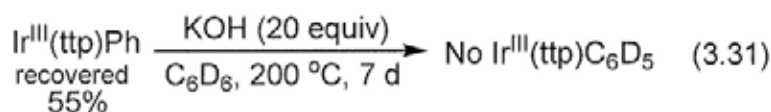
In base-promoted Ar-Br cleavage, a V-shaped Hammett plot was obtained using the Hammett constants σ^o_p[27] When the Hammett constants σ^+_p[27] were used, a similar V-shaped Hammett plot was obtained (Table 3.36; **Appendix II**, Figures 1(a),(b)). The Hammett plots of base-promoted Ar-I and Ar-Cl cleavages also exhibit similar V-shaped patterns using both the Hammett constants σ^o_p and σ^+_p (Tables 3.37 and 3.38; **Appendix II**, Figures 2(a),(b) and 3(a),(b)).

From the Hammett plots, the rates of Ar-X cleavages are promoted by both the electron-donating and electron-withdrawing *para*-substituents due to the enhanced stabilization of the Ir(ttp)-cyclohexadienyl radical (Scheme 3.24, species (**I**)), which is the characteristic of radical *ipso*-substitution reactions (Table 3.5, Scheme 3.16).

Table 3.36 Hammett Plot of Base-Promoted Ar-Br Cleavage by Ir$^{\text{III}}$(ttp)(CO)Cl

$$\text{Ir}^{\text{III}}\text{(ttp)(CO)Cl} + \text{Br}\!-\!\!\langle\!\!\bigcirc\!\!\rangle\!-\!\text{FG}\Big/\text{Br}\!-\!\!\langle\!\!\bigcirc\!\!\rangle \xrightarrow[\text{C}_6\text{H}_6, \, 200\,^\circ\text{C}]{\text{K}_2\text{CO}_3 \text{ (20 equiv)}} \text{Ir}^{\text{III}}\text{(ttp)}\!-\!\!\langle\!\!\bigcirc\!\!\rangle\!-\!\text{FG} + \text{Ir}^{\text{III}}\text{(ttp)}\!-\!\!\langle\!\!\bigcirc\!\!\rangle$$
25 equiv   25 equiv $\log(k_{\text{FG}}/k_{\text{H}})$
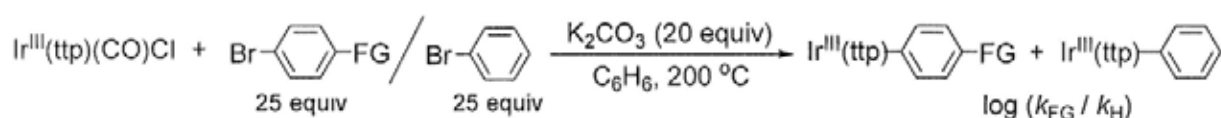
Entry	FG	$\sigma^o_p{}^a$	$\sigma^+_p{}^a$	$\log(k_{\text{FG}}/k_{\text{H}})^b$
1	NMe$_2$	-0.83	-1.70	1.74
2	OMe	-0.27	-0.78	0.81
3		-0.17	-0.31	0.25
4		-0.20	-0.26	0.13
5		-0.07	0.02	0.11
6		0.06	-0.07	0.30
7	Cl	0.23	0.11	0.62
8	Br	0.23	0.15	0.38
9	CO$_2$Me	0.45	0.49	0.75
10	CN	0.66	0.66	0.83
11	NO$_2$	0.78	0.79	1.07

^{a} Hammett constant (Ref 27). ^{b} Ratio obtained by taking the ratio of Ir$^{\text{III}}$(ttp)C$_6$H$_4$(*p*-FG) : Ir$^{\text{III}}$(ttp)Ph in the crude product by ^{1}H NMR spectroscopy.

Table 3.37 Hammett Plot of Base-Promoted Ar-I Cleavage by Ir^{III}(ttp)(CO)Cl

Ir^{III}(ttp)(CO)Cl + I—〈〉—FG / I—〈〉 $\xrightarrow[\text{C}_6\text{H}_6,\ 150\ ^\circ\text{C}]{\text{NaOH (20 equiv)}}$ Ir^{III}(ttp)—〈〉—FG + Ir^{III}(ttp)—〈〉

                25 equiv   25 equiv $\log (k_{FG} / k_H)$
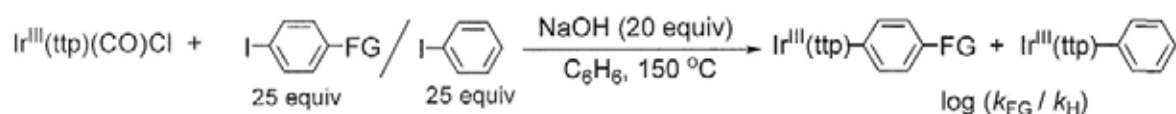
Entry	FG	$\sigma^o_p{}^a$	σ^{+a}_p	$\log (k_{FG} / k_H)^b$
1	OMe	-0.27	-0.78	0.93
2	Me	-0.17	-0.31	0.35
3	F	0.06	-0.07	0.43
4	I	0.18	0.14	0.73
5	Br	0.23	0.15	0.76

^{a} Hammett constant (Ref 27). ^{b} Ratio obtained by taking the ratio of Ir^{III}(ttp)C$_6$H$_4$(p-FG) : Ir^{III}(ttp)Ph in the crude product by ^{1}H NMR spectroscopy.

Table 3.38 Hammett Plot of Base-Promoted Ar-Cl Cleavages by Ir^{III}(ttp)(CO)Cl

Ir^{III}(ttp)(CO)Cl + Cl—〈〉—FG / Cl—〈〉 $\xrightarrow[\text{C}_6\text{H}_6,\ 150\ ^\circ\text{C}]{\text{K}_2\text{CO}_3\text{ (20 equiv)}}$ Ir^{III}(ttp)—〈〉—FG + Ir^{III}(ttp)—〈〉

                100 equiv   100 equiv $\log (k_{FG} / k_H)$
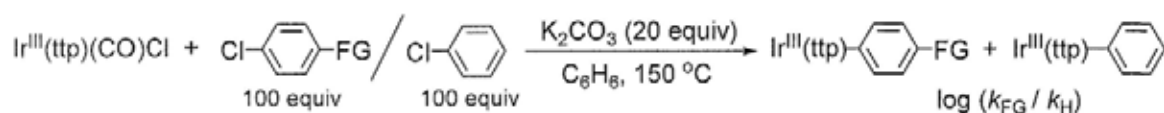
entry	FG	$\sigma^o_p{}^a$	σ^{+a}_p	$\log (k_{FG} / k_H)^b$
1	OMe	-0.27	-0.78	0.64
2	F	0.06	-0.07	0.52
3	Cl	0.23	0.11	0.46
4	CN	0.66	0.66	1.47

^{a} Hammett constant (Ref 27). ^{b} Ratio obtained by taking the ratio of Ir^{III}(ttp)C$_6$H$_4$(p-FG) : Ir^{III}(ttp)Ph in the crude product by ^{1}H NMR spectroscopy.

Mechanisms of Stabilization of Cyclohexadienyl Radicals by *Para*-Substituents. Both the electron-rich (π-donating: NMe$_2$, OMe; σ-donating: ^{t}Bu, Me, SiMe$_3$) and electron-poor (π-donating: F, Cl, Br, I; π-withdrawing: C(O)Me, CO$_2$Me, CN, NO$_2$) *para*-substituents likely stabilize the Ir(ttp)-cyclohexadienyl radical intermediate by the following mechanisms.[61]

(i) π-Donating substituent, e.g. OMe group, extends the resonance stabilization of the Ir(ttp)-cyclohexadienyl radical by donating single electron from the filled oxygen π-orbital to the cyclohexadienyl radical (Scheme 3.25).[61]

Scheme 3.25 Extended Resonance Stabilization of Cyclohexadienyl Radical by π-Donating *Para*-Methoxy Group
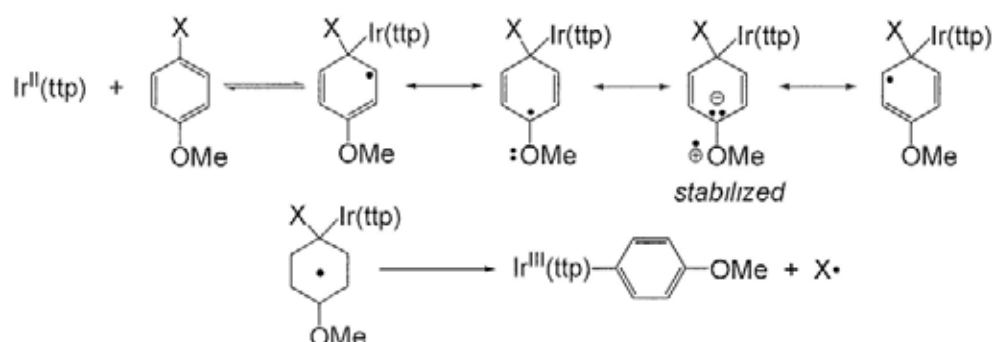
(ii) σ-Donating substituents (e.g. Me, ⁱBu) slightly stabilize the Ir(ttp)-cyclohexadienyl radical by hyperconjugation (Scheme 3.26) [61]

Scheme 3.26 Extended Resonance Stabilization of Cyclohexadienyl Radical by Hyperconjugation with σ-Donating *Para*-Alkyl Groups
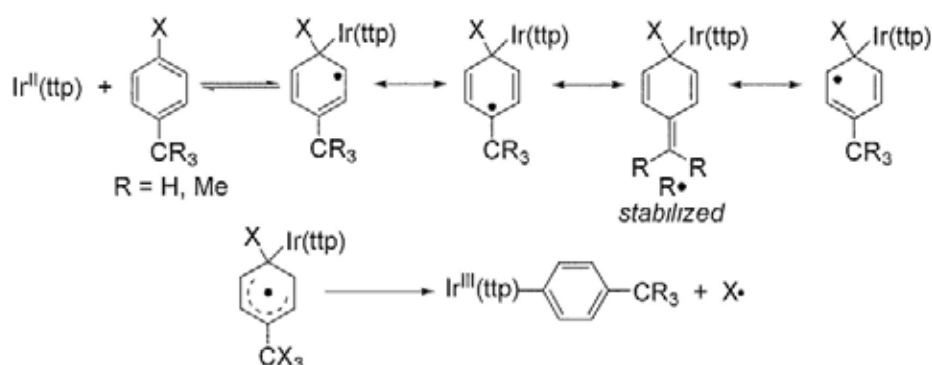
(iii) σ-Donating SiMe₃ group slightly stabilizes the Ir(ttp)-cyclohexadienyl radical via the extended resonance stabilization by donating π-electron to the the low-lying empty d orbital of Si (Scheme 3.27).[61b]

Scheme 3.27 Extended Resonance Stabilization of Cyclohexadienyl Radical by *d*-Orbital Interaction of σ-Donating *Para*-Trimethylsilyl Group

179
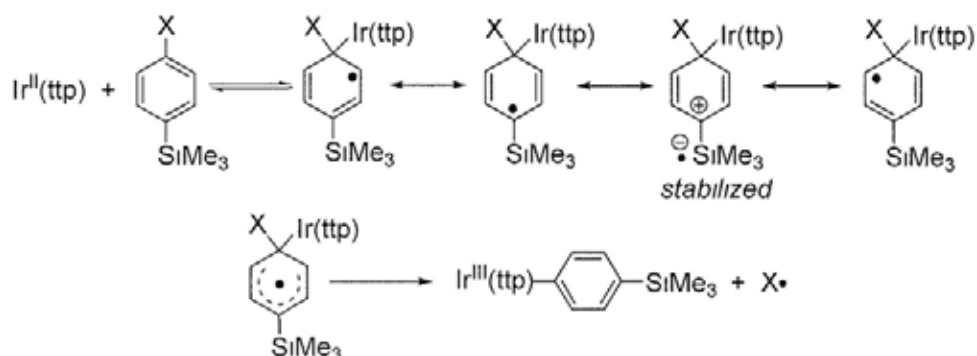
(iv) π-Withdrawing substituent, e.g. NO_2 group, extends the resonance stabilization of the Ir(ttp)-cyclohexadienyl radical by delocalizing the radical to the *para*-substituent (Scheme 3.28).[61]

Scheme 3.28 Extended Resonance Stabilization of Cyclohexadienyl Radical by π-Withdrawing *Para*-Nitro Group
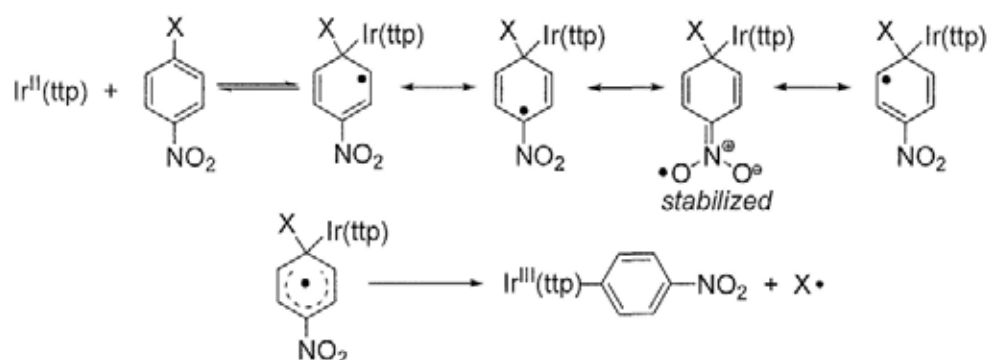
(4) Rate Enhancements in *Para*-Substituted Aryl Halides than *Meta*-Substituted Ones

When an equimolar ratio of *para*- and *meta*-substituted ArBr were reacted with $Ir^{III}(ttp)(CO)Cl$ and K_2CO_3, *para*-substituted aryl iridium porphyrins were always formed more than the *meta*-substituted ones by around 2-7 times (Table 3.39),[62] which is also the characteristic of radical *ipso*-substitution of aryl halides (Scheme 3.15; Table 3.5). The higher reactivities of the *para*-substituted ArX than the *meta*-substituted ones are also indicated by the larger magnitudes of the σ_p^{o} values than the σ_m^{o} ones (Table 3.39).

Table 3.39 Competition Reaction in *Para*- and *Meta*-Substituted Ar-Br Cleavages

entry	FG	$\sigma_p^{o\,a}$	$\sigma_m^{o\,a}$	time/h	*para*-: *meta*-pdt[b]	*para*-pdt yield/%[c]	*para*-pdt yield/%[c]
1	OMe	-0.27	0.12	23	6.9 : 1	84	15
2		-0.17	-0.07	26	1.5 : 1	48	32
3	NO_2	0.78	0.71	19	1.5 : 1	58	37

[a] Hammett constant (Ref 27). [b] Ratio obtained from the crude product by ^1H NMR spectroscopy. [c] Isolated yield.

The *meta*-substituted ArX reacts more slowly than the *para*-substituted ArX, as the *meta*-substituent is the unactivating group and cannot extend the resonance stabilization of the Ir(ttp)-cyclohexadienyl radical (Scheme 3.29).

Scheme 3.29 No Extended Stabilization of Cyclohexadienyl Radical by *Meta*-Substituents

no extra stabilization by FG
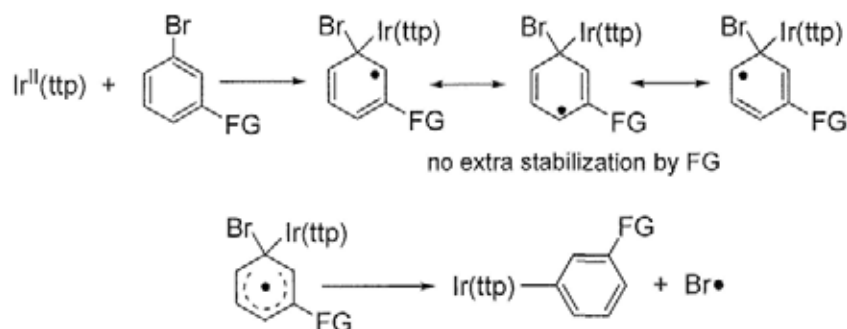
3.2.8.7 Discussions of Radical *Ipso*-Substitution of Aryl Halides by Iridium(II) Porphyrin

The radical chain *ipso*-substitution of ArX with $[Ir^{II}(ttp)]_2$ to form $Ir^{III}(ttp)Ar$ and $Ir^{III}(ttp)X$ is proposed (Sections 3.2.8.3 - 3.2.8.6). Such newly-discovered organometallic reaction exhibits the following characteristics:

(i) Selective Aryl C-X Bond Cleavages without C-H Cleavages

In the base-promoted reactions of ArX (p-FG-C_6H_4X), with $Ir^{III}(ttp)(CO)Cl$, only the Ar-X bonds are cleaved to form $Ir^{III}(ttp)C_6H_4(p$-FG), without the activations of aryl C-H bonds to yield $Ir^{III}(ttp)C_6H_3(FG)(X)$ (Tables 3.24, 3.26, and 3.27). This can be explained by 2 reasons:

(1) Kinetic aspect. Since aryl Ar-X bonds (X = Cl, Br, I, 66-96 kcal mol^{-1}) are weaker than the Ar-H bonds (112-116 cal mol^{-1}) (Table 3.2), it is reasoned that the cleavages of C-X bonds is kinetically more favorable than the cleavages of C-H bonds.

(2) Thermodynamic aspect. The reactions of $[Ir^{II}(ttp)]_2$ with Ph-X to form $Ir^{III}(ttp)$-Ph and $Ir^{III}(ttp)$-X (Scheme 3.30, pathway i) are estimated to be thermodynamically more favorable

than the reactions of $[Ir^{II}(ttp)]_2$ with XC_6H_4-H to form $Ir^{III}(ttp)$-C_6H_4X and $Ir^{III}(ttp)$-X (pathway ii).

Scheme 3.30 Thermodynamic Estimations of Aryl C-X and C-H Cleavages by $[Ir^{II}(ttp)]_2$
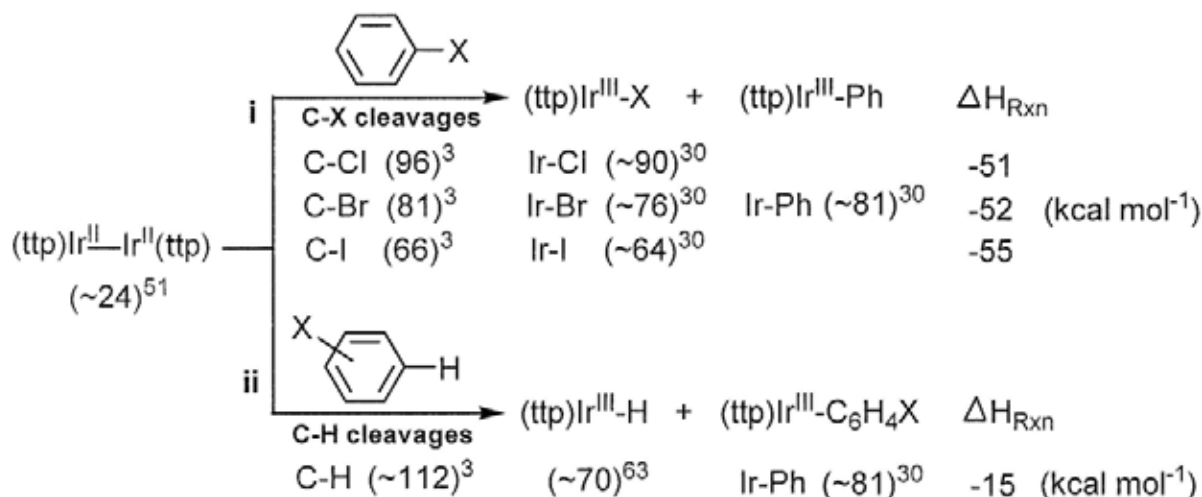
As a result, selective Ar-X bond cleavages by $[Ir^{II}(ttp)]_2$ can be driven both kinetically and thermodynamically.

(ii) Non-Radical-Assisted Elimination of Halogen Atom from Ir(ttp)-Cyclohexadienyl Radical

The elimination of halogen atom (X•) from the Ir(ttp)-cyclohexadienyl radical intermediate (**I**) to form $Ir^{III}(ttp)Ar$ likely occurs without the assistance of $Ir^{II}(ttp)$ radical (Scheme 3.24, pathway iii) due to the following supporting lines of evidence:

(1) Weak $C(sp^3)$-X bonds. The $C(sp^3)$-X bond energies in the halo-cyclohexadienyl radicals (X-C_6H_6•) have been estimated theoretically (Table 3.40).[64] They are much weaker than the corresponding Ph-X bonds, but are still in line with the Ph-X bond energies (F-C_6H_6• > Cl-C_6H_6• > Br-C_6H_6•). It is anticiptated that I-C_6H_6• has an even weaker $C(sp^3)$-X bond. Presumably, X• (X = Cl, Br, I) can eliminates facilely from (**I**) at the reaction temperatures (150-200 °C) by the thermolysis of the weak $C(sp^3)$-X bond, without the $Ir^{II}(ttp)$-assisted abstraction of X•.

Table 3.40 Bond Energies of sp³-C-X bonds in Halo-cyclohexadienyl Radical (X-C₆H₆•)
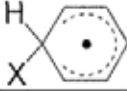
entry		BDE of C(sp³)-X bond / kcal mol⁻¹
1	X = F	33.2-35.9
2	X = Cl	7.2
3	X = Br	< 3.3

(2) Bulkiness of Ir^{II}(ttp). Ir^{II}(ttp) would be too sterically demanding and is thus kinetically unfavorable to abstract X• from (**I**).

(iii) Effect of Nature of PhX on the Rate of Radical-*Ipso* Substitution

The rate of radical *ipso*-substitution of [Ir^{II}(ttp)]$_2$ with PhX is shown to be in the order: PhI > PhBr > PhCl (Table 3.34, entries 3, 6, and 9). Likely, the C(sp³)-X bond strengths in the Ir(ttp)-cyclohexadienyl radical intermediate (**I**) (Scheme 3.24) are in the order: C-I < C-Br < C-Cl (Table 3.40) to dictate the rate of elimination of X• to yield Ir^{III}(ttp)Ph.

(iv) Effect of Reactivity of Halogen Radical on Ir^{III}(ttp)Ph : Ir^{III}(ttp)X Ratio

In the reactions of [Ir^{II}(ttp)]$_2$ with PhX (Table 3.34), the Ir^{III}(ttp)Ph : Ir^{III}(ttp)X ratio is related to the reactivity of X•.

In the Ph-Cl cleavage, the ratio of Ir^{III}(ttp)Ph : Ir^{III}(ttp)Cl is 14.3 : 1 (Table 3.34, entry 9), partly due to the competitive reactions of very reactive Cl• with benzene and PhCl at 200 °C (eq 3.24 and 3.27). Only a small fraction of Cl• reacts with [Ir^{II}(ttp)]$_2$ to give a trace of Ir^{III}(ttp)Cl.

In the Ph-Br cleavage, the Ir^{III}(ttp)Ph : Ir^{III}(ttp)Br ratio is around 1.1 : 1 (Table 3.34, entry 3). The less reactive Br• reacts selectively with [Ir^{II}(ttp)]$_2$ to yield Ir^{III}(ttp)Br (eq 3.28). A trace of Br• also reacts with C₆H₆ to give PhBr (eq 3.25).

In the Ph-I cleavage, the ratio of Ir^{III}(ttp)Ph : Ir^{III}(ttp)I is almost 1:1 (Table 3.34, entry 6). I• is only reactive enough to react with [Ir^{II}(ttp)]$_2$, whereas it is unreactive to react with C₆H₆ to

yield PhI (eq 2.28).

3.2.9 Discussions of Reaction Mechanisms of Aryl C-X Bond Cleavages by Ir^{III}(ttp)(CO)Cl

(i) Base-Promoted Ar-X Cleavages

Since [Ir^{II}(ttp)]$_2$ was identified as the intermediate for Ar-X cleavages to yield Ir^{III}(ttp)Ar and Ir^{III}(ttp)X (Tables 3.34 and 3.35), the reaction mechanisms of the base-promoted Ar-X cleavage by Ir^{III}(ttp)(CO)Cl can then be further summarized as shown in Scheme 3.31.

Ir^{III}(ttp)(CO)Cl undergoes base-promoted reduction to give Ir^{III}(ttp)H (Scheme 3.31, pathway i$_a$ and ii), which then undergoes thermal and base-promoted dehydrogenative dimerization to give [Ir^{II}(ttp)]$_2$ (pathways iii$_a$ and iii$_b$). [Ir^{II}(ttp)]$_2$ cleaves the Ar-X bonds to form Ir^{III}(ttp)Ar and Ir^{III}(ttp)X via radical-chain *ipso*-substitution (pathway iv). Ir^{III}(ttp)X is recycled by base-promoted reduction to regenerate Ir^{III}(ttp)H for further Ar-X cleavages (pathways v and ii).

Scheme 3.31 General Reaction Mechanism of Ar-X Cleavages by Ir^{III}(ttp)(CO)Cl with and without Bases
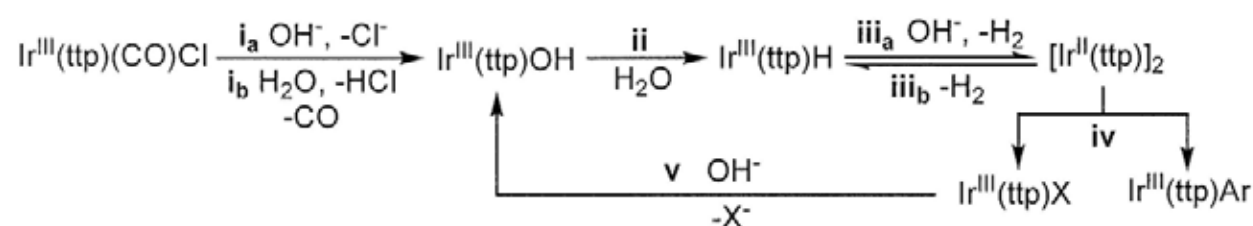
(ii) Ar-X Cleavages in the Absence of Base

In the absence of base, Ir^{III}(ttp)(CO)Cl reacted more slowly with PhX in benzene solvent to yield smaller amounts of Ir^{III}(ttp)Ph and Ir^{III}(ttp)(CO)X (X = Br, I) (Tables 3.10, entries 1, 3, and 5). The mechanism is unclear. It is assumed that Ir^{III}(ttp)(CO)Cl reacts with residual water in benzene and PhX to form a small amount of Ir^{III}(ttp)OH at 200 °C (Scheme 3.31, pathway i$_b$),

which further converts to $Ir^{III}(ttp)H$ and then $[Ir^{II}(ttp)]_2$ (pathways ii and iii$_b$) for Ar-X cleavages (pathway iv), Indeed, $Ir^{III}(ttp)(CO)Cl$ was shown to react with excess water (100 equiv) at 200 °C to yield $Ir^{III}(ttp)H$ in 16% yield (Chapter 2, Section 2.3, Table 2.1, entry 2).

(iii) Optimization of Bases in Ar-X Cleavages

K_2CO_3 was found to be the optimal base for efficient Ar-Cl and Ar-Br cleavages, whereas NaOH was found to be the optimal base for efficient Ar-I cleavage (Table 3.22). This can be attributed to the rate of base-promoted reduction of $Ir^{III}(ttp)(CO)X$ (X = Cl, Br, I) to form $Ir^{III}(ttp)H$ in the observed order: $Ir^{III}(ttp)(CO)Cl \sim Ir^{III}(ttp)(CO)Br > Ir^{III}(ttp)(CO)I$ (Chapter 2, Section 2.3, Table 2.2 and 2.3).

Thus, a weaker base of K_2CO_3 is strong enough for rapid conversions of $Ir^{III}(ttp)(CO)Cl$ and $Ir^{III}(ttp)(CO)Br$ (as an observed intermediate) to $Ir^{III}(ttp)H$ for subsequent Ar-Cl and Ar-Br cleavages, respectively (Tables 3.24, and 3.27). On the other hand, an even stronger base of NaOH is required to promote the rate of reduction of $Ir^{III}(ttp)(CO)I$ (as an observed intermediate) to form more $Ir^{III}(ttp)H$ for subsequent Ar-I cleavage (Table 3.26).

3.3 Conclusions

The base-promoted aryl carbon-halogen bond (Ar-X, X = Cl, Br, I) cleavages by high-valent iridium(III) porphyrin carbonyl chloride ($Ir^{III}(ttp)(CO)Cl$) in benzene solvent have been achieved to give $Ir^{III}(ttp)Ar$. Various *para*-substituted ArX can be reacted with high functional-group compatibilities to give $Ir^{III}(ttp)Ar$ in moderate to high yields. Mechanistic studies suggest that $Ir^{III}(ttp)(CO)Cl$ initially undergoes the base-promoted reduction to form $Ir^{III}(ttp)H$ and then $[Ir^{II}(ttp)]_2$ via the redox reactions (Chapter 2, sections 2.3 and 2.4). $[Ir^{II}(ttp)]_2$ reacts with ArX to form $Ir^{III}(ttp)Ar$ and $Ir^{III}(ttp)X$ via radical chain *ipso*-substitution, involving the elimination of halogen atom (X•) from the *ipso*-iridium-porphyrin-cyclohexadienyl radical intermediate. X• (X = Cl, Br) can further react

with benzene solvent to form PhX. Cl• also reacts with excess PhCl to form 1,4-dichlorobenzene, which is further converted to $Ir^{III}(ttp)(p\text{-}C_6H_4)Ir^{III}(ttp)$.

References

(1) Allred, A. L. *J. Inorg. Nucl. Chem.* **1961**, *17*, 215-221.

(2) Enemærke, R. J.; Christensen, T. B.; Jensen, H.; Daasbjerg, K. *J. Chem. Soc., Perkin Trans. 2*, **2001**, 1620-1630.

(3) Luo, Y.-R. *Comprehensive Handbook of Chemical Bond Energies*; CRC Press: Boca Raton, FL, 2007.

(4) Smith, M. B.; March, J. *March's Advanced Organic Chemistry: Reactions, Mechanisms. And Structure* 6th Ed. New York: J. Wiley, 2007.

(5) (a) Clot, E.; Mégret, C.; Eisenstein, O.; Perutz, R. N. *J. Am. Chem. Soc.* **2009**, *131*, 7817-7827. (b) Evans, M. E.; Burke, C. L.; Yaibuathes, S.; Colt, E.; Eisenstein, O.; Jones, W. D. *J. Am. Chem. Soc.* **2009**, *131*, 13464-13473.

(6) For examples of Ar-F cleavage by transition metal complexes, see: (a) Barrio, P.; Castarlenas, R.; Esteruelas, M. A.; Lledós, A.; Maseras, F.; Oñate, E.; Tomàs, J. *Organometallics* **2001**, *20*, 442-452. (b) Reinhold, M.; McGrady, J. E.; Perutz, R. N. *J. Am. Chem. Soc.* **2004**, *126*, 5268-5276. (c) Schaub, T.; Fischer, P.; Steffen, A.; Braun, T.; Radius, U.; Mix, A. *J. Am. Chem. Soc.* **2008**, *130*, 9304-9317.

(7) For the examples of transition-metal catalyzed cross-coupling reactions, see: (a) Prim, D.; Campagne, J.-M.; Joseph, D.; Andrioletti, B. *Tetrahedron* **2002**, *58*, 2041-2075. (b) van der Boom, M. E.; Milstein, D. *Chem. Rev.* **2003**, *103*, 1759-1792. (c) Martin, R.; Buchwald, S. L. *Acc. Chem. Res.* **2008**, *41*, 1461-1473. (d) Hartwig, J. F. *Acc. Chem. Res.* **2008**, *41*, 1534-1544. (e) Hartwig, J. F. *Nature* **2008**, *455*, 314-322.

(8) Alonso, F.; Beletskaya, I. P.; Yus, M.; *Chem. Rev.* **2002**, *102*, 4009-4091.

(9) Chen, J.; Zhou, S.; Ci, D.; Zhang, J.; Wang, R.; Zhang, J. *Ind. Eng. Chem. Res.* **2009**, *48*,

3812-3819.

(10) For the examples of group 8 transition metals, see: Fe(0): Shi, Y.; Li, M.; Hu, Q.; Li, X.; Sun, H. *Organometallics* **2009**, *28*, 2206-2210.

(11) For the examples of group 9 transition metals, see: (i) Co(I): Chen, Y.; Sun, H.; Flörke, U.; Li, X. *Organometallics* **2008**, *27*, 270-275. (ii) Rh(I): (a) Willems, S. T. H.; Budzelaar, P. H. M.; Moonen, N. N. P.; de Gelder, R.; Smits, J. M. M. Gal, A. W. *Chem. Eur. J.* **2002**, *8*, 1310-1320. (b) Chen, S.; Li, Y.; Zhao, J.; Li, X. *Inorg. Chem.* **2009**, *48*, 1198-1206. (c) Hoogervorst, W. J.; Goubitz, K.; Fraanje, J.; Lutz, M.; Spek, A. L.; Ernsting, J. M.; Elsevier, C. J. *Organometallics* **2004**, *23*, 4550-4563. (d) Ito, J.; Miyakawa, T.; Nishiyama, H. *Organometallics* **2008**, *27*, 3312-3315. (iii) Ir(I): Douvris, C.; Reed, C. A. *Organometallics* **2008**, *27*, 807-810.

(12) For the examples of group 10 transition metals, see: (i) Ni(0): Fahey, D. R. *J. Am. Chem. Soc.* **1970**, *92*, 402-404. (ii) Pd(0): (a) Amatore, C.; Jutand, A. *Acc. Chem. Res.* **2000**, *33*, 314-321. (b) Alcazar-Roman, L. M.; Hartwig, J. F. *Organometallics* **2002**, *21*, 491-502. (c) Barrios-Landeros, F.; Hartwig, J. F. *J. Am. Chem. Soc.* **2005**, *127*, 6944-6945. (iii) Pt(0): G. W. Parshall *J. Am. Chem. Soc.* **1974**, *96*, 2360-2366.

(13) Hartwig, J. F. *Organotransition Metal Chemistry: From Bonding to Catalysis*; Sausalito, CA: University Science Books, 2010.

(14) Tsou, T. T.; Kochi, J. K. *J. Am. Chem. Soc.* **1979**, *101*, 6319-6332.

(15) (a) Blum, J.; Weitzberg, M. *J. Organometal. Chem.* **1976**, *122*, 261-264. (b) Mureinik, R. J.; Weitzberg, M.; Blum, J. *Inorg. Chem.* **1979**, *18*, 915-918.

(16) Edelbach, B. L.; Jones, W. D. *J. Am. Chem. Soc.* **1997**, *119*, 7734-7742.

(17) Funabiki, T.; Nakamura, H.; Yoshida, S. *J. Organomet. Chem.* **1983**, *243*, 95-100.

(18) Ma, K.; Piers, W. E.; Parvez, M. *J. Am. Chem. Soc.* **2006**, *128*, 3303-3312.

(19) Lee, K.-W.; Brown, T. L. *J. Am. Chem. Soc.* **1987**, *109*, 3269-3275.

(20) Roundhill, D. M.; Atherton, S. J. *Inorg. Chem.* **1986**, *25*, 4071-4072.

(21) Halpern, J.; Maher, J. P. *J. Am. Chem. Soc.* **1965**, *87*, 5361-5366.

(22) Roundhill, D. M. *J. Am. Chem. Soc.* **1985**, *107*, 4354-4356.

(23) For reviews of radical *ipso*-substitution, see: (a) Tiecco, M. *Acc. Chem. Res.* **1980**, *13*, 51-57. (b) Traynham, J. G. *Chem. Rev.* **1979**, *79*, 323-330.

(24) (a) Shelton, J. R.; Lipman Jr., A. L. *J. Org. Chem.* **1974**, *39*, 2386-2390. (b) Henriquez, R.; Nonhebel, D. C. *Tetrahedron* **1993**, *49*, 6497-6500.

(25) Benati, L.; Camaggi, C. M.; Zanardi, G. *J. Chem. Soc., Perkin I* **1972**, 2817-2819.

(26) (a) Miller, B.; Walling, C. *J. Am. Chem. Soc.* **1957**, *79*, 4187-4191. (b) Milligan, B.; Bradon, R. L.; M. Rose, J. E.; Hubbert, H. E.; Roe, A. *J. Am. Chem. Soc.* **1962**, *84*, 158-162. (c) Echols, J. T.; Chuang, V. T. C.; Parrish, C. S.; Rose, J. E.; Milligan, B.; *J. Am. Chem. Soc.* **1967**, *89*, 4081-4088. (d) Nakashima, M.; Mok, C. Y.; Noyes, R. M. *J. Am. Chem. Soc.* **1969**, *91*, 7635-7639. (e) Gandour, R. D. *Tetrahedron* **1980**, *36*, 1001-1009.

(27) Hansch, C.; Leo, A.; Taft, R. W. *Chem. Rev.* **1991**, *91*, 165-195.

(28) (a) Davies, D. I.; Hey, D. H.; Summers, B. *J. Chem. Soc. C* **1971**, 2681-2684. (b) Smith, M. B.; March, J. *March's Advanced Organic Chemistry: Reactions, Mechanisms. And Structure* 6th Ed. New York: J. Wiley, 2007, Chapter 14.

(29) (a) Creary, X. *J. Org. Chem.* **1980**, *45*, 280-284. (b) Creary, X.; Mehrsheikh-Mohammadi, M. E.; McDonald, S. *J. Org. Chem.* **1987**, *52*, 3254-3263.

(30) The BDEs of Ir^{III}-X bonds (X = Cl, Br, I, Ph) from $Cp*(PMe_3)Ir^{III}X_2$ are used as the references of BDEs of Ir^{III}-X bonds (X = Cl, Br, I, Ar) in Ir^{III}(ttp)X. See: Stoutland, P. O.; Newman, L. J.; Buchanan, J. M.; Bergman, R. G. *J. Am. Chem. Soc.* **1987**, *109*, 3143-3145.

(31) Gatard, S.; Çelenligil-Çetin, R.; Guo, C.; Foxman, B. M.; Ozerov, O. V. *J. Am. Chem. Soc.* **2006**, *128*, 2808-2809.

(32) Fan, L.; Parkin, S.; Ozerov, O. V. *J. Am. Chem. Soc.* **2005**, *127*, 16772-16773.

(33) Ben-Ari, E.; Gandelman, M.; Rozenberg, H.; Shimon, L. J. W.; Milstein, D. *J. Am. Chem. Soc.* **2003**, *125*, 4714-4715. (b) Ben-Ari, E.; Cohen, R.; Gandelman, M.; Shimon, L. J. W.; Martin, J. M. L.; Milstein, D. *Organometallics* **2006**, *25*, 3190-3210.

(34) (a) Kostas, I. D.; Coutsolelos, A. G.; Charalambidis, G.; Skondra, A. *Tetrahedron Lett.* **2007**, *48*, 6688-6691. (b) Wan, Q.-X.; Liu, Y. *Catal. Lett.* **2009**, *128*, 487-492.

(35) Chiu, P. F. *M. Phil. Thesis*, The Chinese University of Kong Kong, 2006.

(36) The bond energies of transition-metal-carbon and transition-metal-hydrogen bonds (M-C, M-H) generally increase down the groups due to the increase in the thermal stabilities of M-C and M-H complexes. For the examples of reported bond energies of group 9 M-C bonds, see: Ref 3.

(37) K_2CO_3-promoted benzylic C-H bond activations by $Ir^{III}(ttp)(CO)Cl$ was reported. See: Cheung, C. W.; Chan, K. S. *Organometallics* **2008**, *27*, 3043-3055.

(38) The higher oxidizing powers of PhBr and PhI than PhCl can be reflected by the less negative reduction potentials (E) of PhBr and PhI than PhCl (E_{red}(PhI) = -1.28 V, E_{red}(PhBr) = -1.89 V, E_{red}(PhCl) = -2.26 V. See: Ref 2.

(39) The analogous C-H bond activation of benzene by $Ir^{III}(acac)_2OH$ to give $Ir^{III}(acac)_2Ph$ and H_2O has been reported. See: Tenn, W. J.; III; Young, K. J. H.; Oxgaard, J.; Nielsen, R. J.; William A. Goddard, W. A., III; Periana, R. A. *Organometallics* **2006**, *25*, 5173-5175.

(40) The formation of $Ir^{III}(ttp)CH_3$ likely came from the base-promoted reduction of the carbonyl ligand in $Ir^{III}(ttp)(CO)Cl$ by the $Ir^{III}(ttp)H$ intermediate. For the details of the mechanism of $Ir^{III}(ttp)CH_3$ formation, see Ref 37.

(41) The reaction of $Ir^{III}(ttp)(CO)Cl$ with *p*-bromotoluene (1.1 equiv) and Cs_2CO_3 (20 equiv) in benzene-d_6 has been studied in a sealed NMR tube at 150 °C. After 19 hours, $Ir^{III}(ttp)Ph$ was formed quantitatively, without the formation of any $Ir^{III}(ttp)Bn(p$-Br) (δ(benzylic H) ~ -3.6 ppm) in the course of reaction.

(42) Aldehydic C-H bond activations of benzaldehydes by $Ir^{III}(ttp)(CO)Cl$ have been reported. See: Song, X.; Chan, K. S. *Organometallics* **2007**, *26*, 965-970.

(43) Water-soluble iridium(III) porphyrin, $[Ir^{III}(tspp)(H_2O)_2]^{3-}$ has been reported to undergo thermodynamically favorable ligand substitution with CH_3OH to form $[Ir^{III}(tspp)(CH_3OH)_2]^{3-}$. See: Bhagan, S.; Sarkar, S.; Wayland, W. W. *Inorg Chem.* **2010**, *49*, 6734-6739. It is assumed that the non-bulky aldehydic carbonyl group (-CH=O) can also bind strongly to the iridium center of $Ir^{III}(ttp)Ar$.

(44) Benzonitrile can strongly coordinate to iridium(III) porphyrin species. $Ir^{III}(ttp)(CO)Cl$ was shown to react with excess *p*-tolunitrile (*p*-TolCN) at 200 °C to give $Ir^{III}(ttp)(p\text{-TolCN})Cl$.

(45) $Ir^{III}(ttp)Ar$ usually contains more downfield prophyrin's pyrrole proton (δ(pyrrole H) = 8.58-8.61 ppm).

(46) Electron transfer from aniline to oxo(salen)chromium(V) ion, $[Cr^{V}(salen)(O)]^{+}$, to form aniline radical cation and $[Cr^{IV}(salen)(O)]$ has been reported. See: Premsingh, S.; Venkataramanan, N. S.; Rajagopal, S.; Mirza, S. P.; Vairamani, M.; Rao, P. S.; Velavan, K. *Inorg. Chem.* **2004**, *43*, 5744-5753.

(47) The sealed NMR tube experiments are generally slower than the Schlenk tube experiments, even though the reaction conditions are identical. This phenomena has also been observed in the base-promoted C-O bond cleavage of methanol by $Ir^{III}(ttp)(CO)Cl$. See: Cheung, C. W.; Fung, H. S.; Lee, S. Y.; Qian, Y. Y.; Chan, Y. W.; Chan, K. S. *Organometallics* **2010**, *29*, 1343-1354.

(48) $Ir^{I}(ttp)^{-}K^{+}$ in the form of $Ir^{I}(ttp)^{-}[K(18\text{-crown-6})]^{+}$ was prepared for reactivity studies as it was more stable to be observed quantitatively in benzene-d_6 at room temperature to ensure its successful formation. Since $Ir^{I}(ttp)^{-}K^{+}$ was found to rapidly convert to $Ir^{III}(ttp)H$ and $[Ir^{II}(ttp)]_2$ in benzene-d_6 at room temperature (Chapter 2, Section 2.4, eq 2.34), it was not used as the source of iridium(I) porphyrin anion in benzene-d_6.

(49) $Ir^{III}(ttp)Br$ ($1c_1$) (δ(pyrrole) ~ 8.91-8.95 ppm) and $Ir^{III}(ttp)I$ ($1d_1$) (δ(pyrrole) ~ 8.92 ppm) were observed in the reactions in benzene-d_6 by ^1H NMR spectroscopy. They could not be purified by column chromatography as they are unstable to be isolated and unknown species were obtained. Their stabilities may be due to the coordinative unsaturation. Their formation could only be confirmed by HRMS analysis ((a) $[M]^+$ of $Ir^{III}(ttp)Br$ ($1c_1$): theoretical: 940.1747, found: 940.1765; (b) $[M]^+$ of $Ir^{III}(ttp)I$ ($1d_1$): theoretical: 988.1608, found: 988.1611). The more upfield pyrrole proton signals of $Ir^{III}(ttp)Br$ and $Ir^{III}(ttp)I$ than that of $Ir^{III}(ttp)(CO)Br$ (δ(pyrrole) = 9.07 ppm) and $Ir^{III}(ttp)(CO)I$ (δ(pyrrole) = 9.08 ppm) support the absence of coordination of π-withdrawing CO in $Ir^{III}(ttp)Br$ and $Ir^{III}(ttp)I$. Indeed, stable $Ir^{III}(ttp)(py)Br$ (δ(pyrrole) = 8.96 ppm) and $Ir^{III}(ttp)(py)I$ (δ(pyrrole) = 8.96 ppm) without CO ligand were independently prepared and have similar pyrrole proton's chemical shifts as $Ir^{III}(ttp)Br$ and $Ir^{III}(ttp)I$ in benzene-d_6.

(50) Nucleophilic substitution (S_N2) of CH_3-OH by $Ir^I(ttp)^-$ to form $Ir^{III}(ttp)CH_3$ and OH^- has been reported (Ref 47). Likely, S_N2 of CH_3-$OC(O)C_6H_4(p$-Br) by $Ir^I(ttp)^-$ to form $Ir^{III}(ttp)CH_3$ and a better leaving group of benzoate ion, $ArCO_2^-$, is even more favorable.

(51) The equilibrium constant K for the homolysis of $[Ir^{II}(ttp)]_2$ to form 2 $Ir^{II}(ttp)$ monomers in benzene-d_6 at 150 °C and 200 °C can be estimated by using the expression $\Delta G = -RT\ln K$ (where ΔG ~ BDE of Ir-Ir in $[Ir^{II}(ttp)]_2$ ~24 kcal mol^{-1} = 24 x 4.184 x 1000 J mol^{-1} = 100416 J mol^{-1}, R = 8.314 J K^{-1} mol^{-1}, T = 423 K (150 °C) and 473 K (200 °C). K(150 °C) and K(200 °C) are then estimated to be 3.98 x 10^{-13} M and 8.14 x 10^{-12} M, respectively. Thus, only a low concentration of $Ir^{II}(ttp)$ is formed in benzene-d_6 at 150 °C and 200 °C to inititate the Ar-X cleavage reactions. The BDE of Ir-Ir bond in $[Ir^{II}(ttp)]_2$ is estimated to be ~24 kcal mol^{-1} using the reported BDE of Ir-Ir bond in $[Ir^{II}(oep)]_2$. See: Cui, W.; Li, S.; Wayland, B. B. *J. Organomet. Chem.* **2007**, *629*, 3198–3206.

(52) Homolytic aromatic substitution of Ar-H by Cl• to form Ar-Cl has been reported. See: (a) Eibner, A. *Chem. Ber.* **1903**, 1229-1331. (b) Coenen, H. H.; Machulla, H.-J.; Stöcklin. G.

191

J. Am. Chem Soc. **1977**, *99*, 2892-2898.

(53) Homolytic aromatic substitution of Ar-H by Br• to form Ar-Br has been reported. See: (a) Everly, C. R.; Traynham, J. G. *J. Am. Chem. Soc.* **1978**, *100*, 4316-4317. (b) Everly, C. R.; Traynham, J. G. *J. Org. Chem.* **1979**, *44*, 1784-1787.

(54) The theoretical yield of PhBr formed should be 50% from the reaction of Br_2 with C_6H_6 via the Br radical-assisted H atom abstraction from Br-H-cyclohexadienyl radical intermediate (BrC_6H_6•) (Scheme 3.17). However, PhBr in 83% yield was obtained. The high yield may be due to the elimination of H_2 from the BrC_6H_6•. Indeed, the BDE of $C(sp^3)$-H bond in C_6H_7• cyclohexadienyl radical is 22.2 kcal mol^{-1}, which is presumably weak enough to be cleaved thermally via the bimolecular interaction of 2 BrC_6H_6• to form 2 PhBr and H_2 as a thermodynamically favorable pathway (i.e. $2BrC_6H_6$• → $[BrC_6H_5$---H---H---$C_6H_5Br]^{‡}$ → $2PhBr + H_2$). For the BDE of sp^3-C-H bond in C_6H_7•, see: Gao, Y.; DeYonker, N. J.; Garrett, E. C., III; Wilson, A. K.; Cundari, T. R.; Marshall, P. *J. Phys. Chem. A* **2009**, *113*, 6955-6963.

(55) The chlorinated biaryls was likely formed from the dimerization of 2 Cl-cyclohexadienyl radical (ClC_6H_6•) to form dichlorotetrahydrobiphenyls, which then reacts with excess Cl• (as an H atom abstracting agent) to give dichlorobiphenyls. See: Ref 28b.

(56) During the homolytic aromatic substitutions of mono-substituted arenes, both *ortho-* and *para*-attack by radicals are more preferable (Scheme 3.17). However, in the homolytic aromatic substitutions of PhCl by Cl•, *para*-attack is more favorable, since the *ortho*-attack leads to the steric strain from 2 *ortho*-Cl groups in the cyclohexadienyl radical. See: Ref 24b.

(57) To our knowledge, homolytic aromatic substitutions of arenes (ArH) with iodine atom (I•) to form ArI have not been reported. Indeed, I• is unreactive in radical substitution of alkanes (R-H), whereas Cl• and Br• are reactive to react with R-H to give RCl and RBr. See: Ref 4.

(58) The commercial sample of 4-bromo-*tert*-butylbenzene used in the reaction contained no PhBr by GC-MS analysis. Thus, any PhBr detected should come from the reaction.

(59) Only $1,4\text{-}Cl_2C_6H_4$ was formed without $1,2\text{-}Cl_2C_6H_4$ and biaryls in the reaction of $[Ir^{II}(ttp)]_2$ with PhCl. Presumably, the low concentration of Cl• formed in the reactions only favors the least steric and kinetically more favorable *para*-attack of Cl• to PhCl to give $1,4\text{-}Cl_2C_6H_4$, Alternatively, the amounts of other $Cl_2C_6H_4$ and biaryls would be too small to be detected by GC-MS analysis. $1,4\text{-}Cl_2C_6H_4$ did come from the reaction as the commercial sample of PhCl does not contain any $Cl_2C_6H_4$ by GC-MS analysis with reference to the commercial sample of $1,4\text{-}Cl_2C_6H_4$ and $1,2\text{-}Cl_2C_6H_4$ and GC-MS library.

(60) $Ir^{III}(ttp)C_6H_4(p\text{-}Cl)$ was not observed in the reactions of $Ir^{III}(ttp)(CO)Cl$ with PhCl and K_2CO_3 by ^1H NMR spectroscopy (Tables 3.18-3.21). The reason was unclear. Indeed, $[Ir^{II}(ttp)]_2$ did not react with $Ir^{III}(ttp)Ph$ in benzene at 200 °C in 30 minutes to yield any $Ir^{III}(ttp)(p\text{-}C_6H_4)Ir^{III}(ttp)$. Thus, $Ir^{III}(ttp)(p\text{-}C_6H_4)Ir^{III}(ttp)$ should not be formed from the homolytic aromatic substitution of the phenyl group of $Ir^{III}(ttp)Ph$ with $Ir^{II}(ttp)$.

(61) The mode of stabilization of Ir(ttp)-cyclohexadienyl radical by π-donating, σ-donating, and π-withdrawing *para*-substituents have been proposed: (a) Sykes, P. *A Guidebook to Mechanism in Organic Chemistry* 6th Ed, London: Longman, 1986. (b) Ref 29.

(62) The competition reactions between *meta*-substituted ArBr and PhBr in an equimolar ratio with $Ir^{III}(ttp)(CO)Cl$ and K_2CO_3 have also been studied in the same reaction conditions. Indeed, the kinetic ratio between 3-bromoanisole and PhBr was 1.06 : 1.00, whereas the that between 3-bromotoluene and PhBr was 1.03 : 1.00. The results further support that the *meta*-substituted groups are the unactivating group and do not promote the rates of Ar-Br cleavage.

(63) Wayland, B. B. University of Pennsylvania, Philadelphia, PA. Personal communication, 2007.

(64) Berho, F.; Rayez, M.-T.; Lesclaux, R. *J. Phys. Chem. A* **1999**, *103*, 5501-5509.

Chapter 4   Experimental Section

General Procedures

Unless otherwise noted, all reagents were purchased from commercial suppliers and directly used without further purification. Hexane was distilled from anhydrous calcium chloride. Benzene and benzene-d_6 were distilled from sodium and were stored in a Teflon-capped tube under nitrogen prior to use (benzene is a carcinogen and should be handled with care). Triphenylphosphine (PPh_3) was recrystallized from methanol and the triphenylphosphine oxide ($P(O)Ph_3$) present is less than 0.5% yield as determined by ^1H NMR spectroscopy. Iodobenzene was dried with CaH_2 and distilled under vacuum to remove phenol as an impurity. All reactions are undergone without light irradiation by wrapping with aluminum foils. The reactions in Teflon-screw capped Schlenk tubes were heated in the heat blocks on heaters, whereas the reactions in sealed NMR tubes were heated in GC-ovens. Thin layer chromatography was performed on pre-coated silica gel 60 F_{254} plates. $H_2(ttp)$,[1] $[Ir^I(COD)Cl]_2$,[2] $Ir^{III}(ttp)(CO)Cl$,[3] $Ir^{III}(ttp)H$,[4] $[Ir^{II}(ttp)]_2$ dimer,[4] and $Ir^I(ttp)^-[K(18\text{-crown-}6)]^+$[5] have been characterized and were prepared according to the literature procedures. Silica gel (Merck, 70-230 mesh), and neutral alumina (Merck, activity I, 70-230 mesh) added with H_2O (~10:1 v/v), were used for column chromatography.

Without otherwise specified, the residual benzene proton signal of benzene-d_6 solvent was used as an internal standard to estimate the yield of iridium porphyrin species for NMR yield estimations by ^1H NMR spectroscopy.

A trace of residual water was always present in benzene-d_6 ($\delta(H_2O) \sim 0.4$ ppm), and the amount of residual water (equiv with reference to the iridium porphyrin species) in benzene-d_6 in sealed-tube experiments was estimated by ^1H NMR spectroscopy by taking the ratio between the proton signal of residual water and the porphyrin's pyrrole proton signal of iridium porphyrin species.

The yields of di-iridium-porphyrin aryl complexes and $[Ir^{II}(ttp)]_2$ were based on the number of

iridium porphyrin unit incorporated into the products.

The amount (in % NMR yield) of $[Ir^{II}(ttp)]_2$ generated in the reactions in benzene-d_6 could only be roughly estimated since $[Ir^{II}(ttp)]_2$ only partially dissolved in benzene-d_6. $[Ir^{II}(ttp)]_2$ could not be isolated for quantification as it was air-unstable.

Experimental Instrumentation

^1H, ^{13}C, and ^{31}P NMR spectra were recorded on a Brüker DPX-300 at 300 MHz, 75 MHz, and 122 MHz, respectively, or a Brüker AV-400MHz at 400 MHz, 100 MHz, and 162 HMz, respectively. Chemical shifts were referenced with the residual solvent protons in C_6D_6 (δ = 7.15 ppm), $CDCl_3$ (δ = 7.26 ppm), THF-d_8 ($\delta(\beta$-$CH_2)$ = 1.85 ppm), or tetramethylsilane (TMS) (δ = 0.00 ppm) in ^1H NMR spectra as the internal standards, and in $CDCl_3$ (δ = 77.16 ppm), C_6D_6 (δ = 128.06 ppm), or THF-d_8 ($\delta(\beta$-$CH_2)$ = 25.62 ppm) in ^{13}C NMR spectra as the internal standards. H_3PO_4 (85% solution) (δ = 0.00 ppm) in C_6D_6 was referenced as an external standard in ^{31}P NMR spectra. Chemical shifts (δ) were reported as part per million (ppm) in δ scale downfield from TMS. Coupling constants (J) were reported in Hertz (Hz).

High resolution mass spectra (HRMS) were performed on a ThermoFinnigan MAT 95 XL mass spectrometer in fast atom bombardment (FAB) mode using 3-nitrobenzyl alcohol (NBA) matrix and CH_2Cl_2 as solvent, and electrospray ionization (ESI) mode using MeOH : CH_2Cl_2 (1:1) as solvent.

Gas chromatography-mass spectrometric (GC-MS) analysis was conducted on a Shimadzu GCMS-2010Plus using Rtx-5MS column (30 m x 0.25 mm). The column oven temperature and injection temperature were 50.0 and 250 ^oC, repsectively. Helium was used as a carrier gas. Flow control mode was chosen as linear velocity (36.3 cm s^{-1}) with pressure 53.5 kPa. The total flow, column flow, and purge flow were 24.0, 1.0, and 3.0 mL min^{-1}, respectively. Split mode inject with split ratio 20.0 was applied. After injection, the column oven temperature was kept at 50 ^oC for 5 minutes and the temperature was then elevated at a rate of 20 ^oC min^{-1} for 10 minutes until 250 ^oC.

The temperature of 250 °C was further kept for 5 minutes.

Experimental Procedures

(I) Preparation of Various Iridium Porphyrin Species for Reaction Studies

Preparation of Chloro(carbonyl)(5,10,15,20-tetrakis(*p*-tolyl)porphyrinato)iridium(III) [Ir^{III}(ttp)(CO)Cl] (1a).[3] [Ir^{I}(COD)Cl]$_2$[2] (437 mg, 0.65 mmol) and H$_2$(ttp)[1] (436 mg, 0.65 mmol) were heated under reflux in *p*-xylene (200 mL) in 500 mL-round-bottom flask for 3 days. The reaction mixture changed from deep brown to reddish brown, and it was dried under vacuum. The product was purified by column chromatography using CH$_2$Cl$_2$ / hexane (1:2) as an eluent to remove the initial brown fraction and purple fraction. The bright red product fraction was then isolated using CH$_2$Cl$_2$/hexane (4:1) as the eluent. The red fraction was collected, dried, and further purified by recrystallization using CH$_2$Cl$_2$ / methanol. Red solid of Ir^{III}(ttp)(CO)Cl (1a) (385 mg, 0.42 mmol, 64%) was collected. R$_f$ = 0.26 (CH$_2$Cl$_2$/hexane = 1 : 1). ^{1}H NMR (CDCl$_3$, 300 MHz) δ 2.71 (s, 12 H), 7.57 (d, 8 H, J = 8.1 Hz), 8.09 (d, 4 H, J = 7.8 Hz), 8.15 (d, 4 H, J = 7.7 Hz), 8.94 (s, 8 H). ^{1}H NMR (C$_6$D$_6$, 300 MHz) δ 2.37 (s, 12 H), 7.18 (d, 4 H, J = 9.0 Hz), 7.23 (d, 4 H, J = 7.8 Hz), 7.86 (d, 4 H, J = 7.6 Hz), 8.01 (d, 4 H, J = 7.7 Hz), 9.07 (s, 8 H).

Preparation of Chloro(Triphenylphosphine)(5,10,15,20-Tetrakis(*p*-tolyl)porphyrinato)-iridium(III) [Ir^{III}(ttp)(PPh$_3$)Cl] (1b). Ir^{III}(ttp)(CO)Cl (100 mg, 0.11 mmol), PPh$_3$ (142 mg, 0.54 mmol), and benzene (4 mL) were degassed for three freeze-pump-thaw cycles in a Teflon screw capped tube. The reaction mixture was then heated at 200 °C under N$_2$ for 1 day. The solvent was dried, and the reaction mixture was purified by column chromatography with alumina using CHCl$_3$ as the eluent. The major red solution was collected and dried. The product was further recrystallized using CH$_2$Cl$_2$ / hexane to obtain a red solid of Ir^{III}(ttp)(PPh$_3$)Cl (1b) (81.5 mg, 0.070 mmol, 65%). R$_f$ = 0.15 (CHCl$_3$). ^{1}H NMR (C$_6$D$_6$, 300 MHz) δ 2.39 (s, 12 H), 4.27 (dd, 6 H, $^3J_{PH}$ = 9.0 Hz, $^3J_{HH}$ = 8.6 Hz), 6.33 (t, 6 H, $^3J_{HH}$ = 7.4 Hz), 6.55 (t, 3 H, $^3J_{HH}$ = 7.2 Hz), 7.14 (d, 4 H, $^3J_{HH}$ = 7.9 Hz), 7.35 (d, 4 H, $^3J_{HH}$ = 7.5 Hz), 7.78 (d. 4 H, $^3J_{HH}$ = 7.4 Hz), 7.93 (d. 4 H, $^3J_{HH}$ = 7.3 Hz),

8.84 (s, 8 H). ^{13}C NMR (THF-d_8, 300 MHz) δ 21.9, 123.5, 126.0 (d, $^1J_{PC}$ = 53.2 Hz), 127.9 (d, $^2J_{PC}$ = 15.7 Hz), 128.1, 128.6, 130.2, 132.1 (d, $^3J_{PC}$ = 9.0 Hz), 132.4, 134.8, 135.6, 138.1, 140.5, 143.4. ^{31}P NMR (C$_6$D$_6$, 162 MHz) δ -37.5 (br). HRMS (FABMS): Calcd for [C$_{66}$H$_{51}$N$_4$PClIr]$^+$ ([M]$^+$): m/z 1158.3164. Found: m/z. 1158.3199.

Preparation of Bromo(carbonyl)(5,10,15,20-tetrakis(*p*-tolyl)porphyrinato)iridium(III) [Ir^{III}(ttp)(CO)Br] (1c). Ir^{III}(ttp)(CO)Cl (50 mg, 0.054 mmol) and bromobenzene (2 mL) were added to the Teflon screw capped tube and the reaction mixture was degassed for three freeze-pump-thaw cycles. The reaction mixture was heated at 200 ^{o}C under N$_2$ for 2 days to form a deep brown solution. The solvent was removed under vacuum, and the reaction mixture was purified by column chromatography using silica gel and CH$_2$Cl$_2$/hexane (1:1) as an eluent. The major red fraction was collected and dried. The product was purified by recrystallization using CH$_2$Cl$_2$ / methanol. Red solid of Ir^{III}(ttp)(CO)Br (1c) (32 mg, 0.033 mmol, 62%) was collected. R$_f$ = 0.36 (CH$_2$Cl$_2$/hexane = 1 : 1). ^{1}H NMR (CDCl$_3$, 300 MHz) δ 2.71 (s, 12 H), 7.56-7.59 (m, 8 H), 8.10 (d, 4 H, J = 7.5 Hz), 8.13 (d, 4 H, J = 7.2 Hz), 8.93 (s, 8 H). ^{1}H NMR (C$_6$D$_6$, 300 MHz) δ 2.37 (s, 12 H), 7.18 (d, 4 H, J = 7.9 Hz), 7.23 (d, 4 H, J = 8.2 Hz), 7.90 (d, 4 H, J = 7.7 Hz), 8.02 (d, 4 H, J = 7.6 Hz), 9.07 (s, 8 H). ^{13}C NMR (CDCl$_3$, 75 MHz) δ 21.7, 122.4, 127.6, 127.8, 132.0, 132.8, 134.2, 134.6, 137.8, 138.4, 141.3. HRMS (FABMS): Calcd for [C$_{49}$H$_{36}$N$_4$OBrIr]$^+$ ([M]$^+$): m/z 968.1696. Found: m/z. 968.1688.

Preparation of Iodo(carbonyl)(5,10,15,20-tetrakis(*p*-tolyl)porphyrinato)iridium(III) [Ir^{III}(ttp)(CO)I] (1d). Ir^{III}(ttp)(CO)Cl (50 mg, 0.054 mmol) and iodobenzene (2 mL) were added to the Teflon screw capped tube and the reaction mixture was degassed for three freeze-pump-thaw cycles. The reaction mixture was heated at 200 ^{o}C under N$_2$ for 2 days to form a deep brown solution. The solvent was removed under vacuum, and the reaction mixture was purified by column chromatography using silica gel and CH$_2$Cl$_2$/hexane (2:3) as an eluent. The major red fraction was collected and dried. The product was purified by recrystallization using CH$_2$Cl$_2$ / methanol. Red solid of Ir^{III}(ttp)(CO)I (1d) (22 mg, 0.022 mmol, 41%) was collected. R$_f$= 0.48

(CH$_2$Cl$_2$/hexane = 1 : 1). ^{1}H NMR (CDCl$_3$, 300 MHz) δ 2.71 (s, 12 H), 7.55 (d, 4 H, J = 6.6 Hz), 7.57 (d, 4 H, J = 6.3 Hz), 8.09-8.12 (m, 8 H), 8.91 (s, 8 H). ^{1}H NMR (C$_6$D$_6$, 300 MHz) δ 2.37 (s, 12 H), 7.18 (d, 4 H, J = 8.0 Hz), 7.22 (d, 4 H, J = 7.8 Hz), 7.95 (d, 4 H, J = 7.1 Hz), 8.03 (d, 4 H, J = 7.7 Hz), 9.08 (s, 8 H). ^{13}C NMR (CDCl$_3$, 75 MHz) δ 21.7, 122.7, 127.5, 127.9, 132.1, 133.9, 134.7, 137.8, 138.4, 141.5. HRMS (FABMS): Calcd for [C$_{49}$H$_{36}$N$_4$OIIr]$^+$ ([M]$^+$): m/z 1016.1558. Found: m/z. 1016.1556.

Preparation of (5,10,15,20-Tetrakis(*p*-tolyl)porphyrinato)iridium(III) Hexafluoroantimonate [Ir^{III}(ttp)SbF$_6$] (1e). Ir^{III}(ttp)SbF$_6$ was prepared according to the literature procedure of synthesis of Ir^{III}(ttp)BF$_4$.[6] Ir^{III}(ttp)(CO)Cl (50.0 mg, 0.054 mmol) and AgSbF$_6$ (37.2 mg, 0.108 mmol) were added in CH$_2$Cl$_2$ (20 mL) in a 50 mL round-bottom flask, and the reaction mixture was stirred at room temperature for 2 hours. The reaction changed gradually from bright red to orange red. The reaction mixture was filtered to remove the black and grey precipitates, and the solution was added with hexane for recrystallization by slow evaporation using rotary evaporator. The red precipitate was filtered to obtain Ir^{III}(ttp)SbF$_6$ (1e) (~53.3 mg, ~0.049 mmol, ~90%). Ir^{III}(ttp)SbF$_6$ is an inseparable mixture of Ir^{III}(ttp)SbF$_6$ and [Ir^{III}(ttp)(CO)]SbF$_6$ in ~2.6-3.4 : 1 ratio in CDCl$_3$, since the ratio is variable upon each time of preparation of Ir^{III}(ttp)SbF$_6$. R$_f$ = 0.00 (DCM). Only the NMR of Ir^{III}(ttp)SbF$_6$ (Ir^{III}(ttp)SbF$_6$: [Ir^{III}(ttp)(CO)]SbF$_6$ = 3.4 : 1) was shown: ^{1}H NMR (CDCl$_3$, 400 MHz) δ 2.73 (s, 12 H), 7.11 (d, 4 H, $^3J_{HH}$ = 7.7 Hz), 7.64 (d, 4 H, $^3J_{HH}$ = 7.7 Hz), 8.09 (dd, 4 H, $^3J_{HH}$ = 7.6 Hz, $^4J_{HH}$ = 1.6 Hz), 8.16 (dd, 4 H, $^3J_{HH}$ = 7.6 Hz, $^4J_{HH}$ = 1.9 Hz), 9.10 (s, ~6.2 H), 9.12 (s, ~1.8 H). ^{1}H NMR (C$_6$D$_6$, 400 MHz) δ 2.40 (s, 12 H), 7.24 (d, 4 H, $^3J_{HH}$ = 7.6 Hz), 7.32 (d, 4 H, $^3J_{HH}$ = 7.6 Hz), 7.90 (d, 4 H, $^3J_{HH}$ = 7.7 Hz), 8.22 (dd, 4 H, $^3J_{HH}$ = 7.9 Hz, $^4J_{HH}$ = 1.0 Hz), 9.08 (s, 8 H). ^{13}C NMR of Ir^{III}(ttp)SbF$_6$ (CDCl$_3$, 100 MHz) δ 21.7, 123.2, 127.8, 128.4, 132.6, 133.9, 134.7, 137.4, 138.5, 141.6. HRMS ([M]$^+$) of 1e was not taken as the HRMS of analogous Ir^{III}(ttp)BF$_4$[6] only gave Ir(ttp)$^+$ ion ([M-BF$_4$]$^+$).

Preparation of Chloro(pyridino)(5,10,15,20-Tetrakis(*p*-tolyl)porphyrinato)iridium(III) [Ir^{III}(ttp)(py)Cl] (1f). Ir^{III}(ttp)(CO)Cl (50 mg, 0.054 mmol), pyridine (42.8 mg, 43.6 μL, 0.54

mmol, 10 equiv), and benzene (3 mL) were degassed for three freeze-pump-thaw cycles in a Teflon screw capped tube. The reaction mixture was then heated at 200 °C under N_2 for 12 hours. The solvent was dried, and the reaction mixture was purified by column chromatography with alumina using CH_2Cl_2/hexane (3:1) as the eluent. The major orange solution was collected and dried. The product was further recrystallized using CH_2Cl_2/hexane to obtain a deep purple solid of $Ir^{III}(ttp)(py)Cl$ (**1f**) (45.8 mg, 0.047 mmol, 87%). R_f = 0.33 (CH_2Cl_2/hexane = 2 : 1). ^1H NMR ($CDCl_3$, 400 MHz) δ 1.26 (d, 2 H, J = 5.6 Hz), 2.69 (s, 12 H), 5.03 (t, 2 H, J = 6.9 Hz), 6.01 (t, 1 H, J = 7.4 Hz), 7.50 (d, 4 H, J = 7.5 Hz), 7.54 (d, 4 H, J = 7.5 Hz), 7.96 (d, 4 H, J = 7.2 Hz), 8.16 (d, 4 H, J = 7.4 Hz), 8.71 (s, 8 H). ^{13}C NMR ($CDCl_3$, 100 MHz) δ 21.7, 122.2, 122.6, 127.2, 127.8, 131.8, 134.1, 134.4, 134.6, 137.3, 139.1, 142.2, 147.0. HRMS (FABMS): Calcd for $[C_{53}H_{41}N_5ClIr]^+$ ($[M]^+$): m/z 975.2674. Found: m/z 975.2678.

Preparation of Bromo(pyridino)(5,10,15,20-tetrakis(*p*-tolyl)porphyrinato)iridium(III) [Ir^{III}(ttp)(py)Br] (1g). $Ir^{III}(ttp)(CO)Br$ (16.8 mg, 0.017 mmol), pyridine (13.7 mg, 14.0 μL, 0.17 mmol, 10 equiv), and benzene (2 mL) were degassed for three freeze-pump-thaw cycles in a Teflon screw capped tube. The reaction mixture was then heated at 200 °C under N_2 for 19 hours. The product was dried and then purified by column chromatography with alumina using CH_2Cl_2/hexane (2:1) as the eluent. The product was further recrystallized using CH_2Cl_2/hexane to obtain a purple solid of $Ir^{III}(ttp)(py)Br$ (**1g**) (14.8 mg, 0.047 mmol, 84%). R_f = 0.43 (CH_2Cl_2/hexane = 2 : 1). ^1H NMR (C_6D_6, 400 MHz) δ 1.57 (d, 2 H, ^3J = 5.4 Hz), 2.35 (s, 12 H), 3.96 (t, 2 H, ^3J = 7.4 Hz), 4.72 (t, 1 H, ^3J = 7.6 Hz), 7.26 (d, 4 H, ^3J = 7.7 Hz), 7.96 (dd, 4 H, ^3J = 7.7 Hz, ^4J = 1.8 Hz), 8.10 (dd, 4 H, ^3J = 7.6 Hz, ^4J = 1.7 Hz,) 8.96 (s, 8 H). One set of *m*-tolyl's H signal was obscured by residual benzene's H signal. ^{13}C NMR ($CDCl_3$, 100 MHz) δ 21.7, 122.3, 122.6, 127.2, 127.7, 131.9, 133.9, 134.5, 134.7, 137.3, 139.0, 142.2, 146.4. HRMS (FABMS): Calcd for $[C_{53}H_{41}N_5BrIr]^+$ ($[M]^+$): m/z 1019.2169. Found: m/z 1019.2191.

Preparation of Bromo(pyridino)(5,10,15,20-tetrakis(*p*-tolyl)porphyrinato)iridium(III) [Ir^{III}(ttp)(py)I] (1h). $Ir^{III}(ttp)(py)I$ (16.9 mg, 0.017 mmol), pyridine (13.2 mg, 13.4 μL, 0.17 mmol,

10 equiv), and benzene (2 mL) were degassed for three freeze-pump-thaw cycles in a Teflon screw capped tube. The reaction mixture was heated at 200 °C under N_2 for 1 hour. The product was dried and purified by column chromatography with alumina using CH_2Cl_2/hexane (3:2) as the eluent. The product was further recrystallized using CH_2Cl_2/hexane to yield a purple solid of $Ir^{III}(ttp)(py)I$ (**1h**) (14.5 mg, 0.014 mmol, 82%). R_f= 0.48 (CH_2Cl_2/hexane = 2 : 1). ^1H NMR (C_6D_6, 400 MHz) δ 1.56 (d, 2 H, ^3J = 5.7 Hz), 2.35 (s, 12 H), 4.02 (t, 2 H, ^3J = 6.9 Hz), 4.75 (t, 1 H, ^3J = 7.4 Hz), 7.26 (d, 4 H, ^3J = 7.6 Hz), 8.01 (d, 4 H, ^3J = 7.5 Hz), 8.10 (d, 4 H, ^3J = 7.6 Hz) 8.96 (s, 8 H). One set of *m*-tolyl's H signal was obscured by residual benzene's H signal. ^{13}C NMR ($CDCl_3$, 100 MHz) δ 21.7, 122.4, 122.5, 127.2, 127.7, 131.9, 133.7, 134.7, 134.8, 137.3, 139.0, 142.3, 145.1. HRMS (FABMS): Calcd for $[C_{53}H_{41}N_5IIr]^+$ ($[M]^+$): m/z 1067.2030. Found: m/z 1067.2032.

Preparation of Hydrido(5,10,15,20-Tetrakis(*p*-tolyl)porphyrinato)iridium(III) [Ir^{III}(ttp)H] (2a). Ir^{III}(ttp)H[4] was prepared according to the literature procedure of synthesis of Ir^{III}(oep)H.[3a] A suspension of Ir^{III}(ttp)(CO)Cl (100 mg, 0.11 mmol) in THF (50 mL) in a Teflon screw-capped 250 mL round-bottomed flask, a solution of $NaBH_4$ (81.7 mg, 2.16 mmol) in aqueous NaOH (1.0 M, 3.0 mL), and concentrated HCl (~10 mL) in water (200 mL) were purged separately with N_2 for 15 min separately. The solution of $NaBH_4$ was added slowly to the suspension of Ir^{III}(ttp)(CO)Cl via a cannula. The mixture was heated at 50 °C under N_2 for 2 hours to give a deep brown suspension. The mixture was then cooled in ice-water bath under N_2, and the HCl solution was added via a cannula under N_2. The reaction mixture was stirred in ice-water bath under N_2 until the maximal deep brown precipitate and a clear, colorless solution were obtained. The deep brown precipitate was collected and further washed with water to obtain Ir^{III}(ttp)H (**2a**) (83 mg, 0.097 mmol, 88 %). ^1H NMR ($CDCl_3$, 300 MHz) δ -57.6 (s, 1 H), 2.68 (s, 12 H), 7.50 (d, 8 H, J = 7.2 Hz), 8.00 (d, 8 H, J = 6.9 Hz), 8.57 (s, 8 H). ^1H NMR (C_6D_6, 300 MHz) δ -57.5 (s, 1 H), 2.40 (s, 12 H), 7.21 (d, 4 H, J = 7.5 Hz), 7.36 (d, 4 H, J = 7.7 Hz), 7.92 (d, 4 H, J = 7.3 Hz), 8.20 (d, 4 H, J = 7.1 Hz), 8.81 (s, 8 H). ^{13}C NMR (THF-d_8, 75 MHz) δ 21.9, 124.5, 128.3, 128.6, 132.0, 134.9, 138.1, 140.5, 144.8. HRMS (FABMS): Calcd for $[C_{48}H_{37}N_4Ir]^-$ ($[M]^-$): m/z 862.2653. Found: m/z 862.2640.

Preparation of hydrido(triphenylphosphine)(5,10,15,20-Tetrakis(*p*-tolyl)-porphyrinato)-iridium(III) [Ir^III(ttp)(PPh_3)H] (2b).[5] Ir^III(ttp)H (4.7 mg, 0.005 mmol), PPh_3 (1.4 mg, 0.005 mmol), and benzene-d_6 (0.5 mL) were added to the Teflon screw capped NMR tube under N_2. The reaction mixture was degassed for three freeze-pump-thaw cycles and then flame-sealed under vacuum. The color of the reaction mixture changed to deep reddish brown instantaneously at room temperature to give Ir^III(ttp)(PPh_3)H (**2b**) quantitatively as no other iridium porphyrin species were observed by ^{1}H NMR spectroscopy. ^{1}H NMR (C_6D_6, 300 MHz) δ -32.57 (d, 1 H, $^2J_{PH}$ = 258.6 Hz), 2.58 (s, 12 H), 4.51 (br, 6 H), 6.48 (br, 6 H), 6.64 (br, 3 H), 7.50 (d, 4 H, J = 7.7 Hz), 7.81 (d, 4 H, J = 7.7 Hz), 7.90 (d, 4 H, J = 8.0 Hz), 8.75 (s, 8 H). One set of *m*-phenyl's H signal was obscured by C_6H_6 singal. ^{13}C NMR (C_6D_6, 75 MHz) δ 21.4, 123.6, 127.3, 131.4 (d, $^3J_{PC}$ = 10.1 Hz), 132.0, 134.3, 134.7, 136.8, 139.9, 143.9. *Ipso*-, *o*-, and *p*-phenyl's C signals of PPh_3 were shielded by C_6H_6 signals. ^{31}P NMR (C_6D_6, 122 MHz) δ -25.9 (d(br), $^2J_{PH}$ = 258 Hz). HRMS (FABMS): Calcd for [C_66H_52N_4IrP]$^+$ ([M]$^+$): m/z 1124.3553. Found: m/z 1124.3520.

Preparation of (5, 10, 15, 20-Tetrakis(*p*-tolyl)porphyrinato)iridium(II) Dimer [[Ir^II(ttp)]_2] (3). [Ir^II(ttp)]_2[4] was prepared using the literature method for the preparation of [Ir^II(oep)]_2.[7] Ir^III(ttp)H (4.2 mg, 0.005 mmol) and degassed benzene (0.5 mL) were degassed for three freeze-pump-thaw cycles in a Teflon screw capped NMR tube. 2,2,6,6-Tetramethylpiperidinooxy (TEMPO) (1.1 mg, 0.007 mmol) was added into the tube under N_2. The reaction mixture changed to deep brown instantaneously, and it was dried under vacuum for a few hours to reomove the solvent, unreacted TEMPO, and TEMPOH co-product. Degassed benzene-d_6 was then added into the tube under N_2, and the reaction mixture was degassed for three freeze-pump-thaw cycles in the tube and then flame-sealed under vacuum. Deep brown of [Ir^II(ttp)]_2 in pure form was observed by ^{1}H NMR spectroscopy. [Ir^II(ttp)]_2 (**3**) was formed quantitatively as no other iridium porphyrin species were observed. ^{1}H NMR (C_6D_6, 300 MHz) δ 2.46 (s, 12 H), 7.08 (d, 4 H, J = 8.9 Hz), 7.66 (d, 4 H, J = 7.7 Hz), 8.33 (s, 8 H), 9.49 (d, 4 H, J = 7.8 Hz). One set of *m*-phenyl proton signal is obscured by benzene's proton signal (δ 7.15).

Preparation of Potassium (5,10,15,20-Tetrakis(p-tolyl)porphyrinato)iridate(I) [Ir^I(ttp)$^-$K$^+$] (4a). Ir^I(ttp)$^-$K$^+$ was synthesized according to the procedure in synthesis of Ir^I(ttp)$^-$[K(18-crown-6)]$^+$.[5] Ir^{III}(ttp)H (5.0 mg, 0.006 mmol), KOH (6.6 mg, 0.12 mmol), and THF-d_8 (0.5 mL) were degassed for three freeze-pump-thaw cycles in a Teflon screw capped NMR tube and then flame-sealed under vacuum. The reaction mixture was covered by aluminum foil and heated at 120 °C in an oil bath for 6 hours to yield a brown solution of Ir^I(ttp)$^-$K$^+$ (4a) quantitatively using the residual THF's β-protons as the internal standard. ^{1}H NMR (THF-d_8, 400 MHz) δ 2.68 (s, 12 H). 7.51 (d, 8 H, J = 7.6 Hz), 7.92 (d, 8 H, J = 7.5 Hz), 8.17 (s, 8 H). ^{13}C NMR (THF-d_8, 100 MHz) δ 21.8, 128.6, 130.6, 131.7, 134.2, 136.8, 141.2, 146.2.

Preparation of Potassium(18-crown-6) (5,10,15,20-Tetrakis(p-tolyl)-porphyrinato)iridate(I) [Ir^I(ttp)$^-$[K(18-crown-6)$^+$]] (4b). Ir^I(ttp)$^-$[K(18-crown-6)]$^+$ [5] was synthesized according to the procedure in synthesis of Rh^I(ttp)$^-$[K(18-crown-6)]$^+$).[8] Ir^{III}(ttp)H (5.0 mg, 0.006 mmol), KOH (3.3 mg, 0.058 mmol), 18-crown-6 ether (4.6 mg, 0.017 mmol), and THF-d_8 (0.5 mL) were degassed for three freeze-pump-thaw cycles in a Teflon screw capped NMR tube and then flame-sealed under vacuum. The reaction mixture was covered by aluminum foil and heated at 150 °C in an oil bath in 45 minutes to yield a brown solution of Ir^I(ttp)$^-$[K(18-crown-6)]$^+$ (4b) quantitatively using the residual THF's β-protons as the internal standard. The THF-d_8 solvent in the tube could be removed under vacuum before flame-sealing, and degassed benzene-d_6 was added to obtain a stable Ir^I(ttp)$^-$K(18-crown-6)$^+$ (4b). ^{1}H NMR (THF-d_8, 300 MHz) δ 2.62 (s, 12 H). 7.43 (d, 8 H, J = 7.7 Hz), 7.88 (d, 8 H, J = 7.7 Hz), 8.14 (s, 8 H). ^{1}H NMR (C$_6$D$_6$, 300 MHz) δ 2.38 (s, 12 H). 7.28 (d, 8 H, J = 7.7 Hz), 7.95 (d, 8 H, J = 7.9 Hz), 8.58 (s, 8 H).

Preparation of Hydroxo(pyridino)(5,10,15,20-Tetrakis(p-tolyl)porphyrinato)iridium(III) [Ir^{III}(ttp)(py)OH] (5b). Ir^{III}(ttp)(py)Cl (50 mg, 0.054 mmol), AgSbF$_6$ (37.1 mg, 0.11 mmol, 2 equiv), and THF (3 mL) were degassed for three freeze-pump-thaw cycles in a Teflon screw capped tube. The reaction mixture was then heated at 120 °C under N$_2$ for 2 hours to prepare [Ir^{III}(ttp)(py)]SbF$_6$ *in-situ*. Excess CsOH (~162 mg, ~1.08 mmol) was then added into the reaction

mixture under N_2 and the reaction mixture was further heated at 50 °C for 4 hours. The reaction mixture was filtered to remove the grey and black precipitates. The filtrate was then added with excess water and THF were dried under vacuum using rotary evaporator to obtain an orange solid of Ir^{III}(ttp)(py)OH (**5b**) (33.6 mg, 0.035 mmol, 65%). ^{1}H NMR (CDCl$_3$, 400 MHz) δ -10.02 (br, 1 H), 1.47 (br, 2 H), 2.69 (s, 12 H), 5.03 (t, 2 H, J = 6.5 Hz), 6.01 (t, 1 H, J = 7.1 Hz), 7.50 (d, 4 H, J = 7.2 Hz), 7.55 (d, 4 H, J = 7.2 Hz), 7.96 (d, 4 H, J = 6.8 Hz), 8.14 (d, 4 H, J = 6.8 Hz), 8.65 (s, 8 H). ^{13}C NMR (CDCl$_3$, 100 MHz) δ 21.7, 122.5, 127.2, 127.8, 131.8, 133.7, 134.0, 134.6, 137.3, 138.9, 142.6, 147.8. HRMS (FABMS): Calcd for $[C_{53}H_{42}N_5OIr]^+$ ($[M]^+$): m/z 957.3013. Found: m/z 957.3024.

Preparation of β-Hydroxyethyl(5,10,15,20-Tetrakis(*p*-tolyl)porphyrinato)iridium(III) [Ir^{III}(ttp)CH$_2$CH$_2$OH] (7). A suspension of Ir^{III}(ttp)(CO)Cl (84 mg, 0.091 mmol) in THF (20 mL) in a Teflon screw-capped 250 mL round-bottomed flask, and a solution of NaBH$_4$ (68.7 mg, 1.82 mmol) in aqueous NaOH (1.0 M, 1.5 mL), were purged with N_2 for 15 minutes separately. The solution of NaBH$_4$ was added slowly to the suspension of Ir^{III}(ttp)(CO)Cl via a cannula. The mixture was heated at 50 °C under N_2 for 2 hours to give a deep brown solution. The mixture was then cooled to room temperature, and 2-iodoethanol (156.2 mg, 71 μL, 0.91 mmol) was added under N_2. The reaction mixture was further heated at 50 °C for 2 hours. The reaction mixture was dried and purified by column chromatography with alumina using CH$_2$Cl$_2$/hexane (1:2) as an eluent. The major deep brown faction was collected and dried. The product was recrystallized in CH$_2$Cl$_2$ / hexane to obtain a deep brown solid of Ir^{III}(ttp)CH$_2$CH$_2$OH (**7**) (74.5 mg, 0.082 mmol, 90%). R_f = 0.26 (CH$_2$Cl$_2$/hexane = 1 : 1). ^{1}H NMR (400 MHz, CDCl$_3$): δ -5.29 (t, 2 H, ^3J = 7.3 Hz), -2.43 (t, 1 H, ^3J = 6.2 Hz), -2.16 (q, 2 H, ^3J = 6.9 Hz), 2.68 (s, 12 H), 7.52 (d, 8 H, ^3J = 7.9 Hz), 7.98 (dd, 4 H, ^3J = 8.2 Hz, ^4J = 2.2 Hz), 8.02 (dd, 4 H, ^3J = 8.2 Hz, ^4J = 2.3 Hz), 8.54 (s, 8 H). ^{13}C NMR (100 MHz, CDCl$_3$): δ -14.7, 21.7, 59.0, 124.1, 127.6, 127.7, 131.6, 133.6, 134.0, 137.4, 138.6, 143.4. HRMS (FABMS): Calcd for $[C_{50}H_{41}N_4OIr]^+$ ($[M]^+$): m/z 906.2904. Found: m/z 906.2912.

Preparation of *μ*-Oxo Bis((Aqua)(5,10,15,20-Tetrakis(*p*-tolyl)porphyrinato)iridium(III)) **[(H₂O)(ttp)Ir^{III}OIr^{III}(ttp)(OH₂)] (6a).** Ir^{III}(ttp)CH₂CH₂OH (2.6 mg, 0.003 mmol) and benzene-*d₆* (0.5 mL) were degassed in a Teflon screw capped NMR tube for three freeze-pump-thaw cycles and then flame-sealed under vacuum. Residual water (~2.4 equiv) was observed by ^{1}H NMR spectroscopy. The reaction mixture was heated at 120 °C for 23 days to yield a brown (H₂O)Ir^{III}(ttp)OIr^{III}(ttp)(OH₂) (6a) in 72% NMR yield using the residual benzene as the internal standard. Ir^{III}(ttp)C₆D₅ (δ(pyrrole) = 8.79) (most likely generated from the reaction of Ir^{III}(ttp)OH with benzene-*d₆*) and unreacted Ir^{III}(ttp)CH₂CH₂OH (δ(pyrrole) = 8.76) were observed in 7% and 2% NMR yields, respectively. C₂H₄ (δ(C₂H₄) = 5.23) was also observed. The coordinated water in (H₂O)Ir^{III}(ttp)OIr^{III}(ttp)(OH₂) underwent H/D exchange with excess D₂O in benzene-*d₆* at room temperature under air in 1.5 days, and the ratio of D:H in the coordinated water was observed to be ~2.9 : 1 by ^{1}H NMR spectroscopy. The sample of (H₂O)Ir^{III}(ttp)OIr^{III}(ttp)(OH₂) in benzene-*d₆* completely decomposed in air in 3 days. ^{1}H NMR (C₆D₆, 400 MHz) δ -10.89 (s, 4 H), 2.43 (s, 24 H), 7.24 (d, 8 H, ^3J = 7.7 Hz), 7.38 (d, 8 H, ^3J = 7.4 Hz), 7.62 (dd, 8 H, ^3J = 7.4 Hz, ^4J = 1.6 Hz), 7.89 (dd, 8 H, ^3J = 7.7 Hz, ^4J = 1.8 Hz), 8.36 (s, 16 H). ^{13}C NMR (C₆D₆, 100 MHz) δ 21.6, 123.5, 127.4, 130.6, 132.9, 135.1, 136.9, 139.3, 142.4. One *m*-tolyl's carbon signal was shielded by residual benzene peak. HRMS (FABMS): Calcd for [C₉₆H₇₂N₈OIr₂]$^+$ ([M-2H₂O]$^+$): m/z 1737.5092. Found: m/z 1737.5052.

Preparation of Phenyl(triphenylphosphine)(5,10,15,20-tetrakis(*p*-tolyl)porphyrinato)- iridium(III) [Ir^{III}(ttp)(PPh₃)Ph] (2x). Ir^{III}(ttp)Ph (21.6 mg, 0.023 mmol), triphenylphosphine (60 mg, 0.23 mmol, 10 equiv), and benzene (2 mL) were degassed in a Teflon screw capped tube for three freeze-pump-thaw cycles. The reaction mixture was then heated at 120 °C under N₂ for 30 minutes. The reaction mixture was then dried, isolated by column chromatography over alumina using CH₂Cl₂ / hexane (1 : 1) as an eluent, and further recrystallized with CH₂Cl₂ / CH₃OH to obtain a deep reddish brown solid of Ir^{III}(ttp)(PPh₃)Ph (2x) (21.9 mg, 0.018 mmol, 79%). R$_f$ = 0.51 (CH₂Cl₂/hexane = 1 : 1). ^{1}H NMR (CDCl₃, 400 MHz) δ 0.37 (dd, 2 H, $^3J_{HH}$ = 7.0 Hz, $^4J_{PH}$ = 6.4

Hz), 2.65 (s, 12 H), 4.12 (dd, 6 H, $^3J_{PH}$ = 8.1 Hz, $^3J_{HH}$ = 8.1 Hz), 4.71 (t, 2 H, $^3J_{HH}$ = 7.1 Hz), 5.13 (t, 1 H, $^3J_{HH}$ = 7.0 Hz), 6.54 (t, 6 H, $^3J_{HH}$ = 7.0 Hz), 6.85 (t, 3 H, $^3J_{HH}$ = 7.3 Hz), 7.41 (d, 4 H, $^3J_{HH}$ = 7.7 Hz), 7.45 (d, 4 H, $^3J_{HH}$ = 7.7 Hz), 7.63 (d, 4 H, $^3J_{HH}$ = 7.4 Hz), 7.79 (d, 4 H, $^3J_{HH}$ = 7.5 Hz), 8.42 (s, 8 H). ^{13}C NMR (CDCl$_3$, 100 MHz) δ 21.6, 119.2, 122.8, 122.9, 126.9 (d, $^3J_{PC}$ = 8 Hz), 127.0, 127.4, 128.0, 128.9 (d, $^1J_{PC}$ = 25 Hz), 130.9 (d, $^2J_{PC}$ = 11 Hz), 131.7, 133.8, 134.6, 136.9, 139.2, 142.4. HRMS (FABMS): Calcd for [C$_{72}$H$_{56}$N$_4$PIr]$^+$: m/z 1200.3866. Found: m/z 1200.3861.

Preparation of (p-Chlorobenzoyl)(triphenylphosphine)(5,10,15,20-tetrakis(p-tolyl)-porphyrinato)iridium(III)) Ir^{III}(ttp)(PPh$_3$)(C(O)C$_6$H$_4$(p-Cl) (12). Ir^{III}(ttp)CH$_3$ (62 mg, 0.072 mmol), 4-chlorobenzaldehyde (506 mg, 3.6 mmol, 50 equiv), and benzene (2 mL) were degassed in a Teflon screw capped tube for three freeze-pump-thaw cycles. The reaction mixture was heated at 200 °C under N$_2$ for 14 days. The reaction mixture was then dried and was further purified by column chromatography over silica gel using CH$_2$Cl$_2$ / hexane (2 : 1) as an eluent to obtain an orange solid of Ir^{III}(ttp)C(O)C$_6$H$_4$(p-Cl)[6] (42 mg, 0.042 mmol, 58%). Ir^{III}(ttp)C(O)C$_6$H$_4$(p-Cl) was then reacted with PPh$_3$ (110 mg, 0.42 mmol, 10 equiv) in CHCl$_3$ (4 mL) in a Telfon screw capped tube under air at 50 °C for 30 minutes. The deep reddish brown reaction mixture was dried and purified by column chromatography over alumina using CH$_2$Cl$_2$/hexane (1:3) as an eluent to obtain a reddish brown solid of Ir^{III}(ttp)(PPh$_3$)(C(O)C$_6$H$_4$(p-Cl)) (12) (45 mg, 0.036 mmol, 50% (with reference to Ir^{III}(ttp)CH$_3$)). R$_f$ = 0.67 (CH$_2$Cl$_2$/hexane = 1 : 1). ^{1}H NMR (CDCl$_3$, 300 MHz) δ 2.22 (d, 2 H, J = 8.4 Hz), 2.23 (s, 12 H), 4.05 (br, 6 H), 5.85 (d, 2 H, J = 8.0 Hz), 6.54 (t, 6 H, J = 6.8 Hz), 6.85 (t, 3 H, J = 7.2 Hz), 7.48 (d, 8 H, J = 8.0 Hz), 7.69 (d, 4 H, J = 8.0 Hz), 7.80 (d, 4 H, J = 7.6 Hz), 8.48 (s, 8 H). ^{13}C NMR (CDCl$_3$, 75 MHz) δ 21.6, 118.5, 118.6, 122.8, 125.3, 127.0 (d, J = 7.6 Hz), 127.1, 127.6, 127.9, 128.1, 128.3, 130.0 (d, $^1J_{PC}$ = 30.5 Hz), 130.8 (d, $^2J_{PC}$ = 11.5 Hz), 131.7, 133.8, 134.5, 137.0, 139.1, 142.4. HRMS (FABMS): Calcd for [C$_{73}$H$_{56}$N$_4$ClOPIr]$^+$ ([M+H]$^+$): m/z 1263.3503. Found: m/z 1263.3500.

Preparation of Triphenylphosphine Oxide (P(O)Ph$_3$). The typical synthetic method of the preparation of P(O)Ph$_3$ is the oxidation of PPh$_3$ by H$_2$O$_2$.[9] PPh$_3$ (64 mg, 0.24 mmol) and H$_2$O$_2$

(30% solution, 2.5 mL, 24.4 mmol H$_2$O$_2$ (100 equiv)), and benzene (2 mL) were gassed in a Teflon screw capped tube for three freeze-pump-thaw cycles. The reaction mixture was heated at 200 ^{o}C for 12 hours under N$_2$ and then purified by column chromatography over silica gel (pre-treated by adding water, silica gel : water ~ 10 : 1 v/v) using CHCl$_3$ as the eluent. The product was crystallized by CH$_2$Cl$_2$ / hexane to yield a pale yellow solid of P(O)Ph$_3$ (50.7 mg, 0.18 mmol, 76%). R$_f$ = 0.33 (CHCl$_3$). ^{1}H NMR (C$_6$D$_6$, 400 MHz) δ 6.96-7.03 (m, 9 H), 7.74 (ddd, 6 H, $^3J_{PH}$ = 11.5 Hz, $^3J_{HH}$ = 8.1 Hz, $^4J_{HH}$ = 1.5 Hz). The observation of $^4J_{HH}$ is dependent on the concentration of P(O)Ph$_3$. ^{31}P NMR (C$_6$D$_6$, 162 MHz) δ 25.2 (hept, $^3J_{PH}$ = 11.3 Hz). HRMS (ESIMS): Calcd for [C$_{18}$H$_{15}$OPNa]$^+$ ([M+Na]$^+$): m/z 301.0753. Found: m/z 301.0748.

(II) Chapter 2　　Redox Chemistry of Iridium(III) Porphyrins in Basic Media

Reactions of Ir^{III}(ttp)(CO)Cl in Benzene-d_6.

(i) Without Addition of Base and Water at 200 ^{o}C. Ir^{III}(ttp)(CO)Cl (4.7 mg, 0.005 mmol) and benzene-d_6 (0.5 mL) were degassed in a Teflon screw capped NMR tube for three freeze-pump-thaw cycles and then flame-sealed under vacuum. Residual water (~2 equiv) was observed by ^{1}H NMR spectroscopy. The reaction mixture was heated at 200 ^{o}C for 14 days. No Ir^{III}(ttp)H was formed and unreacted Ir^{III}(ttp)(CO)Cl was recovered quantitatively using the residual benzene as an internal standard.

(ii) Addition of Water (100 equiv) at 200 ^{o}C. Ir^{III}(ttp)(CO)Cl (4.7 mg, 0.005 mmol), water (9.2 mg, 9.2 μL, 0.51 mmol), and benzene-d_6 (0.5 mL) were degassed in a Teflon screw capped NMR tube for three freeze-pump-thaw cycles and then flame-sealed under vacuum. The reaction mixture was heated at 200 ^{o}C. After 10 days, Ir^{III}(ttp)H was formed in 16% NMR yield and unreacted Ir^{III}(ttp)(CO)Cl was recovered in 84% NMR yield using the residual benzene as an internal standard.

(iii) Addition of KOH (20 equiv) at 200 ^{o}C. Ir^{III}(ttp)(CO)Cl (4.7 mg, 0.005 mmol), KOH (5.7 mg,

0.10 mmol), and benzene-d_6 (0.5 mL) were degassed in a Teflon screw capped NMR tube for three freeze-pump-thaw cycles and then flame-sealed under vacuum. Residual water (~0.2 equiv) was observed by ^{1}H NMR spectroscopy. The reaction mixture was heated at 200 ^{o}C. The reaction was complete in 1 hour to yield Ir^{III}(ttp)H quantitatively (NMR yield) using the residual benzene as an internal standard.

(iv) Addition of K$_2$CO$_3$ (20 equiv) at 200 ^{o}C. Ir^{III}(ttp)(CO)Cl (4.7 mg, 0.005 mmol), K$_2$CO$_3$ (14.0 mg, 0.10 mmol), and benzene-d_6 (0.5 mL) were degassed in a Teflon screw capped NMR tube for three freeze-pump-thaw cycles and then flame-sealed under vacuum. Residual water (~0.2 equiv) was observed by ^{1}H NMR spectroscopy. The reaction mixture was heated at 200 ^{o}C. The reaction was complete in 30 hours to yield Ir^{III}(ttp)H in 95% NMR yield using the residual benzene as an internal standard.

(v) Addition of KOH (20 equiv) at 120 ^{o}C. Ir^{III}(ttp)(CO)Cl (4.7 mg, 0.005 mmol), KOH (5.7 mg, 0.10 mmol), and benzene-d_6 (0.5 mL) were degassed in a Teflon screw capped NMR tube for three freeze-pump-thaw cycles and then flame-sealed under vacuum. Residual water (~0.3 equiv) was observed by ^{1}H NMR spectroscopy. The reaction mixture was heated at 120 ^{o}C. After 2 hours, Ir^{III}(ttp)H in 55% NMR yield was formed and unreacted Ir^{III}(ttp)(CO)Cl was recovered in 45% NMR yield. The reaction was complete after 5 hours to yield Ir^{III}(ttp)H in 84% NMR yield and Ir^{I}(ttp)$^-$K$^+$ (δ(pyrrole H) = 8.50 ppm) in 9% NMR yield. The yields were estimated using the residual benzene as the internal standard.

(vi) Addition of K$_2$CO$_3$ (20 equiv) at 120 ^{o}C. Ir^{III}(ttp)(CO)Cl (4.7 mg, 0.005 mmol), K$_2$CO$_3$ (14.0 mg, 0.10 mmol), and benzene-d_6 (0.5 mL) were degassed in a Teflon screw capped NMR tube for three freeze-pump-thaw cycles and then flame-sealed under vacuum. Residual water (~0.4 equiv) was observed by ^{1}H NMR spectroscopy. The reaction mixture was heated at 120 ^{o}C. The reaction was complete in 23 days to yield Ir^{III}(ttp)H quantitatively (NMR yield) using the residual benzene as the internal standard.

Reactions of Ir^{III}(ttp)(CO)Br in Benzene-d_6.

(i) Addition of KOH (20 equiv) at 120 °C. Ir^{III}(ttp)(CO)Br (4.9 mg, 0.005 mmol), KOH (5.7 mg, 0.10 mmol), and benzene-d_6 (0.5 mL) were degassed in a Teflon screw capped NMR tube for three freeze-pump-thaw cycles and then flame-sealed under vacuum. Residual water (~0.8 equiv) was observed by ^{1}H NMR spectroscopy. The reaction mixture was heated at 120 °C. The reaction was complete in 5 hours to yield Ir^{III}(ttp)H in 71% NMR yield and Ir^{I}(ttp)$^-$K$^+$ (δ(pyrrole H) = 8.59 ppm) in 11% NMR yield using the residual benzene as the internal standard.

(ii) Addition of K$_2$CO$_3$ (20 equiv) at 200 °C. Ir^{III}(ttp)(CO)Br (4.9 mg, 0.05 mmol), K$_2$CO$_3$ (14.0 mg, 0.10 mmol), and benzene-d_6 (0.5 mL) were degassed in a Teflon screw capped NMR tube for three freeze-pump-thaw cycles and then flame-sealed under vacuum. Residual water (~0.2 equiv) was observed by ^{1}H NMR spectroscopy. The reaction mixture was heated at 200 °C. The reaction was complete in 30 hours to yield Ir^{III}(ttp)H in 97% NMR yield using the residual benzene as the internal standard.

Reactions of Ir^{III}(ttp)(CO)I in Benzene-d_6.

(i) Addition of KOH (20 equiv) at 120 °C. Ir^{III}(ttp)(CO)I (5.2 mg, 0.005 mmol), KOH (5.7 mg, 0.10 mmol), and benzene-d_6 (0.5 mL) were degassed in a Teflon screw capped NMR tube for three freeze-pump-thaw cycles and then flame-sealed under vacuum. Residual water (~0.4 equiv) was observed by ^{1}H NMR spectroscopy. The reaction mixture was heated at 120 °C. The reaction was complete in 11 hours to yield Ir^{III}(ttp)H in 87% NMR yield and [Ir^{II}(ttp)]$_2$ in 9% NMR yield using the residual benzene as the internal standard.

(ii) Addition of K$_2$CO$_3$ (20 equiv) at 200 °C. Ir^{III}(ttp)(CO)I (5.2 mg, 0.005 mmol), K$_2$CO$_3$ (14.0 mg, 0.10 mmol), and benzene-d_6 (0.5 mL) were degassed in a Teflon screw capped NMR tube for three freeze-pump-thaw cycles and then flame-sealed under vacuum. Residual water (~1.1 equiv) was observed by ^{1}H NMR spectroscopy. The reaction mixture was heated at 120 °C. The reaction was complete in 50 hours to yield Ir^{III}(ttp)H in 95% NMR yield using the residual benzene as the

internal standard.

Reactions of Ir^{III}(ttp)SbF$_6$ with Bases

(A) Reactions of Ir^{III}(ttp)SbF$_6$ with CsOH (10 equiv)

(i) **In Sealed NMR Tube.** Ir^{III}(ttp)SbF$_6$ (3.0 mg, 0.003 mmol) and CsOH (4.9 mg, 0.03 mmol) were dried under vacuum in a Teflon screw capped NMR tube for a few hours. Benzene-d_6 (0.5 mL) was then added in the tube under N$_2$ and the reaction mixture was degassed for three freeze-pump-thaw cycles and then flame-sealed under vacuum. The reaction occurred instantaneously at room temperature and the color of the reaction mixture changed from red to orange. After 5 minutes, Ir^{III}(ttp)H was estimated to be 95% NMR yield by taking the ratio of the pyrrole proton signal of Ir^{III}(ttp)H and the total pyrrole proton signals of the observed iridium porphyrins. A trace of unreacted Ir^{III}(ttp)SbF$_6$ in 3% NMR yield was also observed. Residual water (~2.9 equiv) dissolved in the reaction mixture was estimated by ^{1}H NMR spectroscopy.

(ii) **In Telfon Screw Capped Tube.** Ir^{III}(ttp)SbF$_6$ (2.9 mg, 0.003 mmol) and CsOH (4.9 mg, 0.29 mmol) were dried under vacuum in a Teflon screw capped tube for a few hours. Benzene-d_6 was then added into the tube under N$_2$ and the reaction mixture was degassed for three freeze-pump-thaw cycles. The reaction occurred instantaneously under N$_2$ at room temperature and the color of the reaction mixture changed from red to orange. The reaction mixture was then taken for HRMS analysis. Ir^{III}(ttp)OH (**5**) and (ttp)Ir^{III}OIr^{III}(ttp) (**6**) were detected in around 6 : 1 ratio by HRMS. **HRMS** (FABMS): (1) Calcd for [C$_{48}$H$_{37}$N$_4$OIr]$^+$ (**5**) ([M]$^+$ = [Ir^{III}(ttp)OH]$^+$): m/z 878.2591. Found: m/z 878.2574. (2) [C$_{96}$H$_{72}$N$_8$OIr$_2$]$^+$ (**6**) ([M]$^+$ = [(ttp)Ir^{III}OIr^{III}(ttp)]$^+$): m/z 1737.5092 Found: m/z 1737.5052.

(B) Reaction of Ir^{III}(ttp)SbF$_6$ with KOH (20 equiv). Ir^{III}(ttp)SbF$_6$ (3.0 mg, 0.003 mmol) and KOH (3.1 mg, 0.05 mmol) were dried under vacuum in a Teflon screw capped NMR tube for a few hours. Benzene-d_6 (0.5 mL) was then added into the tube under N$_2$ and the reaction mixture was degassed for three freeze-pump-thaw cycles and then flame-sealed under vacuum. No

instantaneous reaction occurred at room temperature. In 1.5 days, the color of the reaction mixture changed to orange, and $Ir^{III}(ttp)H$ and $[Ir^{II}(ttp)]_2$ were observed and estimated to be 75% and 7% NMR yields, respectively, by comparing the ratios of the pyrrole proton signals of the products with the total pyrrole proton signals of the observed iridium porphyrins.

Reactions of $[Ir^{II}(ttp)]_2$ in Benzene-d_6

(i) Reaction of $[Ir^{II}(ttp)]_2$ with KOH (20 equiv) at Room Temperature. $Ir^{III}(ttp)H$ (3.8 mg, 0.004 mmol) and benzene (0.5 mL) were degassed for three freeze-pump-thaw cycles in a Teflon screw capped NMR tube. 2,2,6,6-Tetramethylpiperidinooxy (TEMPO) (0.8 mg, 0.005 mmol) was added into the tube under N_2. The reaction mixture changed to deep brown instantaneously, and it was dried under vacuum for a few hours to remove the solvent, unreacted TEMPO, and TEMPOH co-product. KOH (4.9 mg, 0.088 mmol) and benzene-d_6 (0.5 mL) were added into the tube under N_2, and the reaction mixture was further degassed for three freeze-pump-thaw cycles in the tube and then flame-sealed under vacuum. At room temperature, no reaction occurred in 2 days, and $[Ir^{II}(ttp)]_2$ remained unreacted.

(ii) Reaction of $[Ir^{II}(ttp)]_2$ with H_2O (100 equiv). $Ir^{III}(ttp)H$ (3.8 mg, 0.004 mmol) and benzene (0.5 mL) were degassed for three freeze-pump-thaw cycles in a Teflon screw capped NMR tube. 2,2,6,6-Tetramethylpiperidinooxy (TEMPO) (0.8 mg, 0.005 mmol) was added into the tube under N_2. The reaction mixture changed to deep brown instantaneously, and it was dried under vacuum for a few hours to remove the solvent, unreacted TEMPO, and TEMPOH co-product. Water (7.9 mg, 0.44 mmol) and benzene-d_6 (0.5 mL) were added into the tube under N_2, and the reaction mixture was further degassed for three freeze-pump-thaw cycles in the tube and then flame-sealed under vacuum. At room temperature, no reaction occurred in 2 days. At 200 °C, most of $[Ir^{II}(ttp)]_2$ was decomposed in 7 days, and $Ir^{II}(ttp)H$ was formed in 11% NMR yield as estimated by adding TMS_4Si (0.00058 mmol, from standard TMS_4Si / benzene solution) as the internal standard.

(iii) Thermal Reaction of $[Ir^{II}(ttp)]_2$ at 200 °C. $Ir^{III}(ttp)H$ (3.8 mg, 0.004 mmol) and benzene (0.5

mL) were degassed for three freeze-pump-thaw cycles in a Teflon screw capped NMR tube. 2,2,6,6-Tetramethylpiperidinooxy (TEMPO) (0.8 mg, 0.005 mmol) was added into the tube under N_2. The reaction mixture changed to deep brown instantaneously, and it was dried under vacuum for a few hours to remove the solvent, unreacted TEMPO, and TEMPOH co-product. Benzene-d_6 (0.5 mL) was added into the tube, and the reaction mixture was further degassed for three freeze-pump-thaw cycles in the tube and then flame-sealed under vacuum. At room temperature, no reaction occurred in 2 days. At 200 °C, [Ir^{II}(ttp)]$_2$ was recovered in ~26% yield after 1 hour and the rest of [Ir^{II}(ttp)]$_2$ was decomposed to unknown iridium porphyrin species. The yield of [Ir^{II}(ttp)]$_2$ was estimated by comparing the ratios of pyrrole proton signals of [Ir^{II}(ttp)]$_2$ with the total observed pyrrole proton signals of iridium porphyrin species. After 7 days, a trace of Ir^{III}(ttp)H was formed (5% NMR yield, estimated by using TMS$_4$Si (0.00058 mmol, from standard TMS$_4$Si / benzene solution) as the internal standard).

Reaction of Ir^{III}(ttp)(PPh$_3$)Cl with KOH

(i) In Sealed NMR tube. Ir^{III}(ttp)(PPh$_3$)Cl (4.5 mg, 0.004 mmol), KOH (4.4 mg, 0.08 mmol), and benzene-d_6 (0.5 mL) were degassed for three freeze-pump-thaw cycles in a Teflon screw capped NMR tube and then flame-sealed under vacuum. Residual water (~1.7 equiv) was observed by ^{1}H NMR spectroscopy. The reaction mixture was heated at 200 °C in 4 hours to form a deep red Ir^{III}(ttp)(PPh$_3$)OH and Ir^{III}(ttp)(PPh$_3$)H in 96% and 2% NMR yields, respectively, using residual benzene as the internal standard. The reaction mixture was further heated in 9 hours to form a deep brown solution containing Ir^{III}(ttp)(PPh$_3$)H in ~33% NMR yield. **Characterization of Ir^{III}(ttp)(PPh$_3$)OH (5a):** ^{1}H NMR (C$_6$D$_6$, 300 MHz) ^{1}H NMR (C$_6$D$_6$, 300 MHz) δ -9.35 (s, 1 H, $^3J_{PH}$ = 7.5 Hz), 2.40 (s, 12 H), 4.29 (dd, 6 H, $^3J_{PH}$ = 8.9 Hz, $^3J_{HH}$ = 8.7 Hz), 6.36 (t, 6 H, $^3J_{HH}$ = 7.2 Hz), 6.56 (t, 3 H, $^3J_{HH}$ = 7.1 Hz), 7.17 (d, 4 H, $^3J_{HH}$ = 7.2 Hz), 7.35 (d, 4 H, $^3J_{HH}$ = 7.5 Hz), 7.82 (d, 4 H, $^3J_{HH}$ = 7.5 Hz), 7.92 (d, 4 H, $^3J_{HH}$ = 7.5 Hz), 8.81 (s, 8 H). ^{13}C NMR (C$_6$D$_6$, 100 MHz) δ 21.2, 122.8, 126.7, 126.9 (d, $^1J_{PC}$ = 17 Hz), 131.0, (d, $^3J_{PC}$ = 9 Hz), 131.7, 133.8, 134.9, 136.7, 139.5,

142.9. One set of porphyrin's tolyl *m*-carbon signals and PPh$_3$'s *ipso*- and *p*-phenyl carbon signals were obscured by residual benzene carbon signals. ^{31}P NMR (C$_6$D$_6$, 122 MHz) δ -34.9 (d, $^3J_{PC}$ = 7.2 Hz). HRMS (FABMS): Calcd for [C$_{66}$H$_{52}$N$_4$OPIr]$^+$ ([M]$^+$): m/z 1140.3502. Found: m/z 1140.3545.

(ii) In Telfon-Screw Capped Tube. Ir^{III}(ttp)(PPh$_3$)Cl (5.2 mg, 0.004 mmol), KOH (5.0 mg, 0.10 mmol), and benzene-*d$_6$* (0.5 mL) were degassed for three freeze-pump-thaw cycles in a Teflon screw capped tube. The reaction mixture was heated at 200 ^{o}C in 30 minutes to form Ir^{III}(ttp)(PPh$_3$)H (δ(pyrrole H) = 8.75 ppm), Ir^{III}(ttp)(PPh$_3$)OH (δ(pyrrole H) = 8.81 ppm), and unreacted Ir^{III}(ttp)(PPh$_3$)Cl (δ(pyrrole H) = 8.84 ppm) in 31%, 17%, and 29% NMR yields, respectively, by ^{1}H NMR spectroscopy using a known amount of tetrakis(trimethylsilyl)methane (TMS$_4$Si) as an internal standard. The reaction mixture was subjected to HRMS analysis, and no (Ph$_3$P)(ttp)Ir^{III}OIr^{III}(ttp)(PPh$_3$), (Ph$_3$P)(ttp)Ir^{III}OIr^{III}(ttp), or (ttp)Ir^{III}OIr^{III}(ttp) were detected.

Reaction of Ir^{III}(ttp)(PPh$_3$)H with KOH (20 equiv). Ir^{III}(ttp)H (4.7 mg, 0.005 mmol), PPh$_3$ (1.4 mg, 0.005 mmol), KOH (6.1 mg, 0.11 mmol), and benzene-*d$_6$* (0.5 mL) were added to the Teflon screw capped NMR tube under N$_2$. The reaction mixture was degassed for three freeze-pump-thaw cycles and then flame-sealed under vacuum. The reaction mixture changed to reddish brown instantaneously at room temperature to give Ir^{III}(ttp)(PPh$_3$)H quantitatively. The reaction mixture containing Ir^{III}(ttp)(PPh$_3$)H and KOH was heated at 200 ^{o}C for 3 days. Ir^{III}(ttp)(PPh$_3$)H was recovered in 98% NMR yield using the residual benzene as the internal standard.

Reaction of PPh$_3$ with Possible Oxygen Sources

(i) With Oxygen in Air. PPh$_3$ (8.6 mg, 0.033 mmol) and benzene (1 mL) were heated in air (~ 3 equiv O$_2$) at 200 ^{o}C in a Teflon screw capped tube in 12 hours. The reaction mixture was dried. A quantified amount of TMS$_4$Si was added as an internal standard to calculate the number of moles of products, and benzene-*d$_6$* was further added for ^{1}H NMR spectroscopy. No P(O)Ph$_3$ was formed

(< 1% NMR yield), and unreacted PPh$_3$ was recovered in 89% NMR yield. The number of mole of O$_2$ in air (n) was estimated by using the ideal gas equation: n = (PV)/(RT) x 21%, where P = 101325 Nm^{-2}, V ~13 x 10^{-6} m^3, R = 8.314 J K^{-1} mol^{-1}, T = 298 K, and 21% is the percentage of O$_2$ in air. Thus, n is found to be 0.11 mmol (~3 equiv with reference to PPh$_3$).

(ii) With H$_2$O. PPh$_3$ (8.6 mg, 0.033 mmol), water (3.0 μL, 0.16 mmol, 5 equiv), and benzene (1 mL) were degassed for three freeze-pump-thaw cycles in a Teflon screw capped tube. The reaction was heated under N$_2$ at 200 $^{\circ}$C in 12 hours. A quantified amount of TMS$_4$Si was added as an internal standard to calculate the number of moles of products, and benzene-d_6 was further added for ^{1}H NMR spectroscopy. No P(O)Ph$_3$ was formed (< 1% NMR yield), and unreacted PPh$_3$ was recovered in 94% NMR yield.

(iii) With KOH. PPh$_3$ (8.7 mg, 0.033 mmol), KOH (37.2 mg, 0.66 mmol, 20 equiv), and benzene (1 mL) were degassed for three freeze-pump-thaw cycles in a Teflon screw capped tube. The reaction was heated under N$_2$ at 200 $^{\circ}$C in 12 hours. The reaction mixture was dried. A quantified amount of TMS$_4$Si was added as an internal standard to calculate the number of moles of products, and benzene-d_6 was further added for ^{1}H NMR spectroscopy. No P(O)Ph$_3$ was formed (< 1% NMR yield), and unreacted PPh$_3$ was recovered in 75% NMR yield.

(iv) With H$_2$O$_2$. PPh$_3$ (17.5 mg, 0.067 mmol) H$_2$O$_2$ (30% solution, 15.1 mg, 13.6 μL, 0.1334 mmol of H$_2$O$_2$ (2 equiv)), and benzene (2 mL) were degassed for three freeze-pump-thaw cycles in a Teflon screw capped tube. The reaction was heated under N$_2$ at 200 $^{\circ}$C, and the reaction was complete in 1 hour as determined by thin-layer chromatography. The reaction mixture was dried. A quantified amount of TMS$_4$Si was added as an internal standard to calculate of the number of moles of products, and benzene-d_6 was further added for ^{1}H NMR spectroscopy. P(O)Ph$_3$ was formed in 86% NMR yield.

(v) Without Oxygen Sources. PPh$_3$ (8.6 mg, 0.033 mmol) and benzene (1 mL) were degassed for three freeze-pump-thaw cycles in a Teflon screw capped tube. The reaction was heated under N$_2$ at 200 $^{\circ}$C in 12 hours. The reaction mixture was dried. A quantified amount of TMS$_4$Si was added as

an internal standard to calculate of the number of moles of products, and benzene-d_6 was further added for ^{1}H NMR spectroscopy. No P(O)Ph$_3$ was formed (<1% NMR yield), and unreacted PPh$_3$ was recovered in 75% NMR yield.

(vi) With KOH and H$_2$O$_2$. PPh$_3$ (9.2 mg, 0.035 mmol) H$_2$O$_2$ (30% solution, 7.9 mg, 7.3 μL, 0.070 mmol of H$_2$O$_2$ (2 equiv)), KOH (mg, mmol), and benzene (1 mL) were degassed for three freeze-pump-thaw cycles in a Teflon screw capped tube. Prior to heating, gas bubbles, which is most likely O$_2$, were evolved due to the KOH-catalyzed disproportionation of H$_2$O$_2$ in aqueous solution. The reaction was then heated under N$_2$ at 200 ^{o}C in 1 hour. The reaction mixture was dried. A quantified amount of TMS$_4$Si was added as an internal standard to calculate of the number of moles of products, and benzene-d_6 was further added for ^{1}H NMR spectroscopy. P(O)Ph$_3$ was formed in 2% NMR yield, and unreacted PPh$_3$ was recovered in 80% NMR yield.

Reaction of Ir^{III}(ttp)(CO)Cl with KOH and Excess PPh$_3$ (5 equiv). Ir^{III}(ttp)(CO)Cl (10 mg, 0.011 mmol), KOH (12.1 mg, 0.22 mmol), PPh$_3$ (14.2 mg, 0.054 mmol), and benzene-d_6 (1 mL) were degassed for three freeze-pump-thaw cycles in a Teflon screw capped tube. The reaction was heated under N$_2$ for 3 hours, and the color of the reaction mixture changed from deep red to deep brown. Tetrakis(trimethylsilyl)methane (TMS$_4$Si) (1.4 mg, 0.0044 mmol) was added to the reaction mixture as an internal standard to calculate the number of moles of product formed. Ir^{III}(ttp)(PPh$_3$)H, Ir^{III}(ttp)(PPh$_3$)OH, and P(O)Ph$_3$ were formed in 42%, 7%, and 21% NMR yields, respectively, with reference to Ir^{III}(ttp)(CO)Cl added. Unreacted PPh$_3$ was observed in 70% yield with reference to PPh$_3$ added. The formation of P(O)Ph$_3$ in the reaction was confirmed by ^{1}H NMR spectroscopy by comparing with the authentic sample of P(O)Ph$_3$. **Characterization of P(O)Ph$_3$ formed:** ^{1}H NMR (C$_6$D$_6$, 400 MHz) δ(*o*-phenyl H) 7.75 (dd, $^3J_{PH}$ = 12.0 Hz, $^3J_{HH}$ = 7.6 Hz). The P(O)Ph$_3$'s phenyl's *m*- and *p*-protons are obscured by the excess PPh$_3$'s phenyl's *m*- and *p*-protons. ^{31}P NMR (C$_6$D$_6$, 162 MHz) 24.9 (br). HRMS (ESIMS): Calcd for [C$_{18}$H$_{15}$OPNa]$^+$ ([M+Na]$^+$): m/z 301.0753. Found: m/z 301.0750.

Reaction of Ir^{III}(ttp)(CO)Cl with Excess PPh$_3$ (5 equiv) without Base. Ir^{III}(ttp)(CO)Cl (10.3 mg, 0.011 mmol), PPh$_3$ (14.6 mg, 0.056 mmol), and benzene-d_6 (1 mL) were degassed for three freeze-pump-thaw cycles in a Teflon screw capped tube. The reaction was heated under N$_2$ for 12 hours. TMS$_4$Si (4.1 mg, 0.0128 mmol) was added to the reaction mixture as an internal standard to calculate the number of moles of product formed. Ir^{III}(ttp)(PPh$_3$)Cl was formed quantitatively and P(O)Ph$_3$ was formed in a trace amount (~5% NMR yield) with reference to Ir^{III}(ttp)(CO)Cl added. Unreacted PPh$_3$ and P(O)Ph$_3$ were observed in 69% and 1% NMR yields, respectively, with reference to PPh$_3$ added. The formation of P(O)Ph$_3$ was probably due to the oxidation of PPh$_3$ with residual O$_2$ catalyzed by Ir(por) species.

Detection of Phenol in the Reaction of Ir^{III}(ttp)(CO)Cl of KOH (20 equiv)

(i) At 120 ^{o}C. Ir^{III}(ttp)(CO)Cl (10.0 mg, 0.011 mmol), KOH (12.1 mg, 0.22 mmol), and benzene (1 mL) were degassed in a Teflon screw capped tube for three freeze-pump-thaw cycles. The reaction mixture was heated at 120 ^{o}C under N$_2$ for 9 hours. The solvent was then collected in a liguid-N$_2$ cooled trap under vacuum and subjected to GC-MS analysis. No phenol was detected using the authentic phenol as a reference compound. The solid residue was dissolved in benzene-d_6 for ^{1}H NMR spectroscopy, and only Ir^{III}(ttp)H was observed. All solid residues (left in Teflon-screw capped tube and NMR tube) were washed with CH$_2$Cl$_2$ / HCl (aq). The aqueous layer was removed by dropper, and the volatile organic compounds in the organic layer was then collected in a liquid-N$_2$ cooled trap under vacuum and further subjected to GC-MS analysis. No phenol was detected.

(ii) At 200 ^{o}C. Ir^{III}(ttp)(CO)Cl (10.0 mg, 0.011 mmol), KOH (12.1 mg, 0.22 mmol), and benzene (1 mL) were degassed in a Teflon screw capped tube for three freeze-pump-thaw cycles. The reaction mixture was heated at 200 ^{o}C under N$_2$ for 15 minutes to produce only Ir^{III}(ttp)H observed by ^{1}H NMR spectroscopy. No phenol was detected by GC-MS analysis using the same procedures

adopted in the reaction at 120 °C.

Reaction of [Ir^{II}(ttp)]$_2$ / PPh$_3$ in Benzene-d_6

(i) Without Addition of KOH. Ir^{III}(ttp)H (3.8 mg, 0.004 mmol) and benzene (0.5 mL) were degassed for three freeze-pump-thaw cycles in a Teflon screw capped NMR tube. 2,2,6,6-Tetramethylpiperidinooxy (TEMPO) (1.0 mg, 0.005 mmol) was added into the tube under N$_2$ to form [Ir^{II}(ttp)]$_2$ quantitatively. The reaction mixture was dried under vacuum for a few hours to remove the solvent, unreacted TEMPO, and TEMPOH co-product. PPh$_3$ (1.2 mg, 0.004 mmol) and benzene-d_6 (0.5 mL) were added into the tube, and the reaction mixture was degassed for three freeze-pump-thaw cycles in the tube and then flame-sealed under vacuum. Residual water (~1 equiv) was estimated by ^{1}H NMR spectroscopy. The color of the reaction mixture changed to red instantaneously. Reddish brown precipitate was also formed, probably due to the formation of insoluble [Ir^{II}(ttp)(PPh$_3$)]$_2$. By ^{1}H NMR spectroscopy, all unreacted [Ir^{II}(ttp)]$_2$ was consumed, and scarce Ir^{III}(ttp)(PPh$_3$)OH was observed. The reaction mixture was then heated at 200 °C for 4 hours to yield Ir^{III}(ttp)(PPh$_3$)H and Ir^{III}(ttp)(PPh$_3$)OH in trace amounts (<5% yield) estimated by adding TMS$_4$Si (0.00029 mmol, from standard TMS$_4$Si / benzene solution) as the internal standard (Figure 2.7).

(ii) With Addition of KOH (20 equiv). Ir^{III}(ttp)H (3.8 mg, 0.004 mmol) and benzene (0.5 mL) were degassed for three freeze-pump-thaw cycles in a Teflon screw capped NMR tube. 2,2,6,6-Tetramethylpiperidinooxy (TEMPO) (1.0 mg, 0.005 mmol) was added into the tube under N$_2$ to form [Ir^{II}(ttp)]$_2$ quantitatively. The reaction mixture was dried under vacuum for a few hours to remove the solvent, unreacted TEMPO, and TEMPOH co-product. PPh$_3$ (1.2 mg, 0.004 mmol), KOH (5.0 mg, 0.088 mmol), and benzene-d_6 (0.5 mL) were added into the tube, and the reaction mixture was degassed for three freeze-pump-thaw cycles in the tube and then flame-sealed under vacuum. Residual water (~1 equiv) was observed by ^{1}H NMR spectroscopy. The color of the reaction mixture changed to red instantaneously. Reddish brown precipitate was also formed,

probably due to the formation of insoluble [Ir^{II}(ttp)(PPh$_3$)]$_2$. By ^{1}H NMR spectroscopy, all unreacted [Ir^{II}(ttp)]$_2$ was consumed, and scarce Ir^{III}(ttp)(PPh$_3$)OH was observed. The reaction mixture was then heated at 200 ^{o}C for 4 hours to yield Ir^{III}(ttp)(PPh$_3$)H and Ir^{III}(ttp)(PPh$_3$)OH in 15% and 16% NMR yields, respectively. The yield of Ir^{III}(ttp)(PPh$_3$)OH was estimated by adding TMS$_4$Si (0.00029 mmol, from standard TMS$_4$Si / benzene solution) as the internal standard. The yield of Ir^{III}(ttp)(PPh$_3$)H was estimated by using the yield of Ir^{III}(ttp)(PPh$_3$)OH, and the ratio of porphyrin's pyrrole proton signal ratios of Ir^{III}(ttp)(PPh$_3$)H and Ir^{III}(ttp)(PPh$_3$)OH (1.0 : 1.1) (Figure 2.8).

Reaction of (H$_2$O)(ttp)Ir^{III}OIr^{III}(ttp)(OH$_2$) with KOH. (H$_2$O)Ir^{III}(ttp)OIr^{III}(ttp)(OH$_2$), which was prepared in 72% yield in the reaction of Ir^{III}(ttp)CH$_2$CH$_2$OH in benzene-d_6 at 120 ^{o}C in 23 days in a sealed NMR tube, was added with KOH (3.2 mg, 0.057 mmol) after breaking the toppest part of the sealed NMR tube. The reaction mixture was degassed for three freeze-pump-thaw cycles using a septum and a cannula and then flame-sealed under vacuum. Residual water (~1.9 equiv) was observed by ^{1}H NMR spectroscopy. The reaction was heated in 120 ^{o}C for 10 days to give Ir^{III}(ttp)H in 6% NMR yield and unreacted (H$_2$O)(ttp)Ir^{III}OIr^{III}(ttp)(OH$_2$) was recovered in 94% yield. The reaction mixture was further heated at 200 ^{o}C in 10 days to yield Ir^{III}(ttp)H in 58% yield. The yields were estimated using the residual benzene as the internal standard.

Reaction of Ir^{I}(ttp)$^-$K$^+$ in Benzene-d_6 at Room Temperature. Ir^{III}(ttp)H (5.0 mg, 0.006 mmol), KOH (6.6 mg, 0.12 mmol), and THF-d_8 (0.5 mL) were degassed for three freeze-pump-thaw cycles in a Teflon screw capped NMR tube. The reaction mixture was heated at 120 ^{o}C under N$_2$ in an oil bath for 6 hours to yield Ir^{I}(ttp)$^-$K$^+$ quantitatively. The solvent was dried under vacuum, and benzene-d_6 (0.5 mL) was added under N$_2$. The reaction mixture was further degassed for three freeze-pump-thaw cycles and then flame-sealed under vacuum. At room temperature, the reaction occurred instantaneously to give Ir^{III}(ttp)H and [Ir^{II}(ttp)]$_2$ in approximately 45% and 18% yields,

respectively, by comparing the ratio of pyrrole signals of the products with the total pyrrole proton signals of all iridium porphyrin species observed. The yield of $[Ir^{II}(ttp)]_2$ was only estimated from the observed $[Ir^{II}(ttp)]_2$ dissolved in benzene-d_6 as the solubility of $[Ir^{II}(ttp)]_2$ was not very high and existed as a deep brown solid when it was formed in large amount. Residual water (~0.5 equiv) was estimated in the reaction mixture by ^{1}H NMR spectroscopy.

Reaction of Ir^{III}(ttp)H in Benzene-d_6

(i) Without Base at Room Temperature. Ir^{III}(ttp)H (2.3 mg, 0.003 mmol), and benzene-d_6 (0.5 mL) were degassed for three freeze-pump-thaw cycles in a Teflon screw capped NMR tube and then flame-sealed under vacuum. The course of the reaction at room temperature was monitored by ^{1}H NMR spectroscopy. Ir^{III}(ttp)H was instantaneously converted to $[Ir^{II}(ttp)]_2$ in 1% yield and unreacted Ir^{III}(ttp)H in 99% yield was observed using residual benzene protons as an internal standard. In 7 and 22 days, unreacted $[Ir^{II}(ttp)]_2$ and Ir^{III}(ttp)H in 95% and 5% yields were observed. The yield was estimated using the residual benzene as an internal standard. It is assumed that the residual O$_2$ in benzene-d_6 led to the formation of $[Ir^{II}(ttp)]_2$.

(ii) Without Base at 200 °C. Ir^{III}(ttp)H (4.4 mg, 0.005 mmol) and benzene-d_6 (0.5 mL) were degassed for three freeze-pump-thaw cycles in a Teflon screw capped NMR tube and then flame-sealed under vacuum. The course of the reaction at 200 °C was monitored by ^{1}H NMR spectroscopy. In 2 minutes, $[Ir^{II}(ttp)]_2$ in 19% yield and unreacted Ir^{III}(ttp)H in 81% yield were estimated using residual benzene protons as an internal standard. After 15 minutes, $[Ir^{II}(ttp)]_2$ in 7% yield and unreacted Ir^{III}(ttp)H in 70% yield were observed. After 1.5 hours and afterwards, only Ir^{III}(ttp)H in 72% NMR yield was observed without further reaction. Residual water (~1 equiv) was estimated in the reaction mixture by ^{1}H NMR spectroscopy. The reaction time profile was shown in Figure 2.9.

(iii) With KOH at at 200 °C. Ir^{III}(ttp)H (5.1 mg, 0.006 mmol), KOH (6.6 mg, 0.12 mmol), and benzene-d_6 (0.5 mL) were degassed for three freeze-pump-thaw cycles in a Teflon screw capped

NMR tube and then flame-sealed under vacuum. Residual water (~1.4 equiv) was estimated by ^{1}H NMR spectroscopy. The course of the reaction at 200 °C was monitored by ^{1}H NMR spectroscopy. After 2 minutes, [Ir^{II}(ttp)]$_2$ in 59% yield and unreacted Ir^{II}(ttp)H in 36% yield were estimated using residual benzene protons as an internal standard. After 15 minutes, [Ir^{II}(ttp)]$_2$ in 39% yield and unreacted Ir^{III}(ttp)H in 53% yield were observed. After 1 hour, only Ir^I(ttp)$^-$K$^+$ in 16% yield and unreacted Ir^{III}(ttp)H in 56% yield were observed. After 2 hours and afterwards, Ir^{III}(ttp)H in 74% yield was observed without further reaction. Residual water (~1.4 equiv) was estimated in the reaction mixture by ^{1}H NMR spectroscopy. The reaction profile was shown in Figure 2.10.

(iv) With K$_2$CO$_3$ at at 200 °C. Ir^{III}(ttp)H (4.6 mg, 0.005 mmol), K$_2$CO$_3$ (14.7 mg, 0.11 mmol), and benzene-d_6 were degassed for three freeze-pump-thaw cycles in a Teflon screw capped NMR tube and then flame-sealed under vacuum. The course of the reaction at 200 °C was monitored by ^{1}H NMR spectroscopy. After 2 minutes, [Ir^{II}(ttp)]$_2$ in 55% yield and unreacted Ir^{III}(ttp)H in 40% yield were estimated using residual benzene protons as an internal standard. After 1.5 hours, [Ir^{II}(ttp)]$_2$ in 24% yield and unreacted Ir^{III}(ttp)H in 48% yield were observed. After 15 hours, only Ir^{III}(ttp)H in 64% yield was observed without further reaction. Residual water (~1.8 equiv) was estimated in the reaction mixture by ^{1}H NMR spectroscopy. The reaction profile was shown in Figure 2.11.

(III) Chapter 3   Base-Promoted Aryl Carbon-Halogen Bond Cleavages by Iridium(III)
   Porphyrins

Reactions of Ir^{III}(ttp)(CO)Cl with PhX in Solvent-Free Conditions.

The experimental procedure of the reaction of Ir^{III}(ttp)(CO)Cl with PhCl at 200 °C was described as a typical example.

(a) Reaction of Ir^{III}(ttp)(CO)Cl with PhCl. Ir^{III}(ttp)(CO)Cl (15.0 mg, 0.016 mmol) and PhCl (1 mL) were degassed for three freeze-pump-thaw cycles in a Teflon screw-capped tube. The reaction

mixture was heated at 200 °C under N_2 for 3 days. The solvent was then removed under vacuum and the reddish brown residue was purified by column chromatography over silica gel (pre-treated by adding ~10% v/v water to lower the polarity of the silica gel to successfully isolate Ir^{III}(ttp)Ph) eluted with CH_2Cl_2/hexane (1:3). The major brown fraction was collected to isolate a brown solid of Ir^{III}(ttp)Ph (**8a**) (4.0 mg, 0.004 mmol, 26%). CH_2Cl_2 and hexane (2:1) was then used as an eluent to isolate a red Ir^{III}(ttp)(CO)Cl (6.7 mg, 0.007 mmol, 45%). **Characterization of** Ir^{III}(ttp)Ph (8a): R_f = 0.47 (CH_2Cl_2/hexane = 1 : 1). ^{1}H NMR ($CDCl_3$, 300 MHz) δ 0.55 (d, 2 H, J = 8.1 Hz), 2.68 (s, 12 H), 4.72 (t, 2 H, J = 8.4 Hz), 5.22 (t, 1 H, J = 7.2 Hz), 7.50-7.53 (m, 8 H), 7.99-8.02 (m, 8 H), 8.58 (s, 8 H). ^{13}C NMR ($CDCl_3$, 75 MHz) δ 21.7, 95.3, 120.2, 123.2, 124.2, 127.6, 129.1, 131.6, 133.7, 134.2, 137.4, 138.8, 143.1. HRMS (ESIMS): Calcd for $[C_{54}H_{41}N_4Ir]^+$: m/z 938.2955. Found: m/z 938.2948. The single crystal for X-ray crystallography was grown from CH_2Cl_2 / CH_3OH.

(b) Reaction of Ir^{III}(ttp)(CO)Cl with PhCl and K_2CO_3. Ir^{III}(ttp)(CO)Cl (15.0 mg, 0.016 mmol), K_2CO_3 (45 mg, 0.32 mmol, 20 equiv), and PhCl (1 mL) were heated at 200 °C under N_2 for 12 hours. The crude product was purified by column chromatography over alumina eluted with CH_2Cl_2/hexane (1:3) to isolate a brown solid of Ir^{III}(ttp)Ph (12.6 mg, 0.013 mmol, 84%).

(c) Reactions of Ir^{III}(ttp)(CO)Cl with PhBr. Ir^{III}(ttp)(CO)Cl (15 mg, 0.016 mmol) and PhBr (1 mL) were heated at 200 °C under N_2 for 2 days to give a red solid of Ir^{III}(ttp)(CO)Br (9.6 mg, 0.010 mmol, 62%) upon column chromatography with silica gel using CH_2Cl_2 / hexane (1:1) as an eluent. Ir^{III}(ttp)Ph was observed in 1 day by thin-layer chromatography (R_f = 0.50 (CH_2Cl_2/hexane = 1 : 1), but it decomposed to form black complex upon further heating to 2 days.

(d) Reaction of Ir^{III}(ttp)(CO)Cl with PhBr and K_2CO_3. Ir^{III}(ttp)(CO)Cl (15 mg, 0.016 mmol), K_2CO_3 (45 mg, 0.32 mmol, 20 equiv), and PhBr (1 mL) were heated at 150 °C under N_2 for 12 hours to give Ir^{III}(ttp)Ph (13.7 mg, 0.015 mmol, 91%) upon column chromatography with alumina using CH_2Cl_2 / hexane (1:1) as an eluent..

(e) Reaction of Ir^{III}(ttp)(CO)Cl with PhI. Ir^{III}(ttp)(CO)Cl (15 mg, 0.016 mmol) and PhI (1 mL)

were heated at 200 °C under N_2 for 2 days. The crude product was purified by column chromatography over silica gel eluted with CH_2Cl_2/hexane (2:3) to give a red solid of Ir^{III}(ttp)(CO)I (6.7 mg, 0.007 mmol, 41%). Ir^{III}(ttp)Ph was observed in 1 day by thin-layer chromatography ($R_f = 0.50$ (CH_2Cl_2/hexane = 1 : 1), but it decomposed to form black complex upon further heating to 2 days.

(f) Reaction of Ir^{III}(ttp)(CO)Cl with PhI and K_2CO_3. Ir^{III}(ttp)(CO)Cl (15 mg, 0.016 mmol), K_2CO_3 (45 mg, 0.32 mmol, 20 equiv), and PhI (1 mL) were heated at 150 °C under N_2 for 36 hours. The crude product was purified by column chromatography over alumina eluted with CH_2Cl_2/hexane (1:1) to give Ir^{III}(ttp)Ph (14.0 mg, 0.015 mmol, 93%).

Reactions of Ir^{III}(ttp)(CO)Cl with PhX (1.1 equiv) in Benzene Solvent at 200 °C.

The experimental procedure of the reaction Ir^{III}(ttp)(CO)Cl with PhCl (1.1 equiv) at 200 °C was described as a typical example for the following reactions.

(a) Reaction of Ir^{III}(ttp)(CO)Cl with PhCl (1.1 equiv). Ir^{III}(ttp)(CO)Cl (20 mg, 0.022 mmol), PhCl (2.7 mg, 2.4 μL, 0.024 mmol), and benzene (2 mL) were degassed for three freeze-pump-thaw cycles in a Teflon screw-capped tube. The reaction mixture was heated at 200 °C under N_2 for 7 days. The solvent was then removed under vacuum and the crude products were purified by column chromatography over silica gel eluted with CH_2Cl_2/hexane (2:1). The major red fraction was collected to give Ir^{III}(ttp)(CO)Cl (15.7 mg, 0.017 mmol, 78%). Ir^{III}(ttp)Ph formed in trace amount could not be isolated by column chromatography due to its decomposition in silica gel. The yield of Ir^{III}(ttp)Ph (2% NMR yield) was estimated by using the isolated yield of unreacted Ir^{III}(ttp)(CO)Cl, and the porphyrin's pyrrole proton ratio of Ir^{III}(ttp)(CO)Cl : Ir^{III}(ttp)Ph (~39 : 1) in the crude product mixture estimated by ^{1}H NMR spectroscopy.

(b) Reaction of Ir^{III}(ttp)(CO)Cl with PhCl (1.1 equiv) and K_2CO_3 (20 equiv). Ir^{III}(ttp)(CO)Cl (19.7 mg, 0.021 mmol), K_2CO_3 (59.0 mg, 0.43 mmol), PhCl (2.6 mg, 2.4 μL, 0.023 mmol), and benzene (2 mL) were heated at 200 °C under N_2 for 1 days. The crude products were purified by

221

column chromatography over alumina eluted with CH_2Cl_2 / hexane (1 : 2) to isolate a mixture of $Ir^{III}(ttp)Ph$ (6.2 mg, 0.007 mmol, 31%), $Ir^{III}(ttp)(p-C_6H_4)Ir^{III}(ttp)$ (**9a**) (0.5 mg, 0.0006 mmol, 3%), and $Ir^{III}(ttp)CH_3$ (**10**)[3b] (1.1 mg, 0.0006 mmol, 3%). The products ratio was estimated from the pyrrole proton ratios of the mixed products by ^1H NMR spectroscopy. **Characterization of $Ir^{III}(ttp)(p-C_6H_4)Ir^{III}(ttp)$ (9a):** R_f = 0.32 (CH_2Cl_2/hexane = 1 : 1). ^1H NMR ($CDCl_3$, 400 MHz) δ -2.00 (s, 4 H), 2.66 (s, 24 H), 7.39 (d, 8 H, $^3J_{HH}$ = 7.4 Hz), 7.41 (d, 8 H, $^3J_{HH}$ = 7.8 Hz), 7.44 (dd, 8 H, $^3J_{HH}$ = 7.6 Hz, $^4J_{HH}$ = 1.7 Hz), 7.79 (dd, 8 H, $^3J_{HH}$ = 7.6 Hz, $^4J_{HH}$ = 1.8 Hz), 8.18 (s, 16 H). ^{13}C NMR with complete ^{13}C signals could not be obtained since $Ir^{III}(ttp)(p-C_6H_4)Ir^{III}(ttp)$ was only springly soluble in $CDCl_3$ and THF-d_8. HRMS (FABMS): $[C_{101}^{13}CH_{76}N_8^{193}Ir^{191}Ir]^+$: m/z 1797.5456. Found: m/z 1797.5470. **Characterization of $Ir^{III}(ttp)CH_3$ (10):**[3b] R_f = 0.62 (CH_2Cl_2/hexane = 1 : 1). ^1H NMR (300 MHz, $CDCl_3$) δ -6.30 (s, 3 H), 2,69 (s, 12 H), 7.51-7.53 (m, 8 H), 7.98-8.05 (m, 8 H), 8.51 (s, 8 H). ^{13}C NMR (75 MHz, $CDCl_3$) δ -39.4, 21.7, 124.0, 127.58, 127.62, 131.4, 133.7, 133.9, 137.3, 138.9, 143.4.

(c) Reaction of $Ir^{III}(ttp)(CO)Cl$ with PhBr (1.1 equiv). $Ir^{III}(ttp)(CO)Cl$ (20 mg, 0.022 mmol), PhBr (3.7 mg, 2.5 μL, 0.024 mmol), and benzene (2 mL) were heated at 200 °C under N_2 for 7 days. The crude product was purified by column chromatography over silica gel eluted with CH_2Cl_2/hexane (1:2) to give $Ir^{III}(ttp)CO)Br$ (2.1 mg, 0.002 mmol, 10%), and then eluted with CH_2Cl_2/hexane (2:1) to give $Ir^{III}(ttp)CO)Cl$ (16.2 mg, 0.017 mmol, 81%). $Ir^{III}(ttp)Ph$ (9%, NMR yield) was also formed as it could not be isolated and decomposed in silica gel.

(d) Reaction of $Ir^{III}(ttp)(CO)Cl$ with PhBr (1.1 equiv) and K_2CO_3 (20 equiv). $Ir^{III}(ttp)(CO)Cl$ (20 mg, 0.022 mmol), PhBr (3.7 mg, 2.5 μL, 0.024 mmol), K_2CO_3 (60 mg, 0.43 mmol), and benzene (2 mL) were heated at 200 °C under N_2 for 2 days. The crude product was purified by column chromatography over alumina eluted with CH_2Cl_2/hexane (1:1) to give $Ir^{III}(ttp)Ph$ (20.3 mg, 0.022 mmol, 100%).

(e) Reaction of $Ir^{III}(ttp)(CO)Cl$ with PhI (1.1 equiv). $Ir^{III}(ttp)(CO)Cl$ (20.0 mg, 0.022 mmol), PhI (4.8 mg, 2.6 μL, 0.024 mmol), and benzene (2 mL) were heated at 200 °C under N_2 for 7 days.

The crude product was purified by column chromatography over silica gel eluted with CH$_2$Cl$_2$/hexane (1:2) to give Ir^{III}(ttp)CO)I (1.1 mg, 0.001 mmol, 5%), and then eluted with CH$_2$Cl$_2$/hexane (2:1) to give Ir^{III}(ttp)CO)Cl (15.2 mg, 0.016 mmol, 76%). Ir^{III}(ttp)Ph (19%, NMR yield) was also formed as it could not be isolated and decomposed in silica gel.   .

(f) Reaction of Ir^{III}(ttp)(CO)Cl with PhI (1.1 equiv) and K$_2$CO$_3$ (20 equiv). Ir^{III}(ttp)(CO)Cl (20.0 mg, 0.022 mmol), PhI (4.8 mg, 2.6 μL, 0.024 mmol), K$_2$CO$_3$ (60 mg, 0.43 mmol), and benzene (2 mL) were heated at 200 °C under N$_2$ for 3 days. The crude product was purified by column chromatography over alumina eluted with CH$_2$Cl$_2$/hexane (1:1) to give Ir^{III}(ttp)Ph (16.4 mg, 0.017 mmol, 81%).

Optimization of Base-Promoted Ph-Br Cleavage by Ir^{III}(ttp)(CO)Cl

The experimental procedure of the reaction Ir^{III}(ttp)(CO)Cl with PhBr and KOH at 150 °C was described as a typical example.

(1) Reaction of Ir^{III}(ttp)(CO)Cl with PhBr and KOH. Ir^{III}(ttp)(CO)Cl (15.0 mg, 0.016 mmol), KOH (18.0 mg, 0.32 mmol, 20 equiv), and PhBr (1 mL) were degassed for three freeze-pump-thaw cycles in a Teflon screw capped tube. The reaction was then heated at 150 °C under N$_2$ for 2 hours. The crude product was purified by column chromatography over alumina eluted with CH$_2$Cl$_2$/hexane (1:2) to give Ir^{III}(ttp)Ph (11.3 mg, 0.012 mmol, 75%).

(2) Reaction of Ir^{III}(ttp)(CO)Cl with PhBr and NaOH. Ir^{III}(ttp)(CO)Cl (15.0 mg, 0.016 mmol), NaOH (12.8 mg, 0.32 mmol, 20 equiv), and PhBr (1 mL) were heated at 150 °C under N$_2$ for 2.5 hours to give Ir^{III}(ttp)Ph (11.3 mg, 0.012 mmol, 75%).

(3) Reaction of Ir^{III}(ttp)(CO)Cl with PhBr and Cs$_2$CO$_3$. Ir^{III}(ttp)(CO)Cl (15.0 mg, 0.016 mmol), Cs$_2$CO$_3$ (104.3 mg, 0.32 mmol, 20 equiv), and PhBr (1 mL) were heated at 150 °C under N$_2$ for 3 hours to give Ir^{III}(ttp)Ph (12.6 mg, 0.013 mmol, 83%).

(4) Reaction of Ir^{III}(ttp)(CO)Cl with PhBr and K$_3$PO$_4$. Ir^{III}(ttp)(CO)Cl (15.0 mg, 0.016 mmol), K$_3$PO$_4$ (68 mg, 0.32 mmol, 20 equiv), and PhBr (1 mL) were heated at 150 °C under N$_2$ for 20

hours to give Ir^{III}(ttp)Ph (14.6 mg, 0.016 mmol, 97%).

(5) Reaction of Ir^{III}(ttp)(CO)Cl with PhBr and K_2CO_3.

(a) K_2CO_3 (10 equiv). Ir^{III}(ttp)(CO)Cl (15.0 mg, 0.016 mmol), K_2CO_3 (23 mg, 0.16 mmol), and PhBr (1 mL) were heated at 150 °C under N_2 for 2 days to give Ir^{III}(ttp)Ph (11.1 mg, 0.012 mmol, 74%).

(b) K_2CO_3 (20 equiv). Ir^{III}(ttp)(CO)Cl (15.0 mg, 0.016 mmol), K_2CO_3 (45 mg, 0.32 mmol), and PhBr (1 mL) were heated at 150 °C under N_2 for 12 hours to give Ir^{III}(ttp)Ph (13.7 mg, 0.015 mmol, 91%).

(c) K_2CO_3 (30 equiv). Ir^{III}(ttp)(CO)Cl (15.0 mg, 0.016 mmol), K_2CO_3 (68 mg, 0.48 mmol), and PhBr (1 mL) were heated at 150 °C under N_2 for 6 hours to give Ir^{III}(ttp)Ph (12.6 mg, 0.013 mmol, 84%).

(6) Reaction of Ir^{III}(ttp)(CO)Cl with PhBr (1.1 equiv) and K_2CO_3 (20 equiv) in Benzene at 150 °C. Ir^{III}(ttp)(CO)Cl (20.0 mg, 0.022 mmol), PhBr (3.7 mg, 2.5 μL, 0.024 mmol), K_2CO_3 (60 mg, 0.43 mmol), and benzene (2 mL) were heated at 200 °C under N_2 for 4 days to give Ir^{III}(ttp)Ph (17.6 mg, 0.019 mmol, 87%).

(7) Reaction of Ir^{III}(ttp)(CO)Cl with PhBr (1.1 equiv) and K_2CO_3 (20 equiv) in Benzene at 200 °C. Ir^{III}(ttp)(CO)Cl (20.0 mg, 0.022 mmol), PhBr (3.7 mg, 2.5 μL, 0.024 mmol), K_2CO_3 (60 mg, 0.43 mmol), and benzene (2 mL) were heated at 200 °C under N_2 for 2 days to give Ir^{III}(ttp)Ph (20.3 mg, 0.022 mmol, 100%).

Optimization of Base-Promoted Ph-I Cleavage by Ir^{III}(ttp)(CO)Cl

The experimental procedure of the reaction Ir^{III}(ttp)(CO)Cl with PhI (1.1 equiv) and KOH (20 equiv) at 150 °C was described as a typical example.

(1) Reactions of Ir^{III}(ttp)(CO)Cl with PhI (1.1 equiv) and KOH. Ir^{III}(ttp)(CO)Cl (9.9 mg, 0.011 mmol), KOH (12.0 mg, 0.21 mmol, 20 equiv), PhI (2.4 mg, 1.3 μL, 0.012 mmol), and benzene (1 mL) were degassed for three freeze-pump-thaw cycles in a Teflon screw capped tube. The reaction

was then heated at 150 °C under N$_2$ for 12 hours. The crude product was purified by column chromatography over alumina eluted with CH$_2$Cl$_2$/hexane (1:2) to give Ir^{III}(ttp)Ph (7.0 mg, 0.007 mmol, 70%).

(2) Reaction of Ir^{III}(ttp)(CO)Cl with PhI (1.1 equiv) and Cs$_2$CO$_3$. Ir^{III}(ttp)(CO)Cl (10.6 mg, 0.011 mmol), Cs$_2$CO$_3$ (7.5 mg, 0.23 mmo, 20 equiv), PhI (2.6 mg, 1.4 μL, 0.013 mmol), and benzene (1 mL) were heated at 150 °C under N$_2$ for 1 day to give Ir^{III}(ttp)Ph (8.8 mg, 0.009 mmol, 82%).

(3) Reaction of Ir^{III}(ttp)(CO)Cl with PhI (1.1 equiv) and K$_2$CO$_3$. Ir^{III}(ttp)(CO)Cl (10.0 mg, 0.011 mmol), K$_2$CO$_3$ (30.0 mg, 0.22 mmol, 20 equiv), PhI (2.4 mg, 1.3 μL, 0.012 mmol), and benzene (1 mL) were heated at 150 °C under N$_2$ for 5 days to give Ir^{III}(ttp)Ph (7.9 mg, 0.008 mmol, 78%).

(4) Reaction of Ir^{III}(ttp)(CO)Cl with PhI (1.1 equiv) and K$_3$PO$_4$. Ir^{III}(ttp)(CO)Cl (9.3 mg, 0.010 mmol), K$_3$PO$_4$ (44.0 mg, 0.20 mmol, 20 equiv), PhI (2.2 mg, 1.2 μL, 0.011 mmol), and benzene (1 mL) were heated at 150 °C under N$_2$ for 1.5 days to give Ir^{III}(ttp)Ph (7.7 mg, 0.008 mmol, 82%).

(5) Reaction of Ir^{III}(ttp)(CO)Cl with PhI (1.1 equiv) and NaOH

(a) NaOH (10 equiv) at 150 °C. Ir^{III}(ttp)(CO)Cl (9.5 mg, 0.010 mmol), NaOH (4.1 mg, 0.10 mmol), PhI (2.3 mg, 1.3 μL, 0.011 mmol), and benzene (1 mL) were heated at 200 °C under N$_2$ for 1 day to give Ir^{III}(ttp)Ph (8.4 mg, 0.009 mmol, 87%).

(b) NaOH (20 equiv) at 150 °C. Ir^{III}(ttp)(CO)Cl (10.3 mg, 0.011 mmol), NaOH (8.9 mg, 0.22 mmol), PhI (2.5 mg, 1.4 μL, 0.012 mmol), and benzene (1 mL) were heated at 200 °C under N$_2$ for 12 hours to give Ir^{III}(ttp)Ph (10.3 mg, 0.011 mmol, 99%).

(c) NaOH (30 equiv) at 150 °C. Ir^{III}(ttp)(CO)Cl (9.5 mg, 0.010 mmol), NaOH (12.3 mg, 0.31 mmol), PhI (2.3 mg, 1.3 μL, 0.011 mmol), and benzene (1 mL) were heated at 200 °C under N$_2$ for 9 hours to give Ir^{III}(ttp)Ph (9.2 mg, 0.010 mmol, 95%).

(d) NaOH (20 equiv) at 120 °C. Ir^{III}(ttp)(CO)Cl (9.8 mg, 0.011 mmol), NaOH (8.5 mg, 0.21 mmol), PhI (2.4 mg, 1.3 μL, 0.012 mmol), and benzene (1 mL) were heated at 120 °C under N$_2$ for

20 hours to give Ir^{III}(ttp)Ph (9.0 mg, 0.010 mmol, 90%).

(e) NaOH (20 equiv) at 200 °C. Ir^{III}(ttp)(CO)Cl (9.6 mg, 0.010 mmol), NaOH (8.3 mg, 0.21 mmol), PhI (2.3 mg, 1.3 μL, 0.011 mmol), and benzene (1 mL) were heated at 200 °C under N$_2$ for 2 hours to give Ir^{III}(ttp)Ph (9.4 mg, 0.010 mmol, 97%).

Optimization of Base-Promoted Ph-Cl Cleavage by Ir^{III}(ttp)(CO)Cl

The experimental procedure of the reaction Ir^{III}(ttp)(CO)Cl with PhCl (1.1 equiv) and NaOH (20 equiv) at 200 °C was described as a typical example.

(1) Reaction of Ir^{III}(ttp)(CO)Cl with PhCl (1.1 equiv) and NaOH (20 equiv) at 200 °C. Ir^{III}(ttp)(CO)Cl (9.9 mg, 0.011 mmol), NaOH (8.6 mg, 0.21 mmol), PhCl (1.3 mg, 1.2 μL, 0.012 mmol), and benzene (1 mL) were degassed for three freeze-pump-thaw cycles in a Teflon screw capped tube. The reaction was then heated at 200 °C under N$_2$ for 1 day. The crude product was purified by column chromatography over alumina eluted with CH$_2$Cl$_2$/hexane (1:2) to give Ir^{III}(ttp)Ph (2.0 mg, 0.002 mmol, 20%) and Ir^{III}(ttp)CH$_3$[3b] (0.6 mg, 0.0007 mmol, 6%). The products ratio was estimated by using the pyrrole proton ratios of the products in the isolated products by ^{1}H NMR spectroscopy.

(2) Reaction of Ir^{III}(ttp)(CO)Cl with PhCl (1.1 equiv) and KOH (20 equiv) at 200 °C. Ir^{III}(ttp)(CO)Cl (10.1 mg, 0.011 mmol), KOH (12.3 mg, 0.22 mmol), PhCl (1.4 mg, 1.2 μL, 0.012 mmol), and benzene (1 mL) were heated at 200 °C under N$_2$ for 20 hours to give Ir^{III}(ttp)Ph (1.8 mg, 0.002 mmol, 18%) and Ir^{III}(ttp)CH$_3$ (0.2 mg, 0.0002 mmol, 2%).

(3) Reaction of Ir^{III}(ttp)(CO)Cl with PhCl (1.1 equiv) and K$_3$PO$_4$ (20 equiv) at 200 °C. Ir^{III}(ttp)(CO)Cl (10.0 mg, 0.011 mmol), K$_3$PO$_4$ (46.0 mg, 0.22 mmol), PhCl (1.3 mg, 1.2 μL, 0.012 mmol), and benzene (1 mL) were heated at 200 °C under N$_2$ for 4 days to give Ir^{III}(ttp)Ph (2.0 mg, 0.002 mmol, 20%) and Ir^{III}(ttp)CH$_3$ (1.5 mg, 0.002 mmol, 16%).

(4) Reaction of Ir^{III}(ttp)(CO)Cl with PhCl (1.1 equiv) and K$_2$CO$_3$ (20 equiv) at 200 °C. Ir^{III}(ttp)(CO)Cl (19.7 mg, 0.021 mmol), K$_2$CO$_3$ (59.0 mg, 0.43 mmol), PhCl (2.6 mg, 2.4 μL, 0.023

mmol), and benzene (2 mL) were heated at 200 °C under N_2 for 1 day to give Ir^{III}(ttp)Ph (6.2 mg, 0.007 mmol, 31%), Ir^{III}(ttp)(p-C_6H_4)Ir^{III}(ttp) (0.5 mg, 0.0006 mmol, 3%), and Ir^{III}(ttp)CH_3 (1.1 mg, 0.0006 mmol, 3%).

(5) Reaction of Ir^{III}(ttp)(CO)Cl with PhCl (50 equiv) and K_2CO_3 (20 equiv) at 200 °C. Ir^{III}(ttp)(CO)Cl (9.7 mg, 0.010 mmol), K_2CO_3 (29 mg, 0.21 mmol), PhCl (59 mg, 53 μL, 0.53 mmol), and benzene (1 mL) were heated at 200 °C under N_2 for 12 hours to give Ir^{III}(ttp)Ph (5.6 mg, 0.006 mmol, 57%), Ir^{III}(ttp)(p-C_6H_4)Ir^{III}(ttp) (0.6 mg, 0.0003 mmol, 3%), and Ir^{III}(ttp)CH_3 (0.5 mg, 0.0005 mmol, 5%).

(6) Reaction of Ir^{III}(ttp)(CO)Cl with PhCl (100 equiv) and K_2CO_3 (20 equiv). Ir^{III}(ttp)(CO)Cl (9.7 mg, 0.010 mmol), K_2CO_3 (29 mg, 0.21 mmol), PhCl (118 mg, 107 μL, 1.05 mmol), and benzene (1 mL) were heated at 200 °C under N_2 for 10 hours to give Ir^{III}(ttp)Ph (6.1 mg, 0.007 mmol, 62%). Ir^{III}(ttp)(p-C_6H_4)Ir^{III}(ttp) (2%, NMR yield) was also formed and its yield was estimated by using the yield of Ir^{III}(ttp)Ph and the pyrrole proton ratios of Ir^{III}(ttp)Ph and Ir^{III}(ttp)(p-C_6H_4)Ir^{III}(ttp) (~ 31 : 1) in the crude products by ^{1}H NMR spectroscopy.

(7) Reaction of Ir^{III}(ttp)(CO)Cl with PhCl (300 equiv) and K_2CO_3 (20 equiv). Ir^{III}(ttp)(CO)Cl (10.5 mg, 0.011 mmol), K_2CO_3 (31 mg, 0.23 mmol), PhCl (384 mg, 347 μL, 3.4 mmol), and benzene (1 mL) were heated at 200 °C under N_2 for 12 hours to give Ir^{III}(ttp)Ph (8.4 mg, 0.009 mmol, 79%) and Ir^{III}(ttp)(p-C_6H_4)Ir^{III}(ttp) (1%, NMR yield).

(8) Reaction of Ir^{III}(ttp)(CO)Cl with PhCl (200 equiv) and K_2CO_3 (20 equiv) at 200 °C.

(i) **K_2CO_3 (10 equiv).** Ir^{III}(ttp)(CO)Cl (9.8 mg, 0.011 mmol), K_2CO_3 (15 mg, 0.11 mmol), PhCl (239 mg, 216 μL, 2.1 mmol), and benzene (1 mL) were heated at 200 °C under N_2 for 19 hours to give Ir^{III}(ttp)Ph (6.3 mg, 0.007 mmol, 63%) and Ir^{III}(ttp)(p-C_6H_4)Ir^{III}(ttp) (2%, NMR yield).

(ii) **K_2CO_3 (20 equiv).** Ir^{III}(ttp)(CO)Cl (10.9 mg, 0.012 mmol), K_2CO_3 (33 mg, 0.24 mmol), PhCl (265 mg, 240 μL, 2.4 mmol), and benzene (1 mL) were heated at 200 °C under N_2 for 7 hours to give Ir^{III}(ttp)Ph (8.3 mg, 0.009 mmol, 75%) and Ir^{III}(ttp)(p-C_6H_4)Ir^{III}(ttp) (2%, NMR yield).

(iii) **K_2CO_3 (30 equiv).** Ir^{III}(ttp)(CO)Cl (9.7 mg, 0.010 mmol), K_2CO_3 (43.5 mg, 0.31 mmol),

PhCl (236 mg, 213 μL, 2.1 mmol), and benzene (1 mL) were heated at 200 $^\circ$C under N$_2$ for 11 hours to give Ir^{III}(ttp)Ph (6.3 mg, 0.007 mmol, 64%) and Ir^{III}(ttp)(p-C$_6$H$_4$)Ir^{III}(ttp) (2%, NMR yield).

(9) Reaction of Ir^{III}(ttp)(CO)Cl with PhCl (200 equiv) and K$_2$CO$_3$ (20 equiv) at 150 $^\circ$C.
Ir^{III}(ttp)(CO)Cl (9.8 mg, 0.011 mmol), K$_2$CO$_3$ (29 mg, 0.21 mmol), PhCl (239 mg, 216 μL, 2.1 mmol), and benzene (1 mL) were heated at 200 $^\circ$C under N$_2$ for 22 hours. The crude product was purified by column chromatography over alumina eluted with CH$_2$Cl$_2$/hexane (1:2) to give Ir^{III}(ttp)Ph (7.4 mg, 0.008 mmol, 74%) and Ir^{III}(ttp)(p-C$_6$H$_4$)Ir^{III}(ttp) (5%, NMR yield).

Scope of Base-Promoted Ar-Br Cleavage: Reactions of Various ArBr (1.1 equiv) with Ir^{III}(ttp)(CO)Cl and K$_2$CO$_3$ (20 equiv)

The experimental procedure of the reaction Ir^{III}(ttp)(CO)Cl with 4-bromoanisole and K$_2$CO$_3$ at 200 $^\circ$C was described as a typical example.

(1) Reaction with 4-Bromoanisole. Ir^{III}(ttp)(CO)Cl (20.0 mg, 0.022 mmol), K$_2$CO$_3$ (60 mg, 0.43 mmol), 4-bromoanisole (4.5 mg, 3.0 μL, 0.024 mmol), and benzene (2 mL) were degassed for three freeze-pump-thaw cycles in a Teflon screw capped tube. The reaction was then heated at 200 $^\circ$C under N$_2$ for 9 hours. The crude product was purified by column chromatography over alumina eluted with CH$_2$Cl$_2$/hexane (1:2) to give a deep brown solid of Ir^{III}(ttp)C$_6$H$_4$(p-OMe) (**8c**) (18.6 mg, 0.019 mmol, 89%). R$_f$ = 0.45 (CH$_2$Cl$_2$/hexane = 1 : 1). ^{1}H NMR (CDCl$_3$, 300 MHz) δ 0.46 (d, 2 H, J = 9.3 Hz), 2.68 (s, 12 H), 2.79 (s, 3 H), 4.41 (d, 2 H, J = 9.3 Hz), 7.51 (d, 8 H, J = 7.2 Hz), 8.00 (d, 8 H, J = 6.3 Hz), 8.56 (s, 8 H). ^{13}C NMR (CDCl$_3$, 75 MHz) δ 21.7, 54.1, 83.3, 109.3, 124.1, 127.6, 128.6, 131.5, 133.7, 134.2, 137.4, 138.8, 143.1, 153.8. HRMS (FABMS): Calcd for [C$_{55}$H$_{43}$N$_4$IrO]$^+$: m/z 968.3061. Found: m/z 968.3057. The single crystal for X-way crystallography was grown from CH$_2$Cl$_2$ / CH$_3$OH.

(2) Reaction with 4-Bromo-N,N-Dimethylaniline.

    (a) Without addition of PPh$_3$. Ir^{III}(ttp)(CO)Cl (20 mg, 0.022 mmol), K$_2$CO$_3$ (60 mg, 0.43 mmol,

20 equiv), 4-bromo-N,N-dimethylaniline (4.8 mg, 0.024 mmol, 1.1 equiv), and benzene (2 mL) were heated at 200 °C under N_2 for 6 hours to give a brown solid of Ir^{III}(ttp)C_6H_4(p-NMe$_2$) (**8b**) (16.5 mg, 0.017 mmol, 78%). R_f= 0.54 (CH$_2$Cl$_2$/hexane = 3 : 1). ^{1}H NMR (CDCl$_3$, 400 MHz) δ -2.37 (br, 2 H), -0.74 (br, 2 H), 1.31 (s, 6 H), 2.65 (s, 12 H), 7.28 (d, 4 H, J = 6.4 Hz), 7.29 (br, 4 H), 7.42 (d, 4 H, J = 7.1 Hz), 7.55 (br, 4 H), 7.81 (br, 8 H). ^{13}C NMR was not shown due to the broad C signals, resulting in difficulty in characterization. HRMS (FABMS): Calcd for [C$_{56}$H$_{46}$N$_5$Ir]$^+$: m/z 981.3377. Found: m/z 981.3400. X-ray crystallography of **8b** could not be successfully grown for further characterization.

(b) With addition of PPh$_3$. Ir^{III}(ttp)(CO)Cl (20.0 mg, 0.022 mmol), K$_2$CO$_3$ (60 mg, 0.43 mmol, 20 equiv), 4-bromo-N,N-Dimethylaniline (4.8 mg, 0.024 mmol), and benzene (2 mL) were heated at 200 °C under N_2 for 6 hours. PPh$_3$ (57 mg, 0.22 mmol) was then added under N_2 and the reaction was further heated at 120 °C for 30 minutes to give a reddish brown solid of Ir^{III}(ttp)(PPh$_3$)C$_6$H$_4$(p-NMe$_2$) (**8b$_1$**) (16.7 mg, 0.013 mmol, 62%). R_f= 0.37 (CH$_2$Cl$_2$/hexane = 2 : 1). ^{1}H NMR (CDCl$_3$, 300 MHz) δ 0.32 (dd, 2 H, $^3J_{HH}$ = 8.3 Hz, $^4J_{PH}$ = 5.7 Hz), 1.85 (s, 6 H), 2.66 (s, 12 H), 4.14 (dd, 6 H, $^3J_{PH}$ = 8.1 Hz, $^3J_{HH}$ = 8.1 Hz), 4.30 (d, 2 H, $^3J_{HH}$ = 7.5 Hz), 6.56 (t, 6 H, $^3J_{HH}$ = 6.9 Hz), 6.86 (t, 3 H, $^3J_{HH}$ = 7.2 Hz), 7.43 (d, 4 H, $^3J_{HH}$ = 8.4 Hz), 7.46 (d, 4 H, $^3J_{HH}$ = 8.7 Hz), 7.65 (d, 4 H, $^3J_{HH}$ = 7.5 Hz), 7.84 (d, 4 H, $^3J_{HH}$ = 7.2 Hz), 8.42 (s, 8 H). ^{13}C NMR (CDCl$_3$, 75 MHz) δ 21.6, 40.5, 109.7 (d, $^3J_{PC}$ = 6.8 Hz), 115.0 (d, $^2J_{PC}$ = 139 Hz), 122.8, 126.9 (d, $^3J_{PC}$ = 7.7 Hz), 127.0, 127.4, 127.7, 128.0, 128.9 (d, $^1J_{PC}$ = 24.4 Hz), 131.3 (d, $^2J_{PC}$ = 11.0 Hz), 131.6, 133.8, 134.6, 136.8, 139.3, 142.4, 143.8. HRMS (FABMS): Calcd for [C$_{74}$H$_{61}$N$_5$PIr]$^+$: m/z 1243.4288. Found: m/z 1243.4334.

(3) Reaction with 4-Bromo-*tert*-butylbenzene. Ir^{III}(ttp)(CO)Cl (20.0 mg, 0.022 mmol), K$_2$CO$_3$ (60 mg, 0.43 mmol), 4-bromo-*tert*-butylbenzene (5.1 mg, 4.1 μL, 0.024 mmol), and benzene (2.0 mL) were heated at 200 °C under N_2 for 15 hours to give a deep brown solid of Ir^{III}(ttp)C$_6$H$_4$(p-^{t}Bu) (**8d**) (18.5 mg, 0.019 mmol, 86%). R_f = 0.51 (CH$_2$Cl$_2$/hexane = 1 : 1). ^{1}H NMR (CDCl$_3$, 300 MHz) δ 0.35 (s, 9 H), 0.50 (d, 2 H, J = 8.7 Hz), 2.68 (s, 12 H), 4.73 (d, 2 H, J = 8.4 Hz), 7.51 (d, 8 H, J =

6.0 Hz), 8.01 (d, 8 H, J = 6.0 Hz), 8.56 (s, 8 H). ^{13}C NMR (CDCl$_3$, 75 MHz) δ 21.7, 30.7, 32.6, 90.5, 120.6, 124.2, 127.6, 128.1, 131.5, 133.7, 134.2, 137.4, 138.8, 142.3, 143.2. HRMS (FABMS): Calcd for [C$_{58}$H$_{49}$N$_4$Ir]$^+$: m/z 994.3581. Found: m/z 994.3567.

(4) Reaction with 4-Bromotoluene. Ir^{III}(ttp)(CO)Cl (20.0 mg, 0.022 mmol), K$_2$CO$_3$ (60 mg, 0.43 mmol), 4-bromotoluene (4.1 mg, 0.024 mmol), and benzene (2.0 mL) were heated at 200 ^{o}C under N$_2$ for 11 hours to give a deep brown solid of Ir^{III}(ttp)(*p*-Tol) (**8e**) (15.0 mg, 0.016 mmol, 73%). R$_f$ = 0.47 (CH$_2$Cl$_2$/hexane = 1 : 1). ^{1}H NMR (CDCl$_3$, 300 MHz) δ 0.48 (d, 2 H, J = 8.4 Hz), 1.10 (s, 3 H), 2.68 (s, 12 H), 4.58 (d, 2 H, J = 8.4 Hz), 7.51 (d, 8 H, J = 8.1 Hz), 8.01 (d, 8 H, J = 8.1 Hz), 8.57 (s, 8 H). ^{13}C NMR (CDCl$_3$, 75 MHz) δ 19.3, 21.7, 89.8, 124.2, 124.3, 127.6, 128.6, 129.2, 131.6, 133.8, 134.2, 137.4, 138.8, 143.1. HRMS (FABMS): Calcd for [C$_{55}$H$_{43}$N$_4$Ir]$^+$: m/z 952.3111. Found: m/z 952.3119. The single crystal for X-way crystallography was grown from CH$_2$Cl$_2$ / CH$_3$OH.

(5) Reaction with 1-Bromo-4-(trimethylsilyl)benzene. Ir^{III}(ttp)(CO)Cl (20.0 mg, 0.022 mmol), K$_2$CO$_3$ (60 mg, 0.43 mmol), 1-bromo-4-(trimethylsilyl)benzene (5.5 mg, 4.7 μL, 0.024 mmol), and benzene (2.0 mL) were heated at 200 ^{o}C under N$_2$ for 15 hours to give a deep brown solid of Ir^{III}(ttp)C$_6$H$_4$(*p*-SiMe$_3$) (**8f**) (17.5 mg, 0.017 mmol, 80%). R$_f$ = 0.50 (CH$_2$Cl$_2$/hexane = 1 : 1). ^{1}H NMR (CDCl$_3$, 300 MHz) δ -0.56 (s, 9 H), 0.55 (d, 2 H, J = 8.1 Hz), 2.68 (s, 12 H), 4.82 (d, 2 H, J = 8.4 Hz), 7.51 (d, 8 H, J = 8.4 Hz), 8.00 (d, 4 H, J = 6.0 Hz), 8.02 (d, 4 H, J = 6.1 Hz), 8.58 (s, 8 H). ^{13}C NMR (CDCl$_3$, 75 MHz) δ -1.5, 21.7, 97.4, 124.2, 127.6, 128.4, 128.7, 129.7, 131.6, 133.7, 134.2, 137.4, 138.8, 143.1. HRMS (FABMS): Calcd for [C$_{57}$H$_{49}$N$_4$SiIr]$^+$: m/z 1010.3350. Found: m/z 1010.3315. The single crystal for X-way crystallography was grown from CHCl$_3$ / EtOH.

(6) Reaction with *N*-(4-Bromophenyl)phthalimide. Ir^{III}(ttp)(CO)Cl (40.0 mg, 0.043 mmol), K$_2$CO$_3$ (119 mg, 0.87 mmol), *N*-(4-bromophenyl)phthalimide (14.4 mg, 0.048 mmol), and benzene (4.0 mL) were heated at 200 ^{o}C under N$_2$ for 27 hours to give a deep brown solid of Ir^{III}(ttp)C$_6$H$_4$(*p*-NPht) (**8g**) (31.9 mg, 0.029 mmol, 68%). R$_f$ = 0.48 (CH$_2$Cl$_2$/hexane = 2 : 1). ^{1}H NMR (CDCl$_3$, 300 MHz) δ 0.67 (d, 2 H, J = 8.7 Hz), 2.68 (s, 12 H), 4.80 (d, 2 H, J = 8.7 Hz),

7.50-7.54 (m, 12 H), 8.01 (d, 4 H, J = 6.9 Hz), 8.06 (d, 4 H, J = 6.9 Hz), 8.61 (s, 8 H). ^{13}C NMR (CDCl$_3$, 75 MHz) δ 21.7, 96.1, 120.6, 123.1, 124.0, 124.3, 127.5, 127.7, 129.5, 131.3, 131.6, 133.7, 134.3, 137.4, 138.7, 143.0, 143.5, 167.0. HRMS (FABMS): Calcd for [C$_{62}$H$_{44}$N$_5$O$_2$Ir]$^+$: m/z 1083.3119. Found: m/z 1083.3126.

(7) Reaction with 1-Bromo-4-fluorobenzene. Ir^{III}(ttp)(CO)Cl (19.8 mg, 0.021 mmol), K$_2$CO$_3$ (59 mg, 0.43 mmol), 1-bromo-4-fluorobenzene (4.1 mg, 2.6 μL, 0.024 mmol), and benzene (2.0 mL) were heated at 200 $^{\circ}$C under N$_2$ for 20 hours to give a deep brown solid of Ir^{III}(ttp)C$_6$H$_4$(p-F) **(8h)** (20.3 mg, 0.021 mmol, 99%). R$_f$ = 0.42 (CH$_2$Cl$_2$/hexane = 1 : 1). ^{1}H NMR (CDCl$_3$, 300 MHz) δ 0.44 (dd, 2 H, $^3J_{HH}$ = 8.7 Hz, $^4J_{HF}$ = 6.0 Hz), 2.68 (s, 12 H), 4.54 (dd, 2 H, $^3J_{HH}$ = 9.0 Hz, $^3J_{HF}$ = 9.0 Hz), 7.51 (d, 8 H, J = 7.8 Hz), 7.97 (d, 4 H, J = 8.0 Hz), 8.02 (d, 4 H, J = 8.0 Hz), 8.58 (s, 8 H). ^{13}C NMR (CDCl$_3$, 75 MHz) δ 21.7, 86.7, 110.0 (d, $^2J_{CF}$ = 19.6 Hz), 124.1, 127.6, 129.0 (d, $^3J_{CF}$ = 6.2 Hz), 131.6, 133.7, 134.2, 137.5, 138.7, 143.0, 158.4 (d, $^1J_{CF}$ = 236 Hz). HRMS (FABMS): Calcd for [C$_{54}$H$_{40}$N$_4$IrF]$^+$: m/z 956.2861. Found: m/z 956.2855.

(8) Reaction with 1,4-Dibromobenzene. Ir^{III}(ttp)(CO)Cl (21.4 mg, 0.023 mmol), K$_2$CO$_3$ (64 mg, 0.46 mmol), 1,4-dibromobenzene (6.0 mg, 0.025 mmol), and benzene (2.0 mL) were heated at 200 $^{\circ}$C under N$_2$ for 36 hours to give a deep brown solid of Ir^{III}(ttp)C$_6$H$_4$(p-Br) **(8i)** (17.9 mg, 0.018 mmol, 76%). R$_f$ = 0.52 (CH$_2$Cl$_2$/hexane = 1 : 1). ^{1}H NMR (CDCl$_3$, 300 MHz) δ 0.37 (d, 2 H, J = 8.7 Hz), 2.68 (s, 12 H), 4.85 (d, 2 H, J = 8.4 Hz), 7.52 (d, 8 H, J = 7.5 Hz), 7.99 (d, 4 H, J = 6.6 Hz), 8.02 (d, 4 H, J = 7.7 Hz), 8.59 (s, 8 H). ^{13}C NMR (CDCl$_3$, 75 MHz) δ 21.7, 94.1, 114.5, 124.0, 126.0, 127.7, 130.6, 131.6, 133.7, 134.2, 137.5, 138.6, 142.9. HRMS (FABMS): Calcd for [C$_{54}$H$_{40}$N$_4$BrIr]$^+$ ([M]$^+$): m/z 1016.2060. Found: m/z 1016.2055.

(9) Reaction with 1-Bromo-4-iodobenzene. Ir^{III}(ttp)(CO)Cl (21.5 mg, 0.023 mmol), K$_2$CO$_3$ (64 mg, 0.46 mmol), 1-bromo-4-iodobenzene (7.2 mg, 0.026 mmol), and benzene (2.0 mL) were heated at 200 $^{\circ}$C under N$_2$ for 19 hours to give a deep brown solid of Ir^{III}(ttp)C$_6$H$_4$(p-Br) **(8i)** (20.8 mg, 0.020 mmol, 88%).

(10) Reaction with 1-Bromo-4-chlorobenzene. Ir^{III}(ttp)(CO)Cl (20.9 mg, 0.023 mmol), K$_2$CO$_3$

(62 mg, 0.45 mmol), 1-bromo-4-chlorobenzene (4.8 mg, 0.025 mmol), and benzene (2.0 mL) were heated at 200 °C under N_2 for 1 day to give a deep brown solid of Ir^{III}(ttp)C_6H_4(p-Cl) (**8j**) (15.9 mg, 0.016 mmol, 72%). R_f = 0.45 (CH_2Cl_2/hexane = 1 : 1). ^{1}H NMR ($CDCl_3$, 300 MHz) δ 0.43 (d, 2 H, $^3J_{HH}$ = 9.0 Hz), 2.68 (s, 12 H), 4.72 (d, 2 H, $^3J_{HH}$ = 8.7 Hz), 7.52 (d, 8 H, $^3J_{HH}$ = 7.9 Hz), 7.98 (dd, 4 H, $^3J_{HH}$ = 8.5 Hz, $^4J_{HH}$ = 2.4 Hz), 8.01 (dd, 4 H, $^3J_{HH}$ = 7.9 Hz, $^4J_{HH}$ = 2.1 Hz), 8.59 (s, 8 H). ^{13}C NMR ($CDCl_3$, 75 MHz) δ 21.7, 92.9, 123.2, 124.1, 126.4, 127.7, 130.0, 131.6, 133.7, 134.2, 137.5, 138.7, 143.0. HRMS (FABMS): Calcd for $[C_{54}H_{40}N_4ClIr]^+$ ($[M]^+$): m/z 972.2565. Found: m/z 972.2563.

(11) Reaction with Methyl 4-Bromobenzoate. Ir^{III}(ttp)(CO)Cl (22.7 mg, 0.025mol), K_2CO_3 (68 mg, 0.49 mol), methyl 4-bromobenzoate (5.8 mg, 0.027 mmol), and benzene (2.0 mL) were heated at 200 °C under N_2 for 36 hours to give a deep brown solid of Ir^{III}(ttp)C_6H_4(p-CO_2Me) (**8k**) (20.6 mg, 0.021 mmol, 84%). R_f = 0.49 (CH_2Cl_2/hexane = 2 : 1). ^{1}H NMR ($CDCl_3$, 300 MHz) δ 0.57 (d, 2 H, J = 7.5 Hz), 2.68 (s, 12 H), 3.23 (s, 3 H), 5.32 (d, 2 H, J = 8.4 Hz), 7.53-7.54 (m, 8 H), 7.97 (d, 4 H, J = 8.2 Hz), 8.00 (d, 4 H, J = 8.2 Hz), 8.61 (s, 8 H). ^{13}C NMR ($CDCl_3$, 75 MHz) δ 21.7, 50.9, 88.9, 107.2, 121.8, 123.6, 123.9, 127.6, 127.7, 129.4, 131.6, 133.6, 134.3, 137.5, 138.6, 142.8, 167.0. HRMS (FABMS): Calcd for $[C_{56}H_{43}N_4O_2Ir]^+$ ($[M]^+$): m/z 996.3010. Found: m/z 996.3027.

(12) Reaction with 4-Bromoacetophenone. Ir^{III}(ttp)(CO)Cl (20.0 mg, 0.022 mmol), K_2CO_3 (60 mg, 0.43 mmol), 4-bromoacetophenone (4.7 mg, 0.024 mmol), and benzene (2.0 mL) were heated at 200 °C under N_2 for 19 hours to give a deep brown solid of Ir^{III}(ttp)C_6H_4(p-C(O)Me) (**8l**) (17.4 mg, 0.018 mmol, 82%). R_f = 0.36 (CH_2Cl_2/hexane = 1 : 1). ^{1}H NMR ($CDCl_3$, 300 MHz) δ 0.62 (d, 2 H, J = 8.4 Hz), 1.55 (s, 3 H), 2.68 (s, 12 H), 5.24 (d, 2 H, J = 8.4 Hz), 7.52 (d, 8 H, J = 8.1 Hz), 7.98 (d, 4 H, J = 8.1 Hz), 8.00 (d, 4 H, J = 7.8 Hz), 8.61 (s, 8 H). ^{13}C NMR ($CDCl_3$, 75 MHz) δ 21.7, 24.8, 109.8, 122.5, 123.9, 127.6, 129.4, 131.1, 131.6, 133.6, 134.2, 137.5, 138.6, 142.8, 197.7. HRMS (FABMS): Calcd for $[C_{56}H_{43}N_4IrO]^+$: m/z 980.3061. Found: m/z 980.3050.

(13) Reaction with 4-Bromobenzaldehyde. Ir^{III}(ttp)(CO)Cl (20.0 mg, 0.022 mmol), K_2CO_3 (60 mg, 0.43 mmol), 4-bromobenzaldehyde (4.4 mg, 0.024 mmol), and benzene (2.0 mL) were heated

at 200 °C under N$_2$ for 11 hours to form a brown precipitate. PPh$_3$ (57 mg, 0.22 mmol) was then added under N$_2$ and the reaction was further heated at 120 °C for 30 minutes to give a reddish brown solid of Ir^{III}(ttp)(PPh$_3$)C$_6$H$_4$(p-CHO) (**8m**) (16.2 mg, 0.013 mmol, 61%). R$_f$ = 0.64 (CH$_2$Cl$_2$/hexane = 1 : 1). ^{1}H NMR (CDCl$_3$, 300 MHz) δ 0.49 (dd, 2 H, $^3J_{HH}$ = 8.1 Hz, $^4J_{PH}$ = 5.1 Hz), 2.65 (s, 12 H), 4.09 (dd, 6 H, $^3J_{HH}$ = 8.1 Hz, $^3J_{PH}$ = 8.1 Hz), 5.17 (dd, 2 H, $^3J_{HH}$ = 8.4 Hz, $^4J_{HH}$ = 1.8 Hz), 6.54 (td, 6 H, $^3J_{HH}$ = 7.5 Hz, $^4J_{HH}$ = 1.8 Hz), 6.86 (t, 3 H, $^3J_{HH}$ = 8.4 Hz), 7.42 (d, 4 H, $^3J_{HH}$ = 7.9 Hz), 7.46 (d, 4 H, $^3J_{HH}$ = 8.1 Hz), 7.62 (dd, 4 H, $^3J_{HH}$ = 7.4 Hz, $^4J_{HH}$ = 1.4 Hz), 7.76 (dd, 4 H, $^3J_{HH}$ = 7.6 Hz, $^4J_{HH}$ = 1.4 Hz), 8.46 (s, 8 H), 8.61 (s, 1 H). ^{13}C NMR (CDCl$_3$, 100 MHz) δ 21.6, 122.8, 124.0 (d, $^3J_{PC}$ = 7 Hz), 127.0 (d, $^3J_{PC}$ = 8 Hz), 127.1, 127.5, 128.2, 128.4 (d, $^1J_{PC}$ = 34 Hz), 128.9, 130.8 (d, $^2J_{PC}$ = 11 Hz), 131.8, 133.7, 134.5, 137.1, 138.9, 142.2, 142.7 (d, $^2J_{PC}$ = 136 Hz), 192.1. HRMS (FABMS): Calcd for [C$_{73}$H$_{56}$N$_4$POIr]$^+$ ([M]$^+$): m/z 1228.3815. Found: m/z 1228.3857.

(14) Reaction with 4-Bromobenzotrifluoride. Ir^{III}(ttp)(CO)Cl (20.0 mg, 0.022 mmol), K$_2$CO$_3$ (60 mg, 0.43 mmol), 4-bromobenzotrifluoride (5.4 mg, 3.3 μL, 0.024 mmol), and benzene (2 mL) were heated at 200 °C under N$_2$ for 1 day to give a deep brown solid of Ir^{III}(ttp)C$_6$H$_4$(p-CF$_3$) (**8n**) (15.7 mg, 0.016 mmol, 72%). R$_f$ = 0.44 (CH$_2$Cl$_2$/hexane = 1 : 1). ^{1}H NMR (CDCl$_3$, 300 MHz) δ 0.43 (d, 2 H, J = 8.7 Hz), 2.68 (s, 12 H), 4.72 (d, 2 H, J = 8.4 Hz), 7.52 (d, 8 H, J = 7.8 Hz), 7.99 (d, 4 H, J = 6.9 Hz), 8.01 (d, 4 H, J = 5.7 Hz), 8.59 (s, 8 H). ^{13}C NMR (CDCl$_3$, 100 MHz) δ 21.7, 102.7, 119.5 (q, ^3J = 3.6 Hz), 122.1 (q, ^2J = 31.5 Hz), 124.0, 124.1 (q, ^1J = 269.7 Hz), 127.6, 127.7, 129.3, 131.7, 133.7, 134.2, 137.6, 138.6, 142.9. HRMS (FABMS): Calcd for [C$_{55}$H$_{40}$N$_4$F$_3$Ir]$^+$ ([M]$^+$): m/z 1006.2829. Found: m/z 1006.2825.

(15) Reaction with 4-Bromobenzonitrile. Ir^{III}(ttp)(CO)Cl (30.0 mg, 0.032 mmol), K$_2$CO$_3$ (90 mg, 0.65 mmol), 4-bromobenzonitrile (6.5 mg, 0.036 mmol), and benzene (3.0 mL) were heated at 200 °C under N$_2$ for 1 day. PPh$_3$ (57 mg, 0.22 mmol) was then added and the reaction was further heated at 120 °C for 30 minutes to give a reddish brown solid of Ir^{III}(ttp)(PPh$_3$)C$_6$H$_4$(p-CN) (**8o**) (24.7 mg, 0.0201 mmol, 62%). R$_f$ = 0.64 (CH$_2$Cl$_2$/hexane = 1 : 1). ^{1}H NMR (CDCl$_3$, 300 MHz) δ

0.38 (dd, 2 H, $^3J_{HH}$ = 8.3 Hz, $^4J_{PH}$ = 5.3 Hz,), 2.66 (s, 12 H), 4.08 (dd, 6 H, $^3J_{PH}$ = 8.4 Hz, $^3J_{HH}$ = 8.3 Hz), 4.92 (d, 2 H, $^3J_{HH}$ = 8.0 Hz), 6.54 (t, 6 H, $^3J_{HH}$ = 7.6 Hz), 6.87 (t, 3 H, $^3J_{HH}$ = 7.4 Hz), 7.43 (d, 4 H, $^3J_{HH}$ = 7.8 Hz), 7.46 (d, 4 H, $^3J_{HH}$ = 8.0 Hz), 7.61 (d, 4 H, $^3J_{HH}$ = 7.2 Hz), 7.76 (d, 4 H, $^3J_{HH}$ = 7.6 Hz), 8.46 (s, 8 H). ^{13}C NMR (CDCl$_3$, 75 MHz) δ 21.6, 102.2, 120.0, 122.8, 125.9 (d, $^3J_{PC}$ = 6.8 Hz), 127.0 (d, $^3J_{PC}$ = 8.0 Hz), 127.2, 127.5, 128.2, 128.3 (d, $^1J_{PC}$ = 27.5 Hz), 128.9, 130.8 (d, $^2J_{PC}$ = 10.8 Hz), 131.9, 133.7, 134.5, 137.1, 138.8, 142.1. HRMS (FABMS): Calcd for [C$_{73}$H$_{55}$N$_5$PIr]$^+$ ([M]$^+$): m/z 1225.3819. Found: m/z 1225.3818.

(16) Reaction with 4-Bromo-nitrobenzene. Ir^{III}(ttp)(CO)Cl (20.0 mg, 0.022 mmol), K$_2$CO$_3$ (60 mg, 0.43 mmol), 4-bromo-nitrobenzene (4.8 mg, 0.024 mmol), and benzene (2.0 mL) were heated at 200 °C under N$_2$ for 6 hours to give an orange-brown solid of Ir^{III}(ttp)C$_6$H$_4$(p-NO$_2$) **(8p)** (13.4 mg, 0.014 mmol, 63%). R$_f$ = 0.51 (CH$_2$Cl$_2$/hexane = 2 : 1). ^{1}H NMR (CDCl$_3$, 300 MHz) δ 0.64 (d, 2 H, $^3J_{HH}$ = 9.3 Hz), 2.69 (s, 12 H), 5.55 (d, 2 H, $^3J_{HH}$ = 9.3 Hz), 7.52-7.55 (m, 8 H), 7.97 (dd, 4 H, $^3J_{HH}$ = 7.3 Hz, $^4J_{HH}$ = 2.3 Hz), 8.02 (dd, 4 H, $^3J_{HH}$ = 7.4 Hz, $^4J_{HH}$ = 2.1 Hz), 8.65 (s, 8 H). ^{13}C NMR (THF-d_8, 75 MHz) δ 21.9, 117.6, 121.7, 124.5, 128.4, 128.7, 131.8, 132.4, 134.8, 135.3, 138.6, 140.1, 142.5, 143.9. HRMS (FABMS): Calcd for [C$_{54}$H$_{40}$N$_5$O$_2$Ir]$^+$: m/z 983.2806. Found: m/z 983.2791. The single crystal for X-ray crystallography was grown from CH$_2$Cl$_2$ / CH$_3$OH.

(17) Reaction with 2-Bromonaphthalene. Ir^{III}(ttp)(CO)Cl (20.0 mg, 0.022 mmol), K$_2$CO$_3$ (60 mg, 0.43 mmol), 2-bromonaphthalene (4.9 mg, 0.024 mmol), and benzene (2 mL) were heated at 200 °C under N$_2$ for 19 hours to give a deep brown solid of Ir^{III}(ttp)(2-naphthyl) **(8q)** (18.1 mg, 0.018 mmol, 85%). R$_f$ = 0.46 (CH$_2$Cl$_2$/hexane = 1 : 1). ^{1}H NMR (CDCl$_3$, 400 MHz) δ 0.74 (dd, 1 H, $^3J_{HH}$ = 8.9 Hz, $^4J_{HH}$ = 1.7 Hz), 0.92 (s, 1 H), 2.68 (s, 12 H), 5.21 (d, 1 H, $^3J_{HH}$ = 9.0 Hz), 6.09 (d, 1 H, $^3J_{HH}$ = 9.0 Hz), 6.50-6.90 (m, 3 H), 7.51 (d, 4 H, $^3J_{HH}$ = 7.0 Hz), 7.52 (d, 4 H, $^3J_{HH}$ = 6.9 Hz), 8.01 (d, 4 H, $^3J_{HH}$ = 7.9 Hz), 8.03 (d, 4 H, $^3J_{HH}$ = 7.9 Hz), 8.58 (s, 8 H). ^{13}C NMR (CDCl$_3$, 75 MHz) δ 21.7, 93.7, 121.1, 122.4, 123.1, 124.1, 125.2, 125.8, 127.2, 127.6, 127.9, 128.5, 129.9, 131.6, 133.7, 134.2, 137.4, 138.8, 143.1. HRMS (FABMS): Calcd for [C$_{58}$H$_{43}$N$_4$Ir]$^+$ ([M]$^+$): m/z 988.3111. Found: m/z 988.3115.

(18) Reaction with 3-Bromoanisole. $Ir^{III}(ttp)(CO)Cl$ (19.8 mg, 0.021 mmol), K_2CO_3 (59 mg, 0.43 mmol), 3-bromoanisole (2.5 mg, 0.024 mmol, 1.7 μL), and benzene (2 mL) were heated at 200 °C under N_2 for 17 hours to give a deep brown solid of $Ir^{III}(ttp)C_6H_4(m\text{-OMe})$ (**8u**) (17.3 mg, 0.018 mmol, 83%). R_f = 0.49 (CH_2Cl_2/hexane = 1 : 1). ^1H NMR ($CDCl_3$, 400 MHz) δ 0.21 (d, 1 H, J = 8.3 Hz), 2.59 (s, 3 H), 2.61 (s, 1 H), 2.68 (s, 12 H), 4.60 (t, 1 H, J = 8.1 Hz), 4.82 (dd, 1 H, ^3J = 7.9 Hz, ^4J = 1.7 Hz), 7.52 (d, 8 H, J = 7.0 Hz), 8.01 (d, 8 H, J = 7.7 Hz), 8.59 (s, 8 H). ^{13}C NMR ($CDCl_3$, 100 MHz) δ 21.7, 53.8, 96.2, 107.0, 113.5, 121.7, 123.1, 124.1, 127.61, 127.64, 131.6, 133.9, 134.1, 137.4, 138.8, 143.1, 153.0. HRMS (FABMS): Calcd for $[C_{55}H_{43}N_4OIr]^+$ ($[M]^+$): m/z 968.3061. Found: m/z 968.3042.

(19) Reaction with 3-Bromotoluene. $Ir^{III}(ttp)(CO)Cl$ (19.4 mg, 0.021 mmol), K_2CO_3 (58 mg, 0.42 mmol), 3-bromotoluene (4.0 mg, 0.023 mmol, 2.8 μL), and benzene (2 mL) were heated at 200 °C under N_2 for 14 hours to give a deep brown solid of $Ir^{III}(ttp)(m\text{-Tol})$ (**8v**) (17.0 mg, 0.018 mmol, 85%). R_f = 0.49 (CH_2Cl_2/hexane = 1 : 1). ^1H NMR ($CDCl_3$, 400 MHz) δ 0.31 (s, 1 H), 0.42 (d, 1 H, J = 8.3 Hz), 0.86 (s, 3 H), 2.68 (s, 12 H), 4.60 (t, 1 H, J = 8.0 Hz), 5.04 (d, 1 H, J = 7.1 Hz), 7.50-7.53 (m, 8 H), 8.01 (d, 8 H, J = 8.2 Hz), 8.57 (s, 8 H). ^{13}C NMR ($CDCl_3$, 100 MHz) δ 20.1, 21.7, 94.5, 121.2, 122.7, 124.2, 125.9, 127.6, 129.8, 131.5, 131.9, 133.7, 134.2, 137.4, 138.9, 143.1. HRMS (FABMS): Calcd for $[C_{55}H_{43}N_4Ir]^+$ ($[M]^+$): m/z 952.3111. Found: m/z 952.3100.

(20) Reaction with 3-Bromo-nitrobenzene. $Ir^{III}(ttp)(CO)Cl$ (19.6 mg, 0.021 mmol), K_2CO_3 (59 mg, 0.42 mmol), 3-bromo-nitrobenzene (4.7 mg, 0.023 mmol), and benzene (2 mL) were heated at 200 °C under N_2 for 16 hours to give a deep brown solid of $Ir^{III}(ttp)C_6H_4(m\text{-NO}_2)$ (**8w**) (17.5 mg, 0.018 mmol, 84%). R_f = 0.51 (CH_2Cl_2/hexane = 1 : 1). ^1H NMR ($CDCl_3$, 400 MHz) δ 0.80 (d, 1 H, ^3J = 8.2 Hz), 1.29 (t, 1 H, ^4J = 1.8 Hz), 2.69 (s, 12 H), 4.83 (t, 1 H, ^3J = 8.1 Hz), 6.09 (dd, 1 H, ^3J = 8.0 Hz, ^4J = 1.8 Hz), 7.54 (d, 8 H, J = 7.7 Hz), 8.03 (d, 4 H, J = 6.9 Hz), 8.05 (d, 4 H, J = 7.6 Hz), 8.64 (s, 8 H). ^{13}C NMR ($CDCl_3$, 100 MHz) δ 21.7, 96.5, 115.4, 123.2, 123.4, 124.0, 127.6, 127.8, 131.7, 133.6, 134.3, 135.9, 137.6, 138.5, 142.4, 142.8. HRMS (FABMS): Calcd for $[C_{54}H_{40}N_5O_2Ir]^+$ ($[M]^+$): m/z 983.2806. Found: m/z 983.2803.

Scope of Base-Promoted Aryl C–I Cleavage: Reactions of Various 4-Substituted Aryl Bromides (1.1 equiv) with Ir^{III}(ttp)(CO)Cl and NaOH (20 equiv)

The experimental procedure of the reaction Ir^{III}(ttp)(CO)Cl with 4-iodoanisole (1.1 equiv) and NaOH (20 equiv) at 150 °C was described as a typical example.

(1) Reaction with 4-Iodoanisole. Ir^{III}(ttp)(CO)Cl (10.0 mg, 0.011 mmol), NaOH (8.7 mg, 0.22 mmol), 4-iodoanisole (2.8 mg, 0.012 mmol), and benzene (1 mL) were degassed for three freeze-pump-thaw cycles in a Teflon screw capped tube. The reaction was then heated at 150 °C under N$_2$ for 20 hours. The crude product was purified by column chromatography over alumina eluted with CH$_2$Cl$_2$/hexane (1:2) to give Ir^{III}(ttp)C$_6$H$_4$(*p*-OMe) (**8c**) (9.3 mg, 0.010 mmol, 89%).

(2) Reaction with 4-Iodotoluene. Ir^{III}(ttp)(CO)Cl (10.1 mg, 0.011 mmol), NaOH (8.7 mg, 0.22 mmol), 4-iodotoluene (2.6 mg, 0.012 mmol), and benzene (2 mL) were heated at 200 °C under N$_2$ for 17 hours to give Ir^{III}(ttp)(*p*-Tol) (**8e**) (8.7 mg, 0.0009 mmol, 84%).

(3) Reaction with 1-Fluoro-4-iodobenzene. Ir^{III}(ttp)(CO)Cl (9.8 mg, 0.011 mmol), NaOH (8.5 mg, 0.21 mmol), 1-fluoro-4-iodobenzene (2.6 mg, 1.4 μL, 0.012 mmol), and benzene (2 mL) were heated at 150 °C under N$_2$ for 1 day to give Ir^{III}(ttp)C$_6$H$_4$(*p*-F) (**8h**) (9.7 mg, 0.010 mmol, 96%).

(4) Reaction with 1-Bromo-4-iodobenzene. Ir^{III}(ttp)(CO)Cl (10.1 mg, 0.011 mmol), NaOH (8.7 mg, 0.22 mmol), 1-bromo-4-iodobenzene (3.4 mg, 0.012 mmol), and benzene (2 mL) were heated at 150 °C under N$_2$ for 12 hours to give deep brown solids of Ir^{III}(ttp)C$_6$H$_4$(*p*-Br) (**8i**) (8.6 mg, 0.008 mmol, 77%), Ir^{III}(ttp)C$_6$H$_4$(*p*-I) (**8r**) (0.4 mg, 0.0004 mmol, 3%), and Ir^{III}(ttp)(*p*-C$_6$H$_4$)Ir^{III}(ttp) (**9a**) (1%, NMR yield). The 3 products were isolated in a single fraction and their ratio was estimated from their pyrrole proton signal ratio in the mixed products by ^{1}H NMR spectroscopy.

Characterization of Ir^{III}(ttp)C$_6$H$_4$(*p*-I) (8r): R$_f$ = 0.50 (CH$_2$Cl$_2$/hexane = 1 : 1). ^{1}H NMR (CDCl$_3$, 300 MHz) δ 0.23 (d, 2 H, *J* = 8.7 Hz), 2.68 (s, 12 H), 4.98 (d, 2 H, *J* = 8.4 Hz), 7.52 (d, 8 H, *J* = 7.8 Hz), 7.99 (d, 8 H, *J* = 6.6 Hz), 8.59 (s, 8 H). ^{13}C NMR (CDCl$_3$, 100 MHz) δ 21.7, 85.4, 98.9, 123.7, 127.6, 131.2, 131.5, 133.7, 134.3, 137.4, 138.7, 142.7. HRMS (FABMS): Calcd for

$[C_{54}H_{40}N_4IIr]^+$: m/z 1064.1921. Found: m/z 1064.1927.

(5) Reaction with 1,4-Diiodobenzene. $Ir^{III}(ttp)(CO)Cl$ (9.1 mg, 0.010 mmol), NaOH (7.9 mg, 0.20 mmol), 1,4-diiodobenzene (3.6 mg, 0.011 mmol), and benzene (1 mL) were heated at 200 °C under N_2 for 9 hours to give $Ir^{III}(ttp)C_6H_4(p\text{-}I)$ **(8r)** (9.4 mg, 0.009 mmol, 90%) and $Ir^{III}(ttp)(p\text{-}C_6H_4)Ir^{III}(ttp)$ **(9a)** (0.5 mg, 0.0002 mmol, 3%).

(6) Reaction with 4-Iodo-acetophenone. $Ir^{III}(ttp)(CO)Cl$ (9.3 mg, 0.010 mmol), NaOH (8.0 mg, 0.20 mmol), 4-iodo-acetophenone (2.7 mg, 0.011 mmol), and benzene (1 mL) were heated at 200 °C under N_2 for 12 hours to give $Ir^{III}(ttp)C_6H_4(p\text{-}(CO)Me)$ **(8l)** (8.0 mg, 0.008 mmol, 81%).

(7) Reaction with 4-Iodo-nitrobenzene. $Ir^{III}(ttp)(CO)Cl$ (10.1 mg, 0.011 mmol), NaOH (8.7 mg, 0.22 mmol), 4-iodo-nitrobenzene (3 mg, 0.012 mmol), and benzene (2 mL) were heated at 200 °C under N_2 for 15 hours to give $Ir^{III}(ttp)C_6H_4(p\text{-}NO_2)$ **(8p)** (10.5 mg, 0.011 mmol, 98%).

Scope of Base-Promoted Aryl C-Cl Cleavage: Reactions of 4-Substituted Aryl Chlorides (200 equiv) with $Ir^{III}(ttp)(CO)Cl$ and K_2CO_3 (20 equiv)

The experimental procedure of the reaction $Ir^{III}(ttp)(CO)Cl$ with 4-chloroanisole (200 equiv) and K_2CO_3 (20 equiv) at 150 °C was described as a typical example.

(1) Reaction with 4-Chloroanisole. $Ir^{III}(ttp)(CO)Cl$ (9.6 mg, 0.010 mmol), K_2CO_3 (29 mg, 0.21 mmol, 20 equiv), 4-chloroanisole (296 mg, 254 μL, 2.1 mmol), and benzene (1 mL) were degassed for three freeze-pump-thaw cycles in a Teflon screw capped tube. The reaction was then heated at 150 °C under N_2 for 36 hours. The crude product was purified by column chromatography over alumina eluted with CH_2Cl_2/hexane (1:2) to give $Ir^{III}(ttp)C_6H_4(p\text{-}OMe)$ **(8c)** (7.6 mg, 0.008 mmol, 76%) and $Ir^{III}(ttp)CH_3$[3b] **(10)** (0.3 mg, 0.0003 mmol, 3%).

(2) Reaction with 4-Chlorotoluene. $Ir^{III}(ttp)(CO)Cl$ (9.5 mg, 0.010 mmol), K_2CO_3 (28 mg, 0.21 mmol, 20 equiv), 4-chlorotoluene (260 mg, 243 μL, 2.1 mmol, 200 equiv), and benzene (1 mL) were heated at 150 °C under N_2 for 36 hours to give deep brown solids of $Ir^{III}(ttp)(p\text{-}Tol)$ **(8e)** (3.1 mg, 0.003 mmol, 32%), $Ir^{III}(ttp)Bn(p\text{-}Cl)$ **(11)** (1.8 mg, 0.002 mmol, 18%), and $Ir^{III}(ttp)CH_3$ (0.3

mg, 0.0003 mmol, 3%). **Characterization of Ir^{III}(ttp)Bn(p-Cl) (11):** R_f = 0.67 (CH$_2$Cl$_2$/hexane = 1 : 1). ^{1}H NMR (CDCl$_3$, 300 MHz) δ -4.02 (s, 2 H), 2.69 (s, 12 H), 3.04 (d, 2 H, J = 8.4 Hz), 5.84 (d, 2 H, J = 8.4 Hz), 7.53 (d, 4 H, J = 7.8 Hz), 7.55 (d, 4 H, J = 8.1 Hz), 7.94 (d, 4 H, J = 7.5 Hz), 8.02 (d, 4 H, J = 7.8 Hz), 8.49 (d, 8 H). ^{13}C NMR (CDCl$_3$, 75 MHz) δ -15.7, 21.7, 124.1, 125.3, 126.2, 127.7, 131.4, 133.7, 133.9, 137.3, 138.8, 140.3, 143.2. HRMS (FABMS): Calcd for [C$_{55}$H$_{42}$N$_4$ClIr]$^+$ ([M]$^+$): m/z 986.2722. Found: m/z 986.2730.

(3) Reaction with 1-Chloro-4-fluorobenzene. Ir^{III}(ttp)(CO)Cl (10.4 mg, 0.011 mmol), K$_2$CO$_3$ (31 mg, 0.23 mmol, 20 equiv), 1-chloro-4-fluorobenzene (294 mg, 240 μL, 2.3 mmol), and benzene (1 mL) were heated at 150 ^{o}C under N$_2$ for 36 hours to give Ir^{III}(ttp)C$_6$H$_4$(p-F) (**8h**) (7.2 mg, 0.008 mmol, 67%).

(4) Reaction with 1,4-Dichlorobenzene. Ir^{III}(ttp)(CO)Cl (10.7 mg, 0.012 mmol), K$_2$CO$_3$ (32 mg, 0.23 mmol, 20 equiv), 1,4-dichlorobenzene (340 mg, 2.3 mmol), and benzene (1 mL) were heated at 150 ^{o}C under N$_2$ for 3.5 days to give Ir^{III}(ttp)C$_6$H$_4$(p-Cl) (**8j**) (11.2 mg, 0.012 mmol, 100%).

(5) Reaction with Methyl 4-Chlorobenzoate. Ir^{III}(ttp)(CO)Cl (10.2 mg, 0.011 mmol), K$_2$CO$_3$ (30.5 mg, 0.22 mmol, 20 equiv), methyl 4-chlorobenzoate (376 mg, 2.2 mmol), and benzene (1 mL) were heated at 150 ^{o}C under N$_2$ for 46 hours to give Ir^{III}(ttp)C$_6$H$_4$(p-C(O)Me) (**8k**) (7.7 mg, 0.008 mmol, 70%) and Ir^{III}(ttp)CH$_3$ (0.3 mg, 0.0003 mmol, 3%).

(6) Reaction with 4-Chlorobenzaldehyde. Ir^{III}(ttp)(CO)Cl (10.8 mg, 0.012 mmol), K$_2$CO$_3$ (32 mg, 0.023 mmol, 20 equiv), 4-chlorobenzaldehyde (328 mg, 2.3 mmol), and benzene (1 mL) were heated at 150 ^{o}C under N$_2$ for 22 hours. PPh$_3$ (30.6 mg, 0.12, 10 equiv) was then added under N$_2$ and the reaction was further heated at 120 ^{o}C for 1 hour to give Ir^{III}(ttp)(PPh$_3$)C$_6$H$_4$(p-CHO) (**8m**) (9.9 mg, 0.008 mmol, 69%) and Ir^{III}(ttp)(PPh$_3$)(C(O)C$_6$H$_4$(p-Cl)) (**12**) (<1%).

(7) Reaction with 4-Chlorobenzotrifluoride. Ir^{III}(ttp)(CO)Cl (10.6 mg, 0.011 mmol), K$_2$CO$_3$ (33 mg, 0.23 mmol, 20 equiv), 4-chlorobenzotrifluoride (414 mg, 2.3 mmol), and benzene (1 mL) were heated at 150 ^{o}C under N$_2$ for 7 days to give Ir^{III}(ttp)C$_6$H$_4$(p-CF$_3$) (**8n**) (7.9 mg, 0.008 mmol, 68%).

(8) Reaction with 4-Chlorobenzonitrile. Ir^{III}(ttp)(CO)Cl (10.6 mg, 0.011 mmol), K$_2$CO$_3$ (32 mg,

0.23 mmol, 20 equiv), 4-chlorobenzonitrile (315.6 mg, 2.3 mmol, 200 equiv), and benzene (1 mL) were heated at 150 °C under N_2 for 1 day. PPh$_3$ (30.1 mg, 0.11, 10 equiv) was then added under N_2 and the reaction was further heated at 120 °C for 1 hour. The crude product was purified by column chromatography over alumina eluted with CH_2Cl_2/hexane (1:2) to give Ir^{III}(ttp)(PPh$_3$)C$_6$H$_4$(p-CN) (8o) (7.3 mg, 0.006 mmol, 52%).

Preparations of 1,4-Di-Iridium-Porphyrin Substituted Benzene [Ir^{III}(ttp)(p-C$_6$H$_4$)Ir^{III}(ttp)] (9a)

(A) From 1,4-Diiodobenzene

(1) Conversion of 1,4-Diiodobenzene to Ir^{III}(ttp)C$_6$H$_4$(p-I). Ir^{III}(ttp)(CO)Cl (50.0 mg, 0.054 mmol), K_2CO_3 (149 mg, 1.08 mmol, 20 equiv), 1,4-diiodobenzene (178.4 mg, 0.54 mmol, 10 equiv), and benzene (4 mL) were heated at 200 °C under N_2 for 11 hours. The crude product was purified by column chromatography over alumina eluted with CH_2Cl_2/hexane (1:2) to give Ir^{III}(ttp)C$_6$H$_4$(p-I) (8r) (53.2 mg, 0.050 mmol, 92%).

(2) Conversion of Ir^{III}(ttp)C$_6$H$_4$(p-I) to Ir^{III}(ttp)(p-C$_6$H$_4$)Ir^{III}(ttp). Ir^{III}(ttp)C$_6$H$_4$(p-I) (50.0 mg, 0.047 mmol), K_2CO_3 (130 mg, 0.94 mmol, 20 equiv), Ir^{III}(ttp)(CO)Cl (48.1 mg, 0.052 mmol, 1.1 equiv), and benzene (3 mL) were heated at 200 °C under N_2 for 24 hours. The crude product was purified by column chromatography over alumina eluted with CH_2Cl_2/hexane (1:1) to give Ir^{III}(ttp)(p-C$_6$H$_4$)Ir^{III}(ttp) (9a) (65.9 mg, 0.037 mmol, 78%).

(B) From 1,4-Dibromobenzene: Conversion of Ir^{III}(ttp)C$_6$H$_4$(p-Br) to Ir^{III}(ttp)(p-C$_6$H$_4$)Ir^{III}(ttp). Ir^{III}(ttp)C$_6$H$_4$(p-Br) (prepared from the reaction of Ir^{III}(ttp)(CO)Cl with 1,4-dibromobenzene (1.1 equiv) and K_2CO_3) (50 mg, 0.049 mmol), K_2CO_3 (136 mg, 0.98 mmol, 20 equiv), Ir^{III}(ttp)(CO)Cl (49.8 mg, 0.054 mmol, 1.1 equiv), and benzene (3 mL) were heated at 200 °C under N_2 for 14 hours to give Ir^{III}(ttp)(p-C$_6$H$_4$)Ir^{III}(ttp) (9a) (54.2 mg, 0.029 mmol, 59%).

Preparations of 4,4'-Di-Iridium-Porphyrin Substituted Biphenyl [Ir^{III}(ttp)(p-C$_6$H$_4$)$_2$$Ir^{III}$(ttp)]

(9b)

(A) From 4,4'-Diiodobiphenyl

(1) Conversion of 4,4'-Diiodobiphenyl to Ir^{III}(ttp)(p-C$_6$H$_4$)$_2$(p-I). Ir^{III}(ttp)(CO)Cl (50.0 mg, 0.054 mmol), K$_2$CO$_3$ (149 mg, 1.08 mmol, 20 equiv), 4,4'-diiodobiphenyl (107 mg, 0.32 mmol, 6 equiv), and benzene (3 mL) were heated at 200 °C under N$_2$ for 24 hours. The crude product was purified by column chromatography over alumina eluted with CH$_2$Cl$_2$/hexane (1:2) to give a deep brown solid of Ir^{III}(ttp)(p-C$_6$H$_4$)$_2$(p-I) (**8s**) (46.8 mg, 0.041 mmol, 76%). R$_f$ = 0.57 (CH$_2$Cl$_2$/hexane = 2 : 1). ^{1}H NMR (CDCl$_3$, 300 MHz) δ 0.63 (d, 2 H, J = 8.4 Hz), 2.68 (s, 12 H), 4.95 (d, 2 H, J = 8.7 Hz), 6.28 (d, 2 H, J = 8.4 Hz), 7.14 (d, 2 H, J = 8.4 Hz), 7.51 (d, 4 H, J = 6.9 Hz), 7.53 (d, 4 H, J = 6.9 Hz), 8.01 (d, 8 H, J = 7.5 Hz), 8.60 (s, 8 H). ^{13}C NMR of Ir^{III}(ttp)(p-C$_6$H$_4$)$_2$(p-I) could not be obtained due to its poor solubility in CDCl$_3$ and THF-d_8. HRMS (FABMS): Calcd for [C$_{60}$H$_{44}$N$_4$IIr]$^+$ ([M]$^+$): m/z 1140.2234. Found: m/z 1140.2277.

(2) Conversion of Ir^{III}(ttp)(p-C$_6$H$_4$)$_2$(p-I) to Ir^{III}(ttp)(p-C$_6$H$_4$)$_2$Ir^{III}(ttp). Ir^{III}(ttp)(p-C$_6$H$_4$)$_2$(p-I) (50 mg, 0.044 mmol), K$_2$CO$_3$ (121 mg, 0.88 mmol, 20 equiv), Ir^{III}(ttp)(CO)Cl (44.7 mg, 0.048 mmol, 1.1 equiv), and benzene (3 mL) were heated at 200 °C under N$_2$ for 19 hours. The crude product was purified by column chromatography over alumina eluted with CH$_2$Cl$_2$/hexane (1:1) to give a deep brown solid of Ir^{III}(ttp)(p-C$_6$H$_4$)$_2$Ir^{III}(ttp) (**9b**) (58.4 mg, 0.031 mmol, 71%). R$_f$ = 0.51 (CH$_2$Cl$_2$/hexane = 2 : 1). ^{1}H NMR (CDCl$_3$, 300 MHz) δ 0.06 (d, 4 H, J = 8.7 Hz), 2.62 (s, 24 H), 3.93 (d, 4 H, J = 8.7 Hz), 7.38 (d, 8 H, J = 7.7 Hz), 7.43 (d, 8 H, J = 7.6 Hz), 7.74 (d, 8 H, J = 7.7 Hz), 7.89 (d, 8 H, J = 7.6 Hz), 8.39 (s, 16 H). ^{13}C NMR (CDCl$_3$, 75 MHz) δ 21.6, 92.8, 120.2, 123.9, 127.5, 128.3, 131.3, 133.5, 134.1, 137.2, 138.7, 142.9, 143.5. HRMS (FABMS): Calcd for [C$_{107}$^{13}CH$_{80}$N$_8$^{193}Ir^{191}Ir]$^+$: m/z 1873.5769. Found: m/z 1873.5778. The single crystal for X-way crystallography was grown from CHCl$_3$ / MeOH.

(B) From 4,4'-Dibromobiphenyl

(i) Sequential Synthesis.

(1) Conversion of 4,4'-Dibromobiphenyl to Ir^{III}(ttp)(p-C$_6$H$_4$)$_2$(p-Br). Ir^{III}(ttp)(CO)Cl (50.0 mg, 0.054 mmol), K$_2$CO$_3$ (149 mg, 1.08 mmol, 20 equiv), 4,4'-dibromobiphenyl (127 mg, 0.54 mmol, 10 equiv), and benzene (3 mL) were heated at 200 °C for 15 hours to give a deep brown solid of Ir^{III}(ttp)(p-C$_6$H$_4$)$_2$(p-Br) (**8t**) (43.1 mg, 0.039 mmol, 73%). R$_f$ = 0.45 (CH$_2$Cl$_2$/hexane = 1 : 1). ^{1}H NMR (CDCl$_3$, 300 MHz) δ 0.63 (d, 2 H, J = 8.7 Hz), 2.68 (s, 12 H), 4.95 (d, 2 H, J = 8.7 Hz), 6.41 (d, 2 H, J = 8.7 Hz), 6.96 (d, 2 H, J = 8.7 Hz), 7.51 (d, 4 H, J = 6.6 Hz), 7.53 (d, 4 H, J = 6.6 Hz), 8.02 (d, 8 H, J = 7.5 Hz), 8.60 (s, 8 H). ^{13}C NMR (CDCl$_3$, 75 MHz) δ 21.7, 96.8, 119.6, 121.5, 124.1, 127.1, 127.6, 129.5, 131.0, 131.2, 131.6, 133.7, 134.2, 137.5, 138.7, 139.3, 143.1. HRMS (FABMS): Calcd for [C$_{60}$H$_{44}$N$_4$BrIr]$^+$ ([M]$^+$): m/z 1092.2373. Found: m/z 1092.2369.

(2) Conversion of Ir^{III}(ttp)(p-C$_6$H$_4$)$_2$(p-Br) to Ir^{III}(ttp)(p-C$_6$H$_4$)$_2$Ir^{III}(ttp). Ir^{III}(ttp)(p-C$_6$H$_4$)$_2$(p-Br) (50.0 mg, 0.046 mmol), K$_2$CO$_3$ (126 mg, 0.91 mmol, 20 equiv), Ir^{III}(ttp)(CO)Cl (46.8 mg, 0.051 mmol, 1.1 equiv), and benzene (3 mL) were heated at 200 °C under N$_2$ for 36 hours to give Ir^{III}(ttp)(p-C$_6$H$_4$)$_2$Ir^{III}(ttp) (**9b**) (64.3 mg, 0.034 mmol, 75%).

(ii) 1-Pot Synthesis. 4,4'-Dibromobiphenyl (5.3 mg, 0.017 mmol), Ir^{III}(ttp)(CO)Cl (55 mg, 0.059 mmol, 3.5 equiv), K$_2$CO$_3$ (94 mg, 0.68 mmol, 40 equiv), and benzene (2.0 mL) were heated at 200 °C under N$_2$ for 3 days to give Ir^{III}(ttp)(p-C$_6$H$_4$)$_2$Ir^{III}(ttp) (**9b**) (13.7 mg, 0.007 mmol, 43%).

Monitoring the Intermediates in Base-Promoted Ar-X Cleavages by Ir^{III}(ttp)(CO)Cl.

The experimental procedure of the reaction of Ir^{III}(ttp)(CO)Cl with PhBr (1.1 equiv) and K$_2$CO$_3$ (20 equiv) in sealed NMR tube was described as an typical example.

(A) Reaction with PhBr (1.1 equiv).

(i) Addition of K$_2$CO$_3$. Ir^{III}(ttp)(CO)Cl (4.7 mg, 0.005 mmol), K$_2$CO$_3$ (14 mg, 0.10 mmol, 20 equiv), PhBr (0.9 mg, 0.60 μL, 0.006 mmol, 1.1 equiv), and benzene-d_6 (0.5 mL) were degassed for three freeze-pump-thaw cycles in a Telfon screw capped NMR tube and then flame-sealed under vacuum. The reaction was then heated at 200 °C, and the course of the reaction was monitored by ^{1}H NMR spectroscopy. Ir^{III}(ttp)(CO)Cl was gradually consumed in 10 days to form

Ir^{III}(ttp)Ph in 94% NMR yield without the observations of the intermediates of Ir^{III}(ttp)H and [Ir^{II}(ttp)]$_2$. The yield was estimated using the residual benzene's protons as the internal standard.

(ii) Addition of Cs$_2$CO$_3$. Ir^{III}(ttp)(CO)Cl (4.5 mg, 0.005 mmol), Cs$_2$CO$_3$ (32 mg, 0.10 mmol, 20 equiv), PhBr (0.8 mg, 0.6 μL, 0.005 mmol, 1.1 equiv), and benzene-d_6 (0.5 mL) were heated at 150 °C in a sealed NMR tube, and the course of the reaction was monitored by ^{1}H NMR spectroscopy. Ir^{III}(ttp)H and [Ir^{II}(ttp)]$_2$ were observed as intermediates after 3 hours in the course of reaction. Ir^{III}(ttp)(CO)Cl was gradually consumed after 60 hours to form Ir^{III}(ttp)Ph quantitatively (NMR yield) (Table 3.31).

(B) Reaction with PhI (1.1 equiv) and KOH. Ir^{III}(ttp)(CO)Cl (5.0 mg, 0.005 mmol), KOH (6.1 mg, 0.11 mmol, 20 equiv), PhI (1.2 mg, 0.7 μL, 0.006 mmol, 1.1 equiv), and benzene-d_6 (0.5 mL) were heated at 120 °C in a sealed NMR tube, and the course of the reaction was monitored by ^{1}H NMR spectroscopy. Ir^{III}(ttp)H and [Ir^{II}(ttp)]$_2$ were observed as intermediates in the course of reaction. Ir^{III}(ttp)(CO)Cl was gradually consumed after 38 hours to form Ir^{III}(ttp)Ph quantitatively (NMR yield) (Table 3.32).

(C) Reaction with PhCl (50 quiv) and Cs$_2$CO$_3$. Ir^{III}(ttp)(CO)Cl (4.3 mg, 0.005 mmol), Cs$_2$CO$_3$ (30 mg, 0.09 mmol, 20 equiv), PhCl (26 mg, 24 μL, 0.23 mmol, 50 equiv), and benzene-d_6 (0.5 mL) were heated at 150 °C in a sealed NMR tube, and the course of the reaction was monitored by ^{1}H NMR spectroscopy. Ir^{III}(ttp)H and [Ir^{II}(ttp)]$_2$ were observed as intermediates in the course of reaction. After 18 days, the reaction was incomplete as unreacted Ir^{III}(ttp)H was still observed. The reaction was further heated at 200 °C in 60 hours to form Ir^{III}(ttp)Ph, Ir^{III}(ttp)(p-C$_6$H$_4$)Ir^{III}(ttp), and Ir^{III}(ttp)CH$_3$ in 71%, 6%, and 4% NMR yields, respectively (Table 3.33). It is noted that PhCl in 50 equiv was used instead of the optimal amount of 200 equiv to avoid the proton signals of excess PhCl from overlapping and weakening that from the iridium porphyrin species.

Relative Reactivity of Possible Iridium Porphyrin Intermediates in Ar-X Cleavages.

(A) Cleavage of Ph-Br (1.1 equiv)

The experimental procedures of the reactions of $Ir^I(ttp)^-[K(18-crown-6)]^+$ (**4b**), $Ir^{III}(ttp)H$ (**2a**), and $[Ir^{II}(ttp)]_2$ (**3**) with PhBr (1.1 equiv) in benzene-d_6 were described as typical examples.

(i) Reaction with $Ir^I(ttp)^-$. $Ir^{III}(ttp)H$ (4.8 mg, 0.006 mmol), KOH (3.1 mg, 0.06 mmol, 10 equiv), 18-crown-6 ether (4.4 mg, 0.017 mmol, 3 equiv), and THF (0.5 mL) were degassed for three freeze-pump-thaw cycles in a Teflon screw capped NMR tube. The reaction mixture was covered by aluminum foil and heated at 150 °C under N_2 in 45 minutes to yield $Ir^I(ttp)^-[K(18-crown-6)]^+$ quantitatively. The solvent was dried under vacuum, and PhBr (1.0 mg, 0.6 μL, 0.006 mmol, 1.1 equiv), and benzene-d_6 (0.5 mL) were added under N_2. The reaction mixture was further degassed for three freeze-pump-thaw cycles and then flame-sealed under vacuum. The reaction mixture was heated at 200 °C, and the reaction was monitored by ^1H NMR spectroscopy. After 2 days, $Ir^{III}(ttp)Ph$ was formed in 27% NMR yield and unreacted $Ir^I(ttp)^-$ was recovered in 43% NMR yield using the residual benzene proton as an internal standard. After 14 days, all $Ir^I(ttp)^-[K(18-crown-6)]^+$ was consumed to give $Ir^{III}(ttp)Ph$. The crude product was purified by column chromatography using alumina eluted with CH_2Cl_2 / hexane (1:2) to give $Ir^{III}(ttp)Ph$ (2.0 mg, 0.002 mmol, 38%).

(ii) Reaction with $Ir^{III}(ttp)H$. $Ir^{III}(ttp)H$ (6.0 mg, 0.007 mmol), PhBr (1.2 mg, 0.8 μL, 0.008 mmol, 1.1 equiv), and benzene-d_6 (0.6 mL) were degassed for three freeze-pump-thaw cycles in a Teflon screw capped NMR tube and then flame-sealed under vacuum. The reaction mixture was heated at 200 °C, and the reaction was monitored by ^1H NMR spectroscopy. After 14 hours, all $Ir^{III}(ttp)H$ was consumed to form $Ir^{III}(ttp)Ph$ and $Ir^{III}(ttp)Br$ (**Figure 3.9(a)**). The crude product was purified by column chromatography using alumina eluted with CH_2Cl_2 / hexane (1:2) to give $Ir^{III}(ttp)Ph$ (2.0 mg, 0.002 mmol, 31%). $Ir^{III}(ttp)Br$ was formed in 7% NMR yield estimated by using the isolated yield of $Ir^{III}(ttp)Ph$ and the porphyrin's pyrrole proton ratio of $Ir^{III}(ttp)Ph$: $Ir^{III}(ttp)Br$ (δ(pyrrole) = 8.91-8.95 ppm) (~4.4 : 1) in the crude ^1H NMR spectroscopy. Attempted isolation of $Ir^{III}(ttp)Br$ using CH_2Cl_2 / hexane (2:1) as an eluent was unsuccessful due to the partial

decomposition of $Ir^{III}(ttp)Br$ to form unknown species. The characterizations of $Ir^{III}(ttp)Br$ by ^1H and ^{13}C NMR spectroscopies could not be successfully obtained. Only HRMS analysis could be used to identifty $Ir^{III}(ttp)Br$. **HRMS** (FABMS) of $Ir^{III}(ttp)Br$ (**1c$_1$**): Calcd for $[C_{48}H_{36}N_4BrIr]^+$ ($[M]^+$): m/z 940.1747. Found: m/z 940.1765.

(iii) Reaction with $[Ir^{II}(ttp)]_2$. $Ir^{III}(ttp)H$ (5.7 mg, 0.007 mmol) and benzene (0.5 mL) were degassed for three freeze-pump-thaw cycles in a Teflon screw capped NMR tube. 2,2,6,6-Tetramethylpiperidinooxy (TEMPO) (1.1 mg, 0.007 mmol, 1.1 equiv) was added into the tube under N_2 to form $[Ir^{II}(ttp)]_2$ quantitatively. The solvent, unreacted TEMPO, and TEMPOH co-product were removed under vacuum. PhBr (1.1 mg, 0.8 μL, 0.007 mmol, 1.1 equiv) and benzene-d_6 (0.6 mL) were then added into the tube under N_2, and the reaction mixture was further degassed for three freeze-pump-thaw cycles in the tube and then flame-sealed under vacuum. The reaction mixture was heated at 200 ^{o}C, and the reaction was monitored by ^1H NMR spectroscopy. After 2 minutes, all $[Ir^{II}(ttp)]_2$ were consumed to form $Ir^{III}(ttp)Ph$ and $Ir^{III}(ttp)Br$ (**Figure 3.9(b)**). The crude product was purified by column chromatography using alumina eluted with CH_2Cl_2 / hexane (1:2) to give $Ir^{III}(ttp)Ph$ (2.1 mg, 0.002 mmol, 34%). $Ir^{III}(ttp)Br$ was formed in 32% NMR yield its yield was estimated by using the isolated yield of $Ir^{III}(ttp)Ph$ and the porphyrin's pyrrole proton ratio of $Ir^{III}(ttp)Ph$: $Ir^{III}(ttp)Br$ (~1.06 : 1) in the crude ^1H NMR spectroscopy. Attempted isolation of $Ir^{III}(ttp)Br$ using CH_2Cl_2 / hexane (2:1) as an eluent was unsuccessful due to the partial decomposition of $Ir^{III}(ttp)Br$ to form unknown species.

(B) Cleavage of Ph-I

(i) Reaction with $Ir^I(ttp)^-$. $Ir^I(ttp)^-[K(18\text{-crown-}6)]^+$ was prepared quantitatively from the reaction of $Ir^{III}(ttp)H$ (4.7 mg, 0.005 mmol) with KOH (3.1 mg, 0.05 mmol. 10 equiv) and 18-crown-6 ether (4.3 mg, 0.016 mmol, 3 equiv) in THF (0.5 mL) at 150 ^{o}C for 45 minutes in a Telfon-screw capped NMR tube. THF was then dried, and PhI (1.2 mg, 0.7 μL, 0.006 mmol) and benzene-d_6 (0.5 mL) were added under N_2. The reaction mixture in a sealed NMR tube was heated under vacuum at 200

°C. After 20 days, all $Ir^I(ttp)[K(18\text{-}crown\text{-}6)]^+$ was consumed to yield $Ir^{III}(ttp)Ph$ (1.3 mg, 0.001 mmol, 25%) by column chromatography and unreacted $Ir^I(ttp)^-$ was recovered in 15% NMR yield.

(ii) Reaction with $Ir^{III}(ttp)H$. $Ir^{III}(ttp)H$ (5.7 mg, 0.007 mmol), PhI (1.5 mg, 0.8 μL, 0.007 mmol, 1.1 equiv), and benzene-d_6 (0.6 mL) were heated in a sealed NMR tube under vacuum at 200 °C, and the reaction was monitored by ^1H NMR spectroscopy. Afte 15 minutes, all $Ir^{III}(ttp)H$ was consumed to form $Ir^{III}(ttp)Ph$ and $Ir^{III}(ttp)I$ (δ(pyrrole) = 8.92 ppm) (**Figure 3.10(a)**). $Ir^{III}(ttp)Ph$ (2.1 mg, 0.002 mmol, 34%) was isolated by column chromatography with alumina using CH_2Cl_2/hexane (1:2) as the eluent. The yield of $Ir^{III}(ttp)I$ (19%, NMR yield) was estimated by using the yield of $Ir^{III}(ttp)Ph$ and the ratio of $Ir^{III}(ttp)Ph$: $Ir^{III}(ttp)I$ (~1.8 : 1) by ^1H NMR spectroscopy. Attempted isolation of $Ir^{III}(ttp)I$ using CH_2Cl_2 / hexane (2:1) as an eluent was unsuccessful due to the partial decomposition of $Ir^{III}(ttp)Br$ to form unknown species. The characterization of $Ir^{III}(ttp)I$ by ^1H and ^{13}C NMR spectroscopies could not be successfully obtained, and only HRMS could be adopted. **HRMS** (FABMS) of $Ir^{III}(ttp)I$ (**1d₁**) : Calcd for $[C_{48}H_{36}N_4IIr]^+$ ($[M]^+$): m/z 988.1608. Found: m/z 988.1611.

(iii) Reaction with $[Ir^{II}(ttp)]_2$. $[Ir^{II}(ttp)]_2$ was prepared quantitatively from the reaction of $Ir^{III}(ttp)H$ (5.9 mg, 0.007 mmol) with tetramethylpiperidinooxy (TEMPO) (1.2 mg, 0.008 mmol, 1. equiv) in benzene (0.5 mL) in a Teflon screw capped NMR tube. The solvent was removed under vacuum, and PhI (1.5 mg, 0.8 μL, 0.008 mmol, 1.1 equiv) and benzene-d_6 (0.6 mL) were then added into the tube. The reaction mixture was heated in a sealed NMR tube under vacuum at 200 °C, and the reaction was monitored by ^1H NMR spectroscopy. After 1 minute, all $[Ir^{II}(ttp)]_2$ were consumed to form $Ir^{III}(ttp)Ph$ (2.4 mg, 0.003 mmol, 37%) and $Ir^{III}(ttp)I$ (36%, NMR yield) (**Figure 3.10(b)**). Attempted isolation of $Ir^{III}(ttp)I$ was unsuccessful due to the partial decomposition of $Ir^{III}(ttp)I$ to form unknown species.

(C) Cleavage of Ph-Cl (50 equiv)

(i) Reaction with $Ir^I(ttp)^-$. $Ir^I(ttp)[K(18\text{-}crown\text{-}6)]^+$ was prepared quantitatively from the reaction

of $Ir^{III}(ttp)H$ (4.6 mg, 0.005 mmol) with KOH (3.0 mg, 0.05 mmol, 10 equiv) and 18-crown-6 ether (4.3 mg, 0.016 mmol, 3 equiv) in THF (0.5 mL) at 150 °C for 45 minutes in a Telfon-screw capped NMR tube. THF was then dried, and PhCl (30.0 mg, 27 μL, 0.27 mmol, 50 equiv) and benzene-d_6 (0.5 mL) were added under N_2. The reaction mixture in a sealed NMR tube under vacuum was heated at 200 °C. All $Ir^I(ttp)^-[K(18\text{-crown-6})]^+$ was consumed in 4 days to give $Ir^{III}(ttp)Ph$ (2.5 mg, 0.003 mmol, 50%) by column chromatography.

(ii) Reaction with $Ir^{III}(ttp)H$. $Ir^{III}(ttp)H$ (4.8 mg, 0.006 mmol), PhCl (31.3 mg, 28 μL, 0.28 mmol, 50 equiv), and benzene-d_6 (0.5 mL) were heated in a sealed NMR tube at 200 °C, and the reaction was monitored by ^1H NMR spectroscopy. After 4 days, all $Ir^{III}(ttp)H$ was consumed to form $Ir^{III}(ttp)Ph$ (3.5 mg, 0.004 mmol, 67%) and $Ir^{III}(ttp)(CO)Cl$ (0.2 mg, 0.0002 mmol, 4%) by column chromatography using CH_2Cl_2/hexane (1:2) as an eluent.

(iii) Reaction with $[Ir^{II}(ttp)]_2$. $[Ir^{III}(ttp)]_2$ was prepared quantitatively from the reaction of $Ir^{III}(ttp)H$ (4.5 mg, 0.005 mmol) with TEMPO (0.9 mg, 0.006 mmol) in benzene (0.5 mL) in a Teflon screw capped NMR tube. The solvent was removed under vacuum, and PhCl (29.4 mg, 26.5 μL, 0.26 mmol, 50 equiv) and benzene-d_6 (0.5 mL) were then added into the tube under N_2. The reaction mixture was heated in a sealed NMR tube under vacuum at 200 °C, and the reaction was monitored by ^1H NMR spectroscopy. After 5 hours, all $[Ir^{II}(ttp)]_2$ were consumed to form $Ir^{III}(ttp)Ph$ (2.8 mg, 0.003 mmol, 57%) and $Ir^{III}(ttp)(CO)Cl$ (0.2 mg, 0.0002 mmol, 4%). $Ir^{III}(ttp)(p\text{-}C_6H_4)Ir^{III}(ttp)$ (3%, NMR yield) was also formed and its yield was estimated by using the yield of $Ir^{III}(ttp)Ph$ and the pyrrole proton ratios of $Ir^{III}(ttp)Ph : Ir^{III}(ttp)(p\text{-}C_6H_4)Ir^{III}(ttp)$ in the reaction mixture by ^1H NMR spectroscopy.

(D) Cleavage of $(p\text{-MeO})C_6H_4\text{-Br}$ (1.1 equiv)

(i) Reaction with $Ir^I(ttp)^-$. $Ir^I(ttp)^-[K(18\text{-crown-6})]^+$ was prepared quantitatively from the reaction of $Ir^{III}(ttp)H$ (4.7 mg, 0.005 mmol) with KOH (3.1 mg, 0.05 mmol, 10 equiv) and 18-crown-6 ether (4.3 mg, 0.016 mmol, 3 equiv) in THF (0.5 mL) at 150 °C for 45 minutes in a Telfon-screw capped

NMR tube. THF was then dried, and 4-bromoanisole (1.1 mg, 0.8 μL, 0.006 mmol, 1.1 equiv) and benzene-d_6 (0.5 mL) were added under N$_2$. The reaction mixture in a sealed NMR tube was heated under vacuum at 200 $^\circ$C. After 2 days, Ir^I(ttp)$^-$ was consumed to give only Ir^{III}(ttp)CH$_3$ (3.5 mg, 0.004 mmol, 73%) by column chromatography over alumina using CH$_2$Cl$_2$/hexane (1:2) as an eluent.

(ii) Reaction with Ir^{III}(ttp)H. Ir^{III}(ttp)H (4.8 mg, 0.006 mmol), 4-bromoanisole (1.2 mg, 0.8 μL, 0.006 mmol, 1. equiv), and benzene-d_6 (0.5 mL) were heated in a sealed NMR tube at 200 $^\circ$C, and the reaction was monitored by ^{1}H NMR spectroscopy. After 1 hour, all Ir^{III}(ttp)H was consumed to yield Ir^{III}(ttp)C$_6$H$_4$(p-OMe) (3.3 mg, 0.003 mmol, 61%) by column chromatography over alumina using CH$_2$Cl$_2$/hexane (1:1) as an eluent, and Ir^{III}(ttp)I (28%, NMR yield) by estimation.

(iii) Reaction with [Ir^{II}(ttp)]$_2$. [Ir^{III}(ttp)]$_2$ was prepared quantitatively from the reaction of Ir^{III}(ttp)H (4.8 mg, 0.006 mmol) with tetramethylpiperidinooxy (TEMPO) (1.0 mg, 0.006 mmol) in benzene (0.5 mL) under N$_2$ in a Teflon screw capped NMR tube. The solvent was removed under vacuum, and 4-bromoanisole (1.2 mg, 0.8 μL, 0.006 mmol, 1.1 equiv) and benzene-d_6 (0.5 mL) were then added into the tube. The reaction mixture was heated in a sealed NMR tube under vacuum at 200 $^\circ$C, and the reaction was monitored by ^{1}H NMR spectroscopy. After 2 minutes, all [Ir^{II}(ttp)]$_2$ were consumed to form Ir^{III}(ttp)C$_6$H$_4$(p-OMe) (2.5 mg, 0.003 mmol, 46%) by column chromatography over alumina using CH$_2$Cl$_2$/hexane (1:1) as an eluent, and and Ir^{III}(ttp)Br (31%, NMR yield) by estimation.

(E) Cleavage of (p-NO$_2$)C$_6$H$_4$-Br (1.1 equiv)

(i) Reaction with Ir^I(ttp)$^-$. Ir^I(ttp)$^-$[K(18-crown-6)]$^+$ was prepared quantitatively from the reaction of Ir^{III}(ttp)H (4.7 mg, 0.005 mmol) with KOH (3.1 mg, 0.05 mmol, 10 equiv) and 18-crown-6 ether (3.6 mg, 0.014 mmol, 2.5 equiv) in THF (0.5 mL) at 150 $^\circ$C for 45 minutes in a Telfon-screw capped NMR tube. THF was then dried, and 4-bromo-nitrobenzene (1.2 mg, 0.006 mmol) and benzene-d_6 (0.5 mL) were added under N$_2$. The reaction mixture in a sealed NMR tube was heated

under vacuum at 200 °C. After 2 days, no $Ir^{III}(ttp)C_6H_4(p\text{-}NO_2)$ was observed by ^1H NMR spectroscopy and unreacted $Ir^I(ttp)^-$ was recovered in 73% NMR yield.

(ii) Reaction with $Ir^{III}(ttp)H$. $Ir^{III}(ttp)H$ (4.8 mg, 0.006 mmol), 4-bromo-nitrobenzene (1.2 mg, 0.006 mmol), and benzene-d_6 (0.5 mL) were heated in a sealed NMR tube at 200 °C, and the reaction was monitored by ^1H NMR spectroscopy. After 1 hour, all $Ir^{III}(ttp)H$ was consumed to form $Ir^{III}(ttp)C_6H_4(p\text{-}NO_2)$ (2.4 mg, 0.002 mmol, 44%) by column chromatography over alumina using CH_2Cl_2/hexane (1:1) as an eluent, and $Ir^{III}(ttp)Br$ (14%, NMR yield) by estimation.

(iii) Reaction with $[Ir^{II}(ttp)]_2$. $[Ir^{III}(ttp)]_2$ was prepared quantitatively from the reaction of $Ir^{III}(ttp)H$ (4.8 mg, 0.006 mmol) with TEMPO (1.0 mg, 0.006 mmol) in benzene (0.5 mL) under N_2 in a Teflon screw capped NMR tube. The solvent was removed under vacuum, and 4-bromo-nitrobenzene (1.0 mg, 0.006 mmol) and benzene-d_6 (0.5 mL) were then added into the tube. The reaction mixture was heated in a sealed NMR tube under vacuum at 200 °C, and the reaction was monitored by ^1H NMR spectroscopy. After 2 minutes, all $[Ir^{II}(ttp)]_2$ were consumed to form $Ir^{III}(ttp)C_6H_4(p\text{-}NO_2)$ (2.0 mg, 0.002 mmol, 37%) by column chromatography over alumina using CH_2Cl_2/hexane (1:2) as an eluent, and $Ir^{III}(ttp)Br$ (36% NMR yield) by estimation.

Reactions of Halogen Radical Sources with Arenes

The experimental procedure of the reaction of sulfuryl chloride with benzene at 200 °C was described as a typical example.

(A) Reaction of Sulfuryl Chloride with Benzene. SO_2Cl_2 (25.0 mg, 15 μL, 0.19 mmol) and benzene (1 mL) were degassed for three freeze-pump-thaw cycles in a Teflon screw-capped tube. The reaction mixture was then heated under N_2 at 200 °C in 90 minutes. 4-chlorotoluene was added as an internal standard and the PhCl formed (20%) was quantified by GC-MS analysis. The product yield was calculated with reference to the number of Cl atoms in SO_2Cl_2. The formation of PhCl was confirmed by the commericial sample of PhCl.

(B) Reaction of Bromine with Benzene. Br_2 (6.2 mg, 2 μL, 0.039 mmol) and benzene (1 mL)

were heated in a Teflon screw-capped tube under N_2 at 200 °C in 90 minutes. PhBr (83%) was quantified by GC-MS analysis using 4-bromotoluene as an internal standard, in which the product yields was calculated with reference to the number of Br atoms in Br_2. The formation of PhBr in the reaction was confirmed by the commercial sample of PhBr.

(C) Reaction of Iodine with Benzene. I_2 (158 mg, 0.62 mmol) and benzene (1 mL) were heated in a Teflon screw-capped tube under N_2 at 200 °C in 2 hours. No PhI was detected by GC-MS analysis using the commercial sample of PhI as a reference. The reaction mixture remained deep purple after prolonged heating.

(D) Reaction of Sulfuryl Chloride with PhCl. SO_2Cl_2 (25.0 mg, 15 μL, 0.19 mmol) and excess PhCl (1 mL) were heated in a Teflon screw-capped tube under N_2 at 200 °C in 90 minutes. 1,4-$Cl_2C_6H_4$ (6%), 1,2-$Cl_2C_6H_4$ (4%), 1,3-$Cl_2C_6H_4$ (<1%), and chloro-substituted biphenyls (1%) were detected by GC-MS analysis using 4-chlorotoluene as an internal standard, in which the product yields were calculated with reference to the number of Cl atoms in SO_2Cl_2. The formations of 1,4-$Cl_2C_6H_4$ and 1,2-$Cl_2C_6H_4$ in the reaction were confirmed by the commercial samples, whereas the formations of 1,3-$Cl_2C_6H_4$, and chloro-substituted biphenyls were confirmed by the GC-MS library.

(E) Reaction of $[Ir^{II}(ttp)]_2$ with 4-Bromo-*tert*-Butylbenzene (1.1 equiv) in Benzene. $[Ir^{II}(ttp)]_2$ was prepared quantitatively from the reaction of $Ir^{III}(ttp)H$ (10.3 mg, 0.012 mmol) with tetramethylpiperidinooxy (TEMPO) (2.1 mg, 0.013 mmol) in benzene (1 mL) in a Teflon screw-capped tube. The solvent, unreacted TEMPO, and TEMPOH co-product were removed under vacuum. 4-Bromo-*tert*-butylbenzene (2.8 mg, 2.3 μL, 0.013 mmol) and benzene (1 mL) were then added under N_2. The reaction mixture was degassed for 3 freeze-pump-thaw cycles and was further heated at 200 °C for 5 minutes. The organic fraction was collected by a cold-trap under liquid N_2 and was subjected to GC-MS analysis. PhBr (1% yield, with reference to $Ir^{II}(ttp)$ monomer used) was detected using 4-bromotoluene as an internal standard. The crude products were purified by column chromatography over alumina to yield $Ir^{III}(ttp)C_6H_4(p\text{-}^tBu)$ (5.5 mg,

0.006 mmol, 47%) and $Ir^{III}(ttp)Br$ (~4.4 mg, ~0.005 mmol, ~39%, containing unknown iridium porphyrin species due to the partial decomposition of $Ir^{III}(ttp)Br$ upon column chromatography).

(F) Reaction of $[Ir^{II}(ttp)]_2$ with PhCl. $[Ir^{II}(ttp)]_2$ was prepared quantitatively from the reaction of $Ir^{III}(ttp)H$ (5.6 mg, 0.006 mmol) with tetramethylpiperidinooxy (TEMPO) (1.1 mg, 0.007 mmol) in benzene (0.5 mL) in a Teflon screw-capped tube. The solvent, unreacted TEMPO, and TEMPOH co-product were removed under vacuum. PhCl (1 mL) was then added under N_2. The reaction mixture was degassed for 3 freeze-pump-thaw cycles and was further heated at 200 °C for 30 minutes. The organic fraction was collected by a cold-trap under liquid N_2 and was subjected to GC-MS analysis. $1,4-Cl_2C_6H_4$ (2% yield, with reference to $Ir^{II}(ttp)$ monomer used) was detected using 4-chlorotoluene as an internal standard. The crude products were purified by column chromatography in a single fraction to yield $Ir^{III}(ttp)Ph$ (2.4 mg, 0.003 mmol, 39%) and $Ir^{III}(ttp)(CO)Cl$ (<0.1 mg, 0.00001 mmol, ~1%). $Ir^{III}(ttp)(p-C_6H_4)Ir^{III}(ttp)$ (4%, NMR yield) was also formed as its yield was estimated by using the yield of $Ir^{III}(ttp)Ph$ and the pyrrole proton ratios of $Ir^{III}(ttp)Ph : Ir^{III}(ttp)(p-C_6H_4)Ir^{III}(ttp)$ in the reaction mixture by ^1H NMR spectroscopy.

Reaction of $Ir^{III}(ttp)(CO)Cl$ with 1,4-Dichlorobenzene (1 equiv) and K_2CO_3. $Ir^{III}(ttp)(CO)Cl$ (11.0 mg, 0.012 mmol), K_2CO_3 (33 mg, 0.24 mmol, 20 equiv), 1,4-dichlorobenzene (1.8 mg, 0.012 mmol, 1 equiv), and benzene (1 mL) were degassed for three freeze-pump-thaw cycles in a Teflon-screw capped tube and then heated at 200 °C in 7 hours under N_2 to yield $Ir^{III}(ttp)C_6H_4(p-Cl)$ (1.1 mg, 0.001 mmol, 9%), $Ir^{III}(ttp)CH_3$ (0.1 mg, 0.0002 mmol, 1%), and $Ir^{III}(ttp)(p-C_6H_4)Ir^{III}(ttp)$ (3%, NMR yield). Unreacted $Ir^{III}(ttp)H$ (7%, NMR yield) was also recovered. The NMR yields of products were estimated by using the isolated yield of $Ir^{III}(ttp)C_6H_4(p-Cl)$ and the pyrrole proton ratios of $Ir^{III}(ttp)H : Ir^{III}(ttp)(p-C_6H_4)Ir^{III}(ttp) : Ir^{III}(ttp)C_6H_4(p-Cl)$ in the crude reaction mixture by ^1H NMR spectroscopy.

Competition Reactions in Base-Promoted Ar-X Cleavages by $Ir^{III}(ttp)(CO)Cl$

(A) Reaction of Ir^{III}(ttp)(CO)Cl with 1,4-Dihalo-benzenes (50 equiv) and K$_2$CO$_3$ (20 equiv)

The experimental procedure of the reaction Ir^{III}(ttp)(CO)Cl with 1-bromo-4-iodobenzene and K$_2$CO$_3$ was described as a typical example.

(i) Reaction of Ir^{III}(ttp)(CO)Cl with 1-Bromo-4-iodobenzene. Ir^{III}(ttp)(CO)Cl (20.0 mg, 0.022 mmol), K$_2$CO$_3$ (60 mg, 0.43 mmol), and 1-bromo-4-iodobenzene (306 mg, 1.08 mmol) were degassed for three freeze-pump-thaw cycles in a Teflon screw-capped tube. The reaction was then heated at 200 °C under N$_2$ for 6 hours. The crude product was purified by column chromatography over alumina eluted with CH$_2$Cl$_2$/hexane (1:2) to give only Ir^{III}(ttp)C$_6$H$_4$(p-Br) (**8i**) (18.9 mg, 0.019 mmol, 86%).

(ii) Reaction of Ir^{III}(ttp)(CO)Cl with 1-Bromo-4-chlorobenzene. Ir^{III}(ttp)(CO)Cl (20.0 mg, 0.022 mmol), K$_2$CO$_3$ (60 mg, 0.43 mmol), and 1-bromo-4-chlorobenzene (207 mg, 1.08 mmol) were heated at 200 °C under N$_2$ for 21 hours to give only Ir^{III}(ttp)C$_6$H$_4$(p-Cl) (**8j**) (13.9 mg, 0.014 mmol, 66%).

(iii) Reaction of Ir^{III}(ttp)(CO)Cl with 1-Chloro-4-fluorobenzene. Ir^{III}(ttp)(CO)Cl (20.0 mg, 0.022 mmol), K$_2$CO$_3$ (60 mg, 0.43 mmol), and 1-chloro-4-fluorobenzene (141 mg, 115 µL, 1.08 mmol) were heated at 200 °C under N$_2$ for 1 day to give only Ir^{III}(ttp)C$_6$H$_4$(p-F) (**8h**) (13.6 mg, 0.014 mmol, 66%).

(B) Competition Reactions between *Para*-Substituted ArBr and PhBr

The experimental procedure of the competition reaction between 4-bromoanisole (25 equiv) and PhBr (25 equiv) with Ir^{III}(ttp)(CO)Cl and K$_2$CO$_3$ was described as a typical example.

(i) 4-Bromoanisole. Ir^{III}(ttp)(CO)Cl (10.2 mg, 0.011 mmol), K$_2$CO$_3$ (30 mg, 0.22 mmol, 20 equiv), 4-bromoanisole (51.6 mg, 35 µL, 0.28 mmol, 25 equiv), PhBr (43.3 mg, 29 µL, 0.28 mmol, 25 equiv), and benzene (1 mL) were degassed for three freeze-pump-thaw cycles in a Telfon screw capped tube. The reaction mixture was then heated at 200 °C under N$_2$ for 1 hour. The kinetic ratio of the Ar-Br cleavage products, Ir^{III}(ttp)C$_6$H$_4$(p-OMe) : Ir^{III}(ttp)Ph, in the crude products was

estimated to be 6.44 : 1.00 by ^{1}H NMR spectroscopy using the *ortho* or *meta*-aryl ligand (Ar-Ir)'s proton signals of the 2 products. The crude product was then purified by column chromatography over alumina eluted with CH_2Cl_2/hexane (1:1) to yield Ir^{III}(ttp)C_6H_4(*p*-OMe) (7.7 mg, 0.008 mmol, 72%) and Ir^{III}(ttp)Ph (1.2 mg, 0.001 mmol, 12%) (ratio = 6.0 : 1). The yields of the 2 products were estimated by using the isolated total weight of the products, and the ratio of the porphyrin's pyrrole proton signals of the 2 products in the isolated product mixture by ^{1}H NMR spectroscopy.

(ii) 4-Bromo-*N,N*-Dimethylaniline. Initially, Ir^{III}(ttp)(CO)Cl (12.2 mg, 0.013 mmol), K_2CO_3 (36 mg, 0.26 mmol, 20 equiv), 4-bromo-*N,N*-dimethylaniline (66 mg, 0.33 mmol, 25 equiv), PhBr (51.8 mg, 35 μL, 0.33 mmol, 25 equiv), and benzene (1 mL) were heated at 200 ^{o}C under N_2 for 6 hours. PPh$_3$ (35 mg, 0.13 mmol, 10 equiv) was then added and the reaction mixture was further heated at 120 ^{o}C for 30 minutes to give only Ir^{III}(ttp)(PPh$_3$)C_6H_4(*p*-NMe$_2$) (14.5 mg, 0.012 mmol, 88%) without the formation of Ir^{III}(ttp)(PPh$_3$)Ph. Therefore, the kinetic ratio was estimated indirectly. Next, Ir^{III}(ttp)(CO)Cl (9.7 mg, 0.010 mmol), K_2CO_3 (29 mg, 0.21 mmol, 20 equiv), 4-bromo-*N,N*-dimethylaniline (52 mg, 0.26 mmol, 25 equiv), 4-bromoanisole (49.1 mg, 33 μL, 0.26 mmol, 25 equiv), and benzene (1 mL) were heated at 200 ^{o}C under N_2 for 11 hours. PPh$_3$ (28 mg, 0.10 mmol, 10 equiv) was further added and heated at 120 ^{o}C for 15 minutes. The kinetic ratio of Ir^{III}(ttp)(PPh$_3$)C_6H_4(*p*-NMe$_2$) : Ir^{III}(ttp)(PPh$_3$)C_6H_4(*p*-OMe) was found to be 8.44 : 1.00, with the corresponding isolated yields in 77% and 11% yield (ratio = 7.0 : 1), respectively. By incorporating the kinetic ratio of Ir^{III}(ttp)C_6H_4(*p*-OMe) : Ir^{III}(ttp)Ph (6.44 : 1.00) (from **(i)**) into that of Ir^{III}(ttp)(PPh$_3$)C_6H_4(*p*-NMe$_2$) : Ir^{III}(ttp)(PPh$_3$)C_6H_4(*p*-OMe) (8.44 : 1.00), the kinetic ratio of Ir^{III}(ttp)C_6H_4(*p*-NMe$_2$) : Ir^{III}(ttp)Ph was indirectly estimated to be 54.4 : 1.00.

(iii) 4-Bromotoluene. Ir^{III}(ttp)(CO)Cl (11.6 mg, 0.013 mmol), K_2CO_3 (35 mg, 0.25 mmol, 20 equiv), 4-bromotoluene (54 mg, 0.31 mmol, 25 equiv), PhBr (49.3 mg, 33 μL, 0.31 mmol, 25 equiv), and benzene (1 mL) were heated at 200 ^{o}C under N_2 for 12 hours. The kinetic ratio of Ir^{III}(ttp)(*p*-Tol) : Ir^{III}(ttp)Ph was estimated to be 1.80 : 1.00. The crude product was then purified to yield Ir^{III}(ttp)(*p*-Tol) (10.5 mg, 0.007 mmol, 55%) and Ir^{III}(ttp)Ph (4.0 mg, 0.004 mmol, 34%)

(ratio = 1.6 : 1).

(iv) 4-Bromo-*tert*-butylbenzene. $Ir^{III}(ttp)(CO)Cl$ (20.4 mg, 0.022 mmol), K_2CO_3 (60 mg, 0.44 mmol, 20 equiv), 4-bromo-*tert*-butylbenzene (117.6 mg, 96 μL, 0.55 mmol, 25 equiv), PhBr (86.6 mg, 58 μL, 0.55 mmol, 25 equiv), and benzene (2 mL) were heated at 200 °C under N_2 for 2 days. The kinetic ratio of $Ir^{III}(ttp)C_6H_4(p\text{-}^tBu)$: $Ir^{III}(ttp)Ph$ from the crude products was found to be 1.36 : 1.00 by ^1H NMR spectroscopy. The crude product was then purified to yield $Ir^{III}(ttp)C_6H_4(p\text{-}^tBu)$ (9.3 mg, 0.009 mmol, 42%) and $Ir^{III}(ttp)Ph$ (6.7 mg, 0.007 mmol, 32%).

(v) 1-Bromo-4-fluorobenzene. $Ir^{III}(ttp)(CO)Cl$ (20.0 mg, 0.022 mmol), K_2CO_3 (60 mg, 0.43 mmol, 20 equiv), 1-bromo-4-fluorobenzene (94.6 mg, 59 μL, 0.54 mmol, 25 equiv), PhBr (84.9 mg, 57 μL, 0.54 mmol, 25 equiv), and benzene (2 mL) were heated at 200 °C under N_2 for 2 days. The kinetic ratio of $Ir^{III}(ttp)C_6H_4(p\text{-}F)$: $Ir^{III}(ttp)Ph$ from the crude products was found to be 1.98 : 1.00 by ^1H NMR spectroscopy. The crude product was then purified to yield $Ir^{III}(ttp)C_6H_4(p\text{-}F)$ (11.4 mg, 0.012 mmol, 55%) and $Ir^{III}(ttp)Ph$ (5.6 mg, 0.006 mmol, 27%) (ratio = 2.0 : 1).

(vi) 1-Bromo-4-(trimethylsilyl)benzene. $Ir^{III}(ttp)(CO)Cl$ (9.8 mg, 0.011 mmol), K_2CO_3 (29 mg, 0.22 mmol, 20 equiv), 1-bromo-4-(trimethylsilyl)benzene, (60.7 mg, 52 μL, 0.27 mmol, 25 equiv), PhBr (41.6 mg, 28 μL, 0.27 mmol, 25 equiv), and benzene (1 mL) were heated at 200 °C under N_2 for 12 hours. The kinetic ratio of $Ir^{III}(ttp)C_6H_4(p\text{-}SiMe_3)$: $Ir^{III}(ttp)Ph$ was found to be 1.29 : 1.00. The crude product was then purified to yield $Ir^{III}(ttp)C_6H_4(p\text{-}SiMe_3)$ (4.8 mg, 0.005 mmol, 45%) and $Ir^{III}(ttp)Ph$ (3.6 mg, 0.004 mmol, 36%) (ratio = 1.3 : 1).

(vii) 1-Bromo-4-chlorobenzene. $Ir^{III}(ttp)(CO)Cl$ (20.0 mg, 0.022 mmol), K_2CO_3 (60 mg, 0.43 mmol, 20 equiv), 1-bromo-4-chlorobenzene, (103.5 mg, 0.54 mmol, 25 equiv), PhBr (84.9 mg, 57 μL, 0.54 mmol, 25 equiv), and benzene (2 mL) were heated at 200 °C under N_2 for 15 hours. The kinetic ratio of $Ir^{III}(ttp)C_6H_4(p\text{-}Cl)$: $Ir^{III}(ttp)Ph$ from the crude products was estimated to be 4.13 : 1.00 by ^1H NMR spectroscopy. The crude product was then purified to yield $Ir^{III}(ttp)C_6H_4(p\text{-}Cl)$ (13.9 mg, 0.014 mmol, 66%) and $Ir^{III}(ttp)Ph$ (3.4 mg, 0.004 mmol, 17%) (ratio = 3.9 :1).

(viii) 1,4-Dibromobenzene. $Ir^{III}(ttp)(CO)Cl$ (20.4 mg, 0.022 mmol), K_2CO_3 (61 mg, 0.44 mmol,

20 equiv), 1,4-dibromobenzene, (130 mg, 0.55 mmol, 25 equiv), PhBr (86.6 mg, 58 μL, 0.55 mmol, 25 equiv), and benzene (2 mL) were heated at 200 °C under N_2 for 30 hours. The kinetic ratio of $Ir^{III}(ttp)C_6H_4(p\text{-}Br)$: $Ir^{III}(ttp)Ph$ from the crude products was estimated to be 2.39 : 1.00 by ^1H NMR spectroscopy by averaging the original kinetic ratio (4.77 : 1.00) due to the presence of 2 C-Br bonds in 1,4-diiodobenzene for reaction. The crude product was then purified to yield $Ir^{III}(ttp)C_6H_4(p\text{-}Br)$ (17.0 mg, 0.017 mmol, 76%) and $Ir^{III}(ttp)Ph$ (2.4 mg, 0.003 mmol, 12%) (ratio = 6.3 : 1).

(ix) Methyl 4-Bromobenzoate. $Ir^{III}(ttp)(CO)Cl$ (11.0 mg, 0.012 mmol), K_2CO_3 (33 mg, 0.40 mmol, 20 equiv), methyl 4-bromobenzoate (64 mg, 0.30 mmol, 25 equiv), PhBr (46.7 mg, 31 μL, 0.30 mmol, 25 equiv), and benzene (1 mL) were heated at 200 °C under N_2 for 19 hours. The kinetic ratio of $Ir^{III}(ttp)C_6H_4(p\text{-}CO_2Me)$: $Ir^{III}(ttp)Ph$ from the crude products was found to be 5.63 : 1.00 by ^1H NMR spectroscopy. The crude product was then purified to yield $Ir^{III}(ttp)C_6H_4(p\text{-}CO_2Me)$ (8.7 mg, 0.009 mmol, 76%) and $Ir^{III}(ttp)Ph$ (1 mg, 0.001 mmol, 9%) (ratio = 8.4 : 1).

(x) 4-Bromobenzonitrile. $Ir^{III}(ttp)(CO)Cl$ (10.5 mg, 0.011 mmol), K_2CO_3 (31 mg, 0.23 mmol, 20 equiv), 4-bromobenzonitrile (52 mg, 0.28 mmol, 25 equiv), PhBr (44.6 mg, 30 μL, 0.28 mmol, 25 equiv), and benzene (1 mL) were heated at 200 °C under N_2 for 12 hours. PPh_3 (30 mg, 0.11 mmol) was then added under N_2 and the reaction mixture was further heated at 120 °C for 15 mnutes. The kinetic ratio of $Ir^{III}(ttp)(PPh_3)C_6H_4(p\text{-}CN)$: $Ir^{III}(ttp)(PPh_3)Ph$ was found to be 6.75 : 1.00. The crude product was then purified to yield $Ir^{III}(ttp)(PPh_3)C_6H_4(p\text{-}CN)$ (10.7 mg, 0.009 mmol, 77%) and $Ir^{III}(ttp)(PPh_3)Ph$ (0.7 mg, 0.0006 mmol, 5%) (ratio = 15 : 1).

(xi) 4-Bromo-nitrobenzene. $Ir^{III}(ttp)(CO)Cl$ (12.3 mg, 0.013 mmol), K_2CO_3 (37 mg, 0.27 mmol, 20 equiv), 4-bromo-nitrobenzene (67 mg, 0.33 mmol, 25 equiv), PhBr (52.2 mg, 35 μL, 0.33 mmol, 25 equiv), and benzene (1 mL) were heated at 200 °C under N_2 for 12 hours. The kinetic ratio of $Ir^{III}(ttp)C_6H_4(p\text{-}NO_2)$: $Ir^{III}(ttp)Ph$ was found to be 11.77 : 1.00. The crude product was then purified to yield $Ir^{III}(ttp)C_6H_4(p\text{-}NO_2)$ (11.1 mg, 0.011 mmol, 85%) and $Ir^{III}(ttp)Ph$ (0.8 mg, 0.0009 mmol, 7%) (ratio = 12 : 1).

(C) Competition Reactions between *Para*- and *Meta*-Substituted ArBr

(i) 4-Bromoanisole and 3-Bromoanisole. Ir^{III}(ttp)(CO)Cl (10.4 mg, 0.011 mmol), K_2CO_3 (31 mg, 0.23 mmol, 20 equiv), 4-bromoanisole (52.6 mg, 35 μL, 0.28 mmol, 25 equiv), 3-bromoanisole (52.6 mg, 35.6 μL, 0.28 mmol, 25 equiv), and benzene (1 mL) were heated at 200 °C under N_2 for 23 hours. The kinetic ratio of Ir^{III}(ttp)C_6H_4(*p*-OMe) : and Ir^{III}(ttp)C_6H_4(*m*-OMe) was found to be 6.94 : 1.00. The crude product was then purified to yield Ir^{III}(ttp)C_6H_4(*p*-OMe) (9.1 mg, 0.009 mmol, 84%) and Ir^{III}(ttp)C_6H_4(*m*-OMe) (1.6 mg, 0.002 mmol, 15%) (ratio = 5.6 : 1).

(ii) 4-Bromotoluene and 3-Bromotoluene. Ir^{III}(ttp)(CO)Cl (10.5 mg, 0.011 mmol), K_2CO_3 (31 mg, 0.23 mmol, 20 equiv), 4-bromotoluene (48.6 mg, 0.28 mmol, 25 equiv), 3-bromotoluene (48.6 mg, 34.4 μL, 0.28 mmol, 25 equiv), and benzene (1 mL) were heated at 200 °C under N_2 for 26 hours. The kinetic ratio of Ir^{III}(ttp)(*p*-Tol) : Ir^{III}(ttp)(*m*-Tol) from the crude products was found to be 1.52 : 1.00. The crude product was then purified to yield Ir^{III}(ttp)(*p*-Tol) (5.3 mg, 0.006 mmol, 49%) and Ir^{III}(ttp)(*m*-Tol) (3.4 mg, 0.004 mmol, 31%) (ratio = 1.6 : 1).

(iii) 4-Bromo-nitrobenzene and 3-Bromo-nitrobenzene. Ir^{III}(ttp)(CO)Cl (10.7 mg, 0.012 mmol), K_2CO_3 (32 mg, 0.23 mmol, 20 equiv), 4-bromo-nitrobenzene (58.4 mg, 0.29 mmol, 25 equiv), 3-bromo-nitrobenzene (58.4 mg, 0.29 mmol, 25 equiv), and benzene (1 mL) were heated at 200 °C under N_2 for 19 hours. The kinetic ratio of Ir^{III}(ttp)C_6H_4(*p*-NO$_2$) : Ir^{III}(ttp)C_6H_4(*m*-NO$_2$) was found to be 1.46 : 1.00. The crude product was then purified to yield Ir^{III}(ttp)C_6H_4(*p*-NO$_2$) (6.6 mg, 0.007 mmol, 58%) and Ir^{III}(ttp)C_6H_4(*m*-NO$_2$) (4.2 mg, 0.004 mmol, 37%) (ratio = 1.6 : 1).

(D) Competition Reactions between *Meta*-Substituted ArBr and PhBr

(i) 3-Bromoanisole and PhBr. Ir^{III}(ttp)(CO)Cl (5.6 mg, 0.006 mmol), K_2CO_3 (17 mg, 0.12 mmol, 20 equiv), 3-bromoanisole (28.3 mg, 19 μL, 0.15 mmol, 25 equiv), PhBr (23.8 mg, 16 μL, 0.15 mmol, 25 equiv), and benzene (1 mL) were heated at 200 °C under N_2 for 24 hours. The kinetic ratio of Ir^{III}(ttp)C_6H_4(*m*-OMe) : and Ir^{III}(ttp)Ph was found to be 1.06 : 1.00. The crude product was

then purified to yield $Ir^{III}(ttp)C_6H_4(m\text{-}OMe)$ (2.7 mg, 0.003 mmol, 48%) and $Ir^{III}(ttp)Ph$ (2.7 mg, 0.003 mmol, 48%) (ratio = 1 : 1).

(ii) 4-Bromotoluene and PhBr. $Ir^{III}(ttp)(CO)Cl$ (10.8 mg, 0.012 mmol), K_2CO_3 (32 mg, 0.23 mmol, 20 equiv), 3-bromotoluene (49.9 mg, 35.4 μL, 0.29 mmol, 25 equiv), PhBr (45.8 mg, 31 μL, 0.29 mmol, 25 equiv), and benzene (1 mL) were heated at 200 °C under N_2 for 24 hours. The kinetic ratio of $Ir^{III}(ttp)(m\text{-}Tol)$: $Ir^{III}(ttp)Ph$ was found to be 1.03 : 1.00. The crude product was then purified to yield $Ir^{III}(ttp)(m\text{-}Tol)$ (5.3 mg, 0.006 mmol, 48%) and $Ir^{III}(ttp)Ph$ (4.9 mg, 0.005 mmol, 45%) (ratio = 1.1 : 1).

(E) Competition Reactions with *Para*-Substituted ArI and PhI

(i) 4-Iodoanisole. $Ir^{III}(ttp)(CO)Cl$ (7.5 mg, 0.008 mmol), NaOH (6.5 mg, 0.16 mmol, 20 equiv), 4-iodoanisole (47.5 mg, 0.20 mmol, 25 equiv), PhI (41.4 mg, 22.6 μL, 0.20 mmol, 25 equiv), and benzene (1 mL) were heated at 150 °C under N_2 for 15 hours. The kinetic ratio of $Ir^{III}(ttp)C_6H_4(p\text{-}OMe)$: $Ir^{III}(ttp)Ph$ was found to be 8.51 : 1.00. The crude product was then purified to yield $Ir^{III}(ttp)C_6H_4(p\text{-}OMe)$ (6.3 mg, 0.007 mmol, 80%) and $Ir^{III}(ttp)Ph$ (0.7 mg, 0.0007 mmol, 9%) (ratio = 8.9 : 1).

(ii) 4-Iodotoluene. $Ir^{III}(ttp)(CO)Cl$ (7.5 mg, 0.008 mmol), NaOH (6.5 mg, 0.16 mmol, 20 equiv), 4-iodotoluene (44 mg, 0.20 mmol, 25 equiv), PhI (41.4 mg, 22.6 μL, 0.20 mmol, 25 equiv), and benzene (1 mL) were heated at 150 °C under N_2 for 15 hours. The kinetic ratio of $Ir^{III}(ttp)(p\text{-}Tol)$: $Ir^{III}(ttp)Ph$ was found to be 2.23 : 1.00. The crude product was then purified to yield $Ir^{III}(ttp)(p\text{-}Tol)$ (4.6, 0.005 mmol, 61%) and $Ir^{III}(ttp)Ph$ (2.1 mg, 0.002 mmol, 28%) (ratio = 2.2 : 1).

(iii) 1-Fluoro-4-iodobenzene. $Ir^{III}(ttp)(CO)Cl$ (8.1 mg, 0.009 mmol), NaOH (7 mg, 0.18 mmol, 20 equiv), 1-fluoro-4-iodobenzene (48.6 mg, 0.22 mmol, 25 equiv), PhI (44.7 mg, 24.4 μL, 0.22 mmol, 25 equiv), and benzene (1 mL) were heated at 150 °C under N_2 for 36 hours. The kinetic ratio of $Ir^{III}(ttp)C_6H_4(p\text{-}F)$: $Ir^{III}(ttp)Ph$ was found to be 2.69 : 1.00. The crude product was then purified to yield $Ir^{III}(ttp)C_6H_4(p\text{-}F)$ (5.1, 0.005 mmol, 61%) and $Ir^{III}(ttp)Ph$ (2.1 mg, 0.002 mmol,

26%) (ratio = 2.3 : 1).

(iv) 1,4-Diiodobenzene. Ir^{III}(ttp)(CO)Cl (7.5 mg, 0.008 mmol), NaOH (6.5 mg, 0.16 mmol, 20 equiv), 1-4-diiodobenzene (67 mg, 0.20 mmol, 25 equiv), PhI (41.4 mg, 22.4 μL, 0.20 mmol, 25 equiv), and benzene (1 mL) were heated at 150 °C under N_2 for 21 hours. The kinetic ratio of Ir^{III}(ttp)C_6H_4(p-I) : Ir^{III}(ttp)Ph was found to be 5.35 : 1.00 by ^{1}H NMR spectroscopy by averaging the original kinetic ratio (10.70 : 1) due to the presence of 2 C-I bonds in 1,4-diiodobenzene for reaction. The crude product was then purified to yield Ir^{III}(ttp)C_6H_4(p-I) (6.3 mg, 0.006 mmol, 72%) and Ir^{III}(ttp)Ph (0.6 mg, 0.0006 mmol, 7%) (ratio = 10.3 : 1).

(v) 1-Bromo-4-iodobenzene. Ir^{III}(ttp)(CO)Cl (7.9 mg, 0.009 mmol), NaOH (mg, mmol, 20 equiv), 1-bromo-4-iodobenzene (59.4 mg, 0.21 mmol, 25 equiv), PhI (43.6 mg, 24 μL, 0.21 mmol, 25 equiv), and benzene (1 mL) were heated at 200 °C under N_2 for 29 hours. The kinetic ratio of Ir^{III}(ttp)C_6H_4(p-Br) : Ir^{III}(ttp)Ph from the crude products was estimated to be 5.81 : 1.00 by ^{1}H NMR spectroscopy. The crude product was then purified to yield Ir^{III}(ttp)C_6H_4(p-Br) (5.9 mg, 0.006 mmol, 68%) and Ir^{III}(ttp)Ph (0.9 mg, 0.0009 mmol, 11%) (ratio = 6.2 : 1).

(F) Competition Reactions with *Para*-Substituted ArCl and PhCl

(i) 4-Chloroanisole. Ir^{III}(ttp)(CO)Cl (8.5 mg, 0.009 mmol), K_2CO_3 (25 mg, 0.18 mmol, 20 equiv), 4-chloroanisole (131.1 mg, 113 μL, 0.92 mmol, 100 equiv), PhCl (103.5 mg, 93.5 μL, 0.92 mmol, 100 equiv), and benzene (1 mL) were heated at 150 °C under N_2 for 35 hours. The kinetic ratio of Ir^{III}(ttp)C_6H_4(p-OMe) : Ir^{III}(ttp)Ph was estimated to be 4.39 : 1.00 by ^{1}H NMR spectroscopy. The crude product was then purified to yield Ir^{III}(ttp)C_6H_4(p-OMe) (5.9 mg, 0.006 mmol, 66%), Ir^{III}(ttp)Ph (1.7 mg, 0.002 mmol, 19%) (ratio = 3.5 : 1), and Ir^{III}(ttp)CH_3 (0.2 mg, 0.0003 mmol, 3%).

(ii) 1-Fluoro-4-chlorobenzene. Ir^{III}(ttp)(CO)Cl (8.6 mg, 0.009 mmol), K_2CO_3 (25.7 mg, 0.19 mmol, 20 equiv), 1-fluoro-4-chlorobenzene (121.4 mg, 99 μL, 0.93 mmol, 100 equiv), PhCl (104.7 mg, 95 μL, 0.93 mmol, 100 equiv), and benzene (1 mL) were heated at 150 °C under N_2 for 38

hours. The kinetic ratio of $Ir^{III}(ttp)C_6H_4(p$-$F)$: $Ir^{III}(ttp)Ph$ was found to be 3.29 : 1.00. The crude product was then purified to yield $Ir^{III}(ttp)C_6H_4(p$-$F)$ (4.4 mg, 0.005 mmol, 50%), $Ir^{III}(ttp)Ph$ (1.4 mg, 0.001 mmol, 16%) (ratio = 3.1 : 1), and $Ir^{III}(ttp)CH_3$ (0.3 mg, 0.0003 mmol, 4%).

(iii) 1,4-Dichlorobenzene. $Ir^{III}(ttp)(CO)Cl$ (10.8 mg, 0.012 mmol), K_2CO_3 (32 mg, 0.23 mmol, 20 equiv), 1,4-dichlorobenzene (171.7 mg, 1.17 mmol, 100 equiv), PhCl (131.5 mg, 119 μL, 1.17 mmol, 100 equiv), and benzene (1 mL) were heated at 200 ^{o}C under N_2 for 60 hours. The kinetic ratio of $Ir^{III}(ttp)C_6H_4(p$-$F)$: $Ir^{III}(ttp)Ph$ was found to be 5.74 : 1.00 by ^{1}H NMR spectroscopy by averaging the original kinetic ratio (11.48 : 1) due to the presence of 2 C-Cl bond in 1,4-diichlorobenzene for reaction. The crude product was then purified to yield $Ir^{III}(ttp)C_6H_4(p$-$Cl)$ (8.0 mg, 0.008 mmol, 70%), $Ir^{III}(ttp)Ph$ (0.9 mg, 0.001 mmol, 8%) (ratio = 8.8 : 1), $Ir^{III}(ttp)(p$-$C_6H_4)Ir^{III}(ttp)$ (3%, NMR yield), and $Ir^{III}(ttp)CH_3$ (3%, NMR yield). The NMR yields of $Ir^{III}(ttp)(p$-$C_6H_4)Ir^{III}(ttp)$ and $Ir^{III}(ttp)CH_3$ were estimated by using the yield of $Ir^{III}(ttp)C_6H_4(p$-$Cl)$ and the ratios of pyrrole proton signals of $Ir^{III}(ttp)C_6H_4(p$-$Cl)$: $Ir^{III}(ttp)(p$-$C_6H_4)Ir^{III}(ttp)$: $Ir^{III}(ttp)CH_3$ in the crude products.

(iv) 4-Chlorobenzonitrile. $Ir^{III}(ttp)(CO)Cl$ (10.3 mg, 0.011 mmol), K_2CO_3 (31 mg, 0.22 mmol, 20 equiv), 4-chlorobenzonitrile (153.3 mg, 1.11 mmol, 100 equiv), PhCl (125.4 mg, 113 μL, 1.11 mmol, 100 equiv), and benzene (1 mL) were heated at 200 ^{o}C under N_2 for 3.5 days. PPh$_3$ (29.2 mg, 0.11 mmol, 10 equiv) was added under N_2 and the reaction was further heated at 120 ^{o}C for 30 minutes. The kinetic ratio of $Ir^{III}(ttp)(PPh_3)C_6H_4(p$-$CN)$: $Ir^{III}(ttp)(PPh_3)Ph$ was found to be 29.8 : 1.00 by ^{1}H NMR spectroscopy. The crude product was then purified to yield $Ir^{III}(ttp)(PPh_3)C_6H_4(p$-$CN)$ (4.9 mg, 0.004 mmol, 40%) and a trace of $Ir^{III}(ttp)Ph$.

Studies of Base-Promoted Aryl Exchanges between $Ir^{III}(ttp)Ph$ and Arylating Agents

The experimental procedure of the reaction of $Ir^{III}(ttp)Ph$ with benzene-d_6 and K_2CO_3 were described as a typical example.

(a) Exchange with Benzene-d_6 in the Presence of K_2CO_3. $Ir^{III}(ttp)Ph$ (5.0 mg, 0.005 mmol),

K_2CO_3 (14.7 mg, 0.11 mmol), and benzene-d_6 (0.5 mL) were degassed for three freeze-pump-thaw cycles in a Teflon screw capped NMR tube and then flame-sealed under vacuum. The reaction mixture was heated at 200 ^{o}C, and the reaction was monitored by ^{1}H NMR spectroscopy. After 5 days, no deuterium incoporation occurred to form $Ir^{III}(ttp)C_6D_5$, and $Ir^{III}(ttp)Ph$ (91%, NMR yield) was recovered using the residual benzene proton signal as an internal standard.

(b) Exchange with Benzene-d_6 in the Presnece of KOH. $Ir^{III}(ttp)Ph$ (3.0 mg, 0.003 mmol), KOH (3.6 mg, 0.064 mmol), and benzene-d_6 (0.5 mL) were heated in a sealed NMR tube under vacuum at 200 ^{o}C, and the reaction was monitored by ^{1}H NMR spectroscopy. After 7 days, no deuterium incoporation occurred to give $Ir^{III}(ttp)C_6D_5$, and $Ir^{III}(ttp)Ph$ (55%, NMR yield) was recovered using the residual benzene proton signal as an internal standard.

(c) Exchange with 4-Bromo-nitrobenzene in the Presence of KOH. $Ir^{III}(ttp)Ph$ (2.8 mg, 0.003 mmol), KOH (3.3 mg, 0.060 mmol), 4-bromo-nitrobenzene (15.1 mg, 0.075 mmol, 25 equiv), and benzene-d_6 (0.5 mL) were heated in a sealed NMR tube under vacuum at 200 ^{o}C, and the reaction was monitored by ^{1}H NMR spectroscopy. After 7 days, no $Ir^{III}(ttp)C_6H_4(p\text{-}NO_2)$ was formed, and $Ir^{III}(ttp)Ph$ (77%, NMR yield) was recovered using the residual benzene proton signal as an internal standard.

References for Reported Preparations of Compounds:

(1) Alder, A. D.; Logon, F. R.; Finarelli, J. D.; Goldmacher, J.; Assour, J.; Korsakof, L. *J. Org. Chem.* **1967**, *32*, 476.

(2) van der Ent, A.; Onderdelinden, A. L. *Inorg. Synth.* **1973**, *14*, 92-95.

(3) (a) Ogoshi, H.; Setsune, J.-I.; Yoshida, Z.-I. *J. Organomet. Chem.* **1978**, *159*, 317–328. (b) Yeung, S. K.; Chan, K. S. *Organometallics* **2005**, *24*, 6426-6430.

(4) Cheung, C.W.; Chan, K. S. *Organometallics* **2008**, *27*, 3043–3055.

(5) Cheung, C. W.; Fung, H. S.; Lee, S. Y.; Qian, Y. Y.; Chan, Y. W.; Chan, K. S. *Organometallics* **2010**, *29*, 1343–1354.

(6) Song, X.; Chan, K. S. *Organometallics* **2007**, *26*, 965-970.

(7) Chan, K. S.; Leung, Y.-B. *Inorg. Chem.* **1994**, *33*, 3187.

(8) Wayland, B. B.; Vanvoorhees, S. L.; Wilker, C. *Inorg. Chem.* **1986**, *25*, 4039-4042.

(9) Abu-Omar, M. M.; Espenson, J. H. *J. Am. Chem. Soc.* **1995**, *117*, 272-280.

Appendix

Appendix I   Calculation Procedures

(1) Estimation of redox potentials of HO•/OH⁻ in saturated KOH / DMSO solution and at elevated temperatures

The oxidation potential of HO•/ HO$^{\ominus}$ couple ([OH⁻] = 0.0043 M) in DMSO at 24 °C (297 K) is reported as the standard oxidation potental (E_{ox}^{o})[1]:

$$HO^{\ominus} \xrightarrow[\substack{24\ ^{\circ}C}]{DMSO} HO\bullet\ +\ e^{\ominus} \qquad E_{ox}^{o}\ =\ +0.75\ V$$
$$\substack{0.0043\ M}$$
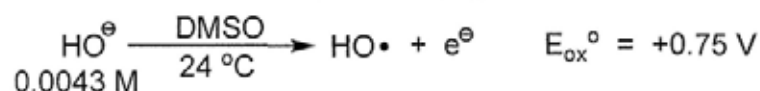
The oxidation potential of HO•/ HO$^{\ominus}$ in DMSO at 25 °C (298 K) in saturated KOH / DMSO solution ([KOH] = 0.037 M)[2] can be estimated using the Nernst equation:

$$\boxed{E\ =\ E^{o}\ -\ \frac{RT}{nF}\ \ln\frac{[HO^{\ominus}]}{[HO\bullet]}}$$

where R = 8.314 J K^{-1} mol^{-1}
T = temperature (K)
n = no. of mole of e⁻ involved in rxn
F = 96485 C mol^{-1}
[HO•] = [HO•] formed in the standard condition
= 0.0043 M

$$E_{ox}(KOH(sat'd,298K))\ \sim\ 0.75\ -\ \frac{8.314(298)}{1(96485)}\left(\ln\frac{0.037}{0.0043}\right)$$
$$\sim\ 0.70\ V$$

Thus, OH⁻ is a more efficient reducing agent in saturated KOH / DMSO solution.

The redox potential of HO• / HO$^{\ominus}$ in DMSO at 120 °C (393 K) and 200 °C (473 K) in saturated KOH / DMSO solution ([DMSO] = 0.037 M) can also be estimated using the Nernst equation:

$$E_{ox}(KOH(sat'd,393K))$$
$$\sim\ 0.75\ -\ \frac{8.314(393)}{1(96485)}\left(\ln\frac{0.037}{0.0043}\right)$$
$$\sim\ 0.68\ V$$

$$E_{ox}(KOH(sat'd,473K))$$
$$\sim\ 0.75\ -\ \frac{8.314(473)}{1(96485)}\left(\ln\frac{0.037}{0.0043}\right)$$
$$\sim\ 0.66\ V$$

Thus, OH⁻ is a much more efficient reducing agent in saturated KOH / DMSO solution when temperature increases.

References:

(1) Goolsby, A. D.; Sawyer, D. T. *Anal. Chem.* **1968**, *40*, 83-86.

(2) Trofimov, B. A.; Vasiltsov, A. M.; Amosova, S. V. *Russ. Chem. Bull.* **1986**, *35*, 682-686.

(2) Estimation of maximal amount of H_2 dissolved in benzene-d_6 in dehydrogenative dimerization of $Ir^{III}(ttp)H$ to $[Ir^{II}(ttp)]_2$ and H_2

The concentration of H_2 in benzene ($[H_2]$, in M) as a function of temperature (T, in K) and H_2 pressure (P, in atm) in a sealed NMR tube is given by the following expression,[1] where P_{atm} is the H_2 pressure in atmosphere at 23 °C, T is the temperature at 23 °C.

$$[H_2]_{T,P} = [2.3421 \times 10^{-3} \text{ M} + (2.2592 \times 10^{-5})\, T(^{o}C)]\, P_{atm}$$

Assume **x** = % yield of H_2 dissolved in benzene-d_6

maximal no. of mole of H_2 formed
= no. of mole of $Ir^{III}(ttp)H$ in benzene-d_6
= 0.005 mmol
= 5×10^{-6} mol

Conc. of mole of $Ir^{III}(ttp)H$ dissolved in benzene-d_6
= $(5 \times 10^{-6}$ mol$)\textbf{x} / 0.5 \times 10^{-3}$ L
= $(0.010\ \textbf{x})$ M

Pressure of H_2 in gas phase
= $[H_2]_{T,P} / [2.3421 \times 10^{-3} \text{ mol L}^{-1} + (2.2592 \times 10^{-5})T]$
= $0.010\textbf{x} / [2.3421 \times 10^{-3} + (2.2592 \times 10^{-5})(23\ ^{o}C)]$
= $0.010\textbf{x} / (2.862 \times 10^{-3})$
= $(3.49\textbf{x})$ atm

Mole of H_2 in gas phase
= $(PV) / (RT)$
= $[(3.49\textbf{x})\ (3 \times 10^{-6})] / [(8.206 \times 10^{-5})(296)]$
= $(4.31 \times 10^{-4}\textbf{x})$ mol

where P = pressure of H_2 (3.49**x** atm)
V = volume of H_2 (~3×10^{-6} m³)
R = 8.206×10^{-5} m³ atm K⁻¹ mol⁻¹
T = 296 K

Total mole of H_2 formed in benzene-d_6
= 5×10^{-6} mol
= $5 \times 10^{-6}\textbf{x} + 4.31 \times 10^{-4}\textbf{x}$
= $(4.36 \times 10^{-4}\textbf{x})$ mol

$4.36 \times 10^{-4}\ \textbf{x} = 5 \times 10^{-6}$
x = 0.011
x = 1.1%

Therefore, the maximal yield of H_2 dissolved in benzene-d_6 is 1.1%, which is out of the detection limit of ^1H NMR spectroscopy.

Reference:

(1) Wayland, B. B; Ba, S.; Sherry, A. E. *Inorg. Chem.* **1992**, *31*, 148-150.

Appendix II   Hammett Plots of Base-Promoted Ar-X (X = Cl, Br, I) Cleavages by $Ir^{III}(ttp)(CO)Cl$

(i) Competition Reactions of Aryl Bromides

$Ir^{III}(ttp)(CO)Cl$ + Br-⟨⟩-FG / Br-⟨⟩ $\xrightarrow[C_6H_6, 200\ ^\circ C]{K_2CO_3\ (20\ equiv)}$ $Ir^{III}(ttp)$-⟨⟩-FG + $Ir^{III}(ttp)$-⟨⟩

25 equiv   25 equiv   log (k_{FG}/k_H)

Figure 1(a) Hammett plot of Ar-Br cleavage using the Hammett constants σ^o_p (Table 3.36).

Figure 1(b) Hammett plot of Ar-Br cleavage using Hammett constants σ^+_p (Table 3.36).

(ii) Competition Reactions of Aryl Iodides
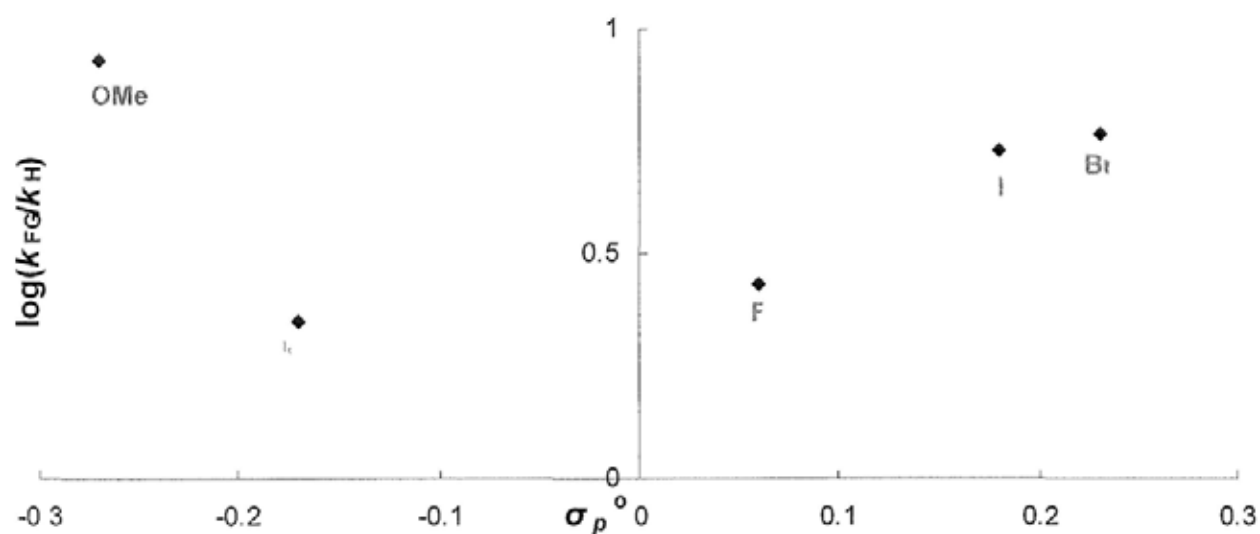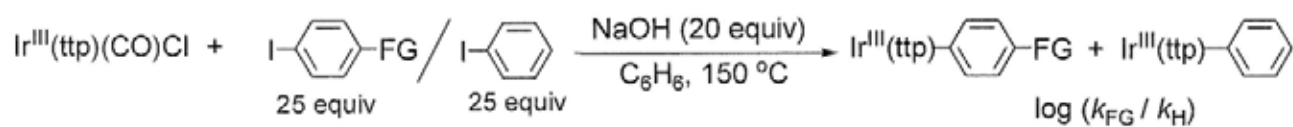
Figure 2(a) Hammett plot of Ar-I cleavage using the Hammett constants σ^o_p (Table 3.37).
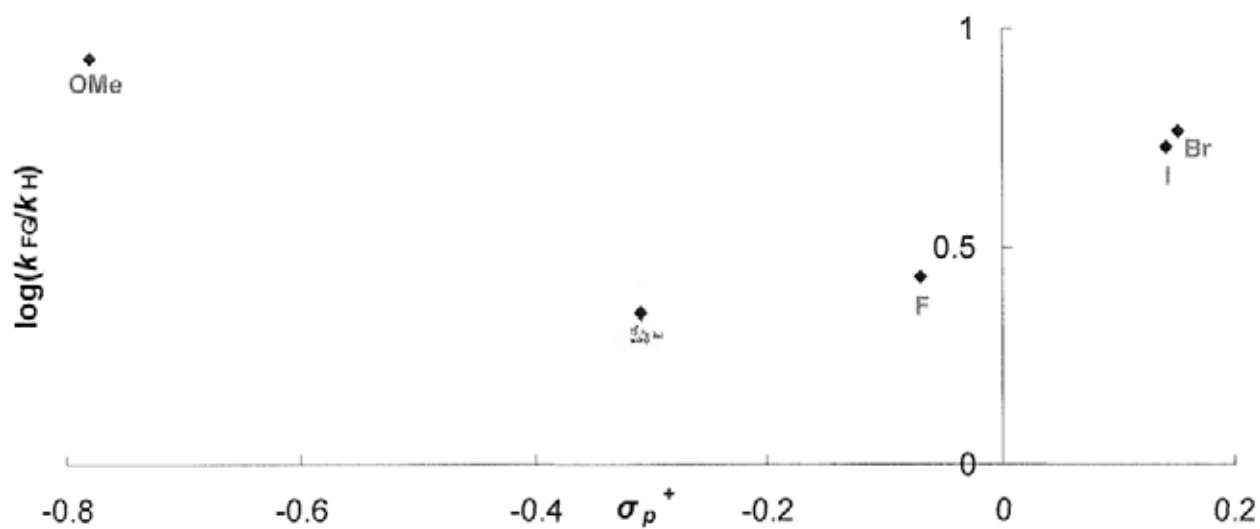
Figure 2(b) Hammett plot of Ar-I cleavage using Hammett constants σ^+_p (Table 3.37).

(iii) Competition Reactions of Aryl Chlorides

$$Ir^{III}(ttp)(CO)Cl \ + \ Cl\text{-}\underset{\text{100 equiv}}{\bigcirc}\text{-}FG \Big/ Cl\text{-}\underset{\text{100 equiv}}{\bigcirc} \xrightarrow[\text{C}_6\text{H}_6,\ 150\ ^\circ\text{C}]{\text{K}_2\text{CO}_3\ (20\ \text{equiv})} Ir^{III}(ttp)\text{-}\bigcirc\text{-}FG \ + \ Ir^{III}(ttp)\text{-}\bigcirc$$

$$\log(k_{FG}/k_H)$$
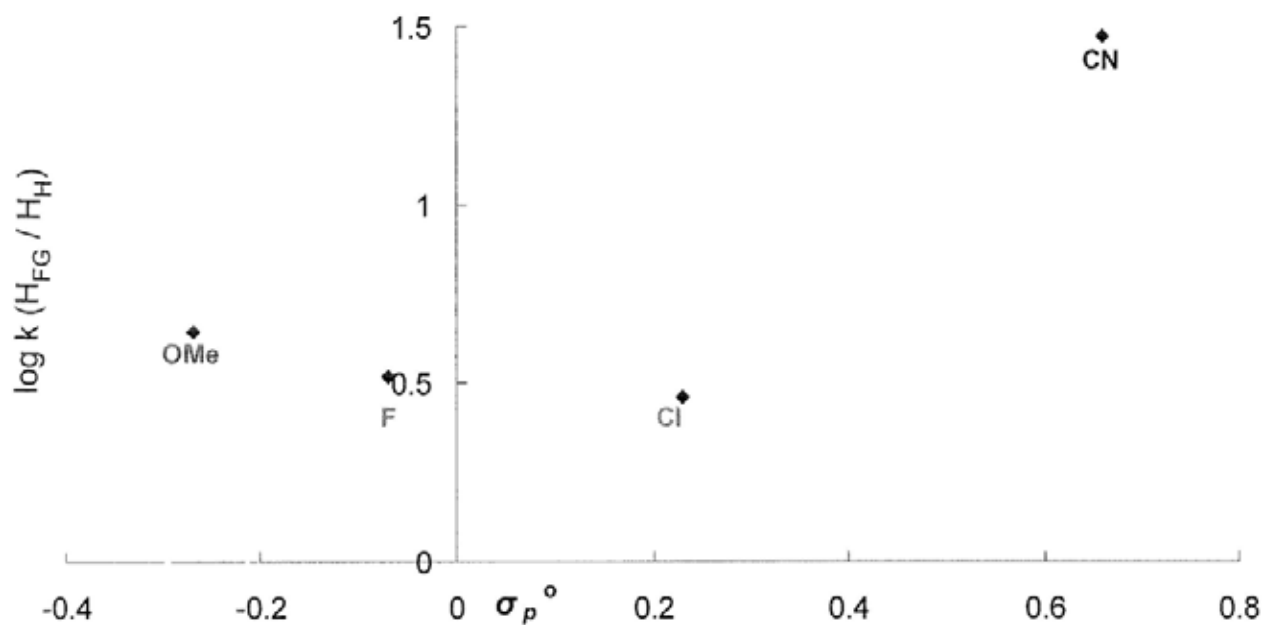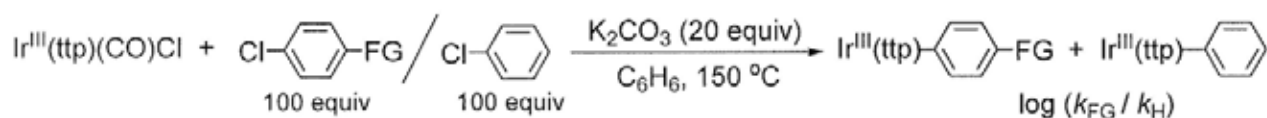
Figure 3(a) Hammett plot of Ar-Cl cleavage using the Hammett constants σ^o_p (Table 3.38).
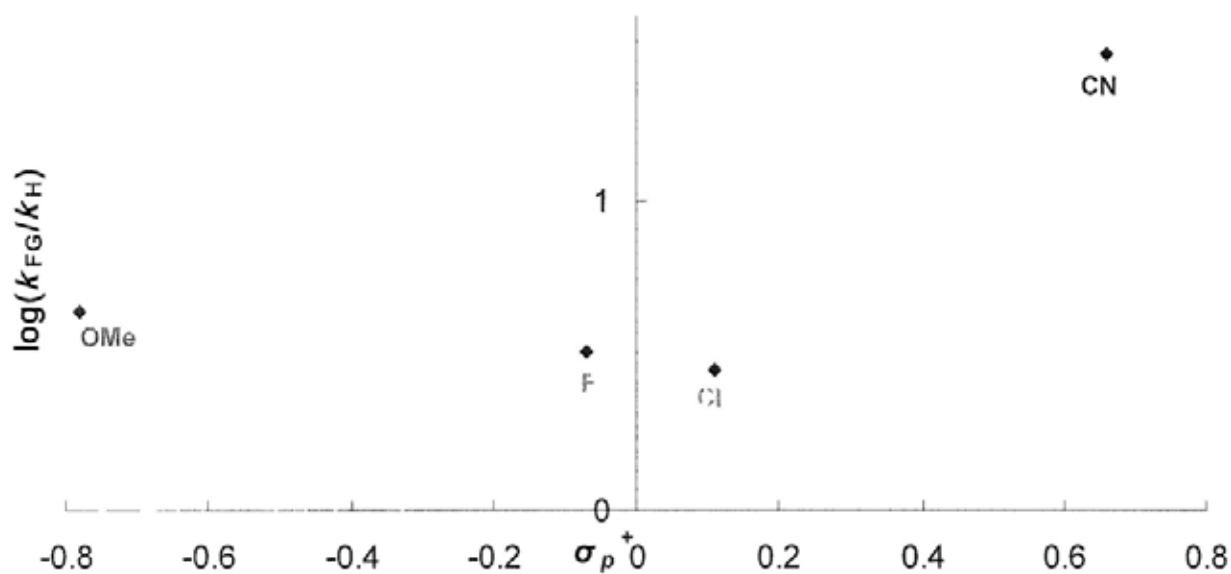
Figure 3(b) Hammett plot of Ar-Cl cleavage using Hammett constants σ^+_p (Table 3.38).

266

Appendix III   X-Ray Crystallographic Data and Structures of $Ir^{III}(ttp)Ar$

(1) X-Ray Data and Structures of $Ir^{III}(ttp)Ar$

(i) $Ir^{III}(ttp)C_6H_4(p\text{-OMe})$ (8c)
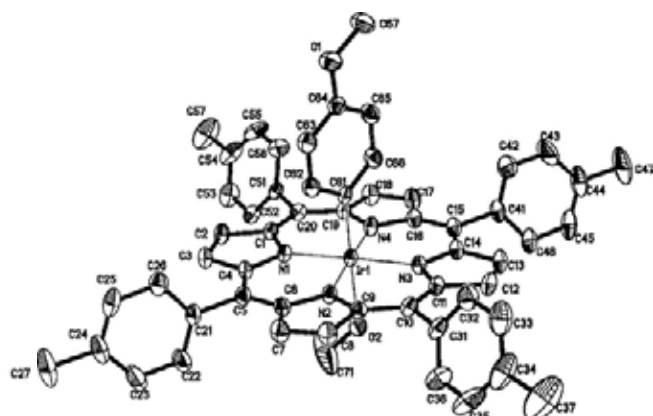
Figure 1 ORTEP presentation of the molecular structure with numbering scheme (left) and wireframe presentation of the molecular structure (right) for $Ir^{III}(ttp)C_6H_4(p\text{-OMe})(CH_3OH)$ (**8c**) (30% probability displacement ellipsoids). Selected bond lengths (Å) Ir(1)–C(61) = 2.023(4).

(ii) $Ir^{III}(ttp)(p\text{-Tol})$ (8e)
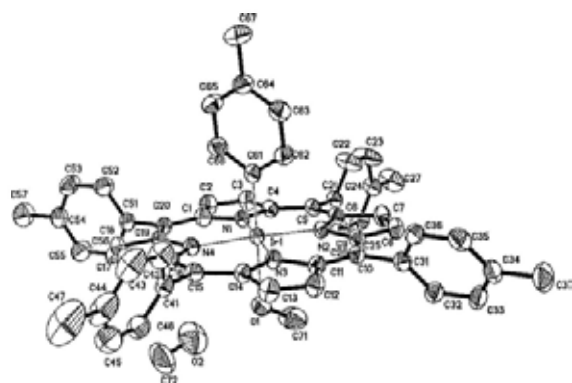
Figure 2 ORTEP presentation of the molecular structure with numbering scheme (left) and wireframe presentation of the molecular structure (right) for $Ir^{III}(ttp)(p\text{-Tol})(CH_3OH)\cdot CH_3OH$ (**8e**) (30% probability displacement ellipsoids). probability displacement ellipsoids). Selected bond lengths (Å) Ir(1)–C(61) = 2.033(5).

(iii) Ir^{III}(ttp)C$_6$H$_4$(p-NO$_2$) (8p)
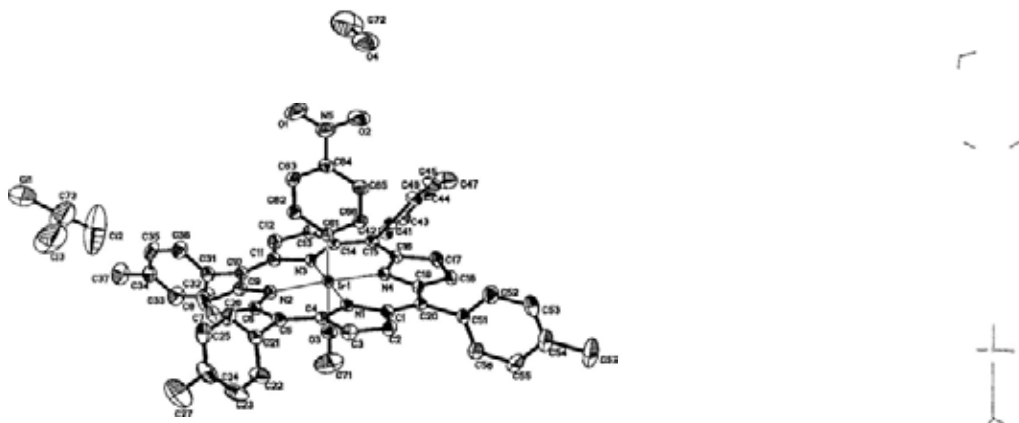
Figure 3 ORTEP presentation of the molecular structure with numbering scheme (left) and wireframe presentation of the molecular structure (right) for Ir^{III}(ttp)C$_6$H$_4$(p-NO$_2$)(CH$_3$OH)•CH$_3$OH•CHCl$_3$ (**8p**) (30% probability displacement ellipsoids). Selected bond lengths (Å) Ir(1)–C(61) = 1.990(6).

(iv) Ir^{III}(ttp)(p-C$_6$H$_4$)$_2$Ir^{III}(ttp) (9b)
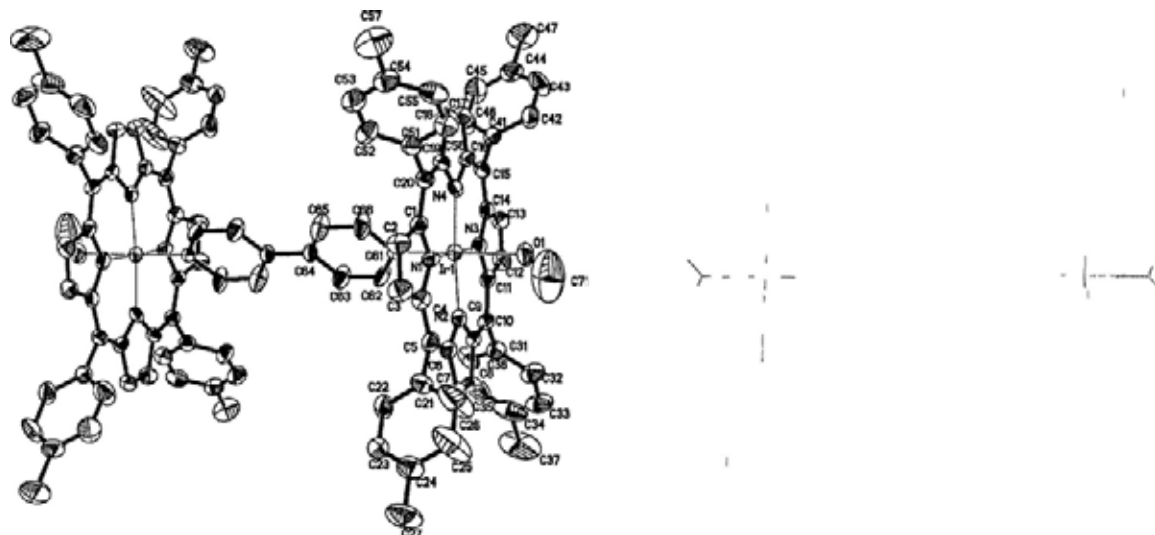
Figure 4 ORTEP presentation of the molecular structure with numbering scheme (left) and wireframe presentation of the molecular structure (right) for (CH$_3$OH)Ir^{III}(ttp)(p-C$_6$H$_4$)$_2$Ir^{III}(ttp)(CH$_3$OH) (**9b**) (30% probability displacement ellipsoids). Selected bond lengths (Å) Ir(1)–C(61) = 2.027(8).

(v) Ir^{III}(ttp)Ph (8a)

Figure 5 ORTEP presentation of the disordered molecular structure with numbering scheme (top) and wireframe presentation of the disordered molecular structure (bottom) for Ir^{III}(ttp)Ph (**8a**) (30% probability displacement ellipsoids). Selected bond lengths (Å) Ir(1)–C(31) = 2.158(11), which is the average value of the Ir(1)-C(31) bond lengths from the two disordered structures.

(vi) Ir^{III}(ttp)C$_6$H$_4$(p-SiMe$_3$) (8f)
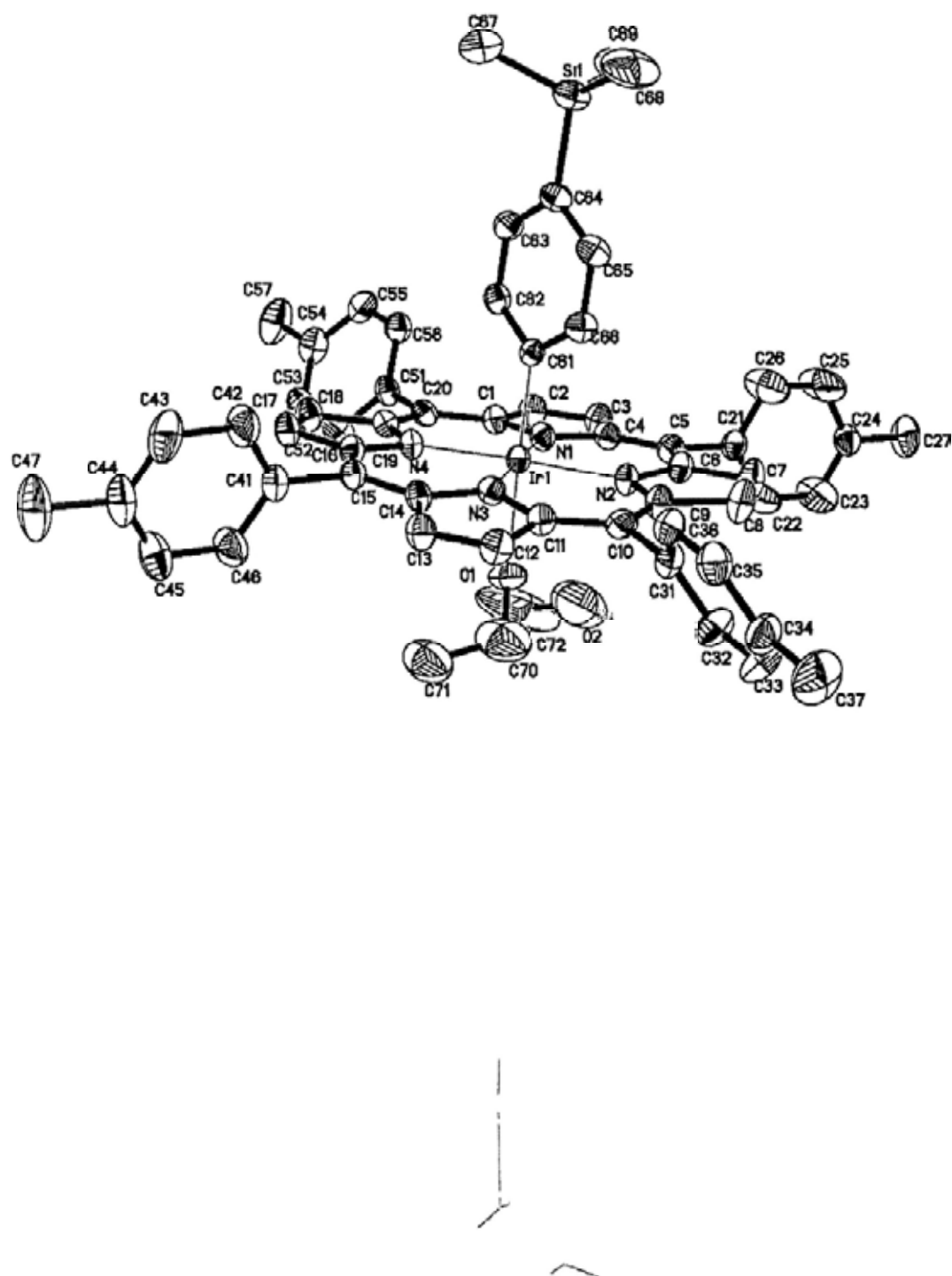
Figure 6 ORTEP presentation of the molecular structure with numbering scheme (top) and wireframe presentation of the molecular structure (bottom) for Ir^{III}(ttp)C$_6$H$_4$(p-SiMe$_3$)(EtOH)•MeOH (**8f**) (30% probability displacement ellipsoids). Selected bond lengths (Å) Ir(1)–C(61) = 2.024(5).

(2) Conformations of Porphyrins in Ir^{III}(ttp)Ar (8a, 8c, 8e, 8f, 8p, 9b)

Ir^{III}(ttp)C$_6$H$_4$(p-OMe) (8c)

Ir^{III}(ttp)(p-Tol) (8e)

Ir^{III}(ttp)C$_6$H$_4$(p-SiMe$_3$) (8f)

Ir^{III}(ttp)Ph (8a) (two disordered structure)

Ir^{III}(ttp)C$_6$H$_4$(p-NO$_2$) (8p)

Ir^{III}(ttp)(p-C$_6$H$_4$)$_2$Ir^{III}(ttp) (9b)
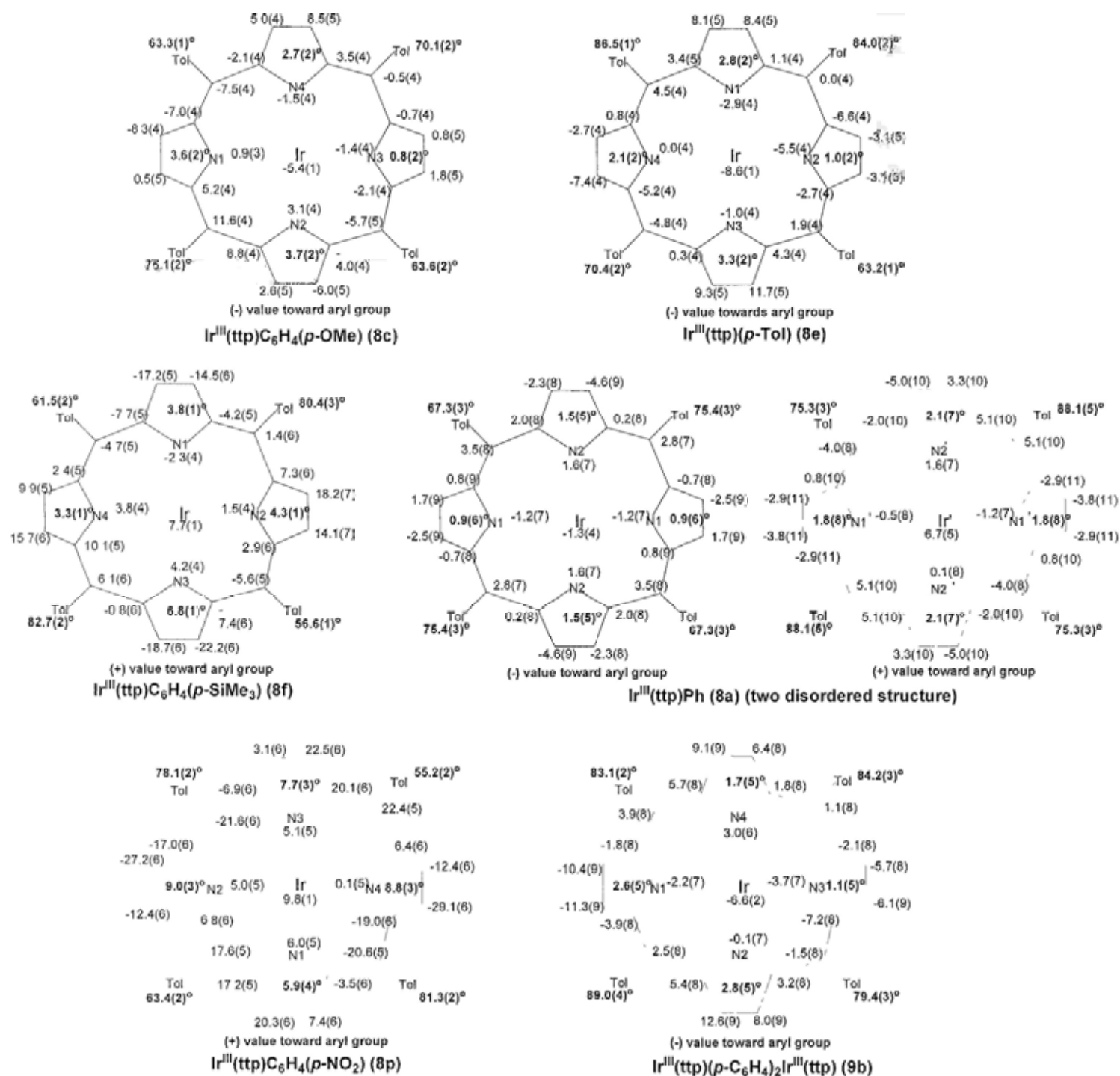
Figure 7 The conformations of porphyrins in Ir^{III}(ttp)C$_6$H$_4$(p-OMe) (**8c**), Ir^{III}(ttp)(p-Tol) (**8e**), Ir^{III}(ttp)C$_6$H$_4$(p-SiMe$_3$) (**8f**), Ir^{III}(ttp)Ph (**8a**), Ir^{III}(ttp)C$_6$H$_4$(p-NO$_2$) (**8p**), Ir^{III}(ttp)(p-C$_6$H$_4$)$_2$Ir^{III}(ttp) (**9b**), showing the displacements of the core atoms and of Ir from the 24-atom least squares planes of porphyrin cores (in pm; negative or positive values correspond to displacement towards the aryl ligand). Absolute values of angles between the pyrrole rings and the least-squares planes, and angles between the tolyl substituents and the least-squares planes, are shown in bold.

(3) Crystal Data and Structure Refinement Parameters for $Ir^{III}(ttp)Ar$

Table 1 Crystal Data and Structure Refinement Parameters for $Ir^{III}(ttp)Ar$ (1)

compounds	$Ir^{III}(ttp)C_6H_4(p\text{-}OMe)$ (8c)	$Ir^{III}(ttp)(p\text{-}Tol)$ (8e)	$Ir^{III}(ttp)C_6H_4(p\text{-}SiMe_3)$ (8f)
color, shape	purple prism	purple prism	purple prism
empirical formula	$C_{55}H_{43}N_4OIr$ $\cdot CH_3OH$	$C_{55}H_{43}N_4Ir$ $\cdot 2CH_3OH$	$C_{57}H_{49}N_4SiIr$ $\cdot CH_3CH_2OH \cdot CH_3OH$
formula wt	1000.18	1016.22	1088.40
temp (K)	293(2)	293(2)	293(2)
Wavelength (Å)	0.71073	0.71073	0.71073
cryst syst	tetragonal	monoclinic	monoclinic
space group	I4 (1)	P2(1) / c	P2(1) / n
unit cell dimens			
a (Å)	19.2067 (10)	11.4621(14)	15.157(3)
b (Å)	19.2067 (10)	17.214(2)	22.886(5)
c (Å)	25.478 (3)	25.013(3)	16.111(3)
α (Å)	90	90	90
β (Å)	90	97.846(3)	107.682(3)
γ (Å)	90	90	90
volume ($Å^3$)	9398.8 (12)	4889.1(10)	5324.4(18)
Z	8	4	4
calcd density (g cm^{-3})	1.414	1.381	1.358
abs coeff (mm^{-1})	2.887	2.776	2.575
$F(000)$	4032	2056	2216
cryst size (mm)	$0.50 \times 0.40 \times 0.30$	$0.50 \times 0.40 \times 0.30$	$0.50 \times 0.40 \times 0.30$
θ range for data collection (deg)	1.33 to 28.03	1.44 to 25.00	1.60 to 25.00
limiting indices	$-20 \leq h \leq 25$ $-25 \leq k \leq 25$ $-28 \leq l \leq 33$	$-13 \leq h \leq 13$ $-20 \leq k \leq 20$ $-16 \leq l \leq 29$	$-18 \leq h \leq 17$ $-27 \leq k \leq 26$ $-19 \leq l \leq 19$
no of rflns collected/unique	31882 / 10629 [R(int) = 0.0350]	25968 / 8610 [R(int) = 0.0364]	28472 / 9345 R(int) = 0.0558]
completeness to $\theta = 28.24$	100.0%	99.9 %	99.9 %
absorp corr	SADABS	SADABS	SADABS
max. and min. transmn	1.000 and 0.697453	1.000 and 0.532193	1.0000 and 0.199487
refinement method	Full-matrix least-squares on F^2	Full-matrix least-squares on F^2	Full-matrix least-squares on F^2
no. of data/restraints/params	10629 / 1 / 568	8610 / 0 / 577	9345 / 1 / 613
GOF	1.044	1.076	1.019
final R indices [$I > 2\sigma(I)$]	$R_1{}^a = 0.0288$ $wR_2{}^b = 0.0603$	$R_1{}^a = 0.0307$ $wR_2{}^b = 0.0693$	$R_1{}^a = 0.0421$ $wR_2{}^b = 0.1102$
R indices (all data)	$R_1{}^a = 0.0409$ $wR_2{}^b = 0.0655$	$R_1{}^a = 0.0544$ $wR_2{}^b = 0.0815$	$R_1{}^a = 0.0594$ $wR_2{}^b = 0.1170$
largest diff peak and hole (e $Å^{-3}$)	1.272 and -0.570	1.117 and -0.671	1.904 and -0.842
$w_1/w_2{}^c$	0.0266/0.3443	0.0378/1.6359	0.0676/0.0000

$^a R_1 = \sum \left(\|F_0| - |F_c\| \right) / \sum |F_0|$. $^b wR_2 = \left\{ \sum \left[w \left(F_0^2 - F_c^2 \right)^2 \right] / \sum \left[w \left(F_0^2 \right)^2 \right] \right\}^{1/2}$. ^{c} Weighting scheme $w^{-1} = \sigma^2 \left(F_0^2 \right) + \left(w_1 P \right)^2 + w_2 P$

where $P = \left(F_0^2 + 2F_c^2 \right) / 3$.

Table 2 Crystal Data and Structure Refinement Parameters for Ir^{III}(ttp)Ar (2)

compounds	Ir^{III}(ttp)Ph (8a)	Ir^{III}(ttp)C_6H_4(p-NO_2) (8p)	Ir^{III}(ttp)(p-C_6H_4)$_2$-Ir^{III}(ttp) (9b)
color, shape	purple prism	purple prism	purple prism
empirical formula	$C_{54}H_{41}N_4Ir$	$C_{54}H_{40}N_5O_2Ir$ •2CH_3OH•$CHCl_3$	$C_{108}H_{80}N_8Ir_2$ •2CH_3OH
formula wt	938.11	1166.56	1938.28
temp (K)	293(2)	293(2)	293(2)
Wavelength (Å)	0.71073	0.71073	0.71073
cryst syst	triclinic	monoclinic	monoclinic
space group	P-1	P2(1) / n	P2(1) / n
unit cell dimens			
a (Å)	11.3189(19)	17.819(3)	15.373(9)
b (Å)	12.050(2)	13.421(3)	19.751(12)
c (Å)	19.000(4)	21.519(4)	17.321(10)
α (Å)	76.108(5)	90	90
β (Å)	72.703(3)	97.439(4)	96.782(10)
γ (Å)	71.709(3)	90	90
volume (Å^3)	2318.3(7)	5103.1(16)	5222 (5)
Z	2	4	2
calcd density (g cm^{-3})	1.344	1.518	1.233
abs coeff (mm^{-1})	2.918	2.826	2.594
F(000)	940	2344	1948
cryst size (mm)	0.40 × 0.30 × 0.20	0.40 × 0.30 × 0.20	0.40 × 0.30 × 0.20
θ range for data collection (deg)	1.14 to 25.00	1.40 to 25.00	1.57 to 25.00
limiting indices	$-13 \leq h \leq 11$ $-14 \leq k \leq 13$ $-22 \leq l \leq 19$	$-21 \leq h \leq 20$ $-15 \leq k \leq 13$ $-25 \leq l \leq 25$	$-18 \leq h \leq 17$ $-23 \leq k \leq 22$ $-20 \leq l \leq 16$
no of rflns collected/unique	12629 / 8154 [R(int) = 0.0264]	27004 / 8956 [R(int) = 0.0430]	27438 / 9192 [R(int) = 0.0842]
completeness to θ = 28.24	99.5%	99.7%	99.9 %
absorp corr	SADABS	SADABS	SADABS
max. and min. transmn	1.0000 and 0.559137	1.000 and 0.631312	1.0000 and 0.322802
refinement method	Full-matrix least-squares on F^2	Full-matrix least-squares on F^2	Full-matrix least-squares on F^2
no. of data/restraints/params	8154 / 36 / 589	8956 / 0 / 631	9192 / 0 / 550
GOF	1.174	1.091	0.902
final R indices [$I > 2\sigma(I)$]	R_1^a = 0.0553 wR_2^b = 0.1586	R_1^a = 0.0379 wR_2^b = 0.0902	R_1^a = 0.0585 wR_2^b = 0.1372
R indices (all data)	R_1^a = 0.0764 wR_2^b = 0.1729	R_1^a = 0.0574 wR_2^b = 0.1016	R_1^a = 0.1000 wR_2^b = 0.1500
largest diff peak and hole (e Å^{-3})	1.951 and -0.949	1.356 and -0.917	2.033 and -1.739
w_1/w_2^c	0.0695/10.3542	0.0383/12.1648	0.0827/0.0000

$^a R_1 = \sum \left(\||F_o|-|F_c\|| \right) / \sum |F_o|$. $^b wR_2 = \left\{ \sum \left[w\left(F_o^2 - F_c^2\right)^2 \right] / \sum \left[w\left(F_o^2\right)^2 \right] \right\}^{1/2}$. ^{c} Weighting scheme $w^{-1} = \sigma^2\left(F_o^2\right) + \left(w_1 P\right)^2 + w_2 P$

where $P = \left(F_o^2 + 2F_c^2\right)/3$.

Appendix IV   CG-MS Analysis Results

(1) GC-MS Analysis of the Commercially Available Chlorobenzene (no 1,4-Dichlorobenzene was found)
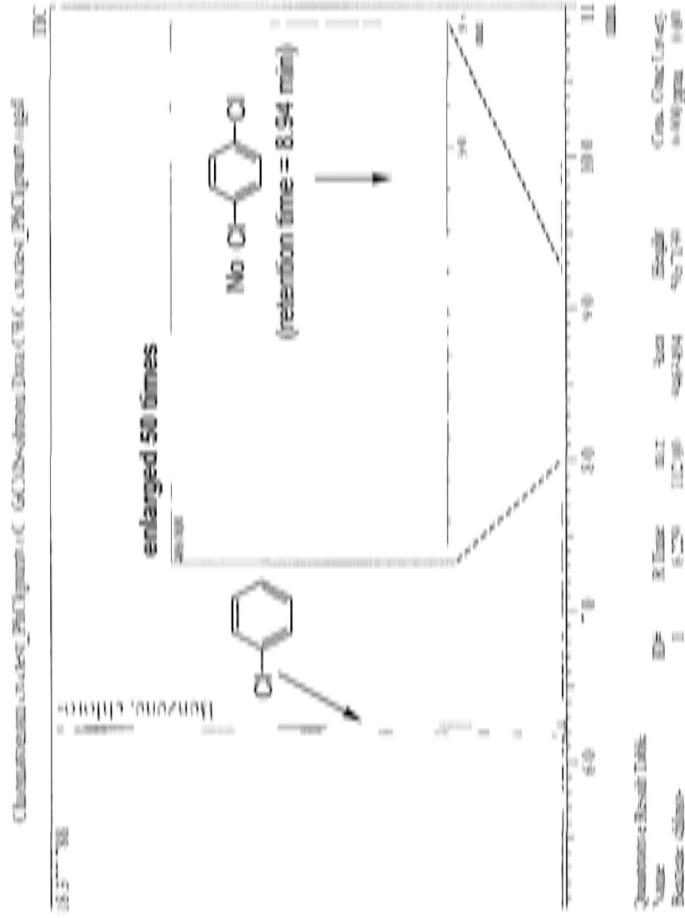
(2) GC-MS Analysis of the Reaction of Sulfuryl Chloride with Benzene at 200 °C to form Chlorobenzene (Chapter 3, eq 3.24)

(4) GC-MS Analysis of the Reaction of Ir^{III}(ttp)(CO)Cl with PbCl (200 equiv) in Benzene at 200 °C to form 1,4-Dichlorobenzene (Chapter 3, Table 3.21, entry 2)

Benzene, 1-chloro-4-methyl-
(internal standard)

(Benzene, 1,4-dichloro-)

(5) GC-MS Analysis of the Reaction of Sulfuryl Chloride with Chlorobenzene at 200 °C to form Dichlorobenzenes and Dichlorobiphenyls (Chapter 3, eq 3.27)

Benzene, 1-chloro-4-methyl-

Benzene, 1,3-dichloro-

Benzene, 1,4-dichloro-

Benzene, 1,2-dichloro-

1,1'-Biphenyl, 2,2'-dichloro-

1,1'-Biphenyl, 4,4'-dichloro-

biphenyl, 3,3'-dichloro-

(5) GC-MS Analysis of the Reaction of Ir^{III}(ttp)(CO)Cl with PhCl (200 equiv) in Benzene at 150 °C to form 1,4-Dichlorobenzene (Chapter 3, Table 3.21, entry 1)

(6) GC-MS Analysis of the Reaction of [Ir^{II}(ttp)]$_2$ and Chlorobenzene at 200 °C to form 1,4-Dichlorobenzene (Chapter 3, eq 3.29)

276

(7) GC-MS Analysis of the Reaction of Bromine with Benzene at 200 °C to form Bromobenzene (Chapter 3, eq 3.25)

Sample Information

Analyzed by	Admin
Analyzed	3/2/2010 6:48 AM
Sample Type	Unknown
Level #	1
Sample Name	cwc2001(2)
Sample ID	[1]=1
IS Amount	1
Sample Amount	1
Dilution Factor	1
Vial #	1
Injection Volume	1
Data File	C:\GCMSsolution\Data\CWC\cwc2001(2).qgd
Run File	C:\GCMSsolution\Data\Project1\cwc2001(2).qg2
Method File	C:\GCMSsolution\Data\Project1\Shine_1.qem
Org Method File	C:\GCMSsolution\Data\Project1\Shine_1.qem
Report File	
Tuning File	C:\GCMSsolution\System\Tune1\o6012009.qgt
Modified by	Admin
Modified	2/2/09 12:22:05 PM

Chromatogram cwc2001(2) C:\GCMSsolution\Data\CWC\cwc2001(2).qgd

18:906:124

Benzene, bromo-

Benzene, 1-bromo-4-methyl- (internal standard)

Quantitative Result Table

Name	ID#	R.Time	m/z	Area	Height	Conc.	Conc.	User
Benzene, bromo-	1	7.831	77.00	2405900	607324	0.000 ppm	0.00	
Benzene, 1-bromo-4-methyl-	2	9.322	91.00	16570719	5776819	0.000 ppm	0.00	

(8) GC-MS Analysis of the Commercially Available 4-Bromo-*tert*-butylbenzene (no Bromobenzene was found)

4-Bromo-*tert*-butylbenzene used: IL (USA), 25 g, 97%

Sample Information

Analyzed by	Admin
Analyzed	11/6/09 1 PM
Sample Type	Unknown
Level #	1
Sample Name	tBuPhB
Sample ID	[1]=1
IS Amount	1
Sample Amount	1
Dilution Factor	1
Vial #	1
Injection Volume	1
Data File	C:\GCMSsolution\Data\CWC\cwc\test_tBuPhBr1.q...
Run File	C:\GCMSsolution\Data\Project1\te_tBtPhBr.qg2
Method File	C:\GCMSsolution\Data\Project1\Shine_1.qem
Org Method File	C:\GCMSsolution\Data\Project1\Shine_1.qem
Report File	
Tuning File	C:\GCMSsolution\System\Tune1_6012709.q...
Modified by	Admin
Modified	11/2/09 1:41:42 PM

Chromatogram cwc\test_tBuPhBr1.C C:\GCMSsolution Data CWC cwc test_tBuPhBt.qgd

Benzene, tert-but...

Propane, 1,2-dibromo-2-methyl-

enlarged 70 times

No—Br

retention time = 7.83 min

Benzene, 1-bromo-4-(1,1-dimethyleth)-

3-tert-butylbromobenzene

Benzene, 3,6-di-tert-butyl-
Benzene, 2,4-dibromo-1,3,5-trimethyl-1-
Di-tert-butylbromobenzene

Quantitative Result Table

Name	ID#	R.Time	m/z	Area	Height	Conc.	Con.
Propane, 1,2-dibromo-2-methyl-	1	7.199	77.00	61251	34890	0.000 ppm	
Benzene, tert-butyl	2	8.662	119.00	144882	90101	0.000 ppm	
3-tert-butylbromobenzene	3	11.147	197.00	981839	596218	0.000 ppm	
Benzene, 1-bromo-4-(1,1-dimethylethyl)-	4	11.47	197.00	9619978	5099122	0.000 ppm	
Bromobenzene, 6-di tert-but-1	5	13.276	253.00	1000.8	7152	0.000 ppm	
Benzene 2,4 dibromo 1,3,5 trimethyl-	6	13.401	27.00	57373	89024	0.000 ppm	
3,5 Di tert-butylbromobenzene	7	13.508	253.00	2.3507	166081	0.000 ppm	

(9) **GC-MS Analysis of the Reaction of [Ir^{II}(ttp)]$_2$ and 4-Bromo-*tert*-butylbenzene (1.1 equiv) in Benzene at 200 °C to form Bromobenzene (Chapter 3, eq 3.28)**

N.B. The manipulation of GC-MS was changed to allow better resolution of PhBr to be detected, which resulted in the increased retention times of all species.

(Retention of PhBr: changed from 7.83 min to 9.57 min)

Appendix V   NMR Spectra

^{1}H NMR Spectrum of Ir^{III}(ttp)(CO)Cl (**1a**) (C$_6$D$_6$)

^{1}H NMR Spectrum of Ir^{III}(ttp)(PPh$_3$)Cl (**1b**) (C$_6$D$_6$)

^{13}C NMR Spectrum of Ir^{III}(ttp)(PPh$_3$)Cl (**1b**) (THF-d_8)

^{1}H NMR Spectrum of Ir^{III}(ttp)(CO)Br (**1c**) (C$_6$D$_6$)

^{13}C NMR Spectrum of Ir^{III}(ttp)(CO)Br (**1c**) (CDCl$_3$)

^{1}H NMR Spectrum of Ir^{III}(ttp)(CO)I (**1d**) (C$_6$D$_6$)
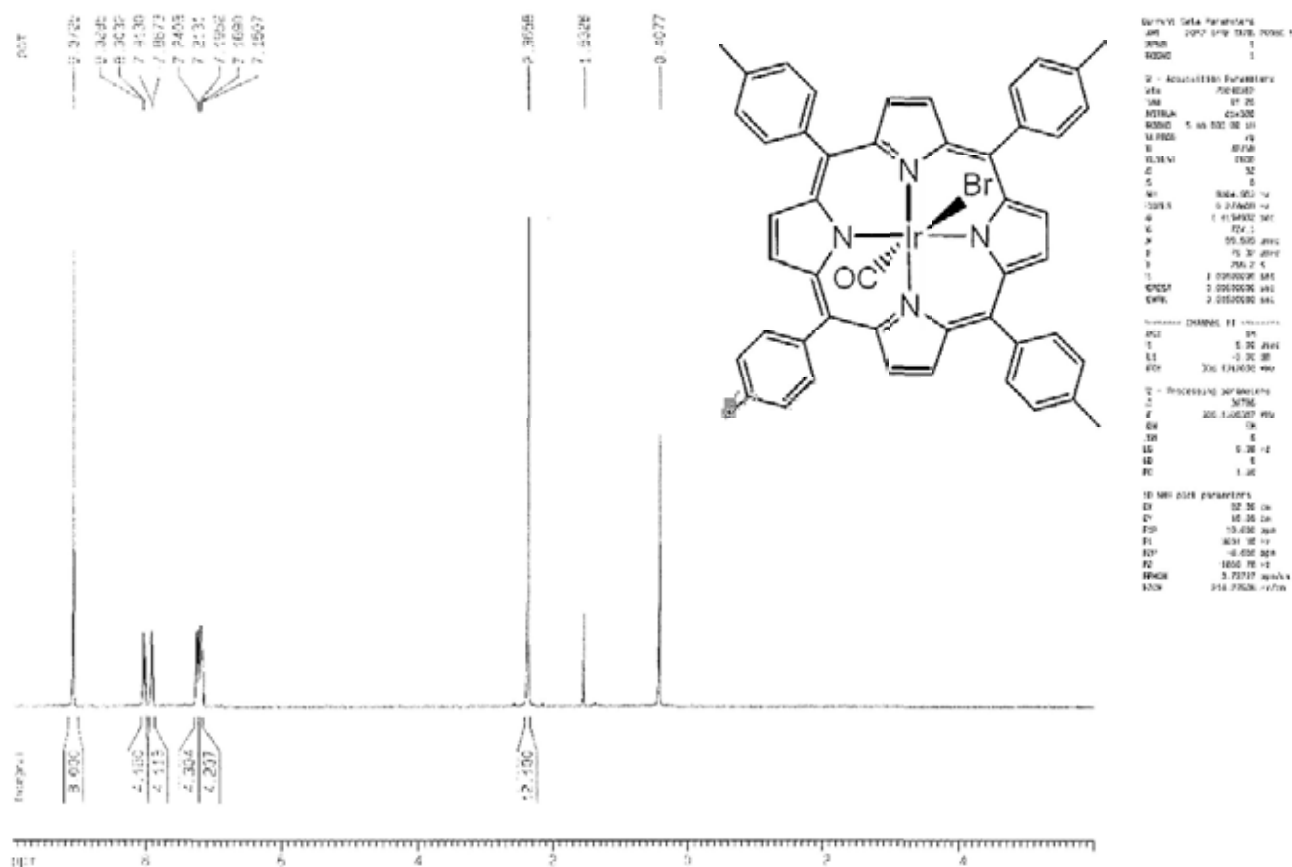
^{13}C NMR Spectrum of Ir^{III}(ttp)(CO)I (**1d**) (CDCl$_3$)

^{1}H NMR Spectrum of Ir^{III}(ttp)SbF$_6$ (**1e**) (CDCl$_3$)

Ir^{III}(ttp)SbF$_6$: [Ir^{III}(ttp)(CO)]SbF$_6$ ~ 3.4 : 1

Ir^{III}(ttp)SbF$_6$

[Ir^{III}(ttp)(CO)]SbF$_6$

285
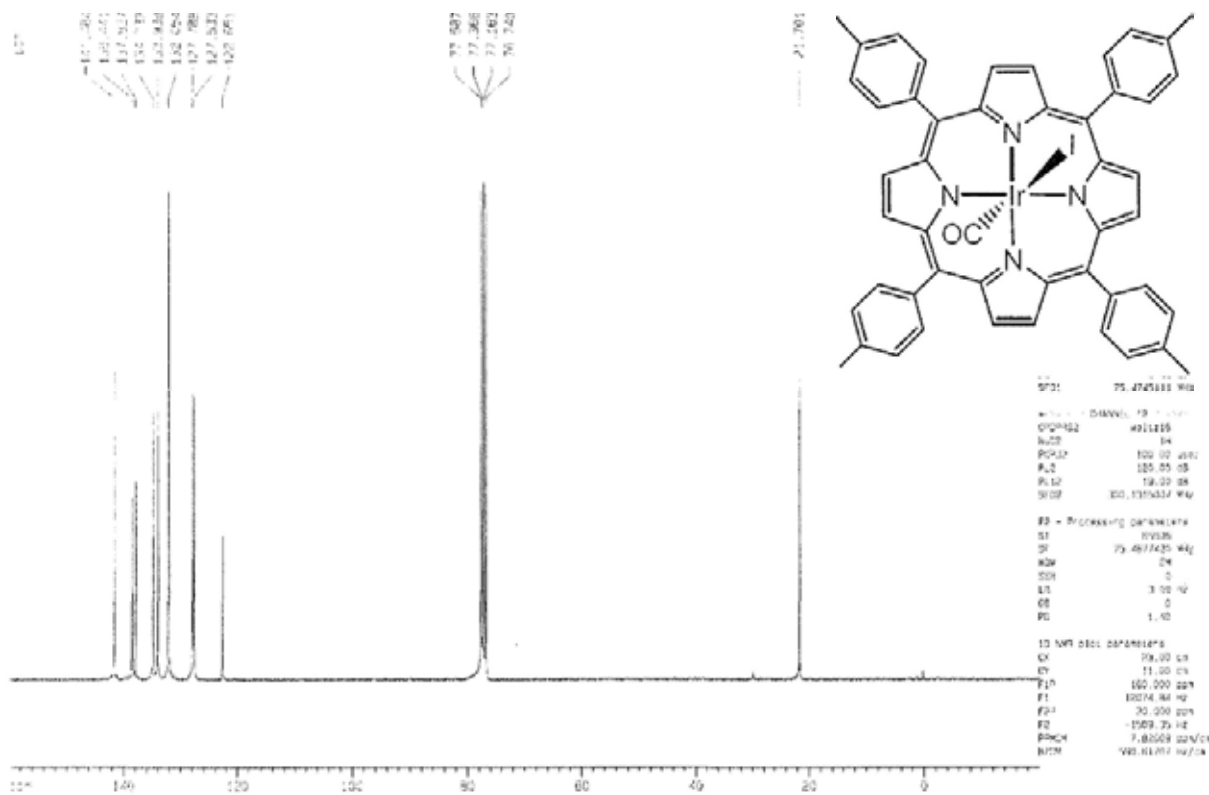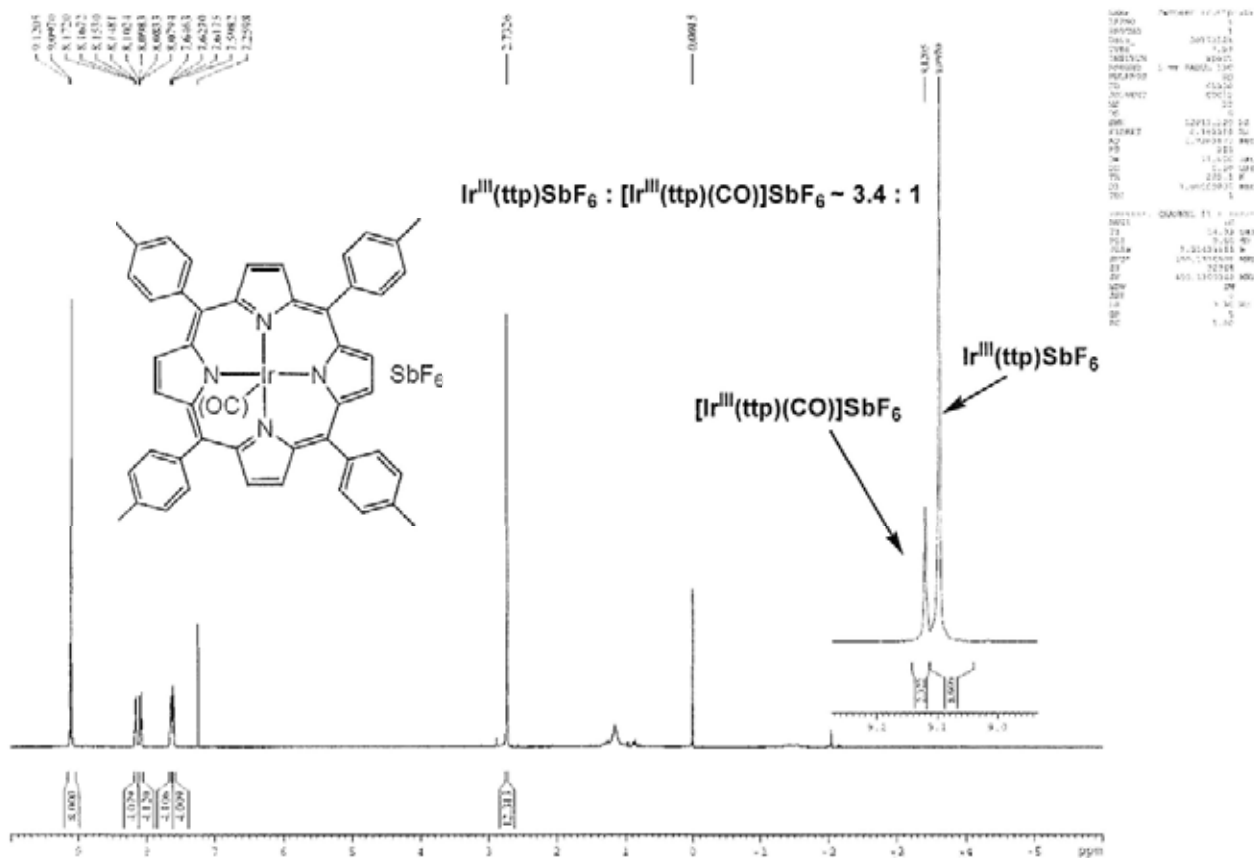
^{1}H NMR Spectrum of Ir^{III}(ttp)SbF$_6$ (1e) (C$_6$D$_6$)

^{13}C NMR Spectrum of Ir^{III}(ttp)SbF$_6$ (1e) (CDCl$_3$)

286
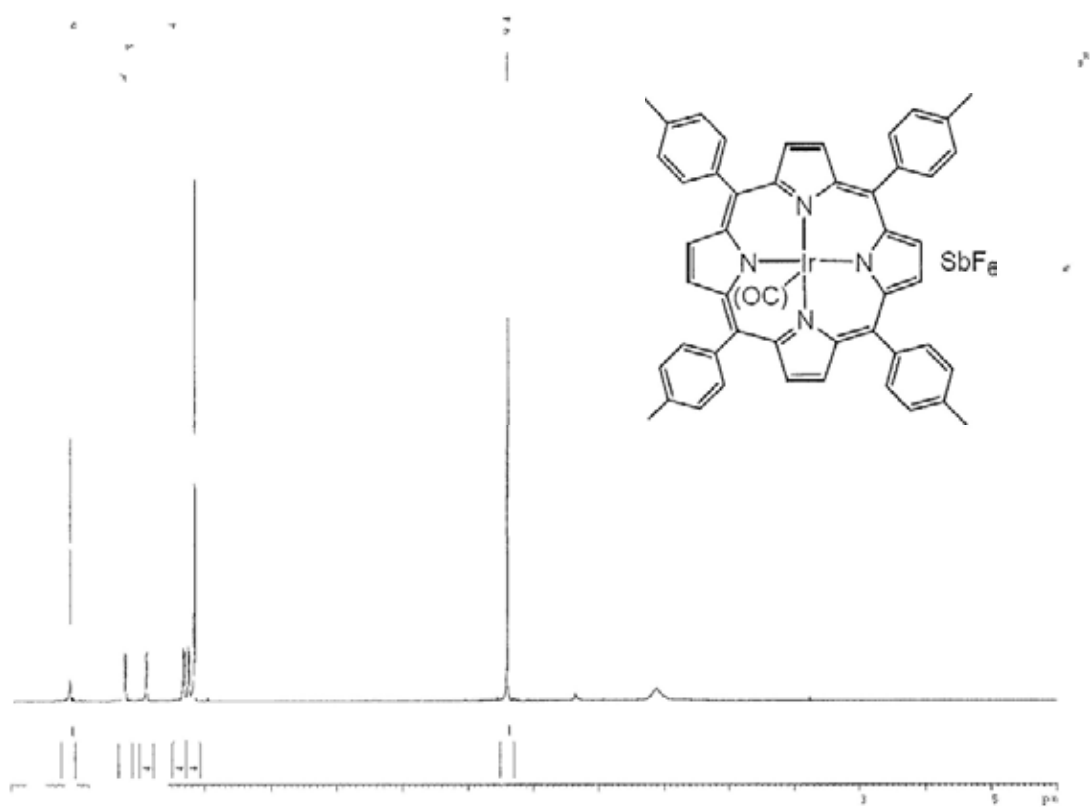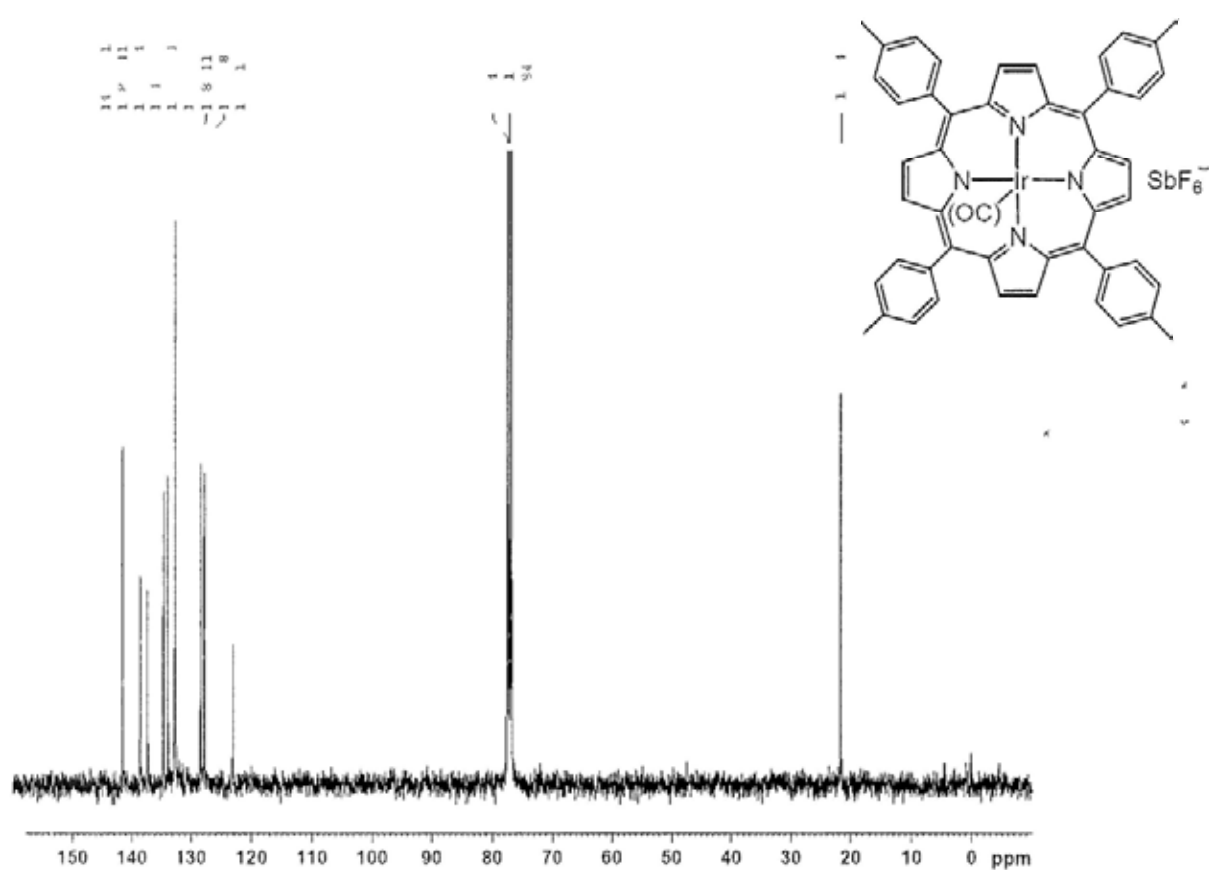
^{1}H NMR Spectrum of Ir^{III}(ttp)(py)Cl (**1f**) (CDCl$_3$)

^{13}C NMR Spectrum of Ir^{III}(ttp)(py)Cl (**1f**) (CDCl$_3$)

287

^{1}H NMR Spectrum of Ir^{III}(ttp)(py)Br (1g) (C$_6$D$_6$)

^{13}C NMR Spectrum of Ir^{III}(ttp)(py)Br (1g) (CDCl$_3$)
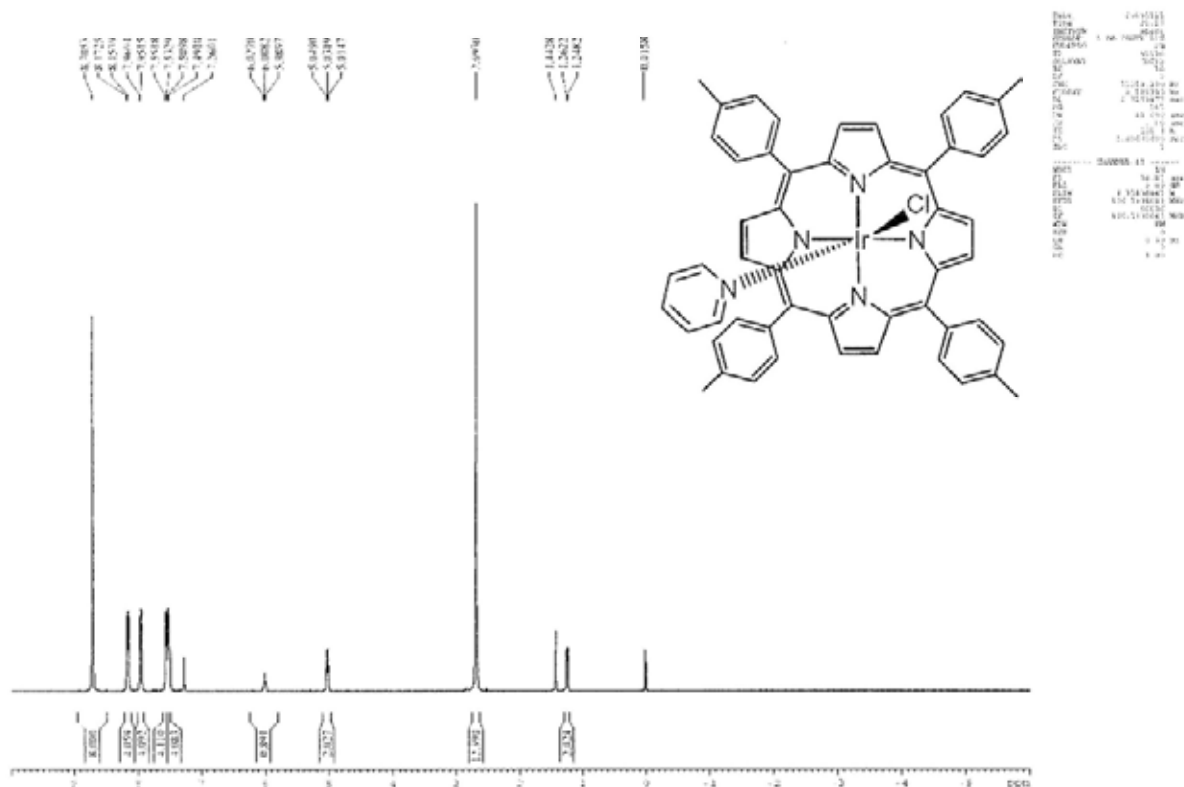
¹H NMR Spectrum of Ir^{III}(ttp)(py)I (**1h**) (C₆D₆)
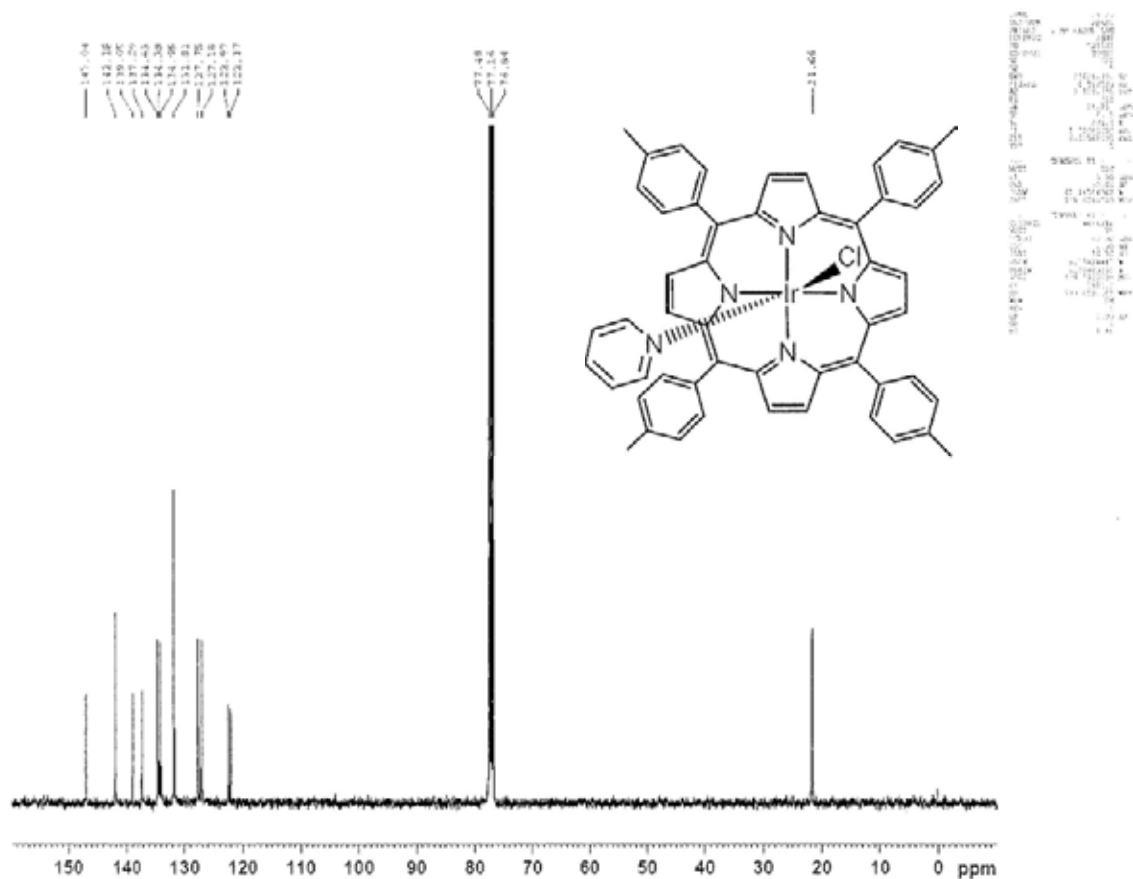
^{1}H NMR Spectrum of Ir^{III}(ttp)(py)I (**1h**) (C$_6$D$_6$)
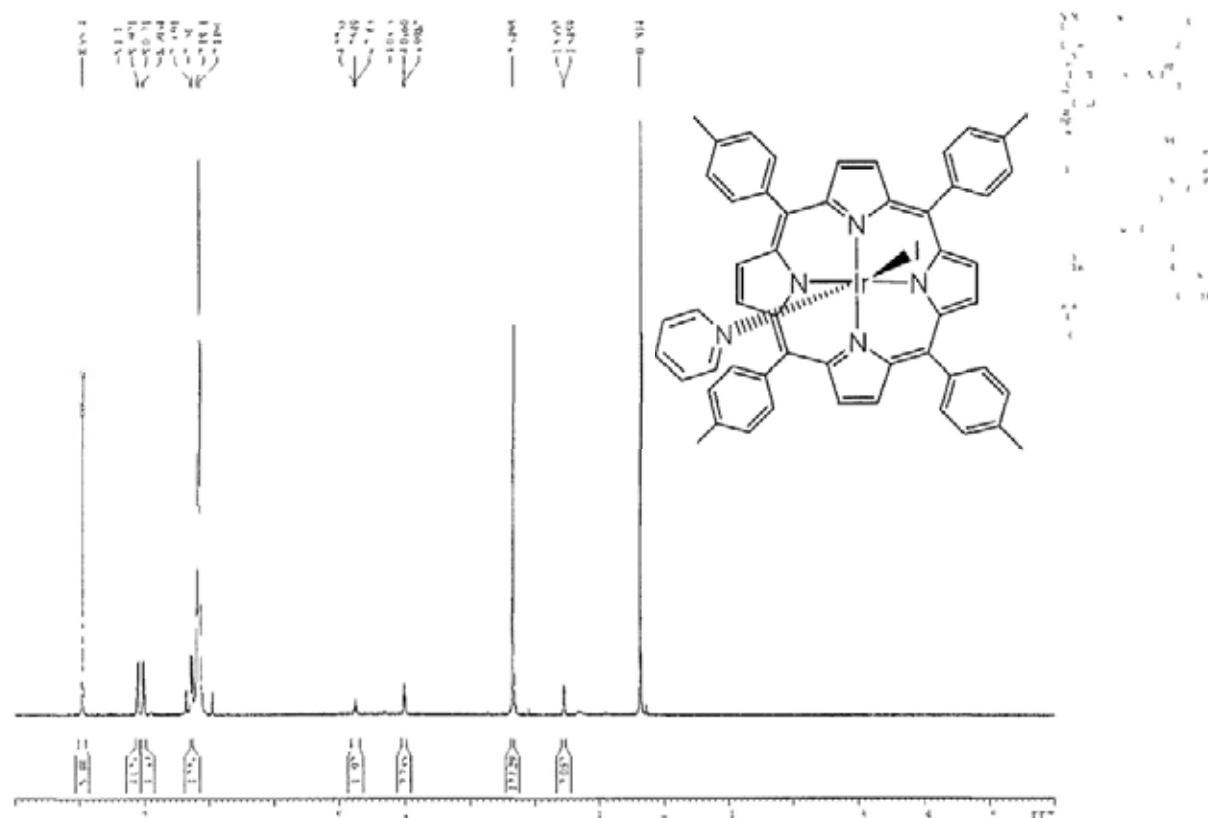
^{13}C NMR Spectrum of Ir^{III}(ttp)(py)I (**1h**) (CDCl$_3$)
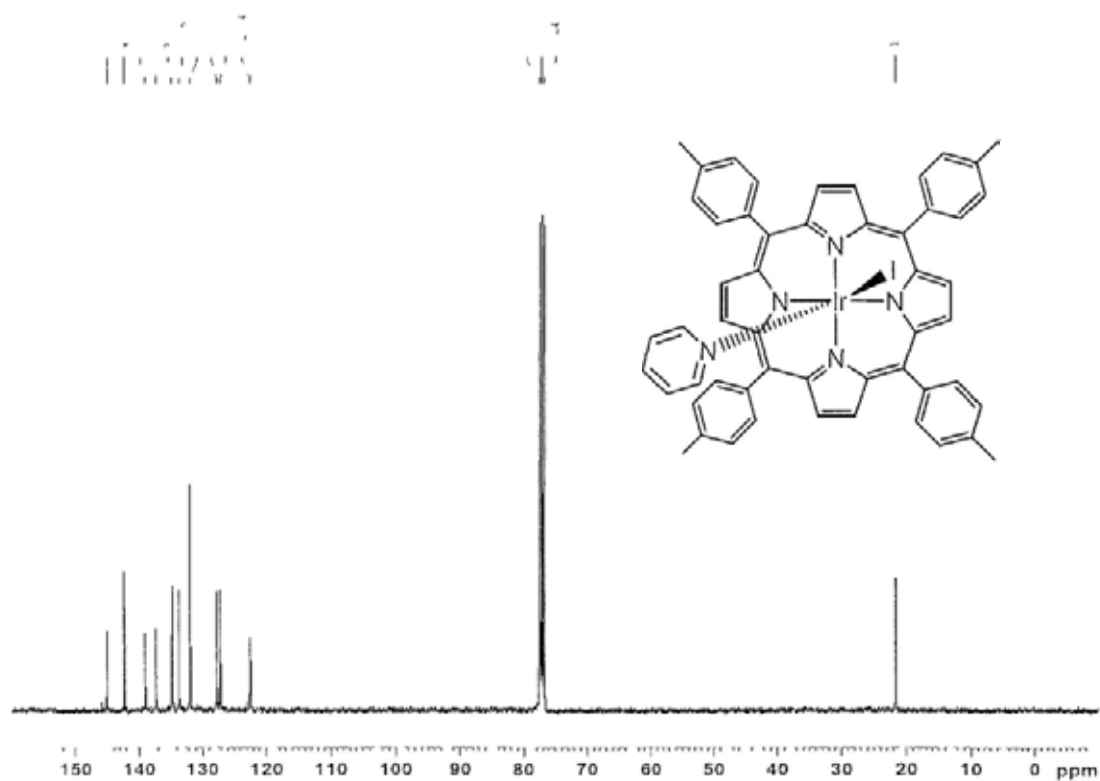
^{1}H NMR Spectrum of Ir^{III}(ttp)H (**2a**) (C$_6$D$_6$)
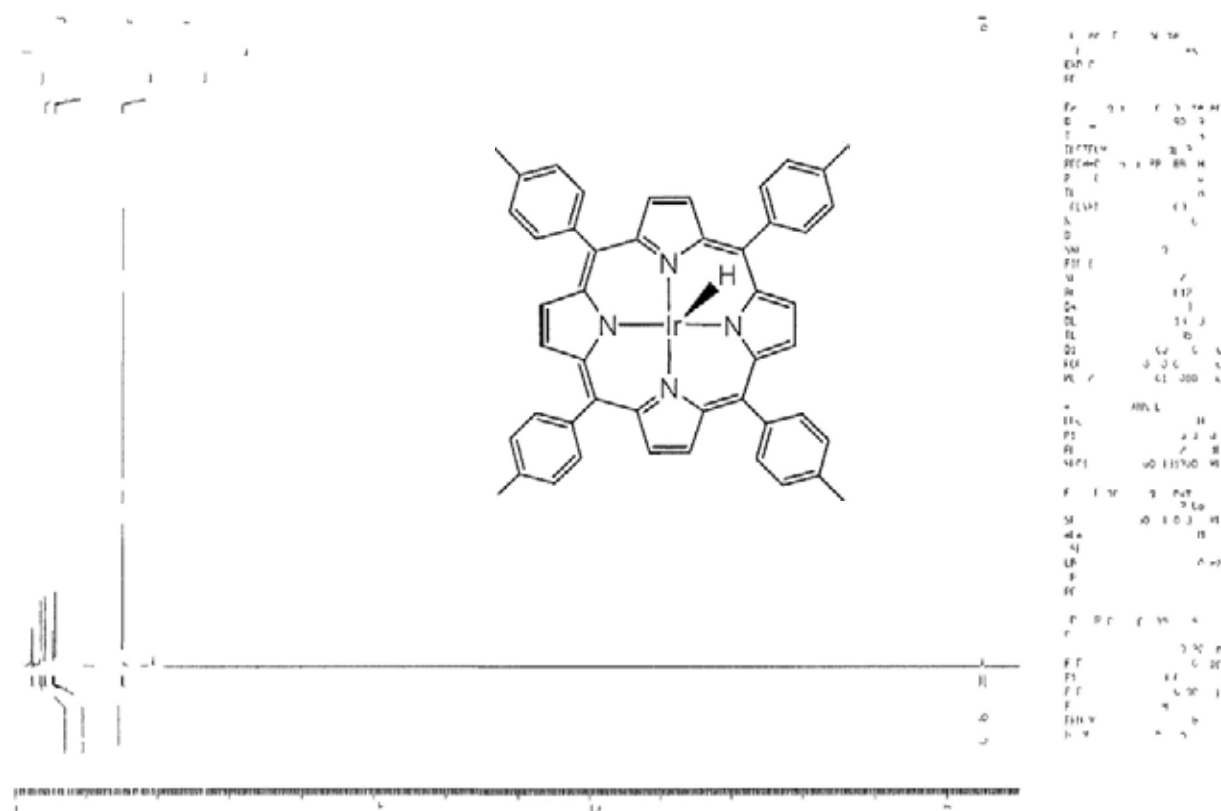
^{1}H NMR Spectrum of Ir^{III}(ttp)(PPh$_3$)H (**2b**) (C$_6$D$_6$)

^{1}H NMR Spectrum of $[Ir^{II}(ttp)]_2$ (**3**) (C_6D_6)

^{1}H NMR Spectrum of $Ir^I(ttp)^-K^+$ (**4a**) (THF-d_8)

¹³C NMR Spectrum of Ir^I(ttp)⁻K⁺ (4a) (THF-d₈)

¹H NMR Spectrum of Ir^I(ttp)⁻[K(18-crown-6)]⁺ (4b) (THF-d₈)

¹H NMR Spectrum of Irᴵ(ttp)⁻[K(18-crown-6)]⁺ (4b) (C₆D₆)

¹H NMR Spectrum of Irᴵᴵᴵ(ttp)(PPh₃)OH (5a) (C₆D₆)

293

13C NMR Spectrum of Ir^{III}(ttp)(PPh₃)OH (5a) (C₆D₆)
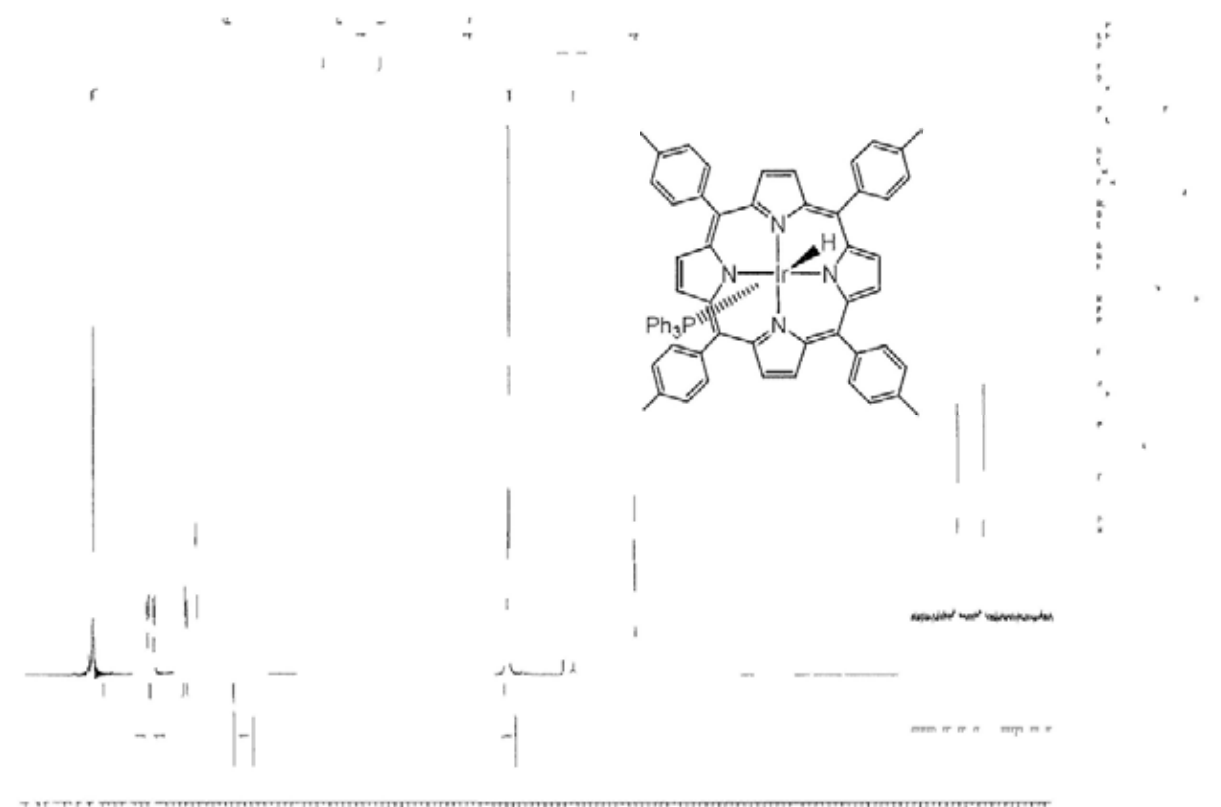
^{13}C NMR Spectrum of Ir^{III}(ttp)(PPh$_3$)OH (**5a**) (C$_6$D$_6$)
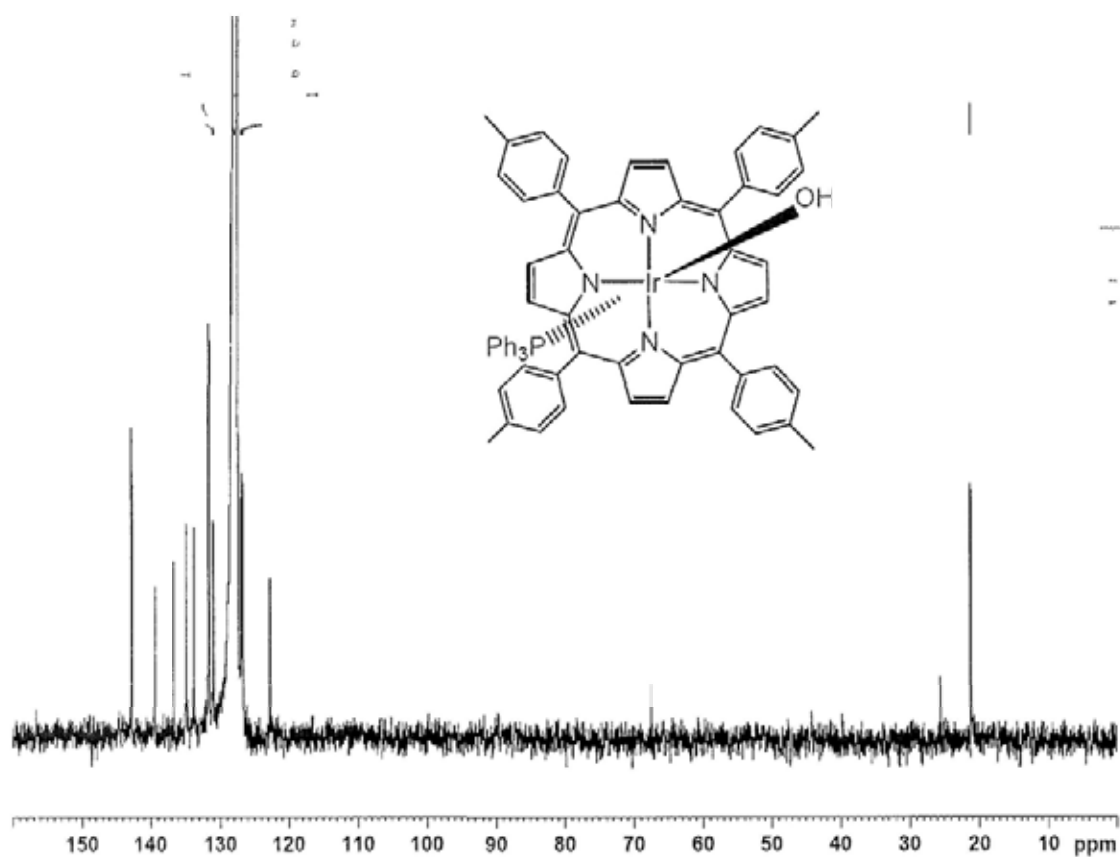
^{1}H NMR Spectrum of Ir^{III}(ttp)(py)OH (**5b**) (CDCl$_3$)
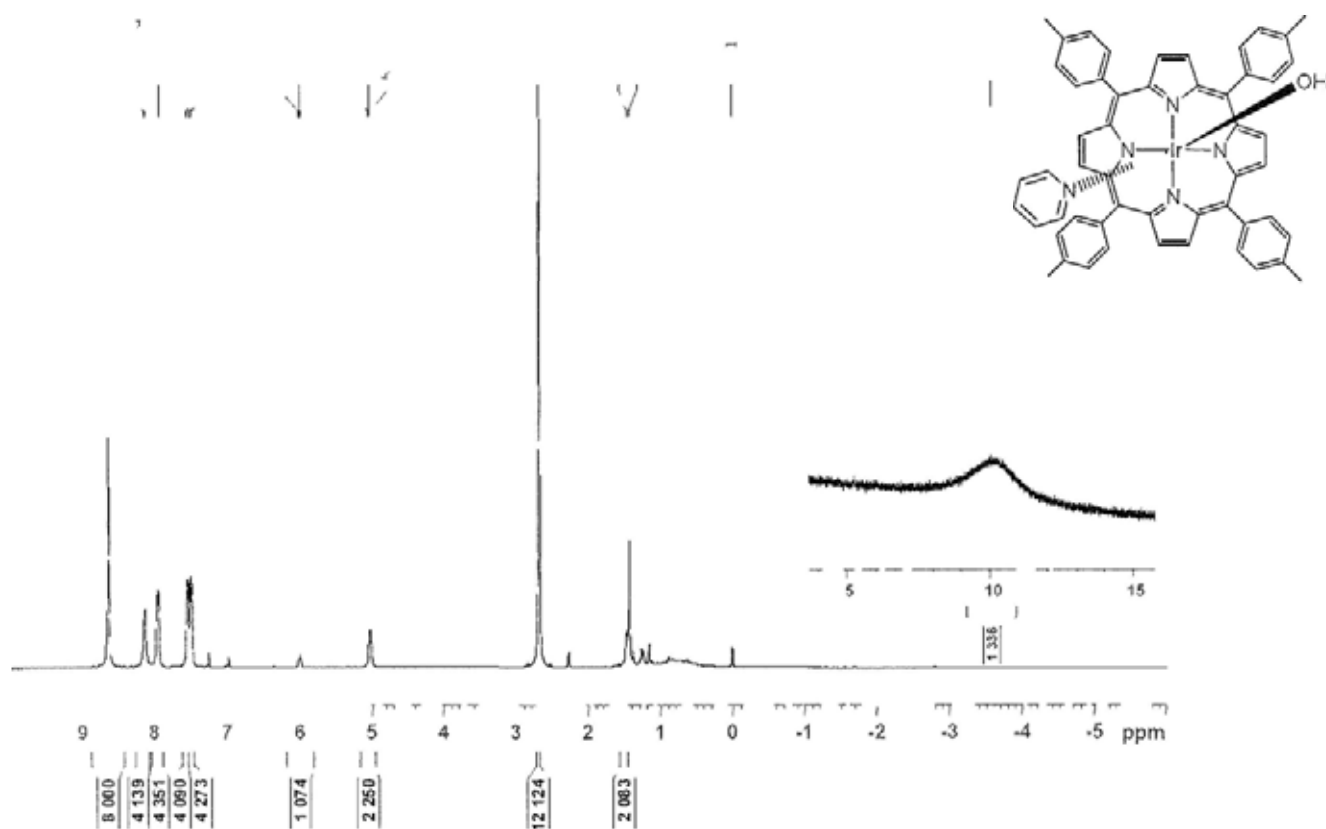
^{13}C NMR Spectrum of Ir^{III}(ttp)(py)OH (**5b**) (CDCl$_3$)

^{1}H NMR Spectrum of (H$_2$O)(ttp)Ir^{III}OIr^{III}(ttp)(OH$_2$) (**6a**) (C$_6$D$_6$)

* Unreacted Ir^{III}(ttp)CH$_2$CH$_2$OH (δ(pyrrole H) = 8 76 ppm) and Ir^{III}(ttp)C$_6$D$_5$ (δ(pyrrole H) = 8 79 ppm) were observed in 2% and 7% yields, respectively, during the preparation of (H$_2$O)(ttp)Ir^{III}OIr^{III}(ttp)(OH$_2$)
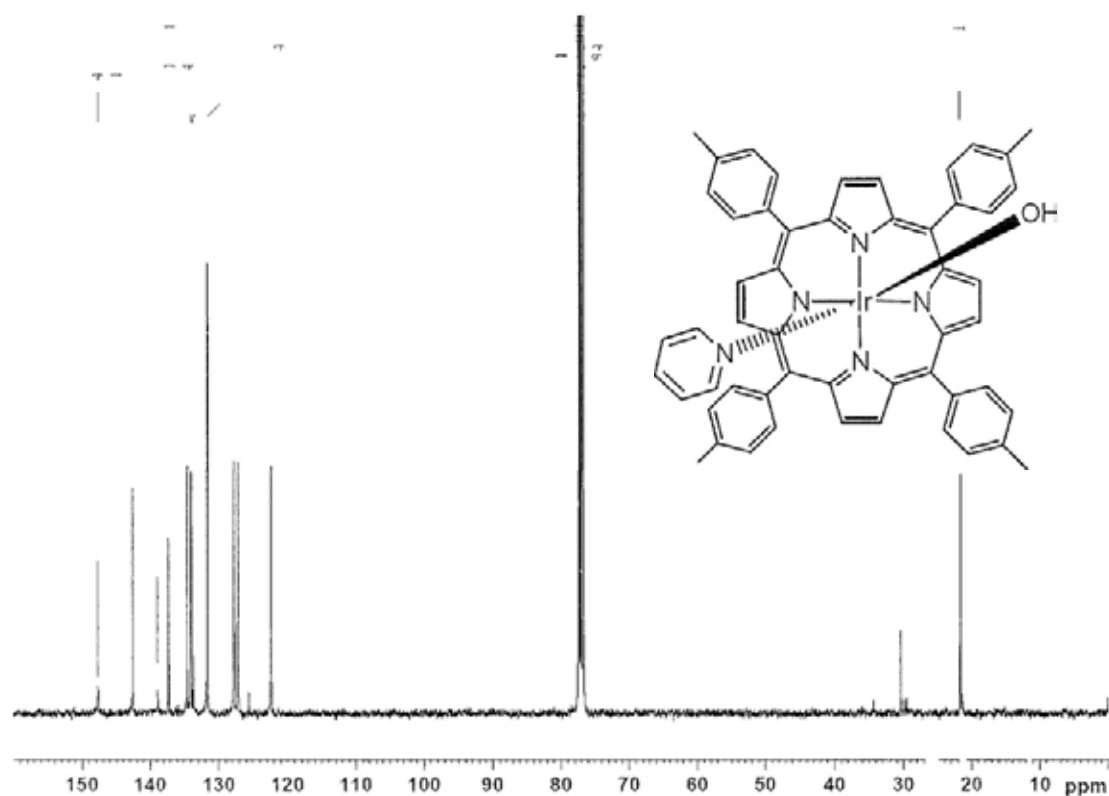
¹³C NMR Spectrum of (H₂O)(ttp)Ir^{III}(OIr^{III}(ttp)(OH₂) (**6a**) (C₆D₆)
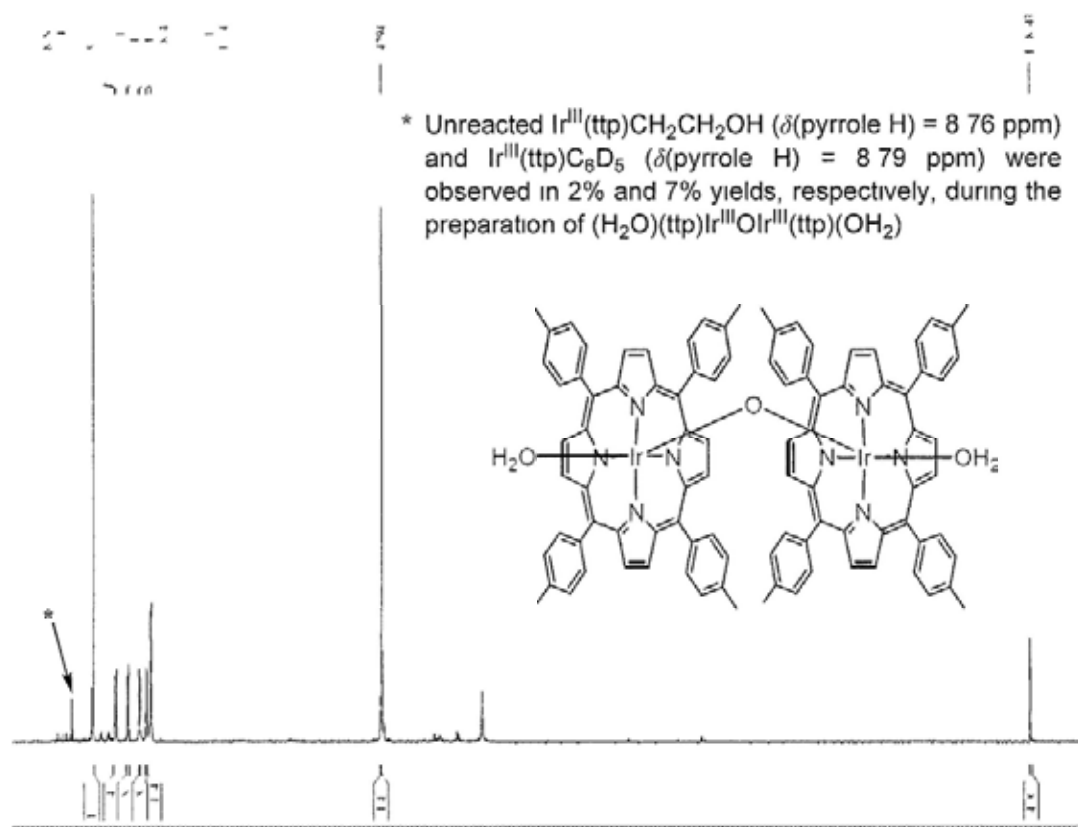
^{13}C NMR Spectrum of (H$_2$O)(ttp)Ir^{III}(OIr^{III}(ttp)(OH$_2$) (**6a**) (C$_6$D$_6$)
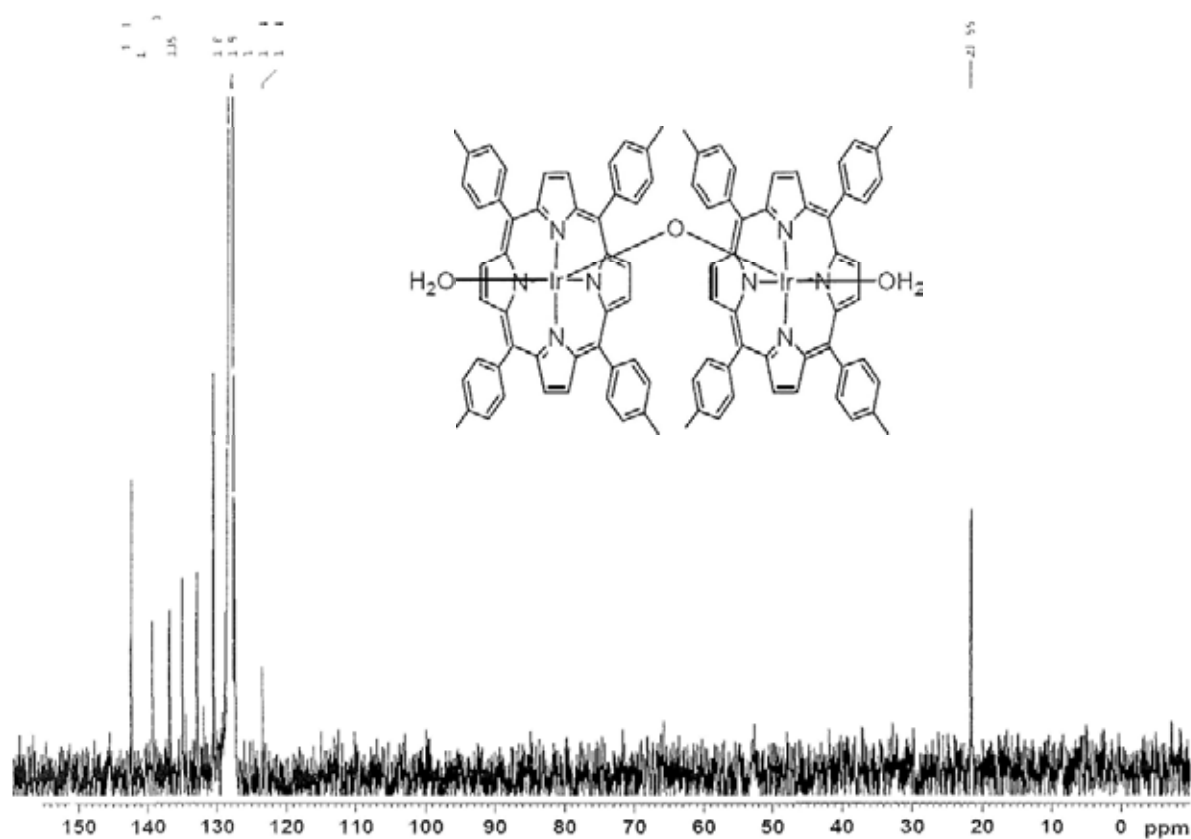
^{1}H NMR Spectrum of Ir^{III}(ttp)CH$_2$CH$_2$OH (**7**) (CDCl$_3$)
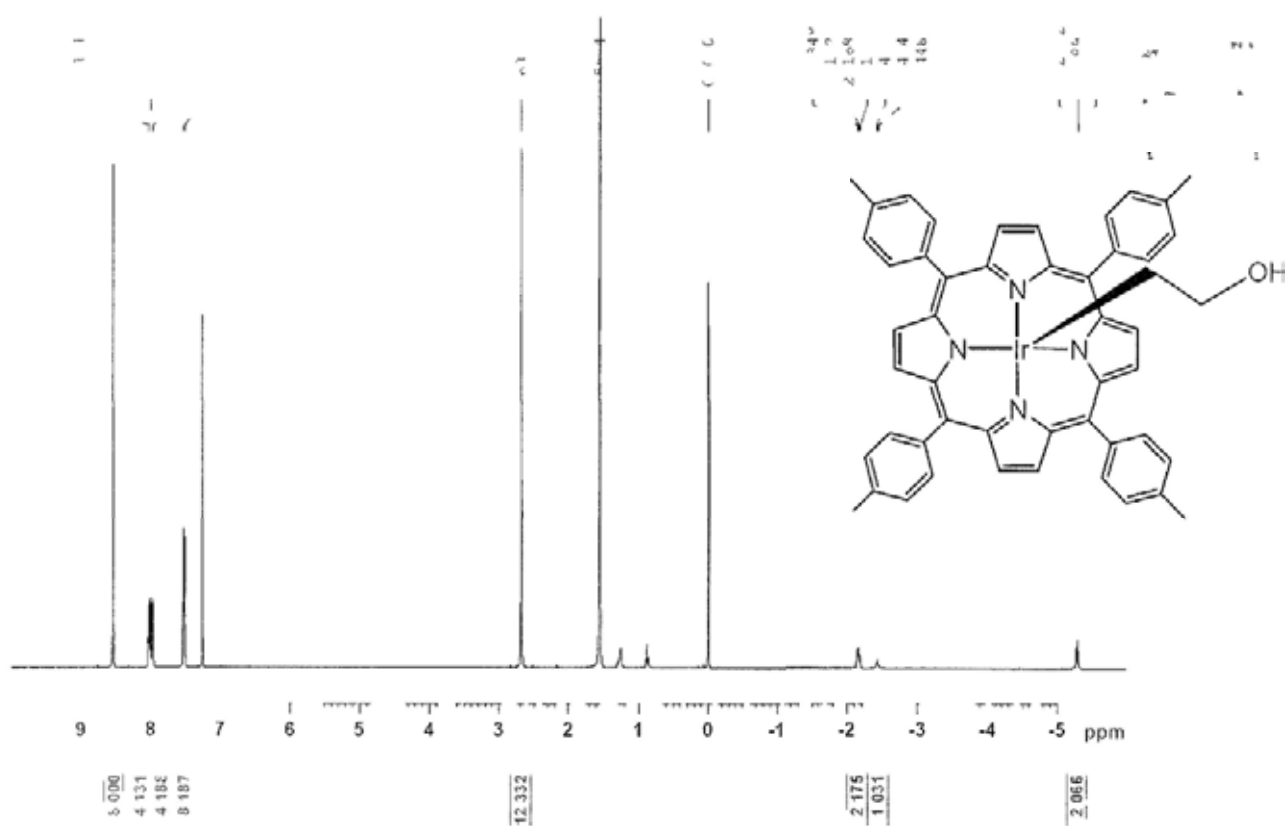
^{13}C NMR Spectrum of Ir^{III}(ttp)CH$_2$CH$_2$OH (**7**) (CDCl$_3$)

^{1}H NMR Spectrum of Ir^{III}(ttp)Ph (**8a**) (CDCl$_3$)

297
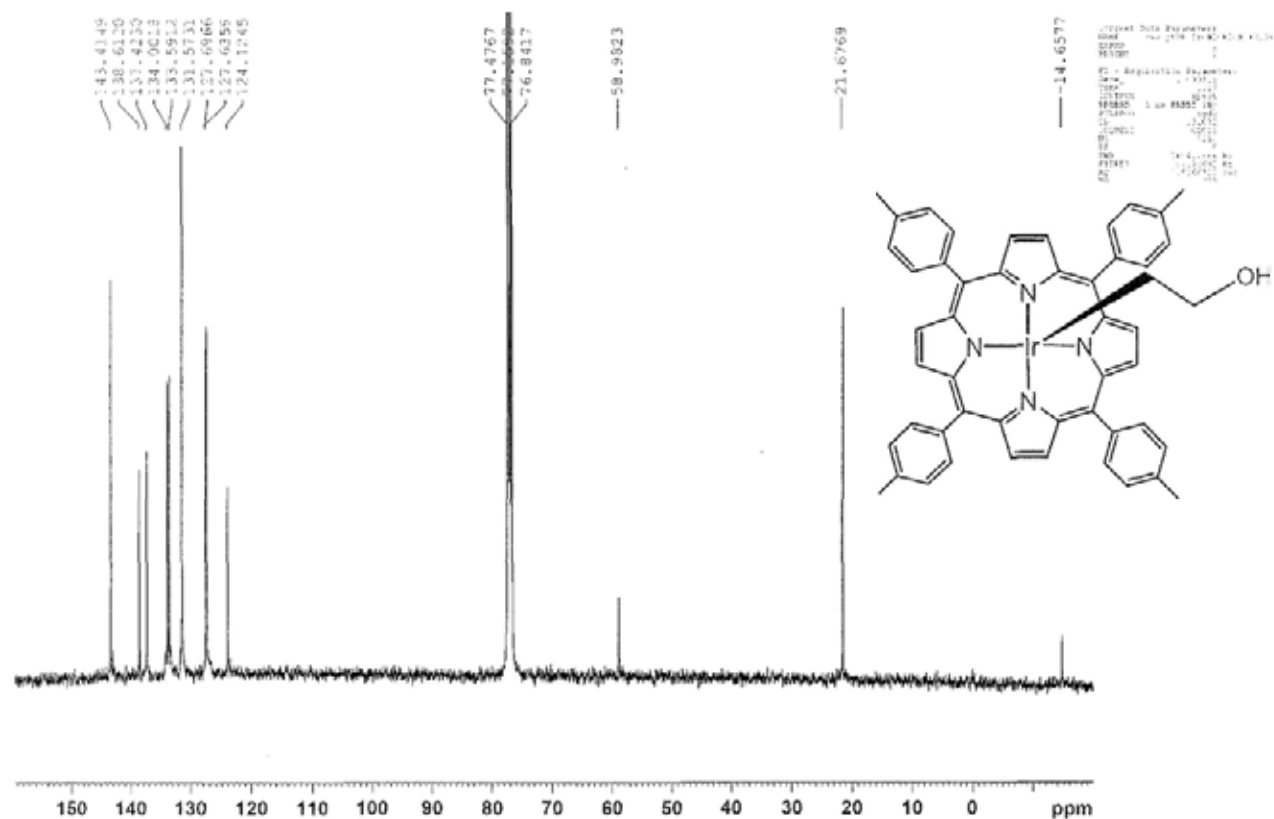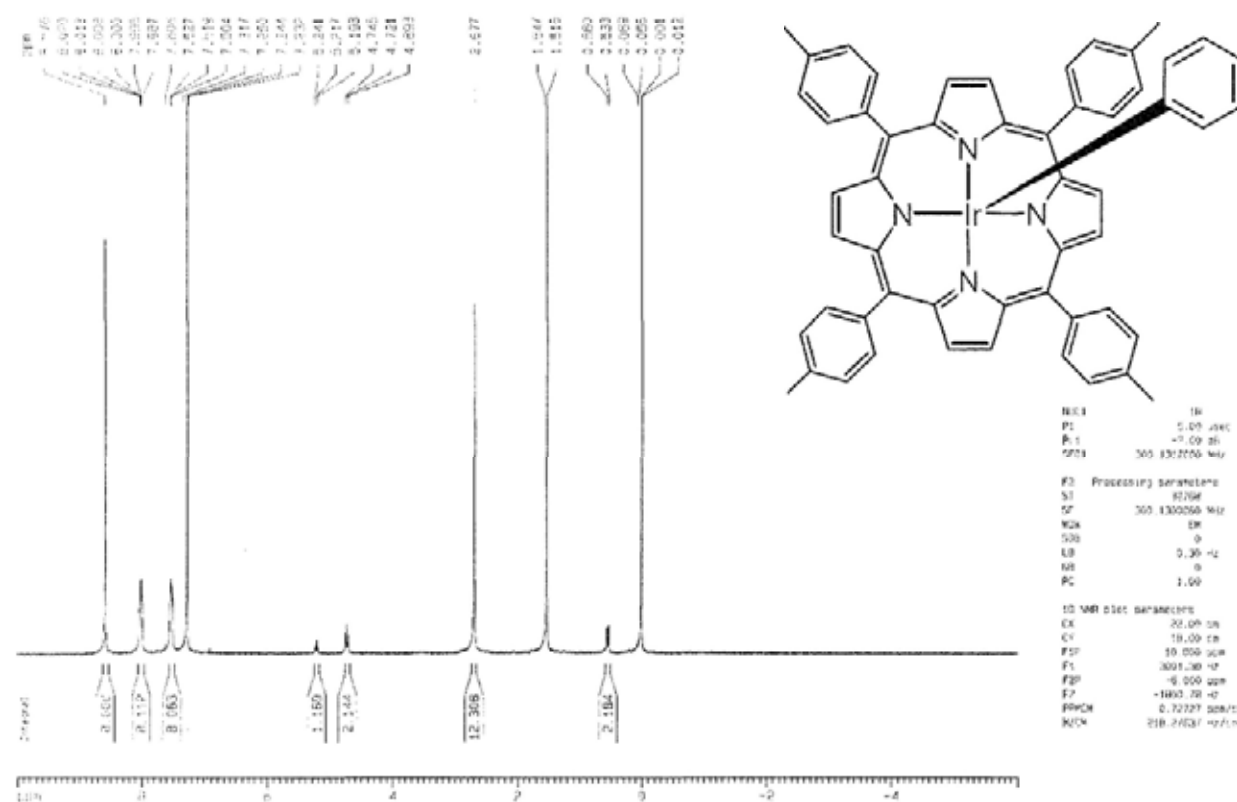
^{13}C NMR Spectrum of Ir^{III}(ttp)Ph (**8a**) (CDCl$_3$)
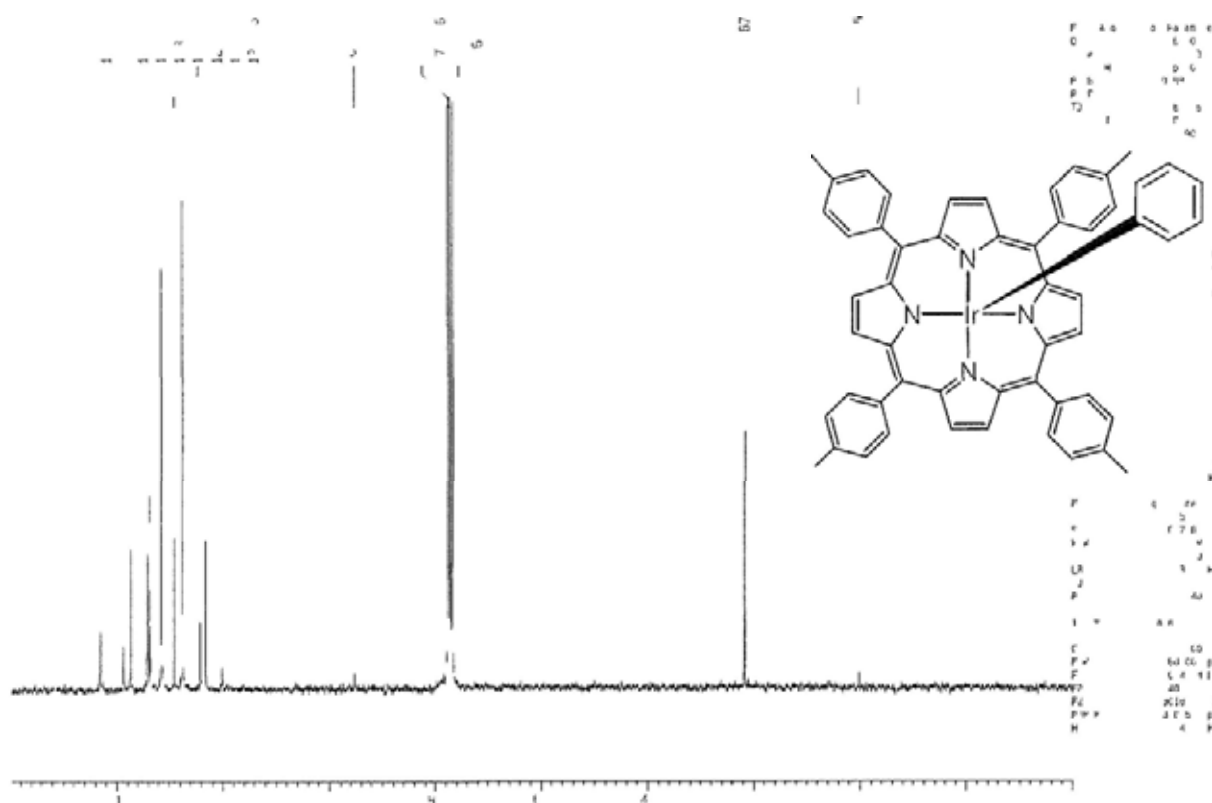
^{1}H NMR Spectrum of Ir^{III}(ttp)C$_6$H$_4$(p-NMe$_2$) (**8b**) (CDCl$_3$)
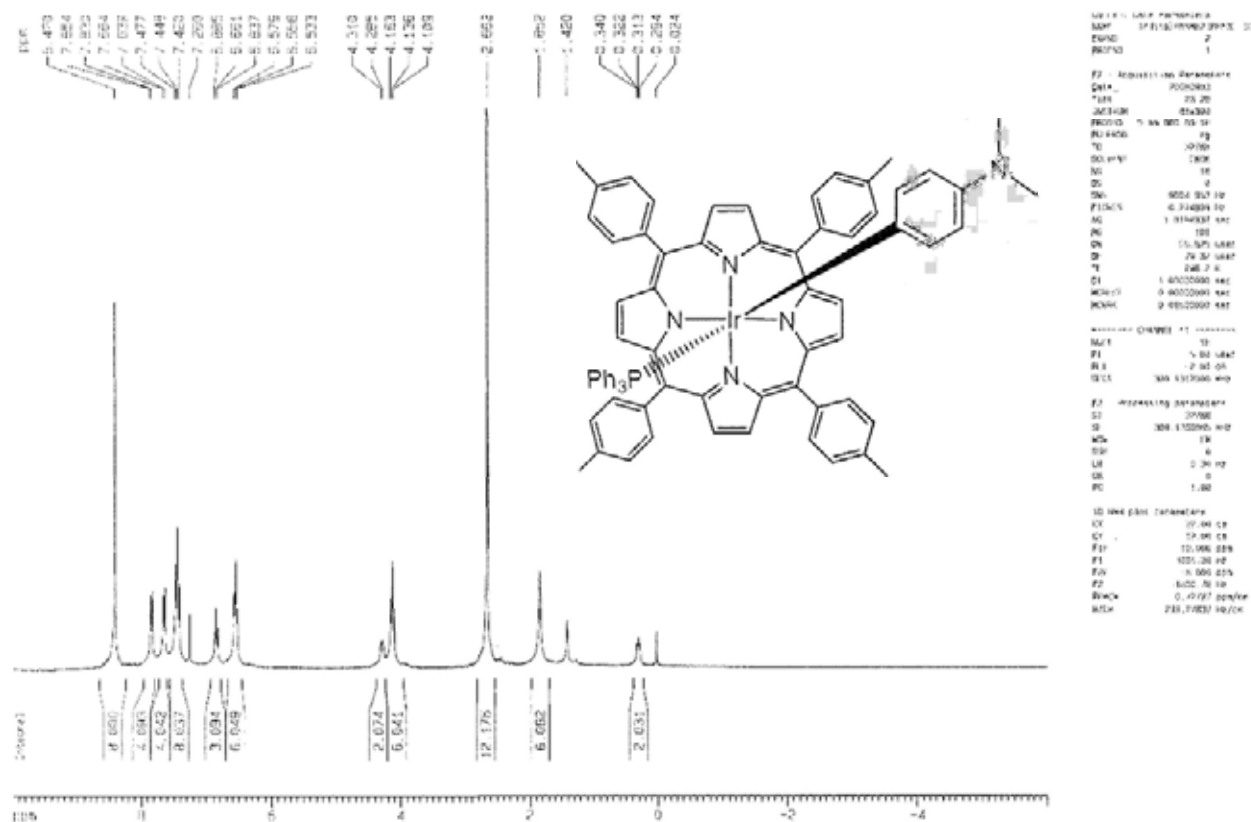
298

^{1}H NMR Spectrum of Ir^{III}(ttp)(PPh$_3$)C$_6$H$_4$(p-NMe$_2$) (8b$_1$) (CDCl$_3$)

^{13}C NMR Spectrum of Ir^{III}(ttp)(PPh$_3$)C$_6$H$_4$(p-NMe$_2$) (8b$_1$) (CDCl$_3$)

299
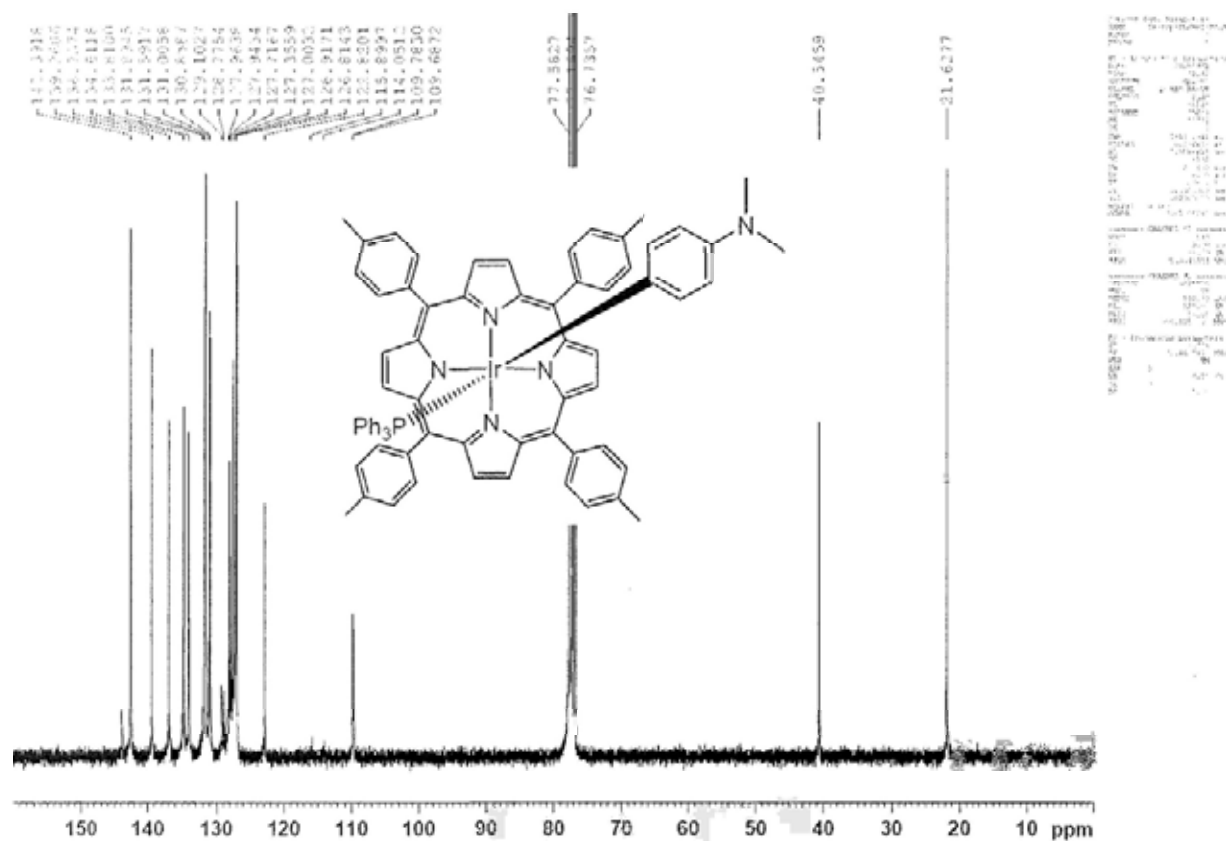
^{1}H NMR Spectrum of Ir^{III}(ttp)C$_6$H$_4$(p-OMe) (8c) (CDCl$_3$)
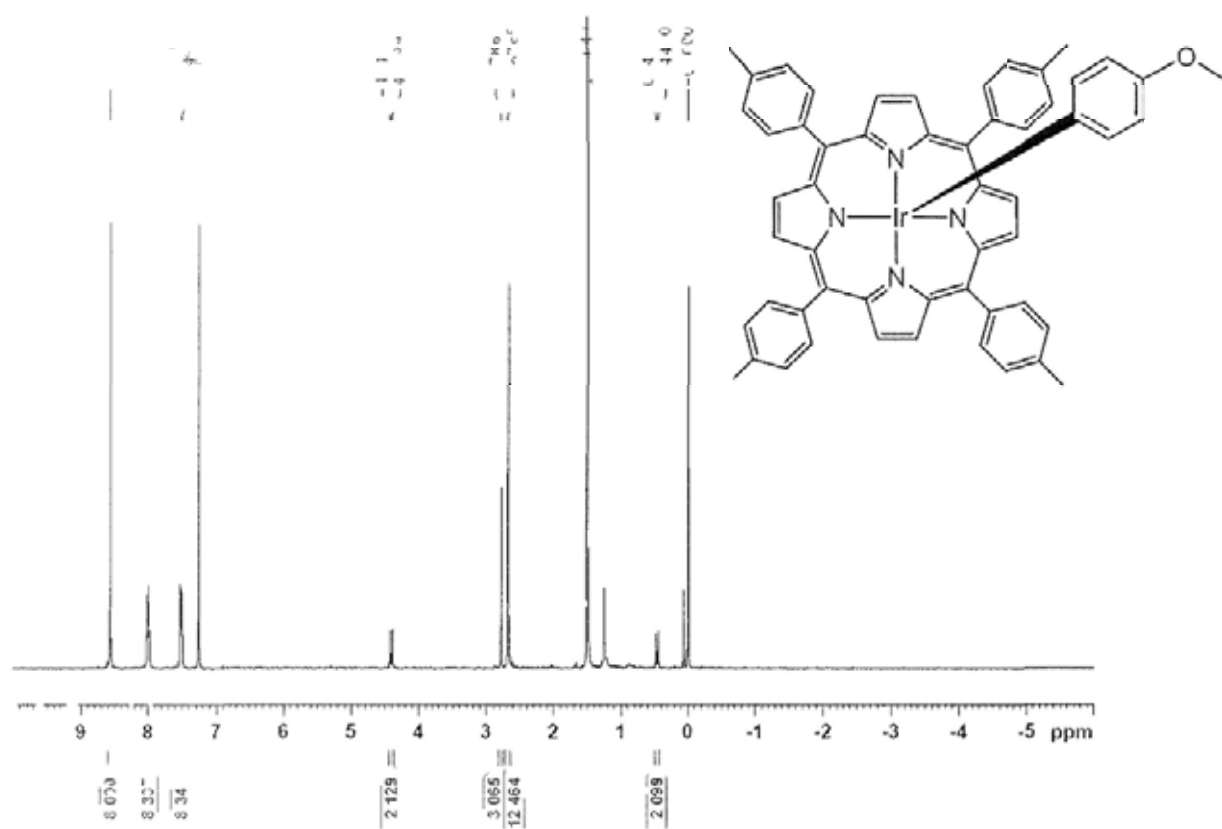
^{13}C NMR Spectrum of Ir^{III}(ttp)C$_6$H$_4$(p-OMe) (8c) (CDCl$_3$)

^{1}H NMR Spectrum of Ir^{III}(ttp)C$_6$H$_4$(p-^{t}Bu) (**8d**) (CDCl$_3$)
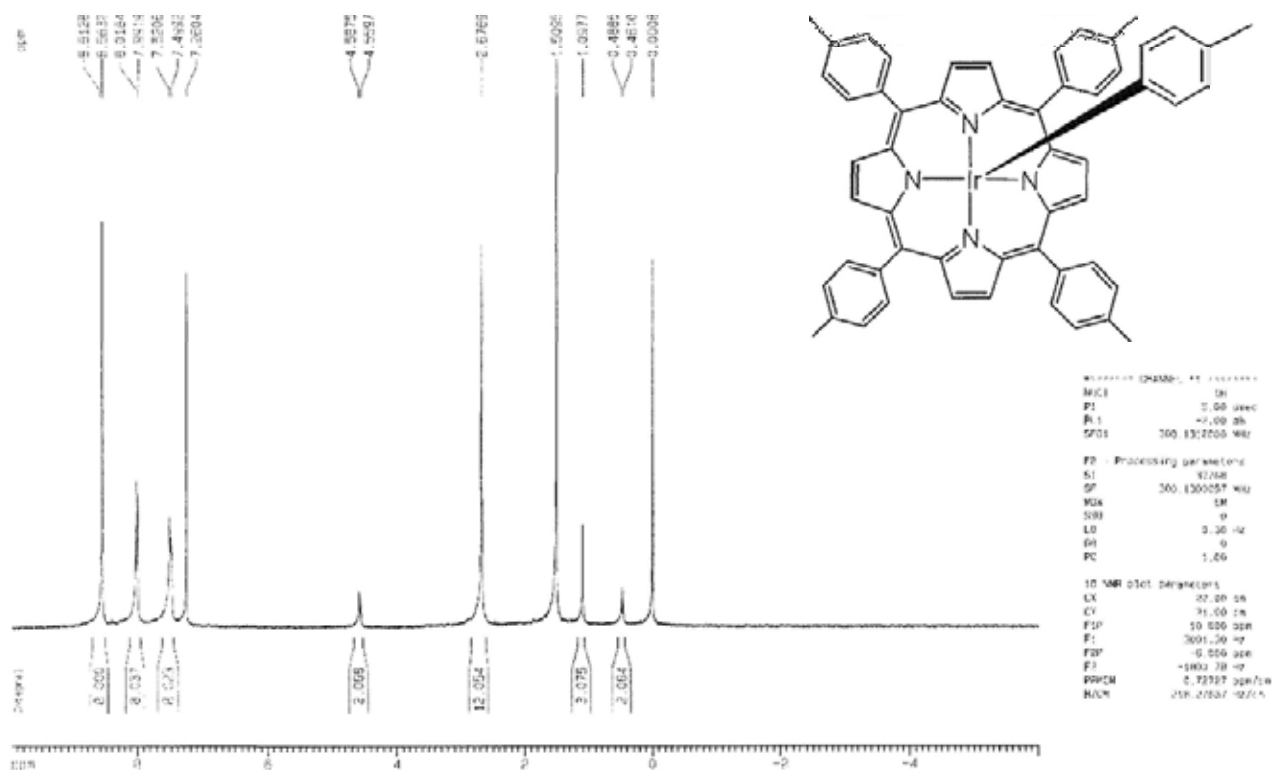
^{13}C NMR Spectrum of Ir^{III}(ttp)C$_6$H$_4$(p-^{t}Bu) (**8d**) (CDCl$_3$)

¹H NMR Spectrum of Ir^{III}(ttp)(*p*-Tol) (**8e**) (CDCl₃)

¹H NMR Spectrum of Ir^{III}(ttp)(*p*-Tol) (**8e**) (CDCl₃)

¹³C NMR Spectrum of Ir^{III}(ttp)(*p*-Tol) (**8e**) (CDCl₃)
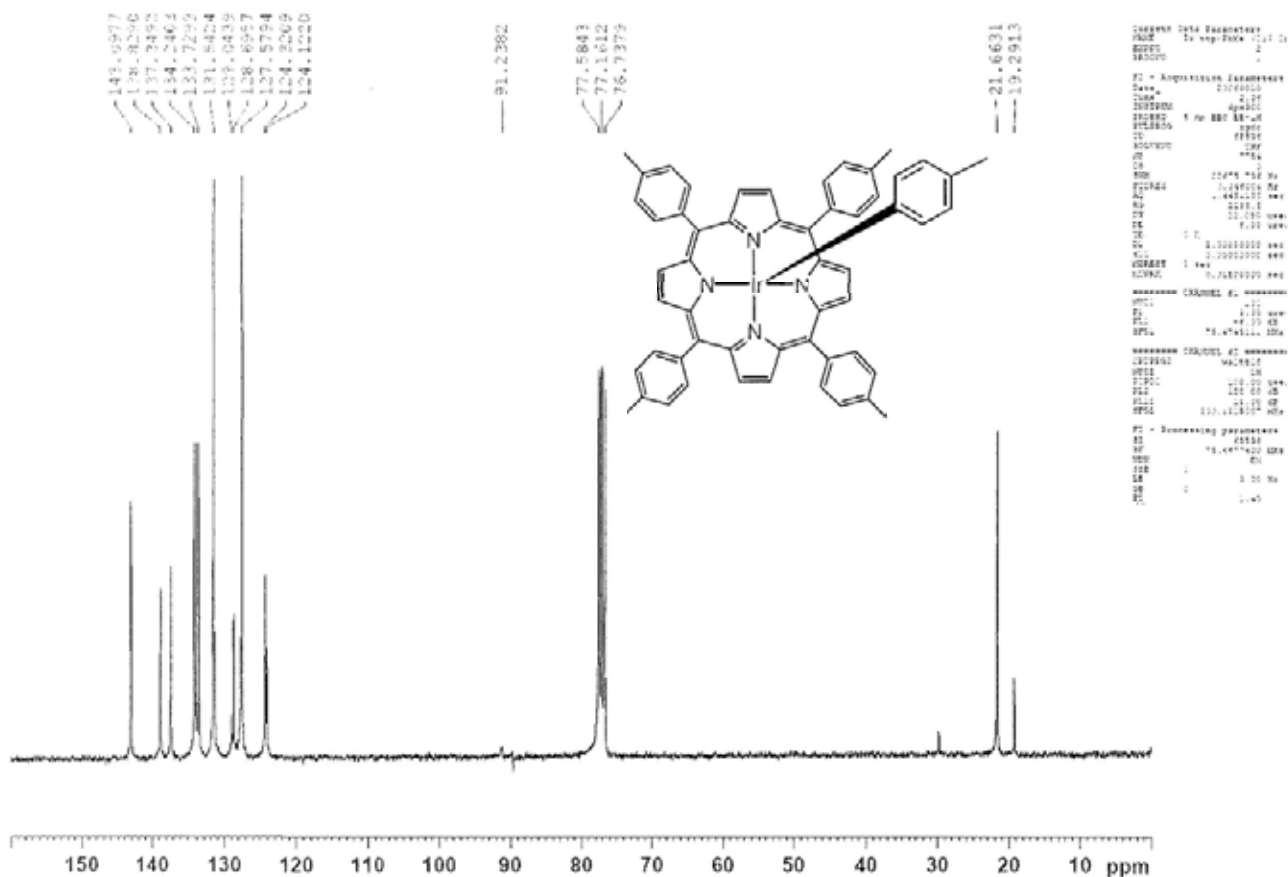
^{1}H NMR Spectrum of Ir^{III}(ttp)C$_6$H$_4$(p-SiMe$_3$) (8f) (CDCl$_3$)
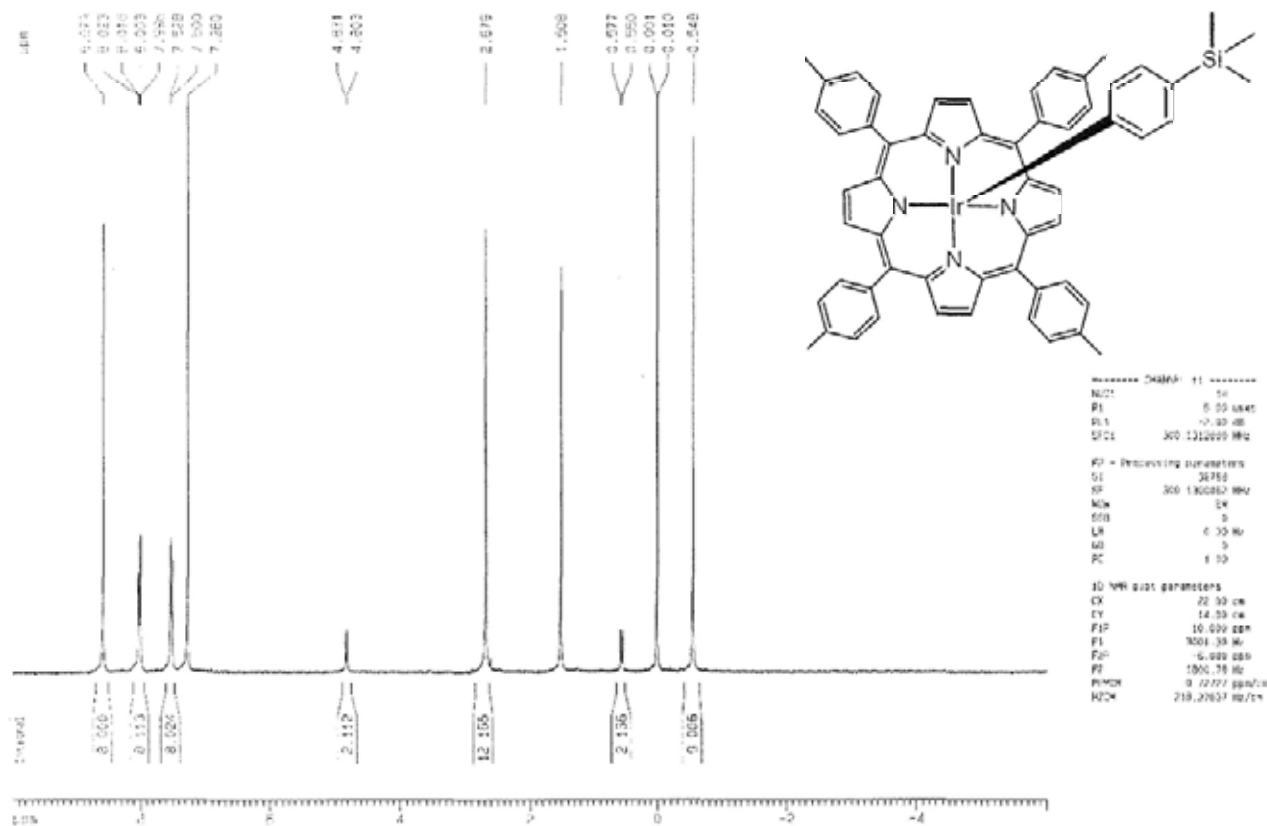
^{13}C NMR Spectrum of Ir^{III}(ttp)C$_6$H$_4$(p-SiMe$_3$) (8f) (CDCl$_3$)
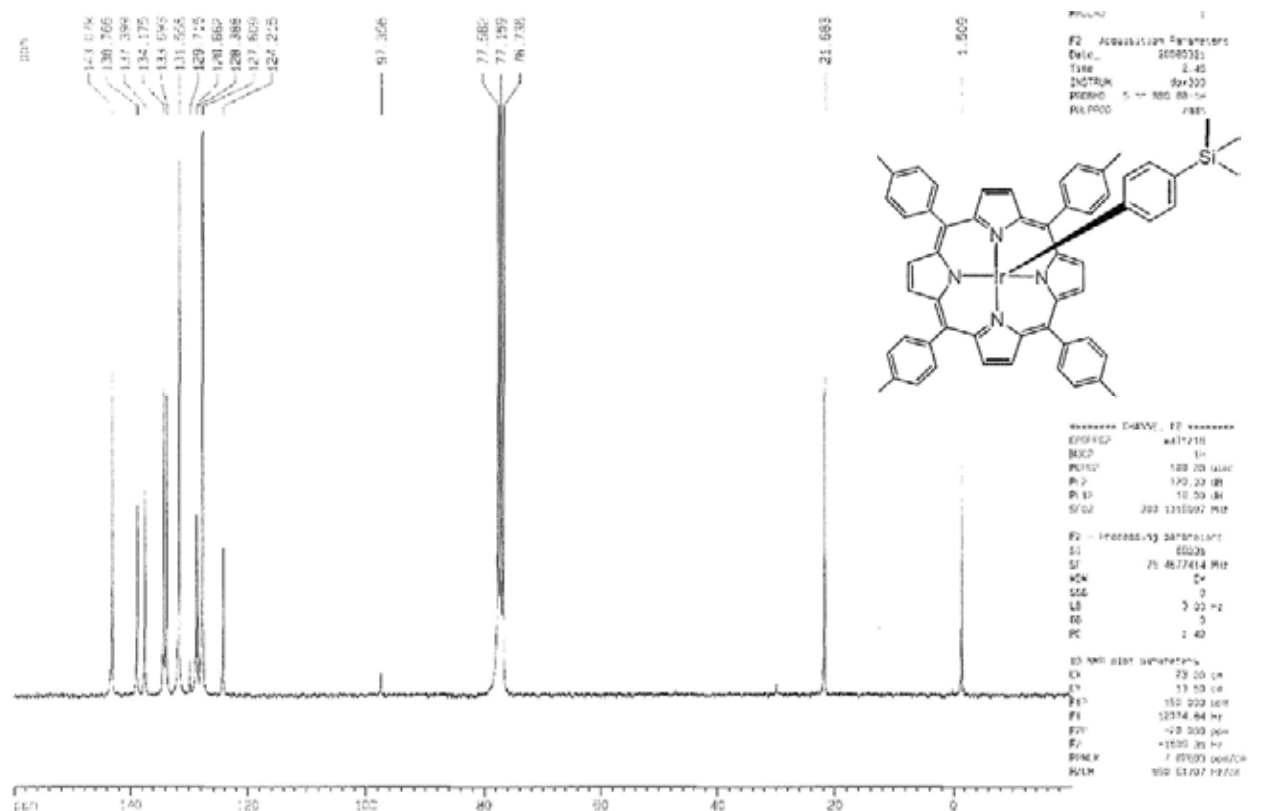
^{1}H NMR Spectrum of Ir^{III}(ttp)C$_6$H$_4$(*p*-NPhth) (**8g**) (CDCl$_3$)
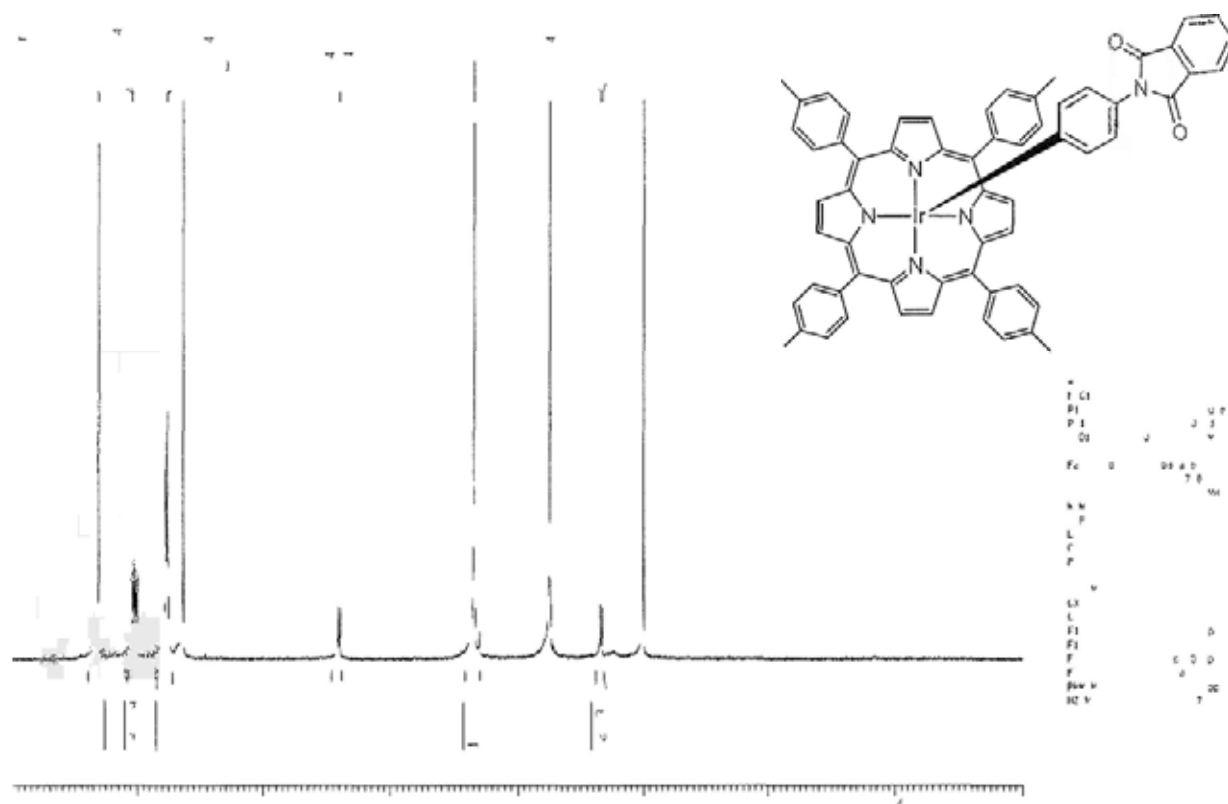
^{13}C NMR Spectrum of Ir^{III}(ttp)C$_6$H$_4$(*p*-NPhth) (**8g**) (CDCl$_3$)

304
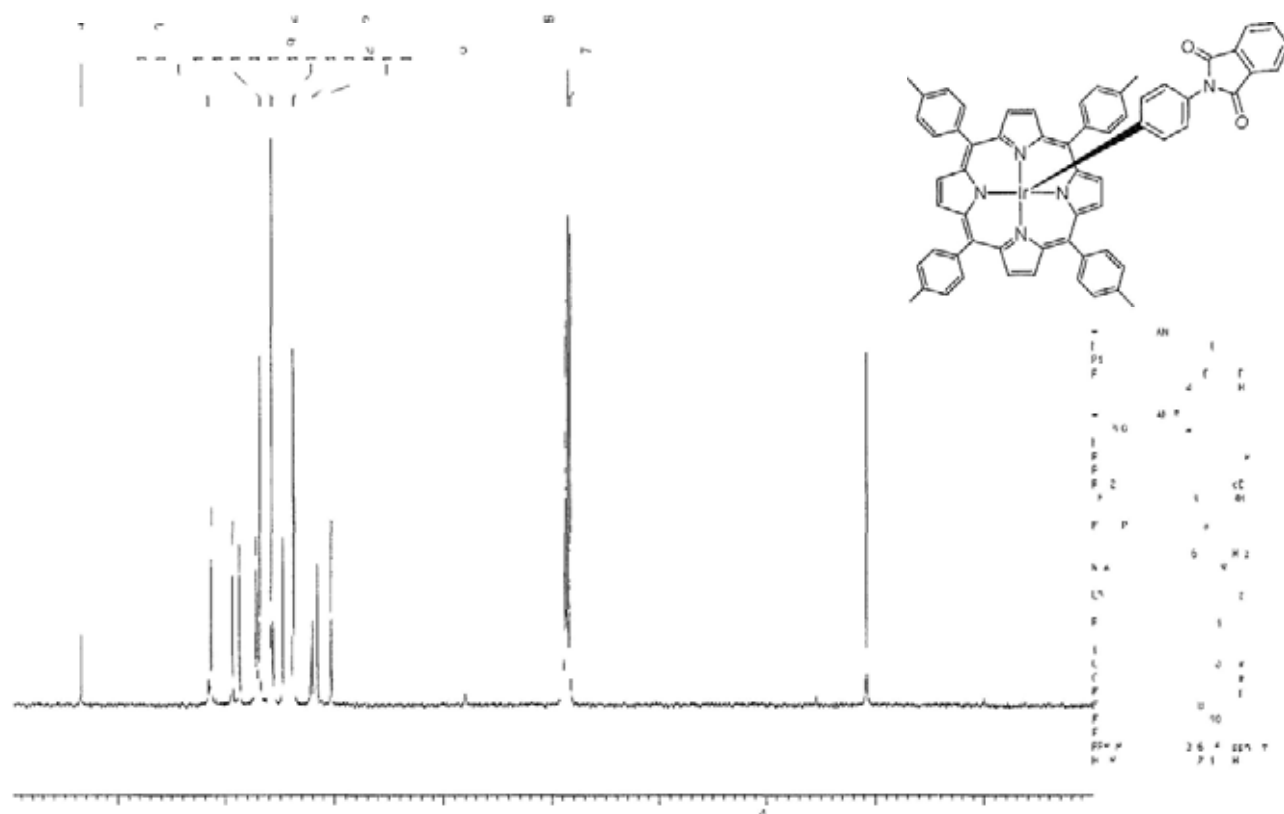
^{1}H NMR Spectrum of Ir^{III}(ttp)C$_6$H$_4$(*p*-F) (**8h**) (CDCl$_3$)
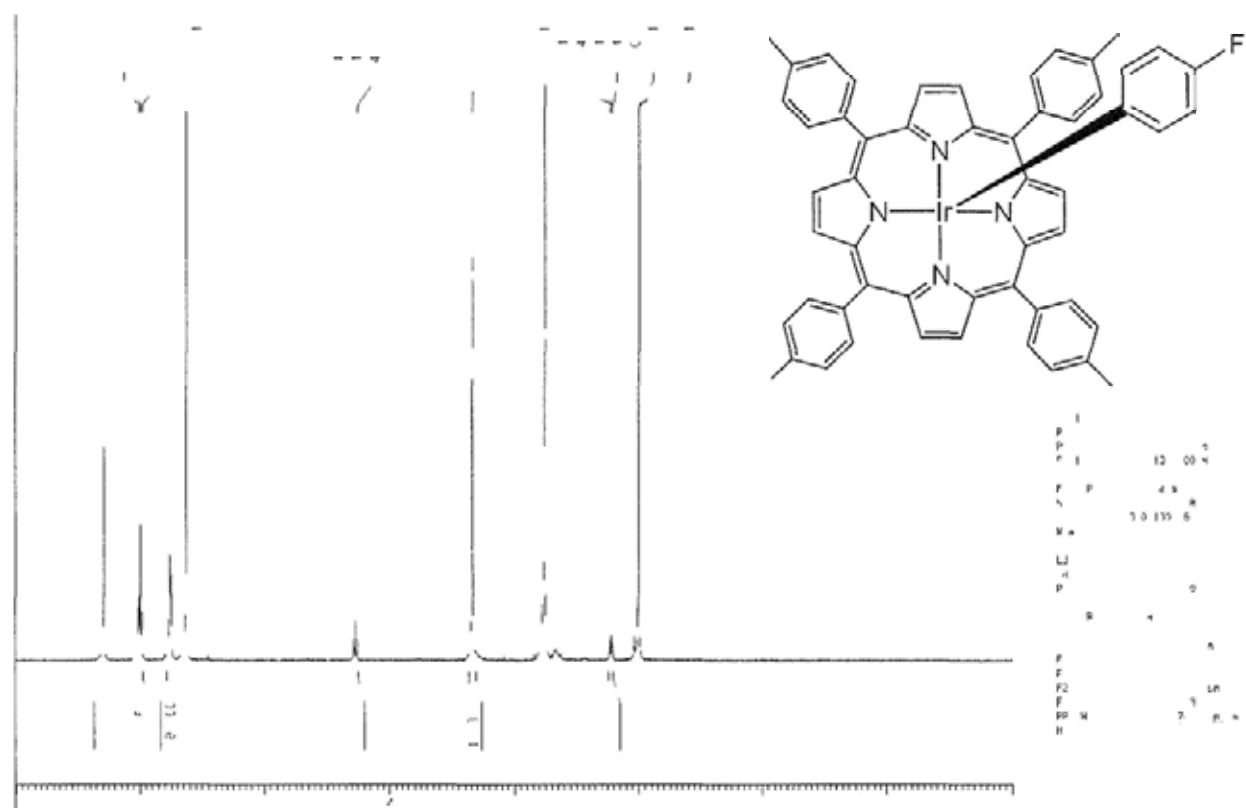
^{13}C NMR Spectrum of Ir^{III}(ttp)C$_6$H$_4$(*p*-F) (**8h**) (CDCl$_3$)
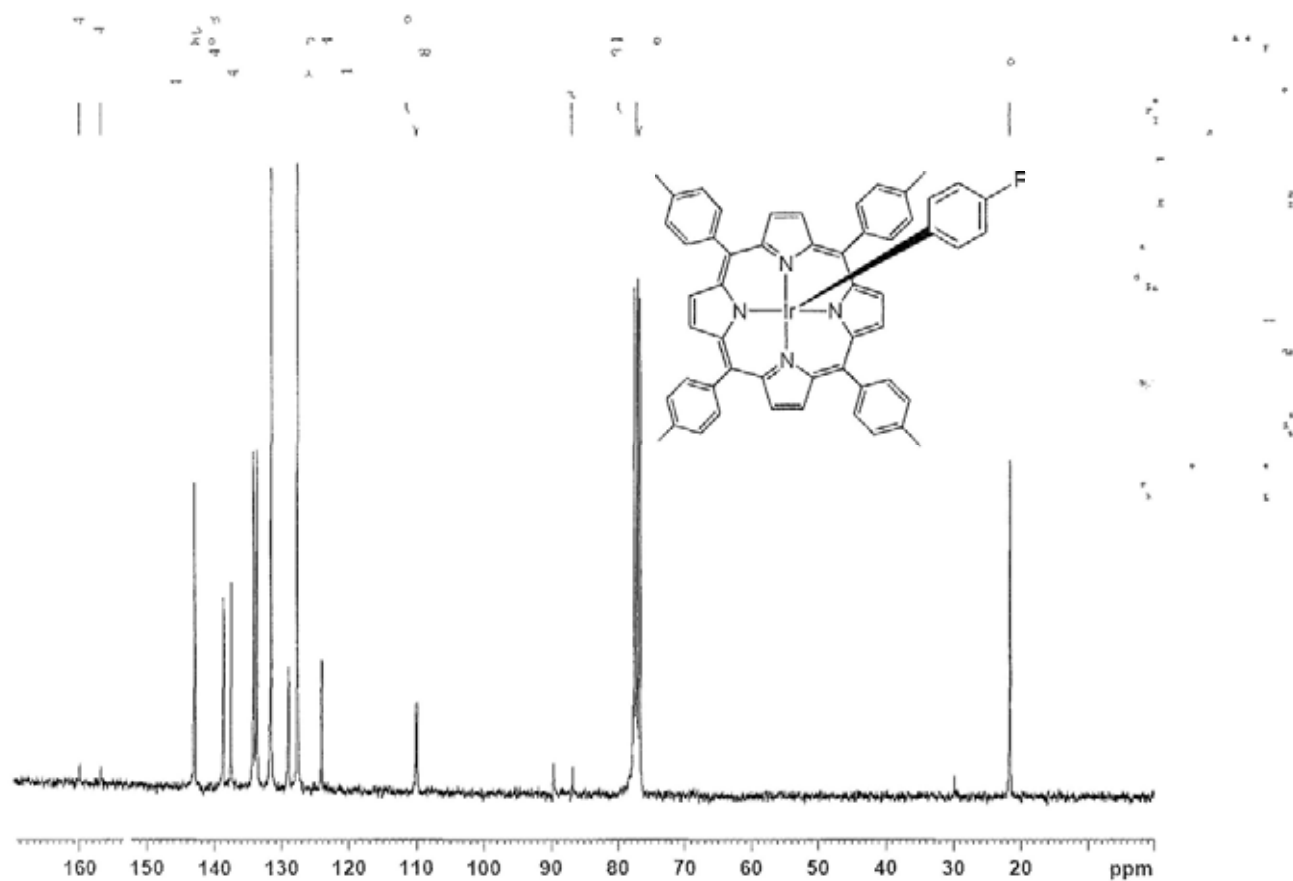
^{1}H NMR Spectrum of Ir^{III}(ttp)C$_6$H$_4$(p-Br) (8i) (CDCl$_3$)
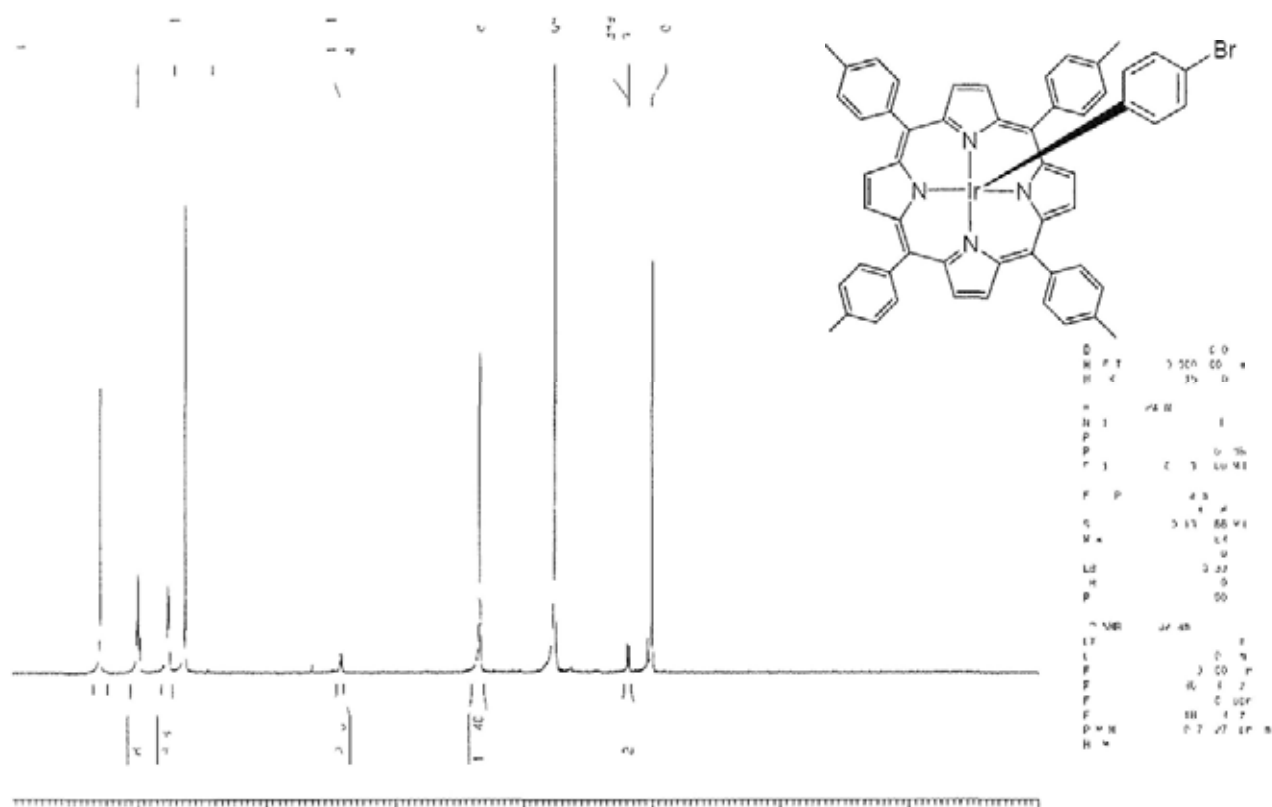
^{13}C NMR Spectrum of Ir^{III}(ttp)C$_6$H$_4$(p-Br) (8i) (CDCl$_3$)

^{1}H NMR Spectrum of Ir^{III}(ttp)C$_6$H$_4$(p-Cl) (8j) (CDCl$_3$)

^{13}C NMR Spectrum of Ir^{III}(ttp)C$_6$H$_4$(p-Cl) (8j) (CDCl$_3$)
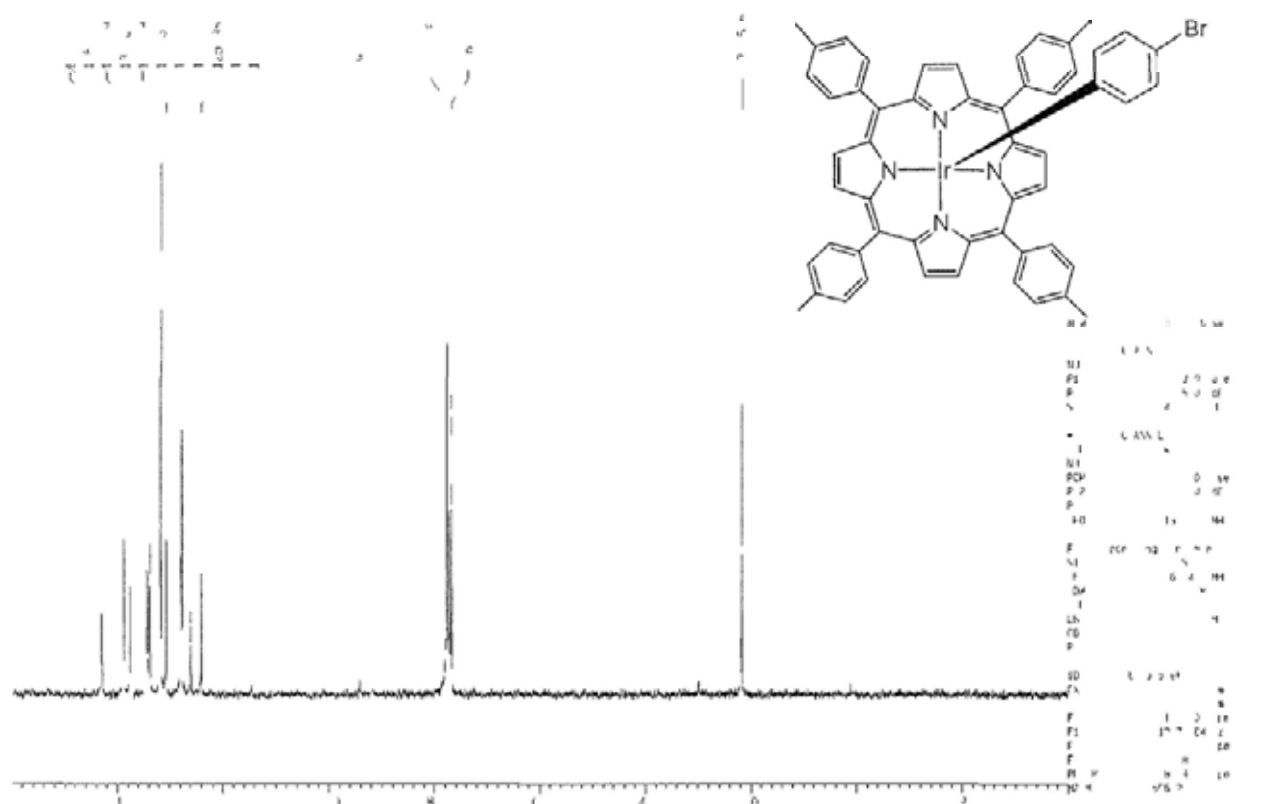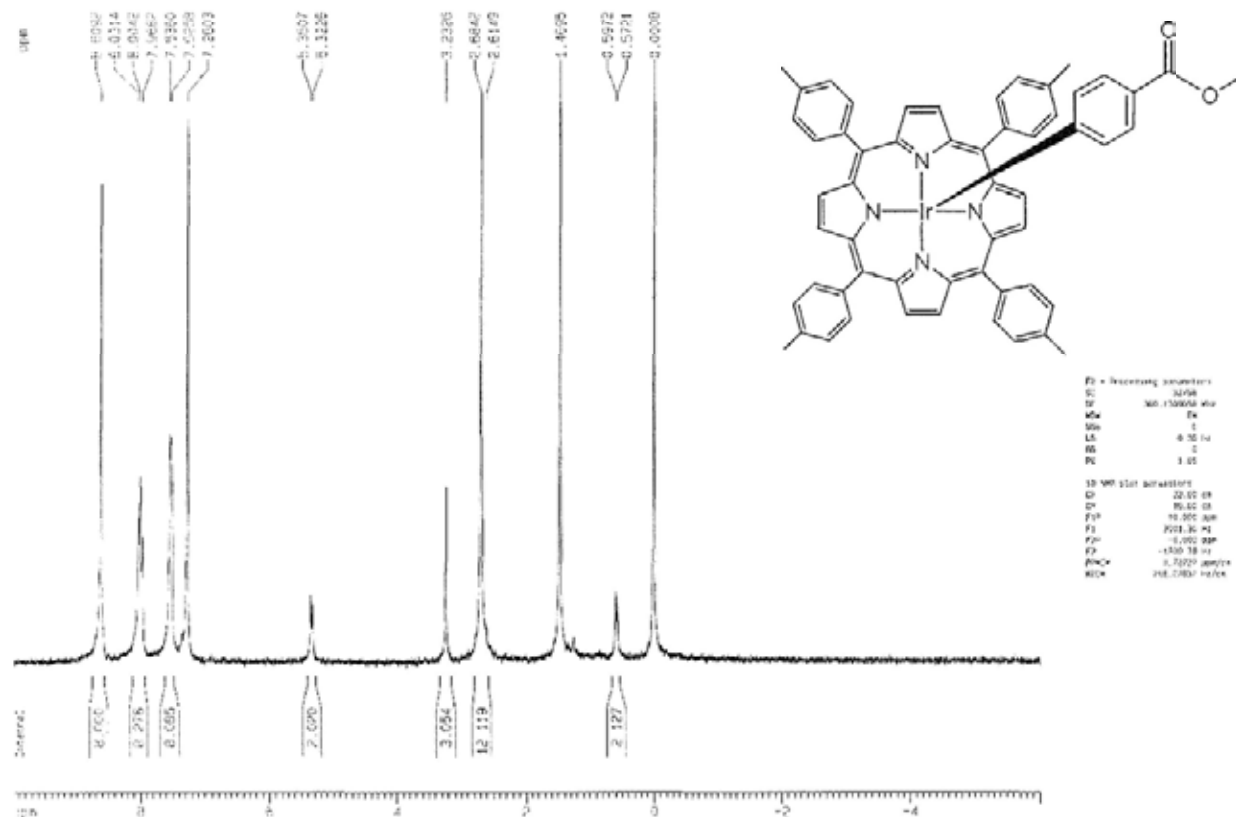
^{1}H NMR Spectrum of Ir^{III}(ttp)C$_6$H$_4$(p-CO$_2$Me) (8k) (CDCl$_3$)

^{13}C NMR Spectrum of Ir^{III}(ttp)C$_6$H$_4$(p-CO$_2$Me) (8k) (CDCl$_3$)

308

¹H NMR Spectrum of Ir^III(ttp)C₆H₄(p-C(O)Me) (8l) (CDCl₃)

¹³C NMR Spectrum of Ir^III(ttp)C₆H₄(p-C(O)Me) (8l) (CDCl₃)

309

^{1}H NMR Spectrum of Ir^{III}(ttp)(PPh$_3$)C$_6$H$_4$(p-CHO) (8m) (CDCl$_3$)

^{13}C NMR Spectrum of Ir^{III}(ttp)(PPh$_3$)C$_6$H$_4$(p-CHO) (8m) (CDCl$_3$)

^{1}H NMR Spectrum of Ir^{III}(ttp)C$_6$H$_4$(p-CF$_3$) (8n) (CDCl$_3$)

^{13}C NMR Spectrum of Ir^{III}(ttp)C$_6$H$_4$(p-CF$_3$) (8n) (CDCl$_3$)

311
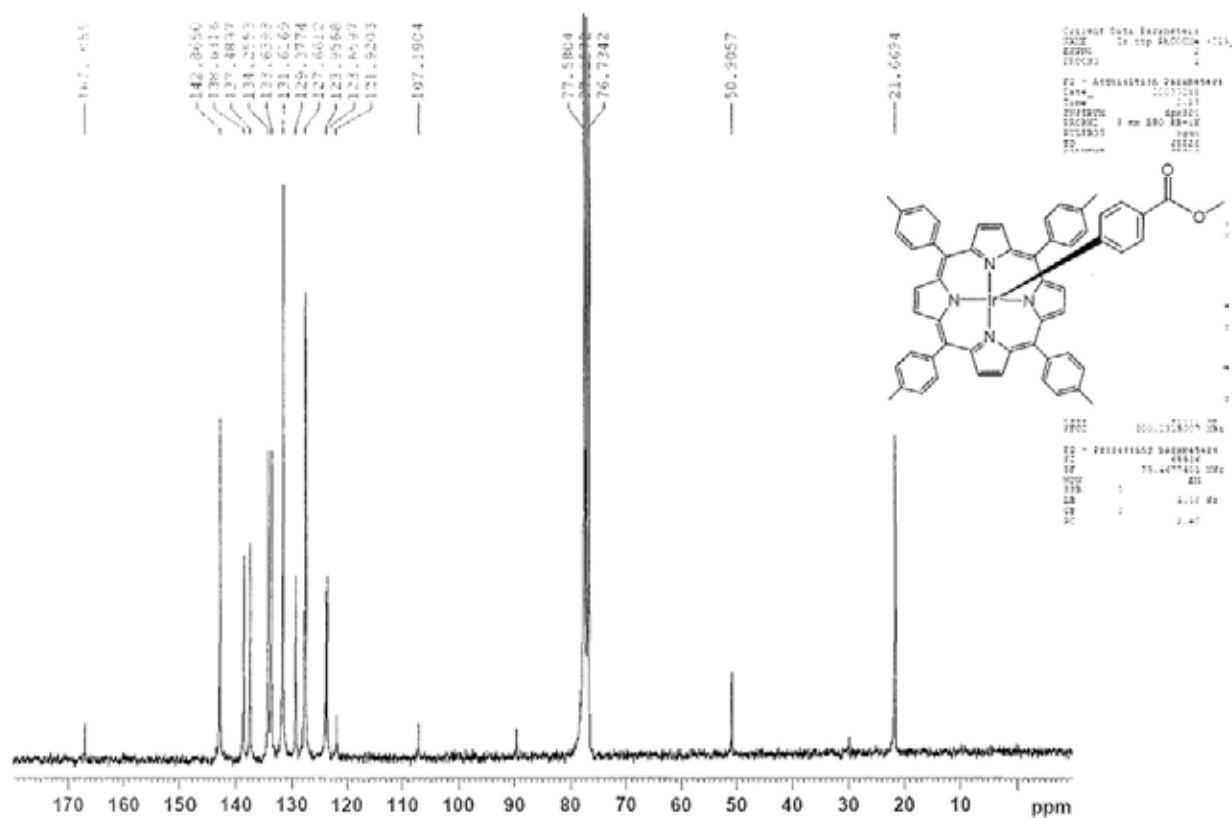
^{13}C NMR Spectrum of Ir^{III}(ttp)C$_6$H$_4$(p-CF$_3$) (8n) (CDCl$_3$) (expanded region)

125.5   125.0   124.5   124.0   123.5   123.0   122.5   122.0   121.5   121.0   120.5   120.0   ppm
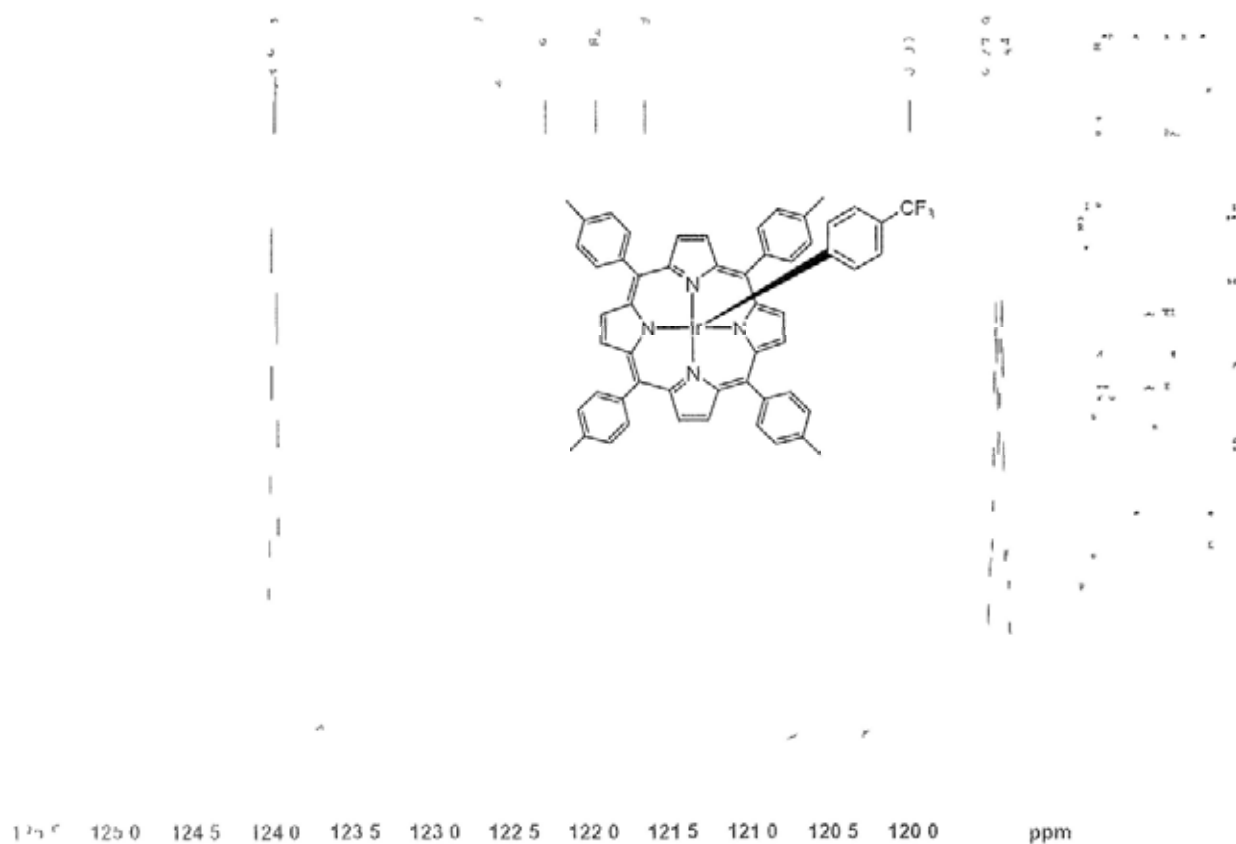
^{1}H NMR Spectrum of Ir^{III}(ttp)(PPh$_3$)C$_6$H$_4$(p-CN) (8o) (CDCl$_3$)
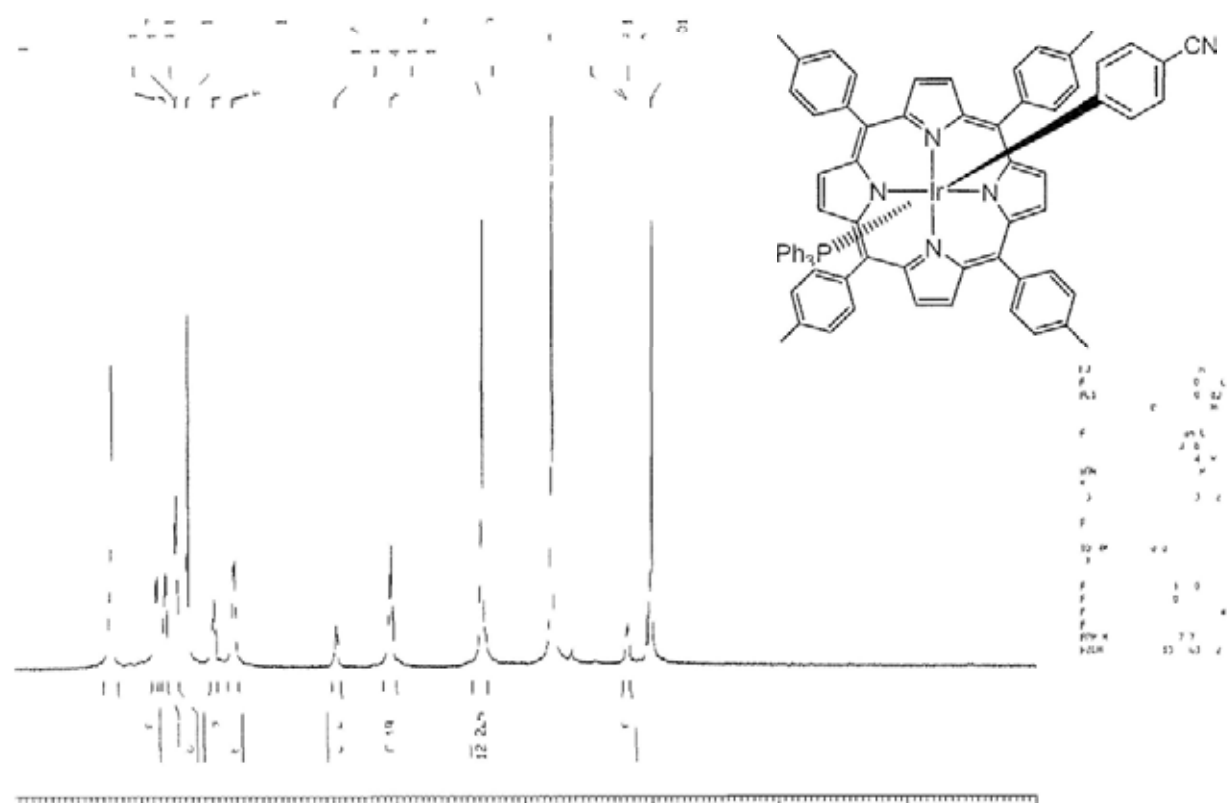
^{13}C NMR Spectrum of Ir^{III}(ttp)(PPh$_3$)C$_6$H$_4$(p-CN) (8o) (CDCl$_3$)
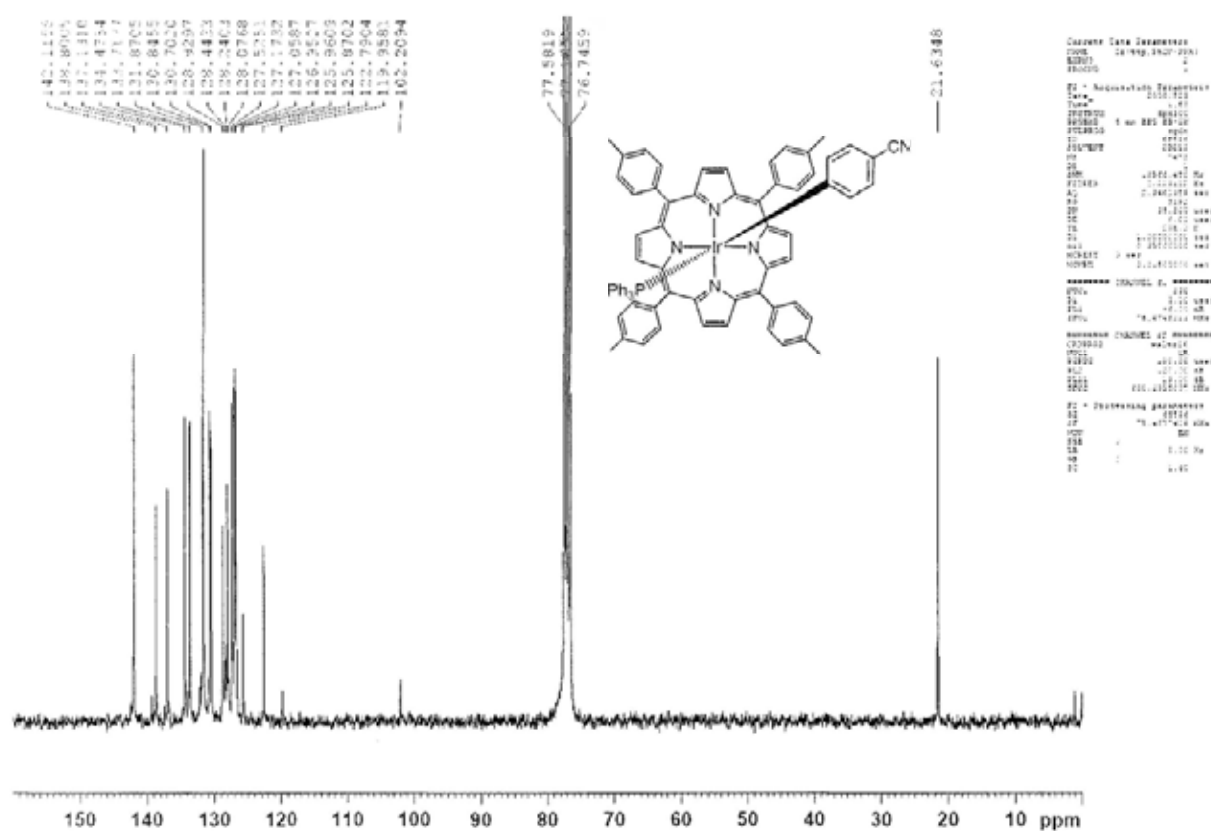
^{1}H NMR Spectrum of Ir^{III}(ttp)C$_6$H$_4$(p-NO$_2$) (8p) (CDCl$_3$)

313
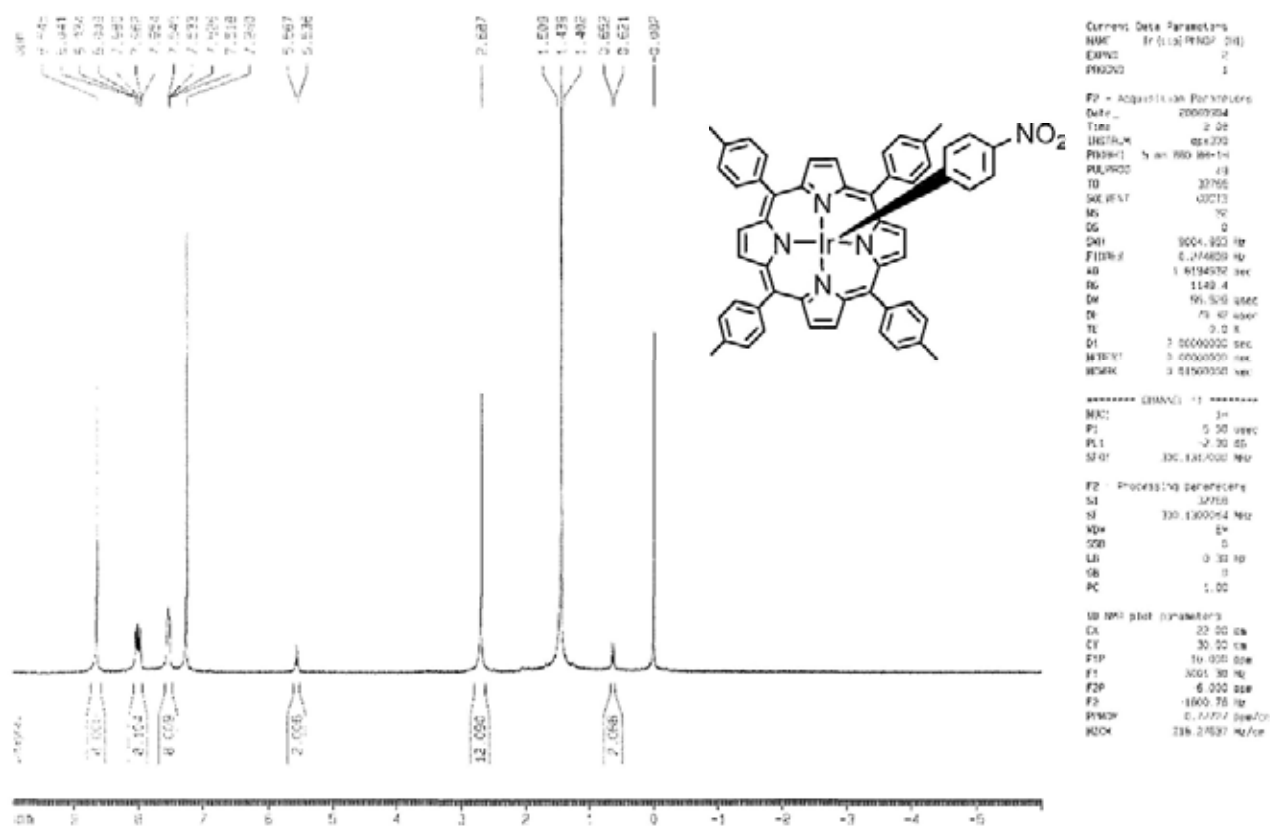
^{13}C NMR Spectrum of Ir^{III}(ttp)C$_6$H$_4$(p-NO$_2$) (8p) (THF-d_8)
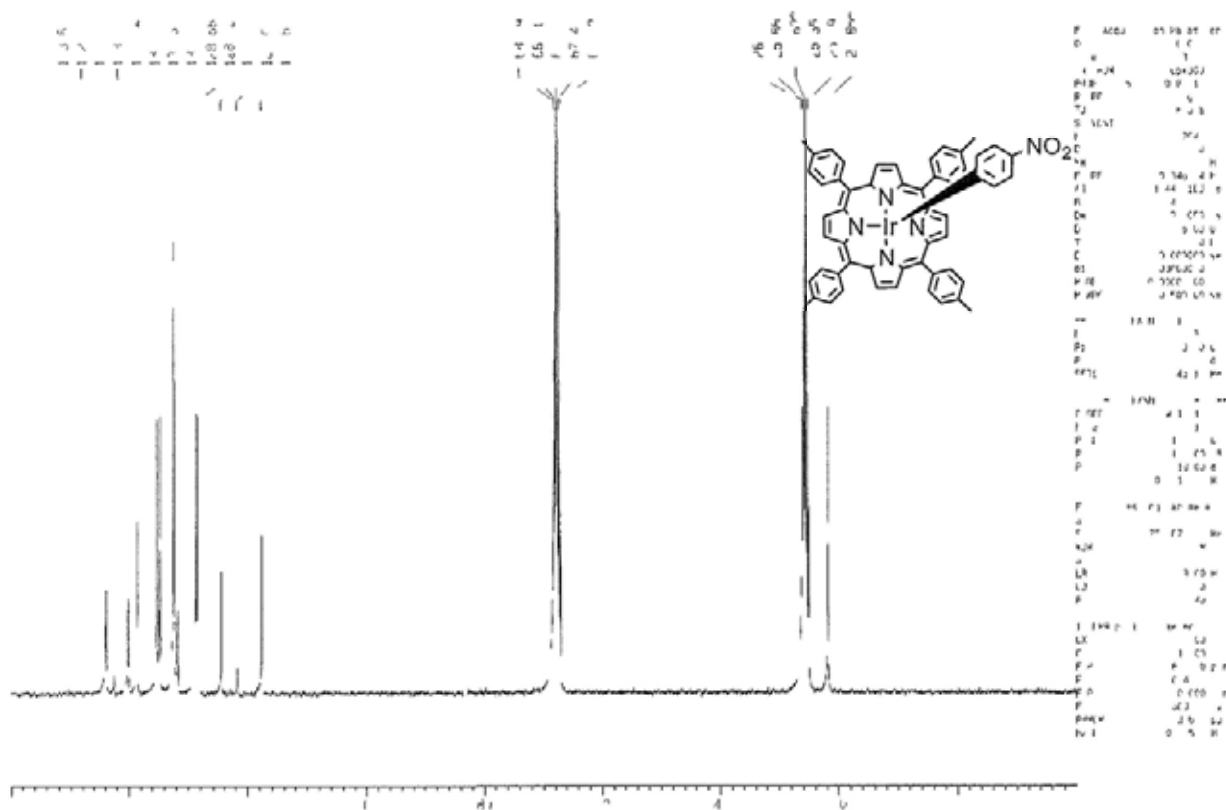
^{1}H NMR Spectrum of Ir^{III}(ttp)(2-naphthyl) (8q) (CDCl$_3$)
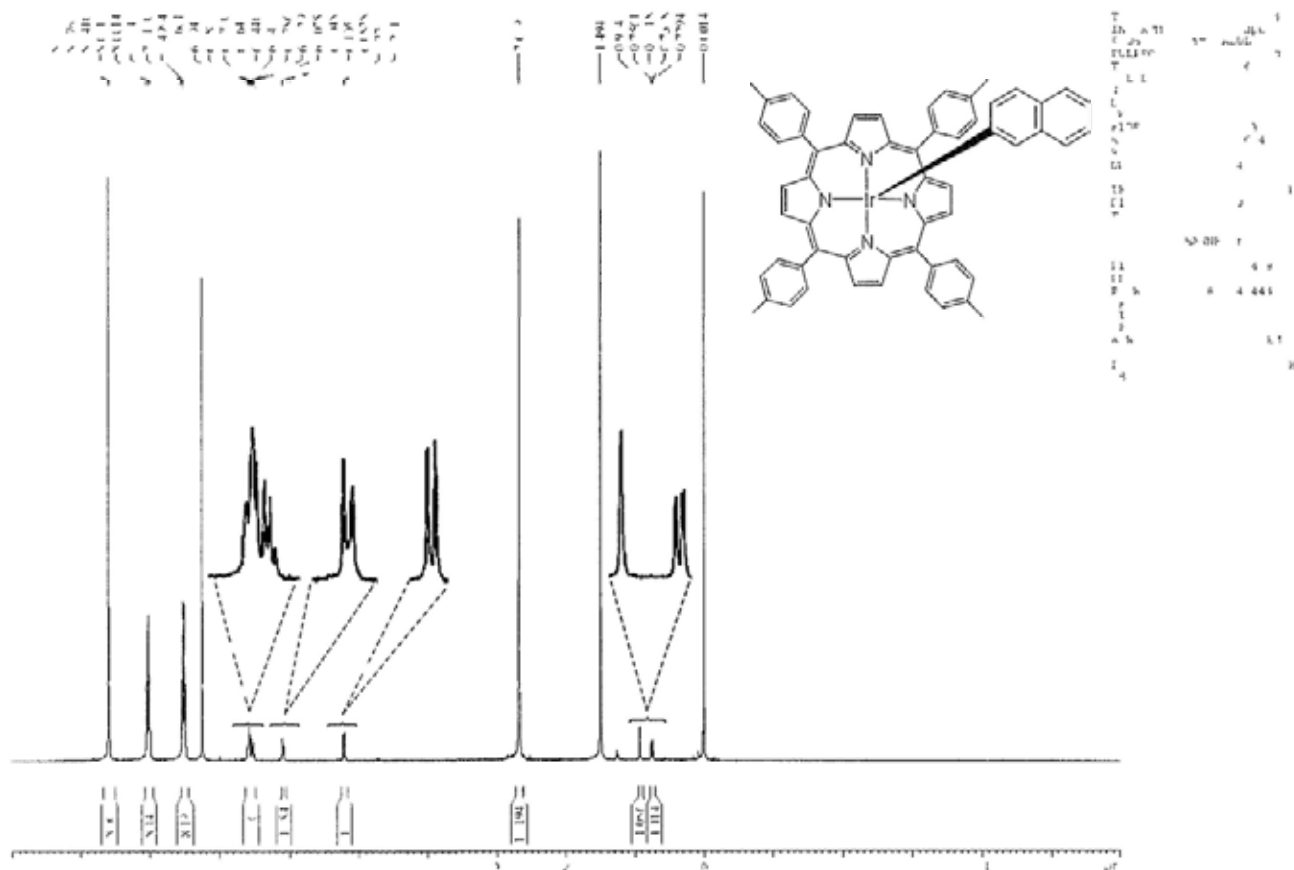
^{13}C NMR Spectrum of Ir^{III}(ttp) (2-naphthyl) (**8q**) (CDCl$_3$)
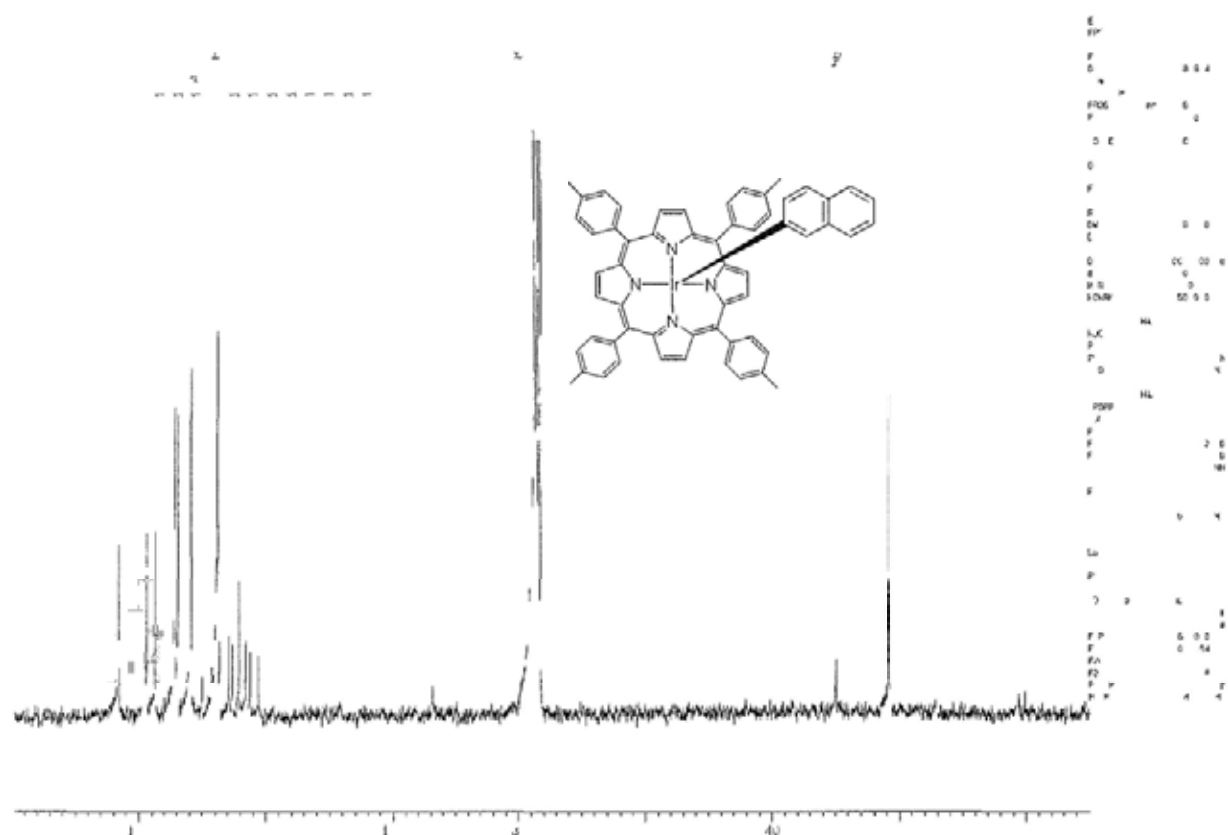
^{1}H NMR Spectrum of Ir^{III}(ttp)C$_6$H$_4$(*p*-I) (**8r**) (CDCl$_3$)
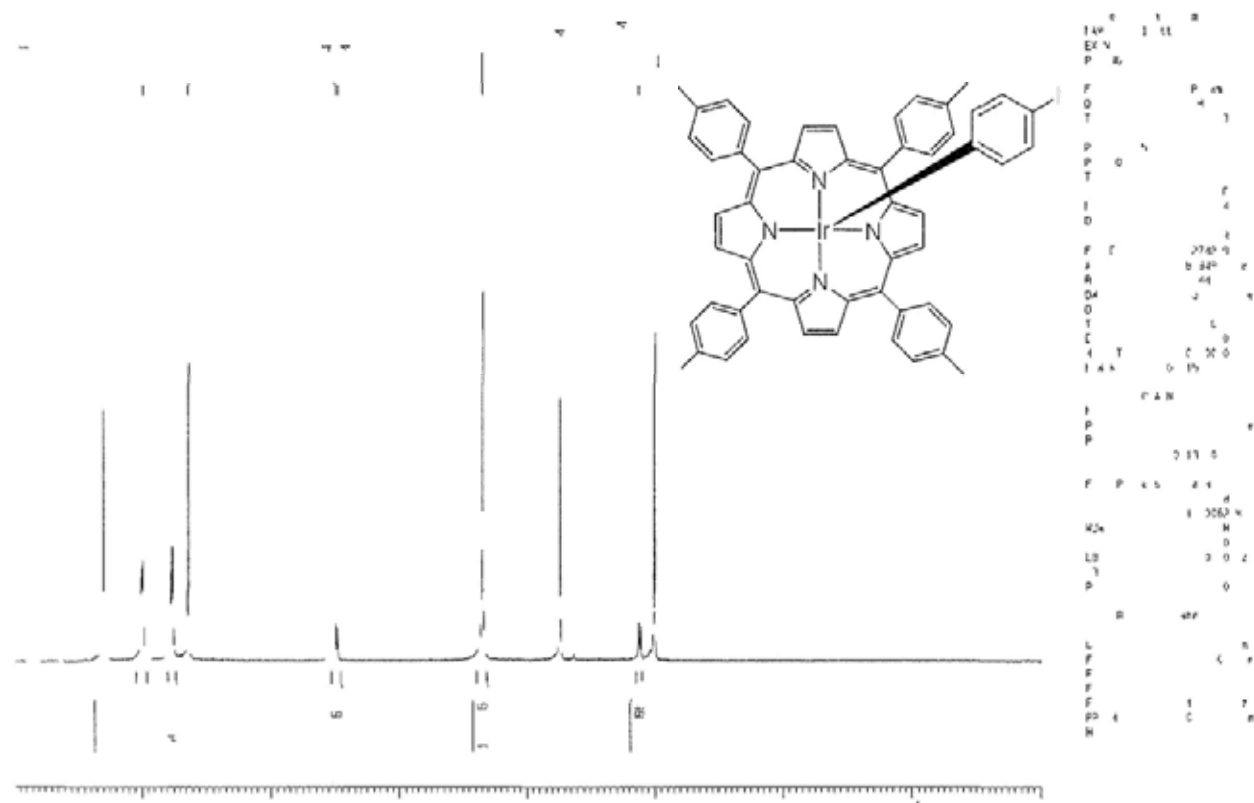
^{13}C NMR Spectrum of Ir^{III}(ttp)C$_6$H$_4$(p-I) (8r) (CDCl$_3$)
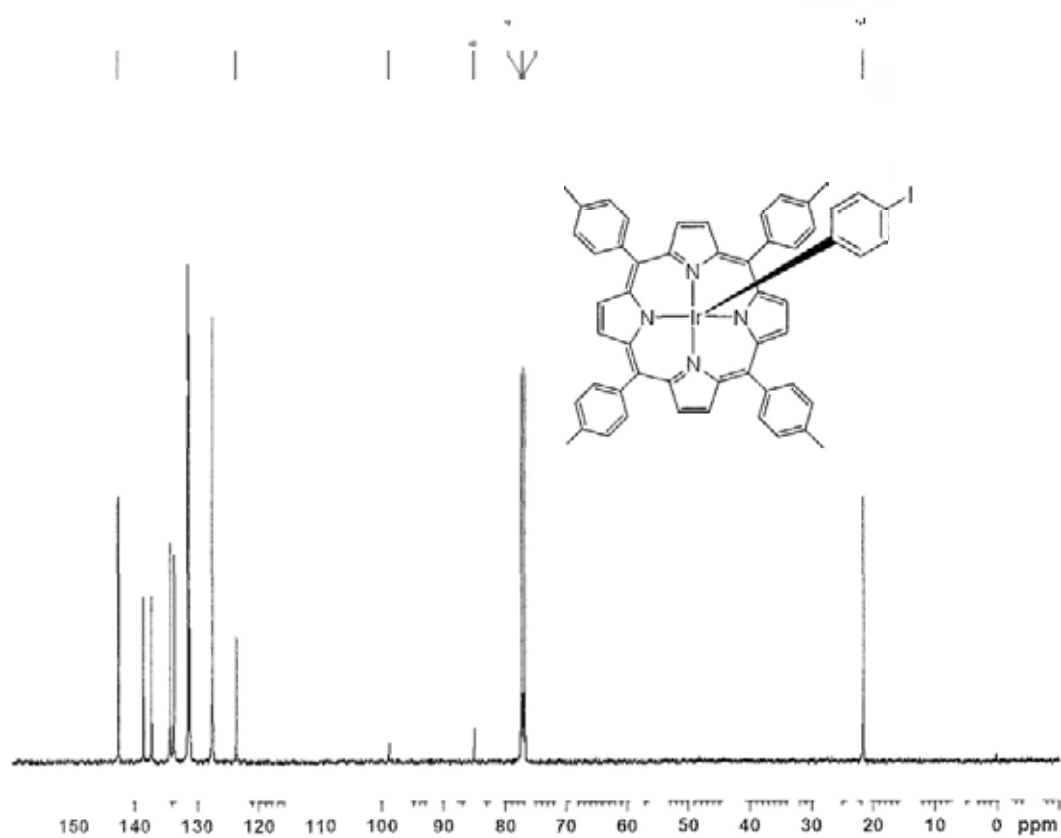
^{1}H NMR Spectrum of Ir^{III}(ttp)(p-C$_6$H$_4$)$_2$(p-I) (8s) (CDCl$_3$)
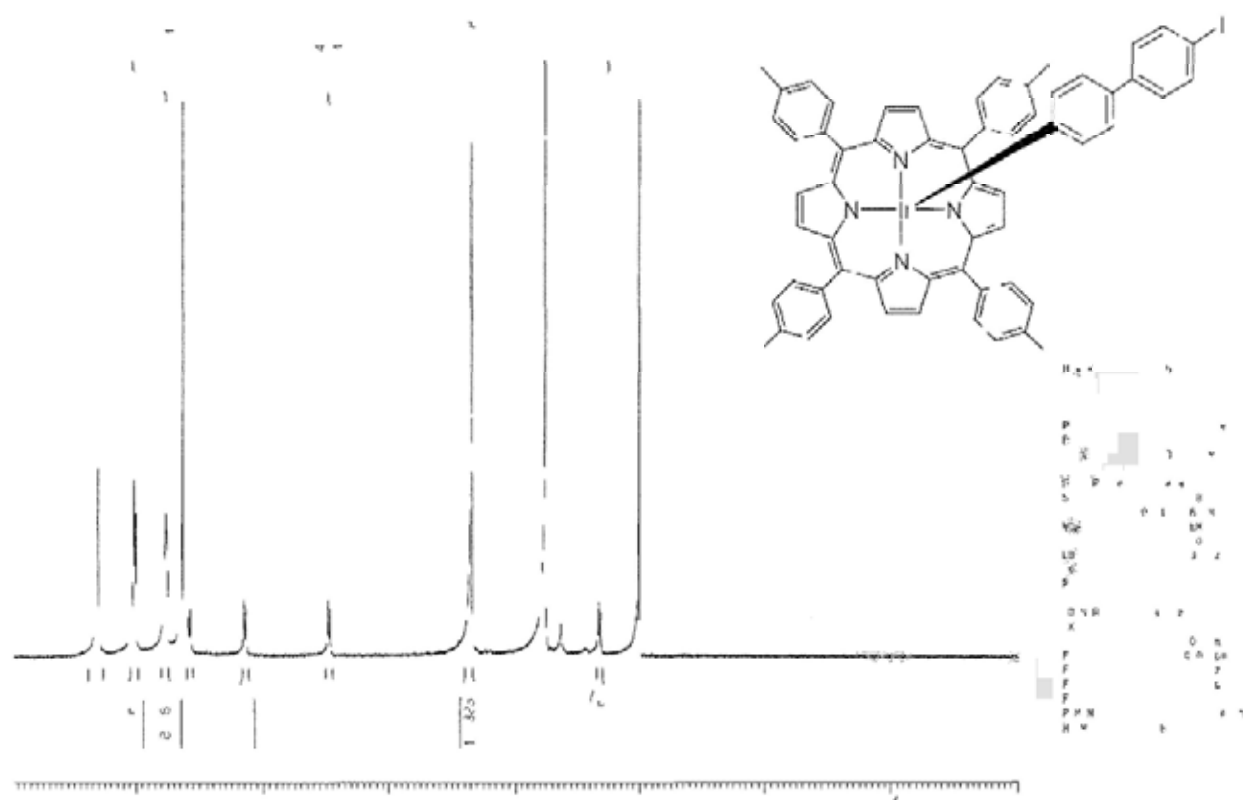
¹H NMR Spectrum of Ir^{III}(ttp)(*p*-C₆H₄)₂(*p*-Br) (**8t**) (CDCl₃)

¹³C NMR Spectrum of Ir^{III}(ttp)(*p*-C₆H₄)₂(*p*-Br) (**8t**) (CDCl₃)

317

¹H NMR Spectrum of Ir^{III}(ttp)C₆H₄(*m*-OMe) (**8u**) (CDCl₃)

¹³C NMR Spectrum of Ir^{III}(ttp)C₆H₄(*m*-OMe) (**8u**) (CDCl₃)

318
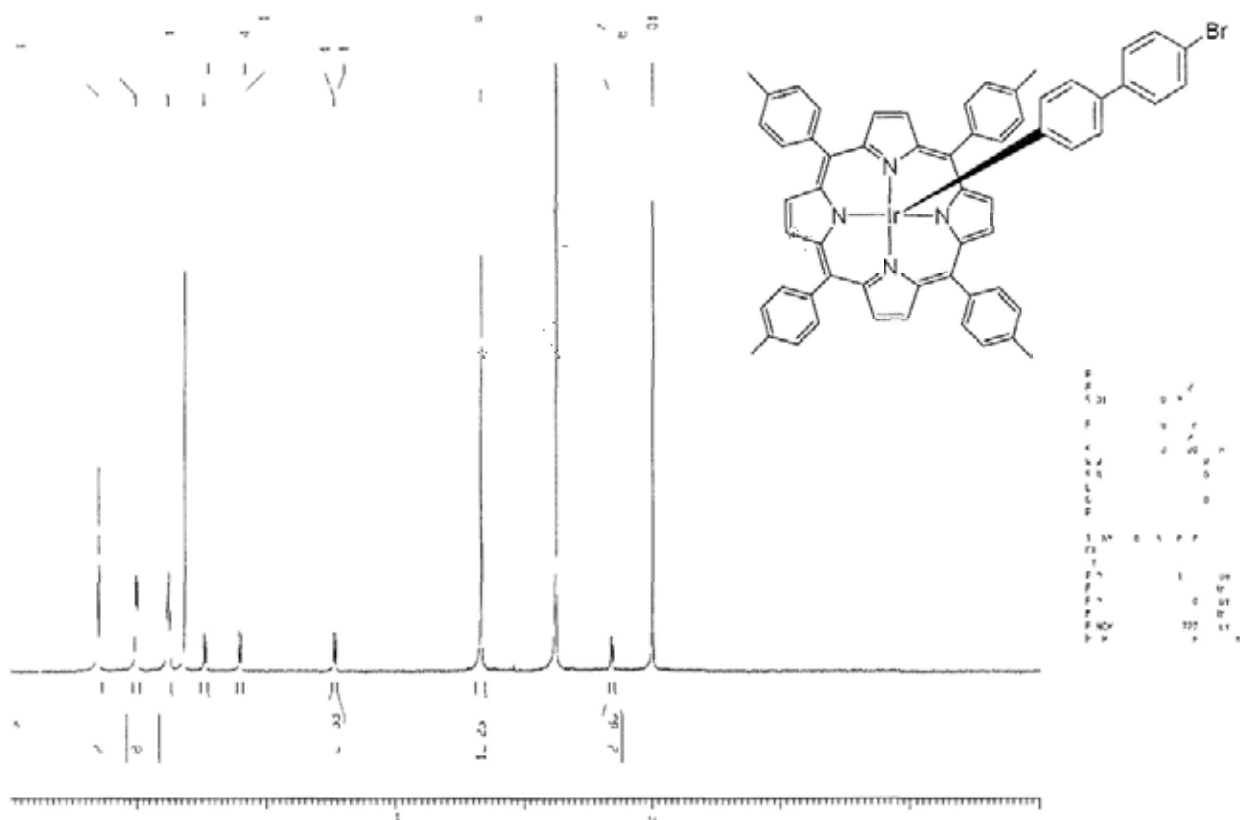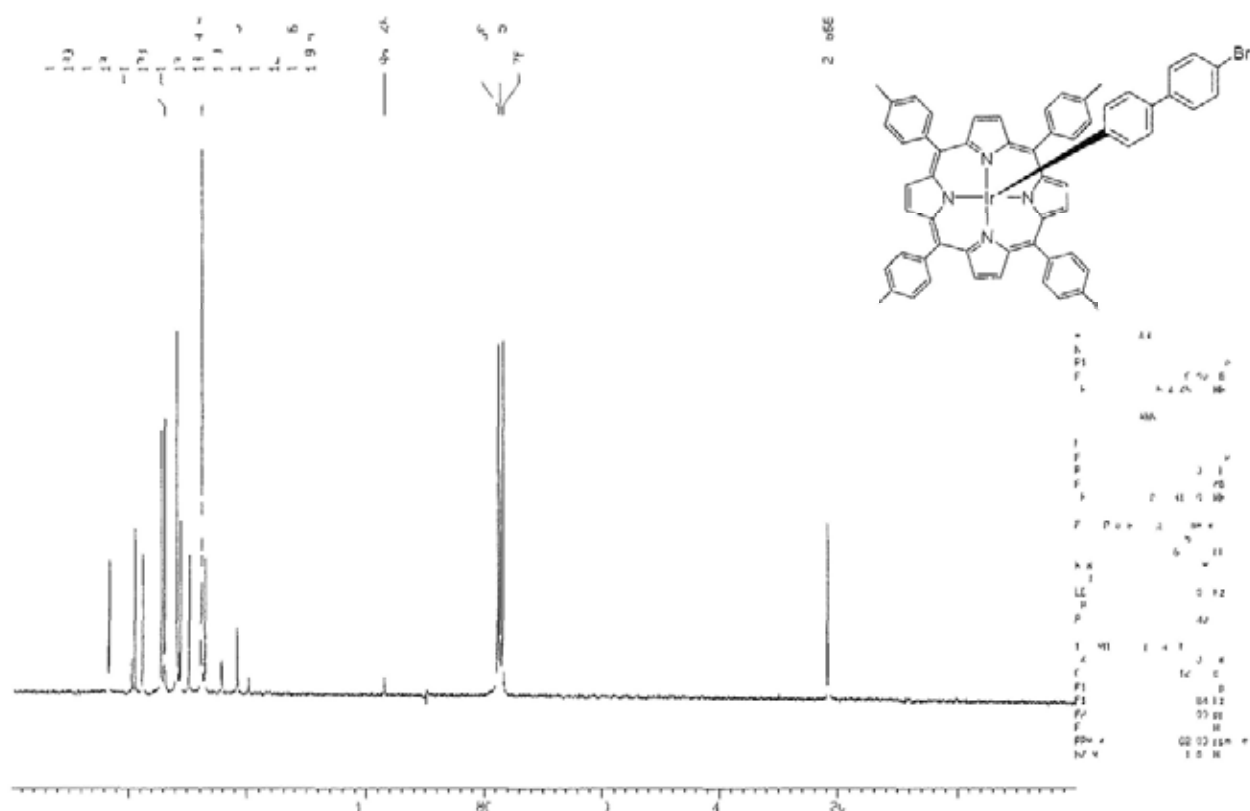
^{1}H NMR Spectrum of Ir^{III}(ttp)(*m*-Tol) (**8v**) (CDCl$_3$)
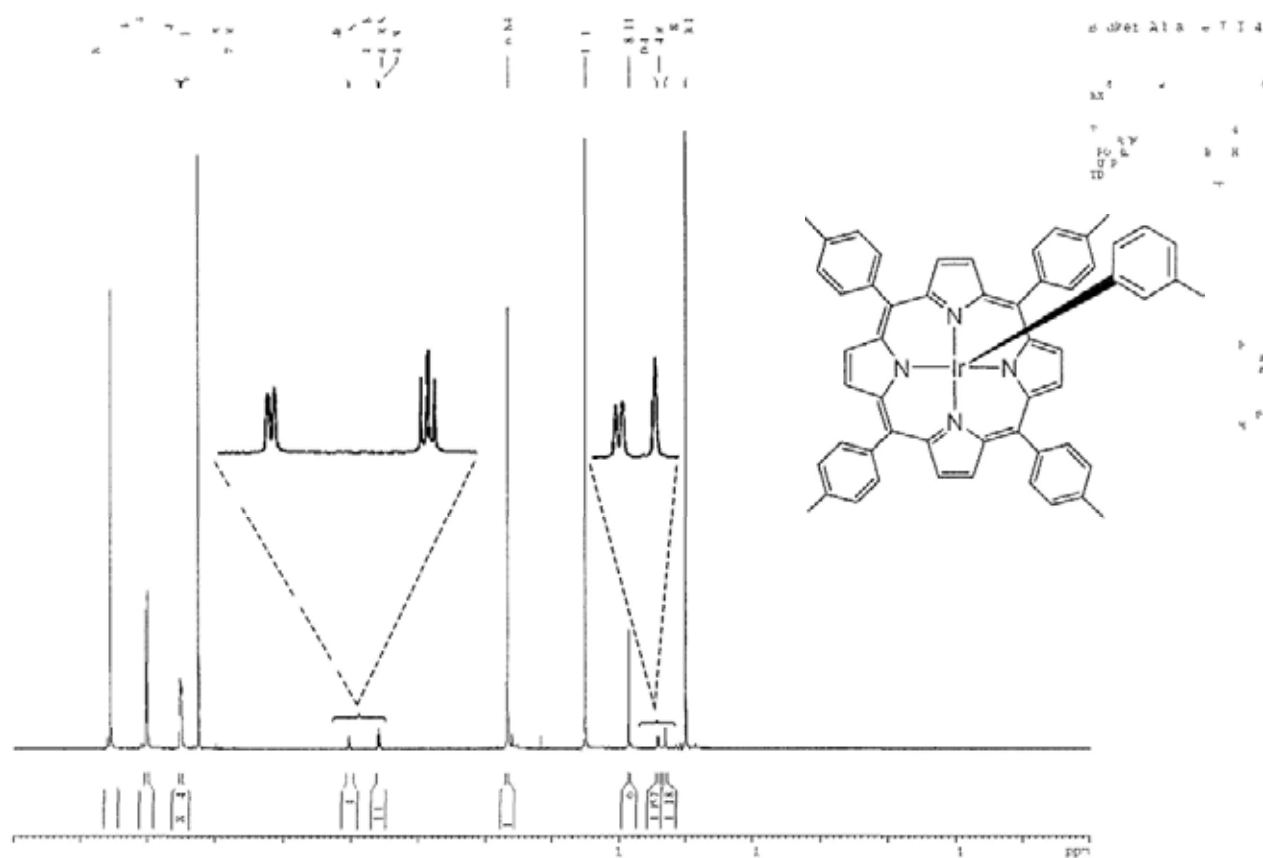
^{13}C NMR Spectrum of Ir^{III}(ttp)(*m*-Tol) (**8v**) (CDCl$_3$)

¹H NMR Spectrum of Ir^{III}(ttp)C₆H₄(*m*-NO₂) (**8w**) (CDCl₃)

^{1}H NMR Spectrum of Ir^{III}(ttp)C$_6$H$_4$(m-NO$_2$) (**8w**) (CDCl$_3$)

^{13}C NMR Spectrum of Ir^{III}(ttp)C$_6$H$_4$(m-NO$_2$) (**8w**) (CDCl$_3$)
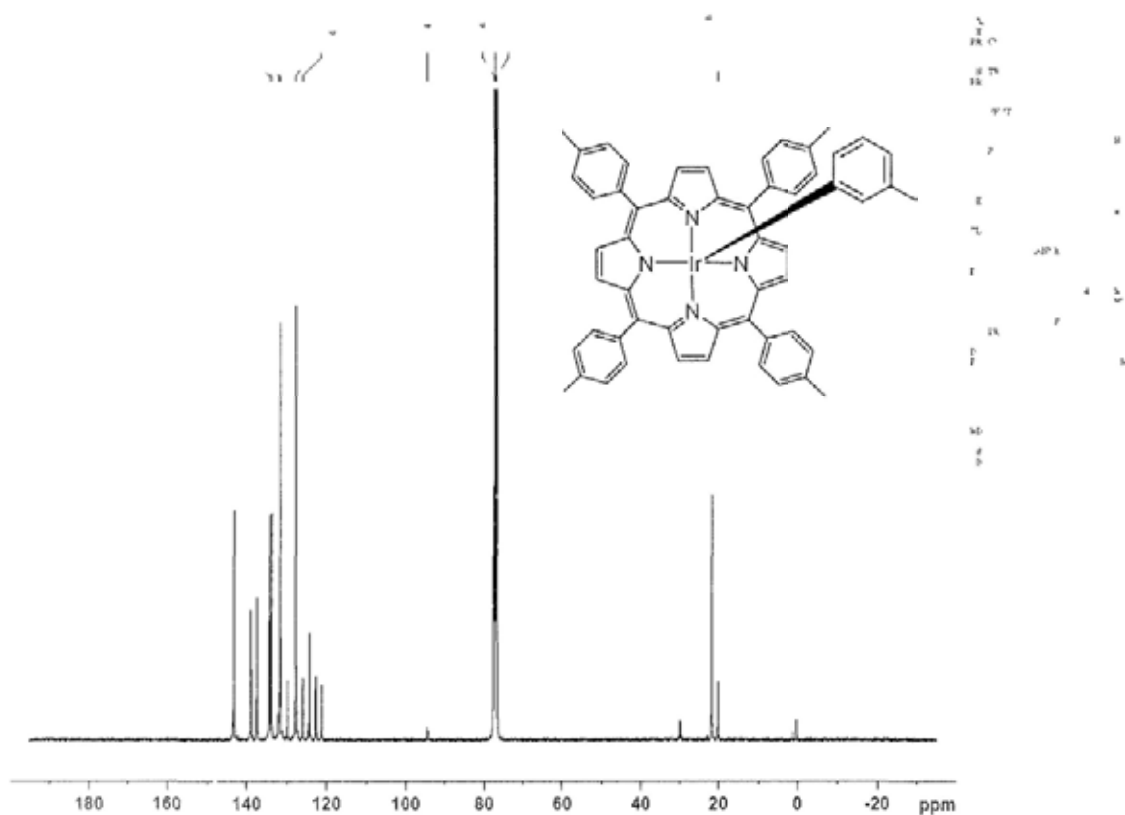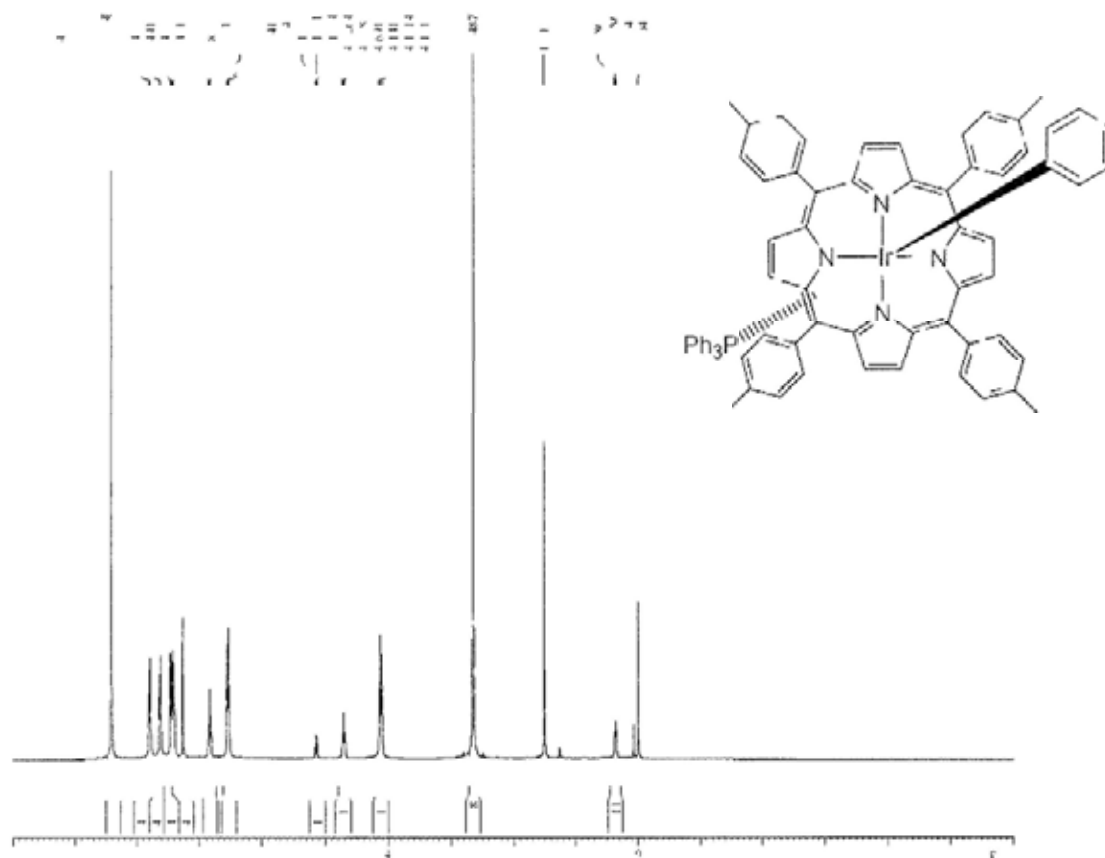
^{1}H NMR Spectrum of Ir^{III}(ttp)(PPh$_3$)Ph (8x) (CDCl$_3$)

^{13}C NMR Spectrum of Ir^{III}(ttp)(PPh$_3$)Ph (8x) (CDCl$_3$)

¹H NMR Spectrum of Ir^{III}(ttp)(p-C₆H₄)Ir^{III}(ttp) **(9a)** (CDCl₃)

¹H NMR Spectrum of Ir^{III}(ttp)(p-C₆H₄)₂Ir^{III}(ttp) **(9b)** (CDCl₃)

322
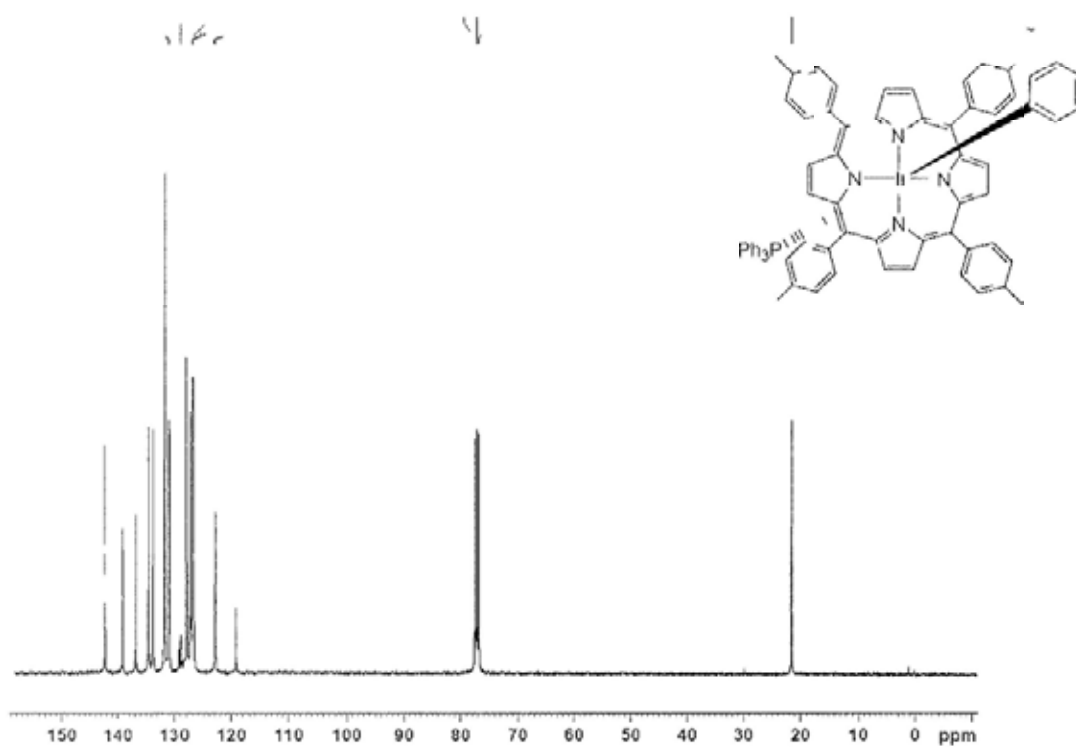
^{13}C NMR Spectrum of Ir^{III}(ttp)(p-C$_6$H$_4$)$_2$Ir^{III}(ttp) (9b) (CDCl$_3$)
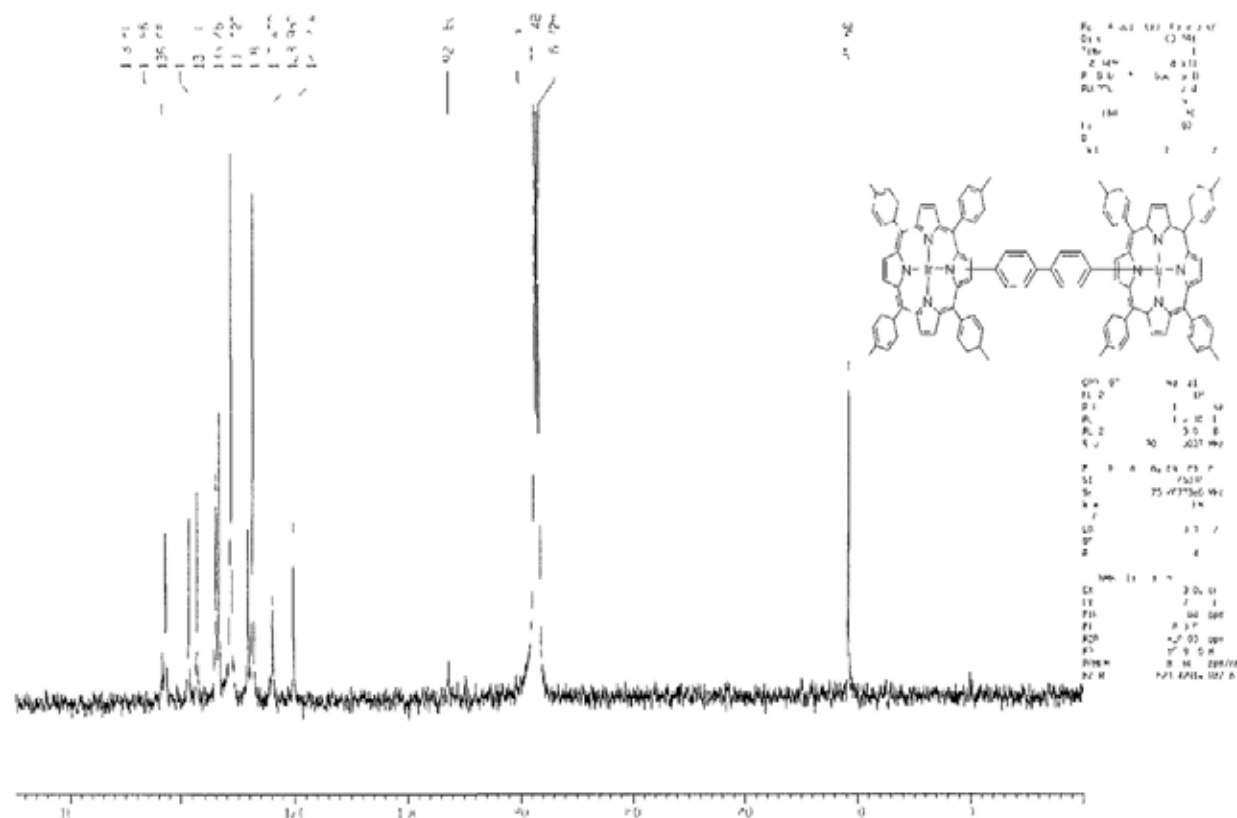
^{1}H NMR Spectrum of Ir^{III}(ttp)CH$_3$ (10) (CDCl$_3$)

323
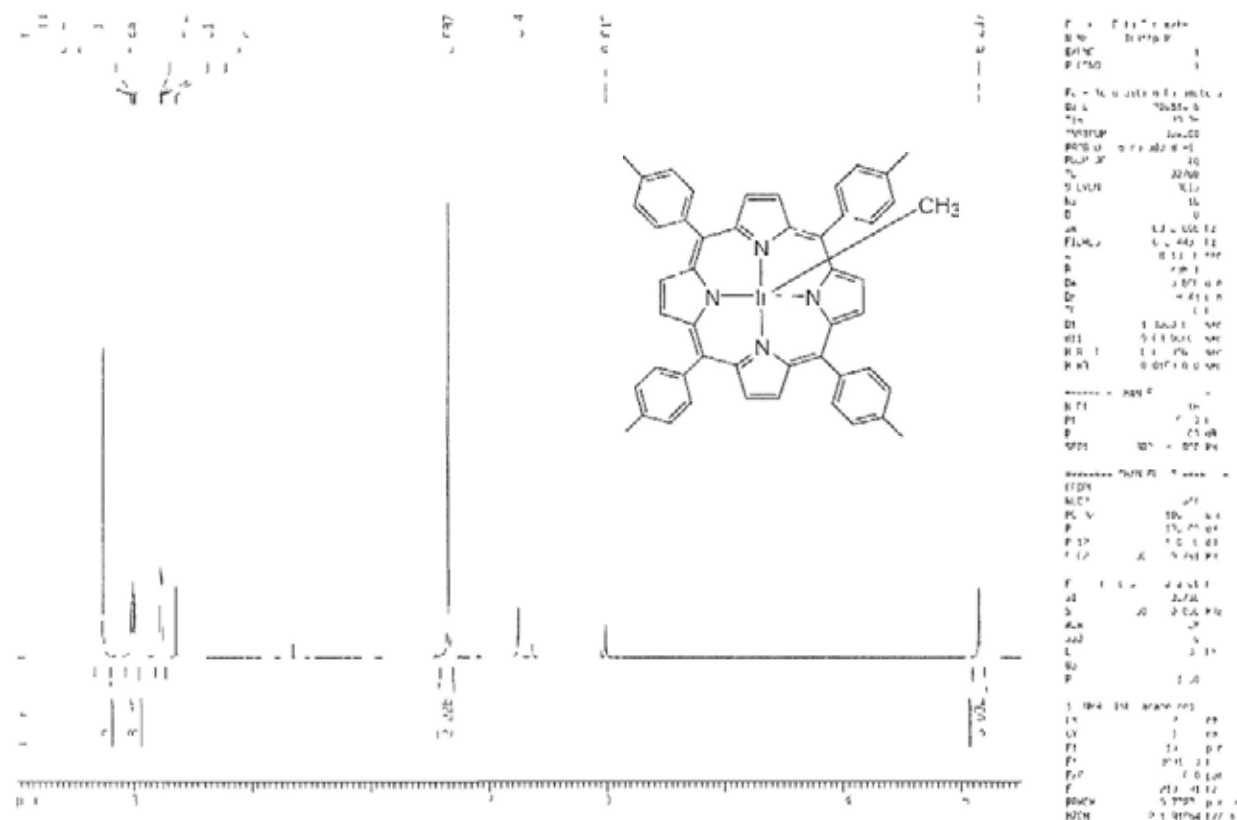
^{1}H NMR Spectrum of Ir^{III}(ttp)Bn(p-Cl) (11) (CDCl$_3$)
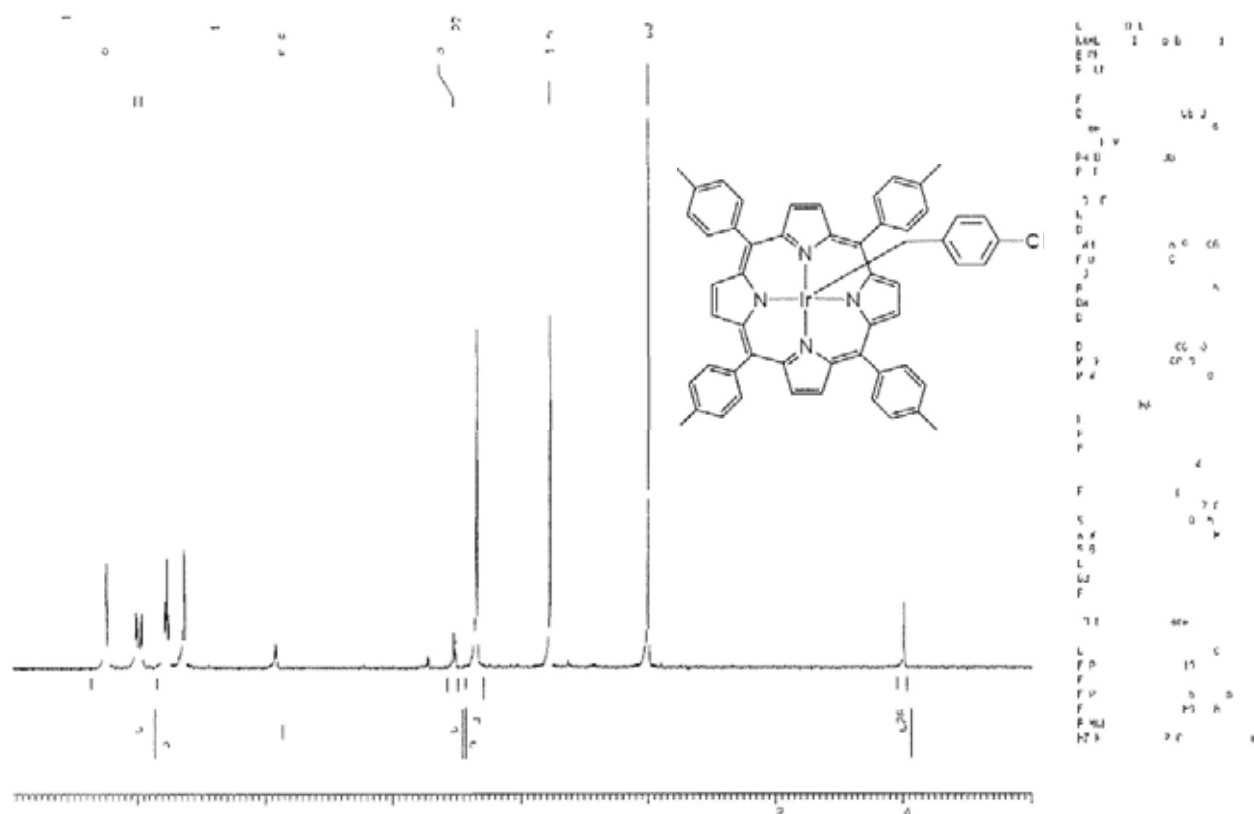
^{13}C NMR Spectrum of Ir^{III}(ttp)Bn(p-Cl) (11) (CDCl$_3$)
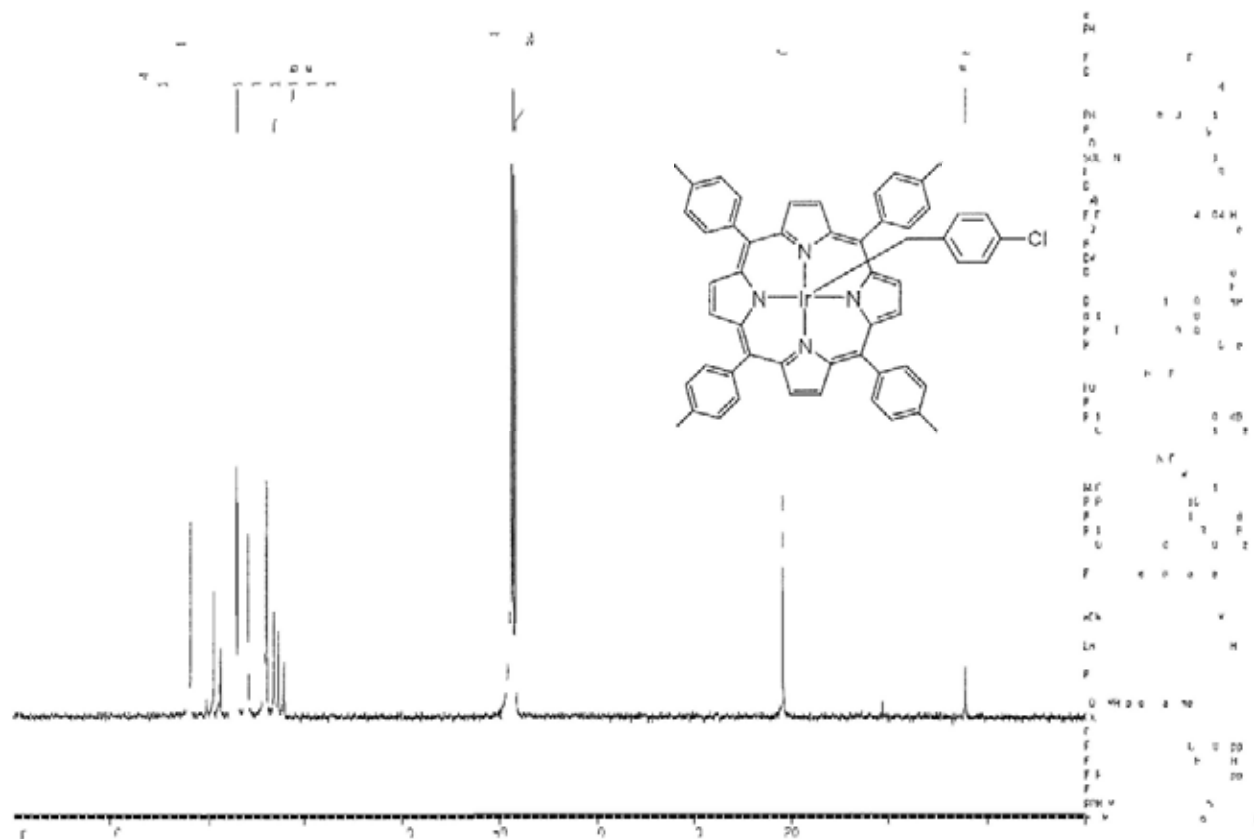
^{1}H NMR Spectrum of Ir^{III}(ttp)(PPh$_3$)C(O)C$_6$H$_4$(*p*-Cl) (**12**) (CDCl$_3$)

^{13}C NMR Spectrum of Ir^{III}(ttp)(PPh$_3$)C(O)C$_6$H$_4$(*p*-Cl) (**12**) (CDCl$_3$)